Studying the Biliary Tree using Organoid-Technology

F.J.M. Roos

Studying the Biliary Tree using Organoid-Technology

F.J.M. Roos

Studying the Biliary Tree using Organoid-Technology

Cover:	Jaap Goslings
Illustratieve bewerkingen:	Jaap Goslings
Layout:	ridderprint.nl
Printing:	ridderprint.nl
ISBN/EAN:	978-94-6458-067-9

The printing of this thesis has been financially supported by the Department of Surgery, Erasmus University Medical Center, Rotterdam; Erasmus University Rotterdam; Nederlandse Vereniging voor Hepatologie; XVIVO; Nederlandse Transplantatie Vereniging; Chipsoft and Medical Delta.

Studying the Biliary Tree using Organoid-Technology

Bestuderen van de galboom middels
organoïd technologie

Proefschrift

ter verkrijging van de graad van doctor aan de

Erasmus Universiteit Rotterdam

op gezag van de

rector magnificus

Prof. dr. A.L. Bredenoord

en volgens besluit van het College voor Promoties.

De openbare verdediging zal plaatsvinden op
donderdag 31 maart 2022 om 15:30 uur

door

Floris Johan Maria Roos

geboren te 's-Gravenhage.

Erasmus University Rotterdam

Promotiecommissie:

Promotoren:	Prof. dr. J.N.M. IJzermans Prof. dr. L.J.W. van der Laan
Overige leden:	Prof. dr. M.P. Peppelenbosch Prof. dr. U.H.W. Beuers Prof. dr. S.W.C. van Mil
Copromotor:	Dr. ing. M.M.A. Verstegen

Paranimfen:	Dr. ir. J. Willemse M.J.M. Roos, BSc

TABLE OF CONTENTS

PART I

INTRODUCTION AND DEFINITIONS

CHAPTER 1

General introduction and outline of thesis, partially based on:

Biliary complications after liver transplantation; recent developments in etiology, diagnosis and endoscopic treatment.

Floris JM Roos, Jan-Werner Poley, Wojciech G Polak, Herold J Metselaar

Best Practice & research: Clinical Gastroenterology 2017 Apr;31(2):227-235.

BACKGROUND

The biliary tree is a complex tubular system containing two major parts: the extrahepatic bile duct (EHBD) which consists of the common bile duct, cystic duct and both of the hepatic ducts, and the intrahepatic bile ducts (IHBD).[1,2] Bile, produced by hepatocytes flows via caniculi into the ducts, passing the epithelial biliary cells (cholangiocytes) on its way.[3] These cholangiocytes provide a protective layer to the hepatic bile and transport bile from the peripheral parts of the intrahepatic ducts to the central large ducts and eventually the extrahepatic bile duct.[4] Genetic and adapted defects in cholangiocytes can cause severe diseases (cholangiopathies).[5] Due to the progressive nature of these destructive diseases, treatment options remain limited with liver transplantation being the only curative option till date.[5,6] Adequate research models are needed to improve our knowledge on these diseases. and to test novel therapies. As the feasibility of 2-D culturing primary cholangiocytes is difficult and limits the feasibility of preclinical models to investigate mechanisms of cholangiocyte-related disease[7], new techniques have been developed including 3-dimensional cholangiocyte (organoid) cell models.[8-10] In this dissertation, I will investigate if cholangiocyte organoids from adult cells are adequate models to study the biliary epithelium. In addition, I will reveal mechanisms of cholangiopathy pathology, provide novel sources for creation of organoids, and demonstrate novel options for treatment.

LIVER ARCHITECTURE AND FUNCTION

Macroscopic architecture

The liver is the largest internal organ in the human body, located in the upper right quadrant of the abdomen, just below the diaphragm, making up for approximately 2.5% of the adult body weight.[11,12] Anatomically the liver is divided into four lobes (including lobus caudatus and quadratus) and a total of eight "Couinaud" segments.[12] The liver receives oxygen-rich blood from the hepatic artery and less oxygenated blood via the portal vein. The vascular discharge is accomplished via hepatic veins draining on the inferior vena cava (Figure 1).[11] The liver is involved in many biological functions, including lipid- and protein synthesis, metabolic breakdown of products, synthesis of blood clotting factors and the production of bile. Bile is a viscous fluid containing waste products produced by hepatocytes, bile acids, electrolytes, proteins and lipids.[4] Due to the toxic, detergent-like composition, bile can disrupt the lipid layer of the plasma membrane and thereby destroy the integrity of cells. Only cholangiocytes and hepatocytes have mechanisms to protect themselves against the toxicity of bile.[4,13]

Bile flows from the smallest canaliculi, located between hepatocytes, via small and bigger bile ducts of the intrahepatic biliary tree to the common bile duct (CBD) and finally to the ampulla of Vater into the duodenal part of the intestines where bile plays a key role in food digestion

(Figure 2).[4] During transport, cholangiocytes modify the bile composition, by secretion of water and electrolytes, to optimize food digestion and energy consumption. The intrahepatic bile ducts are characterized based upon their size and location. The smallest ducts arise at the canals of Hering where they form cholangioles and start to increase in size to form interlobular ducts (15-100 µm), septal ducts (100-300 µm) and segmental ducts (300-400 µm) eventually draining in the right- and left hepatic duct.[14] These ducts are considered the first part of the extrahepatic system and fuse to form the common hepatic duct. After demerging of the cystic duct to the gallbladder, the bile duct is considered the CBD. The biliary tree receives oxygen rich blood via the peribiliary plexus, a network of surrounding blood vessels around the bile duct, which originates from the hepatic artery.[15]

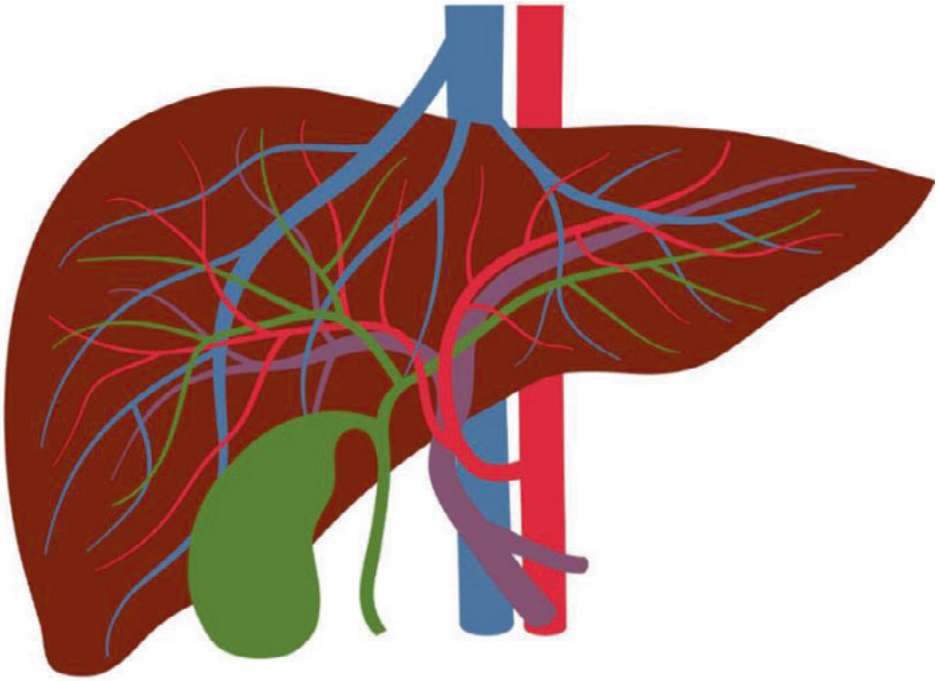

Figure 1. Schematic overview of the liver.
The liver (brown) with its most important structures. In green the biliary system is shown with the gall bladder outside of the liver. Eventually, the bile ducts drain bile into the duodenum (not displayed). The vascular architecture of the liver is shown in purple (portal vein), in red (hepatic artery) and in blue (the inferior caval vein, below and above the liver and the hepatic veins at the liver top).

Microscopic architecture

When looking in more detail, cells within the liver are found to be highly organized in liver lobules.[3] Each hepatic lobule has a central vein, which drains into larger hepatic veins, and is surrounded by multiple portal triads. These portal triads are consistently present at each

corner of the hexagonal liver lobules, and consist of three structures, a hepatic artery, a bile duct and a portal vein. This typical architecture is already present in the hepatoduodenal ligament, indicating a highly organized organ.[3] Blood flows from the portal vein via sinusoids to the central vein. The epithelial cells of the liver (hepatocytes) align the sinusoids and therefore, are able to modify and transport substances, such as albumin and glucoce, directly into the circulation.[3]

Hepatocytes

Hepatocytes are the most common cell type in the liver and are involved in many essential processes, such as protein and glucose storage and synthesis, detoxification, bile salt synthesis and formation of bile.[16,17] The hepatocyte is cubical in shape and has a large round nucleus, which can vary in size (anisokaryosis) a phenomenon that often reflects the degree of polyploidy which is often found in hepatocytes. Moreover, they show functional heterogeneity along the sinusoidal axis (Figure 3).[18] Periportal hepatocytes (zone 1) are specialized in β-oxidation and gluconeogenesis, whereas pericentral hepatocytes (zone 3) are better capable of detoxification, glycolysis and lipogenesis. Metabolic functional differences in hepatocytes, which is largely the result of Wnt-signaling.[18-20] Wnt-signaling is an essential pathway known to be important in embryonic development, cell proliferation and cell differentiation.[21]

In line with their metabolic activities, it has been suggested that hepatocytes also have different self-renewal features based on their location.[22] A highly controversial study described that pericentral diploid Axin2$^+$ hepatocytes are capable to replace 40% the liver to remain homeostasis, within one year.[22] Axin2 is a target gene of the canonical Wnt-pathway[23], which according to this study could be activated in the liver by Wnt-ligands secreted from the central vein, thereby maintaining the niche of these Axin2$^+$ hepatocytes.[22] On the other side of the sinusoidal axis the periportal hepatocytes are located, these specific hepatocytes do not take part in liver homeostasis and have a different gene expression profile compared to the pericentral hepatocytes (being Sox9$^+$ instead of Axin2).[24] A potential specific function, attributed to these cells, is increased proliferation upon chronic injury and thereby contributing to restauration of the hepatocyte compartment.[24]

Cholangiocytes

Although representing a minority of the cells present in the liver (around 3-5%), cholangiocytes account for major physiological functions. They transport and modify bile as well provide a functional barrier to protect hepatocytes from invasion of micro-organisms and toxins present in bile.[4] Cholangiocytes are highly polarized (apical-basolateral) and are either cuboidal (small bile ducts) or columnar (larger bile ducts) in shape, with the nucleus located at the basolateral side. Microvilli and a typical primary cilium are situated on the luminal side of the cells and act as antennae for assessing bile quality.[25-27] This non-motile

cilium harbors a variety of channels and receptors that regulate intracellular signaling,[28] thereby acting as a mechanosensor, osmosensor and chemosensor.[28-30] Based upon the signals from the cilium, cholangiocytes operate a variety of receptors and channels to modify bile.

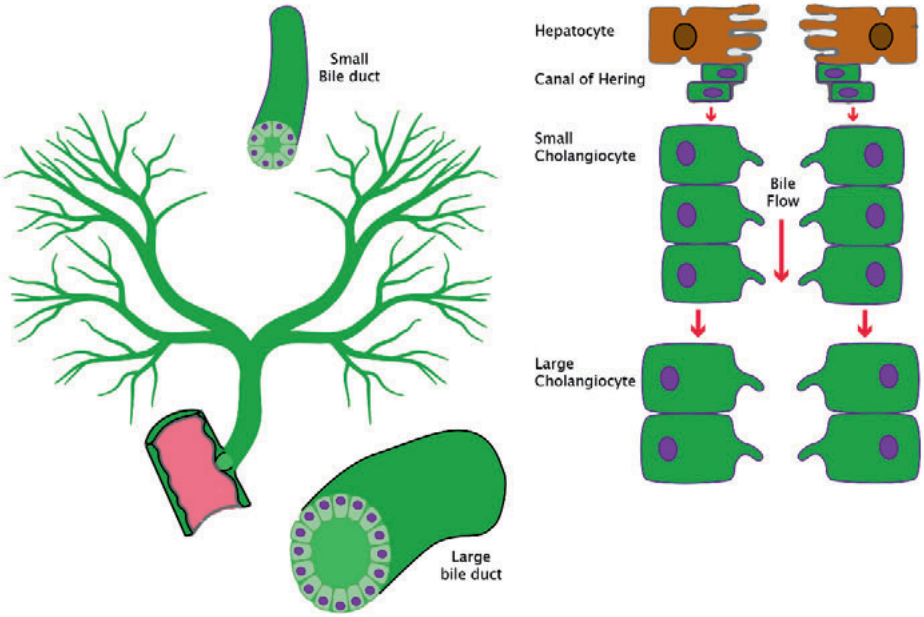

Figure 2. Schematic overview of the biliary tree.
On the left, the branches of the intrahepatic biliary tree are displayed. The bile ducts in the intrahepatic biliary tree are relatively small with a small lumen, when compared to the large bile ducts outside of the liver. Moreover, cholangiocytes (the bile duct epithelial cells) in the small bile ducts have a high nucleus/cytoplasm ratio (see right panel of the figure). The intrahepatic bile ducts drain bile on the right- and left hepatic bile duct. Eventually the hepatic ducts drain upon the common bile duct (CBD) and the duodenum. At the right panel, the bile producing hepatocytes are displayed. Bile is drained in the lumen of the smallest of cholangiocytes, located in the canal of Herring, to the lumen formed by the large cholangiocytes.

In Figure 4**,** a schematic representation of a cholangiocyte is shown. On the luminal side the ion-channels, cystic fibrosis transmembrane conductance regulator (CFTR), calcium-activated chloride channel (CaCC), and anoctamin (ANO)-1 are situated. The latter two can secrete chloride (Cl^-) as well as bicarbonate (HCO_3^-).[4,31] The Anion-Exchange protein 2 (AE2, also known as SLC4A2), exchanges Cl^- for HCO_3^- and the water transportation-channel aquaporin1 (AQP1), are located at the luminal side of the cells.[32] The cholangiocyte's main task is to secrete bicarbonate during the post-prandial period.[33,34] Cholangiocyte transporter activity is

highly regulated. For instance, increased levels of cAMP, as a result of secretin binding to its basolateral receptor, activates, Protein Kinase A (PKA) subsequently activates CFTR.[35,36] Other key-activators of secretin-stimulated bicarbonate secretion include vasoactive intestinal polypeptide (VIP)[37], acetylcholine (ACh)[38], bombesin and phenylephrine.[39] Secretin-stimulated secretion can be inhibited by binding of hormones such as dopamine, gastrin, endothelin and somatostatin to the basolateral somatostatin receptor.[39-41] Increased levels of intracellular calcium (Ca^{2+}), via interaction with nucleotides and luminal P2Y-receptors, will promote release of Ca^{2+} from the Endoplasmatic Reticulum (RA), subsequently resulting in activation of the ANO1 channel and promoting further bicarbonate secretion.[42,43] Cholangiocytes also contribute to absorption of bile acids, glucose, ions and amino acids from bile.[44,45] BAs can be taken up via the Apical Sodium Bile Acid Transporter (ASBT, also known as SLC10A2) at the luminal side of the cell,[46] and excreted basolaterally trough either the multidrug resistance protein 3 (MRP3, also known as ABCC3)[47-49] or the organic solute transporters (OST)α and OSTβ.[50,51] Resorption of water via AQP1 is stimulated via a gradient formed by the sodium (Na^+)-glucose transporter (SGLT1) and the Basolateral glucose-transporter 1 (GLUT1).[52] Ions can be exchanged and transported by a variety of channels such as the luminal transporter Na^+/H^+(NHE3)[53] or the basolateral sodium-potassium-co chloride transporter-1 (NKCC1)[4]. Finally, cholangiocytes are able to transport proteins in both directions by a variety of multidrug resistance proteins.[34]

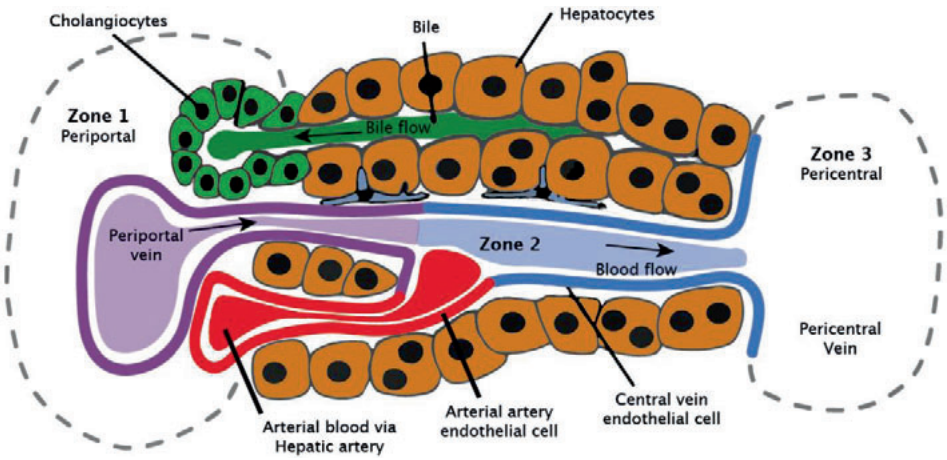

Figure 3. Schematic architecture of hepatocytes and their zonations.
On the left zone 1 (periportal zone -hepatocytes surrounding the portal vein-) and on the right zone 3 (pericentral -hepatocytes surrounding the central vein-) is displayed. Green indicates cholangiocytes and brown hepatocytes. Zone 2 (midlobular zone) is between zone 1 and 3. In purple the portal vein is shown, which along with the hepatic artery (red) drains oxygen rich blood to the central vein (blue).

EMBRYONIC DEVELOPMENT OF THE LIVER

The parenchymal compartment (hepatocytes)

At the start of embryonic development, the blastocyst is formed. This cellular structure contains the trophoblast, which gives rise to extraembryonic tissue, and the inner cell mass, which gives rise to the embryo. The cells within the inner cell mass are pluripotent and will therefore give rise to all cell types of the embryo. During gastrulation, the blastocyst forms three germ layers, ectoderm, mesoderm and endoderm. The definitive endoderm (DE) is patterned into the foregut, midgut and hindgut[54]. Budding of the epithelial wall of the foregut with the septum transversum (mesodermal tissue surrounding the foregut) is essential for proper liver development. In addition, signaling via Fibroblast growth factor 2 (FGF2) from the developing heart, retinoic acid (RA) from the lateral plate mesoderm and bone morphogenetic protein (BMP4)[55], will further promote formation of the liver bud. At gestational week eight, the liver bud will be fully composed of hepatoblasts[56], which are bipotential progenitors capable of differentiating to hepatocytes and intrahepatic cholangiocytes.[57] Proper hepatocyte development and maturation of the liver are further promoted by the transcription factors Forkhead box protein A1 (FOXA1), FOXA2 and GATA4.[58-60]

The biliary tree

The differences between the intra- and extrahepatic bile ducts arise from their distinct embryological origin.[2] An important pathyway for embryonic development in animals in the NOTCH signaling pathway. In the liver, the Notch signaling pathway is essential for development of the intrahepatic bile ducts.[61] It regulates hepatoblast (stem cell) fate decisions by allowing direct cell-communication via a ligand-receptor interaction. The most important ligand for biliary tree formation is Jagged1 (JAG1).[61] Under influence of JAG1/NOTCH2-, transforming growth factor β (TGFβ)-, and fibroblast growth factor (FGF)[55,62] signaling from the portal mesenchyme, hepatoblasts upregulate the expression of Hepatocyte Nuclear Factor 1β (HNF1β), HES1 and SOX9, and begin their differentiation into cholangiocytes as they form the ductal plate.[63,64] The ductal plate is a circular layer of single biliary progenitor cells, and will eventually form the intrahepatic bile ducts.[56] At the beginning of ductal plate formation, the cells express both hepatocyte- and cholangiocyte markers.[56] During growth and additional maturation under influence of WNT/β-catenin, HIPPO-YAP and Hedgehog signaling, they eventually lose their hepatocyte markers and express additional biliary maturation markers.[65-68] Once the ductal plate reaches this current state, cells situated in the portal mesenchyme will start additional growth and vascularize the bile ducts by forming the peribiliary plexus (PBP).[68.69] Recently hepatobiliary hybrid progenitor (HHyP) populations were identified in the proximity of the ductal plate.[24] These cells have a distinct transcriptome compared to the classic hepatoblasts but can also give rise to either

hepatocytes and cholangiocytes, thus they might be contributing to proper cholangiocyte development as well.[70]

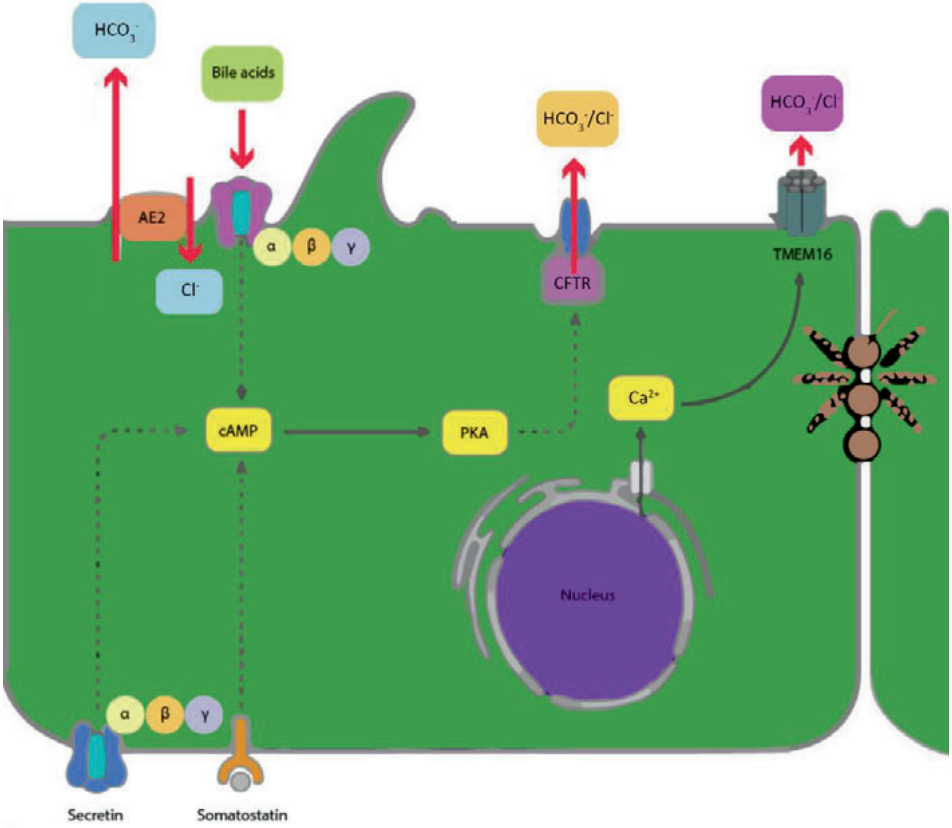

Figure 4. Schematic overview of a cholangiocyte.
In green two (partial) cholangiocytes are displayed, connected via tight junctions. The top side of the figure represents the luminal side of the cholangiocyte with the ion-channel transporters (TMEM16, ANO1 and cystic fibrosis transmembrane conductance regulator -CFTR-). The endoplasmatic reticulum can release Ca^{2+}, that subsequently can activate TMEM16A. Furthermore, the Cl^-/HCO_3^- anion exchanger 2 (AE2) and the primary cilium are displayed. On the bottom of the figure (the basolateral side of the cholangiocytes) the secretin- (SCTR) and somatostatin receptors (SSTR) are shown. Secretin signaling can stimulate cAMP release which subsequently activates CFTR. In contrast, SSTR binding inhibits cAMP. On the top right a tight junction (brown and black) is displayed.

The extrahepatic bile duct has not been as extensively studied as its intrahepatic counterpart and therefore itsdevelopment is not fully clear yet. Known is that the EHBD arises from the

caudal part of the ventral foregut. At embryonic day 8.5, the liver bud will grow out, forming a narrowing, tubular connection to the duodenum and pancreatic buds.[2,71] The pancreaticobiliary progenitors represent a minority of endodermal pancreatic cells that express both SOX17 and pancreatic and duodenal homeobox (PDX)1. Eventually, the extrahepatic bile ducts are formed from these cells under the influence of SOX17 in combination with signaling from Prospero homeobox protein (PROX-1), HES1, HNF-6 and HNF1β.[2]

REGENERATION OF THE LIVER AND BILIARY TREE

After partial hepatectomy

The liver is the only visceral organ in the human body that is capable of regeneration after surgical resection. After 2/3 partial hepatectomy, a massive cellular response is observed, culminating in the restoration of liver mass within a few days. Liver regeneration after partial hepatectomy relies on proliferation and hypertrophy of mature hepatocytes and is divided in three consecutive phases: (1) priming, (2) proliferation and (3) termination.[72] During the priming stage, inflammatory cytokines such as tumor necrosis factor (TNF)-α and interleukin (IL)-6, secreted by Kupffer cells (hepatic macrophages) sensitize hepatocytes to respond to growth factors.[73,74] In the proliferative phase, hepatocytes (re)-enter the G1 cell-cycle due to stimulation of growth factors and interaction with neighbouring cells such as epidermal growth factor (EGF), hepatocyte growth factor (HGF), vascular endothelial growth factor (VEGF) interaction with the endothelium[75] and insulin-like growth factor (IGF)-1[76], secreted for instance by platelets.[77,78] When HGF binds to its receptor (c-MET), β-catenin is quickly translocated to the nucleus of the hepatocyte and induces upregulation of proliferative target genes. Inside the nucleus there is a crosstalk between YAP, Hedgehog and Wnt-signaling, stimulating hepatocyte proliferation and organ formation.[79] This process is finally terminated in the last phase of regeneration by upregulation of TGF-β by the liver and spleen.[80,81]

Hepatocyte homeostasis and regeneration

Depending on the type of liver injury, distinct processes become active in the formation of new hepatocytes. For example, depending on the zonal area (PP or PC) and duration of the injury, different hepatocytes along the sinusoidal axis are activated. The previously mentioned Axin2$^+$ hepatocytes located in the pericentral part of the liver might play a role in homeostasis.[22] In addition to Axin2, this hepatoctyte subset also expresses the embryonic hepatoblast marker Tbx3, and proliferate in a much higher pace compared to other types of hepatocytes as was found by lineage tracing.[22] This was confirmed by additional lineage trancing strategies, which showed that major facilitator superfamily domain containing 2a (Mfsd2a, a gene known to be expressed in periportal hepatocytes) positive hepatocytes were replaced by Mfsd2a$^-$ hepatocytes that migrated from the pericentral area during homeostasis.[82] More recently, these pericentral hepatocytes were found to express LGR5.

Upon injury, the LGR5$^-$ cells swiftly become LGR5 positive.[83] Along with the fact that Wnt-ligands have been found in the endothelium, these results indicate that a local niche of Wnt activated cells could exist around the central vein.[22] Alternatively, hepatocytes located in the periportal zone are also capable of regeneration of hepatocytes upon mild injury.[24] These cells were named hybid hepatocytes (HyHPs) because they express cholangiocyte markers, such as SOX9 and SPP1 in addition to the mature hepatocyte-related gene HNF4α. Since they don't express genes involved in metabolism the primary function of these hybrid hepatocytes, could be regeneration of cholangiocytes and hepatocytes upon injury.[24] Although it seems logical to have a special niche for regenerative cells at the location where there is the highest chance of injury, these cells also have the highest metabolic and synthetic activity.[84] Considering efficiency, it would make more sense for the liver to have a system in which cells have high plasticity and can rapidly switch function. Ideally, this includes primary cells (hepatocytes) that are able to divide and contribute to regeneration within each zone upon need. Several studies suggest that proliferating hepatocytes are located throughout the lobule during homeostasis.[85-88] One of the first publications on this topic showed that these dividing hepatocytes indeed exist. The authors identified these cells as being highly telomerase reverse transcriptase (TERT) positive.[85] Telomerase synthesizes telomere repeats and by doing so could play an essential role in maintaining long-term proliferative capacities of stem-cells. TERT^{high} positive hepatocytes were actively dividing during homeostasis and could also respond by additional proliferation during several forms of drug induced-liver injury. With this, the authors demonstrated that regeneration occurs throughout the whole lobule, but that only a specific subset of hepatocytes contribute this regeneration.[85] Interestingly, subsequent studies showed that hepatocytes throughout the liver contribute equally in regeneration of the liver upon injury and during homeostasis, with no subset of cells having a major proliferative advantage over another.[86-88] Moreover, they demonstrated that in previous lineage Axin2$^+$ tracing models had a bias inserted and thereby interrupting the ingenious allele resulting in haploinsufficiency, eventually leading to a high percentage of hepatocytes being formed from Axin2$^+$ hepatocytes. Thus, this lineage-tracing bias could explain the previous results observed by the authors.[22,88] Additionally, it was demonstrated that the ploidy of hepatocytes, often suggested to be a key aspect that might affect the ability of hepatocytes to proliferate, does not lead to an increase in regenerative capacities.[86] Recent publications did show a proliferative advantage of hepatocytes from a specific zone.[89,90] By using elegant lineage tracing models, it was shown that zone 2 hepatocytes contribute the most to hepatocyte turn-over during homeostasis. Moreover, they showed that zone 2 hepatocytes also contributed to regeneration of zone 1 or zone 3 hepatocytes after injury.[89,90]

In summary, it seems that all hepatocytes can contribute to homeostasis and regeneration after injury. This would be in contrast to the earliest mentioned studies[22,24], and although from a biological perspective it would make more sense to have hepatocytes which can all

divide, a definitive answer is yet to be given. Finally, if injury is too severe to be restored by hepatocytes, the liver might possess a final method for regeneration, namely via a liver stem/progenitor cell (LPCs). Although, it is highly controversial if these "stem cells" actually exist, and if so, what these cells are and where they are located. A possible candidate is the oval cell, located near the canal of Hering.[91] Rat studies revealed that, upon response to injury, these cells differentiate to hepatocytes.[91] Within the reprogrammed cells, there is a subpopulation which share hepatocyte and cholangiocyte markers and show signs of bi-potential differentiation *in vitro*.[10,92] If these cells are actual LPCs and are capable of hepatocyte regeneration *in vivo* is still unknown.

Although the exact mechanisms by which differentiation is regulated is unknown, liver epithelial cells are subjected to a certain plasticity. Cells residing the intrahepatic bile ducts have self-renewal potential and can be (trans)differentiated to hepatocyte-like cell *in vitro*.[93] Moreover, evidence shows that cholangiocytes can act as a facultative (stem) cell compartment and become hepatocytes (in the absence of hepatocyte proliferation) in an *in vivo* model.[94] Although it is unclear if this process is a direct differentiation, it does reveal the enormous plasticity present within the epithelial liver compartments. Additionally, single cell gene expression analysis of liver-resident cells, did not reveal any transcriptomic-profiles resembling signatures that relate to quiescent stem cells (similar to rat oval cells). It was shown tough, that a subpopulation of cholangiocytes might differentiate to hepatocytes under the right circumstances.[95] Thus, it seems reasonable to assume that mature cholangiocytes show a high degree of phenotypic plasticity and can dedifferentiate into cells with more stem cell-like properties (e.q. highly proliferative). However, to compel a more satisfied answer, these types of analysis should also be performed on injured livers. Finally, several studies suggest that it might be a subset of cholangiocytes which can act as a facultative stem cell that can be directed to hepatocytes, it could very well be that all cholangiocytes possess this characteristic.[95,96]

Bile duct homeostasis and regeneration

After partial hepatectomy, not only do the parenchymal cells need to proliferate, but the bile duct cells (obviously) need to regenerate as well. This is supported by the evidence that during regeneration multiple waves of DNA synthesis can be detected, [97,98] suggesting that not only hepatocytes, but also biliary- and other cells undergo accelerated growth and replication. Proliferation of mature cholangiocytes is strongly regulated by a variety of factors such as IL-6, TNF, Ach, bile acids and tumor growth factor (TGF). However, cholangiocytes can also respond to both hormonal cues.[99] Cholangiocytes possess receptors for testosterone and estrogen and start proliferating when activated by these hormones. Estrogen prevents apoptosis, while testosterone increases the mass of intrahepatic bile ducts.[100-102] Similar to liver parenchymal cells, bile ducts regenerate in homeostatic conditions through self-replication of mature cholangiocytes where lost cells are replaced through apoptosis.[24]

Secretin, serotonin, and IL-8 are (or seem to be) important mediators for regulation of cholangiocyte replication.[103,104] Upon severe injury, replication can be achieved by ductal reprogramming of cholangiocytes to a more proliferative/progenitor-like cholangiocyte state. Cholangiocytes can also become activated and proliferative through ischemia-reperfusion injury (IRI), cholestasis, infection and inflammation. During ductal reprogramming, pathways that also regulate biliary organogenesis will become operative and start regulating cell-fate decisions. A key regulating factor in this process is activation of the YAP-Hippo pathway[96,105,106], in close correlation with its downstream target Notch as well as Wnt and Hedgehog signaling. In contrast to hepatocyte proliferation which requires canonical Wnt/β-catenin driven signaling, ductal reprogramming requires non-canonical Wnt-signaling *in vivo.*[105]

If self-replication by cholangiocytes falls short, there are alternatives to restore the biliary epithelium as well (Figure 5). Hepatocytes can transdifferentiate to cholangiocytes in the absence of functional Notch-signaling, making them a facultative (stem) cell for cholangiocytes.[107] However, the question remains if this process concerns a direct transdifferentiation from hepatocytes to cholangiocytes or if this included an unknown pathway via a shared progenitor cell. As stated previously, the existence of a true bipotent LPC is still open for debate; however, this cell could theoretically also contribute to cholangiocyte regeneration. It is important to mention that the discrepancies described in studies on LPCs arise from the differences between *in vitro* and *in vivo* models used and the fact that animal models do not necessarily fully recapitulate the human *in vivo* situation.[91] However, it is clear that both epithelial compartments in the liver have unique and profound cellular plasticity and respond to various conditions.[108]

Cholangiocyte heterogeneity is not unique within the liver, but has also been discovered in the extrahepatic bile ducts. A study demonstrated that cholangiocytes in the gallbladder, the common bile duct and the pancreatic duct each have their own distinguished gene expression profiles.[109] Moreover, this study showed that, in line with their embryonic origin, only intrahepatic cholangiocytes could (trans)differentiate to hepatocytes *in vitro*.[109] Interestingly, a subsequent study from the same group used single cell RNA sequencing to unravel the transcriptome of intrahepatic-, common bile duct-, and gallbladder-derived cholangiocytes.[110] Based upon sequencing of cholangiocytes along all regions of the biliary tree, their data suggests that only one type of cholangiocyte exists across the biliary tree and that local niche-factors (extracellular matrix and bile composition) drive differences in local transcriptomic differences.[110]

Even though cholangiocyte homeostasis in the EHBD also relies on self-replication of biliary cells, the situation upon injury could be different. The large intrahepatic bile ducts and EHBD provide a unique structure which might contain facultative progenitor cells.[111] These crypt-like structures, similar to the stem-cell compartments in the intestine, are called the peribiliary glands (PBGs). PBGs had been described already around a hundred years ago, but

were considered to be mucus secretory glands. This changed in the past decade, when the cell population present in these glands, decade some stem cell properties.[112,113] Despite the fact that more evidence is still needed to prove that the PGB-resident cells are actually stem cells, it is clear that primary cholangiocytes located within the PBGs can become proliferative upon *ex vivo* injury. This eventually results in cell proliferation and repopulation of the injured EHBD with mature cells.[114] Once the ductal barrier function is restored, the PBG cells are inactivated and are non-proliferative again. VEGF signaling along with myofibroblast organization is important for this activation.[114] However, it is unknown if only cells located in the PBGs can become activated upon injury, or if this is a process occurring across the whole EHBD. One theory could be that because the cells located in the PBGs are "relatively deep" inside the EHBD, they are less susceptible for initial injury and regeneration could start within the PBGs, but eventually happens across the whole EHBD.

CHOLANGIOPATHIES

If regeneration of biliary epithelium fails or is impaired, diseases can develop.[115] Diseases of the bile duct are called cholangiopathies, which can either be acquired, as is the case in Primary Sclerosing Cholangitis (PSC), Primary Biliary Cholangitis (PBC) or biliary atresia, or derived from an underlying genetic defect such as cystic fibrosis (CF), neonatal sclerosing cholangitis, or Alagille syndrome (AGS). Most cholangiopathies progress chronically, often ending in end-stage liver disease and resulting in severe morbidity and even mortality.[115,116] Treatment options are limited; therefore, patients often require a life-saving (LT). This is emphasized by the fact that biliary diseases account for the LT indication in 80% of children cases and 20% of adult cases.[5,6] Much is already known about genetic biliary diseases which can provide clues for therapies and underlying pathophysiology of their resembling acquired cholangiopathies.

Alagille Syndrome (AGS)

AGS is an autosomal dominant genetic disorder with an incidence of 1 in 70.000-100.000 births. Due to specific mutations, defective JAG1/NOTCH2 signaling results in incomplete development of the intrahepatic bile ducts from the hepatoblast during embryogenesis.[117-119] In addition to developing jaundice due to impaired bile secretion in the liver, additional malformations in heart, eyes, skeleton and face occur in AGS patients.[120] Although presentation varies, AGS is highly associated with chronic liver disease that often results in end-stage liver disease and 20-50% of patients will require a liver transplantation during life.[121] Clinically, AGS presents itself as a typical "chicken wire fibrosis" as typically seen in alcoholic liver disease (ALD).[122] Thus, NOTCH signaling could also play a role in ALD occurrence. As stated earlier, NOTCH signaling is essential for biliary regeneration and development, but AGS demonstrated that NOTCH signaling is also essential for intrahepatic branching morphogenesis, which could be confirmed in subsequent studies.[117-119] However,

the intrahepatic biliary compartment in mice can be formed in the absence of Notch by the (trans)differentiation of hepatocytes acting as facultative (stem) cells.[108]

Cystic fibrosis (CF)

Cystic fibrosis is a common autosomal recessive disease caused by mutations in the CFTR-gene.[123,124] The primary function of CFTR is secretion of chloride and bicarbonate. It is expressed in multiple epithelia, such as the intestine, the lung, pancreas and the bile ducts, making CF a multi-organ disease.[123,125,126] In the past, CFTR-related biliary complications were seen rarely, due to these complications happening at a late stage in disease. Often the patient was already deceased due to their pulmonary disease, before biliary problems could occur. With the novel therapies and improvement in preventing pulmonary decline, nowadays 5-10% of the CF patients develop cystic fibrosis related cholangiopathy (CFRC).[127,128] In the bile ducts, CFTR is essential for fluid transportation and bile formation; thus dysfunctional CFTR could eventually lead to blockage of bile resulting in cholestasis, secondary biliary cholangitis, and eventually end-stage liver disease.[14] Treatment of CF is based upon addition of small-molecule treatments correcting the different genetic mutations. Treatment options are categorized in either potentiators which restore activation of the CFTR-channel, or correctors which correct the (folding problem of the) protein.[129,130] A recent study demonstrated that 90% of all CF mutations could be successfully corrected with a newly developed cocktail.[131,132] However, most of the *in vitro* and patient-data available has been based upon either lung or intestinal related symptoms. It remains to be investigated if these results can be extrapolated to the biliary system.

Post-transplantation cholangiopathy

Liver transplantation is the only curative treatment option for patients with end-stage liver disease or severe acute liver failure. During LT, the complete liver including (a part of) the EHBD is surgically removed and replaced with either a complete- or a partial liver from a deceased- or living donor. Since the first transplantation in 1963 by Thomas Starzl, the liver transplantation program has come a long way.[133] Sixty years ago it was seen as an experimental procedure, with high mortality and progress was slow. Nowadays, LT has become a routine procedure with excellent long-term outcomes, one- and five-year patient survival is as high 95% and 90%, respectively. This is largely the result of improvements in surgical techniques, patient-screening, novel effective immunosuppressants, and enhanced intensive care units.[134] The improvements have also contributed to a higher demand for LT, resulting in more candidates on the waiting list awaiting transplants than donor organs are available.[135-137] To (partially) overcome the gap between supply and demand, LT programs are using extended criteria organ donors. These grafts are often older, fattier, or are harvested using extensive efforts; this results in an increased complication ratio after liver transplantation.[138]

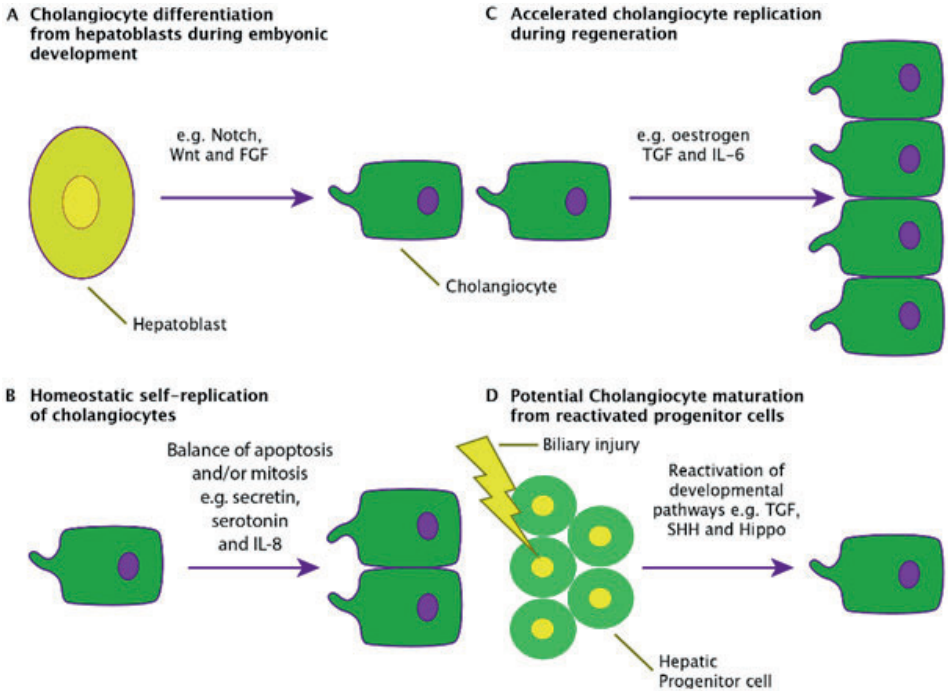

Figure 5. Different (potential) mechanisms of cholangiocyte regeneration.
(a) Cholangiocytes develop via differentiation from hepatoblasts during embryonic development. **(b)** Cholangiocyte homeostasis is achieved due to self-replication of mature cholangiocytes. **(c)** Cholangiocyte regeneration after injury due to accelerated replication (ductal reprogramming). **(d)** Potential regeneration via cholangiocyte differentiation from hepatic progenitor cells that occur after reactivation of developmental pathways.

To optimize diminished donor grafts, current research is focusing on improving methods for allograft preservation before and after collection of the donor organ. For many decades the golden standard for allograft preservation was static cold storage (SCS) in which the organ is cooled down to slow down metabolism and maintain organ viability. However, there is still damage occurring during SCS, therefore new techniques are focusing on either warm- or cold perfusion of the organ grafts using machine perfusion (MP) to minimalize damage.[139-141] Currently, large, randomized trials are being performed to research if MP techniques are superior to SCS in terms of graft- and patient survival as well as graft related complications. The first trials published show very promising results and raise the question if its time to switch standard procedures for graft preservation to machine perfusion techniques.[142-144] However, despite the good overall survival for LT and all the research effects of MP techniques, complications still occur after transplantation. One important group of

transplantation obstacles are the biliary complications represent in 40% of the patients, with the most severe of them being post-transplantation cholangiopathy.[145-148] Post-transplantation cholangiopathy, also known as non-anastomotic bile duct strictures (NAS), ischemic cholangiopathy, or ischemic-type biliary lesions, are strictures or irregularities in the biliary tree beyond one centimeter from the surgical anastomosis in the presence of a patent hepatic artery.[149,150] Incidence of NAS mainly depends on which type of graft is transplanted. In donation after brain death (DBD) donors, the incidence ranges from 4-15%, but in donation after circulatory death (DCD) donors, incidence can be as high as 30-50%.[151,152] NAS is likely a failure of the regenerative capability of the bile duct[153-155], potentially due to specific damage of PBGs.[156] However, this implicates that damage occurs during transplantation. One mechanism of injury can be explained by impaired vascularization of the peribiliary plexus, resulting in damage to the PBGs.[156] Another potential contributing mechanism to cholangiocyte damage, could be the inability to maintain sufficient luminal bicarbonate, the 'bicarbonate umbrella theory'. As stated above, one of the primary goals for cholangiocytes is secretion of bicarbonate to maintain an alkaline pH in bile. If the luminal bicarbonate secretion is impaired, it will leave cholangiocytes vulnerable to conjugated bile acids resulting in apoptosis, senescence, and eventually fibrosis.[157] Over the last couple of years, evidence has emerged that the bicarbonate umbrella plays a crucial role in the development of PBC. A key role is reserved for the Cl^-/HCO_3^- exchanger AE2 which is regulated by microRNA-506.[158-160] Diminished function of either AE2 of microRNA-506 results in lower luminal bicarbonate and eventually cholangiopathy-formation *in vivo*. Interestingly, the standard therapy for PBC is ursodeoxycholic acid (UDCA), which results in both longer overall- as well as transplantation-free survival.[161] When admitted to PBC patients, who have an impaired secretin-induced bicarbonate secretion, UDCA restores prober bicarbonate secretion.[162] Together, these results underline the role played by the bicarbonate umbrella in PBC development. Since a lower pH of bile during liver transplantation is associated with NAS development as well[163], it could be that impaired bicarbonate secretion is a risk factor for NAS.

AN IMPORTANT PLEIOTROPIC ROLE FOR WNT SIGNALING

Wnt-signaling is an evolutionary conserved complex mechanism which is involved in embryogenesis and mature hepatobiliary development. Canonical Wnt/β-catenin signaling is more or less inactive during hepatobiliary homeostasis, but it can be activated when needed for cell-renewal.[164] Moreover, it can play a role in disease development and progression to malignant lesions.[165-168] If canonical Wnt-signaling is inactive, β-catenin levels are low due to degradation by Axin along with APC, CK1α, and GSK3β.[169,170] This combination of proteins is called the destruction complex, which recognizes the phosphorylated β-catenin and degrades it. However, when Wnt-ligands are bound to the Wnt-receptor (Frizzled) and its co-receptors,

the low-density lipoprotein receptor-related protein (LRP) 5 and 6, the Wnt/β-catenin signaling pathway become active.[171-174] Binding of Wnt phosphorylates LRP 5/6 and recruits the protein Dishevelled (DVL) which is capable of binding to the Frizzled receptor.[175,176] Next, Axin binds to the LRP6 receptor, making phosphorylation and subsequent degradation of β-catenin impossible. [175,176] Consequently, β-catenin is translocated to the nucleus where it regulates its downstream effectors, with help of T cell factor/lymphoid enhancer-binding factor (TCF/LEF), (one of) the main Wnt-partner(s).[177] Wnt regulates these downstream effects mostly by activation of target genes involved in proliferation (Myc, Cyclin D1, VEGF, EGFR), dedifferentiation (upregulation of stem-cell related factors, Sox9), and metabolism (Cytochrome P450 enzymes). Interestingly, Wnt- signaling can be enhanced as a result of prolonged activation of Frizzled. A well-known protein capable of enhancing Wnt is R-spondin. Rspondin proteins promote Wnt-signaling via LGR 4, 5 and 6.[178,179] LGR makes sure to increase phosphorylation of the LRP6 complex and more importantly, it ensures that ZNRF3 and RNF43 cannot degrade Frizzled and as a result R-spondin indirectly contributes to Wnt-signaling.[180,181] Other factors which are capable of regulating Wnt are Dickkopf-related proteins (DKK), Wnt inhibitory factor 1, and Frizzled-relate family of proteins (FRPs).[182]
Besides Wnt simulation via β-catenin, Wnt-signaling can also be active independent of β-catenin. These pathways are referred to as non-canonical Wnt-signaling pathways, of which two major variants have been described: the planar cell polarity (PCP) pathway and the Wnt/Calcium pathway.[183,184] In the PCP pathway, Wnt ligands are binding to Frizzled and consequently, they will directly activate Rho-A and Rac, which in turn activate ROCK and JUNK. ROCK and JUNK are important pathways for regulating cell migration and cell polarity (hence, why it is called the PCP pathway).[184-186] In the Wnt/Calcium pathway, the Wnt ligands bind directly to Frizzled and, as a result, a complex is formed which promotes the activation of phospholipase C (PHC).[183] PHC is capable of creating diacylglycerol (DAG) and inositol. DAG activates protein kinase C (PKC) and along with inositol stimulates intracellular levels of calcium. Higher calcium-levels will promote the activity of calcineurin, which plays an important role in cell proliferation and migration.[183] Over the last several years additional pathways have been described in which Wnt ligands can influence cell behavior. However, both the canonical Wnt- and the PCP pathway have been the most extensively studied and show to be important in the context of liver- and biliary development and regeneration. Thus, for the following paragraphs, we will focus on these two pathways.

Wnt signaling in liver development

During embryogenesis, the Wnt/β-catenin pathway is crucial for formation of the liver bud. Throughout gastrulation, the definitive endoderm forms into the foregut, midgut, and the posterior gut. Formation of the hepatic component from the foregut develops in a low gradient of Wnt signaling, tightly regulated by secretion of FRPs from the anterior end of the DE.[181] In the mid- and posterior gut, Wnt signaling is upregulated, thereby enhancing PDX1

expression which will repress HEX signals.[187,188] Subsequently, hepatic development is inhibited in these parts of the DE. However, after hepatic commitment of the anterior part, Wnt signaling is reactivated and helps form the liver bud.[60] Starting from week eight, the liver bud consists of bipotent hepatoblasts which heavily rely on Wnt/β-catenin signaling for proliferation and maturation.[189,190] The latter holds mostly true for the differentiation to hepatocytes. In mice, depletion of the β-catenin gene results in unsuccessful hepatocyte formation from hepatoblasts, along with a decrease in HNF4α and CCAAT-enhancer-binding protein-α (C/EBPα) expression in hepatocytes.[191-193] Both of these proteins are known to be key-regulators for hepatocyte differentiation, making it likely that Wnt/β-catenin influences hepatocyte differentiation via downstream targets. In line with these results, depletion of β-catenin signaling results in a smaller hepatocyte population after birth, indicating the continuous need for Wnt/β-catenin stimulation in hepatocytes, even post-partum.[194-195] For BECs the situation is different. During the late stages of embryonic development, SOX17 expression is highly upregulated which antagonizes the Wnt/β-catenin pathway.[196] Furthermore, if β-catenin is depleted in cholangiocyte progenitors, no differences in bile duct formation are observed in mice experiments.[197] However, some studies suggest that loss of β-catenin can be compensated by upregulating of γ-catenin which would potentially save the biliary phenotype.[198,199]

Wnt-signaling during liver homeostasis

There is a clear hepatocyte zonation in the adult liver which is regulated by canonical Wnt-signaling. For instance, pericentral hepatocytes have high expression of nucleus β-catenin, while periportal hepatocytes express high APC.[60] When, APC is depleted in mice experiments, periportal hepatocytes will start upregulating pericentral hepatocyte markers (for instance urea-cycle associated genes).[196] Vice versa is also true: if β-catenin is knocked down in mice, pericentral hepatocytes will express a periportal hepatocyte-genotype along the complete axis.[200] Finally, a knockout mouse model of LRP5/6 shows no hepatocyte zonation at all. This evidence all indicates that Wnt/β-catenin signaling plays a key role in metabolic zonation.[105] Whether Wnt/β-catenin is also necessary for driving proliferation and maintaining homeostasis of hepatocytes in all zones is yet to be discovered. However, canonical Wnt targets do become upregulated upon hepatocyte proliferation.[96] In contrast, the latest evidence for cholangiocyte homeostasis implies that biliary epithelium does not rely on Wnt/β-catenin signaling for proliferation. Although Wnt-ligands are upregulated, the downstream Wnt targets such as $Axin2^{+}$, are not. Indicating that it is likely that non-canonical Wnt signaling is becoming activated.[96] Subsequent analyses revealed that the PCP pathway and YAP signaling seem especially vital for maintaining the organisation and differentiation of the biliary compartment.[96]

Wnt-signaling during liver regeneration

As previously mentioned, within minutes after partial hepatectomy, β-catenin is severely upregulated and translocated to the nucleus. Here it regulates hepatocyte proliferation via Wnt-target genes.[164,201] Quickly thereafter, this process is halted by the upregulation of APC when a re-activation finally occurs after a couple of hours.[164] This re-activation endures approximately three days before it is inhibited by non-canonical Wnt-signaling, suggesting that hepatocytes have a self-limiting process for hepatocyte proliferation. If hepatocyte-specific loss of β-catenin is modelled, it results in a delay and diminished hepatocyte proliferation after hemihepatectomy. Moreover, if LRP5/6 is knocked-out, a similar delay is observed *in vivo*.[79] Yet, after a couple of days, hepatocyte proliferation starts; this indicates that another unknown mechanism can become active in the absence of canonical Wnt-signaling to restore liver volume after partial hepatectomy.[202] Cholangiocytes undergo ductal reprogramming during chronic injury which is Wnt/β-catenin independent, but require YAP-signaling and Wnt-ligands.[96,105] This has been demonstrated by single-cell RNAsequencing focusing on the biliary compartment in murine livers post-injury and was priory suggested by transdifferentiation models.[203] Both hepatocytes and cholangiocytes can act as facultative (stem) cells for one another.[94,107] However, it is unknown if this would be a direct transdifferentiation or via a shared progenitor. The effects of bile duct ligations in mouse models with depleted LRP5/6 help us to better understand this process. After perturbation via ligation, steady biliary proliferation rates were observed, while hepatocytes showed a reduction in proliferation.[204] Moreover, another study showed that transdifferentiation of hepatocytes to cholangiocytes corresponds to an increase in YAP expression while also upregulating Wnt-ligands, and thereby promoting biliary proliferation in a β-catenin independent manner.[67] In contrast, single-cell analysis indicated that hepatocytes require canonical Wnt for regeneration.[105] The same holds true for hepatocyte development from biliary epithelium. In a diet induced injury mice model, expression of canonical Wnt/β-catenin signaling in biliary cells promoted their (trans)differentiation to hepatocytes.[205] Taking all this evidence together it seems that that non-canonical Wnt/YAP-signaling is important for the biliary compartment, while canonical Wnt signaling is necessary for the hepatocyte lineage.

CHOLANGIOCYTE ORGANOID CULTURES

Organoids are three-dimensional structure derived from (pluripotent) stem cells, progenitor and/or differentiated cells that self-organize through cell-cell and cell-matrix interactions to recapitulate aspects of the native tissue architecture and function *in vitro*.[206] Since the derivation of the first intestinal organoids from adult mouse tissue[207], immense progress has been made in culturing organoids. Nowadays, organoids can be generated from a growing number of sources, including primary cells, stem/progenitor cells, embryonic stem cells (ESCs) and induced pluripotent stem cells (iPSCs).[208] While early reports on the establishment

of organoid systems indicated that organoids are exclusively derived from stem cells; it is now clear that organoids can also be initiated from differentiated cells, such as cholangiocytes.[106] Organoids can therefore be divided into distinct groups based on defining characteristics. These include epithelial organoids, multi-tissue organoids, and multi-organ organoids (Figure 6).[206] As the organoids used for this thesis are epithelial cholangiocyte organoids, the focus is on this type of organoids specifically. Epithelial organoids are derived from a single germ layer (endoderm, mesoderm or ectoderm) and have the ability to self-renew under the appropriate culture conditions. In this context, self-renewal describes the repeated regeneration of organoids from organoid fragments or single cells, allowing for the serial expansion of cultures. Epithelial organoids exemplify this characteristic through the ability of these structures to form from the clonal expansion of a single cell.[10,207,209] As epithelial organoids expand, cells polarize and specialize to reproduce aspects of the native epithelium.[207] Remarkably, upon physical fragmentation or enzymatic and/or chemical dissociation of epithelial organoids into single cells or disordered cell aggregates (followed by secondary culture in expanding conditions), cells reorganize and proliferate to reform organoids.[9,10] As their name implies, epithelial organoids do not harbor mesodermal components normally present in native tissue. That withstanding, in some cases epithelial organoids are co-cultured with supporting cells, however, these cells do not become a part of the epithelial organoid.[210] More broadly, it is suggested that for cells to be constituents of an organoid, they must be functionally integrated into the overall structure and synchronized with the proliferative state of the organoid.

Cholangiocyte organoids from induced pluripotent stem cells

In 2014, Dianat *et al.* described the differentiation of ESCs and iPSCs into functional cholangiocyte-like-cells (CLC).[211] When cultured in 3D conditions, PSC-derived CLCs formed cysts morphologically resembling the cholangiocyte-derived structures reported by LaRusso and colleagues.[212,213] Interestingly, when kept in culture for more than seven days cysts began to bud, forming branched tubular structures.[211] In 2015, the research groups of Vallier and Ghanekar introduced novel protocols for the directed differentiation of PSCs into CLCs, and their 3D culture as epithelial organoids.[8,214] These PSC-derived cholangiocyte organoids displayed key functions and were successfully used to model genetic diseases affecting the bile duct epithelium, such as cystic fibrosis and Alagille syndrome. Notably, researchers were able to rescue the disease phenotypes with pharmacological intervention, validating them as a useful drug screening tool. Organoids were also used to study biliary development through the modulation of key pathways normally active during native bile duct development, proving to be an excellent tool, not only for disease modeling and drug screening, but also for the study of the mechanisms driving bile duct development.[8,210]

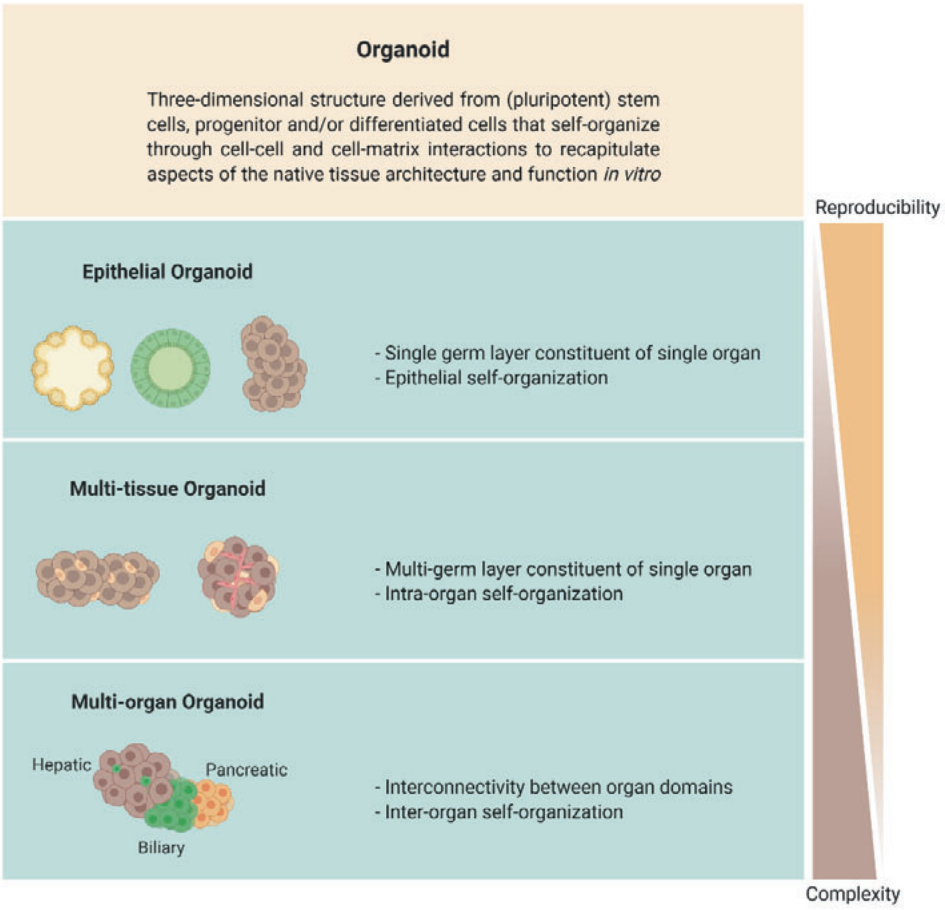

Figure 6. Organoid definition.
Overarching definition of an organoid (top panel) along with the three sub-classifications.[206]

Cholangiocyte organoids from primary tissue

It is now possible to culture self-renewing epithelial organoids from primary tissue intrahepatic biliary tree[10] and the extrahepatic biliary tree.[9,215] To establish cultures, isolated cells or tissue fragments are embedded in a matrix-rich 3D environment, typically Engelbreth-Holm-Swarm-based hydrogels and supplemented with medium containing (non-)canonical WNT stimulating factors, growth factors and small molecules (Figure 7). Within days, 3D structures begin to arise that can be serially passaged for several months.[32,216] Notably, tissue-derived epithelial organoids display high levels of genetic stability and are committed to their tissue of origin, making them an extremely attractive system, not only for *in vitro* testing, but also for therapeutic applications.[217] Therefore, in the studies summarized in this

thesis, tissue-derived cholangiocyte organoids were used to study biliary diseases and the use of these cells in (personalized) regenerative medicine applications.

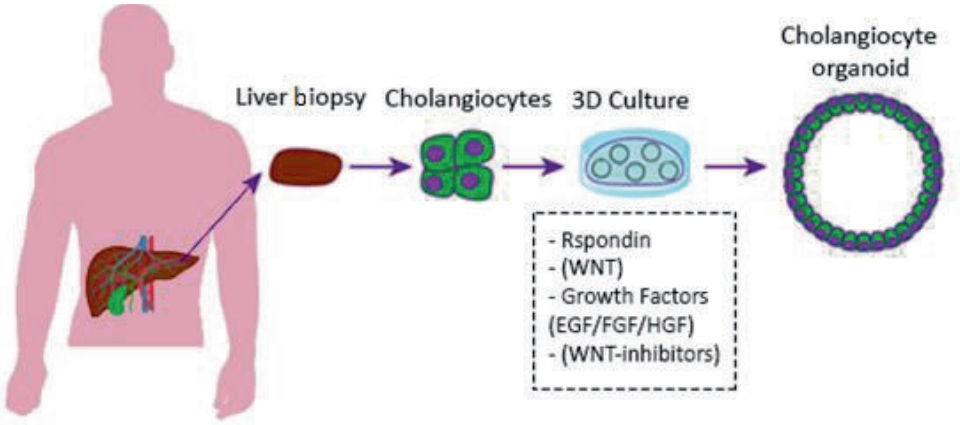

Figure 7. Cholangiocyte organoids cultured from a liver biopsy.

SCOPE AND AIMS OF THIS THESIS

The research presented in this **thesis** focuses on modeling bile duct biology, biliary development and regeneration, and diseases of human bile ducts using organoid-technology. This thesis is divided into four parts:
In **Part I** of this thesis, "Introduction and Definitions", the topic of bile duct biology and *in vitro* models is introduced (**chapter one**). To facilitate scientific communication and consistent interpretation, **chapter two** presents the results of a worldwide survey. Here, through consensus of experts in the field, a new nomenclature for hepatocyte and cholangiocyte organoid systems is proposed, while also providing a clear definition of what an organoid is.
In **Part II** of this thesis, "Disease modeling"; the role of CFTR-related biliary injury and ion-secretion via CFTR was investigated by culturing cholangiocyte organoids as 2D-monolayers.
In **Part III** of this thesis, "Novel Organoid Sources & Models", it was investigated if cholangiocyte organoids can be cultured from bile and extrahepatic bile duct tissue and the complex morphology of the intrahepatic bile ducts was recreated *in vitro.*
In **Part IV** of this thesis, "Regenerative Medicine", the potential of cholangiocyte organoids to repopulate human extrahepatic bile duct scaffolds is studied.

Part II – Disease Modeling

Post transplantation cholangiopathies or non-anastomotic biliary strictures (NAS) are severe complications after liver transplantation and are associated with severe morbidity and mortality. The classic risk-factor for development of NAS is prolonged warm-ischemia time.[218-221] The warm-ischemia time is the period in which the donor-organ lacks sufficient amount of oxygen, while being metabolic active. With the recent introduction of new technologies for optimization of grafts before transplantation, it was discovered that acidic bile (pH <7.0) was strongly associated with NAS development. [163] *In vivo,* bile is buffered by the active secretion of bicarbonate via cholangiocytes, bicarbonite is exchanged with extracellular chloride via Anion-Exchanger (AE)-2. Chloride, in its turn, is secreted from cholangiocytes in bile via cystic fibrosis transmembrane conductance regulator (CFTR) and Anoctamin (ANO)-1. Thus, one can hypothesize that the lack of oxygen in ischemic conditions would inhibit chloride excreting ion-channels in cholangiocytes, resulting in a lack of bicarbonate at the luminal side which would leave cholangiocytes vulnerable to bile. In **chapter three** this question was addressed by culturing cholangiocyte organoids as 2D-monolayers and exposing them to different oxygen conditions. Upon conducting the research described in **chapter three**, it was discovered that CFTR and ANO-1 were able to secrete bicarbonate directly into the lumen of the bile ducts. **Chapter four** elaborates upon this finding by comparing the bicarbonate excreted fraction of CFTR in organoids from different

organs of healthy individuals and of patients with dysfunctional CFTR (cystic fibrosis -CF-patients). Since most CF patients have affected intestines from an early age, and in contrast, CF-related cholangiopathies develop more gradually, and overt liver disease is a late and more sporadic manifestation of CF.[222,223] The research of **chapter four** focused specifically on the instestine and bile ducts and the ion-secretion characteristics of CFTR in these organs were examined.

Part III – Novel Organoid Sources & Models

With the establishment of the intrahepatic cholangiocyte organoid model, long-term culture of human cholangiocyte-like cells became feasible. These cholangiocyte organoids were created from intrahepatic cholangiocytes obtained from liver biopsies. Although very similar, intra- and extrahepatic cholangiocytes might have slightly different functions.[109] To answer this question, organoids were cultured from the extrahepatic bile ducts and compared them to organoids of matching donor controls from the intrahepatic bile duct in **chapter five**. Both the organoid sources rely on tissue biopsies for culturing organoids. Unfortunately, taking a tissue biopsy is invasive and potentially painfull with substantial risk of bleedings. This limits the availability of cholangiocyte organoids to only a subpopulation of patients, namely ones that are undergoing a biopsy or undergoing liver surgery. Because prior research showed that cells from biliary duct tumors (cholangiocarcinoma) could be detected from liquid bile biopsies[224-226], it was hypothesized that organoid-initiating cells might also be present in bile. In **chapter six and seven,** this hypothesis was investigated and subsequtenly it was researched if bile cholangiocyte organoids were capable of repopulating extrahepatic bile ducts. Cholangiocyte organoids consist of a monolayer of epithelial cells in a spheroid like structure. If a transversal section is made of these organoids, it resembles a lumen of a single bile duct, which is very similar to the extrahepatic bile duct. However, cholangiocyte organoids do not represent the complex branching morphogenesis of the intrahepatic part of the biliary tree.[4] Thus, in **chapter eight** cholangiocyte organoids were established that form complex branching bile ducts *in vitro* and investigate if these can be used to study branching related diseases and modeling of embryonic branching development.

Part IV – Regenerative Medicine

Diseases of the extrahepatic bile duct are associated with high percentages of morbidity and even mortality. Current treatment options remain limited, with liver transplantation being the only curative treatment options for patients with end-stage liver failure.[5,6] Among other causes, this is partially due to the lack of sufficient autologous donor tissue for extrahepatic bile ducts. Thus, in **chapter nine** it was investigated if patient-specific cholangiocyte

organoids could be used to functionally repopulate human extrahepatic bile ducts scaffolds as a potential novel strategy for the creation of extrahepatic bile duct replacement tissue.

References introduction

1. Castaing D. Surgical anatomy of the biliary tract. HPB (Oxford). 2008;10(2):72-76.
2. Zong Y, Stanger BZ. Molecular mechanisms of bile duct development. Int. J. Biochem. Cell Biol. 2011;43:257–264.
3. Si-Tayeb K, Lemaigre FP, Duncan SA. Organogenesis and development of the liver. Dev Cell. 2010;18(2):175-189.
4. Boyer JL. Bile formation and secretion. Compr Physiol 2013;3:1035–78.
5. Lazaridis KN, LaRusso NF. The Cholangiopathies. Mayo Clin Proc. 2015;90(6):791-800.
6. Spada M, Riva S, Maggiore G, *et al.* Pediatric liver transplantation. World J Gastroenterol. 2009;15(6):648-674.
7. Sampaziotis F, Segeritz CP, Vallier L. Potential of human induced pluripotent stem cells in studies of liver disease. Hepatology. 2015;62(1):303-311.
8. Sampaziotis F, de Brito MC, Madrigal P, *et al.* Cholangiocytes derived from human induced pluripotent stem cells for disease modeling and drug validation. Nat Biotechnol. 2015;33(8):845-852.
9. Sampaziotis F, Justin AW, Tysoe OC, *et al.* Reconstruction of the mouse extrahepatic biliary tree using primary human extrahepatic cholangiocyte organoids. Nat Med. 2017;23(8):954-963.
10. Huch M, Gehart H, van Boxtel R, *et al.* Long-term culture of genome-stable bipotent stem cells from adult human liver. Cell. 2015;160(1-2):299-312.
11. Juza RM, Pauli EM. Clinical and surgical anatomy of the liver: a review for clinicians. Clin Anat. 2014;27(5):764-769.
12. Abdel-Misih SR, Bloomston M. Liver anatomy. Surg Clin North Am. 2010;90(4):643-653.
13. Li T, Chiang JYL. Bile acid-based therapies for non-alcoholic steatohepatitis and alcoholic liver disease. Hepatobiliary Surg Nutr. 2020;9(2):152-169.
14. Strazzabosco M, Fabris L. Functional anatomy of normal bile ducts. Anat Rec (Hoboken). 2008;291(6):653-660.
15. Terada T, Nakanuma Y. Development of human peribiliary capillary plexus: a lectin-histochemical and immunohistochemical study. Hepatology. 1993;18(3):529-536.
16. Matz-Soja M, Rennert C, Schönefeld K, *et al.* Hedgehog signaling is a potent regulator of liver lipid metabolism and reveals a GLI-code associated with steatosis. Elife. 2016;5:e13308.
17. Kietzmann T. Metabolic zonation of the liver: The oxygen gradient revisited. Biochim Biophys Acta. 2015 May;1851(5):641-56.
18. Jungermann K, Kietzmann T. Zonation of parenchymal and nonparenchymal metabolism in liver. Annu Rev Nutr. 1996;16:179-203.
19. Colletti M, Cicchini C, Conigliaro A, *et al.* Convergence of Wnt signaling on the HNF4alpha-driven transcription in controlling liver zonation [published correction appears in Gastroenterology. 2010 Feb;138(2):793]. Gastroenterology. 2009;137(2):660-672.
20. Burke ZD, Reed KR, Phesse TJ, *et al.* Liver zonation occurs through a β-catenin–dependent, c-Myc–independent mechanism. Gastroenterology. 2009;136(7), 2316-2324e3.
21. Logan CY, Nusse R. The Wnt signaling pathway in development and disease. Annu Rev Cell Dev Biol. 2004;20:781-810.
22. Wang B, Zhao L, Fish M, *et al*. Self-renewing diploid Axin2(+) cells fuel homeostatic renewal of the liver. Nature. 2015;524(7564):180-185.

23. Jho EH, Zhang T, Domon C, *et al.* Wnt/beta-catenin/Tcf signaling induces the transcription of Axin2, a negative regulator of the signaling pathway. Mol Cell Biol. 2002;22(4):1172-1183.
24. Font-Burgada J, Shalapour S, Ramaswamy S, *et al.* Hybrid Periportal Hepatocytes Regenerate the Injured Liver without Giving Rise to Cancer. Cell. 2015;162(4):766-779.
25. Huang BQ, Masyuk TV, Muff MA, *et al.* Isolation and characterization of cholangiocyte primary cilia. Am J Physiol Gastrointest Liver Physiol. 2006;291(3):G500-G509.
26. Ludwig J, Ritman EL, LaRusso NF, *et al.* Anatomy of the human biliary system studied by quantitative computer-aided three-dimensional imaging techniques. Hepatology. 1998;27(4):893-899.
27. Vroman B, LaRusso NF. Development and characterization of polarized primary cultures of rat intrahepatic bile duct epithelial cells. Lab Invest. 1996;74(1):303-313.
28. Masyuk AI, Masyuk TV, Splinter PL, *et al.* Cholangiocyte cilia detect changes in luminal fluid flow and transmit them into intracellular Ca2+ and cAMP signaling. Gastroenterology. 2006;131(3):911-920.
29. Masyuk AI, Gradilone SA, Banales JM, *et al.* Cholangiocyte primary cilia are chemosensory organelles that detect biliary nucleotides via P2Y12 purinergic receptors. Am J Physiol Gastrointest Liver Physiol. 2008;295(4):G725-G734.
30. Masyuk AI, Huang BQ, Radtke BN, *et al.* Ciliary subcellular localization of TGR5 determines the cholangiocyte functional response to bile acid signaling. Am J Physiol Gastrointest Liver Physiol. 2013;304(11):G1013-G1024.
31. Tietz PS, Marinelli RA, Chen XM, *et al.* Agonist-induced coordinated trafficking of functionally related transport proteins for water and ions in cholangiocytes. J Biol Chem. 2003;278(22):20413-20419.
32. Banales JM, Arenas F, Rodríguez-Ortigosa CM, *et al.* Bicarbonate-rich choleresis induced by secretin in normal rat is taurocholate-dependent and involves AE2 anion exchanger. Hepatology. 2006;43(2):266-275.
33. Banales JM, Prieto J, Medina JF. Cholangiocyte anion exchange and biliary bicarbonate excretion. World J Gastroenterol. 2006;12(22):3496-3511.
34. Tabibian JH, Masyuk AI, Masyuk TV, *et al.* Physiology of cholangiocytes. Compr Physiol. 2013;3(1):541-565.
35. Lenzen R, Alpini G, Tavoloni N. Secretin stimulates bile ductular secretory activity through the cAMP system. Am J Physiol. 1992;263(4 Pt 1):G527-G532.
36. Alvaro D, Mennone A, Boyer JL. Role of kinases and phosphatases in the regulation of fluid secretion and Cl-/HCO3- exchange in cholangiocytes [published correction appears in Am J Physiol 1998 Apr;274(4 Pt 1):6605]. Am J Physiol. 1997;273(2 Pt 1):G303-G313.
37. Nyberg B, Einarsson K, Sonnenfeld T. Evidence that vasoactive intestinal peptide induces ductular secretion of bile in humans. Gastroenterology. 1989;96(3):920-924.
38. Hirata K, Nathanson MH. Bile duct epithelia regulate biliary bicarbonate excretion in normal rat liver. Gastroenterology. 2001;121(2):396-406.
39. Kaminski DL, Deshpande YG. Effect of Somatostatin and Bombesin on Secretin-Stimulated Ductular Bile Flow in Dogs. Gastroenterology. 1983;85:1239-47.
40. Glaser SS, Rodgers RE, Phinizy JL, *et al.* Gastrin inhibits secretin-induced ductal secretion by interaction with specific receptors on rat cholangiocytes. Am J Physiol. 1997;273(5):G1061-G1070.

41. Caligiuri A, Glaser S, Rodgers RE, *et al.* Endothelin-1 inhibits secretin-stimulated ductal secretion by interacting with ETA receptors on large cholangiocytes. Am J Physiol. 1998;275(4):G835-G846.
42. Dutta AK, Khimji AK, Kresge C, *et al.* Identification and functional characterization of TMEM16A, a Ca2+-activated Cl- channel activated by extracellular nucleotides, in biliary epithelium. J Biol Chem. 2011;286(1):766-776.
43. Roman RM, Feranchak AP, Salter KD, *et al.* Endogenous ATP release regulates Cl- secretion in cultured human and rat biliary epithelial cells. Am J Physiol. 1999;276(6):G1391-G1400.
44. Hofmann AF. The enterohepatic circulation of bile acids in mammals: form and functions. Front Biosci (Landmark Ed). 2009;14:2584-2598.
45. Lamri Y, Erlinger S, Dumont M, *et al.* Immunoperoxidase localization of ursodeoxycholic acid in rat biliary epithelial cells. Evidence for a cholehepatic circulation. Liver. 1992;12(5):351-354
46. Lazaridis KN, Pham L, Tietz P, *et al.* Rat cholangiocytes absorb bile acids at their apical domain via the ileal sodium-dependent bile acid transporter. J Clin Invest. 1997;100(11):2714-2721.
47. Kool M, van der Linden M, de Haas M, *et al.* MRP3, an organic anion transporter able to transport anti-cancer drugs. Proc Natl Acad Sci U S A. 1999;96(12):6914-6919.
48. Soroka CJ, Lee JM, Azzaroli F, Boyer JL. Cellular localization and up-regulation of multidrug resistance-associated protein 3 in hepatocytes and cholangiocytes during obstructive cholestasis in rat liver. Hepatology. 2001;33(4):783-791.
49. Hirohashi T, Suzuki H, Takikawa H, *et al*. ATP-dependent transport of bile salts by rat multidrug resistance-associated protein 3 (Mrp3). J Biol Chem. 2000;275(4):2905-2910.
50. Ballatori N, Christian WV, Lee JY, *et al.* OSTalpha-OSTbeta: a major basolateral bile acid and steroid transporter in human intestinal, renal, and biliary epithelia. Hepatology. 2005;42(6):1270-1279.
51. Ballatori N, Li N, Fang F, Boyer JL, *et al*. OST alpha-OST beta: a key membrane transporter of bile acids and conjugated steroids. Front Biosci (Landmark Ed). 2009;14:2829-2844.
52. Lazaridis KN, Pham L, Vroman B, *et al.* Kinetic and molecular identification of sodium-dependent glucose transporter in normal rat cholangiocytes. Am J Physiol. 1997;272(5 Pt 1):G1168-G1174.
53. Mennone A, Biemesderfer D, Negoianu D, *et al.* Role of sodium/hydrogen exchanger isoform NHE3 in fluid secretion and absorption in mouse and rat cholangiocytes. Am J Physiol Gastrointest Liver Physiol. 2001;280(2):G247-G254.
54. Tam PP, Kanai-Azuma M, Kanai Y. Early endoderm development in vertebrates: lineage differentiation and morphogenetic function. Current Opinion in Genetics & Development. 2003 Aug;13(4):393-400.
55. Yanai M, Tatsumi N, Hasunuma N, *et al.* FGF signaling segregates biliary cell-lineage from chick hepatoblasts cooperatively with BMP4 and ECM components *in vitro*. Dev Dyn. 2008;237(5):1268-1283.
56. Ober EA, Lemaigre FP. Development of the liver: Insights into organ and tissue morphogenesis. J Hepatol. 2018;68(5):1049-1062.
57. Lemaigre FP. Molecular mechanisms of biliary development. Prog Mol Biol Transl Sci. 2010;97:103-126.
58. Lee CS, Friedman JR, Fulmer JT, *et al.* The initiation of liver development is dependent on Foxa transcription factors. Nature. 2005;435(7044):944-947.
59. Lupien M, Eeckhoute J, Meyer CA, *et al.* FoxA1 translates epigenetic signatures into enhancer-driven lineage-specific transcription. Cell. 2008;132(6):958-970.

60. Lade AG, Monga SP. Beta-catenin signaling in hepatic development and progenitors: which way does the WNT blow?. Dev Dyn. 2011;240(3):486-500.
61. Geisler F, Strazzabosco M. Emerging roles of Notch signaling in liver disease. Hepatology. 2015;61(1):382-392.
62. Clotman F, Jacquemin P, Plumb-Rudewiez N, *et al.* Control of liver cell fate decision by a gradient of TGF beta signaling modulated by Onecut transcription factors. Genes Dev. 2005;19(16):1849-1854.
63. Zong Y, Panikkar A, Xu J, *et al.* Notch signaling controls liver development by regulating biliary differentiation. Development. 2009;136(10):1727-1739.
64. Kodama Y, Hijikata M, Kageyama R, *et al.* The role of notch signaling in the development of intrahepatic bile ducts. Gastroenterology. 2004;127(6):1775-1786.
65. Zhang N, Bai H, David KK, *et al.* The Merlin/NF2 tumor suppressor functions through the YAP oncoprotein to regulate tissue homeostasis in mammals. Dev Cell. 2010;19(1):27-38.
66. Yimlamai D, Christodoulou C, Galli GG, *et al.* Hippo pathway activity influences liver cell fate. Cell. 2014;157(6):1324-1338.
67. Patel SH, Camargo FD, Yimlamai D. Hippo Signaling in the Liver Regulates Organ Size, Cell Fate, and Carcinogenesis. Gastroenterology. 2017;152(3):533-545.
68. Lemaigre FP. Mechanisms of liver development: concepts for understanding liver disorders and design of novel therapies. Gastroenterology. 2009;137(1):62-79.
69. Gérard C, Tys J, Lemaigre FP. Gene regulatory networks in differentiation and direct reprogramming of hepatic cells. Semin Cell Dev Biol. 2017;66:43-50.
70. Segal JM, Kent D, Wesche DJ, *et al.* Single cell analysis of human foetal liver captures the transcriptional profile of hepatobiliary hybrid progenitors. Nat Commun. 2019;10(1):3350.
71. Merino-Azpitarte M, Lozano E, Perugorria MJ, *et al.* SOX17 regulates cholangiocyte differentiation and acts as a tumor suppressor in cholangiocarcinoma. J Hepatol. 2017;67(1):72-83.
72. Fausto N, Riehle KJ. Mechanisms of liver regeneration and their clinical implications. J Hepatobiliary Pancreat Surg. 2005;12(3):181-189.
73. Karin M, Clevers H. Reparative inflammation takes charge of tissue regeneration. Nature. 2016;529(7586):307-315.
74. Michalopoulos GK. Liver regeneration after partial hepatectomy: critical analysis of mechanistic dilemmas. Am J Pathol. 2010;176(1):2-13.
75. Bockhorn M, Goralski M, Prokofiev D, *et al.* VEGF is important for early liver regeneration after partial hepatectomy. J Surg Res. 2007;138(2):291-299.
76. Enguita-Germán M, Fortes P. Targeting the insulin-like growth factor pathway in hepatocellular carcinoma. World J Hepatol. 2014;6(10):716-737.
77. Meyer J, Lejmi E, Fontana P, *et al.* A focus on the role of platelets in liver regeneration: Do platelet-endothelial cell interactions initiate the regenerative process?. J Hepatol. 2015;63(5):1263-1271.
78. Matsuo R, Nakano Y, Ohkohchi N. Platelet administration via the portal vein promotes liver regeneration in rats after 70% hepatectomy. Ann Surg. 2011;253(4):759-763.
79. Yang J, Mowry LE, Nejak-Bowen KN, *et al.* β-catenin signaling in murine liver zonation and regeneration: a Wnt-Wnt situation!. Hepatology. 2014;60(3):964-976.
80. Romero-Gallo J, Sozmen EG, Chytil A, *et al.* Inactivation of TGF-beta signaling in hepatocytes results in an increased proliferative response after partial hepatectomy. Oncogene. 2005;24(18):3028-3041.

81. Lee SC, Jeong HJ, Choi BJ, *et al.* Role of the spleen in liver regeneration in relation to transforming growth factor-β1 and hepatocyte growth factor. J Surg Res. 2015;196(2):270-277.
82. Pu W, Zhang H, Huang X, *et al.* Mfsd2a+ hepatocytes repopulate the liver during injury and regeneration. Nat Commun. 2016;7:13369.
83. Ang CH, Hsu SH, Guo F, *et al.* Lgr5+ pericentral hepatocytes are self-maintained in normal liver regeneration and susceptible to hepatocarcinogenesis. Proc Natl Acad Sci U S A. 2019;116(39):19530-19540.
84. Monga SP. No Zones Left Behind: Democratic Hepatocytes Contribute to Liver Homeostasis and Repair. Cell Stem Cell. 2020;26(1):2-3.
85. Lin S, Nascimento EM, Gajera CR, *et al.* Distributed hepatocytes expressing telomerase repopulate the liver in homeostasis and injury. Nature. 2018;556(7700):244-248.
86. Matsumoto T, Wakefield L, Tarlow BD, *et al*. *In vivo* Lineage Tracing of Polyploid Hepatocytes Reveals Extensive Proliferation during Liver Regeneration. Cell Stem Cell. 2020;26(1):34-47.e3.
87. Chen F, Jimenez RJ, Sharma K, *et al.* Broad Distribution of Hepatocyte Proliferation in Liver Homeostasis and Regeneration. Cell Stem Cell. 2020;26(1):27-33.e4.
88. Sun T, Pikiolek M, Orsini V, *et al.* AXIN2+ Pericentral Hepatocytes Have Limited Contributions to Liver Homeostasis and Regeneration. Cell Stem Cell. 2020;26(1):97-107.e6.
89. Wei Y, Wang YG, Jia Y, *et al.* Liver homeostasis is maintained by midlobular zone 2 hepatocytes. Science. 2021 Feb 26;371(6532):eabb1625.
90. He L, Pu W, Liu X, *et al.* Proliferation tracing reveals regional hepatocyte generation in liver homeostasis and repair. Science. 2021 Feb 26;371(6532):eabc4346.
91. Tsuchiya A, Lu WY. Liver stem cells: Plasticity of the liver epithelium. World J Gastroenterol. 2019;25(9):1037-1049.
92. Huch M, Dorrell C, Boj SF, *et al. In vitro* expansion of single Lgr5+ liver stem cells induced by Wnt-driven regeneration. Nature. 2013;494(7436):247-250.
93. Manco R, Clerbaux LA, Verhulst S, *et al.* Reactive cholangiocytes differentiate into proliferative hepatocytes with efficient DNA repair in mice with chronic liver injury. J Hepatol. 2019;70(6):1180-1191.
94. Raven A, Lu WY, Man TY, *et al.* Cholangiocytes act as facultative liver stem cells during impaired hepatocyte regeneration [published correction appears in Nature. 2018 Mar 14;555(7696):402]. Nature. 2017;547(7663):350-354.
95. Aizarani N, Saviano A, Sagar, *et al.* A human liver cell atlas reveals heterogeneity and epithelial progenitors. Nature. 2019;572(7768):199-204.
96. Pepe-Mooney BJ, Dill MT, Alemany A, *et al.* Single-Cell Analysis of the Liver Epithelium Reveals Dynamic Heterogeneity and an Essential Role for YAP in Homeostasis and Regeneration. Cell Stem Cell. 2019;25(1):23-38.e8.
97. Preziosi ME, Monga SP. Update on the Mechanisms of Liver Regeneration. Semin Liver Dis. 2017;37(2):141-151.
98. Michalopoulos GK, DeFrances MC. Liver regeneration. Science. 1997;276(5309):60-66.
99. Alvaro D, Gigliozzi A, Attili AF. Regulation and deregulation of cholangiocyte proliferation. J Hepatol. 2000;33(2):333-340.
100. Svegliati-Baroni G, Ghiselli R, Marzioni M, *et al.* Estrogens maintain bile duct mass and reduce apoptosis after biliodigestive anastomosis in bile duct ligated rats. J Hepatol. 2006;44(6):1158-1166.

101. Alvaro D, Mancino MG, Onori P, *et al.* Estrogens and the pathophysiology of the biliary tree. World J Gastroenterol. 2006;12(22):3537-3545.
102. Glaser S, DeMorrow S, Francis H, *et al.* Progesterone stimulates the proliferation of female and male cholangiocytes via autocrine/paracrine mechanisms. Am J Physiol Gastrointest Liver Physiol. 2008;295(1):G124-G136.
103. Pinto C, Giordano DM, Maroni L, *et al*. Role of inflammation and proinflammatory cytokines in cholangiocyte pathophysiology. Biochim Biophys Acta Mol Basis Dis. 2018;1864(4 Pt B):1270-1278.
104. Strazzabosco M, Fiorotto R, Cadamuro M, *et al.* Pathophysiologic implications of innate immunity and autoinflammation in the biliary epithelium. Biochim Biophys Acta Mol Basis Dis. 2018;1864(4 Pt B):1374-1379.
105. Planas-Paz L, Sun T, Pikiolek M, *et al.* YAP, but Not RSPO-LGR4/5, Signaling in Biliary Epithelial Cells Promotes a Ductular Reaction in Response to Liver Injury. Cell Stem Cell. 2019;25(1):39-53.e10.
106. Aloia L, McKie MA, Vernaz G, *et al.* Epigenetic remodeling licences adult cholangiocytes for organoid formation and liver regeneration. Nat Cell Biol. 2019;21(11):1321-1333.
107. Schaub JR, Huppert KA, Kurial SNT, *et al.* De novo formation of the biliary system by TGFβ-mediated hepatocyte transdifferentiation. Nature. 2018;557(7704):247-251.
108. Raven A, Forbes SJ. Hepatic progenitors in liver regeneration. J Hepatol. 2018;69(6):1394-1395.
109. Rimland CA, Tilson SG, Morell CM, *et al.* Regional differences in human biliary tissues and corresponding *in vitro* derived organoids [published online ahead of print, 2020 Mar 29]. Hepatology. 2020;10.1002/hep.31252.
110. Sampaziotis F, Muraro D, Tysoe OC, *et al.* Cholangiocyte organoids can repair bile ducts after transplantation in the human liver. Science. 2021 Feb 19;371(6531):839-846.
111. Lanzoni G, Cardinale V, Carpino G. The hepatic, biliary, and pancreatic network of stem/progenitor cell niches in humans: A new reference frame for disease and regeneration. Hepatology. 2016;64(1):277-286.
112. Cardinale V, Wang Y, Carpino G, *et al.* Multipotent stem/progenitor cells in human biliary tree give rise to hepatocytes, cholangiocytes, and pancreatic islets. Hepatology. 2011;54(6):2159-2172.
113. Carpino G, Cardinale V, Onori P, *et al.* Biliary tree stem/progenitor cells in glands of extrahepatic and intraheptic bile ducts: an anatomical in situ study yielding evidence of maturational lineages. J Anat. 2012;220(2):186-199.
114. de Jong IEM, Matton APM, van Praagh JB, *et al.* Peribiliary Glands Are Key in Regeneration of the Human Biliary Epithelium After Severe Bile Duct Injury. Hepatology. 2019;69(4):1719-1734.
115. Lazaridis KN, Strazzabosco M, Larusso NF. The cholangiopathies: disorders of biliary epithelia. Gastroenterology. 2004;127(5):1565-1577.
116. Strazzabosco M, Fabris L, Spirli C. Pathophysiology of cholangiopathies. J Clin Gastroenterol. 2005;39(4 Suppl 2):S90-S102.
117. Li L, Krantz ID, Deng Y, *et al.* Alagille syndrome is caused by mutations in human Jagged1, which encodes a ligand for Notch1. Nat Genet. 1997;16(3):243-251.
118. Oda T, Elkahloun AG, Pike BL, *et al.* Mutations in the human Jagged1 gene are responsible for Alagille syndrome. Nat Genet. 1997;16(3):235-242.
119. McDaniell R, Warthen DM, Sanchez-Lara PA, *et al.* NOTCH2 mutations cause Alagille syndrome, a heterogeneous disorder of the notch signaling pathway. Am J Hum Genet. 2006;79(1):169-173.
120. Lykavieris P, Hadchouel M, Chardot C, *et al*. Outcome of liver disease in children with Alagille syndrome: a study of 163 patients. Gut. 2001;49(3):431-435.

121. Kamath BM, Yin W, Miller H, *et al.* Outcomes of liver transplantation for patients with Alagille syndrome: the studies of pediatric liver transplantation experience. Liver Transpl. 2012;18(8):940-948.
122. Fabris L, Cadamuro M, Guido M, *et al.* Analysis of liver repair mechanisms in Alagille syndrome and biliary atresia reveals a role for notch signaling. Am J Pathol. 2007;171(2):641-653.
123. O'Sullivan BP, Freedman SD. Cystic fibrosis. Lancet. 2009;373(9678):1891-1904.
124. Veit G, Avramescu RG, Chiang AN, *et al.* From CFTR biology toward combinatorial pharmacotherapy: expanded classification of cystic fibrosis mutations. Mol Biol Cell. 2016;27(3):424-433.
125. Cohn JA, Strong TV, Picciotto MR, *et al.* Localization of the cystic fibrosis transmembrane conductance regulator in human bile duct epithelial cells. Gastroenterology. 1993;105(6):1857-1864.
126. Kinnman N, Lindblad A, Housset C, *et al.* Expression of cystic fibrosis transmembrane conductance regulator in liver tissue from patients with cystic fibrosis. Hepatology. 2000;32(2):334-340.
127. Ooi CY, Durie PR. Cystic fibrosis from the gastroenterologist's perspective. Nat Rev Gastroenterol Hepatol. 2016;13(3):175-185.
128. Debray D, Narkewicz MR, Bodewes FAJA, *et al.* Cystic Fibrosis-related Liver Disease: Research Challenges and Future Perspectives. J Pediatr Gastroenterol Nutr. 2017;65(4):443-448.
129. Fajac I, Wainwright CE. New treatments targeting the basic defects in cystic fibrosis. Presse Med. 2017;46(6 Pt 2):e165-e175.
130. Strug LJ, Stephenson AL, Panjwani N, *et al.* Recent advances in developing therapeutics for cystic fibrosis. Hum Mol Genet. 2018;27(R2):R173-R186.
131. Middleton PG, Mall MA, Dřevínek P, *et al.* Elexacaftor-Tezacaftor-Ivacaftor for Cystic Fibrosis with a Single Phe508del Allele. N Engl J Med. 2019;381(19):1809-1819.
132. Heijerman HGM, McKone EF, Downey DG, *et al.* Efficacy and safety of the elexacaftor plus tezacaftor plus ivacaftor combination regimen in people with cystic fibrosis homozygous for the F508del mutation: a double-blind, randomised, phase 3 trial [published correction appears in Lancet. 2020 May 30;395(10238):1694]. Lancet. 2019;394(10212):1940-1948.
133. Starzl TE. History of Liver and Other Splanchnic Organ Transplantation. In: Busuttil RW, Klintmalm GB. editors. Transplantation of the Liver. Philadelphia, PA: W.B. Saunders Company, 1996:3-22.
134. Neuberger J. An update on liver transplantation: A critical review. J Autoimmun. 2016;66:51-59.
135. García-Valdecasas Salgado JC. Non beating heart donors as a possible source for liver transplantation. Acta Chir Belg. 2000;100(6):268-271.
136. Graham JA, Guarrera JV. "Resuscitation" of marginal liver allografts for transplantation with machine perfusion technology. J Hepatol. 2014;61(2):418-431.
137. Jiménez-Romero C, Caso Maestro O, Cambra Molero F, *et al.* Using old liver grafts for liver transplantation: where are the limits?. World J Gastroenterol. 2014;20(31):10691-10702.
138. Selten J, Schlegel A, de Jonge J, *et al.* Hypo- and normothermic perfusion of the liver: Which way to go?. Best Pract Res Clin Gastroenterol. 2017;31(2):171-179.
139. van Golen RF, Reiniers MJ, van Gulik TM, *et al.* Organ cooling in liver transplantation and resection: how low should we go?. Hepatology. 2015;61(1):395-399.
140. Dutkowski P, Krug A, Krysiak M, Dünschede F, Seifert JK, Junginger T. Detection of mitochondrial electron chain carrier redox status by transhepatic light intensity during rat liver reperfusion. Cryobiology. 2003;47(2):125-142.

141. Chang WJ, Chehab M, Kink S, *et al*. Intracellular calcium signaling pathways during liver ischemia and reperfusion. J Invest Surg. 2010;23(4):228-238.
142. Dutkowski P, Schlegel A, de Oliveira M, *et al*. HOPE for human liver grafts obtained from donors after cardiac death. J Hepatol. 2014;60(4):765-772.
143. Nasralla D, Coussios CC, Mergental H, *et al.* A randomized trial of normothermic preservation in liver transplantation. Nature. 2018;557(7703):50-56.
144. van Rijn R, Schurink IJ, de Vries Y, *et al.* Hypothermic Machine Perfusion in Liver Transplantation - A Randomized Trial. N Engl J Med. 2021 Feb 24. doi: 10.1056/NEJMoa2031532. Epub ahead of print. PMID: 33626248.
145. Thethy S, Thomson BNj, Pleass H, *et al.* Management of biliary tract complications after orthotopic liver transplantation. Clin Transplant. 2004;18(6):647-653.
146. Hampe T, Dogan A, Encke J, *et al.* Biliary complications after liver transplantation. Clin Transplant. 2006;20 Suppl 17:93-96.
147. Verdonk RC, Buis CI, Porte RJ, *et al*. Biliary complications after liver transplantation: a review. Scand J Gastroenterol Suppl. 2006;(243):89-101.
148. Wojcicki M, Milkiewicz P, Silva M. Biliary tract complications after liver transplantation: a review. Dig Surg. 2008;25(4):245-257.
149. Sharma S, Gurakar A, Jabbour N. Biliary strictures following liver transplantation: past, present and preventive strategies. Liver Transpl. 2008;14(6):759-769.
150. Verdonk RC, Buis CI, van der Jagt EJ, *et al.* Nonanastomotic biliary strictures after liver transplantation, part 2: management, outcome, and risk factors for disease progression. Liver Transplant. 2007;13(5):725-732.
151. Jay CL, Lyuksemburg V, Ladner DP, *et al.* Ischemic cholangiopathy after controlled donation after cardiac death liver transplantation: a meta-analysis. Ann Surg. 2011;253(2):259-264.
152. Op den Dries S, Sutton ME, Lisman T, *et al.* Protection of bile ducts in liver transplantation: looking beyond ischemia. Transplantation. 2011;92(4):373-379.
153. Hansen T, Hollemann D, Pitton MB, *et al.* Histological examination and evaluation of donor bile ducts received during orthotopic liver transplantation--a morphological clue to ischemic-type biliary lesion?. Virchows Arch. 2012;461(1):41-48.
154. Brunner SM, Junger H, Ruemmele P, *et al.* Bile duct damage after cold storage of deceased donor livers predicts biliary complications after liver transplantation. J Hepatol. 2013;58(6):1133-1139.
155. Karimian N, Op den Dries S, Porte RJ. The origin of biliary strictures after liver transplantation: is it the amount of epithelial injury or insufficient regeneration that counts?. J Hepatol. 2013;58(6):1065-1067.
156. op den Dries S, Westerkamp AC, Karimian N, *et al.* Injury to peribiliary glands and vascular plexus before liver transplantation predicts formation of non-anastomotic biliary strictures. J Hepatol. 2014;60(6):1172-1179.
157. Dyson JK, Beuers U, Jones DEJ, *et al*. Primary sclerosing cholangitis. Lancet. 2018;391(10139):2547-2559.
158. Banales JM, Sáez E, Uriz M, *et al.* Up-regulation of microRNA 506 leads to decreased Cl-/HCO3-anion exchanger 2 expression in biliary epithelium of patients with primary biliary cirrhosis. Hepatology. 2012;56(2):687-697.
159. Prieto J, Qian C, García N, *et al.* Abnormal expression of anion exchanger genes in primary biliary cirrhosis. Gastroenterology. 1993;105(2):572-578.

160. Medina JF, Martínez-Ansó, Vazquez JJ, *et al.* Decreased anion exchanger 2 immunoreactivity in the liver of patients with primary biliary cirrhosis. Hepatology. 1997;25(1):12-17.
161. European Association for the Study of the Liver. EASL Clinical Practice Guidelines: management of cholestatic liver diseases. J Hepatol. 2009;51(2):237-267.
162. Prieto J, Garcia N, Marti-Climent JM, *et al.* Assessment of biliary bicarbonate secretion in humans by positron emission tomography. Gastroenterology 1999;117(1):167–72.
163. Watson CJE, Kosmoliaptsis V, Randle LV, *et al.* Normothermic Perfusion in the Assessment and Preservation of Declined Livers Before Transplantation: Hyperoxia and Vasoplegia-Important Lessons From the First 12 Cases. Transplantation. 2017;101(5):1084-1098.
164. Monga SP, Pediaditakis P, Mule K, *et al.* Changes in WNT/beta-catenin pathway during regulated growth in rat liver regeneration. Hepatology. 2001;33(5):1098-1109.
165. Clevers H, Nusse R. Wnt/β-catenin signaling and disease. Cell. 2012;149(6):1192-1205.
166. Kretzschmar K, Clevers H. Wnt/β-catenin signaling in adult mammalian epithelial stem cells. Dev Biol. 2017;428(2):273-282.
167. Moon RT, Kohn AD, De Ferrari GV, *et al.* WNT and beta-catenin signaling: diseases and therapies. Nat Rev Genet. 2004;5(9):691-701.
168. Nusse R, Clevers H. Wnt/β-Catenin Signaling, Disease, and Emerging Therapeutic Modalities. Cell. 2017;169(6):985-999.
169. Liu C, Li Y, Semenov M, *et al.* Control of beta-catenin phosphorylation/degradation by a dual-kinase mechanism. Cell. 2002;108(6):837-847.
170. Amit S, Hatzubai A, Birman Y, *et al.* Axin-mediated CKI phosphorylation of beta-catenin at Ser 45: a molecular switch for the Wnt pathway. Genes Dev. 2002;16(9):1066-1076.
171. Bhanot P, Brink M, Samos CH, *et al.* A new member of the frizzled family from Drosophila functions as a Wingless receptor. Nature. 1996;382(6588):225-230.
172. Wehrli M, Dougan ST, Caldwell K, *et al.* arrow encodes an LDL-receptor-related protein essential for Wingless signaling [published correction appears in Nature 2001 Apr 12;410(6830):847]. Nature. 2000;407(6803):527-530.
173. Pinson KI, Brennan J, Monkley S, *et al.* An LDL-receptor-related protein mediates Wnt signaling in mice. Nature. 2000;407(6803):535-538.
174. Tamai K, Semenov M, Kato Y, *et al.* LDL-receptor-related proteins in Wnt signal transduction. Nature. 2000;407(6803):530-535.
175. Tamai K, Zeng X, Liu C, *et al.* A mechanism for Wnt coreceptor activation. Mol Cell. 2004;13(1):149-156.
176. MacDonald BT, Tamai K, He X. Wnt/beta-catenin signaling: components, mechanisms, and diseases. Dev Cell. 2009;17(1):9-26.
177. Cadigan KM, Nusse R. Wnt signaling: a common theme in animal development. Genes Dev. 1997;11(24):3286-3305.
178. Carmon KS, Gong X, Lin Q, *et al.* R-spondins function as ligands of the orphan receptors LGR4 and LGR5 to regulate Wnt/beta-catenin signaling. Proc Natl Acad Sci U S A. 2011;108(28):11452-11457.
179. de Lau W, Barker N, Low TY, *et al.* Lgr5 homologues associate with Wnt receptors and mediate R-spondin signaling. Nature. 2011;476(7360):293-297.
180. Hao HX, Xie Y, Zhang Y, *et al.* ZNRF3 promotes Wnt receptor turnover in an R-spondin-sensitive manner. Nature. 2012;485(7397):195-200.

181. Koo BK, Spit M, Jordens I, *et al.* Tumour suppressor RNF43 is a stem-cell E3 ligase that induces endocytosis of Wnt receptors. Nature. 2012;488(7413):665-669.
182. Cruciat CM, Niehrs C. Secreted and transmembrane wnt inhibitors and activators. Cold Spring Harb Perspect Biol. 2013;5(3):a015081.
183. Oishi I, Suzuki H, Onishi N, *et al.* The receptor tyrosine kinase Ror2 is involved in non-canonical Wnt5a/JNK signaling pathway. Genes Cells. 2003;8(7):645-654.
184. Sastre-Perona A, Santisteban P. Role of the wnt pathway in thyroid cancer. Front Endocrinol (Lausanne). 2012;3:31.
185. Pez F, Lopez A, Kim M, *et al.* Wnt signaling and hepatocarcinogenesis: molecular targets for the development of innovative anticancer drugs. J Hepatol. 2013;59(5):1107-1117.
186. Nishita M, Enomoto M, Yamagata K, *et al.* Cell/tissue-tropic functions of Wnt5a signaling in normal and cancer cells. Trends Cell Biol. 2010;20(6):346-354.
187. Goessling W, North TE, Lord AM, *et al.* APC mutant zebrafish uncover a changing temporal requirement for wnt signaling in liver development. Dev Biol. 2008;320(1):161-174.
188. McLin VA, Rankin SA, Zorn AM. Repression of Wnt/beta-catenin signaling in the anterior endoderm is essential for liver and pancreas development. Development. 2007;134(12):2207-2217.
189. Monga SP, Monga HK, Tan X, *et al*. Beta-catenin antisense studies in embryonic liver cultures: role in proliferation, apoptosis, and lineage specification. Gastroenterology. 2003;124(1):202-216.
190. Suksaweang S, Lin CM, Jiang TX, *et al.* Morphogenesis of chicken liver: identification of localized growth zones and the role of beta-catenin/Wnt in size regulation. Dev Biol. 2004;266(1):109-122.
191. Tan X, Yuan Y, Zeng G, *et al.* Beta-catenin deletion in hepatoblasts disrupts hepatic morphogenesis and survival during mouse development. Hepatology. 2008;47(5):1667-1679.
192. Pettinato G, Ramanathan R, Fisher RA, *et al.* Scalable Differentiation of Human iPSCs in a Multicellular Spheroid-based 3D Culture into Hepatocyte-like Cells through Direct Wnt/β-catenin Pathway Inhibition. Sci Rep. 2016;6:32888.
193. Monga SP, Micsenyi A, Germinaro M, *et al*. beta-Catenin regulation during matrigel-induced rat hepatocyte differentiation. Cell Tissue Res. 2006;323(1):71-79.
194. Tan X, Behari J, Cieply B, *et al.* Conditional deletion of beta-catenin reveals its role in liver growth and regeneration. Gastroenterology. 2006;131(5):1561-1572.
195. Tan X, Apte U, Micsenyi A, *et al.* Epidermal growth factor receptor: a novel target of the Wnt/beta-catenin pathway in liver. Gastroenterology. 2005;129(1):285-302.
196. Benhamouche S, Decaens T, Godard C, *et al.* Apc tumor suppressor gene is the "zonation-keeper" of mouse liver. Dev Cell. 2006;10(6):759-770.
197. Cordi S, Godard C, Saandi T, *et al.* Role of β-catenin in development of bile ducts. Differentiation. 2016;91(1-3):42-49.
198. Wickline ED, Awuah PK, Behari J, *et al.* Hepatocyte γ-catenin compensates for conditionally deleted β-catenin at adherens junctions. J Hepatol. 2011;55(6):1256-1262.
199. Wickline ED, Du Y, Stolz DB, *et al.* γ-Catenin at adherens junctions: mechanism and biologic implications in hepatocellular cancer after β-catenin knockdown. Neoplasia. 2013;15(4):421-434.
200. Rocha AS, Vidal V, Mertz M, *et al.* The Angiocrine Factor Rspondin3 Is a Key Determinant of Liver Zonation. Cell Rep. 2015;13(9):1757-1764.
201. Nelsen CJ, Rickheim DG, Timchenko NA, *et al.* Transient expression of cyclin D1 is sufficient to promote hepatocyte replication and liver growth *in vivo*. Cancer Res. 2001;61(23):8564-8568.

202. Yang J, Cusimano A, Monga JK, *et al.* WNT5A inhibits hepatocyte proliferation and concludes β-catenin signaling in liver regeneration. Am J Pathol. 2015;185(8):2194-2205.
203. Michalopoulos GK, Khan Z. Liver Stem Cells: Experimental Findings and Implications for Human Liver Disease. Gastroenterology. 2015;149(4):876-882.
204. Okabe H, Yang J, Sylakowski K, *et al.* Wnt signaling regulates hepatobiliary repair following cholestatic liver injury in mice. Hepatology. 2016;64(5):1652-1666.
205. Michalopoulos GK, Barua L, Bowen WC. Transdifferentiation of rat hepatocytes into biliary cells after bile duct ligation and toxic biliary injury. Hepatology. 2005;41(3):535-544.
206. Marsee A, Roos FJM, Verstegen MMA, *et al*. Building consensus on definition and nomenclature of hepatic, pancreatic, and biliary organoids. Cell Stem Cell. 2021 May 6;28(5):816-832
207. Sato T, Vries RG, Snippert HJ, *et al.* Single Lgr5 stem cells build crypt-villus structures *in vitro* without a mesenchymal niche. Nature. 2009;459(7244):262-265.
208. Kim J, Koo BK, Knoblich JA. Human organoids: model systems for human biology and medicine. Nat Rev Mol Cell Biol. 2020 Oct;21(10):571-584. doi: 10.1038/s41580-020-0259-3. Epub 2020 Jul 7.
209. Hu H, Gehart H, Artegiani B, *et al.* Long-Term Expansion of Functional Mouse and Human Hepatocytes as 3D Organoids. Cell. 2018 Nov 29;175(6):1591-1606.e19.
210. Wang D, Wang J, Bai L, *et al.* Long-Term Expansion of Pancreatic Islet Organoids from Resident Procr+ Progenitors. Cell. 2020 Mar 19;180(6):1198-1211.e19.
211. Dianat N, Dubois-Pot-Schneider H, Steichen C, *et al.* Generation of functional cholangiocyte-like cells from human pluripotent stem cells and HepaRG cells. Hepatology. 2014;60(2):700-714.
212. Banales JM, Masyuk TV, Gradilone SA, *et al.* The cAMP effectors Epac and protein kinase a (PKA) are involved in the hepatic cystogenesis of an animal model of autosomal recessive polycystic kidney disease (ARPKD). Hepatology. 2009;49(1):160-174.
213. Lee SO, Masyuk T, Splinter P, *et al.* MicroRNA15a modulates expression of the cell-cycle regulator Cdc25A and affects hepatic cystogenesis in a rat model of polycystic kidney disease. J Clin Invest. 2008;118(11):3714-3724.
214. Ogawa M, Ogawa S, Bear CE, *et al.* Directed differentiation of cholangiocytes from human pluripotent stem cells. Nat Biotechnol. 2015 Aug;33(8):853-61.
215. Lugli N, Kamileri I, Keogh A, *et al.* R-spondin 1 and noggin facilitate expansion of resident stem cells from non-damaged gallbladders. EMBO Rep. 2016;17(5):769-779.
216. Tysoe OC, Justin AW, Brevini T, *et al.* Isolation and propagation of primary human cholangiocyte organoids for the generation of bioengineered biliary tissue. Nat Protoc. 2019 Jun;14(6):1884-1925.
217. Prior N, Hindley CJ, Rost F, *et al*. Lgr5+ stem and progenitor cells reside at the apex of a heterogeneous embryonic hepatoblast pool. Development. 2019 Jun 12;146(12):dev174557.
218. Taner CB, Bulatao IG, Perry DK, *et al.* Asystole to cross-clamp period predicts development of biliary complications in liver transplantation using donation after cardiac death donors. Transpl Int. 2012;25(8):838-846.
219. Taner CB, Bulatao IG, Willingham DL, *et al.* Events in procurement as risk factors for ischemic cholangiopathy in liver transplantation using donation after cardiac death donors. Liver Transpl. 2012;18(1):100-111.
220. Kalisvaart M, de Haan JE, Polak WG, *et al.* Comparison of Postoperative Outcomes Between Donation After Circulatory Death and Donation After Brain Death Liver Transplantation Using the Comprehensive Complication Index. Ann Surg. 2017;266(5):772-778.

221. Dubbeld J, Hoekstra H, Farid W, *et al.* Similar liver transplantation survival with selected cardiac death donors and brain death donors. Br J Surg. 2010;97(5):744-753.
222. Macias RIR, Banales JM, Sangro B, *et al.* The search for novel diagnostic and prognostic biomarkers in cholangiocarcinoma. Biochim Biophys Acta Mol Basis Dis. 2018 Apr;1864(4 Pt B):1468-1477.
223. Sakiani S, Kleiner DE, Heller T, Koh C. Hepatic manifestations of cystic fibrosis. Clin Liver Dis. 2019;23(2):263-77.
224. Assis DN, Freedman SD. Gastrointestinal disorders in Cystic Fibrosis. Clin Chest Med. 2016;37(1):109-18.
225. Shen N, Zhang D, Yin L, *et al.* Bile cell-free DNA as a novel and powerful liquid biopsy for detecting somatic variants in biliary tract cancer. Oncol Rep. 2019 Aug;42(2):549-560.
226. Lee SJ, Lee YS, Lee MG, *et al.* Triple-tissue sampling during endoscopic retrograde cholangiopancreatography increases the overall diagnostic sensitivity for cholangiocarcinoma. Gut Liver. 2014 Nov;8(6):669-73.

2

CHAPTER 2

Building a Consensus on Definition and Nomenclature of Human Hepatic, Pancreatic and Biliary Organoids.

Floris JM Roos*, Ary Marsee*, Monique MA Verstegen, HPB organoid consortium**, Helmuth Gehart, Eelco de Koning, Frédéric Lemaigre, Stuart J Forbes, Weng Chuan Peng, Meritxell Huch, Takanori Takebe, Ludovic Vallier, Hans Clevers, Luc JW van der Laan×, Bart Spee×

* these authors contributed equally;
** For author list of HPB organoid consortium, please see Table S1;
× shared senior authorship.

Cell Stem Cell 2021 May 6;28(5):816-832.

Abstract

Hepatic, pancreatic and biliary (HPB) organoids have proven to be powerful tools in the study of development, disease and regeneration, with applications ranging from basic research to regenerative medicine. Over the last decade, significant progress has been made in the culture of these three-dimensional (3D) structures. As organoid research intensifies, with laboratories around the world culturing these diverse tissue-like structures, there is need for a clear definition and nomenclature to describe these systems. To facilitate scientific communication and consistent interpretation, we revisit the concept of an organoid and introduce an intuitive classification system and nomenclature for referring to these 3D structures through the consensus of experts in the field. To promote the standardization and validation of HPB organoids, we propose guidelines for establishing, characterizing and benchmarking future systems. Finally, we address some of the major challenges to the clinical application of organoids.

Introduction

Since the derivation of the first tissue-derived intestinal organoids[1,2], immense progress has been made in the field of organoid biology, which is now an established and diverse field of research. These tissue-like 3D structures can be generated from a growing number of sources, including differentiated pluripotent stem cells (PSCs), fetal and adult primary tissue, as well as primary and metastatic tumors.[3] Different types of organoids display fundamental differences in their basic characteristics, complexity and applicability. For example, the extrahepatic bile duct-derived organoids established by Sampaziotis *et al.* take the form of self-renewing epithelial luminal structures, reminiscent of bile ducts *in vivo*.[4] In contrast, the iPSC-derived liver bud organoids developed by Takebe *et al.* take the form of dense multi-cellular structures, which lack long-term self-renewal.[5,6] Rather than expanding, these structures undergo mesenchymal-driven condensation to generate liver tissue with both endodermal and mesodermal components.[7] As the field of organoid biology continues to advance, there is need for consistent definitions and nomenclature to clearly describe these diverse structures. Here we focus on organoids derived from the liver, pancreas and biliary tree, which share a close developmental, anatomical and physiological relationship.[8]

Consistency is currently lacking when referring to tissue-derived hepatic, pancreatic and biliary (HPB) organoids. For example, the intrahepatic bile duct-derived organoid systems are commonly referred to as *liver organoids*[9], *ductal organoids*[10]and *cholangiocyte organoids*[11]. As a result, precise scientific communication is hampered, leading to a variable understanding of a given system. This makes the reproduction of results between institutions more difficult and slows scientific progress. Although renaming organoid systems can be difficult, it is essential to have a common understanding within the community. To accomplish this, we employed a modified Delphi method based on three successive questionnaires (See online supplementary Data: Questionnaire 1-3). Through the consensus of experts in the field, we propose an overarching definition of an organoid, with sub-classifications based on defining characteristics (Figure 1). In addition, we propose nomenclature for tissue-derived epithelial organoids with the goal of achieving clarity and promoting rigor in the field. Importantly, we leave room for future organoid systems that will arise as the field develops. To this end, we propose guidelines for establishing, characterizing and benchmarking future organoids, in turn promoting the standardization and validation of organoid models. In order to provide context and background for this effort, we provide a detailed overview of the recent progress in the culture of organoids derived from the liver, pancreas and biliary tree, as well as PSC-derived organoids differentiated to the hepatic, pancreatic and biliary fate. To conclude, we address some of the hurdles that need to be overcome for organoids to make their way to the clinic.

Defining an Organoid

The concept of an organoid has been around for decades, with many scientific interpretations over the years.[12] However, the term's broad application, from describing small tissue explants[13], to clonally expanding cells that self-organize in 3D culture[2], has made its meaning unclear. To bring clarity to the term organoid and this growing field of research, more than 60 experts (Table S1), representing 16 countries around the world (Figure S1) have come together to define an organoid as a *three-dimensional structure derived from (pluripotent) stem cells, progenitor and/or differentiated cells that self-organize through cell-cell and cell-matrix interactions to recapitulate aspects of the native tissue architecture and function in vitro* (Figure 1). While early reports on the establishment of organoid systems indicated that organoids are exclusively derived from stem cells[14]; it is now clear that organoids can also be initiated from differentiated cells, such as cholangiocytes.[4,15] We propose that organoids can be divided into distinct groups based on defining characteristics. These include epithelial organoids, multi-tissue organoids, and multi-organ organoids (Figure 1). Of note, while we focus on HPB organoids, the proposed classification system can also be applied to organoids of other organs.

Epithelial organoids represent the most widely studied organoid system. These structures are derived from a single germ layer (endoderm, mesoderm or ectoderm) and have the ability to self-renew under the appropriate culture conditions. In this context, self-renewal describes the *repeated regeneration of organoids from organoid fragments or single cells*, allowing for the serial expansion of cultures (Figure 2). Epithelial organoids exemplify this characteristic through the ability of these structures to form from the clonal expansion of a single cell.[2,9,11,16] As epithelial organoids expand, cells polarize and specialize to reproduce aspects of the native epithelium.[2] Remarkably, upon physical fragmentation or enzymatic and/or chemical dissociation of epithelial organoids into single cells or disordered cell aggregates (followed by secondary culture in expanding conditions), cells reorganize and proliferate to reform organoids.[4,9] As their name implies, epithelial organoids do not harbor the mesodermal components normally present in native tissue. That withstanding, in some cases epithelial organoids are co-cultured with supporting cells, however, these cells do not become a part of the epithelial organoid.[17,18] More broadly, we propose that for cells to be constituents of an organoid, they must be functionally integrated into the overall structure and synchronized with the proliferative state of the organoid.

Multi-tissue organoids (Figure 1) are established through the co-culture of stem/progenitor cells derived from at least two germ layers[6], or the co-differentiation of PSCs.[19-21] In the contexts of the liver, pancreas and biliary tree, multi-tissue organoids are composed of cells of endodermal and mesodermal origins. Unlike epithelial organoids, current protocols do not support the self-renewal of multi-tissue organoids, which would require the coordinated expansion of parenchymal and supporting cell types. Instead, cells interact to attain a stable

level of maturity and function.[6,10,21] An advantage of multi-tissue organoids is their tissue-like, hetero-cellular composition. Multi-tissue organoid systems are well-placed for studying the heterotypic cell-cell interactions of multiple cell types normally present in the native tissue. Importantly, these cultures show intra-organ self-organization between epithelial and supporting cell types, similar to that of the native tissue.[6,22]

Multi-organ organoids (Figure 1) are the most complex and least described organoid type, with only one report in the context of HPB organoids.[23] Characteristic to this sub-type is inter-organ developmental self-organization patterns. As demonstrated by Koike *et al.*[23], these systems hold great promise for the study of organogenesis, a process governed by several boundary tissue interactions.[24] HPB multi-organ organoids could be maintained in culture for at least 90 days, not only displaying multiple HPB organ domains, but also showing interconnectivity between them. We anticipate the emergence of additional multi-organ organoid systems in the years to come.

Is a Spheroid an Organoid?

The term spheroid describes 3D cell aggregates that form in the absence of a predefined culture substrate to adhere to.[25] Common techniques to generate spheroids include hanging-drop and ultra-low attachment cultures, which encourage cell-cell interaction, while discouraging cell-substrate/matrix interaction.[26] As a result, cells interact to form a compact sphere, although other shapes are possible.[27] This contrasts with most organoid systems, which self-organize when placed in a matrix-rich 3D environment, such as Matrigel, with which cells can interact.[28-30]

That withstanding, while there is no predefined matrix with which cells can interact during the self-organization of spheroids, extracellular matrix (ECM) cues are involved in their formation. These take the form of long chain ECM fibers containing multiple RGD domains present on cell surfaces.[26] Furthermore, cells secrete their own ECM molecules which likely participate in their organization. In some cases, multicellular spheroid systems have been shown to recapitulate architectural and functional aspects of the original tissue. For example, Bell *et al.* reported the generation of primary human hepatocyte spheroids with bile canaliculi and mature hepatocyte functions.[31] The question therefore arises: when is a spheroid an organoid? Here we propose that a spheroid is an organoid when it is composed of organ-specific cell types and satisfies the overarching definition of an organoid.

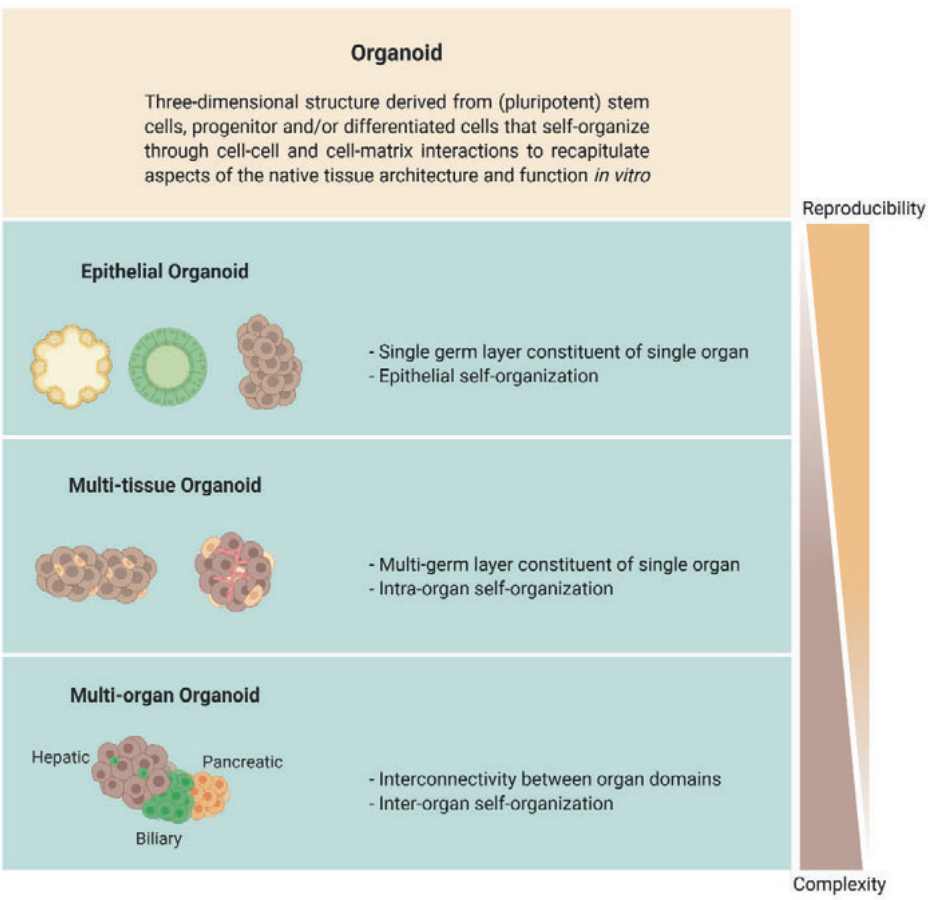

Figure 1. Organoid definition.
Overarching definition of an organoid (top panel) along with the three sub-classification (bottom 3 panels).

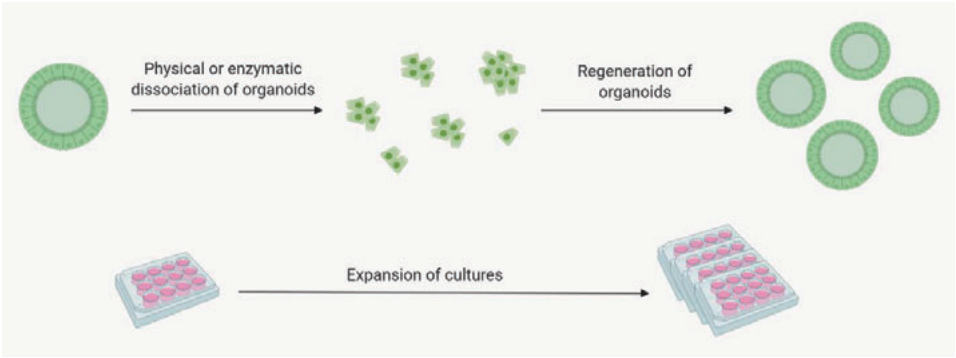

Figure 2. Self-renewal of organoids.
Upon physical or enzymatic and/or chemical dissociation of organoids into fragments or single cells (followed by secondary culture in expanding conditions), cells reorganize and expand, reforming organoids.

Hepatic, Pancreatic and Biliary Organoids Derived from Pluripotent Stem Cells

Since Yamanaka and colleagues reported the efficient reprogramming of mature somatic cells into iPSCs in 2007[32,33], numerous protocols have been developed to direct the differentiation of iPSCs into specific cell types.[34-36] While early endeavors focused on stepwise differentiation protocols exclusively in 2D[37-40], there has been a shift to the 3D culture of PSC-derived cells in recent years.[41] It is now possible to generate epithelial, multi-tissue and multi-organ HPB organoids from iPSCs (Figure 3). Of note, the same techniques can also be applied to ESCs, although their use is more limited due to ethical concerns.[42] In the present section we review recent progress in the culture of hepatic, pancreatic and biliary organoids derived from PSCs.

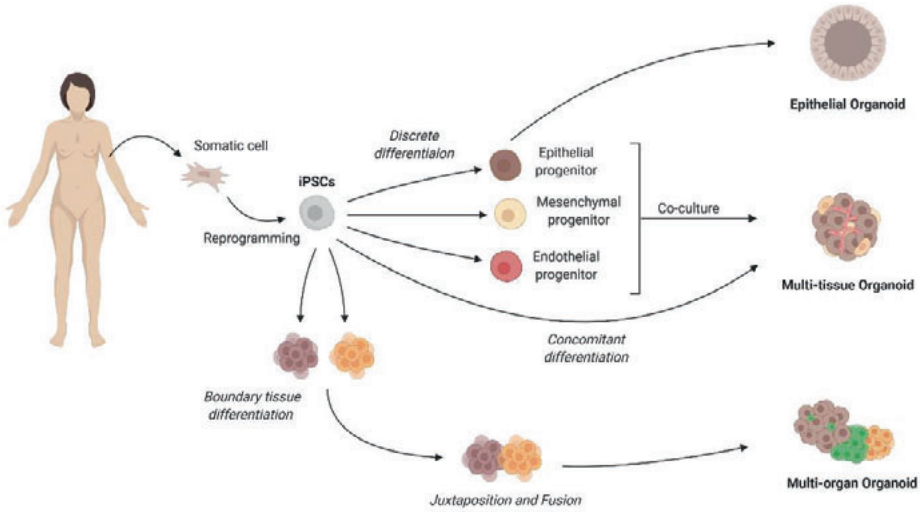

Figure 3. Generation of epithelial, multi-tissue and multi-organ organoids from iPSCs.

PSC-derived Hepatic Organoids

One of the first steps in liver organogenesis is the development of the primordial liver bud, a structure that arises when primitive hepatic endodermal cells of the ventral foregut endoderm delaminate and invade the septum transversum mesenchyme, guided by nascent endothelial cells and the adjacent cardiac mesoderm.[43] Following these principles, Takebe *et al.* reported the generation of multi-tissue "liver bud" organoids from the co-culture of iPSC-derived hepatic endodermal progenitors, human umbilical vein endothelial cells (HUVECs) and mesenchymal stem cells (MSCs).[5] In 2017 the system was reintroduced with both endodermal and mesodermal compartments being derived exclusively from iPSCs.[6] Upon transplantation into immunocompromised mice, liver bud organoids functionally interconnected with the host vasculature and engrafted. *In vivo*, the organoids performed key hepatic functions, rescuing liver function and improving survival of mice challenged with drug-induced liver failure.[5,6] In an effort to model Alagille syndrome (ALGS), a genetic disorder characterized by bile duct paucity and cholestasis, Guan *et al.* established a blend of morphologically diverse iPSC-derived hepatic epithelial organoids.[44] Interestingly, organoids were predominantly composed of either hepatocyte-like-cells (HLCs), cholangiocyte-like-cells (CLCs), or a mixture, containing both HLCs and CLCs. Organoids were self-renewing and could be matured to perform some hepatic functions, including glycogen storage, liver-specific drug metabolism, as well as albumin and bile secretion. Notably, organoids generated using ALGS patient-derived cells formed fewer duct-like structures and had a reduced ability to mediate biliary transport compared to controls, recapitulating the disease phenotype *in vitro*.[44]

In a novel approach, Wu *et al.* generated hepatobiliary multi-tissue organoids from iPSCs by simultaneously inducing both endodermal and mesodermal differentiation. Their protocol promoted the co-differentiation of iPSCs to hepatic, biliary and mesodermal lineages, evident through the CD31-marked tubular network present in the organoids.[21] Similarly, Ouchi *et al.* developed a method to generate hepatic multi-tissue organoids through the co-differentiation of iPSCs or ESCs. Single-cell transcriptomic analysis revealed that their protocol resulted in the co-emergence of HLCs, CLCs, Kupffer-like-cells and stellate-like-cells in the organoids (Ouchi *et al.*, 2019). Interestingly, these systems show the concomitant differentiation of PSCs to both epithelial and mesenchymal cell types under the same culture conditions.[19,21]

Seeking to generate highly expandable sources of hepatic endodermal organoids from PSCs, Wang *et al.*[45], Akbari *et al.*[46] and Mun *et al.*[47] established novel protocols for the derivation and culture of self-renewing ESC- and iPSC-derived hepatic epithelial organoids. In each case organoids expanded as epithelial cysts, morphologically resembling the bile duct-derived organoids described by Huch *et al.*[9], and could be matured to perform some hepatic functions.[45-47] The authors further validated their hepatic organoid models by using them to model rare genetic diseases affecting the liver, such as Citrullinemia type-1[46], as well as hepatotoxicity and steatosis.[47]

In a recent breakthrough, Bin Ramli *et al.*[48] reported the generation of PSC-derived liver epithelial organoids, containing functionally interconnected hepatic and biliary compartments. Morphologically, organoids presented a dense albumin (ALB)$^+$ hepatic core surrounded by cytokeratin (KRT)7$^+$ biliary cysts. Live imaging revealed the transport of the fluorescent compound 5 (and 6)-carboxy-2,7-dichlorofluorescein (CDF) into robust bile canaliculi networks between polarized HLCs, emptying into biliary cysts composed of CLCs. Treatment of organoids with the cholestasis-inducing drug, troglitazone, disrupted the bile canaliculi network.[48] Similarly, Shinozawawa *et al.* reported the generation of iPSC-derived hepatic multi-tissue organoids and their use as a cholestatic drug screening tool. Notably, organoids could be established from cryopreserved iPSC-derived foregut progenitors, allowing for quicker derivation of cultures compared to starting with naïve iPSCs.[20]

PSC-derived Biliary Organoids

In 2014, Dianat *et al.* described the differentiation of ESCs and iPSCs into functional CLCs.[49] When cultured in 3D conditions, PSC-derived CLCs formed cysts morphologically resembling the cholangiocyte-derived structures reported by LaRusso and colleagues.[50,51] Interestingly, when kept in culture for more than seven days cysts began to bud, forming branched tubular structures.[49]

In 2015, the research groups of Vallier and Ghanekar introduced novel protocols for the directed differentiation of PSCs into CLCs, and their 3D culture as epithelial organoids. PSC-derived cholangiocyte organoids displayed key functions and were successfully used to model genetic diseases affecting the bile duct epithelium, such as cystic fibrosis and Alagille syndrome. Importantly, researchers were able to rescue the disease phenotypes with pharmacological intervention, validating them as a drug screening tool. The organoids were also used to study biliary development through the modulation of key pathways normally active during native bile duct development, proving to be an excellent tool, not only for disease modeling and drug screening, but also for the study of the mechanisms driving bile duct development.[52,53]

PSC-derived Pancreatic Organoids

In 2015, Huang *et al.* described the generation of pancreatic epithelial organoids from PSC-derived pancreatic progenitors.[554] Morphologically, organoids resembled cystic structures, consisting of a single, polarized layer of epithelial cells surrounding a central lumen. Characterization of the organoids revealed that culture conditions promoted a progenitor phenotype, with low or undetectable expression of mature ductal, acinar or islet markers. However, ductal and acinar differentiation could be promoted *in vitro* by modifying the culture conditions, or *in vivo* following transplantation into immunodeficient mice. In both cases organoids formed pancreatic exocrine structures containing Carboxypeptidase A1 (CPA1$^+$) acinar and KRT19$^+$ ductal compartments.[54]

Two years later, Hohwieler *et al.* reported the differentiation of iPSCs and ESCs to pancreatic progenitors (PP) and their culture as epithelial organoids.[55] 3D culture conditions promoted the emergence of acinar and ductal lineages, which comprised 34%±15% and 61%±19% of organoid cells, respectively. Functionally, PSC-derived pancreatic organoids exhibited carbonic anhydrase activity at levels comparable to freshly isolated pancreatic ductal cells, as well as detectable levels of amylase, trypsin and elastase activity. Global gene expression analysis revealed that PSC-derived pancreatic organoids clustered closely to human adult pancreatic tissue, as well as primary ductal and acinar cells. When orthotopically transplanted onto the pancreas of immunodeficient mice, organoids functionally engraft, with signs of neovascularization and tri-lineage differentiation, including insulin producing cells.[55]

More recently, Yoshihara *et al.* succeeded in generating human islet-like organoids (HILOs) from iPSCs.[56] HILOs were rich in endocrine cell types, with single-cell transcriptomic analysis revealing the presence of β-, α- and δ-cell rich populations. When transplanted into streptozotocin (STZ)-induced diabetic NOD/SCID mice, HILOs quickly reestablished glucose hemostasis. Furthermore, when genetically engineered to overexpress the immune checkpoint protein, programmed death-ligand1 (PDL1), HILOs could even provide glucose homeostasis in immune-competent mice. PDL1-overexpressing HILOs were shielded from immune destruction, remaining glucose responsive for 50 days. Intriguingly, HILOs treated with the interferon-γ (IFN-γ), which induces PDL1 expression in pancreatic islets, were able to recapitulate the immune evasive properties of transgenic PDL1-overexpressing HILOs, providing glucose homeostasis for 40 days when transplanted into immune competent STZ-induced diabetic mice.[56]

In an attempt to create personalized models of pancreatic cancer Huang *et al.*[57] and Breunig *et al.*[58] developed novel protocols for the generation of pancreatic organoids from iPSCs and their subsequent oncogenic transduction.[57,58] Huang *et al.* generated pancreatic ductal organoids by activating FGF, EGF and non-canonical WNT signaling, while inhibiting canonical WNT signaling. To generate pancreatic acinar organoids, iPSC-derived PP were cultured in canonical WNT-stimulating conditions and hedgehog, NOTCH- and BMP-inhibiting conditions. Both organoid types showed cell-type specific function and expressed either typical ductal markers, SRY-Box transcription factor (SOX)9 and Carbonic anhydrase II (CA2) or acinar markers, pancreatic transcription factor 1 and chymotrypsin C, on a protein-level. When genetically engineered to express one of the cancer-associated forms of KRAS, which bears the G12D mutation, acinar organoids exhibited ductal metaplasia *in vitro* and formed IPMN-like structures *in vivo*.[57] In parallel, Breunig *et al.* demonstrated that different oncogenic mutations, alone or in combination, result in distinct morphological changes and molecular phenotypes in PDOs. For instance, a combination of oncogenic KRAS expression and CDKN2A-loss resulted in PDOs forming PDAC like lesions *in vivo*, while mutant GNAS-expressing PDOs formed IPMN-like lesions following transplantation.[58] Taken together these

studies demonstrate the potential to model diverse cancers by engineering specific oncogenic mutations into iPSC-derived organoids.

Organoids Derived from Primary Tissue of the Human Liver, Pancreas and Biliary Tree

It is now possible to culture self-renewing epithelial organoids from primary tissue of the human liver[9,11], pancreas[59-61] and extrahepatic biliary tree[4,62] (Figure 4 and Table S2). To establish cultures, isolated cells or tissue fragments are embedded in a matrix-rich 3D environment, typically Engelbreth-Holm-Swarm (EHS)-based hydrogels, and supplemented with medium containing growth factors and small molecules. Within days, 3D structures begin to arise that can be serially passaged for several months.[28,30,59] Tissue-derived epithelial organoids display high levels of genetic stability and are committed to their tissue of origin, making them an attractive system, not only for *in vitro* testing, but also for therapeutic applications.[10] In this section, we review the recent progress in the culture of tissue-derived hepatic, pancreatic and biliary organoids.

Building a Consensus on Nomenclature of Tissue-derived Epithelial Organoids

In building a consensus on the nomenclature of HPB organoids we first considered the basic question, what is the most important aspect the nomenclature for organoids should reflect? For example, should it reflect the cell type of origin, the cell type of resemblance *in vitro*, or the anatomical structure the organoid most resembles? In addressing this question, the community considered the following – which aspect is most informative? In the end, consensus was reached that the nomenclature for single cell-type epithelial systems should reflect the cell type of resemblance *in vitro*, and that the cell and tissue of origin should be clearly defined. In this way you know where you begin (tissue and cell of origin) — and where you end (cell type of resemblance *in vitro*). In some cases, the two align. For example, the intra- and extrahepatic cholangiocyte organoid systems are derived from, and resemble cholangiocytes *in vitro*.[4,15] However, for organoid systems capable of transdifferentiation, the cell type of origin is not always reflected *in vitro*.[11,63] For example, in their defined hepatocyte organoid expansion medium, the mouse hepatocyte organoids established by Hu *et al.* expand as condensed structures with typical hepatocyte morphology. However, when cultured under the conditions established by Huch *et al.* for the culture of intrahepatic cholangiocyte organoids, cells transdifferentiate and reorganize, expressing classical cholangiocyte markers and taking on a cystic morphology.[11] Because the cell type of resemblance *in vitro* does not correspond to the cell type of origin in transdifferentiating systems, it is imperative that researchers clearly identify the cell of origin. Recent discoveries have highlighted the extensive degree of plasticity that exists between the epithelial cells of the mouse liver, with numerous reports evidencing cell fate changes between hepatocytes

and cholangiocytes *in vivo*.[64,67] Whether this phenomenon also occurs in humans has yet to be unequivocally established.

For epithelial organoid systems in which multiple cell types arise, consensus was reached that the nomenclature should reflect the anatomical structure that arises. Clear examples of these systems include the gut organoids that arise from single Lgr5$^+$ stem cells to reproduce multiple cell types of the intestinal epithelium[2], or the recently published pancreatic islet organoids that arise from single Procr$^+$ cells.[18] To facilitate clear scientific communication and reproducibility, it will be important for researchers to clearly define the organoid initiating cell population(s) of multi-cell type epithelial organoids when possible.

Intrahepatic Cholangiocyte Organoids (ICOs)

Since the discovery that the Wnt/β-catenin target, Lgr5, marks adult stem cells in the intestine, it was also shown to mark stem cell populations in other tissues.[68,69] This led to the hypothesis that Lgr5 may represent a bona fide marker of adult stem cells in multiple epithelial tissues.[70] However, recent evidence suggests that for organs with low cell turnover, such as the liver, this may not be the case.[71,72] In the homeostatic liver Lgr5 marks pericentral hepatocytes expressing the canonical Wnt/β-catenin target, Axin2.[73] Upon injury, Lgr5 and Axin2 are upregulated in hepatocytes throughout the liver[72], but not in cholangiocytes at any stage during ductular reaction.[71] Interestingly, in 2013 Huch *et al.* described a protocol for the long-term, clonal expansion of single mouse Lgr5$^+$ liver ductal cells as cystic organoids expressing Krt19 and Krt7.[74] Interestingly, mouse intrahepatic cholangiocytes cultured under the described conditions expressed multiple progenitor, hepatocyte and cholangiocyte markers, suggestive of a bipotential nature. Indeed, upon modifying the culture conditions to stimulate hepatic maturation, mouse intrahepatic cholangiocyte organoids (mICOs) expressed markers of mature hepatocytes and could perform some hepatocyte functions.[74] Based on the capacity of ICOs to be differentiated to HLCs, the authors concluded that mICOs were bipotential and derived from a rare Lgr5$^+$ stem cell population of ductular origin that became activated upon carbon tetrachloride (CCl4) injury.[74] It was subsequently demonstrated that the cells of origin were MIC1-1C3$^+$/CD133$^+$/CD26-[75], markers of cholangiocytes as well as biliary progenitors, leaving the question open as to whether the cell of origin was indeed a cholangiocyte, or a stem/progenitor cell. Recently, Huch and colleagues employed a lineage tracing model to formally demonstrate that the organoid-initiating cells are in fact adult intrahepatic cholangiocytes which undergo Tet1-mediated epigenetic reprogramming to assume a stem/progenitor cell state, both *in vitro* and *in vivo*.[15] In support of this, Planas-Paz *et al.* demonstrated that Lgr5 mediated Wnt/β-catenin signaling is absent and unnecessary for Epcam$^+$ cholangiocytes to initiate a ductular reaction *in vivo*. However, upon *in vitro* culture under Wnt/β-catenin-inducing conditions, isolated Epcam$^+$ cholangiocytes form organoids and upregulate Lgr5.[71] Interestingly, Prior *et al.* recently demonstrated that Lgr5 marks a sub-population of truly bi-potent hepatoblasts in the early

mouse embryo (E9.5).[76] Whether the ability of adult cholangiocytes to initiate organoids is restricted to a select subset of cells with increased plasticity, or equally shared amongst biliary epithelial cells (BECs) remains to be determined.

In 2015, the culture of mICOs was adapted to support the culture of human intrahepatic cholangiocyte organoids (hICOs) (Figure 4). To do this, the medium composition was adapted to include forskolin (FSK), a cAMP pathway agonist, and A83-01, an inhibitor of TGFβ receptors ALK4/5/7.[9] Under these conditions $EpCAM^+$ bile duct cells generated organoids with a striking efficiency of 28.4% ± 3.2%. hICOs were highly proliferative, expanding as cystic structures for several months while remaining genetically stable. Interestingly, hICOs expressed a mixture of markers, including LGR5, the hepatocyte marker, HNF4α, and ductal markers KRT19 and ONECUT2. However, hICOs failed to express markers of mature hepatocytes, such as albumin or CYP3A4. In order to exploit the suspected bipotential character of the cells and achieve hepatocyte differentiation, culture media was developed that lacked R-spondin and FSK, but included BMP7, FGF19, dexamethasone and the Notch inhibitor, DAPT. In this hepatocyte differentiation medium hICOs upregulated several hepatocyte markers. Similar to their murine counterparts, hICOs cultured in differentiation medium acquired mature hepatocyte functions, such as albumin and bile acid secretion, glycogen storage, Phase I and II drug metabolism and ammonia detoxification. When transplanted into immunocompromised mice, hICOs could engraft and mature into hepatocytes *in vivo*, although their engraftment efficiency was low (<0.1%).[9] Of note, recent single cell analysis of the human liver has revealed extensive heterogeneity within the biliary compartment, including subsets of cholangiocytes that express classical hepatocyte markers, such as ALB, SERPINA1 and CYP3A4 (although significantly lower compared to hepatocytes).[77] This raises the question: does the hepatocyte differentiation protocol described by Huch and colleagues generate hepatocytes *in vitro*, or are these cells simply cholangiocytes which upregulate some hepatocyte markers and perform certain functions typically attributed to hepatocytes?

Extrahepatic Cholangiocyte Organoids (ECOs)

In 2017 Sampaziotis *et al.* reported the culture of human cholangiocytes derived from the extrahepatic bile ducts as self-renewing organoids.[4] These cells could be isolated by several methods, including brushing of the common bile duct (CBD) during an endoscopic retrograde cholangiopancreatography, a minimally invasive procedure. To initiate ECOs (Figure 4), isolated cholangiocytes were embedded in Matrigel and cultured in medium supplemented with epidermal growth factor (EGF), R-spondin and Dickkopf-related protein 1 (DKK-1). These culture conditions are in contrast to those established for the culture of ICOs, including both a canonical Wnt agonist (R-spondin) and inhibitor (DKK-1). Morphologically, the cells in ECOs had ultrastructural features characteristic of cholangiocytes, including cilia, microvilli and tight junctions. Functional analysis of ECOs revealed that they retained key cholangiocyte

functions, such as transport through multidrug resistance protein-1 (MDR1), luminal extrusion of bile acids, alkaline phosphatase (ALP) and gamma-glutamyltransferase (GGT) activity, and responsiveness to secretin and somatostatin.[4]

To probe the clinical potential of ECOs, the group investigated their potential as a cell source for biliary reconstruction. To do this ECOs were seeded onto polyglycolic acid (PGA) scaffolds and grown until confluence. After successful colonization, the ECO-seeded scaffolds were transplanted into mouse models of CBD and gallbladder injury. Notably, mice transplanted with the resulting tissue constructs survived for up to 104 days without complications. *In vivo*, scaffolds were successfully remodeled into functional biliary tissue expressing biliary markers KRT19, KRT7, HNF-1β, SOX9 and CFTR.[4] More recently, it was demonstrated that ECOs could also be used to regenerate the intrahepatic bile ducts of immunodeficient mice with drug induced cholangiopathy. Control mice not receiving ECOs died within 3 weeks, while mice receiving ECOs survived up to 3 months with resolution of cholangiopathy and normal serum biochemistry.[78]

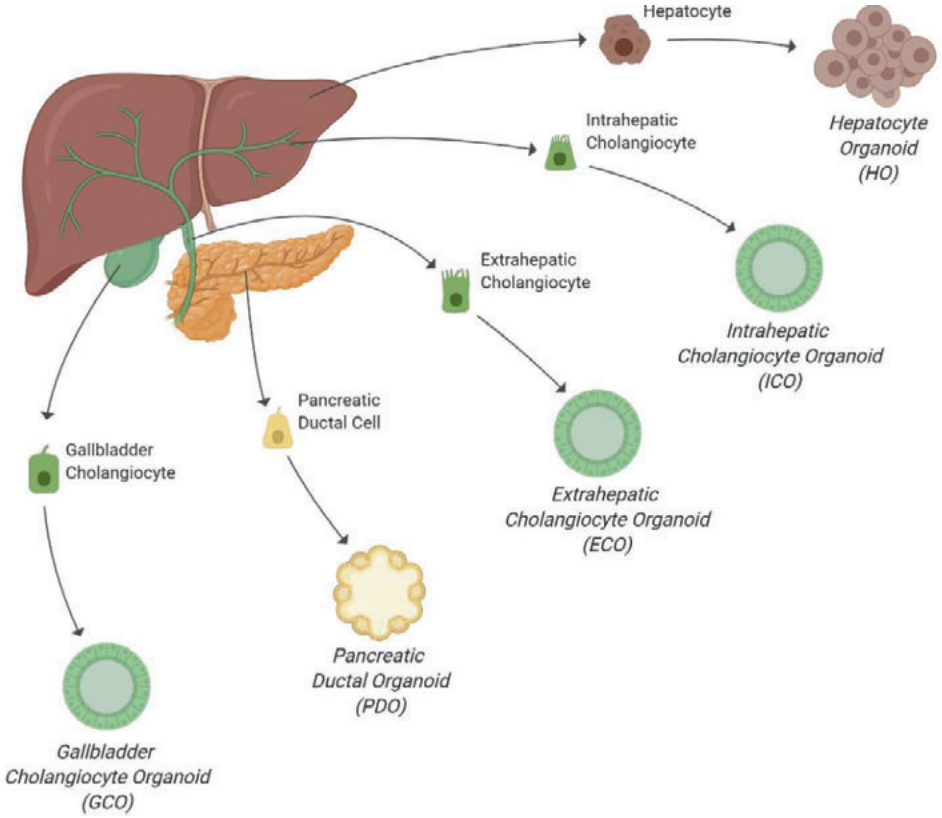

Figure 4. Nomenclature for epithelial organoids derived from primary tissue of the adult liver, pancreas, and biliary tree.

Gallbladder Cholangiocyte Organoids (GCOs)

The protocol established to support the culture of ICOs was quickly applied to other regions of the biliary tree. In 2016, Lugli *et al.* demonstrated that morphologically indistinguishable organoids could be established from fragments of gallbladder and extrahepatic bile duct tissue, although they did not provide a detailed characterization of human gallbladder cholangiocyte organoids (hGCOs) (Figure 4).[62] Mouse GCOs expressed the Wnt-target, Lgr5, as well as biliary makers Cldn3, EpCAM, Prom1, Sox9 and Itga6. Of note, Prom1 and Sox9 have been attributed to both stem cells and mature cholangiocytes. To confirm the origin of the organoids, expression of 413 gallbladder-specific and 190 liver-specific genes were analyzed. mGCOs expressed the gallbladder, but not the liver specific genes and had gene expression profiles that distinguished them from mICOs.[62] In a recent breakthrough, Sampaziotis *et al.* demonstrated that hGCOs could be used to regenerate the intrahepatic bile ducts of the human liver.[78] To accomplish this, the bile ducts of human livers receiving normothermic machine perfusion were infused with GCOs expanded under the conditions described for the culture of ECOs (see next section). Histological analysis of recipient livers revealed that transplanted organoids engrafted in the intrahepatic biliary tree, regenerating ~40-85% of the injected ducts. Furthermore, livers transplanted with GCOs had no evidence of cholangiopathy, while control livers not receiving cells demonstrated evidence of ischemic injury and loss of epithelial continuity.[78]

Regional Diversity of Cholangiocyte Organoids

In an attempt to better understand the differences between cholangiocyte organoids (COs) derived from different regions of the biliary tree, Rimland *et al.* established ICOs, ECOs and GCOs from the intrahepatic bile ducts, common bile duct and gallbladder, respectively.[79] Importantly, each organoid type was derived and cultured under WNT/β-catenin stimulating conditions, allowing for a close comparison. Interestingly, gene and protein expression analyses revealed that ICOs, ECOs and GCOs are remarkably similar, despite some regional differences corresponding to the anatomical location from which cells are isolated.[79] In parallel, Verstegen *et al.* performed comparative analysis of ICOs and ECOs cultured under the conditions established by Huch *et al.* for the culture of ICOs.[80] Under these conditions ICOs and ECOs were highly similar, confirming the findings reported by Rimland and colleagues.[80] It was subsequently demonstrated that bile composition was a large determinant of the regional identity of cholangiocytes located along the biliary tree. Treatment of ICOs, ECOs and GCOs with gallbladder bile caused the cells to acquire overlapping gene expression profiles, providing evidence for a niche-dependent model of regional cholangiocyte identity.[78]

Despite these similarities, only ICOs demonstrated the ability to upregulate hepatocyte markers upon *in vitro* differentiation.[79,80] From an embryological perspective, the selective capacity of ICOs to upregulate hepatocyte markers makes sense. Intrahepatic cholangiocytes

arise from bipotential hepatoblasts, while extrahepatic cholangiocytes arise from the caudal portion of the hepatic diverticulum.[81] This could imply that ICOs, but not ECOs/GCOs have the epigenetic landscape to support hepatocyte (trans)differentiation. Conversely, Sampaziotis *et al.* demonstrated that ECOs and GCOs are interchangeable with ICOs regarding their ability to regenerate the biliary epithelium. When transplanted into the mouse and human liver, ECOs and GCOs engrafted into the intrahepatic bile ducts, regenerating the biliary epithelium, and resolving cholestasis.[78] Notably, engrafted cells lost their extrahepatic gene expression signature and acquired an intrahepatic expression profile. Furthermore, the expression of other hepatic lineage markers was never observed, providing further evidence that extrahepatic cholangiocyte plasticity may be limited the biliary lineage.[78]

Hepatocyte Organoids (HOs)

In 2018 Peng *et al.* reported the long-term 3D culture of primary mouse hepatocytes as organoids. To establish mouse hepatocyte organoids (mHOs), primary hepatocytes were embedded in Matrigel and cultured in medium containing a combination of growth factors, including the small molecule Wnt-agonist, CHIR99021, and the inflammatory cytokine, TNFα.[82] The culture conditions represent a novel approach to directing the expansion of a fastidious cell type through the exploitation of pro-inflammatory signals released during regeneration *in vivo*. In the contexts of liver regeneration, TNFα activates a series of transcription factors including NF-κB, JAK/Stat, AP-1 and YAP, which enhance cell proliferation.[82]

Under the expansion conditions described, mHOs could be expanded for at least eight months. Withdrawal of TNFα resulted in deterioration of cultures. Morphologically, cells in mHOs were polygonal in shape, with larger colonies taking on the appearance of condensed rosette-like structures. Upon transcriptomic analyses, it was shown that mHOs resembled proliferating hepatocytes after partial hepatectomy (PHx).

In order to mature mHOs, the group considered the functional heterogeneity of hepatocytes along the sinusoidal axis (Figure 4). Periportal (PP) hepatocytes (zone 1) are specialized in β-oxidation and gluconeogenesis, whereas pericentral (PC) hepatocytes (zone 3) are better more proficient in xenobiotic detoxification, glycolysis and lipogenesis.[83] These metabolic differences are driven, in part, by the Wnt gradient generated by central vein endothelial cells.[84] In mHOs, PP genes were strongly downregulated, so the group devised two different culture media: one with Wnt/β-catenin activation and one without Wnt/β-catenin activation, to separately induce the expression of either PC or PP genes, allowing for a zonally-defined maturation of mHOs. Functionally, mHOs in both DMs secreted albumin, with the highest levels in the PP-induction medium. Moreover, in both DMs mHOs were functional in low-density-lipoprotein uptake, canicular transport and glycogen storage. Upon transplantation into FAH-/- mice, mHOs engrafted and repopulated up to 80% of the liver parenchyma.

Notably, cells spontaneously established zonated expression profiles depending on their spatial engraftment along the porto-central axis.[82]

In parallel, Hu *et al.* developed a similar protocol for the long-term culture of mouse hepatocytes and human fetal liver cells as organoids.[11] However, rather than inflammatory cytokine-mediated expansion, the group utilized a medium with additional growth factors and the Wnt agonist, R-spondin. The cells comprising mHOs were of typical hepatocyte morphology, as revealed by transmission electron microscopy. Immunofluorescence staining showed that mHOs had strong Alb expression and were negative for the cholangiocyte markers KRT19 and KRT7. In expansion conditions mHOs resembled hepatocytes after PHx, expressing a combination of mature hepatocyte markers, cell-cycle markers and proliferation markers, as well as the fetal (immature) hepatocyte marker alpha fetoprotein (AFP).[11] Similarly, Prior *et al.* showed that single embryonic mouse $Lgr5^+$ bi-potent hepatoblasts could be expanded *in vitro* and fated to either the cholangiocyte or hepatocyte lineage, depending on the culture conditions. When cultured in hICO expansion medium, hepatoblasts would form cholangiocyte organoids. However, when cultured in the hepatocyte medium for expanding human hepatocytes in 2D[85], cells would form hepatocyte organoids (mHOs) which secreted high levels of Albumin while retaining their embryonic nature (by expression of AFP).[76]

Building on their murine work, the protocol for the culture of mHOs was adapted to support the long-term culture of human fetal liver cells as organoids, though the cellular origin of the organoids was never demonstrated. As the plating efficiency was low (<1%), it is possible that a rare stem/progenitor cell is the cell of origin. Fetal liver-derived organoids were distinct from cholangiocyte organoids (COs) and morphologically resembled mHOs. Transmission electron microscopy revealed typical hepatocyte features, including nuclei with prominent nucleoli with fibrillary centers and decondensed chromatin, large numbers of mitochondria, tight junctions and autophagic vacuoles. Remarkably, a network of bile canaliculi leading to small lumens was observed within organoids, indicating that cells were not only polarized, but also interconnected. Similar to mHOs, bulk transcriptomic and functional analysis of fetal-liver derived organoids was more comparable to primary human hepatocytes than to cholangiocytes.[11]

The authors also established organoids morphologically resembling fetal liver-derived organoids from pediatric and adult livers, however their expansion potential was limited (<2.5 months). Importantly, organoids from both fetal and pediatric donors were capable of repopulating the hepatocyte compartment of FAH-/- mice to a significant extent, demonstrating that regardless of the cell-of-origin, cells could complete their differentiation/maturation into hepatocytes *in vivo*. Notably, pediatric and adult liver-derived organoids showed higher engraftment than fetal liver-derived organoids, providing additional evidence that transplant success can be positively correlated with the maturation status of the cell.[11] Taken together, these studies represent a breakthrough in the long-term

culture of primary hepatocytes, a historically fastidious cell type. However, there is need for further improvements in culture conditions in order to support the long-term expansion of adult human hepatocytes as organoids (Figure 4).

Pancreatic Organoids (POs)

In 2013, the group of Grapin-Botton demonstrated that embryonic mouse pancreatic progenitors could be cultured as self-organizing 3D structures with tri-lineage (acinar, ductal and endocrine) differentiation potential. Depending on the culture conditions organoids could be expanded as hollow spheres, or induced to form more complex branching structures which did not allow for passage.[86] The Clevers laboratory went on to establish long-term, self-renewing adult mouse pancreatic ductal organoids (mPDOs) using a protocol similar to that for the culture of mICOs. Under these conditions, mPDOs could be expanded as cystic structures which lacked an endocrine compartment. However, following transplantation endocrine differentiation was stimulated.[87]

In 2015, the culture of mouse pancreatic ductal organoids (mPDOs) was adapted to support the expansion of adult human pancreatic ductal organoids (hPDOs) (Figure 4).[88] Concurrently, Bonfanti *et al.* demonstrated that the 3D culture conditions established for the expansion of adult mPDOs could also support the expansion of fetal mouse and human pancreatic progenitors as organoids. As in previous cases, manipulation of the culture conditions could promote endocrine differentiation, which was shown to be negatively regulated by EGF signaling.[89]

Since their establishment, culture conditions for hPDOs have improved. With the removal of WNT ligands, and the addition of prostaglandin E2 and FSK, hPDOs could be mass expanded long-term.[60] Under these conditions, hPDOs resembled the primary tissue closely on the gene expression level, except for WNT-target and progenitor markers, which were significantly upregulated *in vitro*. When initiated from single pancreatic ductal cells, hPDOs resembled hollow spheres, with occasional budding structures along the periphery of a central lumen composed of a polarized monolayer of epithelial cells.[60] As in the case of cholangiocytes, whether the ability of pancreatic ductal cells to initiate organoids is restricted to a discrete subset of cells, or equally shared amongst pancreatic ductal cells has yet to be determined. Single-cell RNA sequencing (scRNA-seq) has revealed heterogeneity between ductal cells of the pancreas, though the implications for *ex vivo* culture and differentiation potential were not explored.[90]

Tissue-derived acinar cells have also been cultured as organoids under conditions similar to those for the culture of PDOs. However, upon *in vitro* expansion of single acinar cells, cells gradually lost their acinar-cell expression and transdifferentiated into pancreatic ductal organoids.[63] When complete tissue biopsies are used for organoid initiation, larger "budding" structures have also been described (Loomans *et al.*, 2018). In these structures, aldehyde dehydrogenase expressing cells localized in the tips of the budding structures displayed

progenitor characteristics and could be partially differentiated to the endocrine fate. Although no successful mature cells from the endocrine lineage could be established *in vitro*, transplantation of differentiated cells showed formation of ~1% insulin-positive cells *in vivo*.[61] More recently, mouse pancreatic islet organoids were established from newly discovered protein C receptor ($Procr^+$) endocrine precursor cells. When sorted and co-cultured with endothelial cells, this $Procr^+$ population could successfully form organoids under the influence of a medium containing epidermal growth factor, fibroblast growth factor 2, heparin and vascular endothelial growth factor α. When analyzed by single-cell RNA sequencing (scRNA-seq), it was demonstrated that although the majority of cells present were β-cells, all the cell types of the pancreatic islet were present in the organoid and could successfully be used to temporarily cure diabetes in mice.[18]

Organoids Derived from Primary and Metastatic Tumors of the Liver, Pancreas and Biliary Tree

Definition and Nomenclature for Tumor-derived Organoids

Following the discovery that tissue-derived epithelial cells could be cultured as self-renewing organoids, it was demonstrated that neoplastic epithelial cells derived from primary and metastatic tumors of the liver[91,92], pancreas[88], and extrahepatic biliary tree[93] could also be cultured as self-renewing 3D structures. Similar to non-tumor epithelial organoids, tumor-derived organoids self-organize through cell-cell and cell-matrix interactions. However, rather than recapitulating aspects of the healthy tissue, tumor-derived organoids capture the histological organization of the native tumor. Tumor organoids retain the genomic landscape, gene expression profile and tumorigenic potential of the original tumor, providing a novel tool to study cancer *in vitro*.[91] In literature, consistent nomenclature for these systems is lacking and they are commonly referred to as, *tumor organoids*, *canceroids* or *tumoroids*.[3,94] To distinguish tumor-derived organoids from other 3D cancer cell models, consensus was reached on naming these systems *tumor organoids*. Furthermore, it was decided that the nomenclature for tumor organoid systems should reflect the nomenclature of the associated tumor (Figure 5 and Table S3). In this section we review the recent progress in the culture of tumor organoids derived from the liver, pancreas and biliary tree. For details on the applications on tumor organoids the reader is directed elsewhere.[95,96]

Tumor Organoids Derived from Hepatocellular Carcinoma

Malignant tumors of hepatocyte origin are referred to as hepatocellular carcinomas (HCCs). Similar to hepatocytes, culturing neoplastic cells from HCCs is difficult, with the culture of well-differentiated HCCs (<5% proliferative cells) still elusive. However, poorly to moderately differentiated HCCs are amenable to *in vitro* culture as hepatocellular carcinoma organoids (HCCOs) (Figure 5), as demonstrated by the Huch laboratory.[91] Morphologically, HCCOs

resembled dense spheroidal structures. Typical HCC markers, such as AFP were expressed on a protein level. Bulk RNA sequencing revealed high correlation between original tumor samples and the resulting organoid cultures. In depth analysis of tumor-specific mutations revealed organoids presented the same mutations as the original tumor. Importantly, it was shown that upon subcutaneous transplantation of HCCOs, novel tumors with similar histopathological characteristics were formed, demonstrating the HCCOs retain their oncogenic potential after *ex vivo* culture. It is important to note that the culture conditions also supported the outgrowth of cells from combined hepatocellular-cholangiocarcinoma (cHCC-CCA) tumors as organoids (cHCC-CCAO).[91] This is a rare tumor consisting of both hepatocellular- and cholangiocarcinoma (CCA) characteristics, which upon radiological examination often show features of HCC. However, upon pathological examination these tumors show characteristics of both HCC and CCA[97], highlighting the need for tumor characterization prior to culture. A subsequent study by Nuciforo *et al.* demonstrated that similar organoids could be cultured from needle-biopsies of the tumor, making personalize organoid models of HCCs available to a broader patient population.[92] Since only a minority of patients would receive a surgical resection, and since patients receiving resection are less likely to receive systemic therapies[98], tumor-needle biopsies represent a convenient tissue source. More recently, hepatoblastoma organoids were established under the culture conditions described for the culture of HCCOs.[99]

Tumor Organoids Derived from Cholangiocarcinoma

Cholangiocarcinomas (CCAs) represent a heterogenous group of malignancies that can be divided according to their anatomical location (intrahepatic, perihilar and distal). Different subtypes of CCAs display distinct pathological features, prognosis and therapeutic options.[100] As CCA organoid systems are established, it is important to specify the anatomical region of the biliary tree from which the organoids are derived.

In 2017 Huch and colleagues demonstrated the feasibility of culturing neoplastic epithelial cells from intrahepatic cholangiocarcinomas (iCCAs) as organoids (Figure 5). Intrahepatic cholangiocarcinoma organoids (iCCAOs) could be established from both poorly- and well-differentiated tumors. Gene expression analysis revealed that iCCAOs resembled the native tumor *in vitro*. Protein-expression analysis revealed the presence of typical iCCA markers, including KRT7 and KRT19, while HCC markers such as albumin and AFP were absent. Similar to HCCOs, iCCAOs retained the mutational landscape of the original tumor. When subcutaneously transplanted in mice, iCCAOs formed tumors with 100% efficiency (37/37 attempts, n=2 CCA lines), taking on glandular structures similar to primary iCCAs.[91] In parallel, Lampis *et al.* established iCCAOs from a patient with a highly chemo-refractory iCCA. *In vitro*, iCCAOs maintained their chemo-resistant nature, allowing researchers to investigate the possible mechanisms of chemo-resistance *in vivo*.[101]

Building on this work, Saito *et al.* established tumor organoids from other regions of the biliary tree and pancreas. These included gallbladder carcinoma organoids (GBCOs) (Figure 5), pancreatic ductal adenocarcinoma organoids (PDACOs) (Figure 5), and neuro-endocrine carcinoma (NEC) organoids of the ampulla of Vater.[93] However, overall long-term success ratios were low with only 1/3 of tumor cells growing out as organoids. Similar to previous studies performed with intestinal organoids[102] the authors noticed that non-tumor derived organoids proliferated faster than tumor organoids.[93] Thus, novel medium formulations that promoted selective outgrow of tumor cells were devised. Notably, tumor organoids were sensitive to specific-drug therapy compounds depending on the underlying mutation(s).[93]

Tumor Organoids Derived from Pancreatic Tumors

In 2015, the groups of Clevers and Tuveson demonstrated the feasibility of culturing tumorous lesions, both primary and metastatic, as tumor organoids.[88] Unfortunately, most pancreatic ductal adenocarcinomas (PDACs) are diagnosed late. As a result, many patients diagnosed with a PDAC do not undergo surgical resection due to the advanced stage of the disease.[103] To explore the cancer screening potential of pancreatic ductal adenocarcinoma organoids (PDACOs) (Figure 5), the authors demonstrated the feasibility of initiating cultures from biopsies obtained during routine fine needle aspiration (FNA).[88] When screened for common malignant mutations, tumor organoids were found to have mutations similar to the primary tumors from which they were derived. Upon transplantation into mice, healthy control organoids formed ductal structures with low efficacy (~9%), whereas PDACOs formed intraductal neoplasm-like lesions with high efficacy (75%). Over time the lesions progressed and formed invasive metastatic tumors, demonstrating the value of these organoids for modeling disease progression.[88]

More recently, Seino *et al.* revealed the existence of three separate tumor subtypes in 39 PDAC patients, based on WNT and R-spondin niche factor dependencies. Tumor organoids could be established from surgical-resections, FNA and ascites (liquid) biopsies. PDACOs resembled the original tumor, presenting tumor specific mutations, and maintained the ability to form tumors *in vivo* after *ex vivo* culture.[104]

Standardization and Validation of HPB Organoids

Numerous reports describe contrasting methods of generating HPB epithelial organoids from the same cell source.[30, 59,62,79] As a result, the variability of a given system increases. This makes drawing comparisons between studies more difficult, hampering translation of research and calling into question the validity of each system. To further complicate the matter, organoid complexity is increasing at a rapid pace. Nikolaev *et al.* recently reported the generation of perfusable mini-gut and bile duct organoids-on-a chip by applying tissue engineering approaches to build scaffolds within preformed hydrogel networks.[105] As novel organoid systems are developed; it is essential to maintain the clarity the present effort has

sought to bring. To facilitate this, we propose guidelines (Figure 6) for researchers to follow when establishing a novel system or refining an existing one.

First, researchers should clearly define reproducible culture conditions. When possible, we encourage the use of recombinant growth factors or small molecules, rather than conditioned medium in the culture of organoids. Authors should then strive to demonstrate the suspected cell(s) of origin. In animal systems, such as the mouse, this can be done through lineage tracing, but for human systems an alternative method, such as fluorescence-activated cell sorting, could be employed. When this is not possible due to a lack of defined markers with which to sort cells, the tissue of origin should be clearly delineated. Next, the organoid system should be characterized on a morphological, gene expression and functional level, both before and after long-term culture. When performing morphological analysis, a combination of microscopy techniques should be employed, such as light, confocal and electron microscopy. Together, these imaging modalities will allow for a detailed analysis, not only of the organoids' overall structure, but also of individual cells and their histoarchitecture (which should be compared to the primary cells/tissue the organoid resembles *in vitro*). When possible, we encourage the use of emerging technologies, such as single-cell analysis, for organoid characterization. When conducting these analyses, the organoid system should be benchmarked against the tissue and cell of origin/interest and, ideally, compared to previously established systems. To this end, the construction of an open source, high quality data set containing single-cell data of HPB primary tissue and the corresponding organoids would be of great value. For human systems, we propose the use of the Organoid Cell Atlas (https://hca-organoid.eu), which was recently launched as a 'Biological Network' within the Human Cell Atlas.[106] We believe the described guidelines will promote the standardization and validation of organoid systems, optimized to answer the research question at hand. Of note, while the guidelines are presented as a linear roadmap, the order of each step is at the researchers' discretion (Figure 6).

Clinical Application of HPB Organoids (Challenges and Solutions)

Organoids hold great promise in the treatment of many intractable diseases in the form of advanced therapy medicinal products (ATMPs), whereby cells are injected or transplanted as organoid grafts.[107] However, before organoid technology can be translated from bench to bedside as a cell therapy, several challenges must be overcome. Here we address (1) the elimination of animal derived materials in the derivation and culture of organoids, (2) the mass expansion of organoids to clinically relevant numbers, and (3) overcoming immune rejection of organoids upon transplantation. In addition to these hurdles, organoids must meet basic current good manufacturing practices (c-GMPs) to be considered for clinical application, including strict quality control metrics. For more information on cGMP guidelines the reader is directed elsewhere.[108]

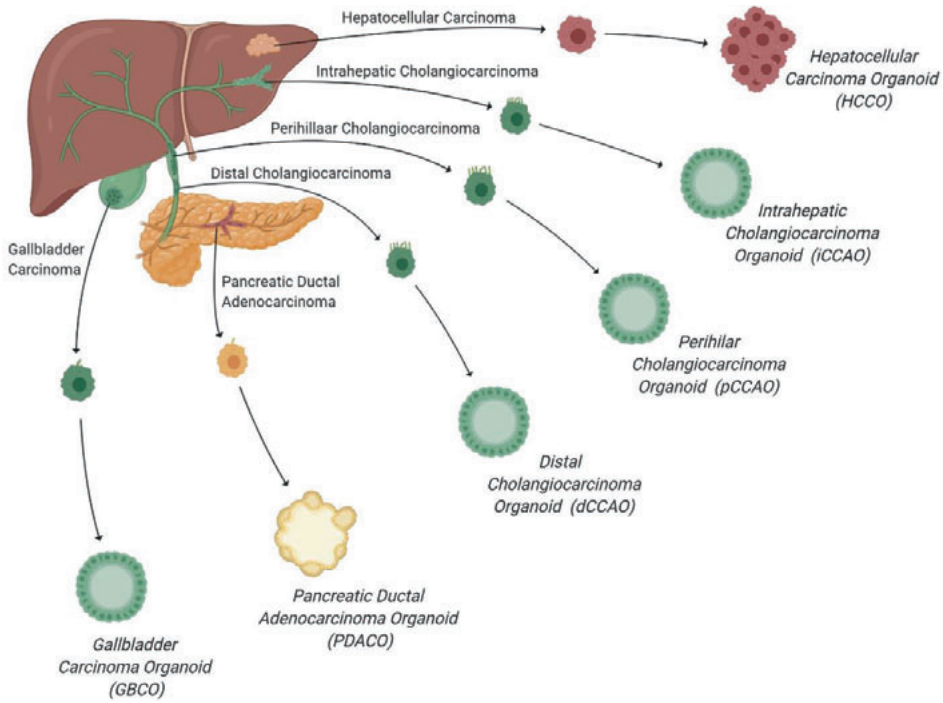

Figure 5. Nomenclature for tumor organoids derived from primary or metastatic tumors of the liver, pancreas, and biliary tree.

Replacing EHS-based Materials

Currently, efficient expansion of organoids requires Matrigel or Basement Membrane Extract (BME).[109,110] However, there are many issues concerning these materials. First and foremost, they are animal-derived, being sourced from Engelbreth-Holm-Swarm (EHS) tumors in mice.[110] As a result, EHS-derived materials will struggle to meet c-GMPs guidelines, which precludes their use in the culture of cells intended for clinical applications. Furthermore, these extracts are not tissue-specific and there are significant batch-to-batch variations, reducing the reliability and reproducibility of results more difficult. Thus, it is imperative to find a replacement for EHS-based materials in order to move organoids to the clinic, as well as to promote the standardization and validation of organoid models.

Several efforts have been made to this end. Broguiere *et al.* reported the culture of ICOs in a hybrid fibrin/laminin-entactin hydrogel.[111] Their results demonstrated that the addition of the laminin-entactin complex at a concentration of 2 mg/mL was sufficient to expand organoids at an efficiency comparable to Matrigel.[111] Building on this, Ye *et al.* utilized synthetic polyisocyanopeptide hydrogels supplemented with recombinant human laminin-

111, the primary constituent of Matrigel, to support the expansion of ICOs.[112] In parallel, Sorrentino *et al.* reported not only the culture, but also the derivation of ICOs in Polyethylene glycol hydrogels functionalized with fibronectin and laminin-111.[113] Intriguingly, replacement of full-length fibronectin with the minimal integrin recognition peptide RGDSPG (Arg-Gly-Asp-Ser-Pro-Gly) produced comparable results, allowing for a great reduction in costs compared to synthesizing full length ECM proteins.[113] Similarly, Georgakopoulos *et al.*, reported that dextran polymers modified with a peptide containing the RGD cell adhesion motif covalently crosslinked with hyaluronic acid supports the establishment as well as culture (up to five passages) of human pancreas organoids.[60] In another approach, Giobbe *et al.* demonstrated that ECM-hydrogels derived from decellularized tissues could support the formation and growth of endoderm-derived human organoids.[114]

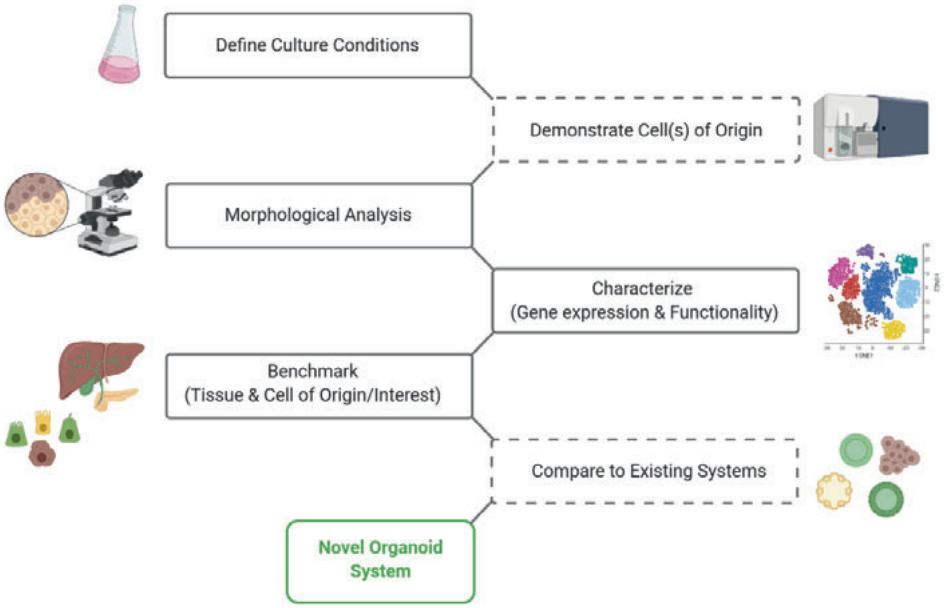

Figure 6. Guidelines for the establishment of novel organoid systems.
Dotted boxes represent facultative steps.

Mass Expansion

Standard organoid culture is an expensive and tedious process, requiring large amounts of materials, labor and time. This limits the use of organoids in large-scale experiments, such as tissue engineering, which can require billions of cells to produce tissue constructs of clinical relevance. In an effort to overcome these limitations, the expansion of organoids in bioreactors is currently being explored.[115-117] Recently, Schneeberger *et al.* used commercial spinner flasks to mass expand intrahepatic cholangiocyte organoids (ICOs).[118] ICOs expanded in stirred suspension achieved an average of a 43-fold induction in two weeks, compared to a 6-fold increase in cell number in static cultures.[118] In another study, Kumar *et al.* used orbital shakers to increase the yield of iPSC-derived kidney organoids 3- to 4-fold compared to static controls.[119] Of note, extended culture of iPSC-derived kidney organoids in stirred suspension caused visual signs of dysplasia, as well as the structural and functional decline of the organoids.[119] While tissue-derived organoids grown under static conditions have been shown to be relatively genetically stable[9,60], it will be important to carefully assess whether suspension culture of tissue-derived organoids compromises their genetic fitness.

Immune Rejection

For organoids to make their way to the clinic they must be immunocompatible. While immunosuppressive drugs can help prevent graft rejection, there are several drawbacks and side effects associated with their use.[120] To circumvent this, autologous cell sources can be applied. For example, tissue-derived organoids can be generated from patient cells isolated by minimally invasive methods and mass expanded *ex vivo*.[30] Recently, it was demonstrated that COs could also be established from bile, circumventing the need for patient biopsies.[121,122] However, minimally invasive isolation methods are not available for each type of organoid, and in emergency situations, such as acute liver failure, there is a need for an off-the-shelf cell source, which means the cells will likely be of allogenic origins.

Fortunately, many encouraging efforts are currently being explored. In one approach, CRISPR-CAS9 gene-editing was used to alter the expression of major histocompatibility complex (MHC) genes, generating immunocompatible allogenic iPSCs.[123] That said, clinical application of gene-editing has its own hurdles to overcome.[124] In another study, Yoshihara *et al.*, demonstrated that pulses of interferon-gamma induced the expression of PDL1 in islet organoids, allowing them to avoid immune destruction when transplanted into diabetic mice with a functional immune system. PDL1 expressing organoids provided sustained blood sugar control without the need for genetic manipulation for at least 40 days.[56]

Concluding Remarks

As organoid technology continues to advance, so must our ability to clearly describe these complex 3D systems. To facilitate effective scientific communication between researchers there is need for consistent nomenclature and precise language, enabling reproducibility and scientific progress. Here, we seek to harmonize the hepatic, pancreatic and biliary organoid communities through the consensus of experts in the field. Together, we developed an intuitive classification system for organoids, and nomenclature for referring to tissue-derived epithelial HPB organoids. Furthermore, in an effort to promote the standardization and validation of organoids we proposed guidelines for researchers to follow when establishing a novel organoid system. We found the process of reaching consensus to be interactive and dynamic, stimulating scientific exchange and a holistic understanding of human HPB organoids. We believe a similar process would help unify and advance other fields.

References

1. Ootani A, Li X, Sangiorgi E, *et al.* Sustained in vitro intestinal epithelial culture within a Wnt-dependent stem cell niche. Nature Medicine. 2009 Jun;15(6):701–6.
2. Sato T, Vries RG, Snippert HJ, *et al.* Single Lgr5 stem cells build crypt-villus structures in vitro without a mesenchymal niche. Nature. 2009 May;459(7244):262–5.
3. Kim J, Koo B-K, Knoblich JA. Human organoids: model systems for human biology and medicine. Nat Rev Mol Cell Biol. 2020 Jul 7;1–14.
4. Sampaziotis F, Justin AW, Tysoe OC, *et al.* Reconstruction of the mouse extrahepatic biliary tree using primary human extrahepatic cholangiocyte organoids. Nat Med. 2017 Aug;23(8):954–63.
5. Takebe T, Sekine K, Enomura M, *et al.* Vascularized and functional human liver from an iPSC-derived organ bud transplant. Nature. 2013 Jul;499(7459):481–4.
6. Takebe T, Sekine K, Kimura M, *et al.* Massive and Reproducible Production of Liver Buds Entirely from Human Pluripotent Stem Cells. Cell Reports. 2017 Dec;21(10):2661–70.
7. Takebe T, Enomura M, Yoshizawa E, *et al.* Vascularized and Complex Organ Buds from Diverse Tissues via Mesenchymal Cell-Driven Condensation. Cell Stem Cell. 2015 May;16(5):556–65.
8. Ghurburrun E, Borbath I, Lemaigre FP, Jacquemin P. Liver and Pancreas: Do Similar Embryonic Development and Tissue Organization Lead to Similar Mechanisms of Tumorigenesis? Gene Expression. 2018 Aug 22;18(3):149–55.
9. Huch M, Gehart H, van Boxtel R, *et al.* Long-Term Culture of Genome-Stable Bipotent Stem Cells from Adult Human Liver. Cell. 2015 Jan;160(1–2):299–312.
10. Prior N, Inacio P, Huch M. Liver organoids: from basic research to therapeutic applications. Gut. 2019 Dec 1;68(12):2228–37.
11. Hu H, Gehart H, Artegiani B, *et al.* Long-Term Expansion of Functional Mouse and Human Hepatocytes as 3D Organoids. Cell. 2018 Nov;175(6):1591-1606.e19.
12. Simian M, Bissell MJ. Organoids: A historical perspective of thinking in three dimensions. Journal of Cell Biology. 2017 Jan 2;216(1):31–40.
13. Shamir ER, Ewald AJ. Three-dimensional organotypic culture: experimental models of mammalian biology and disease. Nature Reviews Molecular Cell Biology. 2014 Oct;15(10):647–64.
14. Lancaster MA, Knoblich JA. Organogenesis in a dish: Modeling development and disease using organoid technologies. Science. 2014 Jul 18;345(6194):1247125–1247125.
15. Aloia L, McKie MA, Vernaz G, *et al.* Epigenetic remodeling licences adult cholangiocytes for organoid formation and liver regeneration. Nat Cell Biol. 2019 Nov;21(11):1321–33.
16. Sato T, Stange DE, Ferrante M, *et al.* Long-term Expansion of Epithelial Organoids From Human Colon, Adenoma, Adenocarcinoma, and Barrett's Epithelium. Gastroenterology. 2011 Nov 1;141(5):1762–72.
17. Palikuqi B, Nguyen D-HT, Li G, *et al.* Adaptable haemodynamic endothelial cells for organogenesis and tumorigenesis. Nature. 2020 Sep;585(7825):426–32.
18. Wang D, Wang J, Bai L, *et al.* Long-Term Expansion of Pancreatic Islet Organoids from Resident Procr+ Progenitors. Cell. 2020 Mar;180(6):1198-1211.e19.
19. Ouchi R, Togo S, Kimura M, *et al.* Modeling Steatohepatitis in Humans with Pluripotent Stem Cell-Derived Organoids. Cell Metabolism. 2019 Aug;30(2):374-384.e6.
20. Shinozawa T, Kimura M, Cai Y, *et al.* High-Fidelity Drug Induced Liver Injury Screen Using Human PSC-derived Organoids. Gastroenterology. 2021 Feb;160(3):831-846.e10.
21. Wu F, Wu D, Ren Y, *et al.* Generation of hepatobiliary organoids from human induced pluripotent stem cells. Journal of Hepatology. 2019 Jun;70(6):1145–58.
22. Vyas D, Baptista PM, Brovold M, *et al.* Self-assembled liver organoids recapitulate hepatobiliary organogenesis *in vitro*. Hepatology. 2018 Feb;67(2):750–61.
23. Koike H, Iwasawa K, Ouchi R, *et al.* Modeling human hepato-biliary-pancreatic organogenesis from the foregut–midgut boundary. Nature. 2019 Oct;574(7776):112–6.

24. Strand DW, Franco OE, Basanta D, *et al.* Perspectives on Tissue Interactions in Development and Disease. Curr Mol Med. 2010 Feb;10(1):95–112.
25. Fennema E, Rivron N, Rouwkema J, *et al.* Spheroid culture as a tool for creating 3D complex tissues. Trends in Biotechnology. 2013 Feb;31(2):108–15.
26. Cui X, Hartanto Y, Zhang H. Advances in multicellular spheroids formation. J R Soc Interface. 2017 Feb 28;14(127):20160877.
27. Achilli TM, Meyer J, Morgan JR. Advances in the formation, use and understanding of multi-cellular spheroids. Expert Opin Biol Ther. 2012 Oct;12(10):1347-60.
28. Hendriks D, Artegiani B, Hu H, *et al*. Establishment of human fetal hepatocyte organoids and CRISPR-Cas9-based gene knockin and knockout in organoid cultures from human liver. Nat Protoc. 2021 Jan;16(1):182-217.
29. Huch M, Koo B-K. Modeling mouse and human development using organoid cultures. Development. 2015 Sep 15;142(18):3113–25.
30. Tysoe OC, Justin AW, Brevini T, *et al.* Isolation and propagation of primary human cholangiocyte organoids for the generation of bioengineered biliary tissue. Nat Protoc. 2019 Jun;14(6):1884–925.
31. Bell CC, Hendriks DFG, Moro SML, *et al.* Characterization of primary human hepatocyte spheroids as a model system for drug-induced liver injury, liver function and disease. Scientific Reports. 2016 May 4;6(1):25187.
32. Takahashi K, Yamanaka S. Induction of Pluripotent Stem Cells from Mouse Embryonic and Adult Fibroblast Cultures by Defined Factors. Cell. 2006 Aug 25;126(4):663–76.
33. Takahashi K, Tanabe K, Ohnuki M, *et al.* Induction of Pluripotent Stem Cells from Adult Human Fibroblasts by Defined Factors. Cell. 2007 Nov 30;131(5):861–72.
34. Osakada F, Ikeda H, Sasai Y, Takahashi M. Stepwise differentiation of pluripotent stem cells into retinal cells. Nature Protocols. 2009 Jun;4(6):811–24.
35. Spence JR, Mayhew CN, Rankin SA, *et al.* Directed differentiation of human pluripotent stem cells into intestinal tissue in vitro. Nature. 2011 Feb;470(7332):105–9.
36. Wong AP, Bear CE, Chin S, *et al.* Directed differentiation of human pluripotent stem cells into mature airway epithelia expressing functional CFTR protein. Nature Biotechnology. 2012 Sep;30(9):876–82.
37. Chen Y-F, Tseng C-Y, Wang H-W, *et al.* Rapid generation of mature hepatocyte-like cells from human induced pluripotent stem cells by an efficient three-step protocol. Hepatology. 2012;55(4):1193–203.
38. Hannan NRF, Segeritz C-P, Touboul T, Vallier L. Production of hepatocyte-like cells from human pluripotent stem cells. Nature Protocols. 2013 Feb;8(2):430–7.
39. Si-Tayeb K, Noto FK, Nagaoka M, *et al.* Highly efficient generation of human hepatocyte–like cells from induced pluripotent stem cells. Hepatology. 2010;51(1):297–305.
40. Yusa K, Rashid ST, Strick-Marchand H, *et al.* Targeted gene correction of α 1 -antitrypsin deficiency in induced pluripotent stem cells. Nature. 2011 Oct;478(7369):391–4.
41. McCauley HA, Wells JM. Pluripotent stem cell-derived organoids: using principles of developmental biology to grow human tissues in a dish. Development. 2017 Mar 15;144(6):958–62.
42. Lo B, Parham L. Ethical Issues in Stem Cell Research. Endocr Rev. 2009 May;30(3):204–13.
43. Ober EA, Lemaigre FP. Development of the liver: Insights into organ and tissue morphogenesis. Journal of Hepatology. 2018 May 1;68(5):1049–62.
44. Guan Y, Xu D, Garfin PM, *et al.* Human hepatic organoids for the analysis of human genetic diseases. JCI Insight. 2017 Sep 7;2(17):e94954.
45. Wang S, Wang X, Tan Z, *et al.* Human ESC-derived expandable hepatic organoids enable therapeutic liver repopulation and pathophysiological modeling of alcoholic liver injury. Cell Res. 2019 Dec;29(12):1009–26.

46. Akbari S, Sevinç GG, Ersoy N, *et al.* Robust, Long-Term Culture of Endoderm-Derived Hepatic Organoids for Disease Modeling. Stem Cell Reports. 2019 Oct;13(4):627–41.
47. Mun SJ, Ryu J-S, Lee M-O, *et al.* Generation of expandable human pluripotent stem cell-derived hepatocyte-like liver organoids. Journal of Hepatology. 2019 Nov;71(5):970–85.
48. Bin Ramli MNB, Lim YS, Koe CT, *et al.* Human Pluripotent Stem Cell-Derived Organoids as Models of Liver Disease. Gastroenterology. 2020 Oct;159(4):1471-1486.e12.
49. Dianat N, Dubois-Pot-Schneider H, Steichen C, *et al.* Generation of functional cholangiocyte-like cells from human pluripotent stem cells and HepaRG cells. Hepatology. 2014;60(2):700–14.
50. Banales JM, Masyuk TV, Gradilone SA, *et al.* The cAMP effectors Epac and protein kinase a (PKA) are involved in the hepatic cystogenesis of an animal model of autosomal recessive polycystic kidney disease (ARPKD). Hepatology. 2009;49(1):160–74.
51. Lee S-O, Masyuk T, Splinter P, *et al.* MicroRNA15a modulates expression of the cell-cycle regulator Cdc25A and affects hepatic cystogenesis in a rat model of polycystic kidney disease. J Clin Invest. 2008 Nov 3;118(11):3714–24.
52. Ogawa M, Ogawa S, Bear CE, *et al.* Directed differentiation of cholangiocytes from human pluripotent stem cells. Nat Biotechnol. 2015 Aug;33(8):853–61.
53. Sampaziotis F, Cardoso de Brito M, Madrigal P, *et al.* Cholangiocytes derived from human induced pluripotent stem cells for disease modeling and drug validation. Nature Biotechnology. 2015 Aug;33(8):845–52.
54. Huang L, Holtzinger A, Jagan I, *et al.* Ductal pancreatic cancer modeling and drug screening using human pluripotent stem cell– and patient-derived tumor organoids. Nature Medicine. 2015 Nov;21(11):1364–71.
55. Hohwieler M, Illing A, Hermann PC, *et al.* Human pluripotent stem cell-derived acinar/ductal organoids generate human pancreas upon orthotopic transplantation and allow disease modeling. Gut. 2017 Mar;66(3):473–86.
56. Yoshihara E, O'Connor C, Gasser E, *et al.* Immune-evasive human islet-like organoids ameliorate diabetes. Nature. 2020 Aug 19;1–6.
57. Huang L, Desai R, Conrad DN, *et al.* Commitment and oncogene-induced plasticity of human stem cell-derived pancreatic acinar and ductal organoids. Cell Stem Cell. 2021 Apr 21:S1934-5909(21)00155-7.
58. Breunig M, Merkle J, Wagner M, et al. Modeling plasticity and dysplasia of pancreatic ductal organoids derived from human pluripotent stem cells. Cell Stem Cell. 2021 Apr 15:S1934-5909(21)00111-9. Broutier L, Andersson-Rolf A, Hindley CJ, *et al.* Culture and establishment of self-renewing human and mouse adult liver and pancreas 3D organoids and their genetic manipulation. Nature Protocols. 2016 Sep;11(9):1724–43.
59. Georgakopoulos N, Prior N, Angres B, *et al.* Long-term expansion, genomic stability and in vivo safety of adult human pancreas organoids. BMC Dev Biol. 2020 Dec;20(1):4.
60. Loomans CJM, Giuliani NW, Balak J, *et al.* Expansion of Adult Human Pancreatic Tissue Yields Organoids Harboring Progenitor Cells with Endocrine Differentiation Potential. Stem Cell Reports. 2018 Mar 13;10(3):712–24.
61. Lugli N, Kamileri I, Keogh A, *et al.* R-spondin 1 and noggin facilitate expansion of resident stem cells from non-damaged gallbladders. EMBO Rep. 2016 May;17(5):769–79.
62. Wollny D, Zhao S, Everlien I, *et al.* Single-Cell Analysis Uncovers Clonal Acinar Cell Heterogeneity in the Adult Pancreas. Developmental Cell. 2016 Nov;39(3):289–301.
63. Deng X, Zhang X, Li W, *et al.* Chronic Liver Injury Induces Conversion of Biliary Epithelial Cells into Hepatocytes. Cell Stem Cell. 2018 Jul;23(1):114-122.e3.
64. Manco R, Clerbaux L-A, Verhulst S, *et al.* Reactive cholangiocytes differentiate into proliferative hepatocytes with efficient DNA repair in mice with chronic liver injury. Journal of Hepatology. 2019 Jun;70(6):1180–91.

65. Raven A, Lu W-Y, Man TY, *et al.* Cholangiocytes act as facultative liver stem cells during impaired hepatocyte regeneration. Nature. 2017 Jul;547(7663):350–4.
66. Schaub JR, Huppert KA, Kurial SNT, *et al.* De novo formation of the biliary system by TGFβ-mediated hepatocyte transdifferentiation. Nature. 2018 May;557(7704):247–51.
67. Leung C, Tan SH, Barker N. Recent Advances in Lgr5+ Stem Cell Research. Trends in Cell Biology. 2018 May 1;28(5):380–91.
68. Schuijers J, Clevers H. Adult mammalian stem cells: the role of Wnt, Lgr5 and R-spondins. EMBO J. 2012 Jun 13;31(12):2685–96.
69. Haegebarth A, Clevers H. Wnt Signaling, Lgr5, and Stem Cells in the Intestine and Skin. The American Journal of Pathology. 2009 Mar 1;174(3):715–21.
70. Planas-Paz L, Sun T, Pikiolek M, *et al.* YAP, but Not RSPO-LGR4/5, Signaling in Biliary Epithelial Cells Promotes a Ductular Reaction in Response to Liver Injury. Cell Stem Cell. 2019 Jul;25(1):39-53.e10.
71. Sun T, Pikiolek M, Orsini V, *et al.* AXIN2+ Pericentral Hepatocytes Have Limited Contributions to Liver Homeostasis and Regeneration. Cell Stem Cell. 2020 Jan;26(1):97-107.e6.
72. Wang B, Zhao L, Fish M, *et al.* Self-renewing diploid Axin2+ cells fuel homeostatic renewal of the liver. Nature. 2015 Aug;524(7564):180–5.
73. Huch M, Dorrell C, Boj SF, *et al.* In vitro expansion of single Lgr5+ liver stem cells induced by Wnt-driven regeneration. Nature. 2013 Feb;494(7436):247–50.
74. Dorrell C, Tarlow B, Wang Y, *et al.* The organoid-initiating cells in mouse pancreas and liver are phenotypically and functionally similar. Stem Cell Research. 2014 Sep;13(2):275–83.
75. Prior N, Hindley CJ, Rost F, *et al.* Lgr5+ stem and progenitor cells reside at the apex of a heterogeneous embryonic hepatoblast pool. Development. 2019 Jun 12;146(12):dev174557.
76. Aizarani N, Saviano A, Sagar, *et al.* A human liver cell atlas reveals heterogeneity and epithelial progenitors. Nature. 2019 Aug;572(7768):199–204.
77. Sampaziotis F, Muraro D, Tysoe OC, *et al.* Cholangiocyte organoids can repair bile ducts after transplantation in the human liver. Science. 2021 Feb 19;371(6531):839–46.
78. Rimland CA, Tilson SG, Morell CM, *et al.* Regional differences in human biliary tissues and corresponding *in vitro* derived organoids. Hepatology. 2021 Jan;73(1):247-267.
79. Verstegen MMA, Roos FJM, Burka K, *et al.* Human extrahepatic and intrahepatic cholangiocyte organoids show region-specific differentiation potential and model cystic fibrosis-related bile duct disease. Scientific Reports. 2020 Dec 14;10(1):21900.
80. Spence JR, Lange AW, Lin S-CJ, K *et al.* Sox17 Regulates Organ Lineage Segregation of Ventral Foregut Progenitor Cells. Developmental Cell. 2009 Jul 21;17(1):62–74.
81. Peng WC, Logan CY, Fish M, *et al.* Inflammatory Cytokine TNFα Promotes the Long-Term Expansion of Primary Hepatocytes in 3D Culture. Cell. 2018 Nov 29;175(6):1607-1619.e15.
82. Schleicher J, Tokarski C, Marbach E, *et al.* Zonation of hepatic fatty acid metabolism — The diversity of its regulation and the benefit of modeling. Biochimica et Biophysica Acta (BBA) - Molecular and Cell Biology of Lipids. 2015 May 1;1851(5):641–56.
83. Kolbe E, Aleithe S, Rennert C, *et al.* Mutual Zonated Interactions of Wnt and Hh Signaling Are Orchestrating the Metabolism of the Adult Liver in Mice and Human. Cell Reports. 2019 Dec 24;29(13):4553-4567.e7.
84. Zhang K, Zhang L, Liu W, *et al.* In Vitro Expansion of Primary Human Hepatocytes with Efficient Liver Repopulation Capacity. Cell Stem Cell. 2018 Dec 6;23(6):806-819.e4.
85. Greggio C, Franceschi FD, Figueiredo-Larsen M, *et al.* Artificial three-dimensional niches deconstruct pancreas development in vitro. Development. 2013 Nov 1;140(21):4452–62.
86. Huch M, Bonfanti P, Boj SF, *et al.* Unlimited in vitro expansion of adult bi-potent pancreas progenitors through the Lgr5/R-spondin axis. The EMBO Journal. 2013 Oct 16;32(20):2708–21.
87. Boj SF, Hwang C-I, Baker LA, *et al.* Organoid Models of Human and Mouse Ductal Pancreatic Cancer. Cell. 2015 Jan;160(1–2):324–38.

88. Bonfanti P, Nobecourt E, Oshima M, *et al.* Ex Vivo Expansion and Differentiation of Human and Mouse Fetal Pancreatic Progenitors Are Modulated by Epidermal Growth Factor. Stem Cells and Development. 2015 Apr 30;24(15):1766–78.
89. Baron M, Veres A, Wolock SL, *et al.* A Single-Cell Transcriptomic Map of the Human and Mouse Pancreas Reveals Inter- and Intra-cell Population Structure. cells. 2016 Oct 26;3(4):346-360.e4.
90. Broutier L, Mastrogiovanni G, Verstegen MM, *et al.* Human primary liver cancer–derived organoid cultures for disease modeling and drug screening. Nature Medicine. 2017 Dec;23(12):1424–35.
91. Nuciforo S, Fofana I, Matter MS, *et al.* Organoid Models of Human Liver Cancers Derived from Tumor Needle Biopsies. Cell Rep. 2018 Jul 31;24(5):1363–76.
92. Saito Y, Muramatsu T, Kanai Y, *et al.* Establishment of Patient-Derived Organoids and Drug Screening for Biliary Tract Carcinoma. Cell Reports. 2019 Apr;27(4):1265-1276.e4.
93. Porter RJ, Murray GI, McLean MH. Current concepts in tumour-derived organoids. British Journal of Cancer. 2020 Jul 30;1–10.
94. Lau HCH, Kranenburg O, Xiao H, Yu J. Organoid models of gastrointestinal cancers in basic and translational research. Nature Reviews Gastroenterology & Hepatology. 2020 Apr;17(4):203–22.
95. Lo Y-H, Karlsson K, Kuo CJ. Applications of organoids for cancer biology and precision medicine. Nature Cancer. 2020 Aug;1(8):761–73.
96. Fowler KJ, Sheybani A, Parker RA, *et al.* Combined hepatocellular and cholangiocarcinoma (biphenotypic) tumors: imaging features and diagnostic accuracy of contrast-enhanced CT and MRI. AJR Am J Roentgenol. 2013 Aug;201(2):332–9.
97. Forner A, Reig M, Bruix J. Hepatocellular carcinoma. The Lancet. 2018 Mar 31;391(10127):1301–14.
98. Saltsman JA, Hammond WJ, Narayan NJC, *et al.* A Human Organoid Model of Aggressive Hepatoblastoma for Disease Modeling and Drug Testing. Cancers (Basel). 2020 Sep 18;12(9):2668.
99. Banales JM, Marin JJG, Lamarca A, *et al.* Cholangiocarcinoma 2020: the next horizon in mechanisms and management. Nature Reviews Gastroenterology & Hepatology. 2020 Sep;17(9):557–88.
100. Lampis A, Carotenuto P, Vlachogiannis G, *et al.* MIR21 Drives Resistance to Heat Shock Protein 90 Inhibition in Cholangiocarcinoma. Gastroenterology. 2018 Mar 1;154(4):1066-1079.e5.
101. van de Wetering M, Francies HE, Francis JM, *et al.* Prospective Derivation of a Living Organoid Biobank of Colorectal Cancer Patients. Cell. 2015 May 7;161(4):933–45.
102. Ryan DP, Hong TS, Bardeesy N. Pancreatic adenocarcinoma. N Engl J Med. 2014 Sep 11;371(11):1039-49.
103. Seino T, Kawasaki S, Shimokawa M, *et al.* Human Pancreatic Tumor Organoids Reveal Loss of Stem Cell Niche Factor Dependence during Disease Progression. Cell Stem Cell. 2018 Mar 1;22(3):454-467.e6.
104. Nikolaev M, Mitrofanova O, Broguiere N, *et al.* Homeostatic mini-intestines through scaffold-guided organoid morphogenesis. Nature. 2020 Sep;585(7826):574–8.
105. Bock C, Boutros M, Camp JG, *et al.* Human Cell Atlas 'Biological Network' Organoids. The Organoid Cell Atlas. Nat Biotechnol. 2021 Jan;39(1):13-17.
106. Hanna E, Rémuzat C, Auquier P, Toumi M. Advanced therapy medicinal products: current and future perspectives. J Mark Access Health Policy. 2016 Apr 25;4.
107. Giancola R, Bonfini T, Iacone A. Cell therapy: cGMP facilities and manufacturing. Muscles Ligaments Tendons J. 2012 Oct 16;2(3):243–7.
108. Arnaoutova I, George J, Kleinman HK, Benton G. Basement Membrane Matrix (BME) has Multiple Uses with Stem Cells. Stem Cell Rev and Rep. 2012 Mar 1;8(1):163–9.
109. Hughes CS, Postovit LM, Lajoie GA. Matrigel: A complex protein mixture required for optimal growth of cell culture. PROTEOMICS. 2010;10(9):1886–90.
110. Broguiere N, Isenmann L, Hirt C, *et al.* Growth of Epithelial Organoids in a Defined Hydrogel. Advanced Materials. 2018;30(43):1801621.

111. Ye S, Boeter JWB, Mihajlovic M, *et al.* A Chemically Defined Hydrogel for Human Liver Organoid Culture. Adv Healthc Mater. 2020 Mar;9(6):e1901658.
112. Sorrentino G, Rezakhani S, Yildiz E, *et al.* Mechano-modulatory synthetic niches for liver organoid derivation. Nature Communications. 2020 Jul 10;11(1):3416.
113. Giobbe GG, Crowley C, Luni C, *et al.* Extracellular matrix hydrogel derived from decellularized tissues enables endodermal organoid culture. Nature Communications. 2019 Dec 11;10(1):5658.
114. Ovando-Roche P, West EL, Branch MJ, *et al.* Use of bioreactors for culturing human retinal organoids improves photoreceptor yields. Stem Cell Research & Therapy. 2018 Jun 13;9(1):156.
115. Phelan MA, Lelkes PI, Swaroop A. Mini and customized low-cost bioreactors for optimized high-throughput generation of tissue organoids. Stem Cell Investig. 2018 Oct 10;5:33.
116. Przepiorski A, Sander V, Tran T, *et al.* A Simple Bioreactor-Based Method to Generate Kidney Organoids from Pluripotent Stem Cells. Stem Cell Reports. 2018 Aug 14;11(2):470–84.
117. Schneeberger K, Sánchez-Romero N, Ye S, *et al.* Large-Scale Production of LGR5-Positive Bipotential Human Liver Stem Cells. Hepatology. 2020;72(1):257–70.
118. Kumar SV, Er PX, Lawlor KT, *et al.* Kidney micro-organoids in suspension culture as a scalable source of human pluripotent stem cell-derived kidney cells. Development. 2019 Mar 1;146(5):dev172361.
119. Fan Y, Tajima A, Goh SK, *et al.* Bioengineering Thymus Organoids to Restore Thymic Function and Induce Donor-Specific Immune Tolerance to Allografts. Molecular Therapy. 2015 Jul 1;23(7):1262–77.
120. Roos FJM, Verstegen MMA, Muñoz Albarinos L, *et al.* Human Bile Contains Cholangiocyte Organoid-Initiating Cells Which Expand as Functional Cholangiocytes in Non-canonical Wnt Stimulating Conditions. Front Cell Dev Biol. 2021 Feb 9;8:630492.
121. Soroka CJ, Assis DN, Alrabadi LS, *et al.* Bile-Derived Organoids From Patients With Primary Sclerosing Cholangitis Recapitulate Their Inflammatory Immune Profile. Hepatology. 2019;70(3):871–82.
122. Xu H, Wang B, Ono M, *et al.* Targeted Disruption of HLA Genes via CRISPR-Cas9 Generates iPSCs with Enhanced Immune Compatibility. Cell Stem Cell. 2019 Apr 4;24(4):566-578.e7.
123. Dai W-J, Zhu L-Y, Yan Z-Y, Xu Y, Wang Q-L, Lu X-J. CRISPR-Cas9 for in vivo Gene Therapy: Promise and Hurdles. Mol Ther Nucleic Acids. 2016;5(8):e349.

Supplementary Information

Supplementary Methods

Expert Invitation

Scientists (hereafter referred to as experts) were invited based on a PUBMED and Google Scholar database search for HPB organoids, regeneration and development. Experts were invited if they had made a significant contribution (either 1st, 2nd or senior authorship) to a peer-reviewed, published manuscript retrieved from the search. From the generated list of experts, select authors with extensive expertise in HPB organoids, regeneration or development were invited to join the steering committee (for members of the steering committee see Table S1). Once invited, all experts had the option to suggest additional experts which would be evaluated by the core team initiating this effort (AM, FJMR, MMAV, LvdL and BS) before receiving an invitation. In a similar fashion, these experts had the option to suggest experts as well. After the first questionnaire round, no additional experts were eligible for invitation.

Building Consensus

To reach consensus, a modified Delphi method based on three successive questionnaires was employed. Consensus was defined as ≥90% agreement on a single question. Questions for which consensus was reached were removed from subsequent questionnaires. Additionally, if an option to a question received <15% of the votes from the expert panel, it was removed from the subsequent questionnaires. Experts had the option to suggest additional answers for each question during the first and second questionnaire. If a suggestion was mentioned by three or more experts, this suggestion was added as an option in the following questionnaire. Furthermore, experts had the option to make additional remarks in the questionnaire, as well as have an open discussion with the core team on their views regarding consensus statements. After each questionnaire, a summary document of the answers was created and sent out to the participating experts, along with an invitation to complete a new questionnaire. Importantly, as per the Delphi method the results of each questionnaire were anonymous. Topics for which consensus was not reached after the third and final questionnaire were deliberated by the steering committee through a round table discussion. Based on the discussion, a final proposition was made by the steering committee for these questions. All experts were given time to review the propositions made by the steering committee, along with the opportunity to discuss their views. In the end, every expert which completed all three questionnaires agreed with the final outcomes and participated in the consensus.

Questionnaires

Questionnaires were created in Google documents (Alphabet Inc., CA). The initial draft of each questionnaire was designed by the core team and evaluated by the steering committee before being sent out to invited experts. Each questionnaire was divided into four categories: (1) Definition of an organoid, (2) Nomenclature for Tissue-derived Hepatic, Pancreatic and Biliary Organoids, (3) Fetal-derived Organoids, and (4) Nomenclature for Tumor-derived Hepatic, Pancreatic and Biliary Organoids. Each questionnaire was designed to reflect the results of the previous questionnaire. Questionnaires and subsequent results can be found in the online supplementary questionnaires 1-3 and results of the questionnaires 1-3.

Results

Table S1. Members of the HPB Consortium

Name	Affiliation	Country	Role
Ary Marsee	Utrecht University	The Netherlands	Core team
Floris Roos	Erasmus MC	The Netherlands	Core team
Monique Verstegen	Erasmus MC	The Netherlands	Core team
Hans Clevers	Hubrecht Institute, Princes Maxima Center, University Medical Center Utrecht	The Netherlands	Steering committee
Ludovic Vallier	University of Cambridge	United Kingdom	Steering committee
Takanori Takebe	Cincinnati Children's Hospital and Tokyo Medical Dental University	USA and Japan	Steering committee
Meritxell Huch	Max Planck Institute of Molecular Cell Biology and Genetics	Germany	Steering committee
Weng Chuan Peng	Princes Maxima Center	The Netherlands	Steering committee
Stuart Forbes	MRC Center for Regenerative Medicine	United Kingdom	Steering committee
Frédéric Lemaigre	Institut de Duve	Belgium	Steering committee
Eelco de Koning	Hubrecht Institute, Leiden University Medical Center, University Medical Center Utrecht	The Netherlands	Steering committee
Helmuth Gehart	Institute for Molecular Health Sciences	Switzerland	Steering committee
Luc van der Laan	Erasmus MC	The Netherlands	Core team
Bart Spee	Utrecht University	The Netherlands	Core team
Sylvia Boj	Hubrecht Organoid Technology (HUB)	The Netherlands	HPB Consortium
Pedro Baptista	Aragon Health Sciences Institute	Spain	HPB Consortium
Kerstin Schneeberger	Utrecht University	The Netherlands	HPB Consortium
Carol Soroka	Yale University	United States	HPB Consortium
Markus Heim	University of Basel	Switzerland	HPB Consortium
Sandro Nuciforo	University of Basel	Switzerland	HPB Consortium
Kenneth Zaret	University of Pennsylvania	United States	HPB Consortium

Yoshimasa Saito	Keio University School of Medicine	Japan	HPB Consortium
Matthias Lutolf	LSCB – Laboratory of Stem Cell Bioengineering - EPFL	Switzerland	HPB Consortium
Vincenzo Cardinale	Sapienza University of Rome	Italy	HPB Consortium
Ben Simons	University of Cambridge	United Kingdom	HPB Consortium
Sven van IJzendoorn	University of Groningen	The Netherlands	HPB Consortium
Akihide Kamiya	Tokai University	Japan	HPB Consortium
Hiromi Chikada	Tokai University	Japan	HPB Consortium
Shuyong Wang	The 8th Medical center of Chinese People's Liberation Army General Hospital	China	HPB Consortium
Seon Ju Mun	Korea Research Institute of Bioscience and Biotechnology	South Korea	HPB Consortium
Myung Jin Son	Korea Research Institute of Bioscience and Biotechnology	South Korea	HPB Consortium
Tamer Tevfik Onder	Koc University	Turkey	HPB Consortium
James Boyer	Yale University	United States	HPB Consortium
Toshiro Sato	Keio University School of Medicine	Japan	HPB Consortium
Nikitas Georgakopou-los	University of Cambridge	United Kingdom	HPB Consortium
Andre Meneses	Universidade Federal Rural da Amazônia	Brazil	HPB Consortium
Laura Broutier	Cancer Research Center of Lyon	France	HPB Consortium
Luke Boulter	University of Edinburgh	United Kingdom	HPB Consortium
Dominic Grün	Max Planck Institute of Immunology and Epigenetics	Germany	HPB Consortium
Jan IJzermans	Erasmus MC	The Netherlands	HPB Consortium
Benedetta Artegiani	Prinses Maxima Centrum	The Netherlands	HPB Consortium
Ruben van Boxtel	Prinses Maxima Centrum	The Netherlands	HPB Consortium
Ewart Kuijk	University of Utrecht	The Netherlands	HPB Consortium
Guido Carpino	Sapienza University of Rome	Italy	HPB Consortium
Gary Peltz	Stanford University School of Medicine	United States	HPB Consortium

Jesus Banales	Ikerbasque Basque Foundation for Science	Spain	HPB Consortium
Nancy Man	University of Hong Kong	Hong Kong, China	HPB Consortium
Luigi Aloia	LMCB – MRC Laboratory for Molecular Cell Biology	United Kingdom	HPB Consortium
Nicholas LaRusso	Mayo Clinic	United States	HPB Consortium
Gregory George	Mayo Clinic	United States	HPB Consortium
Casey Rimland	University of Cambridge	United Kingdom	HPB Consortium
George Yeoh	University of Western Australia Medical School	Australia	HPB Consortium
Anne Grappin-Botton	Max Planck Institute of Molecular Cell Biology and Genetics	Germany	HPB Consortium
Daniel Stange	Universitätsklinikum Carl Gustav Carus der TU Dresden	Germany	HPB Consortium
Nicole Prior	University of Southampton	United Kingdom	HPB Consortium
Nina Tirnitz-Parker	Curtin University	Australia	HPB Consortium
Emma Andersson	Karolinska Institutet	Sweden	HPB Consortium
Chiara Braconi	Glasgow University	United Kingdom	HPB Consortium
Nicholas Hannan	University of Nottingham	United Kingdom	HPB Consortium
Wei Yu Lu	University of Birmingham	United Kingdom	HPB Consortium
Stephen Strom	Karolinska Institutet	Sweden	HPB Consortium
Pau Sancho-Bru	University of Barcelona	Spain	HPB Consortium
Shinichiro Ogawa	University Health Network	Canada	HPB Consortium
Vincenzo Corbo	University of Verona	Italy	HPB Consortium
Madeline Lancaster	MRC Laboratory of Molecular Science	United Kingdom	HPB Consortium
Huili Hu	Shandong University	China	HPB Consortium
Sabine Fuchs	University Medical Center Utrecht	The Netherlands	HPB Consortium
Delilah Hendriks	Hubrecht Institute	The Netherlands	HPB Consortium

Table S2. Nomenclature and key characteristics of human and mouse tissue-derived HPB organoids

	Organoid Type	Cholangiocyte	Hepatocyte	Pancreas ductal	Pancreas islet
	Ref.	(Huch *et al.*, 2013a; Huch *et al.*, 2015; Lugli *et al.*, 2016; Sampaziotis *et al.*, 2017)	(Hu *et al.*, 2018; Peng *et al.*, 2018)	(Huch *et al.*, 2013b; Boj *et al.*, 2015; Loomans *et al.*, 2018; Georgakopoulos *et al.*, 2020)	(Wang *et al.*, 2020)
	Nomen-clature	Cholan-giocyte organoids. Depending on the region: intrahepatic (I), extrahepatic (E) or gallbladder (G)	HOs	PDOs	PIOs
	Abbre-viation	ICOs, ECOs or GCOs	HOs	PDOs	PIOs
Key Characteristics	Organoid Structure	Monolayer of polarized (basolateral-apical) epithelial cells surrounding a lumen.	Polarized cells organized around bile canaliculi network.	Monolayer of polarized (basolateral-apical) epithelial cells	Spheroidal with central pancreatic islet cells with endothelium.
	Cellular Features	Cuboidal or columnar in shape, tight junctions near luminal side and luminal microvilli and primary cilium.	Polygonal in shape, high nucleus to cytoplasm ratio, presence of very low-density lipoproteins, large amounts of smooth and rough ER.	Cuboidal or columnar in shape, tight junctions near luminal side and luminal microvilli and primary cilium.	Consisting of either one or multiple cell types from a pancreatic islet.
	Gene expression	*EpCAM*$^{+}$, *KRT7*$^{+}$, *KRT19*$^{+}$, *CFTR*$^{+}$, *SCTR*$^{+}$, *ALB*$^{-/low}$	*HNF4α*$^{+}$, *ASGR1*$^{+}$, *AHSG*$^{+}$, *ALB*^{high}	*EpCAM*$^{+}$, *CA2*$^{+}$, *KRT19*$^{+}$, *CFTR*$^{+}$, *SCTR*$^{+}$	Depends on cells present. For instance: β-cells: *INS*$^{+}$, *SLC2A1*$^{+}$,
	Functional	Ion and water transport via CFTR, AE2, ANO1 and AQP channels, Alkaline phosphatase and Gamma-GT activity.	Serum protein, bile salt and cholesterol synthesis and secretion; Phase I and phase II- activity.	Ion and water transport via CFTR and ANO1 and AQP channels, secretin signaling.	Metabolically regulated hormone release.

Table S3. Nomenclature and key characteristics of tumor-derived HPB organoids

Tumor Type	Reference	Nomenclature	Abbreviation	Key characteristics
Hepatocellular carcinoma (HCC)	(Broutier *et al.*, 2017; Nuciforo *et al.*, 2018)	Hepatocellular carcinoma organoids	HCCOs	Derived from hepatocellular carcinoma specimens. Presents similar mutations, histoarchitecture and tumorigenic potential as the original tumor.
Cholangio carcinoma (CCA)	(Broutier *et al.*, 2017; Saito *et al.*, 2019)	Cholangio carcinoma organoids. Depending on the region either intrahepatic (I), perihilar (ph) or distal (d)	iCCAOs, phCCAOs, dCCAOs	Derived from cholangiocarcinoma specimens. Presents similar mutations, histoarchitecture and tumorigenic potential as the original tumor.
Gallbladder carcinoma (GBC)	(Saito *et al.*, 2019)	Gallbladder carcinoma organoids	GBCOs	Derived from gallbladder carcinoma specimens. Presents similar mutations, histoarchitecture and tumorigenic potential as the original tumor.
Pancreatic ductal adenocarcinoma (PDAC)	(Boj *et al.*, 2015)	Pancreatic ductal adenocarcinoma organoids	PDACOs	Derived from pancreatic ductal adenocarcinoma specimens. Presents similar mutations, histoarchitecture and tumorigenic potential as the original tumor.

Figure S1. Countries represented in the HPB Consortium.

PART II

DISEASE MODELLING

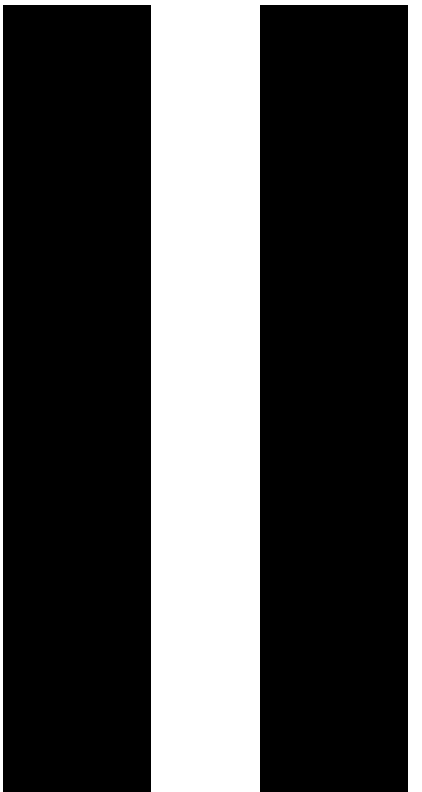

3

CHAPTER 3

Impact of hypoxia and AMPK on CFTR-mediated bicarbonate secretion in human cholangiocyte organoids.

Floris JM Roos, Marcel JC Bijvelds*, Monique MA Verstegen*,
Henk P Roest, Herold J Metselaar, Wojciech G Polak,
Hugo R de Jonge, Jan NM IJzermans, Luc JW van der Laan

* these authors contributed equally.

American Journal of Physiology-Gastrointestinal and Liver Physiology
2021 May 1;320(5):G741-G752.

Abstract

Background and Aims. Cholangiocytes express cystic fibrosis transmembrane conductance regulator (CFTR) which is involved in bicarbonate secretion for the protection against bile toxicity. During liver transplantation prolonged hypoxia of the graft is associated with cholangiocyte loss and biliary complications. Hypoxia is known to diminish CFTR activity in the intestine, but whether it effects CFTR activity in cholangiocytes remains unknown. Thus, the aim of this study is to investigate the effect of hypoxia on CFTR activity in intrahepatic cholangiocyte organoids (ICOs) and test drug-interventions to restore bicarbonate secretion.
Methods. Fifteen different human ICOs were cultured as monolayers and ion channel (CFTR and ANO1) activity was determined using an Ussing chamber assay with or without AMP kinase (AMPK)-inhibitor under hypoxic and oxygenated conditions. Bile-toxicity was tested by apical exposure of cells to fresh human bile.
Results. Overall gene expression analysis showed a high similarity between ICOs and primary cholangiocytes. Under oxygenated conditions, both CFTR and ANO1 channels were responsible for forskolin and UTP activated anion-secretion. Forskolin-stimulation in absence of intracellular chloride showed ion-transport, indicating that bicarbonate could be secreted by CFTR. During hypoxia, CFTR activity significantly decreased ($p=0.01$). Switching from oxygen to hypoxia during CFTR-measurements, reduced CFTR activity ($p=0.03$). Consequently, cell death increased when ICO-monolayers were exposed to bile during hypoxia compared to oxygen ($p=0.04$). Importantly, addition of AMPK-inhibitor restored CFTR-mediated anion-secretion during hypoxia.
Conclusions. ICOs provide an excellent model to study cholangiocyte anion channels and drug-related interventions. Here, we demonstrate that hypoxia affects cholangiocyte ion-secretion, leaving cholangiocytes vulnerable to bile toxicity. The mechanistic insights from this model maybe relevant for hypoxia-related biliary injury during liver transplantation.

Introduction

Severe chronic cholangiopathies, like primary sclerosing cholangitis (PSC) and non-anastomotic bile duct strictures (NAS) are characterized by progressive fibrosis of the bile ducts and are associated with significant morbidity and mortality.[1] Currently, liver transplantation (LT) is the only effective treatment for PSC and PSC accounts for approximately 5% of all LT in the US.[1,2] In recent years our understanding of cholangiopathy development has evolved, but the exact pathophysiology is still unknown. It has been proposed that a loss of ductal bicarbonate secretion contributes to the formation of cholangiopathies. During homeostastis, cholangiocytes modify bile composition by secretion of water, ion and bile acids. Chloride (Cl^-) is secreted into bile by the calcium (Ca^{2+}) activated Cl^- channel Anoctamin 1 (ANO1) or by cystic fibrosis transmembrane conductance regulator (CFTR).[3] Bicarbonate is either secreted indirectly into the bile duct via Cl^- exchange by the Anion-Exchanger 2 (AE2) or could potentially be secreted directly by CFTR.[3] The bicarbonate umbrella theory implies that, if bicarbonate secretion by cholangiocyte is impaired, this could result in insufficient protection to cells from bile toxicity.[4,5] As a results, cholangiocytes will be injured and die, eventually leading to bile duct damage and fibrosis. Fibrosis of the bile duct after LT occurs as NAS, most commonly developing in donation after cardiac arrest livers due to prolonged warm hypoxia time, affecting the bile ducts during liver procurement.[6,7] Hypoxia has been shown to inhibit CFTR activity in multiple tissues.[8,9] Due to the lack of a good functional model for CFTR activity in primary cholangiocytes, the exact effect of hypoxia has not been investigated. Recently, a number of promising 3D-culture models for cholangiocyte-like cells have been established from either primary adult cells, or from induced pluripotent stem cells (IPS).[10-12] Organoids from primary tissue are easily expendable, genetically stable and do not require any differentiation protocols, making adult-tissue derived organoids our preferred choice. Huch *et al.*[10] published a protocol in which they can create intrahepatic cholangiocyte organoids (ICOs) from intrahepatic bile duct cells derived from liver biopsies. We suspected that ICOs might have functional ion-channels, since ICOs swell upon forskolin addition.[10] Forskolin is a cAMP-activator which directly stimulates CFTR anion excretion. Thus, swelling of ICOs might be a result of fluid secretion inside the lumen as a result of an increase in CFTR-mediated chloride secretion. Therefore, the aim of this study is to determine cholangiocyte ion channel activity in ICOs and investigate the effect of hypoxia. The effect of bicarbonate secretion by CFTR on bile-induced cell- death as determined as well as drug testing to ameliorate the effect hypoxia has on transporter-activity.

Materials and Methods

Human liver material and organoid culturing

ICOs were cultured from small liver biopsies (0.5-1.0 cm^3, n=15), collected from donor livers used for LT at the Erasmus MC, according to the previous published culture.[11,13] The medical ethical approval for this research was provided by the Erasmus MC medical ethical committee (MEC-2014-060). A liver biopsy was obtained from the explant liver of a 17-year old cystic fibrosis (CF) patient undergoing liver transplantation at the University Medical Center Groningen. Informed consent was obtained to use these biopsies for research (STEM Study – protocol number 1-402/K). This patient was heterozygous for F508del and R1162X, resulting in a non-functional CFTR transporter. For complete details of the culture methods, see the supplementary materials and methods section.

RNA isolation, cDNA synthesis and RT-qPCR

RNA was isolated by adding 200µL of QIAzol lysis reagent (Qiagen) per 25µL hydrogel droplet and harvested after 10 minutes of addition. RNA-extraction and subsequent cDNA synthesis was performed as previously published.[14] RNA from 2D-grown organoids was collected by adding 300µL of QIAzol lysis reagent directly on top of the cells and mechanically harvesting them after 5 minutes incubation. RNA isolation and cDNA synthesis were similar to 3D-grown organoid cultures. qRT-PCR was performed for mature cholangiocytes markers and channels as well as for hepatocyte-and stem cell-markers.[11] The primer sequences are provided in Table S1. All qRT-PCR data are presented as mean with a 95% confidence interval. qRT-PCR values are relative to the housekeeping gene Glyceraldehyde-3-Phosphate Dehydrogenase (GAPDH) and for visual interpretation multiplied by 10^3 or 10^5.

RNA expression profiling for microarray and microarray analysis

RNA extraction for microarray analysis from ICOs was performed as previously mentioned. A total of 300 ng RNA was reversed transcribed, amplified and biotin-labeled using the Illumina TotalPrep RNA Amplification Kit (Ambion-Life Technologies, Carlsbad CA, USA) according to the manufacturer's guidelines. HumanHT-12 v4 Expression BeadChips (Illumina, San Diego CA, USA) were overnight hybridized with 750 ng cRNA, washed, stained and scanned on an iScan and analyzed using GenomeStudio V2011.1 software (both from Illumina, Inc.). Bead types missing in one or more arrays were excluded and the resulting non-normalized raw probe data set was combined with the raw probe information from the ArrayExpress E-MTAB-4591 data[15] containing embryonic stem cells (ES), freshly plated hepatocytes, primary cholangiocytes and Extrahepatic Cholangiocyte Organoids (ECOs) grown in non-canonical WNT conditions.[15] ECOs from P10 (ECOs_A-C) and from P20 (ECOs_D-F) were combined to one group: ECOs_A-F. Principal component analysis (PCA) and heatmaps were conducted in R using the prcomp and heatmap.2 functions, respectively. Heatmap-selected genes for

hepatocytes and cholangiocytes markers were based on supplementary Figure 6C, Sampaziotis *et al.*[11] For detailed information conducting the PCA and heatmap-plots, see supplementary materials and methods.

Immunohistochemistry (IHC)

Organoids were formalin-fixed (4%) for 24h, paraffin-embedded and sectioned (4 µm) for histological examination. Sections were processed and stained using standard IHC protocols with a specific antibody for CFTR (EMD Millipore Corp: MAB3484, 1:200 dilution). After deparaffinization, antigen retrieval was performed in a TRIS-EDTA (pH 9.0) at boiling temperatures for 10 minutes. Subsequently, sections were incubated with the primary antibody overnight at 4˚C. After washing, sections were incubated with secondary antibody (Envision Flex HRP, Agilent) for 60 minutes at RT prior to incubation with DAB substrate. Slides were analyzed with a bright field microscope and imaged with a Nikon DS camera.

Creating monolayers derived from organoids and Ussing-chamber assay

ICOs from 20, 25µL hydrogel droplets were collected in AdvDMEM/F12, centrifuged (453*g*, 5 min, 4˚C) and the supernatant was removed. Cells were mechanically broken by vigorously pipetting up and down and spun down again. Organoids were made single cell by Trypsin-EDTA incubation for 25 to 40 min, at 37°C. Cells were washed in AdvDMEM/F12 and put through a cell 70µm cell strainer. Approximately $3*10^5$ cells were resuspended in 200 µm AdvDMEM/F12-based expansion medium[10,13] and seeded on transwell inserts (24 well plate 6.5 mm, Corning), precoated with 5% Matrigel in PBS. Each 3-4 days medium was changed. To check confluence, electrophysiological analysis was performed after 4 days and the cells were examined under the microscope daily. Optimal confluence was determined by daily Trans-Epithelial Electrical Resistance (TEER) measurement until electrical resistance went down (after initial gaining TEER).

The confluent monolayers were placed in a Ussing chamber set up[16] to analyze functionality of cholangiocyte-specific transporter channels (CFTR and Ca^{2+} activated Cl^- channel) using Acquire & Analyze Software 2.3 (Physiologic Instruments, San Diego, California) or LabChart 8.1.13 (ADinstruments, Sydney, Australia) and if LabChart was used, graphs were subsequently created in Microsoft Excel (Microsoft, Redmond, USA). For complete details of the set-up, see the supplementary materials and methods section.

Current was clamped and the short circuit current (Isc) was recorded every second. Two 5 millivoltage (mV) pulses were given initially to measure TEER along the epithelial layers ($V=I*R$). TEER measurements of transwells without cells were subtracted from TEER transwells with cells. CFTR-dependent anion secretion was activated by adding 10 µM Forskolin to both sides of the ICOs and inhibited by addition of GlyH-101 (20 µM, apical side). Calcium (Ca^{2+}) activated chloride (Cl^-) channels (CaCC) or anoctamin-1 (ANO1) were stimulated by UTP (50 µM, apical side) and inhibited by T16Ainh-A01 (50 µM, apical side). To

block the uptake of Cl^- by cells via the Na-K-Cl co-transporter-1 (NKCC1) 50 µM bumetanide was added to the basolateral side. To maintain CFTR-activity intact under hypoxic conditions we selected Compound-C (which is a known AMP kinase-inhibitor)[17] as a candidate drug. Compound-C (10 µM) was added to the apical side of the cells under oxygen conditions, 15 minutes before switching to hypoxia. The complete list of reagents used is displayed in Table S2.

Hematoxylin and eosin (H&E) staining of monolayers.
After two weeks of seeding, monolayers were formalin-fixed (4%) for 15 minutes, paraffin-embedded and sectioned (4 µm). Subsequently, an H&E staining was performed according to standard protocols and slides were analyzed with a bright field microscope and imaged with a Nikon DS camera.

Bile exposure and cell survival
To investigate the influence of bile-toxicity on ICOs undiluted bile, spiked with 10 µM Forskolin, was added to the apical side for one hour. Fresh human bile was obtained from an endoscopic retrograde cholangiopancreatography (ERCP) procedure during regular patient treatment (for the details of the-patients of which the bile was used as well as details of the bile composition, please see Table S3). All bile donors consented to donating bile and the use of it was approved by the local MEC (MEC-2016-743). Intactness of the monolayer was determined by TEER-measurements during the experiment and cell-survival was obtained by life-death staining with 10% propidium iodide (PI) (Sigma-Aldrich) and 2% Hoechst (Thermo Fisher Scientific) in AdvDMEM/F12 added directly after the assay and incubated for 30 minutes at 37°C. Subsequently, ICOs were analysed under a EVOS FL Cell fluorescence microscope (Thermo Fisher), using DAPI-signal for Hoechst and red fluorescent protein for PI-signal.

Cell Viability
Cell viability was assessed based on total ATP content using CellTiter-Glo® 3D reagent (Promega, France) according to the manufactures protocol. In short, ICO monolayers were incubated with 300 µL of medium on top of the cells, consisting of a 1:1 dilution of AdvDMEM/F12 and CellTiter-Glo® 3D Reagent. Plates containing the ICO monolayers were gently shaken in the dark for 5 minutes to lyse the samples. Then the samples were incubated for an additional 25 minutes in a 5% CO_2 incubator at 37°C. Subsequently, samples (100 µL) were transferred to a white walled 96 well plate (Perkin Elmer) and the luminescence signal was measured on a LUMIstar OPTIMA microplate reader (BMG LABTECH) with gain set at 1500. The background signal was subtracted from obtained values (3 technical replicates per individual sample, per condition n=4 individual biological samples). The ATP values were

normalized to total RNA content, harvested as described above, as correction for cell numbers.

Statistical analysis

All analyses were conducted using SPSS software (statistical Product and Service solutions, version 22, SSPS Inc, Chicago, IL, USA) and graphs were performed using GraphPad Prism 7.0 (GraphPad Software Inc., USA). Continuous variables were tested using an independent T-test or Mann-Whitney-U test and presented with normal distribution as means with standard deviation and if not normally distributed, they are presented as range. In all tests, a P value of <0.05 was considered significant.

Results

Human organoids derived from intrahepatic biliary cells obtained from liver biopsies resemble cholangiocytes in vitro

Human ICOs (n=15) could be successfully initiated from all liver biopsies according to protocol established by Huch *et al*.[10,13] Donor or explant characteristics are shown in Table 1. As indicated in Figure 1A, gene expression profiles of ICOs closely resemble primary cholangiocytes (PC) and showed clear similarities with the recently described ECOs. An important difference between these organoid types is that ICOs are driven by canonical WNT-signaling and ECOs depend on non-canonical WNT-signaling.[10,11] When looking at known cholangiocyte- and hepatocyte-abundant genes, again ICOs show high expression of cholangiocyte genes, while clearly lacking the expression of hepatocyte specific genes (Figure 1B). These results were confirmed using qRT-PCR on ICOs, showing high expression of cholangiocyte-genes keratin (KRT)19 and KRT7 while lacking clear expression of the hepatocyte-genes albumin and CYP3A4 (Figure 1C).[10] Thus, the previously termed bipotential liver-derived organoids could be probably renamed to ICOs.[10] An important side note to make is the observation that mature cholangiocyte markers, such as CFTR, are lower expressed in ICOs compared to PCs and organoids cultured in the non-canonical WNT stimulation protocol (ECOs).

This is likely due to the status of cholangiocyte-maturation ICOs reflect *in vitro*, cause although derived from PCs, due to their canonical WNT-stimulating culture conditions they represent cholangiocytes undergoing ductal reprogramming (a more proliferative cholangiocyte) *in vitro.*[18]

ICOs have cholangiocyte anion transport activity

Gene expression of different cholangiocyte transporter channels were analysed by qRT-PCR. As shown in Figure 1D, all ICOs showed clearly detectable mRNA levels of CFTR, ANO1, aquaporin 1 (AQP1), apical sodium-depended bile acid transporter (ASBT), NKCC1 and SLC4a2, better known as AE2. Expression of CFTR-protein was confirmed using immunohistochemistry staining using a CFTR-specific antibody (Figure 2A), however no typical luminal specific staining could be observed, but this is likely due to forskolin addition in the medium which stretches out the cells and disguises typical columnar cholangiocyte morphology. Apical bicarbonate and chloride secretion is controlled by both Ca^{2+}- and cAMP-linked neuro-endocrine input that regulates the activity of anion transport channels, including ANO1 and CFTR.[3] To investigate ion-transport properties of ICOs. Organoids were harvested and grown as monolayers before mounting them in Ussing Chambers (Figure 2B).[17] Day 12 after seeding was determined to be the optimal day for read-out with mean TEER for ICO monolayers being 73.3±16.1Ω*cm^2 (Figure 2C), which is in line with TEER-data published for primary mouse cholangiocytes, but significantly lower compared to IPS cholangiocytes

and rat cholangiocytes.[19-21] Next we found that addition of forskolin, a cAMP activator, which subsequent could stimulate CFTR activity, to both sides of the cells resulted in an increase of Isc-signal as a result of ion-transportation. When CFTR inhibitor, GlyH-101, was added, a decrease in Isc was observed (Figure 2D). Indicating that ICOs have functional CFTR-channels which can be activated and inhibited. Stimulation with UTP resulted in a high and rapid increase of Isc signal which could be specifically inhibited by T16Ainh-A01 (Figure 2D). Demonstrating that ICOs also have functional ANO1 ion-channels. Addition of UTP to the contra-luminal (basolateral) bathing medium did not elicit an Isc-signal (data not shown), attesting the highly polarized distribution of (P2Y2-type) purinergic receptors in ICOs. Finally, to test if forskolin was only stimulating CFTR-mediated ion release in our model.[22] We decided to stimulate an ICO monolayer created from a CF-patient with forskolin. As shown in Figure S1, forskolin addition did not stimulate any ion-transport, but upon apical UTP addition a sharp increase in Isc, comparable to healthy controls, was observed. Indicating that the cells grew properly as a monolayer and that forskolin only stimulates cAMP mediated CFTR function in our model.

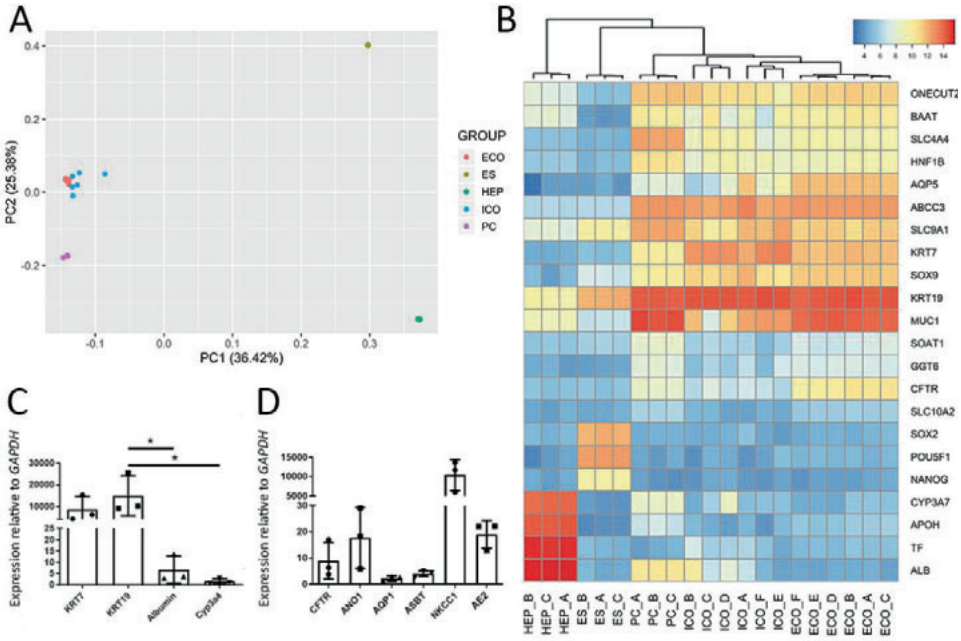

Figure 1. ICOs resemble primary cholangiocytes.

(a) Principal Component Analysis (PCA) of intrahepatic cholangiocyte organoids (ICOs, n=6), extrahepatic cholangiocyte organoids (ECOs, n=6), primary cholangiocytes (PC, n=3), primary human freshly plated hepatocytes (HEP, n=3), and embryonic stem cells (ES, n=3) based on all probes (n=26120) that remained after filtering. ICOs cluster closely with ECOs, indicating a high correlation on expression profiles. Moreover, both ICOs and ECOs cluster relatively close to primary cholangiocytes and distant

from primary hepatocytes and embryonic stem cells, indicating their resemblance to cholangiocyes. **(b)** Heatmap and clustering based on representative biliary, hepatic and stem cell genes. Groups analysed are similar to A. Based on this gene-set ICOs and ECOs both closely cluster to PC and display key cholangiocyte-markers (Cytokeratin (CK) 19 and CK7), while lack or have limited expression of hepatocyte markers (albumin and Cyp3a7). Color key represents the log2 transformed signal intensities after variance stabilizing normalization. **(c)** Gene expression analysis of ICOs by qRT-PCR of cholangiocyte markers (CK 19 and CK7) and hepatocyte markers (albumin and Cyp3a4). Expression of cholangiocyte markers relative to housekeeping gene, GAPDH were significantly upregulated ($p<0.001$) compared to hepatocyte markers (n=3, individual biological samples). * Indicates significant difference ($P<0.05$). **(d)** Gene expression analysis of key cholangiocyte channels in ICOs by qRT-PCR (n=3, individual biological samples).

CFTR can transport both chloride and bicarbonate anions

In respiratory and intestinal epithelia, bicarbonate secretion is thought to account for <25% of total CFTR-mediated anion secretion.[23] To assess the contribution of bicarbonate to CFTR-mediated anion transport in cholangiocytes, forskolin-dependent Isc signal in the presence of bumetanide was tested. Bumetanide inhibits NKCC1-mediated basolateral chloride uptake[24] and only marginally affected the forskolin-induced Isc-response (Figure 3A, B). In the absence of extracellular Cl^- (i.e. in nominally chloride-free medium), the forskolin-depended Isc signal was similar to the signal obtained in chloride-containing (Meyler) medium (10.58± 0.71 versus 12.35 ± 9.1 μA/cm^2, p=0.56, Figure 2C and 3C, D). In contrast, the UTP-dependent ANO1 activation was clearly affected in chloride-free medium versus Meyler conditions (6.285 ± 0.36 vs. 23.99 ±3.49 μA/cm^2, p=0.02, Figure 2C and 3C,E). A similar affect for the ANO1 channel was observed when chloride influx was blocked by bumetanide (24.6 ± 2.89 vs. 10.18 ± 3.92 μA/cm^2, p=0.009). These data suggest that CFTR, but not ANO1, can directly mediate bicarbonate secretion in ICOs.

Hypoxia affects ion channel activity

We investigated whether the CFTR-function is affected by hypoxia in ICOs. To study this, first the monolayer was exposed to oxygen for 30 minutes, after forskolin-stimulation, (Figure 4A, Δ1), and subsequently switched to hypoxic conditions (Figure 4A, Δ2). In all samples a rapid decrease in Isc-signal was observed 22.11±10.98 μA/cm^2 at the end of oxygenation vs.16.21±10.92 μA/cm^2 at the end of hypoxia p=0.03, Figure 4A, B) indicating that hypoxia inhibits CFTR-activity. After switching back to oxygenated condition, CFTR-activity partially restored as demonstrated by an increase in Isc, Figure 4A). To confirm true hypoxia was reached during the experiment, a qRT-PCR was performed to analyse the induction of hypoxia-induced factor (HIF)-1α gene expression, which is upregulated during hypoxia.[25,26] As shown in Figure S2, HIF-1α gene expression started increasing after one hour of hypoxia (0.96±0.22 vs. 1.04±0.25, p=0.05), while 30 minutes of hypoxia exposure was too short to provoke a response in gene expression. This observation was similar to previous

experiments,[27] confirming hypoxia conditions are achieved in the Ussing chamber measurements. Subsequently, to test the kinetics by which hypoxia affects CFTR activity, the forskolin-stimulated Isc was obtained in ICOs that were kept hypoxic for half an hour. After this period, forskolin was added and when a plateau-phase was reached (end of hypoxia, Figure 4C, Δ3), the hypoxic gas was switched to oxygen-rich gas (Figure 4C, end of reoxygenation, Δ4). A significant increase in Isc (13.01± 6.08 vs. 19.83± 8.74 μA/cm^2, p=0.008, Figure 4C, F) was measured in all ICOs after oxygen-exposure. Isc-responses to forskolin were also measured by exposing either monolayers solely to oxygen or to hypoxia. In line with previous results, mean forskolin-stimulated Isc in the oxygenated group (11.26± 5.46 μA/cm^2, Figure 4D) was significantly higher compared to forskolin-stimulated Isc signal during hypoxia (5.680± 2.79 μA/cm^2, p=0.01, Figure 4D). Furthermore, overall TEER of the ICO monolayer was not affected by hypoxia during the course of the measurement; mean TEER of ICOs during hypoxia was 78.4±27.6Ω*cm^2, which did not differ from oxygen conditions (p=0.77, Figure 4E). In control experiments, exposure to hypoxia for one hour without stimulation of CFTR did not show a decrease in Isc signal or TEER (Figure S3). These experiments indicate that the integrity of the cells is not affected by hypoxia during this time frame. Finally, hypoxia did not only affect CFTR but also ANO1 activity. As shown in Figure 4G and 4H, ANO1 stimulated with UTP, became less active after switching to hypoxic conditions (6.387± 1.21 μA/cm^2 vs. 0.193± 3.02 μA/cm^2, p=0.03). Combined, these results suggest that hypoxia not only reduces the bicarbonate secretion, in ICOs by lowering direct transport via CFTR, but also by indirect transport via Cl^- (secreted by CFTR and ANO1) exchange for HCO_3^- by AE2.

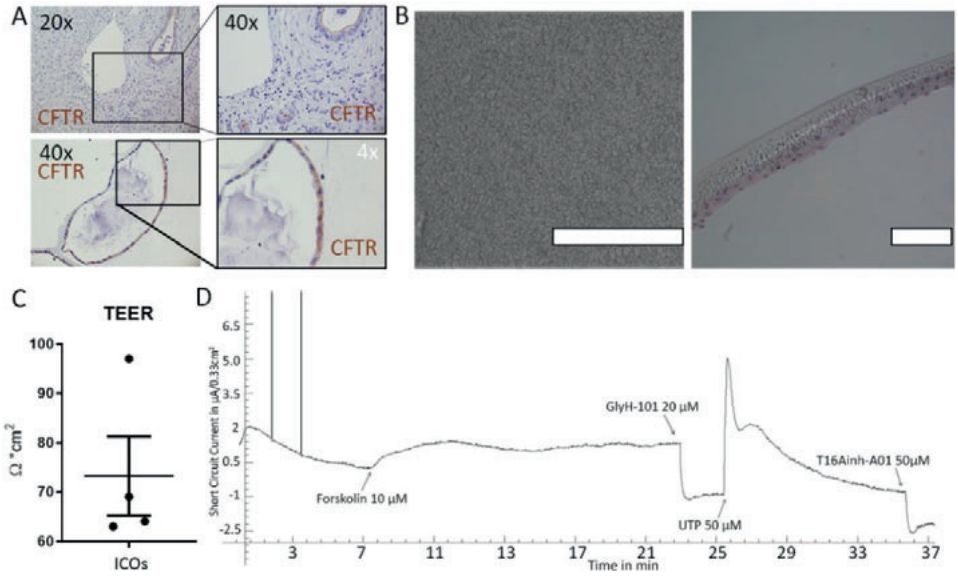

Figure 2. ICOs have functional cholangiocyte ion-channels.
(a) Immunohistochemistry staining of Cystic Fibrosis Transmembrane Conductance regulator (CFTR) on liver biopsies and ICOs, scale bars indicate 200 µm. **(b)** Left panel a detail picture of an ICO monolayer after 12 days of culture. On the right panel hematoxylin and eosin staining of an ICO monolayer after 12 days culture. Scale bars indicate 200 µm. **(c)** Trans epithelial electrical resistance (TEER) of ICO monolayers in Ussing Chamber set-up (n=4, individual biological samples). **(d)** Recording of short circuit current (Isc) in Ussing Chamber set-up. CFTR could be stimulated by Forskolin and inhibited by GlyH-101. Calcium activated Chloride Channels (CaCC, ANO1) could be activated by UTP and inhibited by T16Ainh-A01.

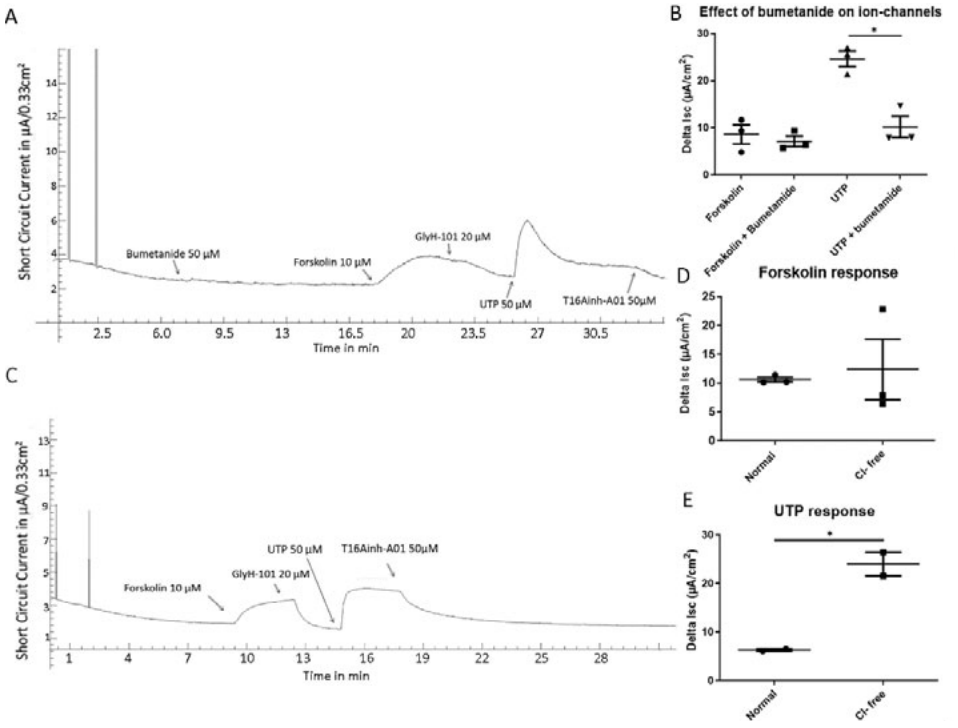

Figure 3. CFTR excretes bicarbonate in ICOs.
(a) If basolateral chloride-influx via Sodium-Potassium-Chloride-Cotransporter (NKCC)-1 was blocked via bumetanide, forskolin-stimulate Isc was similar to the response without bumetanide (n=3, individual biological samples). However, as displayed in **(b)** the response to UTP was around 40% when chloride-influx was blocked basolateral. **(c)** In ICOs measured in chloride-free medium, forskolin-induced Isc is similar to Meylers medium (n=3, individual biological samples), as displayed in **(d)**, indicating that in absence of chloride-influx, CFTR likely can secrete bicarbonate. **(e)** Stimulation of the ANO1 gave a significant lower response in the chloride-free medium (n=2, individual biological samples) compared to the Meylers medium (Figure 2C), as shown in by two-sided ANOVA (p=0.02). * Indicates significant difference (P<0.05).

Hypoxia reduces ICO resistance against bile cytotoxicity

To test if ICOs become more susceptible to bile toxicity, fresh human bile samples were added to the hypoxia-model. ICOs were either exposed to oxygen-rich or hypoxia surroundings with or without bile for one hour. Similar to the situation *in vivo,* cells were exposed to bile from the apical side. TEER-measurements with 5mV pulses were performed each 90 seconds to determine monolayer-integrity. To achieve maximum secretion of bicarbonate from the start of the experiment, bile was spiked with forskolin 10 µM before addition to ICOs. Without forskolin-administration, bile exposure resulted in substantial cell death even under oxygen-rich conditions (data not shown). The influence of hypoxia with and without bile on ICOs is visible in Figure 5A. The red line represents a monolayer of cells under hypoxic conditions without bile addition. The black line represents a monolayer with bile addition to the luminal side during hypoxia. Both lines are pre-stimulated with forskolin 10µM before Isc is displayed. As shown in Figure 5A, no decrease in forskolin-stimulated Isc, or an increase in Isc-responses to 5mV pulses can be seen for the red line over time, as indicated by the dotted red arrows. In contrast, the black line does show a decrease in forskolin-stimulated Isc over time while also showing an increased response to 5mV pulses, as displayed by the black dotted arrows. Thus, these results indicate a lower excretion of CFTR-mediated ions due to loss of confluence of the ICO monolayer, suggesting cell-death. These results could be confirmed by calculating the ΔTEER between the beginning and the end of each experiment. As shown in Figure 5B, the largest decrease in ΔTEER was observed in the hypoxia with bile group, however it did not reach statistical significance, compared to the other three groups (23.3±10.2% vs. 10.4±3. vs.10.8±7.2 and 9.3±3.1, p=0.13). Subsequently, the cell viability of ICO-monolayers was accessed. As shown in Figure 5C, exposition to bile and especially in combination with hypoxic conditions significantly affects cell viability. The oxygenated group had the highest cell viability levels (mean 105.7±SD65.8) and this was significantly higher compared to all other conditions. Cells exposed to only hypoxia demonstrated the second highest value of cell viability (mean 36.0±SD9.4) and both oxygen and hypoxia measurements were also significantly higher compared to oxygen with bile (mean 21.12±SD9.89) and hypoxia with bile (mean 11.36±SD1.21) conditions. Interestingly, quantification of cell-death on ICO monolayers, as determined by PI-positive cells, confirm these results (Figure 5D). Quantification of the PI positive cells showed that cell-death was the highest after exposure to bile under hypoxic conditions (mean 5.6% ±SD3.8 oxygen without bile vs. 75.6% ±SD12.0 for hypoxia with bile $p<0.0001$, Figure 5E). Thus, under oxygen ICO monolayers were significantly more resistant to bile toxicity (Figure 5E). Taken together, this evidence indicates that during hypoxia ICOs are more susceptible to bile-induced cell death and loss of barrier function.

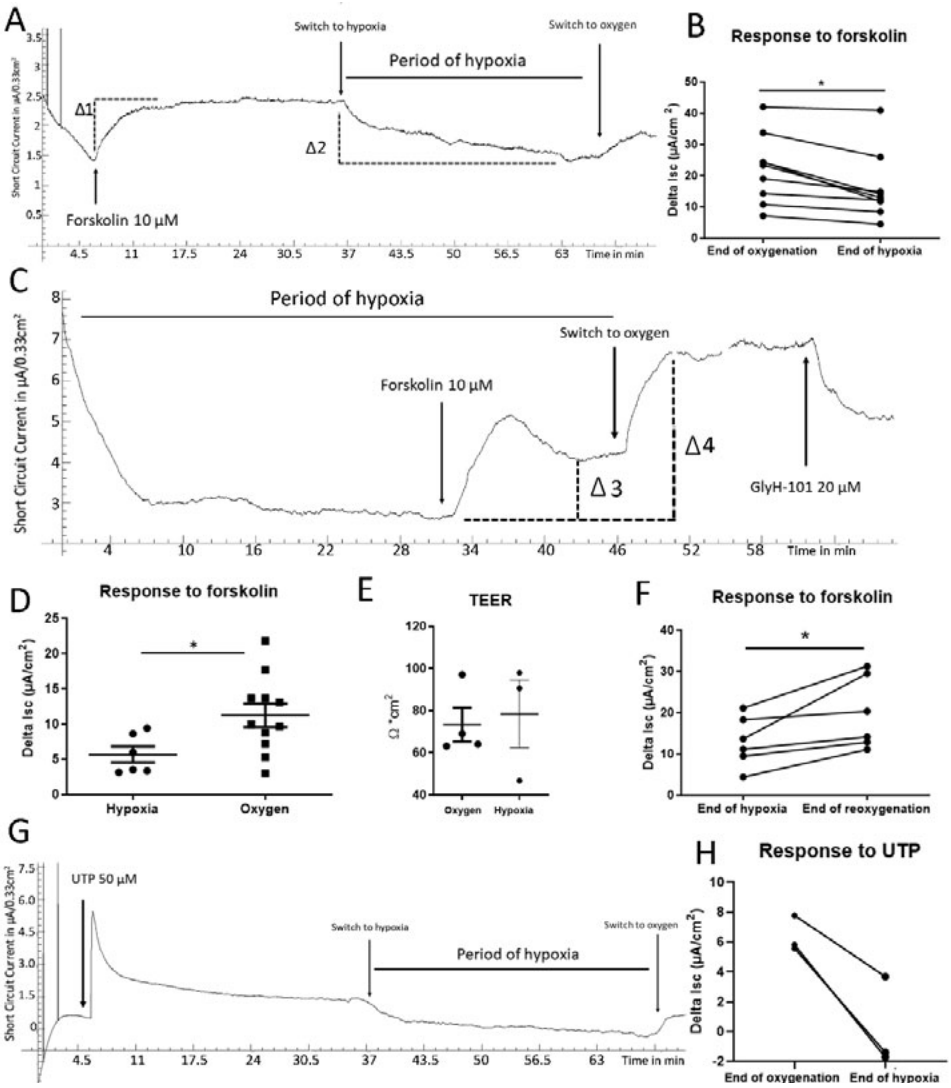

Figure 4. Hypoxia impairs cholangiocyte ion-channel activity.

(a) ICOs are stimulated with forskolin for 30 minutes during oxygenation (end of oxygenation, Δ1) before switching to hypoxia for 30 minutes, when the forskolin-depended Isc decreases (end of hypoxia, Δ2). Afterwards oxygen is reinserted, resulting in an increase in Isc, demonstrating that inhibition of CFTR by hypoxia is at least partially reversible. **(b)** The average forskolin-stimulated Isc significantly decreased during hypoxia (Δ2) (n=8, individual biological samples along with one technical duplicate making n=9, two-tailed paired T-test, p=0.03). **(c)** After 30 min of hypoxia (95%N_2/5%CO_2) ICOs are stimulated with forskolin until Isc plateau (end of hypoxia, Δ3), next ICOs are exposed to oxygen (95%O_2/5%CO_2) which results in a further increase in Isc during oxygenation (Δ4). After a total of one hour, channel activity was still sensitive to inhibited by GlyH-101. **(d)** Forskolin-stimulation during

oxygen is significantly higher compared to the hypoxia response (Δ1 versus Δ3, n=6, individual biological samples vs. n=11, 8 individual biological samples, Two-tailed T-test, p=0.008). **(e)** TEER measurements of ICO-monolayers during hypoxia compared to the TEER measurements during oxygen did not significantly change (n=3, individual biological samples voor N_2 conditions). **(f)** The forskolin-stimulate Isc at the end of hypoxia in ICOs (n=6, individual biological samples) significantly increased after switching to oxygen (Δ4, Two-tailed T-test, p=0.01). **(g)** In ICOs, ANO1 is activated by UTP stimulation for 30 minutes under oxygen and switched to hypoxia resulting in a diminished activity. After 30 minutes oxygen is inserted back into the model, showing that inactivation by hypoxia of ANO1 can be partially restored. **(h)** After stimulation with UTP (ANO1 acitivation) in ICO-monolayers under oxygen, Isc is significantly decreased after exposure to hypoxia (n=3, individual biological samples). *Indicates significant difference (P<0.05).

AMPK inhibitor preserves CFTR function during hypoxia

Regulation of CFTR-activity is known to involve kinase activity. Protein Kinase A activates CFTR and 5'-AMP-activated protein kinase A (AMPK) inhibits CFTR activity.[28] AMPK is upregulated when ATP-concentration in the cell lowers, which is the case if oxidative metabolism is diminished.[29] As hypoxia reduces CFTR activity, the influence of AMPK on CFTR-regulation was further explored. Therefore, we tested AMPK-agonist metformin and AMPK-inhibitor compound-C. ICO monolayers were pre-incubated with metformin or compound-C for 15 minutes to the apical side prior to the switch from the oxygen-rich to the hypoxic condition. Pretreatment with metformin did not affect the CFTR-activity when switching to hypoxia (data not shown). As shown in Figure 6A, pretreatment with compound-C partially prevented loss of CFTR-activity during hypoxia (Figure 6A). Overall, the administration of compound-C resulted in a significantly lower decrease of forskolin-stimulated Isc under hypoxic conditions compared to no administration of compound-C (-3.15± 0. 38 vs. 0.37± 1.88 μA/cm^2, p=0.03, Figure 6B). Importantly, compound-C did not influence chloride or bicarbonate mediated ion secretion on ICO monolayers (Figure S4), but was capable of significantly upregulating CFTR gene expression during hypoxia compared to all other conditions (Figure S5). Together, these results suggest that, AMPK activity is upregulated during hypoxia and contributes to in the inhibition of CFTR-activity. AMPK-inhibition by compound-C partially prevent this loss of CFTR-activity during hypoxia and keeps the forskolin-stimulated Isc-signal intact (Figure 6C).

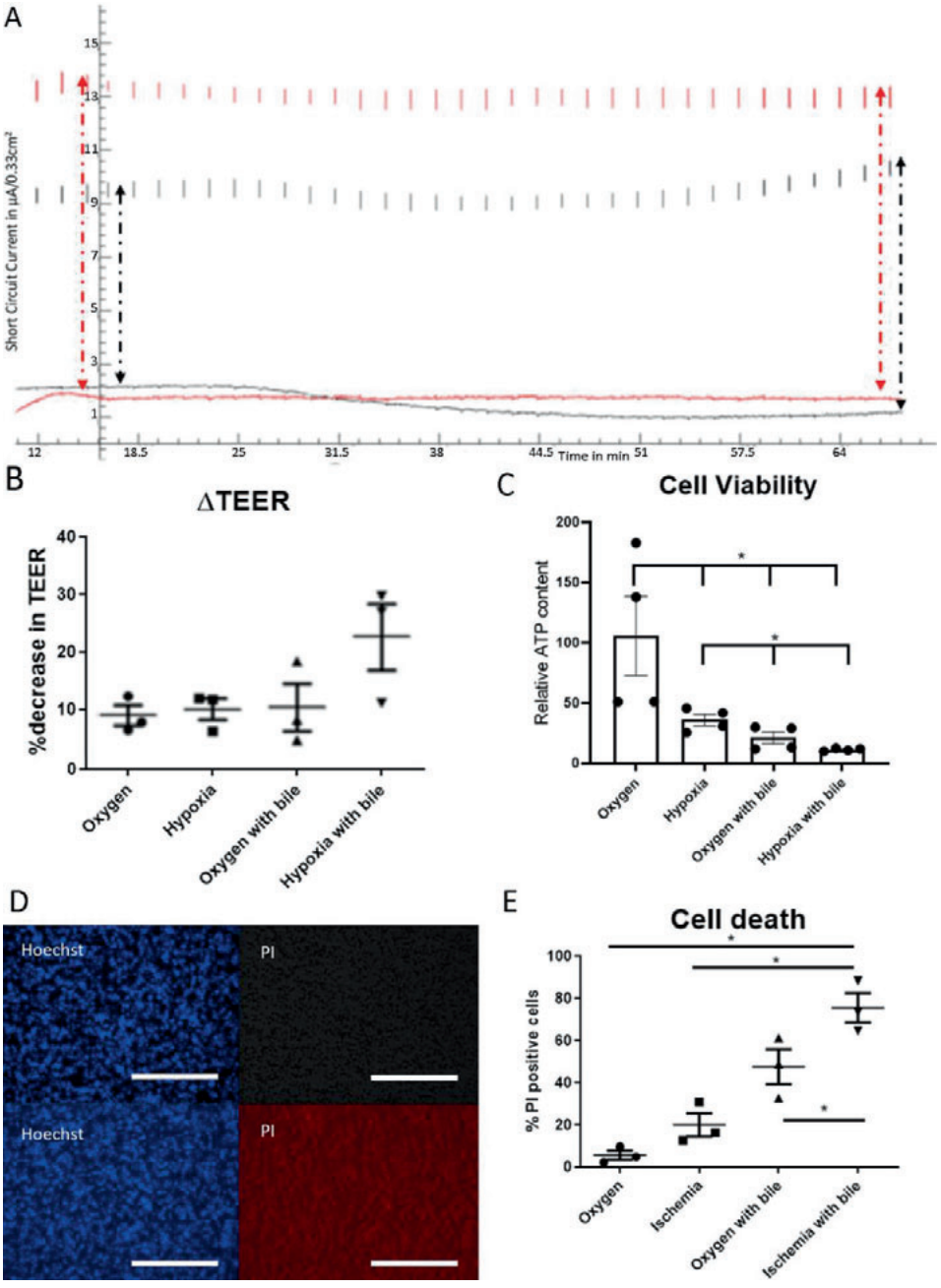
A
Short Circuit Current in µA/0.33cm²
Time in min
B
ΔTEER
%decrease in TEER
Oxygen
Hypoxia
Oxygen with bile
Hypoxia with bile
C
Cell Viability
Relative ATP content
D
Hoechst
PI
E
Cell death
% PI positive cells
Ischemia
Ischemia with bile

Figure 5. Bile induced cell death increases under hypoxic conditions.
(a) The red line represents a ICO under hypoxic conditions without bile addition. The black line represents a ICO with bile addition to the luminal side under hypoxic conditions. Both lines are stimulated with forskolin 10μM. For the red line no Isc decrease or an increase in Isc-response to 5 Millivoltage (mV) pulses is detected. Only the top edges of the Isc-responses to the 5mV-spikes are displayed. The black line shows a decrease in Isc over time and also an increase in Isc-response to 5 mV-pulses indicating decresed TEER (as displayed in B) and less intactness of the monolayer. Dotted black and red arrows indicate the responses in Isc to 5mV pulses, showing a clear increase in the Isc response for the black line over time. **(b)** Decrease in percentage of TEER as calculated between time is 0 minutes and time is 60 minutes (n=3, individual biological samples for all conditions). **(c)** The relative cell viability was measured by ATP content. ATP content was normalized to total RNA content. Shown is the mean ± SD of four independent biological replicates. Cell viability was significantly reduced by hypoxia and bile exposure. Viability was significantly lowest under hypoxia combined with bile. **(d)** A representative Figure of a staining with propidium iodide (PI, red) staining death cells and Hoechst (blue) staining nuclei. Top row shows PI and Hoechst staining for cells exposed to one hour of oxygen, while the bottom row shows hypoxia with bile addition. Scale bar indicates 100 μm. **(e)** A higher percentage of PI positive cells was detected in the hypoxia with bile group compared to all other groups, two-sided ANOVA-test (n=3, individual biological samples, p=0.04). * Indicates significant difference (P<0.05).

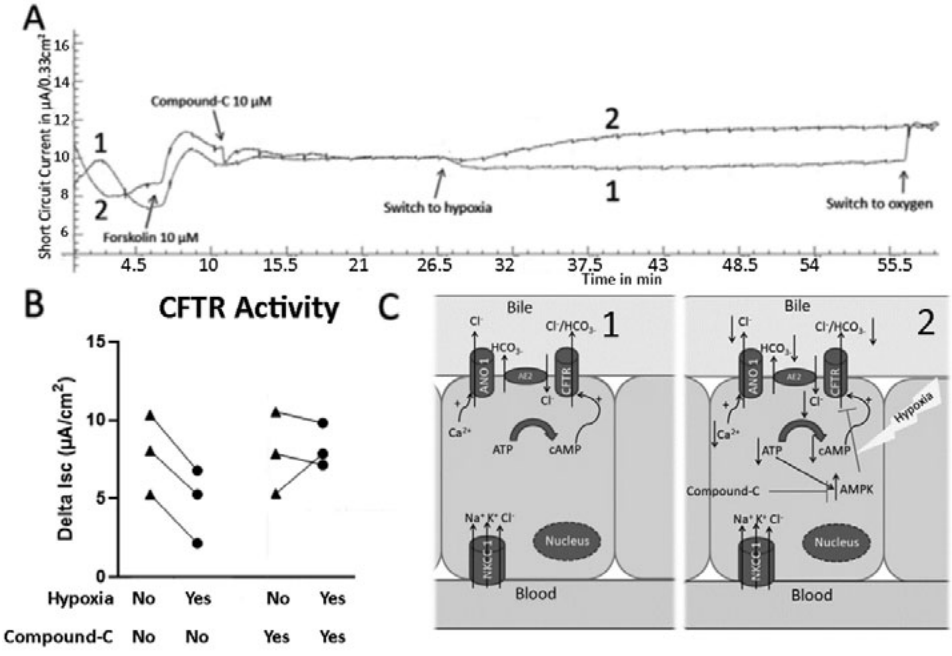

Figure 6. Inactivation of the CFTR channel during hypoxia is restored by AMP-activated protein kinase (AMPK) inhibitor.

(a) Line 1 represents ICOs without addition of compound-C, line 2 is with addition of compound-C. After forskolin-stimulation under oxygen conditions, ICO line 2 was stimulated with Compound-C (10µM apical), 15 minutes before switching to hypoxia. After 30 minutes of oxygen exposure ICOs were switched to hypoxia showing a decrease in Isc for line 1. Line 2 remains stable over time and slightly increases. After 30 minutes ICOs are again exposed to oxygen**. (b)** ICOs with compound-C have a significantly lower decrease (delta) in forskolin-stimulated Isc after switching to hypoxia compared to ICOs without compound-C (n=3, individual biological samples, p=0.03, ANOVA two-sided). **(c)** Schematic overview of the hypothesis. In 1, the normal situation is presented. The endoplasmic reticulum (ER) creates calcium (Ca^{2+}) which can activate the ANO1 channel, while cAMP activates CFTR. Both results directly and indirectly in buffering of the bile with HCO_3^-. In 2, the situation during hypoxia is displayed. Both CFTR and the ANO1 channel become less active resulting in a lower pH of the bile, by lack of bicarbonate, and therefore cholangiocyte cell death (possible by apoptosis). Inhibition of AMPK by compound-C partially restores CFTR function and is able to mobilize HCO3- into the bile. * Indicates significant difference ($P<0.05$).

Discussion

The recently developed 3D-culture systems have made it possible to initiate and long-term propagate organoids from human adult liver tissue, providing new possibilities for disease modeling *in vitro*.[10] Here, we demonstrate that organoids from liver-biopsies cultured according to the protocol established by Huch *et al.*[10] closely resemble primary cholangiocytes in terms of gene expression and functionality. ICOs express the typical progenitor/mature cholangiocyte markers CK19, CK7 and CFTR. Moreover, we show that ICOs have functional, cholangiocyte ion-channels, including CFTR and ANO1, highlighting their cholangiocyte resemblance. Although ICOs do not fully resemble mature primary cholangiocytes, as they retain markers of stemness and represent a more proliferating cholangiocyte *in vitro* [18], they are the first cholangiocyte-like cells grown from primary tissue.[10] Since, ICOs are derived from peripheral liver biopsies they likely have cholangiocytes from the small bile ducts as their starting population. Although functional differences in transporter activity have been described between small and large cholangiocytes for rat cholangiocytes[30], there is no data to support this diversity in humans. Moreover, it is unclear if ICOs would actually resemble small or large cholangioytes *in vitro.* Previous research indicates that although regional-specific gene expression profiles can be found *in vitro,* the microenvironment drives ICOs to a certain phenotype which is more consistent with cholangiocyte organoids cultured from a different part of the biliary tree, than with primary cholangiocytes from the native tissue.[31] In contrast, functional differences still exist between organoids cultured from the intra- and extrahepatic bile duct.[31] Indicating that some regional-diversity still exist *in vitro,* which could be of importance since there is clear regional diversity along the biliary tree for cholangiopathies.[32-34]

A previous publication showed that CFTR is functional in cholangiocytes derived from human induced pluripotent stem cells.[12] However, the differentiation protocols for cholangiocyte-IPS is extensive and difficult and only part of the cells differentiate to cholangiocytes. ICOs are cultured in the same medium for 2D and 3D-cultures, can be expended easily and have cholangiocyte-like properties and functionality even without differentiation, making it our preferred choice.

Our study provides the first evidence for a direct role of CFTR in biliary bicarbonate secretion. The bicarbonate umbrella theory hypothesizes that diminished excretion of chloride by CFTR, via exchange by AE2, indirectly result in less apical excretion of bicarbonate. Indeed, several studies have shown that diminished function of AE2 contributes to cholangiopathy development.[4,35] Here we show that chloride secretion during hypoxia is not only diminished by CFTR but also by ANO1. Evidence for direct secretion of bicarbonate by CFTR has been previously reported in pancreas, airway and intestine, but not for cholangiocytes.[36] Unfortunately, we were unable to directly measure changes in pH, Cl^- or HCO_3^- within our model, which would have been a valid addition, instead we used two indirect methods for

measuring HCO_3^- secretion. By blocking both the influx of Cl^- or removing Cl^- completely from the medium, we were able to maintain Isc after forskolin stimulation both with and without compound-C drug administration. Indicating that is highly likely that cAMP activation can lead to bicarbonate secretion to the apical lumen via CFTR. This provides new insights for the dual role of CFTR, directly and indirectly, in establishing the bicarbonate umbrella and cholangiopathy pathophysiology, by protecting cholangiocytes from bile toxicity.

In our model we focused upon the direct stimulation of CFTR by cAMP via adenyl cyclase (AC) activation due to forskolin addition.[37] However, it is important to notice that cAMP levels in cholangiocytes can also be upregulated via soluble G-protein-insensitive AC (sAC). sAC is regulated by intracellular levels of HCO_3^- and can act independently of secretin.[38] Since there is no evidence that sAC is less active during hypoxia,[39] we focused on the role hypoxia plays in cAMP-stimulated CFTR secretion.

It has previously been reported that CFTR gene expression is downregulated in the liver during hypoxia in mouse models[8], but our study provides the first evidence that both CFTR and ANO1 anion transport function is inhibited during hypoxia. Hypoxia often occurs during organ procurement and ischemia-reperfusion-injury during LT is associated with NAS development.[6] Ischemic-injury is primary determined by the magnitude and duration of interruption of oxygen supply. Reperfusion-injury is mostly a result of reactive oxygen species damage and pro-inflammatory neutrophils infiltrating the damaged tissue.[40] Our study mainly focused on hypoxia and the effects on ion-channel activity. We observed that if ICOs are exposed to fresh human bile, cellular damage was more severe during hypoxia related dysfunction of ion channels. A clear limitation of our study is that the evidence provided within this study is solely based upon our *in vitro* model. Although human ICO monolayers represent monolayers of human biliary epithelium, they do not recapitulate the complete *in vivo* environment of human bile ducts. For instance, there are no blood vessels or immune-cells present. Thus, certain aspects of hypoxia-related biliary injury, such as reactive oxygen species derived from neutrophils are overlooked and are not investigated within our study.

An important novel finding in our study is that addition of the drug compound-C is able to prevent the hypoxia-induced decrease in CFTR activity. This AMP kinase inhibitors might provide a new avenue to prevention bile duct injury and biliary fibrosis after LT. Since our experiments are performed at 37°C, it is warm ischemia damage. In the clinical setting it has been shown that the total period of warm ischemia time contributes to the development of bile duct fibrosis after LT. Therefore, the American Society of Surgeons recommend no more than 30 minutes of donor-warm ischemia time.[41] Donor warm ischemia time is the damage that develops during collection of the donor graft from donation after circulatory death donors. Our results indicate that increased cell death by hepatic bile occurs after approximately 30 minutes in the absence of oxygen, which is in concordance with the clinical experience. Prevention of diminished CFTR activity could be of great importance to prevent cholangiocyte injury. Therefore, AMP kinase-inhibitors could potentially be applied during

graft preservation to prevent bile duct injury during the second period of warm ischemia after transplantation and reperfusion.
In conclusion, we show that ICOs resemble primary cholangiocytes and are a useful model to study cholangiocyte anion exchange channels. Using this model, we demonstrate the direct impact of hypoxia on the activity of these channels and how the lack of bicarbonate section renders the cholangiocyte-like cells vulnerable for bile toxicity. The effect of hypoxia involves AMP Kinase signaling and can be partially reversed by adding compound-C suggesting new opportunities to prevent bile duct injury during graft preservation in LT.

Table 1. Donor demographics corresponding to the fifteen different ICO cultures.

Donor #	Donor-type	Age	Gender
1	DBD donor	69	F
2	DBD donor	48	M
3	DBD donor	70	F
4	DCD donor	44	M
5	DCD donor	52	M
6	DBD donor	74	M
7	DBD donor	55	F
8	DBD donor	52	F
9*	DCD Donor	50	F
10*	DBD Donor	51	F
11*	DBD Donor	54	F
12*	DCD Donor	56	F
13*	Explant liver of a cryptogenic cirrhosis patient	67	F
14*	DCD Donor (not transplanted)	×	×
15	Explant liver of a CF Patient	17	M

Abbreviations: ICO: intrahepatic cholangiocyte organoids, CF: Cystic Fibrosis, M: Male, F: Female, DBD: Donation after Brainstem Death, DCD: Donation after Circulatory Death, *used only for microarray analysis, ×data is unknown.

References

1. Dyson JK, Beuers U, Jones DEJ, *et al.* Primary sclerosing cholangitis. Lancet. 2018 Jun 23;391(10139):2547-2559.
2. Perkins JD. Are we reporting the same thing? Liver Transpl. 2007 Mar;13(3):465-6.
3. Boyer JL. Bile formation and secretion. Compr Physiol. 2013 Jul;3(3):1035-78.
4. Beuers U, Maroni L, Elferink RO. The biliary HCO(3)(-) umbrella: experimental evidence revisited. Curr Opin Gastroenterol. 2012 May;28(3):253-7.
5. Beuers U, Hohenester S, de Buy Wenniger LJ, *et al.* The biliary HCO(3)(-) umbrella: a unifying hypothesis on pathogenetic and therapeutic aspects of fibrosing cholangiopathies. Hepatology. 2010 Oct;52(4):1489-96.
6. Roos FJM, Poley JW, Polak WG, *et al.* Biliary complications after liver transplantation; recent developments in etiology, diagnosis and endoscopic treatment. Best Pract Res Clin Gastroenterol. 2017 Apr;31(2):227-235.
7. Enestvedt CK, Malik S, Reese PP, *et al.* Biliary complications adversely affect patient and graft survival after liver retransplantation. Liver Transpl. 2013 Sep;19(9):965-72.
8. Guimbellot JS, Fortenberry JA, Siegal GP, *et al.* Role of oxygen availability in CFTR expression and function.Am J Respir Cell Mol Biol.2008 Nov;39(5):514-21.
9. Uramoto H, Okada T, Okada Y. Protective role of cardiac CFTR activation upon early reperfusion against myocardial infarction. Cell Physiol Biochem. 2012;30(4):1023-38.
10. Huch M, Gehart H, Boxtel van R, *et al.* Long-term culture of genome-stable bipotent stem cells from adult human liver. Cell. 2015 Jan 15;160(1-2):299-312.
11. Sampaziotis F, Justin AW, Tysoe OC, *et al.* Reconstruction of the mouse extrahepatic biliary tree using primary human extrahepatic cholangiocyte organoids. Nat Med. 2017 Aug;23(8):954-963.
12. Sampaziotis F, de Brito MC, Madrigal P *et al.* Cholangiocytes derived from human induced pluripotent stem cells for disease modeling and drug validation. Nat Biotechnol. 2015 Aug;33(8):845-852.
13. Broutier L, Andersson-Rolf A, Hindley CJ, *et al.* Culture and establishment of self-renewing human and mouse adult liver and pancreas 3D organoids and their genetic manipulation. Nat Protoc. 2016 Sep;11(9):1724-43.
14. Roest HP, Ooms LSS, Gillis AJM, *et al.* Cell-free MicroRNA miR-505-3p in Graft Preservation Fluid Is an Independent Predictor of Delayed Graft Function After Kidney Transplantation. Transplantation. 2019 Feb;103(2):329-335.
15. Sampaziotis F, Justin AW, Tysoe OC, *et al.* Reconstruction of the mouse extrahepatic biliary tree using primary human extrahepatic cholangiocyte organoids. ArrayExpress Data, E-MTAB-4591. https://www.ebi.ac.uk/arrayexpress/experiments/E-MTAB-4591/
16. Li H, Sheppard DN, Hug MJ. Transepithelial electrical measurements with the Ussing chamber. J Cyst Fibros. 2004 Aug;3 Suppl 2:123-6.
17. Liu X, Chhipa RR, Nakano I, Dasgupta B. The AMPK inhibitor compound C is a potent AMPK-independent antiglioma agent. Mol Cancer Ther. 2014 Mar;13(3):596-605.
18. Aloia L, Alexander McKie M, Vernaz G, *et al.* Epigenetic remodeling licences adult cholangiocytes for organoid formation and liver regeneration. Nat Cell Biol. 2019 Nov;21(11):1321-1333.

19. Fiorotto R, Amenduni M, Mariotti V, *et al*. Src kinase inhibition reduces inflammatory and cytoskeletal changes in ΔF508 human cholangiocytes and improves cystic fibrosis transmembrane conductance regulator correctors efficacy. Hepatology. 2018 Mar;67(3):972-988.
20. Dutta AK, Woo K, Khimji AK, *et al*. Mechanosensitive Cl- secretion in biliary epithelium mediated through TMEM16A. Am J Physiol Gastrointest Liver Physiol. 2013 Jan 1;304(1):G87-98.
21. Chinet T, Fouassier L, Dray-Charier N, *et al.* Regulation of electrogenic anion secretion in normal and cystic fibrosis gallbladder mucosa. Hepatology. 1999 Jan;29(1):5-13.
22. Alvaro D, Alpini G, Jezequel AM, *et al.* Role and mechanisms of action of acetylcholine in the regulation of rat cholangiocyte secretory functions. J Clin Invest. 1997 Sep 15;100(6):1349-62.
23. Tang L, Fatehi M, Linsdell P. Mechanism of direct bicarbonate transport by the CFTR anion channel. J Cyst Fibros. 2009 Mar;8(2):115-21.
24. Walker NM, Flagella M, Gawenis LR, *et al.* An alternate pathway of cAMP-stimulated Cl secretion across the NKCC1-null murine duodenum. Gastroenterology. 2002 Aug;123(2):531-41.
25. Wang GL, Jiang BH, Rue EA, *et al.* Hypoxia-inducible factor 1 is a basic-helix-loop-helix-PAS heterodimer regulated by cellular O2 tension. Proc Natl Acad Sci U S A. 1995 Jun 6;92(12):5510-4.
26. Iyer NV, Kotch LE, Agani F, *et al.* Cellular and developmental control of O2 homeostasis by hypoxia-inducible factor 1α. *Genes Dev.* 15; 12(2): 149–162, 1998.
27. Blum JI, Bijli KM, Murphy TC, *et al.* Time-dependent PPARγ Modulation of HIF-1α Signaling in Hypoxic Pulmonary Artery Smooth Muscle Cells. Am J Med Sci. 2016 Jul;352(1):71-9.
28. Siwiak M, Edelman A, Zielenkiewicz P. Structural models of CFTR-AMPK and CFTR-PKA interactions: R-domain flexibility is a key factor in CFTR regulation. J Mol Model. 2012 Jan;18(1):83-90.
29. Mihaylova MM, Shaw RJ. The AMPK signaling pathway coordinates cell growth, autophagy and metabolism. Nat Cell Biol. 2011 Sep 2;13(9):1016-23.
30. Alpini G, Glaser S, Robertson W, *et al.* Large but not small intrahepatic bile ducts are involved in secretin-regulated ductal bile secretion. Am J Physiol. 1997 May;272(5 Pt 1):G1064-74.
31. Rimland CA, Tilson SG, Morell CM, *et al*. Regional Differences in Human Biliary Tissues and Corresponding In Vitro-Derived Organoids. Hepatology. 2021 Jan;73(1):247-267.
32. Kelly DA, Davenport M. Current management of biliary atresia. Arch Dis Child. 2007 Dec;92(12):1132-5.
33. Karimian N, Op den Dries S, Porte RJ. The origin of biliary strictures after liver transplantation: is it the amount of epithelial injury or insufficient regeneration that counts? J Hepatol. 2013 Jun;58(6):1065-7.
34. Chapman R, Cullen S. Etiopathogenesis of primary sclerosing cholangitis. World J Gastroenterol. 2008 Jun 7;14(21):3350-9.
35. Rodrigues PM, Perugorria MJ, Santos-Laso A, *et al.* Primary biliary cholangitis: A tale of epigenetically-induced secretory failure? J Hepatol. 2018 Dec;69(6):1371-1383.
36. Kunzelmann K, Schreiber R, Hadorn HB. Bicarbonate in cystic fibrosis. J Cyst Fibros. 2017 Nov;16(6):653-662.
37. Alasbahi RH, Melzig MF. Forskolin and derivatives as tools for studying the role of cAMP. Pharmazie. 2012 Jan;67(1):5-13.
38. Chang JC, Go S, de Waart DR, *et al.* Soluble Adenylyl Cyclase Regulates Bile Salt-Induced Apoptosis in Human Cholangiocytes.Hepatology. 2016 Aug;64(2):522-34.
39. Nunes AR, Holmes AP, Sample V, *et al.* Bicarbonate-sensitive soluble and transmembrane adenylyl cyclases in peripheral chemoreceptors. Respir Physiol Neurobiol. 2013 Aug 15;188(2):83-93.

40. Kalogeris T, Baines CP, Krenz M, *et al.* Cell biology of ischemia/reperfusion injury. Int Rev Cell Mol Biol. 2012;298:229-317.
41. de Vera ME, Lopez-Solis R, Dvorchik I, *et al.* Liver transplantation using donation after cardiac death donors: long-term follow-up from a single center. Am J Transplant. 2009 Apr;9(4):773-81.

Supplementary Information

Materials and Methods

Human liver material and organoid culturing

Intrahepatic cholangiocyte organoids (ICOs) were cultured from small liver biopsies (0.5-1.0 cm^3, n=15) collected from donor livers used for LT at the Erasmus MC, according to the protocol established by Huch *et al.*[1] The medical ethical committee (MEC) approval for this research was provided by the Erasmus MC medical ethical committee (MEC-2014-060).

For this, biopsies (0.5-1.0 cm^3) were digested using a collagenase solution in (2.5 mg/mL collagenase A1, Roche) EBBS (Hyclone, Thermoscientific) for 30 min at 37 ˚C. Digestion was stopped by adding cold Advanced (Adv)DMEM/F12 (supplemented with 1% penicillin/streptomycin, Life Technologies; 1% Hepes 1 M, Fisher Scientific; 1% Ultra-glutamine 200mM, Fisher Scientific and 0.2% Primocin, Invivogen) and filtered through a 70 µm Nylon cell strainer. The cell suspension was spun down for 5 minutes, 4˚C at 453g. Pellet was harvested and mixed with Matrigel (Corning Incorporation) or Basement Membrane Extract (BME) (Cultrex) and specific medium was added according to protocol.[2] Medium was changed twice a week and organoids were passaged in a 1:2-1:8 ratio according to growth. Cultures were negative for mycoplasma contamination (data not shown). All experiments were performed with ICO organoid cultures between passage six and ten.

RNA expression profiling for microarray and microarray analysis

Total RNA was isolated from ICOs using the miRNEAsy mini kit (Qiagen, Hilden, Germany) according to the manufacturer's protocol and eluted in 30 µL of RNAse-free water. RNA concentration and integrity were determined using a Nanodrop 2000 (Thermo Fisher Scientific, Waltham MA, USA) and a Bioanalyzer 2100 (Agilent Technologies, Santa Clara CA, USA), respectively. A total of 300 ng RNA was reversed transcribed, amplified and biotin-labeled using the Illumina TotalPrep RNA Amplification Kit (Ambion-Life Technologies, Carlsbad CA, USA) according to the manufacturer's guidelines. HumanHT-12 v4 Expression BeadChips (Illumina, San Diego CA, USA) were overnight hybridized with 750 ng cRNA, washed, stained and scanned on an iScan and analyzed using GenomeStudio V2011.1 software (both from Illumina, Inc.). Bead types missing in one or more arrays were excluded and the resulting non-normalized raw probe data set was combined with the raw probe information from the ArrayExpress E-MTAB-4591 data[3], containing embryonic stem cells (ES), freshly plated hepatocytes, primary cholangiocytes and Extrahepatic Cholangiocyte Organoids (ECOs).[3] ECOs from P10 (ECOs_A-C) and from P20 (ECOs_D-F) were combined to one group: ECOs_A-F. The file, describing, for each probe, AVG_Signal and Detection Pval, was loaded into R using the limma package by Ritchie *et al.*[4]. Probes that were present at least once (Detection Pval <0.01) were considered as being expressed (26,120 probes) and

used for further analysis. Following filtering, the data were background subtracted, normalized and log2 transformed using the vsn package.[5] Principal component analysis (PCA) and heatmaps were conducted in R using the prcomp and heatmap.2 functions, respectively. Heatmap- selected genes for hepatocytes and cholangiocytes markers were based on supplementary Figure 6C, Sampaziotis *et al.*[6].

Ussing chamber set-up

ICOs from 20, 25µL hydrogel droplets were collected in Advanced (Adv)DMEM/F12, centrifuged (453g, 5 min, 4˚C) and the supernatant was removed. Cells were mechanically broken by vigorously pipetting up and down and spun down again. Organoids were made single cell by Trypsin-EDTA incubation for 25 to 40 min, at 37°C. Cells were washed in AdvDMEM/F12 and put through a cell 70µm cell strainer. Approximately $3*10^5$ cells were resuspended in 200 µm AdvDMEM/F12-based expansion medium[2] and seeded on transwell inserts (24 well plate 6.5 mm, Corning), precoated with 5% Matrigel in PBS. Medium was changed twice weekly. To check confluence, electrophysiological analysis was performed after 4 days and the cells were examined under the microscope daily.

The confluent transwells were placed in a Ussing chamber set up[7] to analyze functionality of cholangiocyte-specific transporter channels (CFTR and Ca^{2+} activated Cl^- channel) using Acquire & Analyze Software 2.3 (Physiologic Instruments, San Diego, California) or LabChart 8.1.13 (ADinstruments, Sydney, Australia) and if LabChart was used, graphs were subsequently created in Microsoft Excel (Microsoft, Redmond, USA). The temperature of the chambers in the set up was kept 37 °C by warm water bath circulation. Each chamber, of a total of 4, was filled with 3 mL modified Meyler solution (128 mmol/liter NaCl, 4.7 mmol/liter KCl, 1.3 mmol/liter $CaCl_2$, 1.0 mmol/liter $MgCl_2$, 0.3 mmol/liter Na_2HPO_4, 0.4 mmol/liter NaH_2PO_4, 20 mmol/liter $NaHCO_3$, 10 mmol/liter HEPES, supplemented with glucose (10 mmol/liter) at pH 7.3). In case cells were analysed in chloride-free conditions, chloride-free Meyler solution was used (130 mmol/liter $C_2H_5NaO_4S$, 4.7 mmol/liter KNO_3, 20 mmol/liter $NaHCO_3$, 1.3 mmol/liter $C_4H_6O_4Ca$, 1 mmol/liter $MgSO_4$ and 10 mmol/liter HEPES, supplemented with glucose (10 mmol/liter)). Under oxygen conditions ICOs were exposed to 95%O_2, 5%CO_2. Hypoxic conditions were achieved by exposing ICOs to 95%N_2, 5%CO_2. In some experiments, the conditions were switched during the experiment from hypoxic to oxygen. Current was clamped and the short circuit current (Isc) was recorded every second. Two 5 millivoltage (mV) pulses were given initially to measure transepithelial endothelial resistance (TEER) along the epithelial layers (V=I*R). TEER without cells were subtracted from TEER with cells. CFTR-dependent anion secretion was activated by adding 10 µM Forskolin to both sides of the ICOs and inhibited by addition of GlyH-101 (20 µM, apical side). Calcium (Ca^{2+}) activated chloride (Cl^-) channels (CaCC) or anoctamin-1 (ANO1) were stimulated by UTP (50 µM, apical side) and inhibited by T16Ainh-A01 (50 µM, apical side). To block the uptake of Cl^- by cells via the Na-K-Cl co-transporter-1 (NKCC1) 50 µM bumetanide was added to the

basolateral side. To maintain CFTR-activity intact under hypoxic conditions we selected Compound-C (which is a known AMP kinase-inhibitor)[8] as a candidate drug. Compound-C (10 μM) was added to the apical side of the cells under oxygen conditions, 15 minutes before switching to hypoxia. The complete list of reagents used is displayed in Table S2.

Results

Table S1. List of genes and primers used.

Gene	Primer sequence (5' à 3')	
SLC4A2/AE2	F	ACCCTCATGTCAGACAAGCAA
	R	TCCTCTCGCTTCTTGAGCATC
ALB	F	CTGCCTGCCTGTTGCCAAAGC
	R	GGCAAGGTCCGCCCTGTCATC
ANO1	F	CTCCTGGACGAGGTGGTATGG
	R	GAACGCCACGTAAAAGATGG
AQP1	F	GGCCAGCGAGTTCAAGAAGAA
	R	TCACACCATCAGCCAGGTCAT
ASBT	F	GCCCCAAAAAGCAAAGATCA
	R	GCTATGAGCACAATGAGGATGG
CFTR	F	CCTTGTCCATTTTCCTTGTG
	R	GAGGAGGGTAAGAAGCTTGG
KRT7	F	GGGGACGACCTCCGGAATAC
	R	CTTGGCACGCTGGTTCTTGA
KRT19	F	CGCGGCGTATCCGTGTCCTC
	R	AGCCTGTTCCGTCTCAAACTTGGT
Cyp3a4	F	TGTGCCTGAGAACACCAGAG
	R	GTGGTGGAAATAGTCCCGTG
GAPDH	F	AGAAGGCTGGGGCTCATTTG
	R	AGGGGCCATCCACAGTCTTC
HIF-1α	F	TGCTCATCAGTTGCCACTTC
	R	TCCTCACACGCAAATAGCTG
NKCC1	F	ACCAAGGATGTGGTAGTAAGTGTGG
	R	GGATTCTTTTTTCAACAGTGGTTGA

Table S2. Reagents used in Ussing Chamber Assay.

Reagent	Concentration	Company	Cat Number
Forskolin	10 µM	Sigma	F6886
GlyH-101	20 µM	Calbiochem	219671
UTP	50 µM	Sigma	94370
T16A-A01	50 µM	Tocris	4538
Compound-C	10 µM	Calbiochem	CAS 66405-64-3
Bumetanide	50 µM	Sigma	B3023

Table S3. Donor demographics corresponding to the bile which was collected from patients via ERCP.

Amount of bile collected (mL)	Underlying disease	Age (years)	Gender	UDCA Usage
7	Papiladenoma	54	F	-
4	AS	50	M	-
3.5	AS	20	M	-
6	AS	57	F	-
7	Bile stones	26	F	-

Abbreviations: AS: Anastomotic bile duct Stricture after Liver Transplantation, F: Female, M: Male, UDCA: Ursodeoxycholic acid

Characterization of the pooled bile sample: Cholesterol: 0.9 mM (0.5-10.3mM)[9,10] Triglyceriden: 0.2 mM, pH: 7.65 (7.5-8.05)[11]

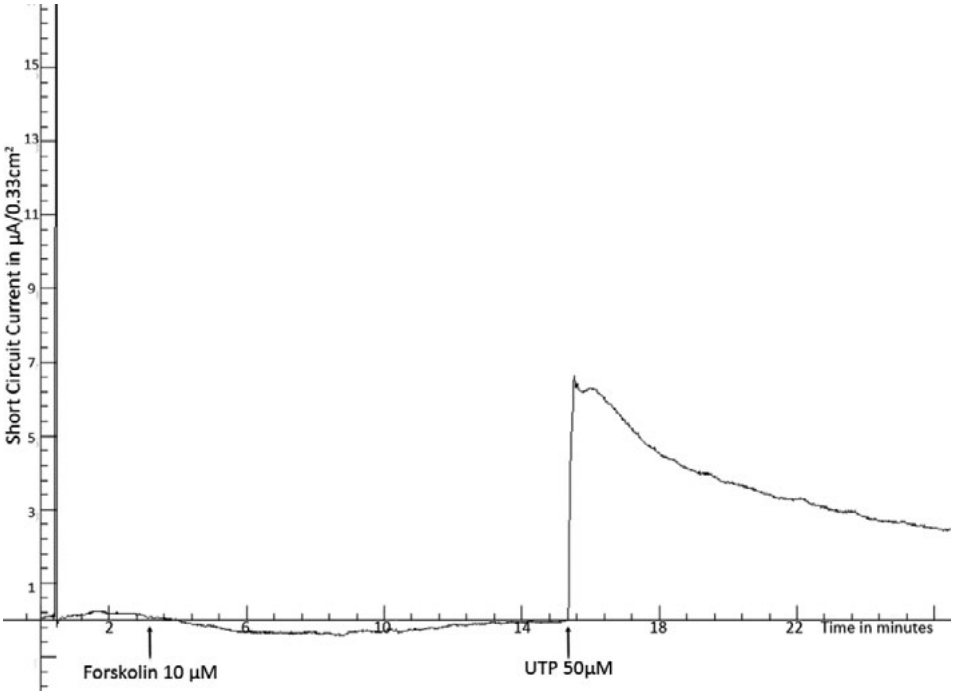

Figure S1. cAMP-activator (forskolin) gives no response in Isc in a patient without functional CFTR. Isc represent a monolayer of ICO-derived cells from a patient without functional CFTR (cystic fibrosis heterozygous mutation F508del and R1162X). As displayed, upon forskolin addition no increase in Isc is observed, in line with a dysfunctional CFTR-channel. In contrast upon UTP addition a rapid increase in Isc due to ANO1 activation is observed. Indicating that within this experimental set-up, forskolin stimulation only is capable of directly activating CFTR and not ANO1.

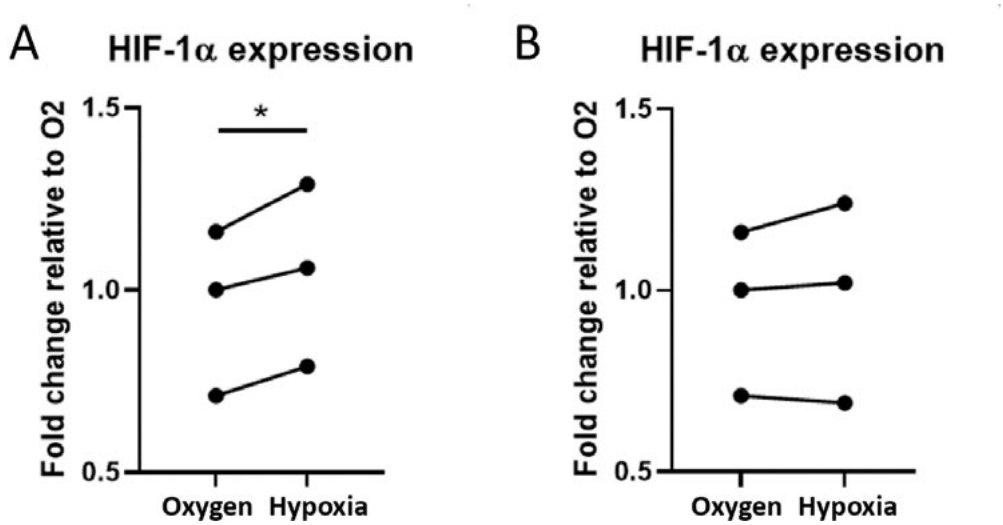

Figure S2. Hypoxic conditions are reached by exposing cells to nitrogen/carbon dioxide gas.
(a) Gene expression of hypoxia induced factor (HIF)-1α as measured by qRT-PCR on ICO monolayers exposed to either gas with oxygen or without oxygen (hypoxia group), both groups n=3, individual biological samples. HIF-1α is upregulated after one hour of hypoxia in comparison to one hour of oxygen according to fold change (Mann-Whitney-U, p=0.05). **(b)** Gene expression of HIF-1α as measured by qRT-PCR on ICO monolayers (n=3, individual biological samples) exposed to either oxygen (one hour) or 30 minutes of hypoxia.

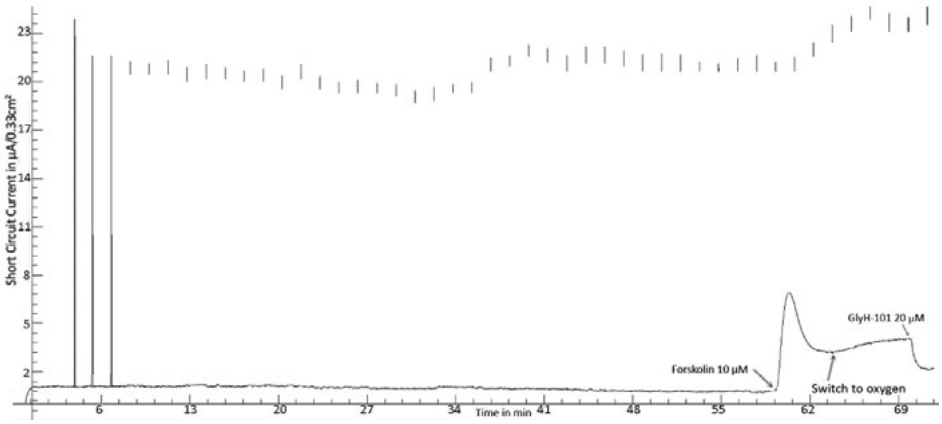

Figure S3. Without bile, long-term hypoxia exposure does not change electrical resistance/barrier function.

Organoids cultured as ICO monolayers exposed to one hour of hypoxia with 5 mV pulses resulting in current spikes every 90 seconds. After one-hour forskolin was added and waited for a plateau-phase, next the cells were exposed to oxygen resulting in a clear increase in current which could still be inhibited by GlyH-101. Comparing TEER at T=5 minutes (92.08Ω*cm^2) and T=60 minutes (88.33Ω*cm^2) showing that long-term exposure to hypoxia does not lead to a significant loss in electrical resistance.

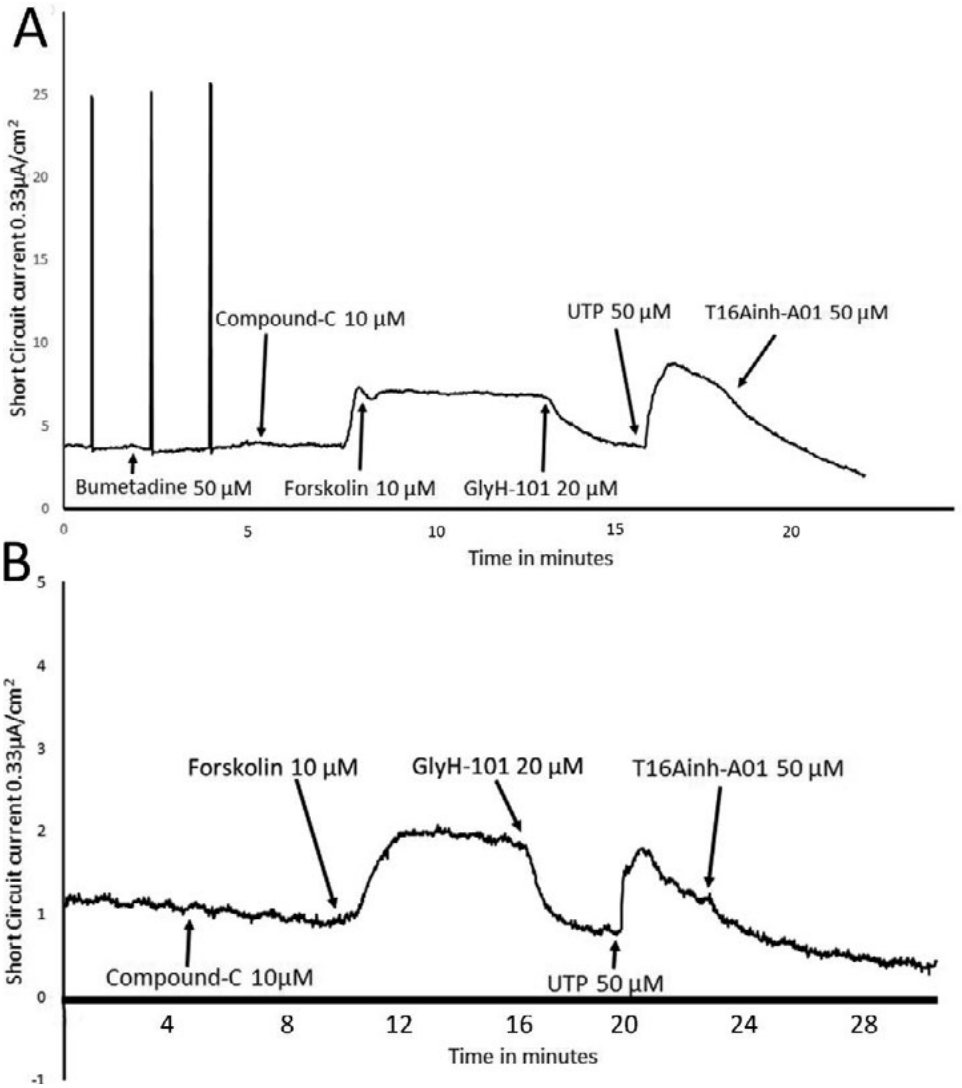

Figure S4. Compound-C exposure does not influence ion-transport on ICO monolayers.
(a) Blocking basolateral chloride-influx via Sodium-Potassium-Chloride-Cotransporter (NKCC)-1 via bumetanide, prior to compound-C addition, results in similar forskolin-stimulated Isc as observed without exposure to compound-C (Figure 3A). Interestingly, the UTP-response was also similar to the response without compound-C, but with bumetamide addition, as shown in Figure 3A, indicating that compound-C does not influence chloride secretion. **(b)** ICO monolayer as measured under chloride-free conditions. Stimulation by forskolin, after compound-C addition, causes increased Isc, while GlyH-101 is still capable of decreasing short-circuit current activity. Similarly, UTP stimulation increases Isc in similar fashion without compound-C addition (Figure 3C), indicating bicarbonate -dependent CFTR- and ANO1-activity on ICO monolayers while being exposed to compound-C.

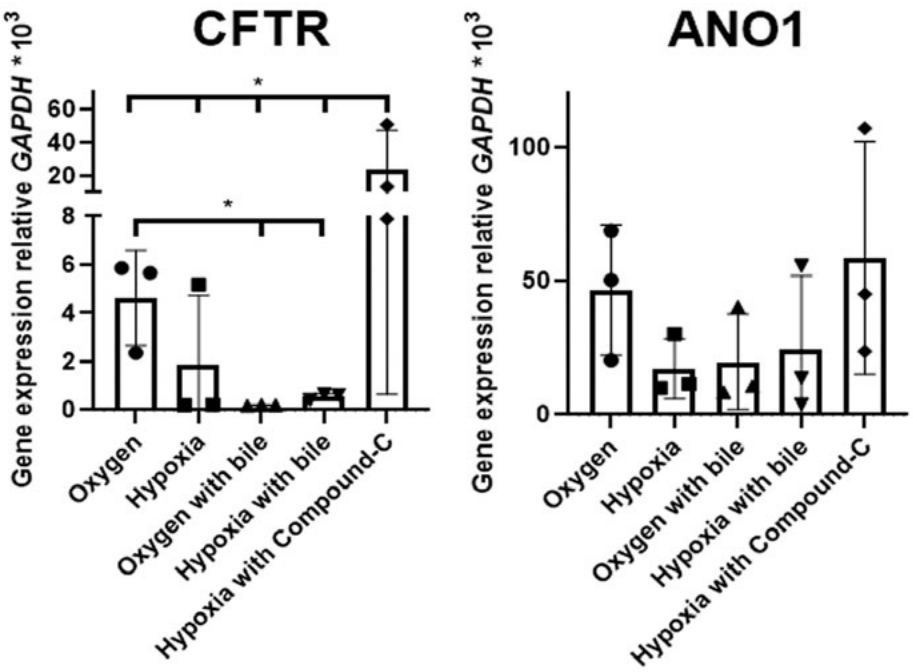

Figure S5. Compound-C stimulates CFTR gene expression.

Gene expression levels of CFTR and ANO1 relative to the housekeeping gene GAPDH $*10^3$ as analysed by qRT-PCR on ICO monolayers (n=3, individual biological samples) under different conditions. *Indicates significant difference ($p<0.05$).

References

1. Huch M, Gehart H, van Boxtel R, *et al.* Long-term culture of genome-stable bipotent stem cells from adult human liver. Cell. 2015 Jan 15;160(1-2):299-312.
2. Broutier L, Andersson-Rolf A, Hindley CJ, *et al.* Culture and establishment of self-renewing human and mouse adult liver and pancreas 3D organoids and their genetic manipulation. Nat Protoc. 2016 Sep;11(9):1724-43.
3. Sampaziotis F, Justin AW, Tysoe OC, *et al.* Reconstruction of the mouse extrahepatic biliary tree using primary human extrahepatic cholangiocyte organoids. Dataset: ArrayExpress Data, E-MTAB-4591, 2017.
   https://www.ebi.ac.uk/arrayexpress/experiments/E-MTAB-4591/
4. Ritchie ME, Phipson B, Wu D, *et al.* limma powers differential expression analyses for RNA-sequencing and microarray studies. Nucleic Acids Res. 2015 Apr 20;43(7):e47.
5. Huber W, von Heydebreck A, Sültmann H, *et al.* Variance stabilization applied to microarray data calibration and to the quantification of differential expression. Bioinformatics. 2002;18 Suppl 1:S96-104.
6. Sampaziotis F, Justin AW, Tysoe OC, *et al.* Reconstruction of the mouse extrahepatic biliary tree using primary human extrahepatic cholangiocyte organoids. Nat Med. 2017 Aug;23(8):954-963.
7. Li H, Sheppard DN, Hug MJ. Transepithelial electrical measurements with the Ussing chamber. J Cyst Fibros. 2004 Aug;3 Suppl 2:123-6.
8. Liu X, Chhipa RR, Nakano I, *et al.* The AMPK inhibitor compound C is a potent AMPK-independent antiglioma agent. Mol Cancer Ther. 2014 Mar;13(3):596-605.
9. Boyer JL. Bile formation and secretion. Compr Physiol. 2013 Jul;3(3):1035-78.
10. Keulemans YC, Mok KS, de Wit LT, *et al.* Hepatic bile versus gallbladder bile: a comparison of protein and lipid concentration and composition in cholesterol gallstone patients. Hepatology. 1998 Jul;28(1):11-6.
11. Sutor DJ, Wilkie LI. Diurnal variations in the pH of pathological gallbladder bile. Gut. 1976;17(12):971-974.

4

CHAPTER 4

Rescue of chloride and bicarbonate transport by elexacaftor-ivacaftor-tezacaftor in organoid-derived CF intestinal and cholangiocyte monolayers.

Marcel JC Bijvelds, Floris JM Roos, Kelly F Meijsen, Henk P Roest, Monique MA Verstegen, Hetty M Janssens, Luc JW van der Laan, Hugo R de Jonge

Journal of Cystic Fibrosis 2021 Dec 15:S1569-1993(21)02165-2.

Abstract

Background. In cystic fibrosis (CF), loss of CF transmembrane conductance regulator (CFTR)-dependent bicarbonate secretion precipitates the accumulation of viscous mucus in the lumen of respiratory and gastrointestinal epithelial tissues. We investigated whether the combination of elexacaftor (ELX), ivacaftor (IVA) and tezacaftor (TEZ), apart from its well-documented effect on chloride transport, also restores Phe508del-CFTR-mediated bicarbonate transport.

Methods. Epithelial monolayers were cultured from intestinal and biliary (cholangiocyte) organoids of homozygous Phe508del-CFTR patients and controls. Transcriptome sequencing was performed, and bicarbonate and chloride transport were assessed in the presence or absence of ELX/IVA/TEZ, using the intestinal current measurement technique.

Results. ELX/IVA/TEZ markedly enhanced bicarbonate and chloride transport across intestinal epithelium. In biliary epithelium, it failed to enhance CFTR-mediated bicarbonate transport but effectively rescued CFTR-mediated chloride transport, known to be requisite for bicarbonate secretion through the chloride-bicarbonate exchanger AE2 (SLC4A2), which was highly expressed by cholangiocytes. Biliary but not intestinal epithelial cells expressed an alternative anion channel, anoctamin-1/TMEM16A (ANO1), and secreted bicarbonate and chloride upon purinergic receptor stimulation.

Conclusions. ELX/IVA/TEZ has the potential to restore both chloride and bicarbonate secretion across CF intestinal and biliary epithelia and may counter luminal hyper-acidification in these tissues.

Introduction

Accumulation of viscous mucus in the respiratory, intestinal, and biliary tract is a hallmark of cystic fibrosis (CF) and is the primary cause of defective mucociliary clearance in the airways and of luminal obstruction in gastrointestinal epithelia.[1-4] It was shown that proper unfolding of mucins, the polymeric glycoproteins that form the main constituent of mucus in these tissues, requires concurrent bicarbonate secretion.[4,5] Bicarbonate is transported by the CF-gene encoded cystic fibrosis transmembrane conductance regulator (CFTR) channel and by chloride-bicarbonate exchangers that are functionally coupled to CFTR.[6] In the absence of bicarbonate secretion, the mucins released by the epithelium remain densely packed and attached to the epithelial surface.

Despite the evident importance of the loss of CFTR-dependent bicarbonate transport in the pathophysiology of CF, and in contrast to the plethora of studies investigating the chloride transport defect, few studies have specifically addressed the rescue of bicarbonate transport.[7] Indeed, most functional CFTR assays currently used for diagnostic and surveillance purposes, e.g. measurement of sweat chloride, forskolin-induced swelling, intestinal current measurement (ICM) and nasal potential difference, solely measure chloride or do not discriminate between chloride and bicarbonate transport. This distinction may be of importance because molecular modeling of CFTR has indicated that access of bicarbonate and chloride to the channel pore may proceed through separate routes in the inner vestibule.[8] Consequently, it is conceivable that conformational changes in this region affect bicarbonate and chloride transport differently. Congruently, it has been shown that modulator drugs, i.e. small-molecule compounds that aim to restore mutant CFTR function by changing protein folding and/or conformation, may have different effects on chloride vs. bicarbonate transport.[9]

CFTR is highly expressed in the intestinal epithelium, and in the liver, it is expressed exclusively in the biliary tree.[10-12] Both these epithelial tissues secrete bicarbonate as well as chloride, stimulated by hormones that trigger cyclic AMP-dependent protein kinase-mediated phosphorylation of CFTR.[10,13] In both tissues, hyper-acidification of the luminal surface, resulting from loss of CFTR-dependent bicarbonate secretion, is thought to play a key role in the CF-typical accumulation of viscous mucus, luminal obstruction, and inflammation.[1-4] Intestinal disease affects most CF patients from an early age, whereas, in contrast, cholangiopathies develop more gradually, and overt liver disease is a late and more sporadic manifestation of CF.[3,11] This may explain why few studies have addressed the effect of CFTR modulators on biliary function.[12,14] However, in view of the changing demographics of CF, effective management of liver disease is becoming increasingly important and such studies seem warranted.

In the present study we asked to what extent a combination of 3 CFTR modulators elexacaftor (ELX), ivacaftor (IVA) and tezacaftor (TEZ), which has been shown to restore anion channel function and to improve clinical outcome in CF patients carrying the Phe508del allele, restores bicarbonate and chloride transport across intestinal and biliary CF epithelia.[15,16] For this purpose, we cultured intestinal and cholangiocyte organoids from tissue of homozygous Phe508del-CFTR patients and assessed the effect of this drug combination on chloride and bicarbonate transport across epithelial monolayers, using a modified ICM protocol.

Materials and Methods

Organoid culture

Organoids, produced from ileal biopsies of a CF patient (homozygous Phe508del-CFTR) and non-CF control, were initiated and cultured routinely in culture medium containing the growth factors Wnt3a, Noggin, R-Spondin 1 and epidermal growth factor (EGF) in Matrigel (Corning) matrix, according to established protocols.[17] Intrahepatic cholangiocyte organoids (ICO) were cultured from liver explant tissue of a CF patient (homozygous Phe508del-CFTR) and tissue of deceased non-CF donors. ICO were initiated and routinely cultured in growth medium containing the growth factors R-Spondin 1, EGF and DKK1 in basement membrane extract matrix (BME; Cultrex), according to protocols described in detail elsewhere.[18] To stimulate growth of CF organoids, the ICO culture medium was supplemented with forskolin (2 µmol/L; Sigma-Aldrich). Organoid cultures were passaged on a weekly basis at a 1:2-1:8 ratio, depending on the rate of expansion. All cultures used were regularly checked for and found to be free of mycoplasma contamination. Tissue donors or their next of kin consented to tissue collection and the study was approved by the institutional review board of the Erasmus MC (MEC-2014-060).

Seeding of epithelial monolayers

For culture of epithelial monolayers, extracellular matrix-embedded, intestinal and biliary organoids were suspended in advanced DMEM (4°C; Gibco) and washed by centrifugation (5 min, 1.500 g) to remove the matrix. Intestinal organoids were dissociated by brief (45 sec., 37°C) incubation in trypsin (0.25%) solution (Gibco), followed by repeated (30x) aspiration through a 200 µL pipette tip (Greiner). Biliary organoids were, similarly, dissociated by repeated aspiration through a pipette tip, but in the absence of trypsin. Dissociation was monitored by microscopy (Zeiss Primovert, final magnification: 40x), and the above procedure was repeated until most organoids had dissociated into small cell clusters. For intestinal preparations, trypsin activity was quenched by addition of fetal calf serum (10%) in advanced DMEM, and cells were washed in advanced DMEM and filtered through a cell strainer (70 µm; Falcon). Both intestinal and biliary cells were finally collected by centrifugation and suspended in complete organoid culture medium, supplemented with CHIR99021 (10 µmol/L; Sigma-Aldrich) and Y-27632 (10 µmol/L; R&D Systems). Cells were counted using a hemocytometer and seeded (intestinal: $6*10^5$; biliary $7.5*10^5$ cells/cm^2) on permeable inserts (Transwell #3470; Corning) that had been pretreated with diluted Matrigel (1:20 in phosphate buffered saline, 0.2 mL/cm^2, 2 hours, 37°C). Culture medium was as for extracellular matrix-embedded organoids, except that CHIR99021 and Y-27632 were added during the first two days after seeding of intestinal cultures, and that forskolin was absent from the medium of biliary cultures. Cells were cultured until a confluent monolayer was obtained (10-14 days). For assessing the formation of a continuous epithelial monolayer,

cultures were examined by microscopy and the transepithelial electrical resistance was monitored using chopstick electrodes (EVOM2; World Precision Instruments).

Transcriptome sequencing and analysis

Organoid-derived epithelial monolayers were transferred to QIAzol lysis reagent (Qiagen) and RNA was extracted using the miRNeasy kit (Qiagen) as reported elsewhere. Transcriptome sequencing was performed at the Beijing Genomics Institute (BGI). In brief, after RNA integrity was verified (RIN >9.0; Agilent 2100 Bioanalyzer), mRNA (200 ng) was isolated from total RNA (Truseq RNA sample preparation kit; Illumina), fragmented and subsequently used for cDNA synthesis (Superscript II cDNA synthesis kit; Invitrogen). End-repaired cDNA was purified (Agencourt Ampure XP beads; Beckman Coulter) and amplified by PCR. The resulting cDNA library was sequenced using an HiSeq 2000 sequencer and TruSeq SBS Kit v3-HS reagent kit (Illumina) resulting in 22-28 million, 100 nucleotides long, paired-end reads. Sequencing data were uploaded to the Galaxy Web platform public server usegalaxy.org quality checked with FASTQC, adapter trimmed (Cutadapt v1.16.5) and mapped using HISAT2 (v2.1.0.) against the human reference genome GRCh38. Mapped reads were converted to counts using FeatureCounts (v2.0.1) applying the built-in hg38 genome annotation file, and RPKM normalized.

Electrophysiological assessment of epithelial anion transport

CF and non-CF monolayers were incubated with ELX (VX-445, 3 µmol/L; MedChem Express), IVA (VX-770; 0.3 µmol/L; SelleckChem) and TEZ (VX-661, 3 µmol/L; SelleckChem), or vehicle (DMSO, 0.2%) for 20 hours. Subsequently, filters were mounted in Ussing chamber sliders (P2302T; Physiologic Instruments, San Diego) and inserted in P2300 type Ussing chambers (Physiologic Instruments). The monolayers were bathed in either of 3 solutions. (1) To assess combined chloride and bicarbonate transport, Meyler solution (mmol/L: 128 NaCl, 4.7 KCl, 1.3 $CaCl_2$, 1.0 $MgCl_2$, 20 $NaHCO_3$, 0.4 NaH_2PO_4, 0.3 Na_2HPO_4, 10 HEPES, 10 glucose) was used. (2) For assessing chloride transport, a similarly formulated solution was used, except that $NaHCO_3$ was replaced by Na-isethionate. The pH of this solution was set at 7.35 by titration with NaOH. The only CFTR-permeating anion in this solution is chloride. (3) For assessing bicarbonate transport, NaCl was replaced by Na-isethionate, KCl by KNO_3, and $CaCl_2$ and $MgCl_2$ by the acetic acid salts of these metal ions. The only physiologically relevant CFTR substrate in this solution is bicarbonate. Osmolality of the bathing solutions was assessed before experimentation and ranged between 304-312 osmole/kg. The appropriate CFTR modulator combinations (or vehicle) were added and solutions were maintained at 37°C, gassed with 95% O_2, 5% CO_2 or O_2 only (in case a bicarbonate-free solution was used). The transepithelial potential difference was clamped at 0 mV with a VVC-MC8 voltage clamp module (Physiologic Instruments), and the resulting short-circuit current (Isc) was recorded using a PowerLab 8/35 AD converter (AD instruments) and associated software (LabChart 8;

AD Instruments). CFTR-mediated Isc responses in organoid-derived monolayers were stimulated by addition of forskolin (10 µmol/L). CFTRinh172 (20 µmol/L; SelleckChem) was used to block CFTR activity and UTP (50 µmol/L; Sigma) was added to the luminal (apical) bath to stimulate Ca^{2+}-dependent chloride channels (CaCC).

Statistical analysis

Data are represented as means ± standard error. Differences between means were statistically analyzed by ANOVA, using the Sidak correction to control for multiple comparisons, except for the effect of T16Ainh-A01 which was statistically evaluated using Student's t-test (Prism 9; Graphpad software).

Results

Expression of ion transporters in biliary vs. intestinal epithelial monolayers

Gene expression was analyzed by transcriptome sequencing of representative CF and non-CF monolayer cultures of cholangiocyte and intestinal organoids (Fig. 1). Congruent with functional assays (see below), *CFTR* was robustly expressed in both intestinal and biliary epithelial monolayers, whereas only the latter contained a significant transcript number of the CaCC anoctamin-1/TMEM16A (*ANO1*). Both intestinal and biliary cells expressed the purinergic receptors $P2Y_1$ (*P2RY1*) and $P2Y_2$ (*P2RY2*). AE2 (*SLC4A2*), which is situated at the basolateral pole in intestinal cells, but mediates apical bicarbonate efflux in cholangiocytes, was ubiquitously expressed in both intestinal and biliary monolayers. Cholangiocytes also expressed the chloride-bicarbonate exchanger AE3 (*SLC4A3*). In contrast to AE2, the chloride-bicarbonate exchangers DRA (*SLC26A3*) and PAT1 (*SLC26A6*) are in the apical membrane of enterocytes. Intriguingly, exceptionally high levels of *SLC26A3* transcript were detected in CF monolayers. Biliary monolayers of both genotypes expressed *SLC26A6* but contained negligible amounts of *SLC26A3* transcript. The sodium-potassium-chloride cotransporter (NKCC1; SLC12A2) and the sodium bicarbonate cotransporter 1 (NBCe1; SLC4A4) mediate cellular uptake of chloride and bicarbonate, respectively, across the basolateral membrane. In addition, both intestinal and biliary monolayers contain transcripts coding for another bicarbonate transporter, NBCn1 (SLC4A7). The major carbonic anhydrase in both cell types is CA9, but intestinal cells also contain low amounts of *CA1* and *CA2* transcripts. Members of the SLC9 family are sodium-proton exchangers that serve to counter acid loading.

ELX/IVA/TEZ partially restores Phe508del-CFTR-mediated chloride and bicarbonate transport in intestinal epithelial monolayers

The ICM technique was adapted to assess CFTR-dependent anion secretion across epithelial monolayers cultured from intestinal organoids.[19] In non-CF monolayers, forskolin elicited a robust Isc response that was blocked by CFTRinh172, indicating that the response is mediated by CFTR (Fig. 2A). Forskolin also elicited an Isc response when the assay was performed in media containing either only chloride or only bicarbonate as the CFTR-permeating anion, consistent with the notion that CFTR mediates both bicarbonate and chloride transport. However, the forskolin-mediated Isc response in bicarbonate medium amounted to only ca. one third of the response in chloride containing medium. In CF monolayers (homozygous Phe508del), the forskolin-mediated Isc responses were small, indicating low levels of residual CFTR activity (Fig. 2B, DMSO-treated). Treatment with the combination of ELX, IVA and TEZ (ELX/IVA/TEZ) significantly increased the forskolin-dependent Isc response of the CF monolayers, which reached levels amounting to ca. 50% of the response in organoids expressing wild type CFTR (Fig. 2B, 2C). ELX/IVA/TEZ enhanced both CFTR-mediated chloride and bicarbonate transport. The ratio of the Isc responses in chloride and bicarbonate medium

in ELX/IVA/TEZ-treated CF monolayers (3.3±0.3, n=6) was similar as in non-CF monolayers (3.6±0.2, n=6; Fig. 2D). In accordance with low ANO1 expression (Fig. 1), UTP did not elicit an appreciable Isc response in intestinal monolayers (not shown).

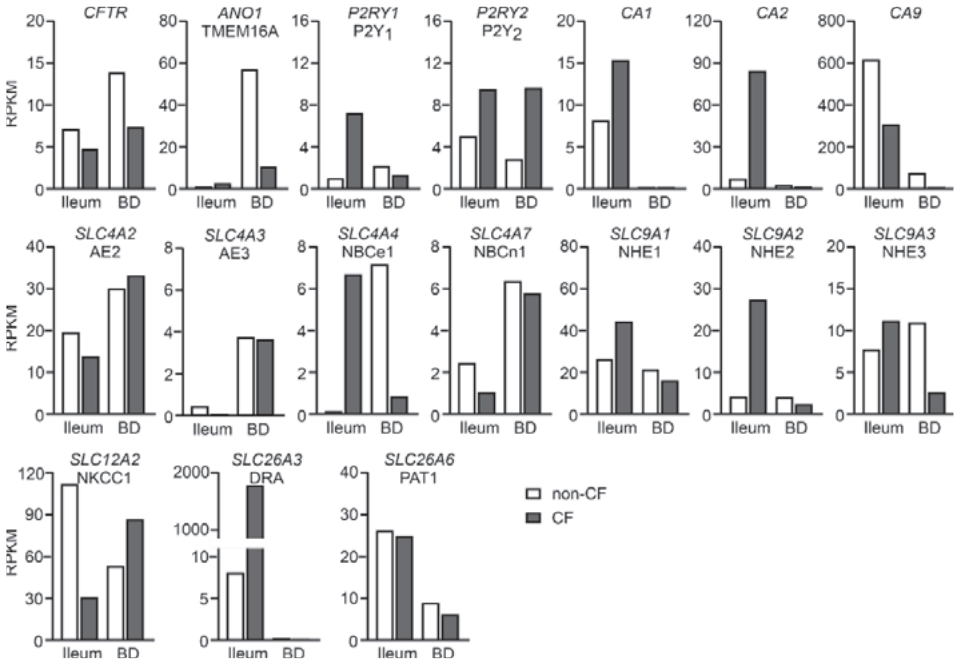

Figure 1. Expression of genes involved in transepithelial anion transport

Expression of genes involved in transepithelial anion transport in epithelial monolayers of organoids cultured from ileum or bile duct (BD) of CF and non-CF donors (n=1 per group). Transcript levels are visualized using normalized read counts (RPKM).

ELX/IVA/TEZ partially restores Phe508del-CFTR-mediated chloride transport in biliary epithelial monolayers

In non-CF biliary epithelial monolayers, forskolin elicited a highly transient Isc response that was followed by a substantially lower but more sustained response, amounting to 30-50% of the preceding peak Isc. Additional experiments showed that removal of chloride from the luminal bathing solution, led to a more sustained forskolin-dependent Isc response (Fig. 3A, middle panel). This suggests that in the presence of luminal chloride, the electrochemical driving force for anion extrusion is rapidly dissipated, putatively because of a comparatively low activity of chloride importers located in the basolateral plasma membrane. In non-CF biliary monolayers, other than in intestinal monolayers, the Isc response in bicarbonate medium exceeded the response in chloride medium. In CF monolayers, the forskolin-dependent Isc was considerably lower than in the non-CF specimens, but some CFTRinh172-

sensitive Isc response was apparent (Fig. 3B, DMSO-treated). ELX/IVA/TEZ markedly enhanced the forskolin-dependent Isc in CF monolayers when assayed in chloride-containing medium, whereas no statistically significant effect was observed when the assay solution contained only bicarbonate as the CFTR substrate (Fig. 3B, 3C).

UTP, through activation of purinergic receptors, stimulates biliary secretion through CaCCs, independent from CFTR.[20] Indeed, in biliary monolayers, in contrast to intestinal cells, luminal UTP elicited a substantial Isc response, which was blocked by the anoctamin-1 inhibitor T16Ainh-A01 (Fig. 3D). UTP-dependent chloride and bicarbonate secretory responses were similar in non-CF and CF monolayers (not treated with ELX/IVA/TEZ; Fig. 3E, 3F).

Because ELX/IVA/TEZ enhanced the forskolin-dependent Isc in CF monolayers only when assayed in chloride-containing medium, the ratio of the Isc responses in chloride and bicarbonate medium in ELX/IVA/TEZ-treated CF monolayers was substantially higher than in non-CF monolayers (Fig. 3G). In non-CF monolayers, the ratio of the Isc responses in chloride and bicarbonate medium after UTP stimulation was significantly higher than for the forskolin-dependent responses, and more similar to the ratio observed in CF monolayers (Fig. 3G).

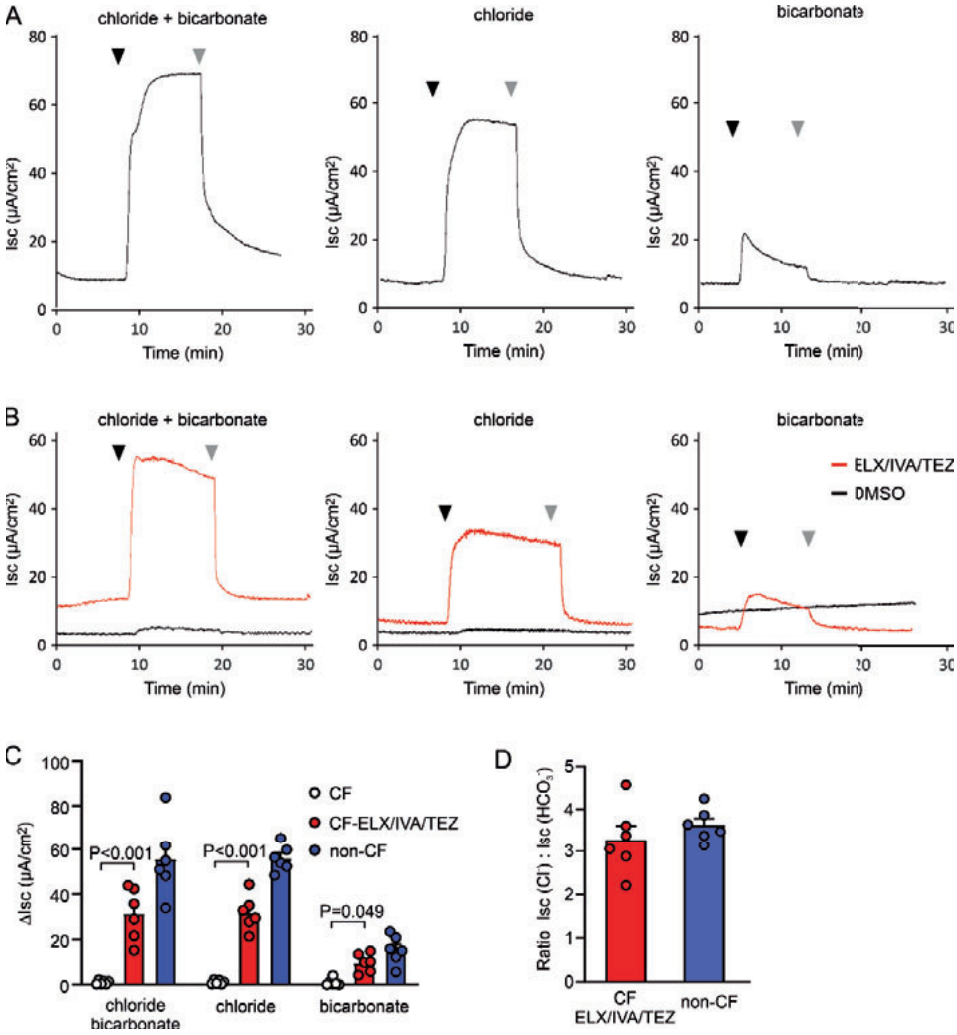

Figure 2. CFTR-mediated Isc responses of CF and non-CF intestinal epithelial monolayers.

CFTR-mediated Isc responses of CF and non-CF intestinal epithelial monolayers. Monolayers were bathed in medium containing both chloride and bicarbonate, only chloride, or only bicarbonate, as indicated. CF monolayers were assayed both in the presence or absence of ELX/IVA/TEZ. Forskolin was added (black arrowheads) to stimulate CFTR activity. Shaded arrowheads denote addition of CFTRinh172. **(a)** Representative examples of non-CF monolayers. **(b)** Representative examples of CF monolayers. **(c)** Aggregate data showing peak forskolin-dependent Isc responses. **(d)** Ratio of the forskolin-dependent Isc responses in chloride and bicarbonate medium. For both genotypes, organoids were derived from tissue of a single donor. Each data point represents one technical replicate (n=6 for each group).

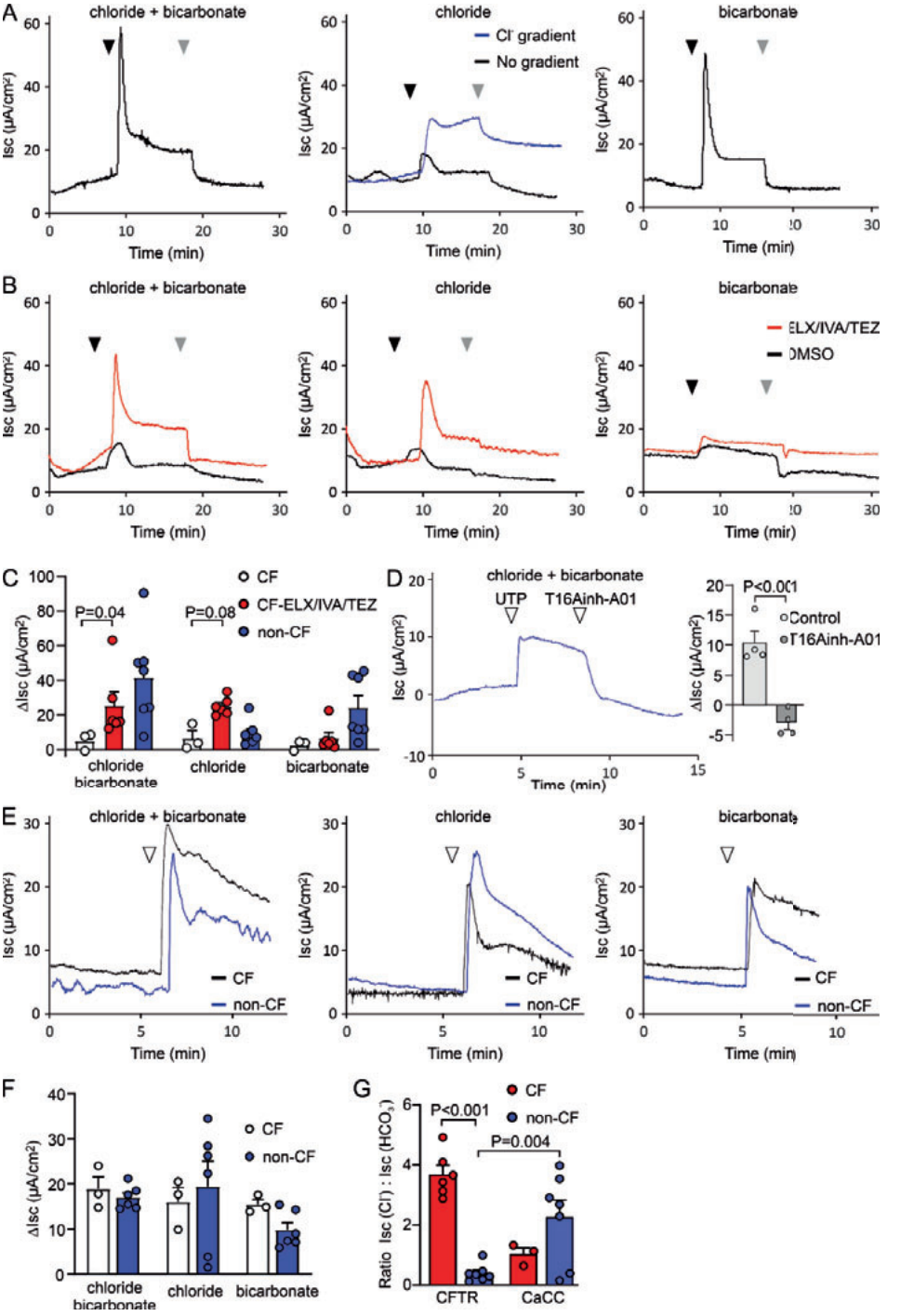
A
chloride + bicarbonate
chloride
Cl⁻ gradient
No gradient
bicarbonate
Isc (µA/cm²)
Time (min)
B
chloride + bicarbonate
chloride
bicarbonate
ELX/IVA/TEZ
DMSO
C
CF
CF-ELX/IVA/TEZ
non-CF
P=0.04
P=0.08
ΔIsc (µA/cm²)
chloride bicarbonate
chloride
bicarbonate
D
chloride + bicarbonate
UTP
T16Ainh-A01
P<0.001
Control
T16Ainh-A01
E
chloride + bicarbonate
chloride
bicarbonate
CF
non-CF
F
CF
non-CF
chloride bicarbonate
chloride
bicarbonate
G
CF
non-CF
P<0.001
P=0.004
Ratio Isc (Cl⁻) : Isc (HCO₃⁻)
CFTR
CaCC

Figure 3 CFTR- and UTP-mediated Isc responses of CF and non-CF biliary epithelial monolayers.
CFTR- and UTP-mediated Isc responses of CF and non-CF biliary epithelial monolayers. Monolayers were bathed in medium containing both chloride and bicarbonate, only chloride, or only bicarbonate, as indicated. Non-CF monolayers were also assayed in the absence of luminal chloride. CF monolayers were assayed both in the presence or absence of ELX/IVA/TEZ. Forskolin was added (black arrowheads) to stimulate CFTR activity. Shaded arrowheads denote addition of CFTRinh172. **(a)** Non-CF monolayers. **(b)** CF monolayers **(c)** Aggregate data of peak forskolin-dependent Isc responses. **(d)** Representative experiment showing the effect of UTP and subsequent addition of T16Ainh-A01 on the Isc response of non-CF monolayers. The bar graph depicts UTP-dependent Isc responses in the presence or absence of T16Ainh-A01. **(e)** UTP (arrowheads) was added to stimulate CaCC-mediated anion secretion across CF and non-CF monolayers. **(f)** Aggregate data of peak UTP-dependent Isc responses. **(g)** Ratio of the CFTR-mediated, forskolin- and CaCC-mediated, UTP-dependent Isc responses in chloride and bicarbonate medium. For CF monolayers, forskolin-dependent responses were assessed in the presence of ELX/IVA/TEZ. For both genotypes, organoids were derived from tissue of a single donor. Each data point represents one technical replicate (n=3-7 per group).

Discussion

In this study we show that ELX/IVA/TEZ partially restored Phe508del-CFTR function in primary cultures of CF intestinal and biliary epithelium. In intestinal epithelium, ELX/IVA/TEZ significantly increased both Phe508del-CFTR-mediated chloride and bicarbonate transport. In biliary epithelium, ELX/IVA/TEZ enhanced Phe508del-CFTR-mediated chloride transport but did not significantly improve bicarbonate transport. In contrast to intestinal cells, cholangiocytes displayed CFTR-independent, CaCC-mediated chloride and bicarbonate transport.

ELX and TEZ are small-molecule compounds that improve (co-translational) folding of the Phe508del-CFTR molecule. They bind to different regions of the nascent protein, and, when combined, increase the level of mature Phe508del-CFTR more than monotherapy with either compound.[16] ELX also acutely enhances Phe508del-CFTR-mediated chloride transport, indicating it also improves channel gating, which is further improved by IVA.[21] Administered in combination, these drugs were shown to improve CFTR-mediated chloride and fluid transport, and lung function in patients, even in those carrying only a single Phe508del allele.[15,16] However, it has not been ascertained whether this drug combination also enhances CFTR-dependent bicarbonate transport, required to counter CF-typical hyper-acidification of luminal surfaces and for detachment of mucus from the epithelial surface.[4,5] To answer this question, we assessed chloride and bicarbonate transport across epithelial monolayers derived from organoid cultures of CF (homozygous Phe508del) intestinal and biliary tissue. Other than in spheroids cultured in an extracellular matrix, both the basolateral (serosal) and the apical (luminal) compartment of such monolayer cultures are readily accessible, enabling ion substitution experiments to assess bicarbonate transport separately from chloride transport.

In intestinal monolayers, we found that ELX/IVA/TEZ partially restored both Phe508del-CFTR-mediated chloride and bicarbonate transport, whereas CFTR-mediated Isc responses were virtually absent in untreated CF monolayers. After treatment with ELX/IVA/TEZ, both the chloride- and bicarbonate-mediated Isc response dramatically increased, reaching ca. 50% of the response observed in non-CF monolayers. This resulted in a similar chloride over bicarbonate transport ratio as observed for wild type CFTR (Fig. 2D). This ratio is comparable with values reported in studies on intestinal and respiratory epithelium, in which similar electrophysiological assays were performed, using ion substitution to distinguish CFTR-mediated chloride and bicarbonate transport.[22,23] It also closely approximates previously reported estimates for the chloride over bicarbonate permeability ratio of CFTR.[24-26] Consequently, it appears that binding of the modulator compounds changes the conformation of Phe508del-CFTR such that its ion selectivity closely mimics that of the wild type channel. Previously, it was shown that the folding correctors lumacaftor (LUM; VX-809)

and TEZ (in the absence of ELX) decrease the chloride over bicarbonate permeability of Phe508del-CFTR expressed in FRT cells.[9] However, in contrast to the present study, this previous study assayed Phe508del-CFTR-mediated bicarbonate and chloride transport in the absence of IVA and ELX. Both these compounds improve the gating of the mutant channel, and it is conceivable that their co-application corrects putative effects of LUM or TEZ monotherapy on the relative bicarbonate and chloride conductance of the channel pore.[21] In fact, in our hands, LUM alone did not significantly enhance the forskolin-dependent Isc in CF monolayers, indicating that it cannot overcome the Phe508del-CFTR-typical gating defect in these patient-derived cells, possibly because they express low levels of CFTR in comparison to transfected FRT cells; LUM needs to be combined with a compound that restores CFTR channel gating, like IVA, to achieve an appreciable response.

ELX/IVA/TEZ also significantly enhanced CFTR-mediated anion secretion across biliary monolayers. It had a most pronounced effect on chloride transport, whereas it did not significantly enhance CFTR-mediated bicarbonate transport. However, cholangiocytes secrete bicarbonate mainly through an apically located electroneutral chloride-bicarbonate exchange mechanism (AE2; SLC4A2). According to this model, CFTR is required for extrusion of chloride entering the cells via the exchanger, enabling continued bicarbonate secretion via AE2.[27] This model implies that restoration of Phe508del-CFTR-mediated chloride secretion suffices to restore biliary bicarbonate secretion.

Consistent with expression of purinergic receptors and a CaCC, we demonstrated that CF monolayers secrete chloride as well as bicarbonate after stimulation by UTP. Because the response was blocked by T16Ainh-A01, it is most plausibly mediated by anoctamin-1. UTP stimulated secretion in the presence of CFTRinh172 and absence of ELX/IVA/TEZ, suggesting that this pathway offers an alternative route for bicarbonate and chloride secretion that may compensate for loss of CFTR. However, previous work suggests that purinergic receptors on cholangiocytes are activated through an autocrine mechanism, and that ATP release depends on CFTR, although the mechanism of CFTR-dependent ATP secretion was not resolved.[28] Therefore, CaCC-mediated anion secretion in vivo may ultimately depend on correction of the Phe508del-CFTR defect.

Our data on non-CF biliary monolayers indicate that, apart from facilitating AE2 operation, CFTR also directly mediates bicarbonate efflux, at a rate that, under the presently used conditions, can exceed chloride transport. Unexpectedly, CFTR-mediated bicarbonate transport was almost absent from CF monolayers, both before and after ELX/IVA/TEZ treatment. The cause of this disparity is speculative. Firstly, we cannot exclude the remote possibility that ELX/IVA/TEZ specifically promotes the permeation of chloride through the channel pore in biliary monolayers, but does not restore the permeation of bicarbonate. If so, it is unlikely to be a direct effect of ELX/IVA/TEZ on CFTR folding or anion conductance as

the apparent shift in the chloride over bicarbonate transport ratio was not observed in similarly treated intestinal monolayers. However, it remains possible that in non-CF biliary monolayers, but not in the CF monolayers, intracellular chloride concentrations reach a sufficiently low level to activate WNK1 and NBCe1, chloride-sensing proteins capable of promoting CFTR-mediated bicarbonate transport.[29] Furthermore, transcriptome analysis showed that, in biliary CF monolayers, expression of NBCe1 and the principle carbonic anhydrase CA9 was substantially lower than in non-CF monolayers. However, differential gene expression cannot fully explain the disparity in transport properties between genotypes, because the low expression of these genes in the CF cells did not impose a similar limit on CaCC-mediated bicarbonate transport. Rather, this implies that the regulation of components of the bicarbonate secretory route, e.g. NBCe1, of which the surface expression is controlled by the WNK/SPAK- and IRBIT pathways, differs between the Ca^{2+} and cAMP signaling pathways, or that CFTR and the CaCC are expressed in different cell types.[29,30] Further, we cannot rule out the possibility that the marked differences in CFTR-mediated bicarbonate transport between CF and non-CF cholangiocyte organoids reflect inter-individual differences, implying that studies on additional CF donor tissue and organoids are indicated. Finally, because the conditions during in vitro cell culture can never fully recapitulate circumstances in vivo, the expression and function of ion transporters may differ between organoids/monolayers and native tissue.

Our data indicate that ELX/IVA/TEZ strongly enhances Phe508del-CFTR-mediated chloride and bicarbonate transport in (small) intestinal epithelial cells, and chloride secretion in biliary epithelial cells. Because CFTR-mediated chloride efflux from both enterocytes and cholangiocytes is thought to promote further bicarbonate secretion through coupling to electrically silent chloride-bicarbonate exchangers (which are not assessed in ICM), the actual level of bicarbonate secretion upon CFTR activation is probably substantially higher than is apparent from the Isc responses.[10,13,27] Consequently, this combination of CFTR modulators is likely to counter luminal hyper-acidification not only in the intestine, but also in the biliary tract.

References

1. Quinton PM. Role of epithelial HCO_3^- transport in mucin secretion: lessons from cystic fibrosis. Am J Physiol Cell Physiol. 2010;299(6):C1222-33.
2. Hansson GC. Mucus and mucins in diseases of the intestinal and respiratory tracts. J Intern Med. 2019;285(5):479-90.
3. Sakiani S, Kleiner DE, Heller T, Koh C. Hepatic manifestations of cystic fibrosis. Clin Liver Dis. 2019;23(2):263-77.
4. Gustafsson JK, Ermund A, Ambort D, *et al*. Bicarbonate and functional CFTR channel are required for proper mucin secretion and link cystic fibrosis with its mucus phenotype. J Exp Med. 2012;209(7):1263-72.
5. Hoegger MJ, Fischer AJ, McMenimen JD, *et al*. Impaired mucus detachment disrupts mucociliary transport in a piglet model of cystic fibrosis. Science. 2014;345(6198):818-22.
6. El Khouri E, Touré A. Functional interaction of the cystic fibrosis transmembrane conductance regulator with members of the SLC26 family of anion transporters (SLC26A8 and SLC26A9): physiological and pathophysiological relevance. Int J Biochem Cell Biol. 2014;52:58-67.
7. Xiao F, Li J, Singh AK, *et al.* Rescue of epithelial HCO_3^- secretion in murine intestine by apical membrane expression of the cystic fibrosis transmembrane conductance regulator mutant F508del. J Physiol (Lond). 2012;590(Pt 21):5317-34.
8. Mornon JP, Hoffmann B, Jonic S, *et al*. Full-open and closed CFTR channels, with lateral tunnels from the cytoplasm and an alternative position of the F508 region, as revealed by molecular dynamics. Cell Mol Life Sci. 2015;72(7):1377-403.
9. Fiore M, Picco C, Moran O. Correctors modify the bicarbonate permeability of F508del-CFTR. Sci Rep. 2020;10(1):8440.
10. Seidler UE. Gastrointestinal HCO_3^- transport and epithelial protection in the gut: new techniques, transport pathways and regulatory pathways. Curr Opin Pharmacol. 2013;13(6):900-8.
11. Assis DN, Freedman SD. Gastrointestinal disorders in Cystic Fibrosis. Clin Chest Med. 2016;37(1):109-18.
12. Zsembery A, Jessner W, Sitter G, *et al*. Correction of CFTR malfunction and stimulation of Ca-activated Cl channels restore HCO3- secretion in cystic fibrosis bile ductular cells. Hepatology. 2002;35(1):95-104.
13. Kanno N, LeSage G, Glaser S, Alpini G. Regulation of cholangiocyte bicarbonate secretion. Am J Physiol. 2001;281(3):G612-G25.
14. Fiorotto R, Amenduni M, Mariotti V, *et al*. Src kinase inhibition reduces inflammatory and cytoskeletal changes in DeltaF508 human cholangiocytes and improves cystic fibrosis transmembrane conductance regulator correctors efficacy. Hepatology. 2018;67(3):972-88.
15. Middleton PG, Mall MA, Dřevínek P, *et al.* Elexacaftor-Tezacaftor-Ivacaftor for cystic fibrosis with a single Phe508del allele. N Engl J Med. 2019;381(19):1809-19.
16. Keating D, Marigowda G, Burr L, *et al.* VX-445-Tezacaftor-Ivacaftor in patients with cystic fibrosis and one or two Phe508del alleles. N Engl J Med. 2018;379(17):1612-20.
17. Dekkers JF, Berkers G, Kruisselbrink E, *et al.* Characterizing responses to CFTR-modulating drugs using rectal organoids derived from subjects with cystic fibrosis. Sci Transl Med. 2016;8(344):344ra84.
18. Tysoe OC, Justin AW, Brevini T, *et al.* Isolation and propagation of primary human cholangiocyte organoids for the generation of bioengineered biliary tissue. Nat Protoc. 2019 Jun;14(6):1884-1925.
19. Zomer-van Ommen DD, de Poel E, Kruisselbrink E, *et al*. Comparison of ex vivo and in vitro intestinal cystic fibrosis models to measure CFTR-dependent ion channel activity. J Cyst Fibros. 2018 May;17(3):316-324.

20. Li Q, Dutta A, Kresge C, *et al*. Bile acids stimulate cholangiocyte fluid secretion by activation of transmembrane member 16A Cl^- channels. Hepatology. 2018;68(1):187-99.
21. Veit G, Vaccarin C, Lukacs GL. Elexacaftor co-potentiates the activity of F508del and gating mutants of CFTR. J Cyst Fibros. 2021; Sep;20(5):895-898.
22. Shamsuddin AK, Quinton PM. Native small airways secrete bicarbonate. Am J Respir Cell Mol Biol. 2014;50(4):796-804.
23. Tuo B, Riederer B, Wang Z, *et al*. Involvement of the anion exchanger SLC26A6 in prostaglandin E2- but not forskolin-stimulated duodenal HCO_3^- Secretion. Gastroenterology. 2006;130(2):349-58.
24. Poulsen JH, Fischer H, Illek B, Machen TE. Bicarbonate conductance and pH regulatory capability of cystic fibrosis transmembrane conductance regulator. Proc Natl Acad Sci U S A. 1994;91(12):5340-4.
25. Linsdell P, Tabcharani JA, Rommens JM, *et al*. Permeability of wild-type and mutant cystic fibrosis transmembrane conductance regulator chloride channels to polyatomic anions. J Gen Physiol. 1997;110(4):355-64.
26. Tang L, Fatehi M, Linsdell P. Mechanism of direct bicarbonate transport by the CFTR anion channel. J Cyst Fibros. 2009;8(2):115-21.
27. Beuers U, Maroni L, Elferink RO. The biliary HCO3- umbrella: experimental evidence revisited. Curr Opin Gastroenterol. 2012;28(3):253-7.
28. Minagawa N, Nagata J, Shibao K, *et al*. Cyclic AMP regulates bicarbonate secretion in cholangiocytes through release of ATP into bile. Gastroenterology. 2007;133(5):1592-602.
29. Lüscher BP, Vachel L, Ohana E, Muallem S. Cl- as a bona fide signaling ion. Am J Physiol. 2020;318:C125-C36.
30. Sondo E, Caci E, Galietta LJ. The TMEM16A chloride channel as an alternative therapeutic target in cystic fibrosis. Int J Biochem Cell Biol. 2014;52:73-6.

PART III

NOVEL ORGANOID SOURCES AND MODELS

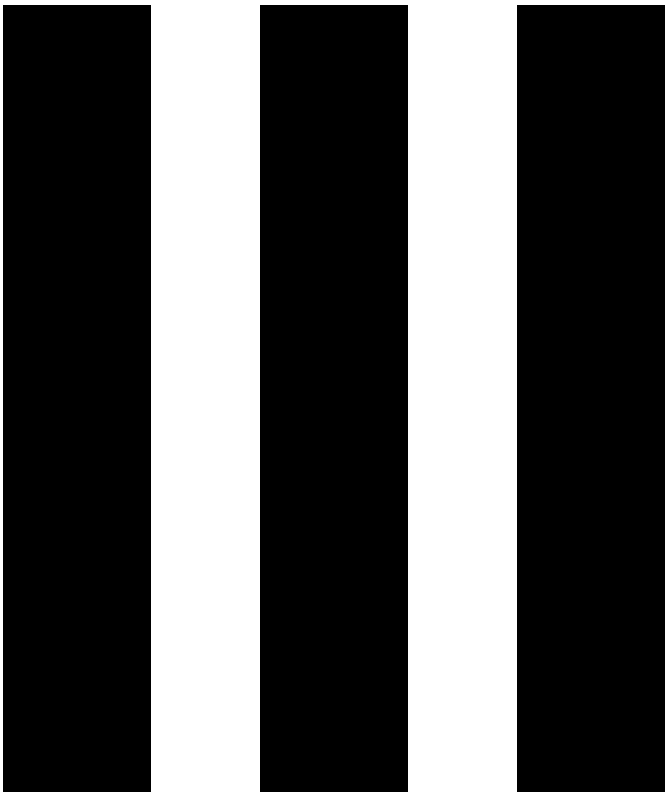

5

CHAPTER 5

Human extrahepatic and intrahepatic cholangiocyte organoids show region-specific differentiation potential and model cystic fibrosis-related bile duct disease.

Monique MA Verstegen, Floris JM Roos*, Ksenia Burka*, Helmuth Gehart, Myrthe Jager, Maaike de Wolf, Marcel JC Bijvelds, Hugo R de Jonge, Arif I Ardisasmita, Nick A van Huizen, Henk P Roest, Jeroen de Jonge, Michael Koch, Francesco Pampaloni, Sabine A Fuchs, Imre F Schene, Theo M Luider, Hubert PJ van der Doef, Frank AJA Bodewes, Ruben HJ de Kleine, Bart Spee, Gert-Jan Kremers, Hans Clevers, Jan NM IJzermans, Edwin Cuppen, Luc JW van der Laan

* these authors contributed equally.

Scientific Reports 2020 Dec 14;10(1):21900.

Abstract

The development, homeostasis, and repair of intrahepatic and extrahepatic bile ducts are thought to involve distinct mechanisms including proliferation and maturation of cholangiocyte and progenitor cells. This study aimed to characterize human extrahepatic cholangiocyte organoids (ECO) using canonical WNT-stimulated culture medium previously developed for intrahepatic cholangiocyte organoids (ICO). Paired ECO and ICO were derived from common bile duct and liver tissue, respectively. Characterization showed both organoid types were highly similar, though some differences in size and gene expression were observed. Both ECO and ICO have cholangiocyte fate differentiation capacity. However, unlike ICO, ECO lack the potential for differentiation to a hepatocyte-like fate. Importantly, ECO derived from a cystic fibrosis patient showed no CFTR channel activity but normal chloride channel and MDR1 transporter activity. In conclusion, this study shows that ECO and ICO have distinct lineage fate and that ECO provide a competent model to study extrahepatic bile duct diseases like cystic fibrosis.

Introduction

Integrity of the biliary tree is imperative for liver function. Diseases that affect the bile duct integrity are common and often life-threatening. Although the adult liver is well-known for its regenerative capacity, the cellular events that drive repair of the bile duct system is not fully elucidated. Mature cholangiocytes are known to have self-renewal capacity, both to maintain homeostasis and in response to bile duct injury[1-4]. In larger bile ducts, including in the extrahepatic bile ducts (eBD), peribiliary glands are thought to harbor biliary stem/progenitor cells. Evidence suggests that these peribiliary glands provide a proliferative response upon damage of the bile duct providing new cholangiocytes to restore the biliary lining[5]. These biliary progenitor cells have a different embryological origin than the bipotent progenitors found in the liver and share a common developmental origin with the pancreas and duodenum[6,7]. This distinct developmental lineage might explain the differences in morphology, function and proliferation between intra- and extrahepatic cholangiocytes[8-11].
With the development of the 3D organoid culture technique[12], epithelial cells, including those found in the liver[13,14] can be expanded *in vitro* driven by canonical WNT-signaling. The original liver organoids were shown to be derived from LGR5 and EpCAM double positive cells located in the intrahepatic bile ducts (iBD), both for human and mouse. More recently, work from the human liver cell atlas further specified the liver organoid-initiating cells as the TROP2 intermediate-EpCAM positive subset of cholangiocytes which share characteristics with biliary stem/progenitor cells [15]. Therefore, the original liver organoids [14] are derived from iBD cells and should correctively be termed IntrahepaticCholangiocyte Organoids (ICO). However, these ICO organoids might not recapitulate unique features of eBD cells and might therefore not be the favorable source to be used to model extrahepatic biliary diseases like cholangiocyte dysfunctions, biliary strictures and atresia.
More recently, a novel culture method was published by Sampaziotis and colleagues[16], to expand primary cholangiocyte-like cells as organoids by stimulation of the non-canonical WNT signaling of the planar cell polarity pathway. These organoids retained many biliary characteristics in culture and apart from their application in disease modeling, they were used to bioengineer artificial ducts that could be successfully transplanted in mice. However, these non-canonical WNT stimulated cholangiocyte organoids, unlike conventional ICO, do not express stem cell markers/WNT-target genes (including LGR5), but do express markers of mature cholangiocytes. In parallel with our studies, Rimland *et al*. recently showed that cholangiocyte organoids isolated from intrahepatic ducts were different when compared to cholangiocyte organoids derived from common bile duct, gallbladder, and pancreatic duct. Strikingly, they found that only a limited number of regional-specific gene markers of the tissue were conserved in the organoids, possibly driven by the culture conditions they were subjected to[17]. Only expression of common bile duct specific gene, HOXB2, was retained in

organoids derived from the common bile duct and not in those derived from pancreas duct or gall bladder.

The aim of this study was to establish WNT-dependent organoids from human eBD and compare these to paired ICO from liver samples of the same donor. Here we report that WNT-stimulated Extrahepatic Cholangiocyte Organoids (ECO) have distinct differentiation capacity to hepatocyte-fate when compared to ICO. As proof of qualifying as model for eBD disease, we showcase ECO from a cystic fibrosis (CF) patient.

Materials and Methods

Human organoid culture initiation and expansion

Tissue samples (<=0.5 cm^3) of donor extrahepatic (common) bile duct (eBD) and donor liver biopsies (n>40) were collected during liver transplantation at the Erasmus Medical Center Rotterdam. Use of both tissues for research purposes was approved by the Medical Ethical Council of the Erasmus MC and informed consent was given (MEC-2014-060). Liver and eBD biopsies were obtained from a 17-year old male Cystic Fibrosis (CF) patient undergoing liver transplantation at the University Medical Center Groningen. Informed consent was obtained to use these biopsies for research (STEM Study – protocol number 1-402/K, informed consent was obtained from a parent). This patient was compound heterozygous for F508del and R1162X, resulting in a non-functional CFTR transporter. Biopsies were stored in organ preservation fluid (University of Wisconsin Belzer UW Cold Storage Solution, Bridge of Life Ltd. London, UK) and transported at 4˚C. The biopsies were used to initiate ECO and ICO cultures which were initiated as described for human liver tissue[14,18]. In short, the biopsies (liver and eBD) were washed in Advanced DMEM/F-12 medium supplemented with penicillin/streptomycin (with 10.000 U/mL, Life Technologies), HEPES (1M, Life Technologies), Ultraglutamine (200mM, Life Technologies). Both liver and eBD biopsies were minced and digested in a collagenase solution (2.5 mg/mL collagenase Type A, Sigma Aldrich in Advanced DMEM/F-12 medium), rocking at 37˚C for 20 minutes. Single cell solutions were gained by passaging over a 70 µm nylon mesh cell strainer and washed in Advanced DMEM/F-12 medium (5 minutes, 1500 rpm at 4˚C) after which the pellet was diluted in ice cold Matrigel (Corning) and seeded in 25 µL droplets in 48-wells plates. After solidifying of the Matrigel, 250 µl culture initiating medium was added and cells were incubated at 37˚C, 5% CO_2 for three days. Culture initiating medium consisted of Advanced DMEM/F12 medium (Invitrogen) supplemented with 1% N2, 1% B27 (both Gibco), 1.25 mM N-Acetylcystein (Sigma), 10 nM gastrin (Sigma), 50 ng/mL EGF (Peprotech), 100 ng/mL FGF10 Peprotech), 25 ng/mL HGF (Peprotech), 10% R-spondin (conditioned medium), 10nM nicotinamide (Sigma), 5 µM A83.01 (Tocris), 10 µM forskolin (Tocris), 25 ng/mL Noggin (conditioned medium), 30% WNT (conditioned medium), 10µM Y27632 (Sigma), and hES cell cloning recovery solution (Stemgent). After three days, the initiation medium was changed to expansion medium (EM), deprived of noggin, WNT, Y27632 and hES cell cloning recovery solution. Organoid formation was seen within two or three days after culture initiation and medium was refreshed every 3 days. Organoids were split (1:3) every 7 days. To prepare viably frozen stocks (from different passages), organoids were mechanically dissociated and mixed with recovery cell culture freezing medium (Gibco) according to the manufacturers protocol and stored at -196˚C.

DNA-synthesis and cell cycle analysis

Cell proliferation was analyzed by direct measurement of DNA synthesis using the Click-iT EdU Alexa Fluor 488 Flow Cytometry kit (Thermo Fisher). For this, organoids of different passage numbers were incubated with the thymidine analogue 5-ethynyl-2'-deoxyuridine (EdU) during 4 hours at 37˚C, 5% CO_2 after which the organoids were harvested and made single cell using trypsin-EDTA incubation (15 minutes at 37˚C). The cells were further processed according to the manufacturer's protocol. The percentage of S-phase cells in the organoids was determined using standard flow cytometry methods (FACSCalibur, BD Biosciences).

Organoid growth rate analysis

Organoid growth rates were determined using a custom-made pipeline for bright field-based image segmentation (Hof *et al.*, *in submission*) in three pairs of ICO and ECO (passage 7 to 16). In brief, organoids were split, seeded in 5 µL of Matrigel into 96-well plates at similar densities, overlaid with 100 µl of expansion medium, and were cultured for 84 hours before imaging. Organoids were imaged for 30 hours at 1 hour intervals using bright field microscopy (microscope: Zeiss AxioObserver.Z1; objective lens: Zeiss Plan-Apochromat 5x/0.16; tiling: 2x2; z-planes: 10; z-spacing: 65 µm). The recorded time-lapse image stacks were pre-processed with Fiji (ImageJ version 1.51n, Java version 1.8.0_6 (64-bit)) by reducing the dimensionality of the raw data set from 4 (2x2) tiles with 10 z-planes each to 1 stitched image with 1 z-plane per time frame using the plugin Grid/Collection stitching[19]. The resulting image stacks were subsequently segmented based on projected luminal areas of the organoids by using the Fiji plugin Morphological Segmentation (MorphoLibJ[20]. Segmented luminal areas were measured with the Fiji plugin Region Morphometry (MorphoLibJ[19]. The luminal areas of individual organoids were normalized to the average luminal area over the first 5 time-points. Organoids which were not detected in all 31-time frames were manually excluded from the analysis. Data is displayed as mean ± SEM in the corresponding graph.

Hepatocyte differentiation

Organoids were expanded for 5-7 days before initiation of hepatocyte differentiation. Differentiation to hepatocyte fate was initiated with the addition of 25 ng/mL BMP7 (Peprotech) to the expansion medium and lasted 5 days. Subsequently, organoids were passaged with a 1:1.5 split ratio and medium was changed to human hepatocyte differentiation medium based on the original differentiation protocol as published by Huch *et al.,*[14] and Gehart *et al.* (World Interlectual Property Organization Patent WO2017149025A1). Medium was changed every 2-3 days for a total of 10 days after which the organoids were analyzed for hepatocyte-specific markers.

Cholangiocyte differentiation

The protocol used to differentiate organoids to cholangiocytes was adapted from the previously published protocol for iPSC differentiation to cholangiocytes[21]. From the last steps onwards, describing the differentiation from the hepatoblast phenotype to cholangiocytes, this protocol was used to differentiate the eBD and iBD organoids to cholangiocytes. In detail, organoids were expanded for 7 days in Matrigel to near-full wells. Culture medium was then switched to differentiation medium, consisting of AdDMEM/F12 supplemented with B27 (1x, Gibco), fibroblast growth factor 10 (FGF10, 50ng/mL, Peprotech), Activin-A (50 ng/mL, Gibco), and retinoic acid (3µM, Sigma-Aldrich). After 4 days, medium was changed to William's E medium (Gibco, Life Technologies) supplemented with nicotinamide (10mM, Sigma-Aldrich), sodium bicarbonate (17 mM, Sigma-Aldrich), 2-phospho-i-ascorbic acid tri-sodium salt (0.2 mM, Sigma-Aldrich), sodium pyruvate (6.3 mM, Invitrogen), glucose (14 mM, Sigma-Aldrich), HEPES (20 mM, Invitrogen), ITS+ premix (BD Biosciences), dexamethasone (0.1 M, R&D Systems), epidermal growth factor (EGF, 20 ng/mL, R&D Systems), Ultraglutamine (2 mM, Invitrogen), and penicillin (100 U/mL)/ streptomycin (100g/mL). Differentiation was blocked by adding 50 µM DAPT (Sigma) to the culture medium. The medium was refreshed every 2 days for a total of 10 days after which the organoids were analyzed.

RNA sequencing

Organoids (ICO and ECO, before and after differentiation to the hepatocyte and cholangiocyte phenotypes) were collected in lysis buffer (QIAzol lysing reagent, Qiagen) and total RNA was collected using the miRNeasy mini kit (Qiagen). The amount and integrity of RNA was analyzed using the Agilent 2100 Bioanalyser (Agilent). RNA sequencing libraries were generated from 100 ng of total RNA using the TruSeq Stranded Total RNA Library Prep Human/Mouse/Rat kit (Illumina) and sequenced 2 x 75bp on the Illumina Nextseq500. Sequencing reads were subsequently aligned against the human reference genome (GRCh37) using STAR 2.4.2a 21and counted with HTSeq 0.6.1 22. Differential expression analysis was done using DESeq 1.20.0 23. Genes were considered to be significantly differentially expressed when Padjusted < 0.05 (Benjamini Hochberg FDR correction). The GSEA analysis was performed using the software from Broad Institute (v4.0.3).

Forskolin-Indiced Swelling assay (FIS)

To assess CFTR functionality, Forskolin-Induced Swelling (FIS) of organoids was performed essentially as described by Dekkers *et al.*[22,23]. In brief, ICO and ECO were seeded in 96-well cell culture plates (circa 50/well), in a 5 µL droplet of Matrigel. After 2 days, organoids were loaded with calcein-green (Invitrogen; acetoxymethyl ester; 5 µmol/L; 1 hour) suspended in modified Meyler solution. Calcein-fluorescent, viable organoids were maintained at 37°C in 5% CO_2 and visualized on a confocal microscope equipped with a computer-controlled

moveable stage (5x objective; Leica TCS SP5). After CFTR phosphorylation/activation was triggered by addition of forskolin (5 µM), images were acquired at 6 min. intervals for 2 hours. CFTR-mediated anion secretion stimulates osmotic fluid transport into the enclosed organoid lumen, leading to a volume increase. To assess organoid swelling, the area enclosed by the fluorescent cells lining the organoids was quantified on the ImageJ platform (NIH, USA), using a software module developed by the Optical Imaging Center of the Erasmus MC, which fully automates image analysis. Data depict the cumulative increase in volume over 1 hour. In the graphic display of the data, each data point represents the average of triplicate wells.

Ussing chamber assay

Ussing chamber assays were performed essentially as described elsewhere[24]. In short, organoids were dissociated into single cells and seeded on a permeable support (Transwell 3470; Corning) that were coated with Matrigel (1:20 in PBS) and cultured in EM organoid medium. After the cells had formed a confluent monolayer (circa 10 days after seeding), filters were inserted in Ussing chambers (P2302T/P2300; Physiologic Instruments, San Diego, CA), and bathed in modified Meyler solution (128 mM NaCl, 4.7 mM KCl, 1.3 mM $CaCl_2$, 1.0 mM $MgCl_2$, 0.3 mM Na_2HPO_4, 0.4 mM NaH_2PO_4, 20 mmol/liter $NaHCO_3$, 10 mM HEPES), supplemented with glucose (10 mM), in 95% O_2, 5% CO_2, pH 7.3, at 37 °C. The transepithelial potential difference (PD) was clamped at 0 mV using a VCC MC8 voltage clamp module (Physiologic Instruments), and the resulting short-circuit current (Isc) was digitally recorded using an analog-to-digital signal converter and associated software (Acquire and Analyze 2.3; Physiologic Instruments). Anion secretion was stimulated by addition of the adenylyl cyclase activator forskolin (10 µmol/liter, Sigma-Aldrich) or the purinergic receptor agonist UTP (50 µmol/liter, Sigma-Aldrich) to the luminal bathing solution. Forskolin-induced and UTP-induced secretion was inhibited by Glyh-101 (20 µmol/liter, Sigma-Aldrich) and T16inh-A01 (50 µmol/liter, Sigma-Aldrich), respectively.

Rhodamine 123 assay

To determine the presence of calcium channels, including multidrug resistance protein 1B (MDR1b – important in the biliary excretion of large hydrophobic components – member of the P-glycoprotein membrane transporter family), Rhodamine 123 (Rh123) was added to the cultures. Rh123 is a fluorescent chemical compound that can be transported by these transporter channels[25]. For this, cold Advanced DMEM/F12 medium was used to remove Matrigel and collagen from the cultures that were subsequently pretreated with DMSO or 10 µM Verapamil (Sigma-Aldrich – MDR1b inhibitor) for 30 minutes, followed by 5 minutes of incubation with 100 µM Rh123 (Sigma-Aldrich). The organoids were washed 3 times with expansion medium. Fluorescence (excitation wavelength: 511 nm; emission wavelength: 534 nm) was visualized with a Leica SPE-II confocal system, 30 minutes after washing and analyzed with ImageJ.

Flow cytometry

To assess TROP2 expression, paired ICO and ECO (passage 5) from three donors were dissociated using Trypsin/EDTA (15 minutes at 37˚C), washed in 8mL in Advanced DMEM/F-12 medium (1500 rpm, 5 min, 4˚C) and cells were re-suspended in EBSS to make a single cell suspension. TROP2 antibody (Invitrogen; rabbit monoclonal conjugated to Alexa Fluor-488, clone MR54, used 1:100) was added (30 min, on ice) and cells were subsequently measured on a FACS Canto flow cytometer (BD Biosciences).

Flow cytometric analysis of the starting cell populations, liver (n=3) and extrahepatic bile duct biopsies (n=3), collected during liver transplantation were treated similar to organoid initiation as described above. Instead of adding Matrigel to initiate the organoid cultures, the cells were stained for flow cytometry using monoclonal antibodies against human LGR5 (1:100, Clone 8F2, BD Biosciences) and human EpCAM (1:100, Clone 9C4. Biolegend), conjugated directly with PerCP and PerCP/Cy5.5, respectively. Cells were measured on a FACS CantoII flow cytometer (BD Biosciences) and analysed using FACS Diva software. Cells from ICO and ECO were harvested by trypsin-treatment (10 min, 37˚C), subsequently washed in Advanded DMEM/F-12 and stained with EpCAM and LGR5 to be analysed by flow cytometry.

Immunohistochemistry

Organoids were formalin-fixed (4%) for 24h, paraffin-embedded and sectioned (5 µm) for histological examination. To analyze the general morphology, sections were stained with hematoxylin-eosin (H&E) and analyzed using a bright field microscope. Additional sections were processed and stained using standard IHC protocols with specific antibodies for cytokeratin 19 (KRT19) and Mucin-1 (Muc-1). After deparaffinization, antigen retrieval was performed in a citrate buffer (pH 6) at boiling temperatures for 10 minutes. Subsequently, sections were incubated with primary antibodies (MUC-1 clone E29, Fisher Scientific 1:500, and KRT-19 clone RCK108, Agilent Dako, 1:250) overnight at 4˚C. After washing, sections were incubated with secondary antibody (Envision Flex HRP, Agilent) for 60 minutes at RT prior to incubation with DAB substrate. Slides were analyzed with a bright field microscope and imaged with a Nikon DS camera. To determine cell proliferation, stainings were done on sections using standard immunofluorescence (IF) protocols, using a specific antibody for Ki67 (1:100, kind gift from PARTS, Department of Pathology, Erasmus MC, Rotterdam).

CFTR Western blot analysis

To demonstrate the near absence of the CFTR protein in the CF-eBD organoids, Western blot analysis was performed. Cells from ECO derived from CF patients and healthy donors were harvested, collected by centrifugation, and lysed in ice-cold RIPA buffer (Cell Signaling Technology) supplemented with a protease inhibitor cocktail (Roche). Total protein content was measured photometrically using the RC-DC protein assay (Bio-Rad Laboratories, Inc., CA). Cell lysates were subjected to sodium dodecylsulfate polyacrylamide gel electrophoresis (SDS-PAGE) (8.0% acryl amide), and proteins were transferred to polyvinylidene fluoride

membrane (120 V, 70 min.). Nonspecific binding sites were blocked for with Western blot blocking buffer (1 h, RT; ThermoFisher Scientific). The CFTR primary antibodies '570' and '596' antibodies were obtained through the Cystic Fibrosis Foundation Therapeutics initiative (www.cftrfolding.org/CFFTReagents.htm) and used at a 1:400 dilution in Western blot blocking buffer (16h, at 4 °C)[22,26]. After washing in Tris-buffered saline with Tween-20 (TBST), the membrane was incubated with donkey polyclonal anti-mouse immunoglobulin (Ig)G-H&L HRP (Abcam, 1:10.000; 1 h) in Western blot blocking buffer. After washing, the reaction was visualized using Chemiluminescence (ChemiDoc, Bio-Rad). Normalization was done to ß-actin (C4 HRP, sc-47778, Santa Cruz Biotechnology, USA) expression using Image Studio lite version 5.2 (LI-COR Biosciences, NE).

Statistical analysis and data access

All values are represented as mean ± SEM. All statistical analysis were performed using GraphPad Prism 7, R statistical environment or Python 3 with NumPy, Pandas and SciPy libraries 28. A two-sided Student's t-test was done to test statistical significance between means (qRT-PCR) and Two-tailed t-test was performed to analyse relative ICO and ECO sizes. A p-value <0.05 was considered statistically significant. RNA sequencing data was submitted to EGA under study ID: EGAS00001003792. All methods were carried out in accordance with relevant guidelines and regulations of the Erasmus MC – University Medical Center Rotterdam and The Netherlands.

Results

Efficient organoid initiation from the human common bile duct

Samples from donor liver and the extrahepatic bile duct were dissociated and used for culture initiation (Figure 1A). EpCAM and LGR5 frequencies were determined in the cells that were isolated from eBD and liver biopsies. Flow cytometric analysis show that EpCAM levels were low 1.2±1.6% in eBD and 0.9±0.7% (average±SD) in liver starting populations as anticipated and as previously shown[27]. Cells isolated from ICO and ECO expressed ~100% EpCAM as shown before[14] (Figure S1). LGR5 expression was too low to be detected by flow cytometry (not shown). Organoids could be initiated from human CBD tissue with >95% success rate from over 40 biopsies from both male and female organ donors or patients with a wide age range (16-70 years). On average, the first ECO were visible in cultures at 7 days (6.8 days ± 1.0 SD). Organoids were grown 3-dimentional in hydrogels (Matrigel) and after initiation organoid cultures were passaged one to two times per week (split 1:3). Organoid initiation efficiency and expansion potential was similar to paired ICO cultured from liver biopsies from the same donor (data not shown). In accordance with previous results[14], ECO could be viably frozen and thawed and in general, behaved similarly to ICO. Several organoid lines were biobanked early, but many ECO cultures (n=15) were passaged over 30 times for a period of 8 months or longer without clear signs of exhaustion. The ICO and ECO cultures were morphologically similar and no apparent histological differences were found (Figure 1B-I). Both cultures remained proliferative at late passages (>6 months), with 11.0 ± 2.1% and 17.3 ± 2.4% (mean ± SEM) of the cells in S-phase at P10, respectively. Additional Ki67 stainings of ECO and ICO organoid sections confirmed this (Figure 1J and Figure S2), and were similar to previously described percentages for ICO [14]. Despite similar proliferation rates, the increase of relative organoids sizes as measured by time-lapse bright-field microscopy was significant differences for paired organoid types (Figure 1K). Organoid size was measured starting 3.5 days after splitting and followed for 30 hours. After 12 hours of measuring the size of ICO were significantly larger than ECO from the same donor (n=100 organoids per type, $P<0.001$). As shown in Figure 1L, both organoid types express the trophoblast cell surface protein 2 (TROP2) protein which is associated with organoid-initiating cells and no significant difference was found in TROP2 protein expression (Figure 1M, 99.1%±1.2% in ECO and 98.5%±1.0% in ICO; $p=0.67$). Together, these results show that organoids are initiated efficiently from human eBD and iBD and have similar characteristics with only a small but significant difference in organoid size expansion.

Gene expression analyses of ECO and ICO

When looking at the expression of specific genes known to be markers for intrahepatic organoid-initiation cells identified by single cell RNA sequencing and cell sorting[15], all genes were present and no significant difference in expression was observed between ECO and ICO

(Figure 1N). These genes include epithelial cell adhesion molecule (EpCAM), leucine-rich repeat-containing G-protein coupled receptor 5 (LGR5), the low-density lipoprotein receptor-related protein (LRP5/6) co-receptor group[12], tumor-associated calcium signal inducer 2 (TACSTD2 or TROP2), SRY-Box 9 (SOX9), Cytokeratin 19 (KRT19), fibroblast growth factor receptor 2 (FGFR2), transmembrane 4 L Six Family member 4 (TM4SF4) and others[15]. Though all these markers were found positive in organoids, some genes were highly expressed (TM4SF4, KRT19) and some genes relatively low (LGR5 and OCT4).

Extending the gene expression analysis of specific genes associated with bi-potential progenitors, or progenitors with hepatocyte-fate or cholangiocyte-fate, again as described in the human liver atlas study[15], did not show any significant different expressed between ICO or ECO (Figure 2A). Looking at the global gene expression of three paired organoid sets and one additional non-paired ICO, revealed a high degree of similarity and only small differences. As shown in Figure 2B, this RNA sequencing analyses showed that only 29 genes were significantly differentially expressed (P-adjusted <0.05), of which 13 were expressed at higher levels in ECO and 16 were expressed at higher levels in ICO. Among the genes that were more abundantly expressed in ECO were Aquaporin5 (AQP5), a classic water transporter-channel known to be expressed on cholangiocytes and pancreatic epithelium and to a lesser degree by hepatocytes, and Insulin Like Growth Factor Binding Protein 1 (IGFBP1) known to be involved in ductular reactions of the biliary epithelium in response to liver damage[28]. Genes associated with the alcohol dehydrogenase pathway (ALDH1A3, AADAC) and lipid metabolism (STS), typically expressed in hepatocytes, are differentially expressed and upregulated in ICO. In particular ALDH1A3, highly expressed in ICO, is known to be involved in the biosynthesis of retinoic acid (RA) and RA signaling transduction. Interestingly, a previous study with lung organoids showed that inhibition of RA pathway causes an increased ALDH expression and an increase in the size of organoids[29]. Thus, higher ALDH expression in ICO may explain their larger organoid size as compared to ECO (Figure 1K), however, this requires further experimental proof. Other hepatocyte-related genes as CYP3A4 and HNF4a were not differently expressed in ICO and ECO (Figure 2B). The regional-specific gene for common bile duct tissue which was retained in common bile duct organoids[17], HOXB2, was not significantly different between ECO and ICO (not shown). This same study reported that PROM1, SOX9 and Albumin were significantly higher expressed in intrahepatic versus extrahepatic bile duct organoids. These differences were not confirmed in our ICO and ECO (data not shown) and may be related to the different culture conditions. Taken together, although these results show that gene expression in ICO and ECO was generally quite similar, several genes were found to be differentially expressed.

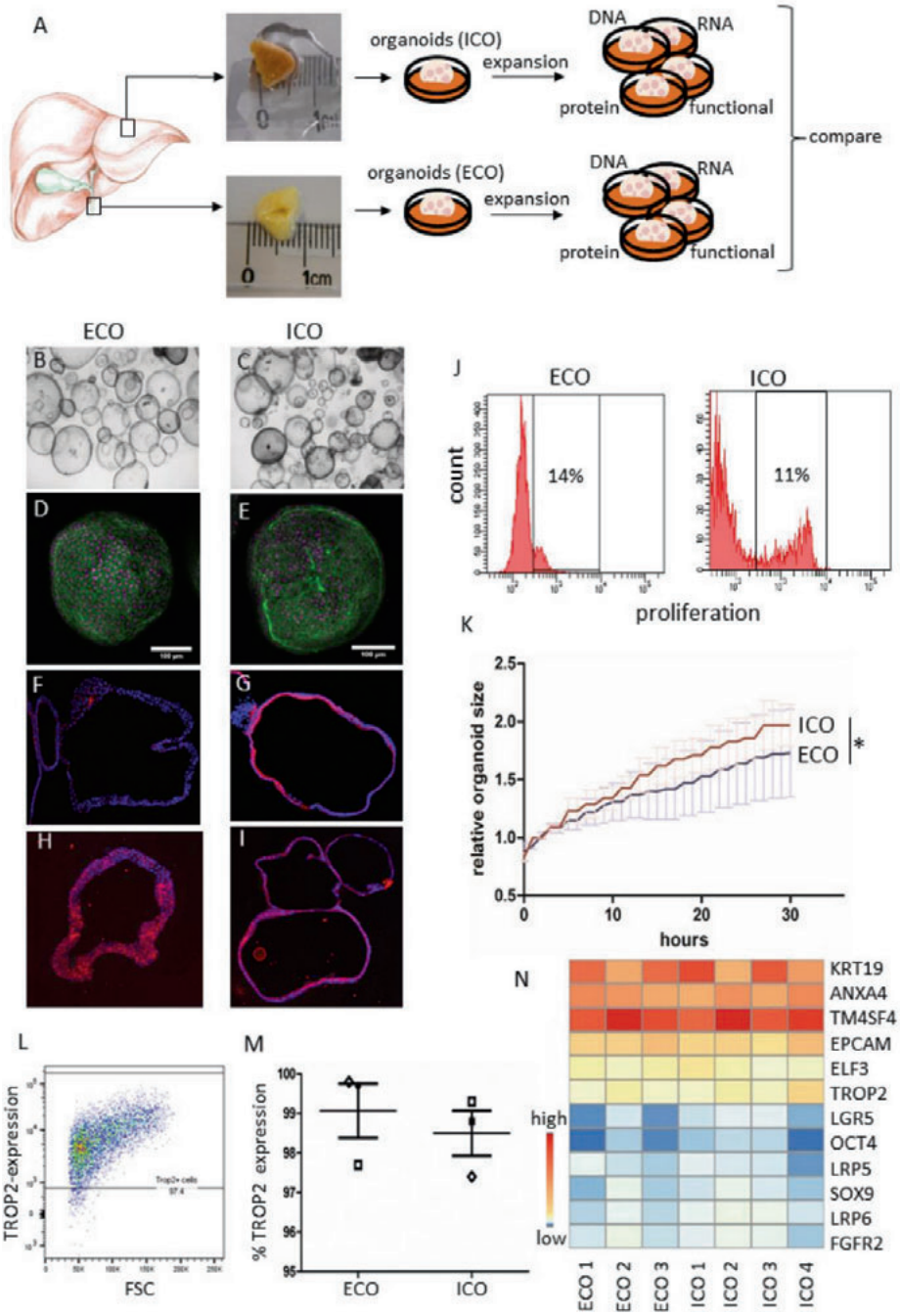
A
organoids (ICO)
expansion
DNA
RNA
protein
functional
compare
organoids (ECO)
expansion
DNA
RNA
protein
functional
0
1cm
ECO
ICO
B
C
D
E
F
G
H
I
J
ECO
ICO
count
14%
11%
proliferation
K
relative organoid size
ICO
ECO
*
hours
L
TROP2-expression
FSC
M
% TROP2 expression
ECO
ICO
N
KRT19
ANXA4
TM4SF4
EPCAM
ELF3
TROP2
LGR5
OCT4
LRP5
SOX9
LRP6
FGFR2
high
low
ECO 1
ECO 2
ECO 3
ICO 1
ICO 2
ICO 3
ICO 4

Figure 1. Culture initiation and characteristics of liver- and extrahepatic bile duct-derived organoids. **(a)** Schematic representation of organoid culture initiation from liver biopsies (intrahepatic bile duct; iDO) and extrahepatic bile duct (eDO). Organoids were cultured and passaged weekly (1:3 for over 30 passages/ > 8 mo) and harvested at different passages for further analysis. ECO were cultured as efficiently as liver-derived ICO. Both look similar at the microscopic level **(b,c)**, when stained with phalloidin/DAPI **(d,e)**, and in FFPE sections stained by immunofluorescent KRT7 **(f,g**—10×**)** and KRT19 **(h, i**—10×**)**. EdU-incorporation showed a similar percentage of proliferating cells (11–14% in S-phase) in both organoid types at passage 10. Shown is one representative result of three paired donor lines tested **(j)**. The individual percentages are shown in Figure S2. Despite no significant difference in proliferation ($p = 0.122$), a significant difference in organoid size was found when analyzing individual organoids for 30 hours **(k)** Shown is mean ± SEM of 100 organoids from paired ECO and ICO of three different donors. TROP2 protein expression was found in almost 100% of the organoid cells, both for ECO and ICO **(l, m)** (three paired organoid lines). Expression heatmap of selected genes described by Aizarani *et al.*, as markers for liver progenitors[15]. The expression levels per gene were collected from the normalized RNA sequencing analysis performed on four ICO and three ECO lines, and visualized as Z-score. Though the level of expression varied per gene, no significant difference in expression was found between ICO and ECO **(n)**.

Cholangiocyte-related ion transport activity in ECO and ICO

To execute their function to modify hepatocyte-derived bile, cholangiocytes harbor a number of transporter-channels on their apical membranes. This include the cAMP-activated CFTR channel and the Ca^{2+}-activated Cl^- channel CaCCs. As shown in Figure 3, basolateral forskolin stimulation of ECO or ICO cells grown as a 2D monolayer, induced a short-circuit current (Isc). This Isc signal could be completely inhibited by the CFTR-inhibitor GlyH-101(N-(2-naphthalenyl)-((3,5-dibromo-2,4-dihydroxyphenyl)methylene)glycine hydrazide)[30].

Furthermore, apical UTP, which elicits Ca^{2+} mobilization through activation of purinergic (P2Y) receptors, induced an Isc that was inhibited by the CaCC inhibitor T16inh-A01 (Figure 3A). No differences were found in activation of the CaCC by UTP and subsequent inhibition by T16inh-A01. Of note, although in both organoids' types clear CFTR activity was measured, the most pronounced response to forskolin was observed in ECO. This observation was further supported with another CFTR measure, the 3D forskolin-induced swelling (FIS) assay. In this FIS assay, due to changed osmolarity upon forskolin stimulation, water is transported inside the lumen, causing the organoids to swell. Figure 3B (ECO) and Figure 3C (ICO) show the organoid size before and after 120 minutes forskolin stimulation. Both ECO and ICO showed swelling upon forskolin activation, demonstrating also polarization of the cells and luminal expression of the CFTR channel in the organoids. Automated quantification of the organoid-size over time confirmed significantly more swelling in ECO compared to ICO (Figure 3D, $P<0.0001$).

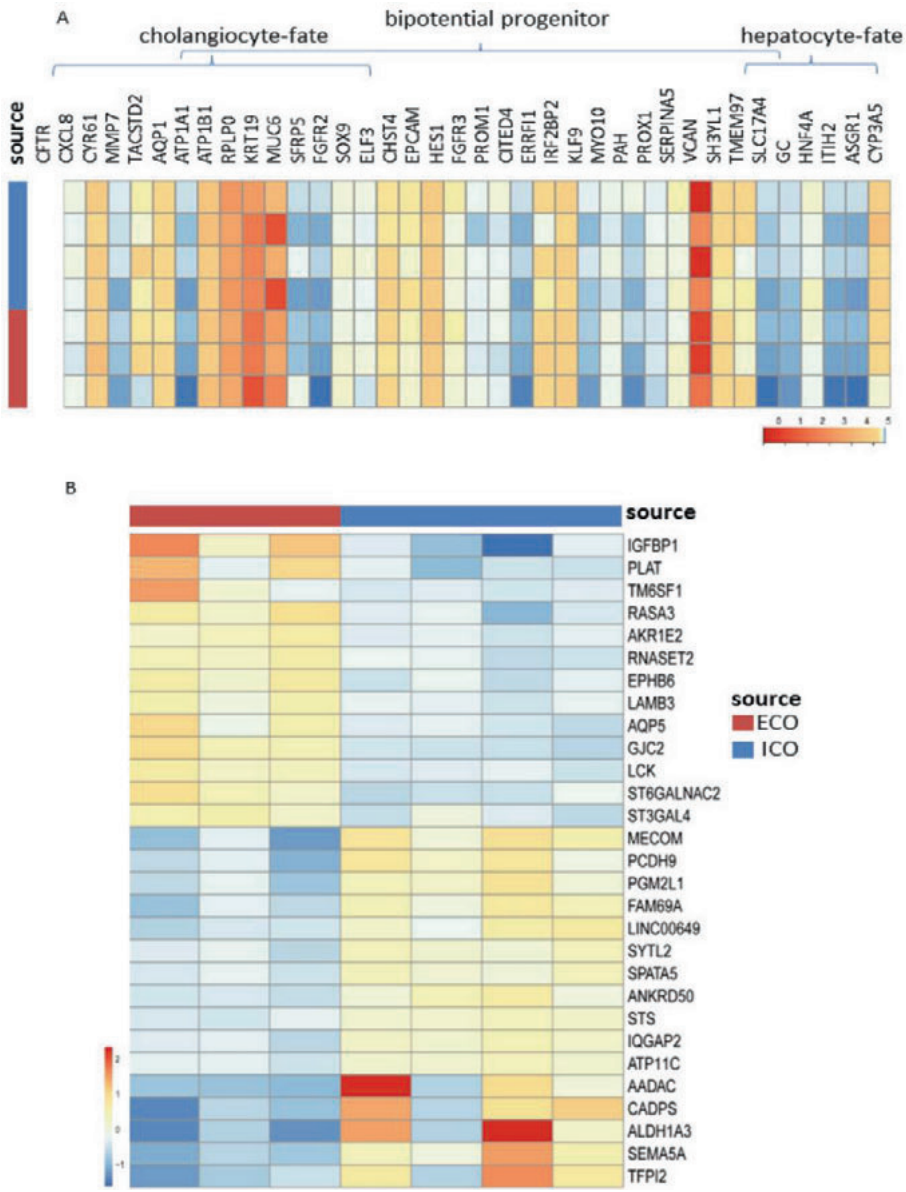

Figure 2. Limited differences in gene expression between ECO and ICO.

(a) Gene expression analysis of three paired ICO and ECO and one additional ICO line was performed using RNAseq. Selected genes, as described by Aizarani *et al.*[15] that are expressed in EpCAM-positive cells and associated with progenitors, hepatocyte-fate or cholangiocyte-fate. Shown are normalized (bulk) RNA sequencing results of the undifferentiated ECO and ICO for this specific gene set. Expression of the progenitor, hepatocyte-fate- and cholangiocyte-fate associated genes was similar between ECO

and ICO. The expression heatmap shows Z-scores that are color-coded as shown. No significant differences between ICO and ECO for this gene set was observed. **(b)** The expression heatmap indicates clusters of genes that are differentially expressed (29 in total, p adjusted < 0.05), 13 are higher expressed in ECO and 16 higher in ICO. This analysis reveals that although both organoid types are very similar in gene expression profiles, there are some differences albeit in a relatively low number of genes.

Cholangiocyte-fate differentiation potential is similar for ECO and ICO

Different protocols have been developed for differentiation to a cholangiocyte-like phenotype, both for iPSC and ICOs. As the starting cell population prior to differentiation already have many cholangiocyte-like properties (i.e. ion and water channel activities), this cholangiocyte-fate differentiation can also be considered maturation. As shown in Figure 4A, after 14 days culture in differentiation medium, organoids became denser, had thicker outer walls and stopped proliferating as shown in Figure 4B, at gene expression level, stem cell and proliferation markers LGR5 and Ki67 were significantly downregulated in DM-chol both for ECO and ICO, confirming loss of stemness and proliferation. To benchmark the cholangiocyte-differentiated ICO and ECO, RNA expression profiles from bile duct tissue, published by Rimland *et al*.[17], were used. For this, 20 genes known to be highly expressed in cholangiocytes were used. Gene expression clustering of ICO, ECO and the bile duct tissue showed that in both ICO and ECO in DM-cholangiocyte conditions, these cholangiocyte genes were upregulated (Figure 4C).

The P-glycoprotein (Pgp) membrane transporter family member MDR1, is an apical transporter known to be expressed by cholangiocytes. Differentiated ECO readily took up the tracer dye and actively transported this to the luminal side via MDR1, resulting in a fluorescent organoid lumen (Figure 4D). MDR1 dependency was confirmed by blocking luminal transport of Rh123 with the MDR1 antagonist Verapamil, resulting in accumulation of dye in the cell cytoplasm. Similar results were observed for ICO in DM-chol (not shown). Finally, we confirmed that cholangiocyte-lineage differentiation is highly dependent on Notch signaling (Figure 4E). For this, a specific small molecular inhibitor of the Notch pathway, DAPT, was added during the differentiation culture in DM-chol. Clearly the cholangiocyte-specific genes AQP1, AE2 and HNF1β which were upregulated during DM-chol, were completely downregulated by treatment with DAPT. Also, the Notch-related genes NOTCH2 and JAG1 were downregulated by DAPT (Figure 4E) These results indicate that organoids initiated from both eBD and iBD can be driven to a similar adult cholangiocyte-like phenotype.

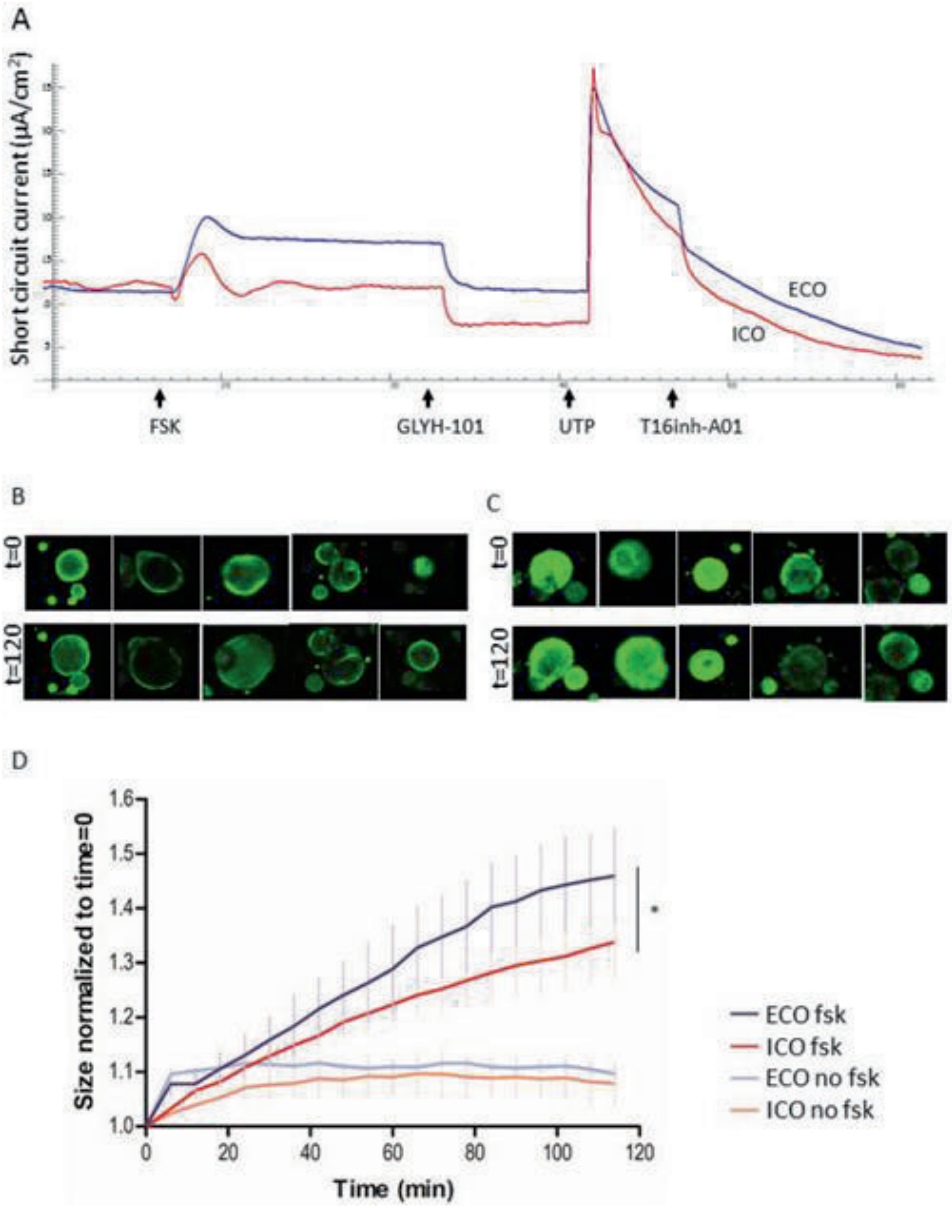

Figure 3. Forskolin-induced ion channel activity is more prominent in ECO then ICO.
(a) A representative Ussing experiment shows CFTR stimulation by forskolin (FSK, 5 μM) in ECO (blue line) and ICO (red line) organoids. GlyH-101 inhibits the CFTR transporter channel specifically. Ca^{2+}-activated Cl^- channels (CaCC) are stimulated by UTP and inhibited by CaCC inhibitor T16inh-A01 (arrows)

demonstrating the presence of functional CFTR and Ca^{2+}-activated Cl^- channels in these organoids. Functionality of CFTR in 3D grown organoids was shown by FIS. **(b, c)** Representative pictures of five individual calcein green-labeled ECO and ICO before (t = 0) and after (t = 120) forskolin stimulation show the swelling in time. **(d)** Qualification of organoid size in time showed that ECO swell ignificantly larger upon forskolin-activation than ICO (*p < 0.0001).

Different hepatocyte-fate differentiation potential of ECO and ICO.

Previous studies demonstrated that ICO have the potential to differentiate to the hepatocyte lineage[14]. As shown in Figure 5, culturing organoids in hepatocyte differentiation medium (DM-hep) results in a clear morphological change compared to organoids in expansion medium (EM) in both ICO and ECO. Histological sections of the ECO and ICO grown in DM-hep medium for 14 days, show increasing cellular density within the individual organoids (Figure 5A). Comparative gene expression analysis of EM and DM-hep of 35 genes specific for hepatocytes, cholangiocytes or progenitor cells selected from the human liver atlas[15] is shown in Figure 5B. Gene expression of primary hepatocytes (PHH) as published by Schneeberger *et al*.[31] were included as a benchmark for hepatocyte-fate differentiation. Expression of the hepatocyte-specific genes were clearly different between ICO and ECO. In the DM-hep condition ECO showed less upregulation of hepatocyte-specific genes as compared to ICO, whereas progenitor- and cholangiocyte-related genes were not significantly different. Of note, one of the ICO lines showed less prominent hepatocyte-fate differentiation but it is well known that differentiation potential varies between individual donors. Assessing general differences in ICO and ECO gene expression showed that undifferentiated organoids in EM have only limited number of significantly different genes (16 genes significantly higher in ICO and 13 in ECO, shown in Figure 2B). As shown in Figure 5C, in the DM-chol condition the difference in gene expression between ICO and ECO completely disappeared (1 significantly different gene). However, in the DM-hep condition clearly heterogeneity in gene expression profiles increased. In ECO 136 genes were significantly higher and 89 genes were found significantly higher in ICO (Figure 5C), indicating a difference in response to the DM-hep condition between these organoid types. The expression of hepatocyte-specific genes ALB (Figure 5D) and CYP3A4 (Figure 5E) was further confirmed in 3 independent differentiation experiments and quantified by qRT-PCR. Again, though progenitor-related gene KRT19 was not significantly different regulated between ICO and ECO (Figure 5F), again only ICO showed significant upregulation of ALB and CYP3A4 in the DM-hep condition whereas ECO clearly did not upregulate ALB and CYP3A4. This was also confirmed on a functional level testing CYP3A4 activity in an enzymatic assay (Figure 5G). Also here, only ICO and not ECO showed a significant increase in CYP3A4 activity in DM-hep condition. Together these results indicate that though both ECO and ICO have similar cholangiocyte lineage potential (Figure 4), only ICO and not ECO show hepatocyte lineage potential. This indicate both organoid types retain some regional specific differentiation potential, with the extrahepatic bile duct region lacking clear hepatocyte-fate differentiation.

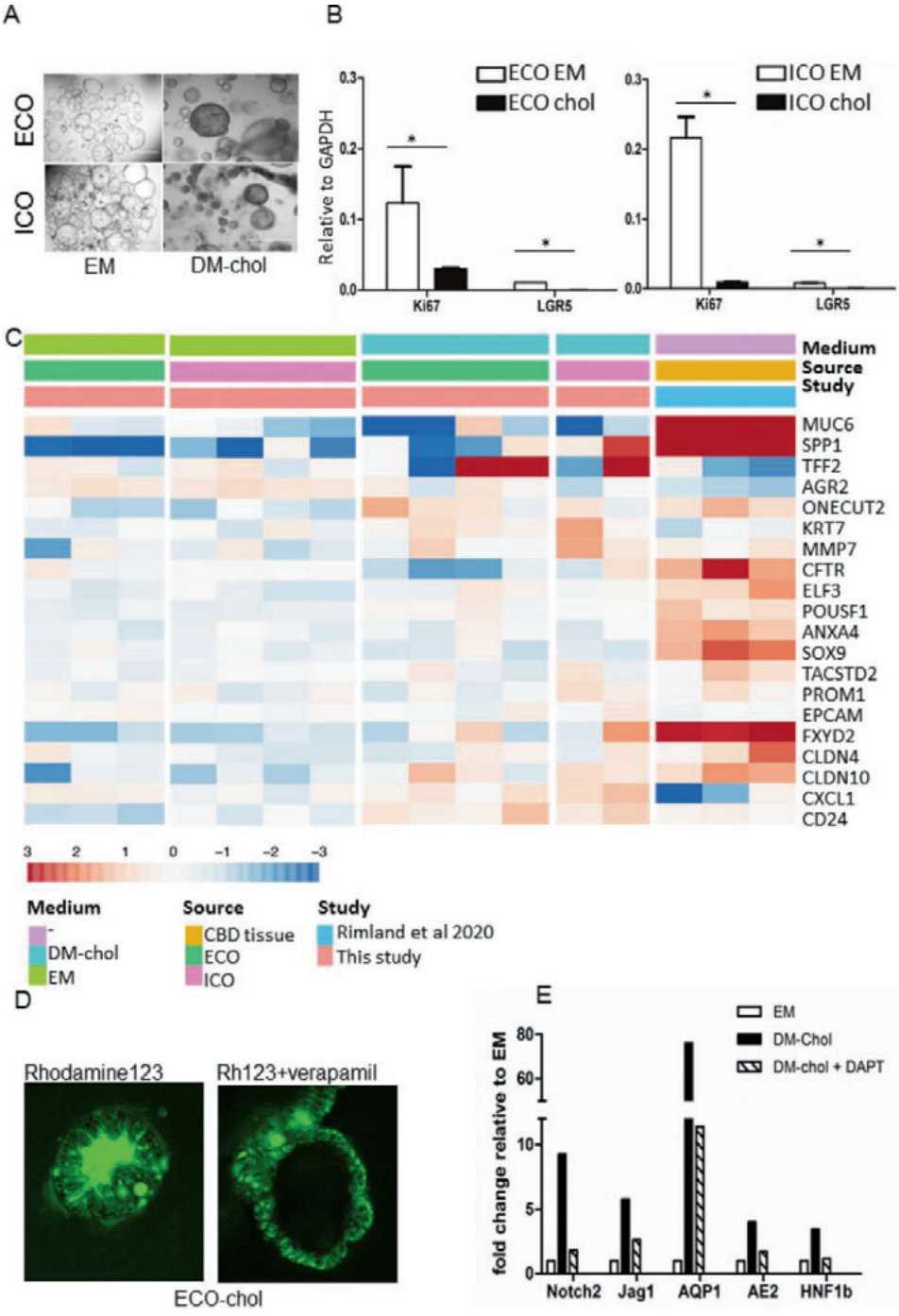
A
ECO
ICO
EM
DM-chol
B
ECO EM
ECO chol
ICO EM
ICO chol
Relative to GAPDH
Ki67
LGR5
C
Medium
Source
Study
MUC6
SPP1
TFF2
AGR2
ONECUT2
KRT7
MMP7
CFTR
ELF3
POUSF1
ANXA4
SOX9
TACSTD2
PROM1
EPCAM
FXYD2
CLDN4
CLDN10
CXCL1
CD24
Medium
DM-chol
EM
Source
CBD tissue
ECO
ICO
Study
Rimland et al 2020
This study
D
Rhodamine123
Rh123+verapamil
ECO-chol
E
EM
DM-Chol
DM-chol + DAPT
fold change relative to EM
Notch2
Jag1
AQP1
AE2
HNF1b

Figure 4. Both ECO and ICO have cholangiocyte-fate differentiation potential.
(a) Both ECO and ICO have cholangiocyte-fate differentiation potential. Culturing organoids in cholangiocyte differentiation medium (DM-chol) for 14 days result in morphological changes, Organoids became denser, had thicker outer walls as compared to EM condition and stopped proliferating. Shown are representative bright field microscopic images (bar = 1000 um). **(b)** At gene expression level, stem cell/WNT-target gene and proliferation markers LGR5 and Ki67 were significantly downregulated in DM-chol both for ECO and ICO. **(c)** Gene expression clustering is based on 20 genes selected for their high expression in cholangiocytes by single cell RNA sequencing. For benchmarking the cholangiocyte-differentiated ICO and ECO bile duct tissue gene expression profiles were used (Rimland *et al.*[17]). Both ICO and ECO showed clear upregulation of cholangiocyte genes in DM-chol conditions. **(d)** Fluorescent tracer dye was used to determine transporter channel activity in DM-chol ECO. As shown in left panel, Rhodamine123 is actively transported into the lumen of ECO-chol. This luminal transport of rhodamine was completely inhibited by MDR1 inhibitor, verapamil (10 nM, right panel). **(e)** Blocking the Notch-pathway by DAPT, inhibit cholangiocyte-fate differentiation of ECO. This confirms that Notch signals are important drives of cholangiocyte lineage development *in vitro*.

Modeling cystic fibrosis biliary disease in ECO

To determine the feasibility to use ECO as a model for bile duct diseases, organoids were initiated from eBD tissue collected from a CF patient at time of liver transplantation. This patient was known to carry a compound heterozygous mutation in the CFTR gene, resulting in a non-functional CFTR protein. Western blot analysis of protein lysate from organoids confirmed the absence of mature CFTR protein (band at 170 kDa) in the CF-ECO (Figure 6A, and complete blot displayed in Figure S3) which was clearly visible in the healthy ECO. Immature CFTR (band at 130 kDa) was detected in both CF and healthy organoids as expected. Initiation and expansion of the CF-ECO was similar efficient compared to ECO from healthy donors. As shown in Figure 6B, EdU incorporation assays showed similar levels level of cell proliferation, with 18% of cells S-phase for CF-ECO, as compared to healthy ECO (14%, Figure 1J). Functional transporter assays in Ussing chambers showed a clear lack of forskolin-activated CFTR-mediated chloride currents (Figure 6C). To demonstrate that this non-responsiveness was specific for the CFTR channel, the Ca^{2+} activated Cl^- channel was activated with UTP at the apical side of the cells. Upon UTP addition, the channel was clearly activated in the CF-ECO cells and could be specifically inhibited by CaCC channel inhibitor T16inh-A01. As previously showed in Figure 3, ECO of healthy donors show clear activity of both CFTR and the Ca^{2+} activated Cl^- channel.

The CFTR channel is known to co-localized with other transporter channels, like MDR1 [23]. To test whether the CFTR deficiency in organoids effects the function of other channels we needed to differentiate CF-ECO in DM-chol condition in order to measure MDR1 activity. As shown in Figure 6D, the CF-ECO showed comparable cholangiocyte-fate differentiation as the healthy counterparts. The morphological changes in CF-ECO appeared smaller. In DM-chol conditions less dense organoids were observed as compared to healthy donor ECO (Figure 4). This difference could be attributed to changes in water export due to dysfunctional CFTR

channel activity. As shown in Figure 6E, changes in gene expression of CF-ECO in DM-chol condition were similar to normal ECO (Figure 4). Stem cell and proliferation markers, LGR5 and Ki67 were down regulated upon differentiation. Conversely, expression of mature cholangiocyte markers KRT19, NOTCH2, and HNF1β were upregulated (Figure 6E). Although the MDR1 pump and the CFTR channel are co-localized[32], MDR1 functionality was not diminished in ECO of CF patient (Figure 6F). Efficient transport of the Rhodamine123 was seen in the CF-ECO which again could be blocked by specific inhibitor, Verapamil. Combined these results provide evidence that ECO can be used as a patient-specific model for bile duct diseases like CF and encourage further research on CF physiology and personalized drug testing.

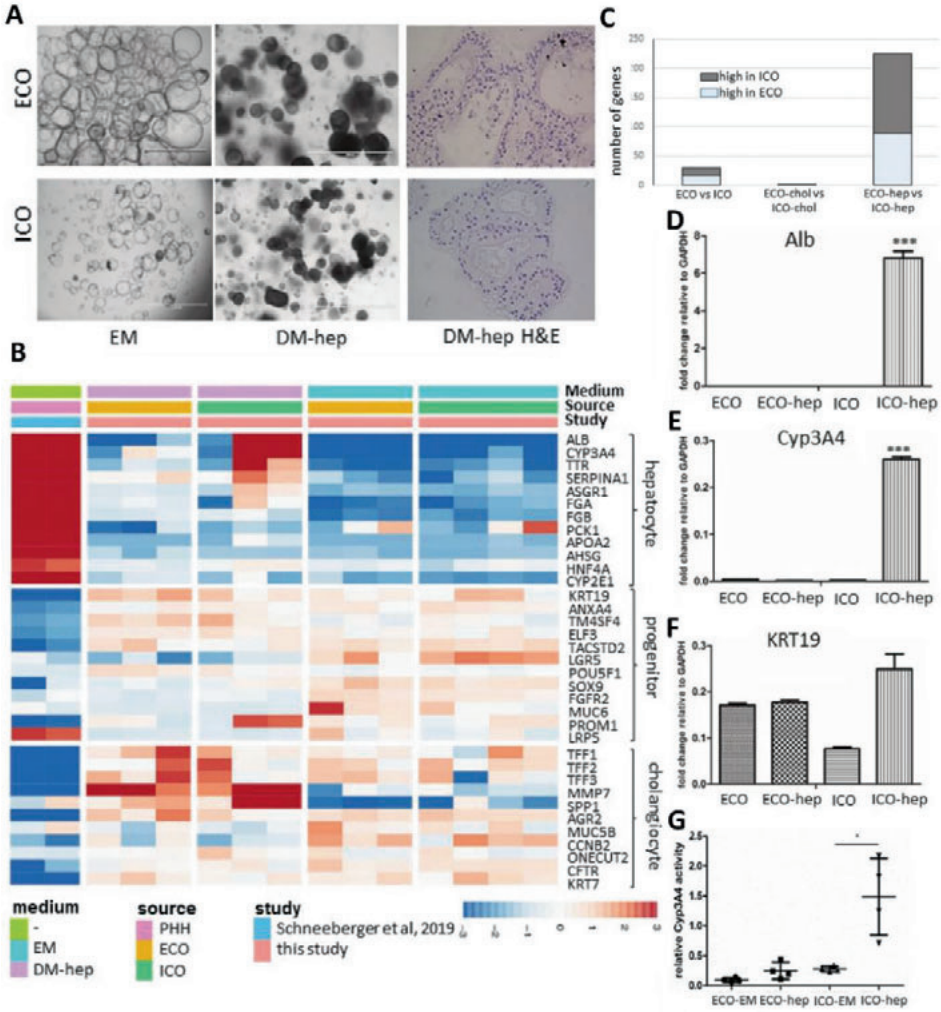

Figure 5. ECO lack hepatocyte-fate differentiation potential.
(a) Culturing organoids in hepatocyte differentiation medium (DM-hep) for 14 days result in morphological changes. Organoids became denser (DM-hep) and stopped proliferating (bar = 1000 um). H&E staining of 5 µm organoid Sections (40×) show multiple cell layers and dense cellular structure in DM-hep. **(b)** Bulk RNA sequencing analysis was performed and 35 selected genes associated with heptatocyte, cholangiocyte and liver progenitor cells[15] provided an expression heatmap showing the relative expression of ECO and ICO organoids that were differentiated to hepatocyte-fate. Relative gene expression levels are indicated in color, with blue for down-regulated genes and red for upregulated genes. None of the ECO-hep organoids clearly expressed hepatocyte-specific genes, whereas 2 of the 3 ICO-hep organoids showed expression to a hepatocyte-like phenotype. Primary hepatocytes (PHH, adapted from Schneeberger *et al.*[31]), served as positive controls. **(c)** Assessing general differences in ICO and ECO gene expression showed that in DM-hep condition the difference between ICO and ECO is biggest whereas small differences in gene expression was observed in DM-chol. **(d)** Gene expression levels of hepatocyte-specific genes albumin and Cyp3A4 **(e)** were further confirmed by qRT-PCR analyses in independent experiments. Both albumin and Cyp3A4 were again found increased in ICO and not in ECO. **(f)**. KRT19 expression levels did not differ significantly between these organoid types. Significance is indicated as ***$p < 0.0005$. **(g)** As a functional measure of hepatocyte metabolic activity, Cyp3A4 activity was measured using a commercially available kit. The relative Cyp3A4 activity was significantly higher in DM-hep conditions for ICO but not for ECO. Significance is indicated as *$p < 0.01$

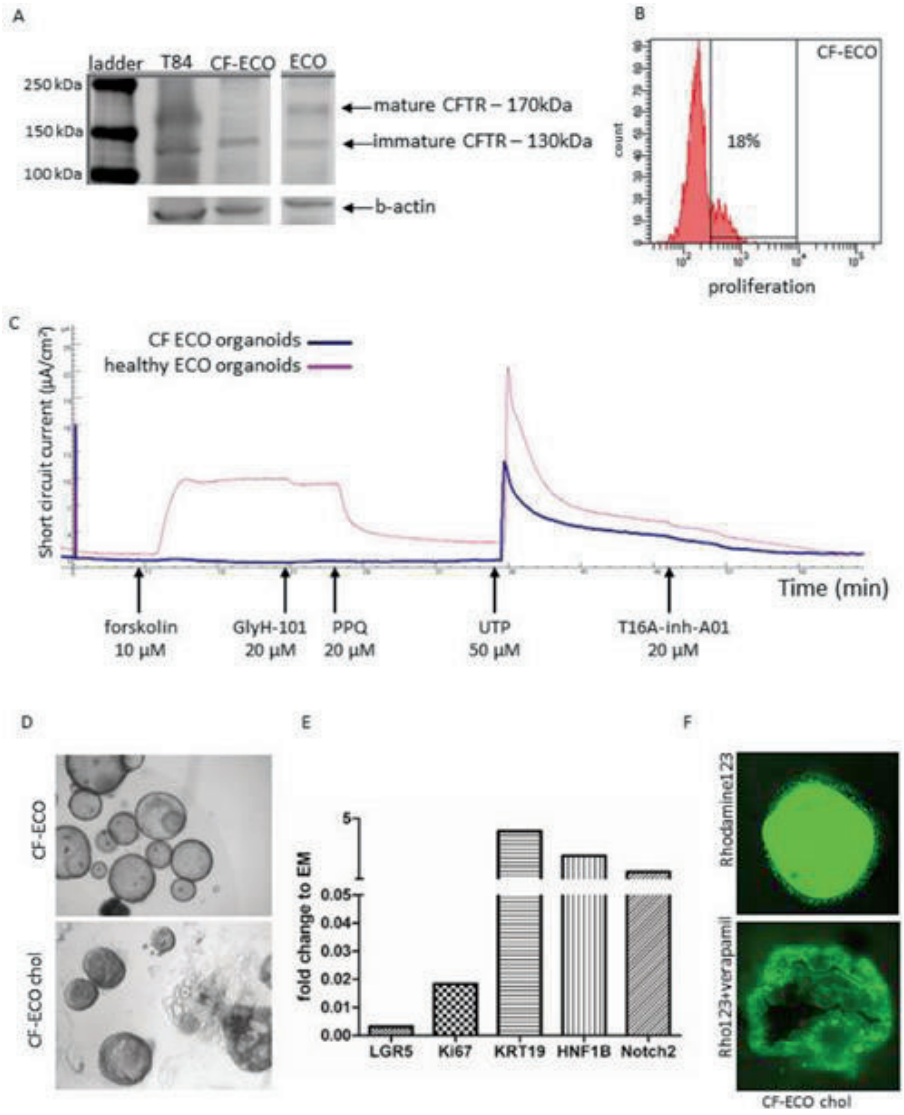

Figure 6. Patient-derived ECO can model cystic fibrosis biliary disease.

(a) ECO cultures were initiated from CF patient extrahepatic bile duct tissue. ECO from healthy donors were used as positive controls. Western blot analysis showed clear expression of wild type mature CFTR protein (170 kDa) in healthy control ECO, whereas this protein was absent in CF-ECO. Instead, only an immature CFTR (band of 130 kDa) was present in CF-ECO.The immature band was also detected in healthy ECO organoids and in a T84 control cell line (colon carcinoma cell line expressing mature CFTR). Shown is a cropped blot and β-actin served as a loading control. The full blot is provided in Figure S3. **(b)** The CF-ECO showed similar cell proliferate speed as healthy ECO; 18% at passage 15 as

demonstrated with EdU incorporation using flow cytometry. **(c)** Functional transporter assays were done using CF-ECO (blue line) and healthy ECO (pink line) in an Ussing chamber assay. As expected, CF-ECO cells do not respond to CFTR stimulation with forskolin, whereas healthy ECO stimulated with forskolin showed a clear current which was inhibited by CFTR inhibitors, GlyH-101 and pyrimido-pyrrolo-quinoxalinedione (PPQ). These inhibitors had no effect on the CF-ECO. Stimulation with UTP shows functionality of other Ca^{2+}-dependent Cl^- channels in both ECO (CF and healthy) and both are responsive to the specific inhibitor of this channel, T16A-inh-A01. **(d)** Representative cultures of undifferentiated CF-ECO (upper panel,) and CF-ECO that are differentiated to cholangiocytes (DM-chol, lower panel). **(e)** Changes in gene expression of CF-ECO after cholangiocyte-fate differention. Changes are similar to healthy ECO. **(f)** Functional transport of Rhodamine123 via transported channels was shown in CF-ECO organoids differentiated to cholangiocyte fate. This signal is specific for MDR1 as it could be complete blocked by Verapamil. Shown is one of two experiments and MDR1 activity was comparable to healthy ECO.

Discussion

The development, homeostasis, and repair of iBD and eBD involves distinct mechanisms, either involving cholangiocyte or progenitor cell proliferation or maturation. In this study, organoids were successfully initiated from human eBD and pair-wise compared to the well-established iBD-organoids[14]. Overall, these two types of organoids, ECO and ICO, behaved highly similar in terms of gene expression, proliferation capacity and function capacities. Despite these similarities, we observed regional-specific differences in their differentiation potential. As reported earlier, ICO have clear bipotent differentiation capacity. However, here we found that ECO are committed to differentiation to cholangiocyte-fate and lack the ability to differentiate to a hepatocyte-like phenotype. A similar observation was recently reported by Rimland *et al.*[17]. They also demonstrate that differences exist between ICO and ECO which is mostly reflected in the exclusive capacity of ICO to differentiate in the direction of hepatocyte lineage. Considering the differences in embryonic origin ECO may also be bipotent, not in respect to hepatocyte-fate, but with the potential for pancreatic-lineage and cholangiocyte-lineage differentiation potential. Although this has also been suggested by others[6,7], it requires further research to confirm this. As shown in Figure 2, only few genes were differentially expressed between ECO and ICO lines. Currently, a follow-up study has started to find markers that distinguish between the organoid-initiating cells of each type at a single-cell resolution and show their localization and distribution in primary liver and bile duct tissue. Recent advances in stem cell biology and novel culture technology enabled the large-scale expansion of primary biliary epithelium by generating complex 3D stem cell-derived constructs or organoids from liver biopsies[14]. Whether these organoids arise from LGR5-positive or negative cells, remains to be determined. Lineage tracking studies in Lgr5-creERT2 reporter mice suggests that LGR5-negative cells could be activated upon liver injury induction and at that point start to express LGR5[33]. This implies plasticity of liver ductal cells that respond to the need of parenchymal cells. These liver-organoids, or more specifically, ICO enabled detailed analysis of intrahepatic biliary epithelium. In parallel, mature cholangiocytes were derived from human induced pluripotent cells (iPSC) to act as model for biliary disease and drug screening[21]. However, both liver-derived organoids and iPSC-based cholangiocytes could not provide insight into the (stem) cell populations present in eBD. With the availability of eBD biopsies collected during liver transplantation, we embarked on characterizing organoids from the extrahepatic biliary epithelium (eBD) and compared them to paired organoids initiated from iBD of the same donor. The non-canonical WNT-stimulated extrahepatic cholangiocyte organoids as described by Sampaziotis[16], isolated from eBD are potent cells for regenerative medicine applications[16,34]. However, these cholangiocyte organoids are assumedly derived from mature primary cholangiocytes (not stem/progenitor cells) and are not dependent on canonical WNT signaling like the LGR5-positive ICO[14] and ECO. Although cholangiocyte organoid cultures are interesting in their own right they are not

representative of extrahepatic LGR5-positive stem cell populations which reside in the peribiliary glands and which are dependent on canonical Wnt signaling[35,36]. As the ECO resemble biliary progenitor cells that are present in the bile ducts, they can specifically be employed in studies focusing on stem cell defects leading to biliary diseases and developmental biology research. The results described in this study may reflect intrinsic differences between intra- and extrahepatic resident (stem/progenitor) cells. It is known that differences in phenotype and functionality between mature cholangiocyte populations depend on their localization along the biliary tree[17,27]. With the development of novel technology as single cell RNA sequencing, now the cellular composition of the liver can be reconstructed based on distinct gene expression profiles of individual cell types[15,37]. Sequencing single EpCAM-positive liver cells showed they are a heterogeneous set of cells including mature cholangiocytes as well as potential progenitor cell subpopulations which both express cell surface markers TROP2 (or TACSTD2), FGFR2, TM4SF4, and CLDN1. Further analyses indicated that the cell population with intermediate expression of TROP2 ($EpCAM^{+}$ $TROP2^{int}$) to indicate the true progenitor population with both hepatocyte and cholangiocyte differentiation potential[15]. Interestingly, an earlier study on TROP2 in eBD reported that though TROP2 is non expressed in peribiliary glands, upon damage of the bile ducts TROP2 is clearly upregulated in these glands epithelial cells[38]. Although novel culture techniques provide evidence for long-term expansion of primary hepatocytes[39,40] and primary cholangiocytes[14,16], both cell types remain challenging to maintain in culture while keeping their mature functions[13,14,35]. Expansion of ECO could provide in this shortcoming. In addition to cell expansion for use in tissue engineering, as was recently demonstrated by recellularization of decellularized human eBD[41], we demonstrate that ECO, have the potential to be used as a model for bile duct-related diseases as CF. To show proof of concept, ECO were cultured from eBD tissue from a CF patient and assessed for disease-typical features. Transporter channels were functional in ECO derived from healthy donor bile duct as demonstrated by activating and blocking specific transporter function (CFTR and MDR1[42]), whereas CFTR channel activity was impaired in the CF patient-derived ECO. Of note, we also showed that healthy ECO respond significantly higher to forskolin-activation as ICO, indicating that ECO better mimic biliary epithelium that is affected in CF patients. Modeling diseases as CF using ECO will help to study not only pathways involved in fluid transport and epithelial function, but also provide the opportunity to test (toxic) effects of bile acids and beneficial effects of CFTR targeted drugs.

In conclusion, this study shows the feasibility to culture WNT-driven organoids from small tissue biopsies of human eBD and that these ECO can be differentiated to functional cholangiocyte-like cells. This opens the avenue for use in pre-clinical toxicology studies, development and testing of novel treatments in a personalized setting, and tissue engineering for patient-specific clinical applications.

References

1. Boulter, L, Govaere O, Bird TG, *et al.* Macrophage derived Wnt signaling opposes Notch signaling in a Numb mediated manner to specify HPC fate in chronic liver disease in human and mouse. Nat Med. 2012 Mar 4;18(4):572-9.
2. Lu WY, Bird TG, Boulter L*., et al.* Hepatic progenitor cells of biliary origin with liver repopulation capacity. Nat Cell Biol. 2015 Aug;17(8):971-983.
3. Boulter L, Lu WY, Forbes SJ. Differentiation of progenitors in the liver: a matter of local choice. J Clin Invest. 2013 May;123(5):1867-73.
4. Tabibian JH, Masyuk AI, Masyuk TV, *et al.* Physiology of cholangiocytes. Compr Physiol. 2013 Jan;3(1):541-65.
5. de Jong IEM, van Leeuwen OB, *et al.* Repopulating the biliary tree from the peribiliary glands. Biochim Biophys Acta Mol Basis Dis. 2018 Apr;1864(4 Pt B):1524-1531.
6. Si-Tayeb K, Lemaigre FP, Duncan SA. Organogenesis and development of the liver. Dev Cell. 2010 Feb 16;18(2):175-89.
7. Raynaud P, Carpentier R, Antoniou A, *et al.* Biliary differentiation and bile duct morphogenesis in development and disease. Int J Biochem Cell Biol. 2011 Feb;43(2):245-56.
8. Maroni L, Haibo B, Ray D, *et al.* Functional and structural features of cholangiocytes in health and disease. Cell Mol Gastroenterol Hepatol. 2015 Jul 1;1(4):368-380.
9. Benedetti A, Bassotti C, Rapino K, *et al.* A morphometric study of the epithelium lining the rat intrahepatic biliary tree. J Hepatol. 1996 Mar;24(3):335-42.
10. Alpini G, Roberts S, Kuntz SM, *et al.* Morphological, molecular, and functional heterogeneity of cholangiocytes from normal rat liver. Gastroenterology. 1996 May;110(5):1636-43.
11. Sato K, Meng F, Giang T, *et al*. Mechanisms of cholangiocyte responses to injury. Biochim Biophys Acta Mol Basis Dis. 2018 Apr;1864(4 Pt B):1262-1269.
12. Clevers H, Loh KM, Nusse R. Stem cell signaling. An integral program for tissue renewal and regeneration: Wnt signaling and stem cell control. Science. 2014 Oct 3;346(6205):1248012.
13. Huch M, Dorrell C, Boj SF, *et al.* In vitro expansion of single Lgr5+ liver stem cells induced by Wnt-driven regeneration. Nature. 2013 Feb 14;494(7436):247-50.
14. Huch M, Gehart H, van Boxtel R, *et al.* Long-term culture of genome-stable bipotent stem cells from adult human liver. Cell. 2015 Jan 15;160(1-2):299-312.
15. Aizarani N, Saviano A, Sagar, *et al.* A human liver cell atlas reveals heterogeneity and epithelial progenitors. Nature. 2019 Aug;572(7768):199-204.
16. Sampaziotis F, Justin AW, Tysoe OC, *et al.* Reconstruction of the mouse extrahepatic biliary tree using primary human extrahepatic cholangiocyte organoids. Nat Med. 2017 Aug;23(8):954-963.
17. Rimland CA, Tilson SG, Morell CM, *et al.* Regional differences in human biliary tissues and corresponding *in vitro* derived organoids. Hepatology. 2021 Jan;73(1):247-267.
18. Broutier L, Andersson-Rolf A, Hindley CJ, *et al.* Culture and establishment of self-renewing human and mouse adult liver and pancreas 3D organoids and their genetic manipulation. Nat Protoc. 2016 Sep;11(9):1724-43.
19. Preibisch S, Saalfeld S, Tomancak P. Globally optimal stitching of tiled 3D microscopic image acquisitions. Bioinformatics. 2009 Jun 1;25(11):1463-5.
20. Legland D, Arganda-Carreras I, Andrey P. MorphoLibJ: integrated library and plugins for mathematical morphology with ImageJ. Bioinformatics. 2016 Nov 15;32(22):3532-3534.
21. Sampaziotis F, de Brito MC, Madrigal P*, et al.* Cholangiocytes derived from human induced pluripotent stem cells for disease modeling and drug validation. Nat Biotechnol. 2015 Aug;33(8):845-852.
22. Dekkers JF, Wiegerinck CL, de Jonge HR, *et al.* A functional CFTR assay using primary cystic fibrosis intestinal organoids. Nat Med. 2013 Jul;19(7):939-45.

23. Vidović D, Carlon MS, da Cunha MF, *et al.* rAAV-CFTRDeltaR Rescues the Cystic Fibrosis Phenotype in Human Intestinal Organoids and Cystic Fibrosis Mice. Am J Respir Crit Care Med. 2016 Feb 1;193(3):288-98.
24. Bijvelds MJ, Bot AG, Escher JC, *et al*. Activation of intestinal Cl- secretion by lubiprostone requires the cystic fibrosis transmembrane conductance regulator. Gastroenterology. 2009 Sep;137(3):976-85.
25. Justin AW, Saeb-Parsy K, Markaki AE, *et al.* Advances in the generation of bioengineered bile ducts. Biochim Biophys Acta Mol Basis Dis. 2018 Apr;1864(4 Pt B):1532-1538.
26. van Meegen MA, Terheggen SW, Koymans KJ, *et al.* CFTR-mutation specific applications of CFTR-directed monoclonal antibodies. J Cyst Fibros. 2013 Sep;12(5):487-96.
27. Schmelzer E, Zhang L, Bruce A, *et al.* Human hepatic stem cells from fetal and postnatal donors. J Exp Med. 2007 Aug 6;204(8):1973-87.
28. Raven A, Lu WY, Man TY, *et al.* Cholangiocytes act as facultative liver stem cells during impaired hepatocyte regeneration. Nature. 2017 Jul 20;547(7663):350-354.
29. Ng-Blichfeldt JP, Schrik A, Kortekaas RK, *et al.* Retinoic acid signaling balances adult distal lung epithelial progenitor cell growth and differentiation. EBioMedicine. 2018 Oct;36:461-474.
30. Barman PP, Choisy SC, Gadeberg HC, *et al.* Cardiac ion channel current modulation by the CFTR inhibitor GlyH-101. Biochem Biophys Res Commun. 2011 Apr 29;408(1):12-7.
31. Schneeberger K, Sánchez-Romero N, Ye S*, et al.* Large-Scale Production of LGR5-Positive Bipotential Human Liver Stem Cells. Hepatology. 2020 Jul;72(1):257-270.
32. Scoazec JY, Bringuier AF, Medina JF, *et al.* The plasma membrane polarity of human biliary epithelial cells: in situ immunohistochemical analysis and functional implications. J Hepatol. 1997 Mar;26(3):543-53.
33. Cao W, Chen K, Bolkestein M, *et al.* Dynamics of Proliferative and Quiescent Stem Cells in Liver Homeostasis and Injury. Gastroenterology. 2017 Oct;153(4):1133-1147.
34. Sampaziotis, F. Building better bile ducts. Science. 2018 Mar 9;359(6380):1113.
35. Huch M, Bonfanti P, Boj SF*, et al.* Unlimited in vitro expansion of adult bi-potent pancreas progenitors through the Lgr5/R-spondin axis. EMBO J. 2013 Oct 16;32(20):2708-21.
36. Huch M, Boj SF, Clevers H. Lgr5(+) liver stem cells, hepatic organoids and regenerative medicine. Regen Med. 2013 Jul;8(4):385-7.
37. MacParland SA, Liu JC, Ma XZ*, et al.* Single cell RNA sequencing of human liver reveals distinct intrahepatic macrophage populations. Nat Commun. 2018 Oct 22;9(1):4383.
38. Matsui S, Harada K, Miyata N, *et al.* Characterization of Peribiliary Gland–Constituting Cells Based on Differential Expression of Trophoblast Cell Surface Protein 2 in Biliary Tract. Am J Pathol. 2018 Sep;188(9):2059-2073.
39. Hu H, Gehart H, Artegiani B, *et al.* Long-Term Expansion of Functional Mouse and Human Hepatocytes as 3D Organoids. Cell. 2018 Nov 29;175(6):1591-1606.e19.
40. Zhang K, Zhang L, Liu W*, et al. In vitro* Expansion of Primary Human Hepatocytes with Efficient Liver Repopulation Capacity. Cell Stem Cell. 2018 Dec 6;23(6):806-819.e4.
41. Willemse J, Roos FJM, Voogt IJ, *et al.* Scaffolds obtained from decellularized human extrahepatic bile ducts support organoids to establish functional biliary tissue in a dish. Biotechnol Bioeng. 2021 Feb;118(2):836-851.
42. Hoof T, Demmer A, Hadam MR, *et al.* Cystic fibrosis-type mutational analysis in the ATP-binding cassette transporter signature of human P-glycoprotein MDR1. J Biol Chem. 1994 Aug 12;269(32):20575-83.

Supplementary Information

Results

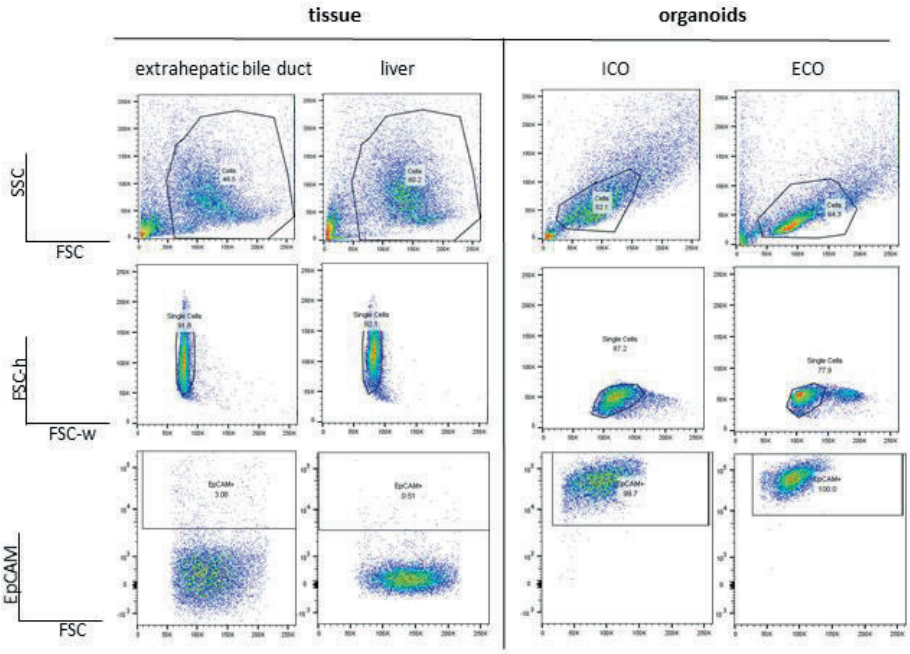

	EpCAM+ % individual	EpCAM+ (%±SD)
Biopsy/start population		
Extrahepatic bile duct (n=3)	3.1 / 0.4 / 0.2	1.2±1.6
Liver (n=3)	0.5 / 1.7 / 0.5	0.9±0.7
Organoids		
ECO (n=2)	99.6 / 99.9	
ICO (n=3)	99.7 / 99.5 / 99.6	99.6±0.1

Figure S1. Representative dotplots of flow cytometric analysis.
Biopsies of donor liver (n=3) and extrahepatic bile duct (n=3), as well as ICO (n=3) and ECO (n=2) were assessed for the expression of EpCAM positive cells by flow cytometry. Gating strategy is shown by the scatter pattern gate, and single cells gating (FCS-h vs FSC-w). Average EpCAM positivity (percentage of life single-cell events ± SD) is presented in the table.

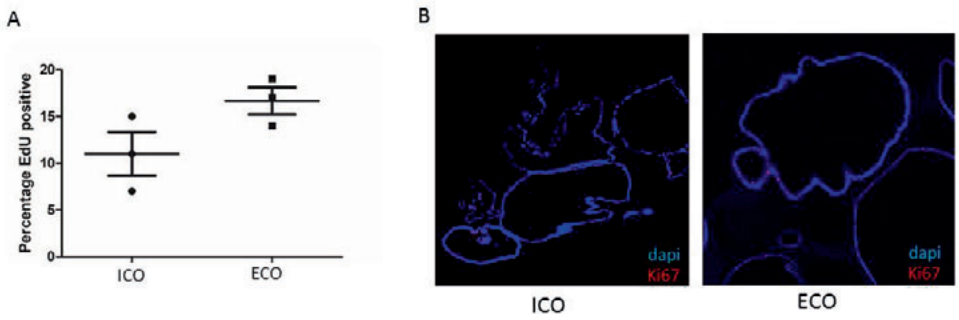

Figure S2. Proliferation rate of ECO and ICO.

(a) EdU incorporation was analysed in paired ECO and ICO from the same donor (n=3) by flow cytometry. The average of proliferating cells (S-phase) was 11.0±2.1% and 17.3±2.4% (mean±SEM) in ICO and ECO, respectively. Differences were not significantly different between these organoid types (p= 0.122). To confirm, FFPE sections of ECO and ICO were stained with a monoclonal antibody for the proliferation marker Ki67 using immunofluorescence. **(b)** Representative images show a similar Ki67positive cells in both organoid types (red = Ki67, blue = dapi).

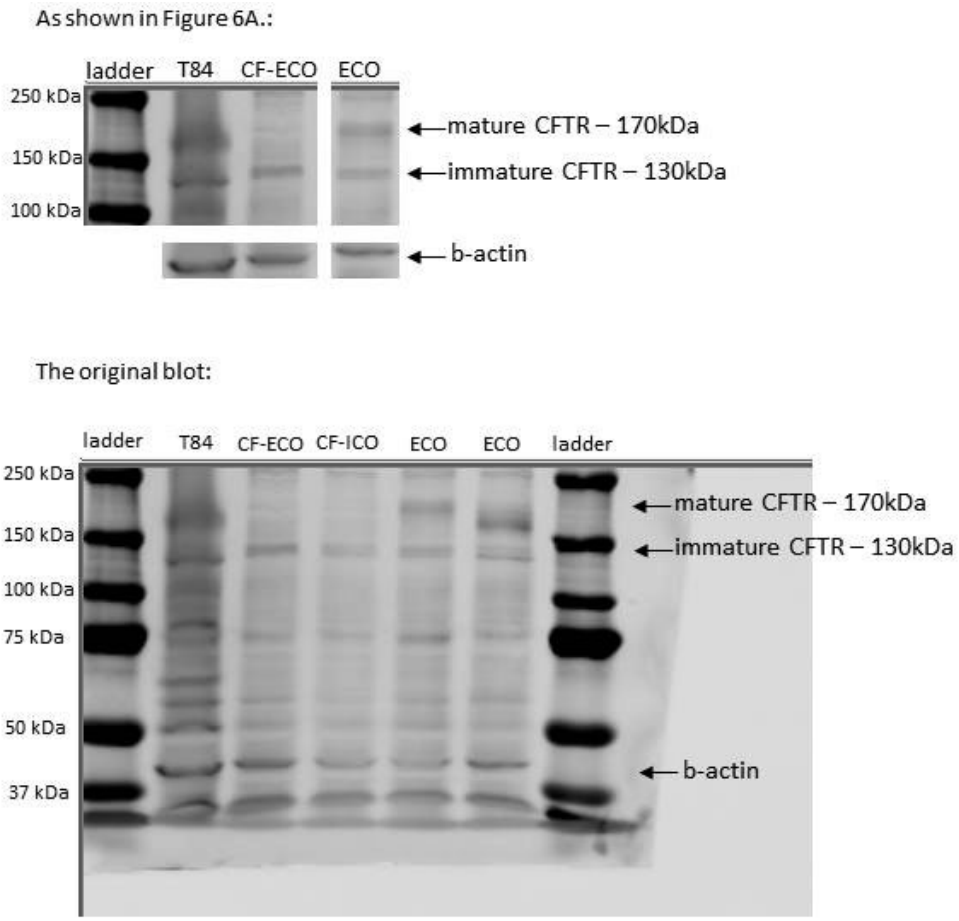

Figure S3. Complete Western blot analysis of CFTR-protein. We show the cropped details of the blot in the manuscript (Figure 6A). In this supplemental figure, we provide the complete Western blot.

6

CHAPTER 6

Cholangiocyte organoids from human bile retain a local phenotype and can repopulate bile ducts *in vitro*.

Floris JM Roos*, Haoyu Wu*, Jorke Willemse, Ruby Lieshout, Laura A Muñoz Albarinos, Petra de Ruiter, Yik Y Kan, Jan-Werner Poley, Marco J Bruno, Jeroen de Jonge, Richard C Bàrtfai, Hendrik Marks, Jan NM IJzermans, Monique MA Verstegen×, Luc JW van der Laan×

* these authors contributed equally;
× shared senior authorship.

Clinical and Translational Medicine 2021;11(12):e566.

Abstract

The well-established 3D organoid culture method enabled efficient expansion of cholangiocyte-like cells from intrahepatic-(IHBD) and extrahepatic bile duct (EHBD) tissue biopsies. The extensive expansion capacity of these organoids enables various applications, from cholangiocyte disease modeling to bile duct tissue engineering. Recent research demonstrated feasibility of culturing cholangiocyte organoids from bile, which was minimal-invasive collected via endoscopic retrograde pancreaticography (ERCP). However, a detailed analysis of these bile cholangiocyte organoids (BCOs) and the cellular region of origin was not yet demonstrated. In this study, we characterize BCOs and mirror them to the already established organoids initiated from IHBD- and EHBD-tissue. We demonstrate successful organoid-initiation from extrahepatic bile collected from gallbladder after resection and by ERCP or percutaneous transhepatic cholangiopathy from a variety of patients.

BCOs initiated from these three sources of bile all show features similar to in vivo cholangiocytes. The regional-specific characteristics of the BCOs are reflected by the exclusive expression of regional common bile duct genes (HOXB2 and HOXB3) by ERCP-derived BCOs and gallbladder-derived BCOs expressing gallbladder-specific genes. Moreover, BCOs have limited hepatocyte-fate differentiation potential compared to intrahepatic cholangiocyte organoids. These results indicate that organoid-initiating cells in bile are likely of local (extrahepatic) origin and are not of intrahepatic origin. Regarding functionality of organoid initiating cells in bile, we demonstrate that BCOs efficiently repopulate decellularised EHBD scaffolds and restore the monolayer of cholangiocyte-like cells *in vitro*.

Conclusion. Bile samples obtained through minimally-invasive procedures provide a safe and effective alternative source of cholangiocyte organoids. The shedding of (organoid-initiating) cholangiocytes in bile provides a convenient source of organoids for regenerative medicine.

Introduction

The biliary tree is a complex tubular system representing the extrahepatic bile duct (EHBD) and the intrahepatic bile ducts (IHBD).[1] In addition to the difference in anatomical location, both these ductal structures originate from distinct progenitor cells during embryonic development.[2] The IHBD arises from bipotential hepatoblasts, while the EHBD develops from a shared pancreaticobiliary progenitor.[2,3] Despite the divergent origin, a single layer of highly specialized epithelial cells, cholangiocytes, are lining the ducts of the entire biliary tree.[1] Cholangiocytes are responsible for modifying bile composition and form an important barrier between the cytotoxic bile and surrounding tissues. Defects in cholangiocytes can result in severe diseases (cholangiopathies), often developing into end-stage liver diseases, for which liver transplantation is the only curative therapy.[3] The regional diversity present in cholangiocytes is also reflected in different cholangiopathies.[4,5] For instance, Alagille Syndrome is only affecting intrahepatic cholangiocytes, in line with the underlying autosomal mutation that prevents proper hepatoblast differentiation to intrahepatic bile ducts. Other examples are primary sclerosing cholangitis (PSC) and non-anastomotic bile duct strictures, diseases that are predominantly affecting the EHBD.[4-6] The presence of regional diversity in the extrahepatic biliary tree was recently confirmed by Rimland *et al.*, where the authors showed distinct gene expression profiles in cholangiocytes covering different parts of the EHBD.[7] In this study 3D cholangiocyte organoids were cultured from both IHBD as well as EHBD and it is demonstrated that only intrahepatic cholangiocyte organoids (ICOs) could (partially) differentiate to hepatocyte-like cells. This result reflects the embryonic origin of this type of cholangiocytes.[7] Initially, cholangiocyte organoids were initiated from liver biopsies, and described as liver-derived bipotent stem cells *in vitro*.[8] However, elaborated studies demonstrate that mature cholangiocytes, undergoing widespread (epi)genetic remodeling into a highly proliferative state, are the organoid-initiating cell type and not adult (biliary) stem cells. Due to canonical-WNT stimulating culture conditions, cholangiocyte organoids start expressing adult stem cell markers/WNT-target genes (*LGR5*) which are substantially overexpressed when compared to *in vivo* cholangiocytes.[9-12] By doing so, cholangiocyte organoids acquire a phenotype comparable to rapid proliferating cholangiocytes *in vivo* (ductal reprogramming).

As ICOs maintain patient-specific characteristics upon expansion, they provide a powerful tool to study the biology and pathophysiology of cholangiocytes.[8] The downside of this culture platform is that ICOs are generally initiated from liver biopsies which are collected during potentially harmful interventions, or during liver transplantation. This limits the use of COs in disease modeling and studying disease progression to a limited subset of patients, i.e. patients that undergo liver transplantation due to end-stage liver disease. To overcome these hurdles, an elegant and minimally invasive alternative to initiate patient-specific organoids was shown by Soroka *et al*.[13]. Here, the authors expanded bile cholangiocyte

organoids (BCOs) from bile samples collected during routine clinical procedures via endoscopic retrograde cholangiopancreaticography (ERCP).[13] However, it is still unclear from which region in the biliary tree (intra- or extra-hepatic) the BCO-initiating cells originate from. Furthermore, a recent study demonstrated that cholangiocyte organoids derived from human EHBD and cultured in non-canonical WNT-stimulating conditions, could efficiently repopulate collagen scaffolds that were successfully transplanted into mice as functional EHBDs.[14] However, whether this is feasible with patient-derived COs cultured in canonical-WNT stimulating conditions obtained from *in vivo* collected bile, is still unknown.

Therefore, the aim of our study is to further characterize the properties of bile cholangiocyte organoids with a focus on determining the anatomical origin of BCOs. Moreover, in addition to ERCP as source of BCOs, we extent the sources of bile with collection via percutaneous transhepatic cholangiopathy drainage (PTCD) and directly from resected gallbladders. As a proof of principle, we show efficient repopulation of human bile duct scaffolds using BCOs collected via ERCP from patients and demonstrate that human EHBD scaffold can help sustain organoids to form a functional cholangiocyte monolayer *in vitro*. Based upon this evidence, the feasibility for the use of BCOs in personalized regenerative medicine is near.

Materials and Methods

Bile, brush and tissue collection

Bile samples (1 mL per patient) were obtained *in vivo* from patients suffering from biliary diseases (Table 1 and Table S1) and which were undergoing ERCP (n=54) or PTCD (n=3) for regular treatment regimens at the Erasmus MC, Rotterdam, the Netherlands. An additional brush specimen (n=2) was collected from the common bile duct (CBD) via ERCP if the patient already underwent brush cytology for standard diagnostics. Bile samples collected *in vivo* were transported at 4˚C and processed within 1 hour after collection. All patients gave written informed consent to use the bile collected during these procedures for research purposes. This study was approved by the local Erasmus MC Medical Ethical Committee and registered under number MEC-2016-743.Bile (3 mL) was collected from gallbladders from donor (n=6) or explanted livers (n=8) obtained during liver transplantation procedures performed at the Erasmus MC, Rotterdam and was stored at 4˚C and processed within 24 hours after collection. All patients or next of kin gave written informed consent to use the tissue for research purposes. This study was approved by the local MEC of the Erasmus MC under number MEC-2014-060.

Tissue biopsies from liver (circa 0.5-3 cm^3, n=4), extrahepatic bile duct (EHBD, circa 0.5-3 cm^3, n=4), and gallbladders (n=3, scraped cells) were obtained from donor livers (n=5) or explant livers (n=2) during liver transplant procedures performed at the Erasmus MC, Rotterdam, the Netherlands. For complete methodology see supplementary materials and methods.

Initiation and culture expansion of organoids

Organoids from liver- and EHBD biopsies were processed, initiated and expanded as previously published by Rimland *et al.*[7] and Huch *et al.*[8]. For detailed methodology and culture conditions see supplementary materials and methods and table S2.

Organoids from bile (BCOs) were initiated according to an adapted protocol from Soroka *et al.*[13] for culturing BCOs from bile collected via ERCP. For detailed methodology and culture conditions see supplementary material and methods and table S2. All experiments were performed with passage five organoids unless otherwise stated. When referred to ECO-cultures in experiments, these cultures resemble canonical-WNT stimulated ECOs (tissue obtained according to Rimland *et al.* and cultured in the Huch *et al.* conditions, table S2)[7,8] unless otherwise stated.

Flow Cytometry

Flow cytometry analysis was performed to evaluate the presence and frequency of $EPCAM^+$ cells in the collected bile samples from ERCP patients. Bile cells were stained with antibodies against human CD326 (EpCAM) (Biolegend 324203; mouse monoclonal – FITC conjugated, 1:100) according to the manufacturer's instructions. Flow cytometry analysis was performed

using a Canto flow cytometer (BD Biosciences) and cell populations were analysed using Flowjo (version v10.6.1, BD).

RNA extraction, cDNA synthesis and RT-qPCR

Total RNA was collected after removal of the culture medium by adding 700µL of QIAzol lysis reagent (Qiagen) to a 24 well containing organoids (two 25µL BME/matrigel domes). RNA was isolated using the miRNeasy kit (Qiagen) according to the manufacturer's protocol[16] and the concentration was measured using a NANOdrop 2000 (ThermoFisher). cDNA from 500ng RNA was prepared using 5x PrimeScript RT Master Mix in a 2720 thermal cycler (Applied Biosystems). RT-qPCR was performed with the primer sets provided in Table S3. All RT-qPCR data are presented as mean with a 95% confidence interval or as standard error of the mean. RT-qPCR values are relative to the housekeeping gene Glyceraldehyde-3-Phosphate Dehydrogenase *(GAPDH)* or Hypoxanthine-guanine-fosforibosyl-transferase *(HPRT)*.

Immunofluorescence (IF) staining

To evaluate protein expression of the organoids, IF was performed with selected antibodies for cytokeratin (KRT)-7, KRT-19, SRY Box (SOX)9, Albumin, Mucin-1 (MUC-1), Secretin Receptor (SCTR) and cystic fibrosis transmembrane conductance regulator (CFTR) (complete list of antibodies and dilutions used are displayed in Table S4), as previously described for ICOs[8]. For detailed methodology see supplementary materials and methods.

Ussing chamber assay

COs cultured from tissue and bile were seeded on a transwell culture plate (24 well plate 6.5mm, Corning) to grow COs in a 2D fashion. Upon forming a confluent monolayer, transwells were placed in an Ussing chamber (Physiologic instruments) set up to analyze functional cholangiocyte-specific transporter channels (CFTR and Ca^{2+}- activated Cl^- channel) using Acquire & Analyze Software 2.3 (Physiologic Instruments, San Diego, California). For detailed methodology see supplementary materials and methods.

ϒ-Glutamyltransferase (GGT) assay

Supernatant (10µL) of BCOs (n=3) and, as a positive control, of ECOs cultured in non-canonical WNT conditions (n=3), was collected. These specific ECOs were chosen since they were shown to excrete the same amount of GGT as primary cholangiocytes.[14] GGT activity was determined using a colorimetric assay kit (MAK089; Sigma-Aldrich), performed according to the manufacturer's protocol.

Rhodamine-123 transport functionality

Functionality of the Multi Drug Resistance (MDR)-1 transporter was assessed using the Rhodamine-123 assay.[17] Specificity was determined by blocking MDR-1 transporter with

Verapamil (10 µM, Sigma Aldrich) for 30 min at 37˚C prior to Rhodamine-123 incubation (100 µM, Sigma Aldrich). Subsequent confocal images were acquired using a Leica SP5 confocal microscope (LEICA) equipped with a 488 nm laser and a 20x zoom dipping lens.

Cell proliferation assessment

Cell proliferation characteristics of BCOs, ICOs and ECOs were measured by PrestoBlue Metabolic Assay (Life Technologies) and 5-Ethynyl-2'-deoxyuridine (EdU)-incorporation (ThermoFisher). For detailed methodology and gating strategy see supplementary materials and methods and Figure S3A and B.

RNA sequencing data obtaining and analysis

RNA was isolated from 3 biological replicates from different types of organoids (ERCP bile, GB bile, ICO, and ECO). 500 ng of total RNA was used for library construction using KAPA RNA Hyper + RiboErase HMR kit (Roche 08098140702). RNA-sequencing (RNAseq) libraries were sequenced paired-end (2 x 38bp) on Illumina NextSeq 500 platform. After sequencing, the qualities of the reads were checked using fastqc. An average of 20 million paired-end reads were aligned to human genome (hg38) using STAR[18] (2.7.0f) with default settings. BAM files were sorted and indexed using SAMtools[19] (1.7). The number of mapped fragments was quantified at gene level using featurecount[20] (1.6.4) with the following parameters, -p -g gene_name, based on Gencode annotation (v30). The R package DESeq2[21] (1.22.2 on R 3.5.1) was used for differential gene expression analysis and for generating principal components analysis (PCA) and heatmap plots. Genes with less than 2 fragments were removed from the differential gene expression analysis. All the differentially expressed genes are determined according to adj-*P*<0.05. Vst normalized counts were generated using vst function from DESeq2, and transformed to Z-scores. Pheatmap package was used to generate heatmap plots using either vst normalized counts or Z-scores as input. Pathway analyses were performed by Enrichr web tool[22] using the significantly differentially expressed genes as input with default settings. RNAseq data from gallbladder- and common bile duct tissue as published by Rimland *et al.*[7] was used as a reference gene set for cholangiocytes and RNAseq data from 2D cultured primary hepatocytes was obtained from Schneeberger *et al.*[23] as a reference gene set for hepatocyte gene expression. For comparing the transcriptome between the ERCP-BCOs cultured in 3D (hydrogel) and ERCP-BCOs that were cultured on scaffolds, RNA samples were isolated from 3 biological replicates. The library construction was done as mentioned before, and the libraries were sequenced pair-end (2x 42bp). The analysis was performed using the same strategy as mentioned before, but using the tools with different versions (STAR version=2.7.6a, SAMtools version=1.7, featureCounts version=2.0.1, R version=3.6.1, DEseq2 version=1.26.0). In particular, before generating the count table, subsampling was applied to have the samples with comparable sequencing depths using SAMtools. Differentially expressed genes are determined based on adj-P<0.05 and |log2(Fold change)| > 1. The R package fgsea[24] (1.12.0) was used for gene set enrichment

analysis (GSEA). Genes up-regulated in either 3D (hydrogel, BME) or scaffold culture system were used as input, and then compared to the differentially gene set published by Rimland *et al*.[7] (Tissue vs. organoid of common bile duct). Cell cycle related genes (involved in G2M and S phases) from R package Seurat (3.2.3)[25] were used for the heatmap. RNAsequencing data from this study was disposed to the GEO dataset (number: GSE156519).

Upregulation of hepatocyte-related genes

BCOs, ICOs and ECOs (from the same patient, n=3 individual patients) were differentiated to hepatocyte-faith. The hepatocyte differentiation protocol used, was adapted from Huch *et al.*[8] with slight modifications (Helmuth *et al.* patent: WO2017149025A1)[26]. For detailed methodology see supplementary materials and methods.

Repopulation of EHBD scaffolds

Decellularised human EHBD scaffolds were reseeded with BCOs. For this, EHBD tissue (n=3, length: 4cm) was obtained from research livers that were deemed unsuitable for transplantation. EHBD scaffolds were created according to the previously published protocol by Willemse *et al.*[27] using a Triton-X-100 based decellularisation method. EHBD scaffolds were reseeded with single-cells derived from ERCP-BCOs (passage 5-9) and cultured for 21 days. For detailed methodology see supplementary materials and methods.

Statistical analyses

All statistical analyses were conducted using SPSS (software version 21, SSPS Inc, Chicago, IL, USA). Qualitative data were analysed with the $\chi 2$ or Fisher exacts tests and were presented with numbers and percentages. Continuous variables were tested using an independent T-test or Mann-Whitney-U test and presented with normal distribution as means with standard deviation and if not normally distributed, they are presented as range. In all tests, a P value of <0.05 is considered significant.

Results

Human bile harbors organoid-initiating cells

Human bile was collected using the ERCP or PTCD procedure or from gallbladders after resection (Figure 1A, B). After obtaining and washing the cell fraction from bile, organoid cultures were initiated. Furthermore, cells obtained by CBD brushes were included and cultured as organoids. BCOs could be initiated from healthy individuals as well as from a variety of patients with different underlying biliary diseases (Table 1, Table S1), although with mixed success rates between sources. Upon initial issues with bacterial infections, vancomycin was added to the culture medium to prevent loss of cultures without losing viable cells (Figure S1). In addition, to prevent fungal infections, which were frequently observed in patients suffering from PSC or CCA, BCO cultures of these patients were supplemented with 1% antibiotic-antimycotic instead of vancomycin for the first three days, as previously published.[13] As shown in Figure 1C, after addition of treatment for micro-organisms, organoid-initiation was successful in 78% (42/54) of bile samples from ERCP. The success rate for brushes was 100% (2/2) and for bile samples from PTCD 67% (2/3). Organoids collected from *ex vivo* bile (resected gallbladders, >12 hours after surgery) could be cultured with a lower 33% (2/6) success rate. This is possibly due to the longer storage time of the bile as compared to the rapidly processed ERCP and PTCD bile (cultured within 1 hour after collection). Indeed, gallbladder bile processed within 12 hours after resection had a 75% (6/8) success rate of BCO initiation (Figure 1C) and ERCP-derived bile stored for 4 hours before processing yielded no viable organoids (Figure S2). Furthermore, we could not find any difference in successful culture percentages between different underlying (biliary) conditions or between cultures derived from livers transplanted after brain death- or circulatory death donation. As shown in Figure 1B, organoids from bile and brushes have a cystic morphology, similar to previous publications of organoids cultured from intra- or extrahepatic bile duct tissue.[7,8] BCOs could be passaged long-term (>passage 15, >5 months) and could be viably frozen at different time points (Table 1). Previous research showed for ICOs that the organoid-initiating cells are $EpCAM^+$ cells and likely a subset of cholangiocytes.[8] As shown in Figure 1D, approximately 50% (mean 44.27% ±19.74, n=3) of the cells present within bile are $EpCAM^+$. These $EpCAM^+$ cells in bile are the likely organoid-initiating cells, however direct evidence is still lacking. Direct cells sorting of $EpCAM^+$ or $EpCAM^-$ cells from bile using flow cytometry failed to yield viable cells for organoid-initiation, thus indicating that likely due to cell-stress related difficulties we are unable to grow organoids from $EpCAM^+$ cells from bile (Figure S2C). In summary, human bile samples are an effective source for cholangiocyte organoids.

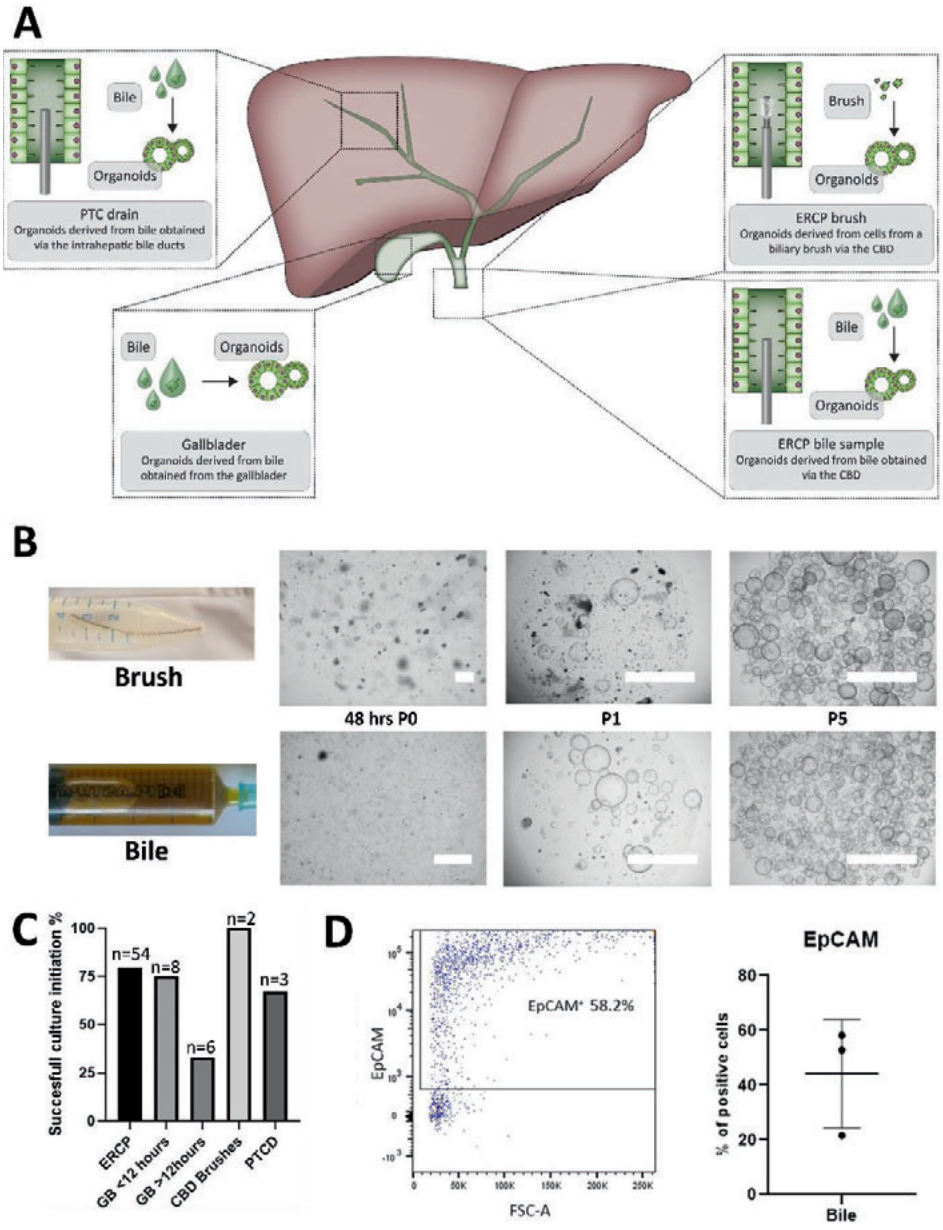

Figure 1. Culture of bile cholangiocyte organoids.

(a) Schematic overview of initiation of bile cholangiocyte organoids (BCOs) from different sources of bile and from endoscopic retrograde cholangiopancreatography (ERCP)-brushes of the common bile duct (CBD). **(b)** Representative organoid cultures from ERCP-brushes and ERCP-derived bile at different passages. Passage 0 (48 hours after culture initiation), P1 (picture taken 72 hours after passage 1) and

P5 (picture taken 120 hours after passage 5) (p), scale bars indicate 1000µm. **(c)** Successful culture percentage from different sources of bile and CBD brushes. **(d)** Flow cytometry analysis of cells within ERCP-derived bile (n=3) revealed that a mean 44.3%±19.7 are of biliary (EpCAM^{+}) origin.

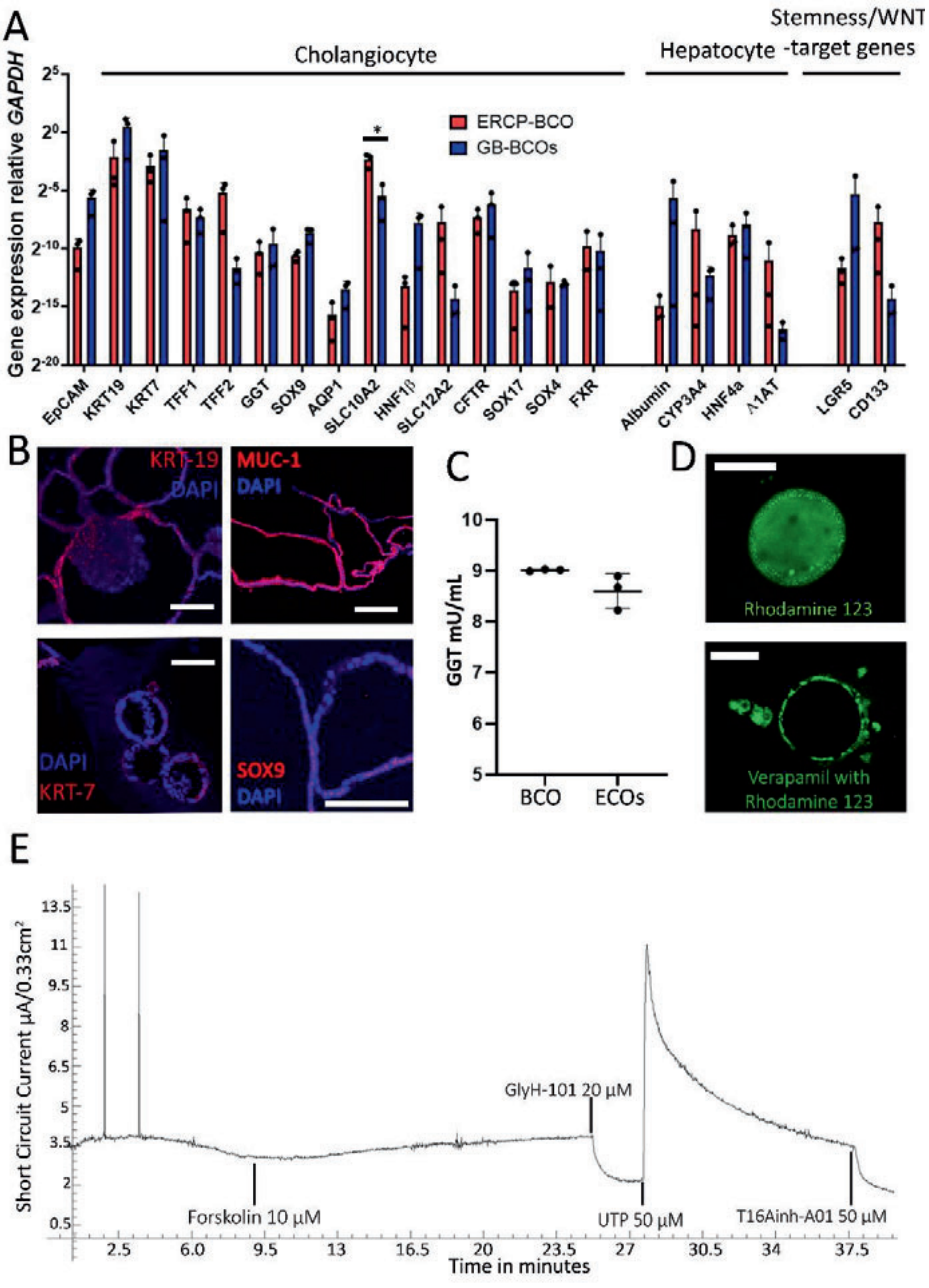

Figure 2. Bile cholangiocyte organoids represent functional cholangiocyte-like cells *in vitro.*
(a) Expression of typical cholangiocyte, hepatocyte and stemness/WNT-target associated genes relative to *GAPDH* (presented as 2^{-dct} method) analysed using RT-qPCR in BCOs (n=6, BCO1-3 and BCO5-7). Mature cholangiocyte markers (*KRT7* and *KRT19*, *TFF1*, *TFF2*) were expressed relatively high compared to the expression of hepatocyte and stemness/WNT-target genes. **(b)** Protein expression by immunofluorescence of the cholangiocyte markers: KRT-19, KRT-7, MUC-1 and SOX9 (red) and nuclei (DAPI, blue) on BCOs (n=3, BCO1, 5 and 7), scale bars indicate 100 µm except for SOX9 where it indicates 200 µm. Images displayed are from BCO 5 and 7. **(c)** Gamma-glutamyltransferase activity of BCO supernatant as measured by fluorescence is similar between BCOs (n=3, BCO5-7) and ECOs (ECO8-10, n=3) grown in non-canonical WNT stimulating conditions (Sampaziotis *et al.* Nat Med 2017). **(d)** BCOs (n=3, BCO1, 5 and 7) have clear MDR-1 activity as Rhodamine 123 was actively transported out of the cells into the lumen of the organoid. Specificity was confirmed by inhibition with Verapamil, scale bars indicate 100 µm. **(e)** Representative ion-channel functionality of 2D-grown BCOs (n=4, BCO1-3 and 5) in an Ussing chamber. Stimulation with cAMP-activator forskolin (both sides), resulted in an increase in short circuit current. This was completely blocked by cystic fibrosis transmembrane conductance regulator (CFTR)-inhibitor, GlyH-101, demonstrating specific CFTR-mediated activity. It also shows calcium-dependent chloride excretion ion-channel activity, specifically stimulated by UTP and inhibited by T16Ainh-A01, indicating anoctamin-1 activity. *Indicates a significant difference ($p<0.05$).

Bile cholangiocyte organoids resemble functional cholangiocyte-like cells in vitro
All bile cholangiocyte cultures from either ERCP (n=3) or gallbladder (n=3) were analysed on gene expression by RT-qPCR and by normalized read counts from RNAseq data of BCOs compared to open access data from primary cholangiocytes and hepatocytes.[7,23] Overall, it is clear that the BCOs follow the transcriptomic profile of cholangiocytes and have limited expression of classical hepatocyte markers compared to primary hepatocytes (Figure S4A-C). Typical biliary markers such as *KRT7*, *KRT19*, sodium-depended bile acid transporter (*ASBT,* also known as *SLC10A2*), *SOX9*, *CFTR*, hepatocyte nuclear factor (*HNF*)*-1β*, and Trefoil factor (*TFF*)*1* and *TFF2* were detected (Figure 2A and S4A). Interestingly, ERCP-derived BCOs (bile collected from the common bile duct) expressed *TFF2* at somewhat higher levels when analysed by RNA-seq., while gallbladder-derived BCOs did not, but showed more expression of *SOX17* (Figure 2A and S4A and B). These, results are in line with a recent publication demonstrating the local differences between cholangiocytes.[28] Gallbladder-BCOs had a high expression of *albumin* (2/3 samples) and a low expression of *CYP3A4*, while ERCP-derived BCOs show the opposite expression profiles (Figure 2A and S4C). Although, this high expression of *albumin* in GB-BCOs could not be confirmed by RNAseq analysis, and did not reach statistical significance, a difference between ERCP- and GB-obtained BCOs still seems to be present (Figure S4C). In addition, ERCP-BCOs showed higher expression of the apical *SLC10A2* transporter and the luminal *SLC12A2* – also known as *NKCC1*- receptor when compared to GB-BCOs (Figure 2A and S4A). Additionally, both BCOs express the WNT-target gene leucine-rich-repeat-containing-G-protein-coupled receptor (*LGR*)*5* (Figure 2A and S4A) known to be higher expressed in cholangiocyte organoids compared to primary

cholangiocytes (Figure S4C).[9,11] Overall, it is clear that BCOs not fully represent mature cholangiocytes, which is reflected in less expression of functional markers *AQP1*, *GGT* and *CFTR* (Figure S4A), similar to previous results.[7] Immunofluorescence revealed protein expression of KRT-7, KRT-19, CFTR, MUC-1, SCTR and SOX9 (Figure 2B and Figure S4D), but the absence of ALB (Figure S4E) in BCOs. In addition, functionality of BCOs was assessed by determining Y-Glutamyltransferase (GGT) activity, multidrug resistance protein-1 (MDR1) activity and ion channel activity. Figure 2C demonstrates that GGT expression levels of BCOs were similar to those found in ECOs cultured in non-canonical WNT stimulating conditions (mean 9.01±SD0.2 vs. mean 8.60±SD0.13, P=0.1). Previously published data showed that these specific ECOs have a similar GGT expression level when compared to primary cholangiocytes[14], providing indirect evidence that GGT levels produced by BCOs might be similar to cholangiocytes. MDR-1 activity was assessed by the ability to transfer Rhodamine-123 into the lumen of the organoids. Upon incubation, Rhodamine-123 was transported into the organoid lumen (Figure 2D). By blocking the MDR1 channel with MDR1 antagonist verapamil, this luminal accumulation was prevented, confirming functional MDR1 transporter channel activity in BCOs. The presence of functional cholangiocyte-specific ion channels in BCOs was analysed on organoids grown on a 2D-monolayer, using an Ussing chamber setup. Incubation with forskolin (cAMP-activator) caused an increase in short circuit current (Isc), which could be inhibited by GlyH-101 (CFTR-inhibitor). It is important to state that prior to forskolin stimulation, forskolin was still present in the culture medium. Therefore, upon addition Isc responses (sometimes) can be limited, however the specific inhibitor by GlyH-101, undoubtedly demonstrated the presence of functional CFTR-receptors. Incubation with uridine 5'-triphosphate (UTP) resulted in an increase in Ca^{2+} -dependent channel activation (via purinergic R) which could be inhibited by T16Ainh-A01 (Figure 2E). These results indicate the presence of functional cholangiocyte ion-channels CFTR and Anoctamin-1 (ANO1). All together, these results indicate that BCOs maintain several functional characteristics of cholangiocytes *in vitro*, but do not represent a fully mature cholangiocyte.

Organoid-specific and regional gene profiles indicate BCOs are of local (extrahepatic) origin

One of the major questions considering bile organoids is whether they originate from an intrahepatic location or from cholangiocytes of the extrahepatic bile ducts. To investigate this, we compared the transcriptomes of BCOs, both ERCP or gallbladder derived, to ICOs and ECOs. As displayed in Figure S5A and B, Principal component analysis (PCA) of top 500 most variable genes between ERCP-BCOs and gallbladder BCOs does not result in specific clustering of either type of BCOs to either ICOs or ECOs. Thus, further analysis was performed focusing on differently expressed (DE) genes between ICOs and ECOs. These ICO- and ECO- unique gene-sets are shown in Figure 4A. As shown in Figure 4A and Figure S5C and D, two out of three ICOs had a unique expression profile compared to BCOs and ECOs. One ICO-line (ICO3)

did had absence of ECO-specific genes, but did not show the unique ICO-regional gene expression (Figure 4A and Figure S5E), that are mostly absent in BCOs from both sources as well (Figure S5E and F), indicating similarities between ECOs and BCOs. Next, we looked at regional gene expression profiles that are preserved in cholangiocyte organoids of different parts of the biliary tree tissue as was previously published.[7] These genes were also specifically analysed in BCOs derived from ERCP and gallbladders. As shown in Figure 4B and C, the typical CBD regional genes *HOXB2* and *HOXB3*[7] are highly expressed in ECOs and ERCP-BCOs, but significantly lower in ICOs and GB-derived BCOs (Figure 4D). Interestingly, in GB-derived BCOs, expression of regional-preserved gallbladder specific genes[7] were more pronounced compared to all other sources of organoids (Figure 4E). Finally, we investigated the transcriptomic difference between ERCP-derived and GB–derived BCOs. With this analysis we could identify 279 DE genes (Sup. File 2, in the online version of this manuscript), indicating that different sources of bile organoids have unique expression profiles and enriched pathways (Figure S6). Overall, these gene expression analyses of organoids from different sources indicate that they are highly comparable, but BCOs resemble ECOs more closely when looked at regional-specific genes. Moreover, different regions of the extrahepatic bile duct are partially preserved in organoids cultured from bile obtained from these regions, showing a high indication that the (majority of) organoid initiating cells come from locally obtained cells, however some contamination from intrahepatic bile duct cells cannot be excluded.

Table 1. Patient and organoid culture characteristics

Culture type	Age patient (years)	Gender	Cell Source	Donor Type or Indication ERCP/surgery	Frozen in after passage
ECO* 8	13	M	GB	DBD	5
BCO 1, ICO 1, ECO 1	27	M	Liver, EHBD, GB Bile	DBD	8
BCO 5	33	F	ERCP Bile	Bile Leakage	18
BCO 6	46	M	ERCP Bile	PSC	26
ECO* 9	50	M	GB	Bile stones	5
BCO 3, ICO 3, ECO 3	56	F	Liver, EHBD, GB Bile	Liver Explant of a cirrhotic PSC liver	10
ECO* 10	59	M	GB	DBD	5
BCO 2, ICO 2, ECO 2	59	F	Liver, EHBD, GB Bile	DBD	10
BCO 4, ICO 4, ECO 4	66	F	Liver, EHBD, GB Bile	Liver Explant of cirrhotic HCV liver with HCC	6
BCO 7	68	F	ERCP Bile	Bile stones	18

Abbreviations: AS: Anastomotic bile duct Stricture, BCO: Bile Cholangiocyte Organoid, DBD: Donation after Brainstem Death, ECO: Extrahepatic Cholangiocyte Organoids, EHBD: Extrahepatic Bile Duct, ERCP: Endoscopic Retrograde Cholangiopancreaticography, F: Female, GB: Gallbladder, GB Bile: Gallbladder Bile, ICO: Intrahepatic Cholangiocyte Organoids M: Male, PSC: Primary Sclerosing Cholangitis, HCV: Hepatitis C Virus, HCC: Hepatocellular Carcinoma. * Indicates that these organoids are cultured using the previously published protocol (Sampaziotis *et al*., Nat. Medicine 2017) stimulating non-canonical WNT culture conditions.

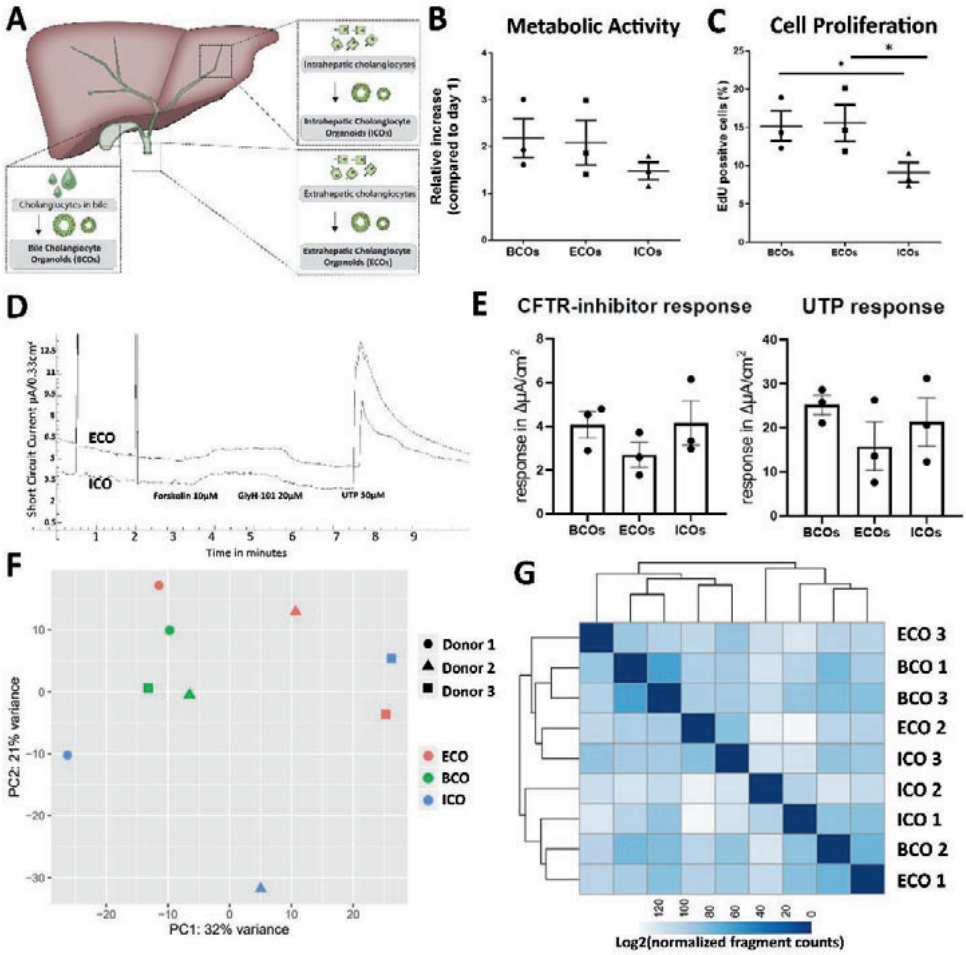

Figure 3. Paired analysis of ICOs, ECOs and BCOs from same donors reveals global similarity and specific differences in cell proliferation.

(a) Schematic layout of culture of BCOs, ICOs and ECOs from the same three donors (all experiments performed with donors 1-3). **(b)** Metabolic activity in the three organoid types as measured by PrestoBlue at day 4 did not increase when compared to day 1 after passaging. **(c)** Cell proliferation as

measured by EdU incorporation. Both BCOs and ECOs have a higher number of EdU positive cells compared to ICOs (15.17%±SD3.38 vs. 15.53%±SD4.18 vs. 9.1%±SD2.21, p=0.03). **(d)** Representative ion-channel functionality of 2D-grown ECOs (top line) and ICOs (bottom line) in an Ussing chamber. Stimulation with cAMP-activator, forskolin (addition to both sides), resulted in an increase in short circuit current. This was completely blocked by CFTR-inhibitor, GlyH-101, addition to the luminal side demonstrating CFTR-mediated activity. Also, the calcium-dependent chloride excretion ion-channel activity (anoctamin-1) could be specifically stimulated by UTP. **(e)** Quantification of the Ussing chamber data showed that both CFTR-activity (as defined by inhibition of the CFTR channel-activity), and anoctamin-1-activity (as defined by UTP stimulation) were similar between cholangiocyte organoids from all three sources. **(f)** Principal component analysis (PCA) based on top 500 most variable genes determined by RNA-seq of organoids from all three sources (n=3), showed no clear clustering based upon donor, however the BCO samples do seem to cluster. **(g)** Heatmap-clustering showing sample-to-sample distances on the same samples as used in the PCA plot. Scale bar represents the distance between samples. The lower the distance is, the more correlated the samples are. This shows no clear clustering on either source or donor.

BCOs and ECOs both lack potential to acquire hepatocyte-related properties

Previous studies showed that ICOs but not ECOs have the potential to upregulate hepatocyte-specific genes in "Hepatic medium (HM)" conditions (Figure 5A).[7,29] Since the gene-expression profiling results indicate that BCOs more closely resemble ECOs, we investigate their ability to acquire hepatocyte-like potential under these conditions.[7,8,29,30] To account for inter-donor variation, we initiated BCOs, ICOs and ECOs from tissue and bile collected from the same patients (n=4). In line with previous studies[7,28], big differences in the ability of ICOs to upregulate hepatocyte-related markers, a*lbumin* and *CYP3A4,* in HM conditions were observed between donors. Only two of the four ICO-lines showed a clear upregulation of these hepatocyte markers (Figure 5B). For the analysis of differentiation of BCOs and ECOs only the good differentiating donors were included. As shown in Figure 5B, only ICOs and not BCOs or ECOs, could upregulate all four hepatocyte markers (*Albumin, CYP3A4, HNF4α* and *A1AT)* in individual donors when cultured in HM condition. Also, downregulation of stem cell/WNT-target genes *LGR5* and *CD133* was most profound in ICOs compared to BCOs (Figure 5C). Only one BCO-line showed 33-times upregulation of *Albumin* in HM conditions compared to the 120-times in ICOs from the same donor and is maybe due to contamination of intrahepatic cholangiocytes in this BCO line. When cultured under cholangiocyte-maturation conditions, all organoids from all sources behaved similar (Figure S7). Overall, our results indicate that none of the ECOs could potentially acquire hepatocytes-like properties, which is in line with previous results.[7,28] Moreover, we demonstrate that BCOs have little to no ability to upregulate hepatocyte-markers as well, confirming that the (bulk of) organoid initiating cells for BCOs are most likely of extrahepatic origin.

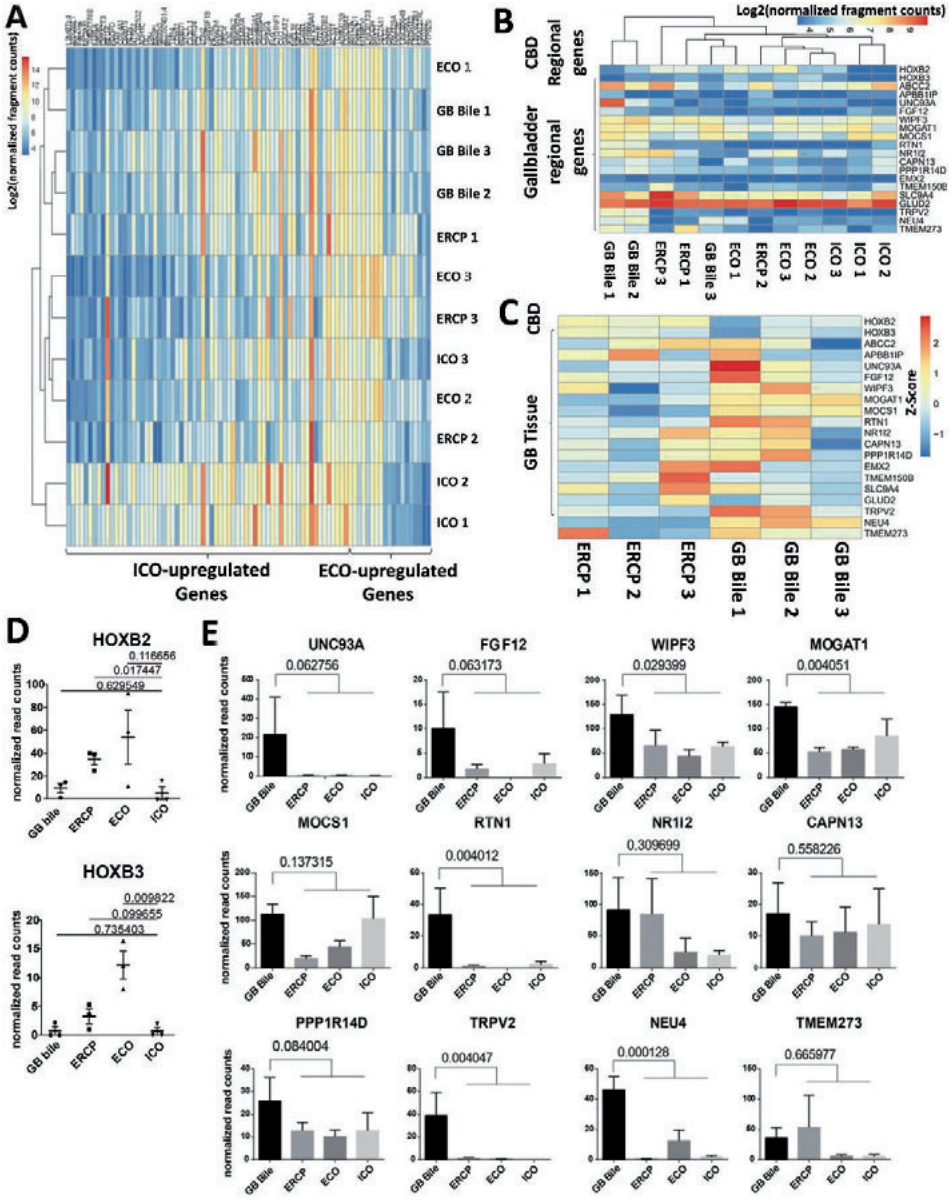

Figure 4. Regional specific gene expression suggest BCOs are of local extrahepatic originate.
(a) Heatmap of the differentially expressed (DE) genes between ICOs and ECOs (n=3, for detail of genes supplementary data file 2), on all organoid samples, showing that ECOs and BCOs cluster more closely. Moreover, BCOs lack the typical ICO-specific, but do express the ECO-specific genes. **(b)** Heatmap of regional specific genes preserved in cholangiocyte organoids derived from the common bile duct and gallbladder[7]. We confirm that ICOs lack expression of *HOXB2* and *HOXB3* as reported[7]. Both ECOs and

ERCP-derived BCOs express common bile duct genes. Moreover, it was clearly shown that in two (GB bile 1 and 2) out of three samples derived from gallbladder bile, expression of gallbladder tissue related genes was upregulated compared to other organoids. **(c)** Heatmap showing Z-score of the same gene set from **b** on BCOs from ERCP-bile and gallbladder-bile showing expression of either CBD-specific or gallbladder tissue-specific genes, demonstrating regional diversity between BCO sources. **(d)** Normalized read counts for BCOs (from either GB bile or ERCP), ICOs and ECOs for common bile duct specific markers *HOXB2* and *HOXB3* shows higher expression in ECOs (for *HOXB3*) and ERCP (*HOXB2*) derived samples compared to ICOs. **(e)** Normalized read counts for BCOs (from either GB bile or ERCP), ICOs and ECOs for 12 GB-tissue specific genes. Significantly higher expression of 5 of the 12 GB genes was observed in GB-BCOs as compared to ERCP-BCOs or ICOs and ECOs. Error bars represent the SEM from three biological replicates. P-values displayed are calculated via t-test and corrected for multiple testing. All experiments in Figure 4 are performed with donor 1-3 and 5-7.

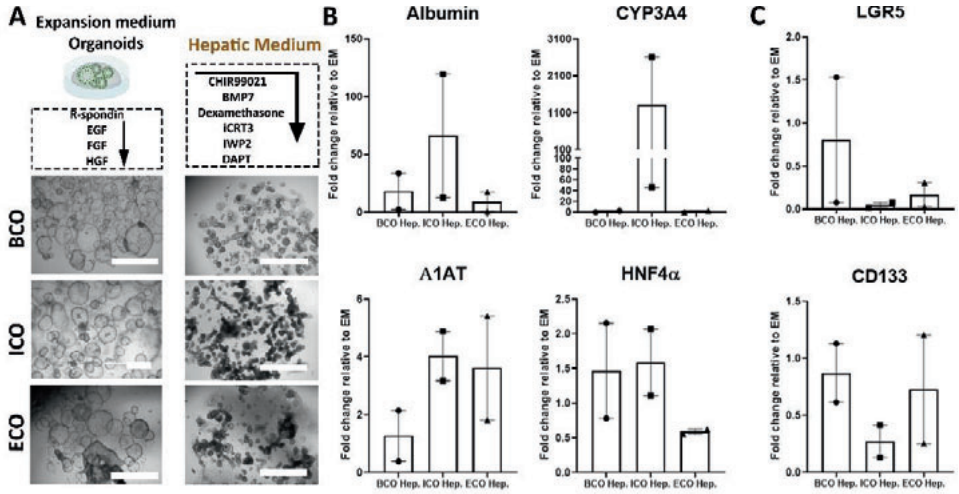

Figure 5. BCOs, similar to ECOs, lack the ability to acquire hepatocyte-like properties.
(a) Schematic overview and pictures of cholangiocyte-organoids from gallbladder-derived BCO, ICOs or ECOs (all experiments in Figure 5 are at least performed in three biological replicates with donors 1-4) grown in either in expansion medium containing canonical-WNT stimulatory factors (left) or after 14 days in hepatic medium (HM, right). Scale bar indicates 2mm. **(b)** Gene-expression by RT-qPCR for the hepatocyte-related genes (*Albumin*, *HNF4α*, *CYP3A4* and *A1AT*) in organoids cultured in HM (n=2). As indicated only ICOs could upregulate all four hepatocyte related genes in individual donors, whereas BCOs and ECOs do not. **(c)** Gene-expression by RT-qPCR relative to the housekeeper gene HPRT1 for stemness/WNT-target markers (*LGR5* and *CD133*) from all three sources (n=2) showing downregulation of stemness/WNT-target markers for ICOs in HM compared to paired samples in expansion medium.

BCOs can pave bile ducts scaffolds and acquire tissue-like cholangiocytes properties in vitro

Since most likely BCOs are of extrahepatic origin, we investigated if they could repopulate EHBD scaffold. In Figure 6A a schematic overview of the experiment is presented. The

absence of cells in the EHBD scaffolds after decellularization was confirmed using hematoxylin and eosin (H&E) (Figure 6B, left panel). Repopulation of the EHBD scaffolds with ERCP-derived BCOs resulted in full coverage of the luminal side of the scaffold surface by a confluent monolayer of cholangiocyte-like cells after 21 days (Figure 6B, right panel).Cells showed columnar morphology with nuclei on the basolateral side of the cells, while cytoplasm was more prominent at the luminal side, consistent to the histology of bile ducts *in vivo* (Figure 6B, right panel).[31] Cross sectional imaging of immunofluorescence staining showed the presence of mature cholangiocyte proteins KRT-7, KRT-19, CFTR and SCTR (Figure 6C and S8A). No upregulation of albumin protein expression was observed (Figure S8A). Whole mount confocal imaging of reseeded EHBDs shows nearly complete paving of the bile duct lining by BCO cells. Furthermore, the ostia located in large bile ducts (peribiliary glands) were repopulated by the cells. All cells stained positive for F-actin (stained by Phalloidin) and most cells expressed cholangiocyte marker KRT-7 (Figure 6D and S8B, online Video S1) and KRT-19 (Figure 6E and online Video S2).

To gain more insight in cholangiocyte-like phenotype of the BCO cultured as a monolayer on a human EHBD scaffold, bulk RNA-seq was performed to look at global gene expression profiles and to compare to those of BCOs cultured in a normal BME hydrogel. As shown in Figure 6F, principal component analysis demonstrates that gene-expression profiles of BCO cells grown on scaffolds or in a hydrogel display clear differences. Similar differences were also seen using heatmap analyses (Figure S8C). Importantly, 54% of variance in gene expression (PC1) was related to the substrate (scaffold versus hydrogel), whereas 23% of variance (PC2) was related to the organoid donor (Figure 6F). Overall, when looking in depth at specific cholangiocyte, hepatocyte- and cell cycle related genes, it is clear that there is no upregulation of hepatocyte-related genes (Figure S8E and F), but a significant downregulation of *KRT19* upon repopulation of the scaffolds was observed (Figure S8E and F). This is in line with a previous study and our own data of (Figure S4A) that shows that *KRT19* expression in cholangiocyte organoids is higher compared to primary cholangiocytes (Figure S4A).[11] In addition, the WNT-target gene *LGR5* and cell-cycle related genes are severely downregulated in BCOs cultured upon scaffolds (Figure S8D-F), likely as the result of formation of a confluent monolayer and maturation of the cells due to the local environment. Finally, we performed GSEA of BCOs cultured on bile duct scaffolds (Figure 6G, top panel) and in a hydrogel (Figure 6G, bottom panel) comparing the DE genes between primary cholangiocytes and organoids from the common bile duct (CBD) that were described by Rimland *et al.*[7]. It is clear that the unique gene-expression profile of the repopulated scaffolds shows a significant similarity to that of cholangiocytes from the CBD (p=0.003), while the BCOs cultured in a hydrogel seem to overlap with organoids cultured from the CBD. Collectively, these results provide evidence that cells obtained from bile, and that are expanded as organoids, can efficiently repopulate human bile duct scaffolds without deviation from the biliary lineage and as such obtain gene-expression profiles more closely resembling primary cholangiocytes *in situ*.

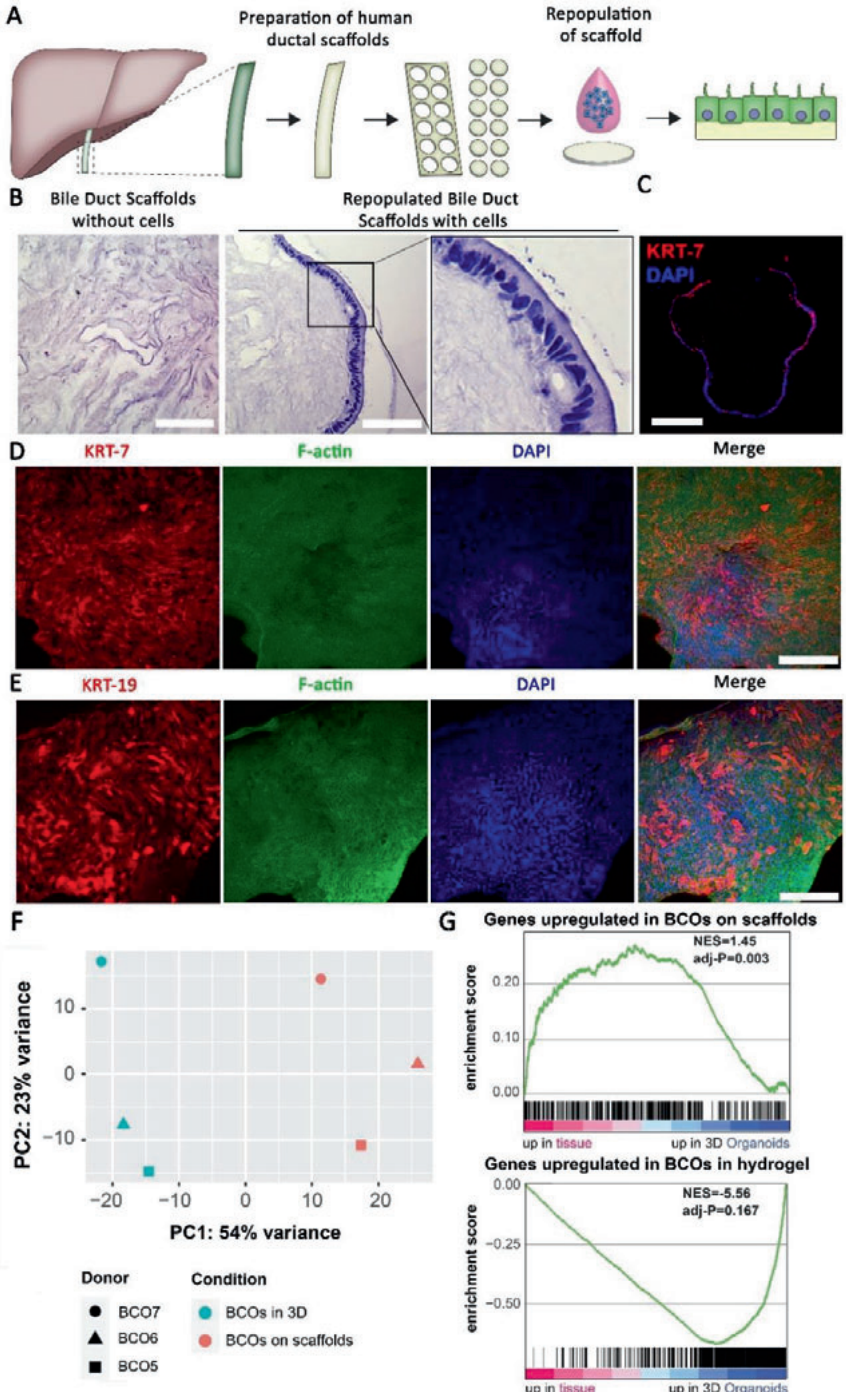
A
Preparation of human ductal scaffolds
Repopulation of scaffold
B
Bile Duct Scaffolds without cells
Repopulated Bile Duct Scaffolds with cells
C
KRT-7
DAPI
D
KRT-7
F-actin
DAPI
Merge
E
KRT-19
F-actin
DAPI
Merge
F
PC2: 23% variance
PC1: 54% variance
Donor
BCO7
BCO6
BCO5
Condition
BCOs in 3D
BCOs on scaffolds
G
Genes upregulated in BCOs on scaffolds
NES=1.45
adj-P=0.003
enrichment score
up in tissue
up in 3D Organoids
Genes upregulated in BCOs in hydrogel
NES=-5.56
adj-P=0.167
enrichment score

Figure 6. BCOs can pave human extrahepatic bile ducts scaffolds and acquire tissue-like cholangiocytes expression-profiles *in vitro*.

(a) Schematic overview of the experiment. Extrahepatic bile ducts (EHBDs) were removed from their cholangiocyte lining using a Tritox-X-100 based protocol and small punches (circular discs, Ø 3mm) were created which were then incubated for 21 days with a BCO cell suspension (consisting of approximately $50{\cdot}10^3$ single cells). All experiments are performed in triple (both technical and biological, BCO5-7). **(b)** H&E confirmed that all cells were efficiently removed from the EHBD scaffolds (left panel) and that single-cells derived from BCOs repopulate the luminal side of the EHBD scaffolds in a columnar manner (nuclei facing the basolateral side, right panel), scale bars indicate 200µm (left panel) and 50µm for the right panel. **(c)** The recellularised bile duct scaffolds expressed the cholangiocyte marker KRT-7 (red). Nuclei are stained with DAPI (blue) and scale bar indicates 200 µm. **(d)** Whole mount confocal imaging of reseeded EHBDs shows nearly complete repopulation of the bile duct lining by BCOs. This included repopulation of the ostia. Most cells expressed cholangiocyte marker KRT-7 (Red) whereas all cells stained positive for Phalloidin (F-actin, green) and DAPI (nuclei, blue). Scale bars indicate 200µm. **(e)** Similar analysis were done by whole mount confocal imaging of cholangiocyte marker KRT-19, co-stained with Phalloidin (F-actin, green) and DAPI (nuclei, blue). A large subset of cells stained positive for KRT-19 (red) after repopulation. Scale bars indicate 100µm. **(f)** PCA plot generated based on RNA-seq. data of BCO samples cultured on scaffolds and in 3D-hydrogel conditions (n=3 both conditions), showing that the PC1 is mainly determined by the different culture conditions and PC2 mainly by donor. **(g)** GSEA analysis of differently expressed genes (supplementary file 3) between BCOs on scaffolds (upper panel) and BCOs grown in a hydrogel (bottom panel). This gene-set was compared to the DEgenes from primary cholangiocytes and organoids from the CBD as previously published.[7] Clearly, BCOs on scaffolds show the highest similarity to primary cholangiocytes of the CBD (p=0.003), while BCOs in hydrogel show a trend to clustering with the CBD organoid profile.

Discussion

In this study, we demonstrate that cholangiocyte organoids can be readily cultured from bile and brushes collected *in* and *ex vivo.* Organoids were cultured from patients and healthy donors, and could be expanded long-term (>25 weeks, >15 passages) without losing their morphological characteristics using canonical-WNT stimulating conditions. These BCOs closely resemble ECOs in their gene- and protein expression patterns, functionality and inability to differentiate to hepatocytes. Furthermore, we show that BCOs are capable of repairing damaged human extrahepatic bile duct scaffolds. These findings highlight the potential of BCOs as a patient-specific minimally invasive cell source for tissue engineering and regenerative medicine applications.

Progress in understanding the pathophysiology and discovering new therapies for biliary diseases have been limited by the lack of functional cholangiocyte-like cells *in vitro*. Cholangiocyte organoids, as first described by Huch *et al.*[8,15], have the potential to overcome this problem. Since bile is shown to be a source for cholangiocyte organoids[13], it becomes feasible to collect patient samples in a minimally invasive manner during their routine clinical procedures rather than depending on invasive trough-cut biopsies. Thus, BCOs extend organoid-initiation beyond patients who receive a liver transplantation or undergo a risky liver biopsy procedure, to patients with rare diseases and following them over time. When cultured in canonical-WNT stimulating conditions, BCOs show a higher proliferation rate compared to ICOs, making them potentially more suitable for use in large-scale experiments. Hence, BCOs provide an attractive model to study cholangiocyte biology and (rare) cholangiopathies. Results from our study indicate that organoids obtained from bile (for the majority) have a local origin and retain characteristics of the local bile duct tissue. Two examples of this are the BCOs derived from bile samples from the common bile duct (by ERCP) and the BCOs derived from gallbladder bile. By comparing the gene expression for organoids with the regional specific signature genes that are preserved in organoids identified by Rimland *et al.*[7], we found that ERCP-derived BCOs upregulated the common bile duct-specific genes *HOXB2* and *HOXB3*. Moreover, gallbladder bile-derived BCOs showed specific upregulation of signature genes expressed in gallbladder-tissue. Further evidence that BCOs are not derived from intrahepatic bile ducts comes from the fact that they lack the potential to acquire hepatocyte-like properties. As shown by two previous studies, only ICOs but not ECOs have this potential.[7,29] This difference in cell fate may be related to their embryonic origin.[6] In agreement with this data, we could confirm that only ICOs, but not ECOs from the same patient, are capable of upregulating hepatocyte-specific genes.[7,29] In contrast, one BCO line was capable of upregulating albumin expression, although to significantly lower levels compared to the ICO counterpart. Thus, it could be that some intrahepatic cholangiocytes could still end up as organoid-initiating cells in BCOs. Essentially, our results highlight the resemblance between ECOs and BCOs, suggesting that BCOs should be used to

study the EHBD and EHBD-related cholangiopathies. However, a question that needs to be addressed is why these cholangiocytes are present in bile. It could be due to local turnover or due to mechanical disruption of the epithelium as a result of the procedure. But an alternative explanation would be that these cholangiocytes are harmed by the local disease and as a result detach and end up in the bile. However, this probably would not be harmful for regenerative experiments, since a recent publication showed that cholangiocyte-organoid initiation likely drives stressed cholangiocytes to a healthier status and thereby enhancing their regenerative potential after organoid initiation.[28] Moreover, we demonstrate that there are no large differences between organoids from bile or from healthy donor biopsies. Interestingly, BCOs could allow scientists and clinicians to follow patients during their inevitable disease-progression. In addition, it would be valuable to research if CCA-organoids can be cultured from bile. Research indicated that tumor organoids can be cultured from tissue specimens obtained from surgical resections or biopsies, while maintaining their resemblance to the *in vivo* tumor and can be used for personalized drug screening options.[32-35] It is known that CCA cells are detectable in bile.[36-39] Thus, it is likely that bile could provide a minimally invasive method to establish CCA organoids, with opportunities to follow CCA development over time. This could accommodate personalized treatment for a larger patient group, especially from patients suffering of CCA in the EHBD, and adjustment of therapy as the tumor progresses and changes.[39,40]

We are not the first group to report on BCOs, Soroka and colleagues showed that BCOs can be cultured from ERCP samples.[13] In their publication, they provided evidence that some of the inflammatory immune profiles of PSC patients were recapitulated *in vitro.*[13] By elaborating on their previous work, we show that BCOs can be formed from multiple sources of bile and from CBD brushes. In line with their results, we demonstrate that BCOs resemble cholangiocyte-like cells *in vitro*. In contrast, we failed to show a superiority for ECOs in function and expression of cholangiocyte-specific channels (CFTR) compared to BCO and ICOs, as was suggested.[13] Instead, we demonstrate that the transcriptomic profile is highly comparable between organoids from different sources of the same donors (Figure 3G). Soroka *et al.* accessed expression profiles between BCOs and ICOs from different donors, thus this might explain the discrepancies found between the studies. Moreover, our research focused on the underlying biology of BCOs as well as using them for tissue-engineering purposes thus providing a valuable addition to the study by Soroka *et al.*[13].

We are the first to demonstrate that BCOs cultured in canonical-WNT conditions can also be used for repopulation of the EHBD by seeding them on empty human scaffolds. These empty scaffolds were created as a model for bile duct damage using a method called decellularization.[27] We demonstrate that recellularisation by BCOs results in the formation of a confluent monolayer with cholangiocyte-like cells. Importantly, BCOs are less proliferative as well as lose their *LGR5* expression when cultured upon EHBD scaffolds. Furthermore, their gene-expression profile seems to move to tissue-like cholangiocyte as a result of interacting

with these scaffolds. Thus, we are the first group that demonstrate the need for appropriate scaffolds for the recreation of EHBD-constructs. This is in line with previous studies that demonstrated the need for appropriate niches to differentiate and maturate cells.[41-45] Of note, a recent study indicates that cholangiocytes and cholangiocyte-organoids are plastic and can adapt their phenotype to local niches in the biliary tree.[28] As a proof of concept, the authors demonstrate that ECOs can successfully restore intrahepatic bile ducts as intrahepatic cholangiocytes. Similar to their study, after repopulation by BCOs there was no upregulation of hepatocyte-related markers.[28] Moreover, we demonstrate that BCOs are unable to upregulate these hepatocyte-related makers *in vitro*. Therefore, it is likely that no other cells from the hepatic-lineage will be formed when BCOs are used for tissue-engineering purposes. Additionally, it could be that BCOs can also be used to regenerate the intrahepatic bile ducts *in vivo*, making BCOs a potential suitable candidate for cholangiopathy treatment.[28,45]

Since, we recently showed that our repopulated scaffolds with BCOs are properly polarized by cilia staining and that they become functional constructs by demonstrating TEER and ion-channel functionality[27], the next goal would be to create a 3D construct. Cholangiocyte-organoids cultured in non-canonical WNT-stimulated conditions have previously shown feasibility to repopulate 3D constructs and function as EHBD *in vivo*.[14,46] Thus, it is likely that BCOs can also repopulate 3D constructs. It is important to emphasize that we only decellularised and repopulated the epithelial compartment of the EHBD. For large constructs to function after transplantation a steady supply of nutrients and oxygen is required. Thus, spontaneous vascularization of the constructs would be necessary. Recent evidence emerged that this might be the case. Both Sampaziotis *et al.*[14] and Struecker *et al.*[47] showed signs of spontaneous vascularization of EHBD constructs as well as long-term survival of the animals without biliary complications. Moreover, it was shown that some mesenchymal supportive cells might become spontaneously present as well.[14] It would have been of great value to see if BCOs can engraft *in vivo* as well. Although previous studies showed that this is the case for mouse gallbladder-derived cholangiocyte organoids cultured in canonical-WNT stimulating conditions[48], there is still a need to demonstrate this for human BCOs as well. Our laboratory lacks the animal micro-surgery expertise and medical ethical approval to perform bile duct transplantations in mice, but in collaboration with expert labs these can hopefully be performed in the future. Furthermore, clinical applications of organoids are still (partially) limited by the use of non GMP-compliant mouse tumor ECM extracts, such as matrigel and BME. Recent studies have shown that organoids can be cultured in more clinically relevant hydrogels derived from porcine small intestine submocase[49] or Cellulose Nanofibril.[50] Thus, in theory, patient-derived BCOs cultured in these ECM hydrogels could effectively create EHBDs *in vitro,* which might be transplanted back into the patient of which the bile is obtained.

In conclusion, our study shows that bile obtained from multiple sources from a wide range of patients can be used to culture cholangiocyte organoids from the extrahepatic bile duct. This opens new doors to study extrahepatic biliary diseases and regenerative medicine of the extrahepatic bile duct without the need of invasively collected biopsies.

References

1. Tabibian JH, Masyuk AI, Masyuk T V, *et al.* Physiology of cholangiocytes. Compr. Physiol. 2013;3:1–49.
2. Zong Y, Stanger BZ. Molecular mechanisms of bile duct development. Int. J. Biochem. Cell Biol. 2011;43:257–264.
3. Banales JM, Huebert RC, Karlsen T, *et al.* Cholangiocyte pathobiology. Nat Rev Gastroenterol Hepatol. 2019 May;16(5):269-281.
4. Karimian N, Op den Dries S, Porte RJ. The origin of biliary strictures after liver transplantation: is it the amount of epithelial injury or insufficient regeneration that counts? J. Hepatol. 2013;58:1065–7.
5. Chapman R, Cullen S. Etiopathogenesis of primary sclerosing cholangitis. World J. Gastroenterol. 2008;14:3350–3359.
6. Fabris L, Fiorotto R, Spirli C, *et al.* Pathobiology of inherited biliary diseases: a roadmap to understand acquired liver diseases. Nat Rev Gastroenterol Hepatol. 2019 Aug;16(8):497-511.
7. Rimland CA, Tilson SG, Morell CM, *et al.* Regional differences in human biliary tissues and corresponding in vitro derived organoids. Regional Differences in Human Biliary Tissues and Corresponding In Vitro-Derived Organoids. Hepatology. 2021 Jan;73(1):247-267.
8. Huch M, Gehart H, Boxtel R van, *et al.* Long-term culture of genome-stable bipotent stem cells from adult human liver. Cell. 2015;1–14.
9. Planas-Paz L, Sun T, Pikiolek M, *et al.* YAP, but Not RSPO-LGR4/5, Signaling in Biliary Epithelial Cells Promotes a Ductular Reaction in Response to Liver Injury. Cell Stem Cell. 2019 Jul 3;25(1):39-53.e10.
10. Pepe-Mooney BJ, Dill MT, Alemany A, *et al.* Accepted Article This article is protected by copyright. All rights reserved Single-Cell Analysis of the Liver Epithelium Reveals Dynamic Heterogeneity and an Essential Role for YAP in Homeostasis and Regeneration. Cell Stem Cell. 2019 Jul 3;25(1):23-38.e8.
11. Aizarani N, Saviano A, Sagar, *et al*. A human liver cell atlas reveals heterogeneity and epithelial progenitors. Nature. 2019 Aug;572(7768):199-204.
12. Aloia L, McKie MA, Vernaz G, *et al.* Epigenetic remodeling licences adult cholangiocytes for organoid formation and liver regeneration. Nat Cell Biol. 2019 Nov;21(11):1321-1333.
13. Soroka CJ, Assis DN, Alrabadi LS, *et al.* Bile-Derived Organoids From Patients With Primary Sclerosing Cholangitis Recapitulate Their Inflammatory Immune Profile. Hepatology. 2019 Sep;70(3):871-882.
14. Sampaziotis F, Justin AW, Tysoe OC, *et al*. Reconstruction of the mouse extrahepatic biliary tree using primary human extrahepatic cholangiocyte organoids. Nat. Med. 2017;23:954–963.
15. Broutier L, Andersson-Rolf A, Hindley CJ, *et al*. Culture and establishment of self-renewing human and mouse adult liver and pancreas 3D organoids and their genetic manipulation. Nat. Protoc. 2016;11:1724–1743.
16. Roest HP, Ooms LSS, Gillis AJM, *et al.* Cell-free MicroRNA miR-505-3p in Graft Preservation Fluid Is an Independent Predictor of Delayed Graft Function After Kidney Transplantation. Transplantation. 2019 Feb;103(2):329-335.

17. Sampaziotis F, de Brito MC, Madrigal P, *et al.* Cholangiocytes derived from human induced pluripotent stem cells for disease modeling and drug validation. Nat Biotechnol. 2015 Aug;33(8):845-852.
18. Dobin A, Davis CA, Schlesinger F, *et al.* STAR: ultrafast universal RNA-seq aligner. Bioinformatics. 2013;29(1):15-21.
19. Li H, Handsaker B, Wysoker A, *et al.* The Sequence Alignment/Map format and SAMtools. Bioinformatics. 2009;25(16):2078-2079.
20. Liao Y, Smyth GK, Shi W. featureCounts: an efficient general purpose program for assigning sequence reads to genomic features. Bioinformatics. 2014;30(7):923-930.
21. Love MI, Huber W, Anders S. Moderated estimation of fold change and dispersion for RNA-seq data with DESeq2. Genome Biol. 2014;15(12):550.
22. Kuleshov MV, Jones MR, Rouillard AD, *et al*. Enrichr: a comprehensive gene set enrichment analysis web server 2016 update. Nucleic Acids Res. 2016;44(W1):W90-W97.
23. Schneeberger K, Sánchez-Romero N, Ye S, *et al.* Large-Scale Production of LGR5-Positive Bipotential Human Liver Stem Cells. Hepatology. 2020 Jul;72(1):257-270.
24. Korotkevich G, Sukhov V, Sergushichev A. Fast gene set enrichment analysis. BioRxiv. 2019, doi: 10.1101/060012.
25. Stuart T, Butler A, Hoffman P, *et al.* Comprehensive Integration of Single-Cell Data. Cell. 2019 Jun 13;177(7):1888-1902.e21.
26. Clevers H, Gehart H. WO2017149025 - IMPROVED DIFFERENTIATION METHOD. Retrieved from Https://patentscope.wipo.int/search/en/detail.jsf?docId=WO2017149025&tab=PCTBIBLIO, accessed upon May 1st 2020.
27. Willemse J, Roos FJM, Voogt IJ, *et al.* Scaffolds obtained from decellularized human extrahepatic bile ducts support organoids to establish functional biliary tissue in a dish. Biotechnol Bioeng. 2021 Feb;118(2):836-851.
28. Sampaziotis F, Muraro D, Tysoe OC, *et al.* Cholangiocyte organoids can repair bile ducts after transplantation in the human liver. Science. 2021 Feb 19;371(6531):839-846.
29. Verstegen MMA, Roos FJM, Burka K, *et al.* Human extrahepatic and intrahepatic cholangiocyte organoids show region-specific differentiation potential and model cystic fibrosis-related bile duct disease. Sci Rep. 2020 Dec 14;10(1):21900
30. Raven A, Lu WY, Man TY, *et al.* Cholangiocytes act as facultative liver stem cells during impaired hepatocyte regeneration. Nature. 2017 Jul 20;547(7663):350-354.
31. Boyer JL. Bile formation and secretion. Comprehensive Physiology. 2013;3(3):1035–1078
32. Broutier L, Mastrogiovanni G, Verstegen MMA, *et al.* Human primary liver cancer-derived organoid cultures for disease modeling and drug screening. Nat Med. 2017 Dec;23(12):1424-1435.
33. Nuciforo S, Fofana I, Matter MS, *et al.* Organoid Models of Human Liver Cancers Derived from Tumor Needle Biopsies. Cell Rep. 2018 Jul 31; 24(5): 1363–1376.
34. Saito Y, Muramatsu T, Kanai Y, *et al.* Establishment of Patient-Derived Organoids and Drug Screening for Biliary Tract Carcinoma. 2019, Cell Reports 27, 1265–1276
35. Kopper O, de Witte CJ, Lõhmussaar K, *et al.* An organoid platform for ovarian cancer captures intra- and interpatient heterogeneity. Nat Med. 2019 May;25(5):838-849.
36. Macias RIR, Banales JM, Sangro B, *et al.* The search for novel diagnostic and prognostic biomarkers in cholangiocarcinoma. Biochim Biophys Acta Mol Basis Dis. 2018 Apr;1864(4 Pt B):1468-1477.

37. Shen N, Zhang D, Yin L, *et al.* Bile cell-free DNA as a novel and powerful liquid biopsy for detecting somatic variants in biliary tract cancer. Oncol Rep. 2019 Aug;42(2):549-560.
38. Lee SJ, Lee YS, Lee MG, *et al.* Triple-tissue sampling during endoscopic retrograde cholangiopancreatography increases the overall diagnostic sensitivity for cholangiocarcinoma. Gut Liver. 2014 Nov;8(6):669-73.
39. Razumilava N, Gores GJ. Cholangiocarcinoma. Lancet. 2014 Jun 21;383(9935):2168-79.
40. Rizvi S, Gores GJ. Pathogenesis, diagnosis, and management of cholangiocarcinoma. Gastroenterology. 2013 Dec;145(6):1215-29.
41. Badylak SF, Freytes DO, Gilbert TW. Extracellular matrix as a biological scaffold material: Structure and function. Acta Biomater. 2009 Jan;5(1):1-13.
42. Gjorevski N, Sachs N, Manfrin A, *et al.* Designer matrices for intestinal stem cell and organoid culture. Nature. 2016 Nov 24;539(7630):560-564.
43. Nikolaev M, Mitrofanova O, Broguiere N, *et al.* Homeostatic mini-intestines through scaffold-guided organoid morphogenesis. Nature. 2020 Sep;585(7826):574-578.
44. Lorvellec M, Scottoni F, Crowley C, *et al.* Mouse decellularised liver scaffold improves human embryonic and induced pluripotent stem cells differentiation into hepatocyte-like cells. PLoS One. 2017 Dec 20;12(12):e0189586.
45. Willemse J, Lieshout R, van der Laan LJW, *et al.* From organoids to organs: Bioengineering liver grafts from hepatic stem cells and matrix. Best Pract Res Clin Gastroenterol. 2017 Apr;31(2):151-159.
46. Tysoe OC, Justin AW, Brevini T, *et al.* Isolation and propagation of primary human cholangiocyte organoids for the generation of bioengineered biliary tissue. Nat Protoc. 2019 Jun;14(6):1884-1925.
47. Struecker B, Hillebrandt KH, Raschzok N, *et al.* Implantation of a Tissue-Engineered Neo-Bile Duct in Domestic Pigs. Eur Surg Res. 2016;56(1-2):61-75.
48. Lugli N, Kamileri I, Keogh A, *et al.* R-spondin 1 and noggin facilitate expansion of resident stem cells from non-damaged gallbladders. EMBO Rep. 2016;17(5):769-779.
49. Giobbe GG, Crowley C, Luni C, *et al.* Extracellular matrix hydrogel derived from decellularized tissues enables endodermal organoid culture. Nat Commun. 2019 Dec 11;10(1):5658.
50. Krüger M, Oosterhoff LA, van Wolferen ME, *et al.* Cellulose Nanofibril Hydrogel Promotes Hepatic Differentiation of Human Liver Organoids. Adv Healthc Mater. 2020 Mar;9(6):e1901658.

Supplementary Information

Materials and Methods

Tissue collection

Biopsies were stored at 4˚C in University of Wisconsin (UW, Bridge to Life Ltd. Belzer Cold Storage Solution) preservation solution during transport. For a complete overview of characteristics of patients or donors from whom (liquid) biopsies were obtained and successfully cultured as organoids, see Table 1 and Table S1. All patients or their next of kin gave written informed consent to use their tissue collected during liver transplantation for research purposes. The use of tissue biopsies and livers deemed unsuitable for transplantation was approved by the Medical Ethical Committee (MEC) of the Erasmus MC, (MEC-2012-090, MEC-2014-060).

Initiation and culture expansion of tissue-derived organoids

Biopsies were digested by incubation with 4 mL collagenase digesting solution (2.5 mg/mL collagenase A1, Roche) in Earle's Balanced Salt Solution (EBSS, Hyclone, Thermoscientific) for 30 min at 37 ˚C. Digestion solution was diluted by adding cold Advanced (Adv)DMEM/F12 (GIBCO, supplemented with 100µg/mL penicillin/streptomycin, Life Technologies; HEPES 1M, Fisher Scientific; 1% Ultraglutamine 200mM, Fisher Scientific and 100µg/mL Primocin, Invivogen) and centrifuged for 5 minutes, 4˚C at 453g. The cell suspension was filtered through a 70 µm Nylon cell strainer and centrifuged for 5 minutes, 4˚C at 453g. Supernatant was removed and the cell pellet was suspended in cold (4°C) 25µL matrigel (Corning Incorporation) or 25µL Basement Membrane Extract (BME, Cultrex) diluted with 30% of AdvDMEM/F12 which was allowed to solidify for 30-45 minutes at 37°C before 250µL start-up expansion medium (SEM, table S2)[1] was added. SEM was replaced with canonical-WNT stimulating expansion medium (EM, table S2) after three days.[1] In addition to extrahepatic cholangiocyte organoids (ECOs) cultured in canonical-WNT conditions (table S2), ECOs were created from gallbladder tissue biopsies cultured in non-canonical WNT-stimulation conditions as a positive control for the γ-glutamyltranspeptidase assay. These organoids were created in a similar manner as described above, only cultured in the non-canonical WNT stimulating medium as published by Sampaziotis *et al.* (n=3).[2]

Initiation and culture expansion of bile-derived organoids

In short, bile was washed twice in 8 mL cold AdvDMEM/F12 and centrifugation for 5 minutes at 4°C at 453g. Subsequently, the supernatant was removed, the cell pellet was suspended in 3 mL of AdvDMEM/F12, and filtered through a 100 µm cell strainer to get a single cell suspension. After a third wash with 3 mL of AdvDMEM/F12, the cell pellet was collected and seeded either in 25µL matrigel (Corning Incorporation) or 70% BME (Cultrex) diluted with

AdvDMEM/F12. SEM (250µL) was added for the first three days and then changed to EM according to the previously published protocol and table S2.[1,3]
If bile was collected via ERCP or PTCD from patients having symptoms of bacterial cholangitis (either jaundice, fever or severe stomach ache), the medium was supplemented with vancomycin, (50µg/mL) during the first three days of culture. The effect of this treatment on organoid culture was evaluated in a dose dependent manner using AlamarBlue (ThermoFisher) assay, performed according to the manufacturer's instructions, and showed no effect on cell viability (Figure S1). Cultures initiated from PSC or cholangiocarcinoma (CCA) patient bile were supplemented with 1% Antibiotic-Antimycotic (Gibco), instead of vancomycin, during the first three days as published previously[4] to minimalize the risk of fungal infection. EM was refreshed every 3 or 4 days on all cultures and they were passaged in a 1:2-1:8 ratio according to proliferation rate. All organoid cultures described were tested and found negative for mycoplasma (data not shown).

Time window for efficient organoid initiation
To evaluate the optimal timeframe to process bile after collection, ERCP-obtained bile was divided into two aliquots of 1 mL. One aliquot was processed immediately after collection (< 1 hour), the other sample was stored for four hours at 4˚C before organoid culture initiation. After 7 days of culture, the numbers of organoids larger than 100 µm in diameter were assessed (Invitrogen™ EVOS™ FL Digital Inverted Fluorescence Microscope).

Immunofluorescence (IF) staining
Organoids were fixed for 10 minutes using 4% paraformaldehyde removing the hydrogel. Samples were paraffin embedded and cut as 4 µm thick slides. Next, they were permeabilized with 0.1% Triton X-100 diluted in PBS for 15 minutes. Subsequently, they were exposed to 10% serum diluted in 1% BSA-PBS to prevent a-specific antibody binding. Primary antibodies were added to the organoids and incubated overnight at 4˚C. Finally, incubation with the secondary antibody (Table S3) took place for 60 minutes at room temperature and cell nuclei were stained with DAPI (Vectashield, Vectorlabs) and analysis took place on a SP5 confocal microscope (LEICA) equipped with a 405, 488 and 561 nm laser. Images were analysed using ImageJ (version 1.52p, supplemented with FIJI).

Ussing chamber assay
Prior to seeding of the cells, transwell inserts were coated with 5% matrigel in PBS for 2 hours. Fully expanded domes of organoids (20 fully grown domes of 25µL) were collected in AdvDMEM/F12 and centrifuged (453*g*, 5 min, 4˚C). After removal of the supernatant, organoids were mechanically broken by vigorously up and down pipetting. The organoid suspension was spun down again and the cell pellet was made single cell by digestion in Trypsin-EDTA (TE) for 25 to 40 min at 37°C. Cells were washed in AdvDMEM/F12 and sieved

through a cell 70 µm cell strainer. Approximately $3x10^5$ cells were suspended in 200 µL EM and seeded on transwell inserts. Medium was changed every 3-4 days. To check confluency, the cells were examined by daily microscopy and electrophysiological analysis was performed after 4 days. Upon forming a confluence monolayer, transwells were placed in an Ussing chamber (Physiologic instruments) set up to analyze functional cholangiocyte-specific transporter channels (Cystic Fibrosis Transmembrane Conductance Regulator –CFTR- and calcium - activated chloride channel) using Acquire & Analyze Software 2.3 (Physiologic Instruments, San Diego, California). The temperature of the chambers was kept at 37°C by warm water bath circulation and chambers were gassed with 95%O_2, 5%CO_2. Each chamber consisted of 3mL modified Meyler solution (128 mmol/liter NaCl, 4.7 mmol/liter KCl, 1.3 mmol/liter $CaCl_2$, 1.0 mmol/liter $MgCl_2$, 0.3 mmol/liter Na_2HPO_4, 0.4 mmol/liter NaH_2PO_4, 20 mmol/liter $NaHCO_3$, 10 mmol/liter HEPES, supplemented with glucose (10 mmol/liter) at pH 7.3). Current was clamped and every second short circuit current (Isc) was recorded. CFTR-dependent anion secretion was activated by adding Forskolin (3µL, 10mM) to both sides of the cells, and GlyH-101 (3µL, 20mM, apical). Calcium (Ca^{2+}) activated chloride (Cl^-) channels (CaCC) were stimulated by UTP (3µL, 50mM, apical) and inhibited by T16Ainhibitor-A01 (3-5 µL, 50mM, apical). The Isc measurements are presented as measured (µA/0.33cm^2).

Metabolic activity measurement

Metabolic activity in organoids from bile and intra- and extrahepatic bile duct biopsies (n=3 all sources) was determined using the PrestoBlue metabolic assay. In short, 400 µL of diluted PrestoBlue (10% in AdvDMEM/F12) was added per 25 µL dome (48 well plate culture suspension, Corning). After 4 hours of 37˚C incubation, 100 µl of PrestoBlue solution per dome was transferred to a white walled 96 well plate (Perkin Elmer) and fluorescence intensity was measured using a plate reader (CytoFluor Series 4000, Applied Biosystems) with the excitation/emission wavelengths set to 530/590nm. BME without cells was measured to assess the background fluorescent signal. This measurement was repeated after three days of subsequent culture and the relative increase in PrestoBlue per dome was calculated.

Cell proliferation

EdU-incorporation was performed according to the manufacturer's protocol. In short: EdU (10µM) was added to the medium and incubated for 4 hours at 37˚C degrees. The organoids were dissociated into single cell suspension as described earlier and suspended in 200µL of 1%BSA-PBS to be analysed by flow cytometry (Canto flow cytometer, BD Biosciences). The gating strategy is shown in Figure S3. Subset analysis was done using Flowjo (version v10.6.1, BD) analysis software.

Upregulation of hepatocyte-specific markers/hepatocyte (trans)differentiation

In principle, upregulation of hepatocyte-specific markers/hepatocyte (trans)differentiation by the novel defined culture conditions is based upon removal of WNT/β-catenin stimulators and blocking of notch-related cholangiocyte differentiation. To achieve upregulation of hepatocyte-associated markers. Organoids were passaged once at 7 days during differentiation and the total differentiation protocol took 14 days (including pre-treatment with BMP7). Differentiation was confirmed by gene and protein expression analysis of genes associated with hepatocyte maturation (*Albumin*, *HNF4α*, *CYP3A4* and alpha-1-anti trypsin – *A1AT*-)[5] and stemness/WNT-target genes (*LGR5* and *CD133*)[5] by RT-qPCR. These data are presented in fold change manner comparing them to their expansion medium controls.

Cholangiocyte maturation

Cholangiocyte-maturation medium for cholangiocyte organoids (COs) was based upon the induced-pluripotent stem cell (IPS) protocol for cholangiocyte-differentiation as established by Sampaziotis *et al.*[5,6] and adapted by Verstegen MMA *et al.*[7] for tissue-derived cholangiocyte organoid cultures. This two-step protocol largely followed the principles of differentiation hepatoblast-like IPS to cholangiocytes. Bile cholangiocyte organoids (BCOs), ECOs and Intrahepatic cholangiocyte organoids (ICOs) from three donors were exposed to these culture conditions and compared to their expansion culture conditions.[1] In detail, all cholangiocyte organoids were expanded for 7 days in basement membrane extract diluted in 10% Williams-E medium (WE, Gibco, Life Technologies) to near-full wells. Culture medium was then switched to maturation medium, consisting of AdvDMEM/F12 supplemented with 1:50 B27 (Gibco), 50 ng/mL FGF10 (Peprotech), 50 ng/mL Activin-A (Gibco) and 3 µM retinoic acid (Sigma-Aldrich). After 4 days, medium was changed to WE supplemented with 10 mM nicotinamide (Sigma-Aldrich), 17 mM sodium bicarbonate (Sigma-Aldrich), 0.2 mM 2-phospho-i-ascorbic acid tri-sodium salt (Sigma-Aldrich), 6.3 mM sodium pyruvate (Invitrogen), 14 mM glucose (Sigma-Aldrich), 20 mM HEPES (Fisher Scientific), ITS+ premix (BD Biosciences), 0.1 M dexamethasone (R&D), 20 ng/mL EGF (R&D), 2 mM Ultraglutamine (Invitrogen), and penicillin (100 U/mL) & streptomycin (100g/mL). The medium was refreshed every 2 days for a total of 10 days after which the organoids were analysed. Maturation *in vitro* was assessed by gene expression profiles using RT-qPCR and immunofluorescence for protein-expression of mature cholangiocyte markers (cytokeratin –*KRT-7*, *KRT19*, *AQP1* and *CFTR*) as well as looking at progenitor/stem cell/WNT-target markers (*LGR5* and *SOX9*).[6]

Repopulation of EHBD scaffolds

EHBD scaffolds were prepared as previously published.[8] After procurement of donor livers deemed unsuitable for transplantation, EHBD (n=3, length: 4cm) were surgically removed, stored in 0.9% saline solution and frozen at -20°C. Decellularisation was started after complete thawing of EHBD tissue. Subsequently, cells were removed by submersion in 4%

Triton-X-100 + 1NH_3. The Triton solution was refreshed every 30 minutes for a total of 10 cycles. Afterwards, the EHBD segments were washed with dH_2O until all detergent was removed. This was followed by DNase type1 treatment in 0.9% NaCl + 100mM $CaCl_2$ + 100mM $MgCl_2$ treatment. Complete decellularisation was confirmed with hematoxylin and eosin (H&E) staining. H&E-stained slides were imaged with Zeiss Axiokop 20 microscope and captured with a Nikon DS-U1 camera. EHBD scaffolds were prepared using a dermal biopsy punch (Ø 3mm). These discs were reseeded by incubation with single cell suspensions made from BCOs. This cell suspension ($5.0 \cdot 10^3$ cells/µL, 10 µL) was pipetted on top of the ductal scaffolds and incubated for 4 hours at 37°C to settle. After this, 500 µL EM supplemented with 10 µM Y27632 was added. After 3 days, the medium was changed with 500 µL EM without Y27632. Medium was refreshed every 2-3 days. Reseeded scaffolds were cultured for 21 days and subsequently fixed in 4% paraformaldehyde for 20 minutes. Subsequently, immunofluorescence staining with the primary antibodies, KRT-7, SCTR, CFTR and Albumin was performed on sections as previously described under the immunofluorescence section in the methods. Furthermore, repopulation efficacy was determined by whole mount confocal microscopy to assess KRT-7 and KRT-19 protein expression. For this, reseeded EHBD samples were stained with fluorescently labeled antibodies in a similar manner as described earlier. Additional cytoskeletal staining with Phalloidin Alexa Fluor™ 488 (1:200, ThermoFisher) and nuclear staining with DAPI was performed. Samples were imaged using a Leica 20X water dipping lens on Leica DM6000 CFS microscope with a LEICA TCS SP5 II confocal system. Images were processed using ImageJ.

Results

Table S1. Characteristics of additional *in vivo* collected bile and brush samples with successful organoid initiation.

Age patient (years)	Gender	Bile Source	Indication for intervention
48	M	ERCP	AS
63	M	ERCP	AS
66	M	ERCP	Mirizzi Syndrome
31	M	Brush	PSC
41	M	ERCP	AS
77	F	PTCD	CCA
71	M	ERCP	NAS
64	M	ERCP	AS
26	F	ERCP	AS
57	F	ERCP	AS
66	M	ERCP	AS
73	M	PTCD	NAS
79	F	ERCP	CCA
60	M	ERCP	AS
20	M	ERCP	PSC
66	F	ERCP	CCA
49	M	ERCP	AS
68	M	ERCP	AS
66	F	ERCP	CCA
48	M	ERCP	AS
52	M	ERCP and brush	CCA
58	M	ERCP	AS
57	F	ERCP	AS
57	F	PTCD	CCA
71	M	ERCP	NAS
55	M	ERCP	PSC
71	M	ERCP	Bile Stones
63	M	ERCP	CCA
73	F	ERCP	Bile Stones
61	M	ERCP	AS
59	F	ERCP	PSC

26	F	ERCP	Bile Stones
58	F	ERCP	AS
70	M	ERCP	Bile Stones
72	M	ERCP	Bile Stones
20	M	ERCP	AS
54	F	ERCP	AS
54	M	ERCP	Bile Stones
63	M	ERCP	AS
85	M	ERCP	Bile Stones
50	M	ERCP	AS
54	F	ERCP	Papiladenoma
30	M	ERCP	PSC

Abbreviations: AS: Anastomotic bile duct Stricture, CCA: Cholangiocarcinoma, ERCP: Endoscopic Retrograde Cholangiopancreaticography, F: Female, M: Male, NAS: Non-Anastomotic bile duct Stricture, PSC: Primary Sclerosing Cholangitis, PTCD: Percutaneous Transhepatic Cholangiography Drainage.

Table S2. Culture conditions used within this manuscript.

Medium formulation for Start Up Medium (SEM) and Expansion Medium (EM) per mL. Medium components with a * are only added to SEM.

Component	Concentration	Brand
Supplemented AdvDMEM/F12**		Gibco
N2	1%	Gibco
B27	2%	Gibco
N-Acetylcystein	1,25 mM	Sigma
gastrin	10 nM	Sigma
EGF	50 ng/mL	Peprotech
FGF10	100 ng/mL	Peprotech
HGF	25 ng/mL	Peprotech
nicotinamide	10nM	Sigma
A83.01	5 µM	Tocris
Forskolin	10 µM	Torcris
R-Spondin	10%	Conditioned medium
WNT*	30% WNT	Conditioned medium
Noggin*	25 ng/mL	Conditioned medium
Y27632*	10µM	Tocris
hES cell cloning recovery solution*	1:1000 dilution	Stemgent

** supplemented AdvDMEM/F12 (Gibco) contains 1M HEPES (Invitrogen), 1x L-Ultraglutamine, 10000U/mL penicillin and streptomycine (both Invitrogen) and 500mg/mL Primocin (invivogen).

Medium formulation for non-canonical WNT stimulating conditions per mL.

Component	Concentration	Brand
William's-E		Gibco
EGF	20 ng/mL	Peprotech
nicotinamide	10nM	Sigma
sodium pyruvate	6.3 mM	Invitrogen
sodium bicarbonate	17 mM	Sigma
ascorbic acid	0.2 mM	Sigma
glucose	14 mM	Sigma
Ultraglutamine	2mM	Invitrogen
dexamethasone	0.1 µM	R&D systems
DKK1	100 ng/mL	R&D systems
ITS+ premix	1x	BD Biosciences
R-Spondin	10%	Conditioned medium
penicillin and streptomycine	10000U/mL	Invitrogen
HEPES	20mM	Invitrogen

Table S3. List of genes and primers used.

Gene		Primer sequence (5' à 3')	Gene		Primer sequence (5' à 3')
KRT7	F	GGGGACGACCTCCGGAATAC	HNF4α	F	GTACTCCTGCAGATTTAGCC
	R	CTTGGCACGCTGGTTCTTGA		R	CTGTCCTCATAGCTTGACCT
KRT19	F	GCACTACAGCCACTACTACACGA	GGT	F	GGTGGACATCATAGGTGGGGA
	R	CTCATGCGCAGAGCCTGTT		R	ATGACGGCAGCACCTCACTT
HNF1B	F	TCACAGATACCAGCAGCATCAGT	SLC10A2	F	GGTGGCCTTTGACATCCTCCC
	R	GGGCATCACCAGGCTTGTA		R	GCATCATTCCGAGGGCAAGC
HPRT1	F	GCTATAAATTCTTTGCTGACCTGCG	SOX9	F	ACCAGTACCCGCACTTGCAC
	R	CTTCGTGGGGTCCTTTTCACC		R	GCGCCTTGAAGATGGCGTTG
ALB	F	CTGCCTGCCTGTTGCCAAAGC	EpCAM	F	GACTTTTGCCGCAGCTCAGGA
	R	GGCAAGGTCCGCCCTGTCATC		R	AGCAGTTTACGGCCAGCTTGT
GAPDH	F	CTTTTGCGTCGCCAGCCGAG	CFTR	F	TGGCGGTCACTCGGCAATTT
	R	CCAGGCGCCCAATACGACCA		R	TCCAGCAACCGCCAACAACT
A1AT	F	AGGAGAGCAGGAAAGGACA	LGR5	F	GTCAGCTGCTCCCGAATCCC
	R	CTCAGCCAGGGAGACAGG		R	TGAAACAGCTTGGGGGCACA
AQP1	F	GGCCAGCGAGTTCAAGAAGAA	TFF1	F	ACAAGCTGCTGTACACGGACA
	R	TCACACCATCAGCCAGGTCAT		R	AAGTTTCCAGGGCCGGGCAAT
SLC12A2	F	ACCAAGGATGTGGTAGTAAGTGTGG	TFF2	F	TCTGTCCTGCCTCCCTGATCCA
	R	GGATTCTTTTTTCAACAGTGGTTGA		R	AAGTTTCCAGGGCCGGGCAAT
CYP3A4	F	AGCAAAGAGCAACACAGAGCTGAA	CD133	F	CCTGGGGCTGCTGTTTATTA
	R	ATCACCAACAGGGAGATTGC		R	CTCTGGCACGTGAATCCCGGT
SOX17	F	ATACGCCAGTGACGACCAGA	SOX4	F	CCCAGCAAGAAGGCGAGTTA
	R	TCCACGACTTGCCCAGCATC		R	CCTTCCAGTTCGTGTCCTCC
FXR	F	GGGACAGAACCTGGAAGTGG			
	R	GCCTGTATACATACATTCAGCCA			

Table S4. List of antibodies used.

Antibody	Raised	Manufacturer-Reference	Dilution
Albumin	Mouse - monoclonal	Sigma-Aldrich: A6684	1:500
SOX9	Mouse - monoclonal	ATLAS antibodies: 02712	1:200
KRT-7	Mouse - monoclonal	DAKO: M7018	1:100
KRT-19	Mouse - monoclonal	DAKO: M0888	1:100
CFTR	Mouse - monoclonal	EMD Millipore Corp: MAB3484	1:100
MUC-1	Mouse	ThermoFisher Scientific: MA5-14077	1:500
SCTR	Rabbit	Abcam: AB234830	1:100
Alexa Fluor 555	Goat – polyclonal (anti-mouse)	ThermoFisher Scientific: A21422	1:200
Alexa Fluor 488	Goat – polyclonal (anti-rabbit)	ThermoFisher Scientific: A32731	1:200

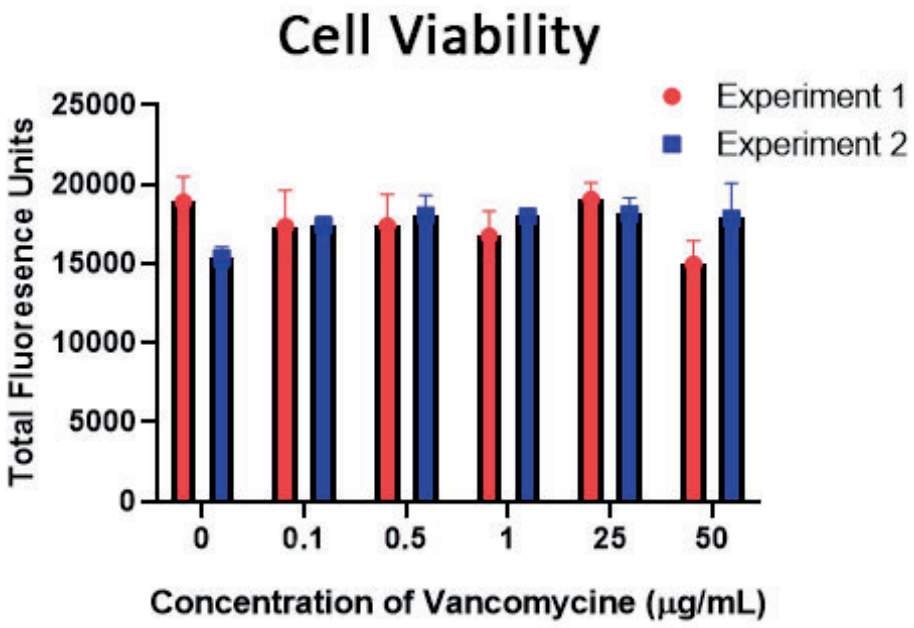

Figure S1. Organoid Viability with vancomycin medium supplementation.
AlamarBlue Fluorescence one week after initiation of bile organoid culture with different concentrations of Vancomycin (n=2 experiments, per concentration 3 technical replicates). No difference in AlamarBlue activity was observed in these experiments, indicating similar cell viability and no harm of vancomycin in BCO cultures.

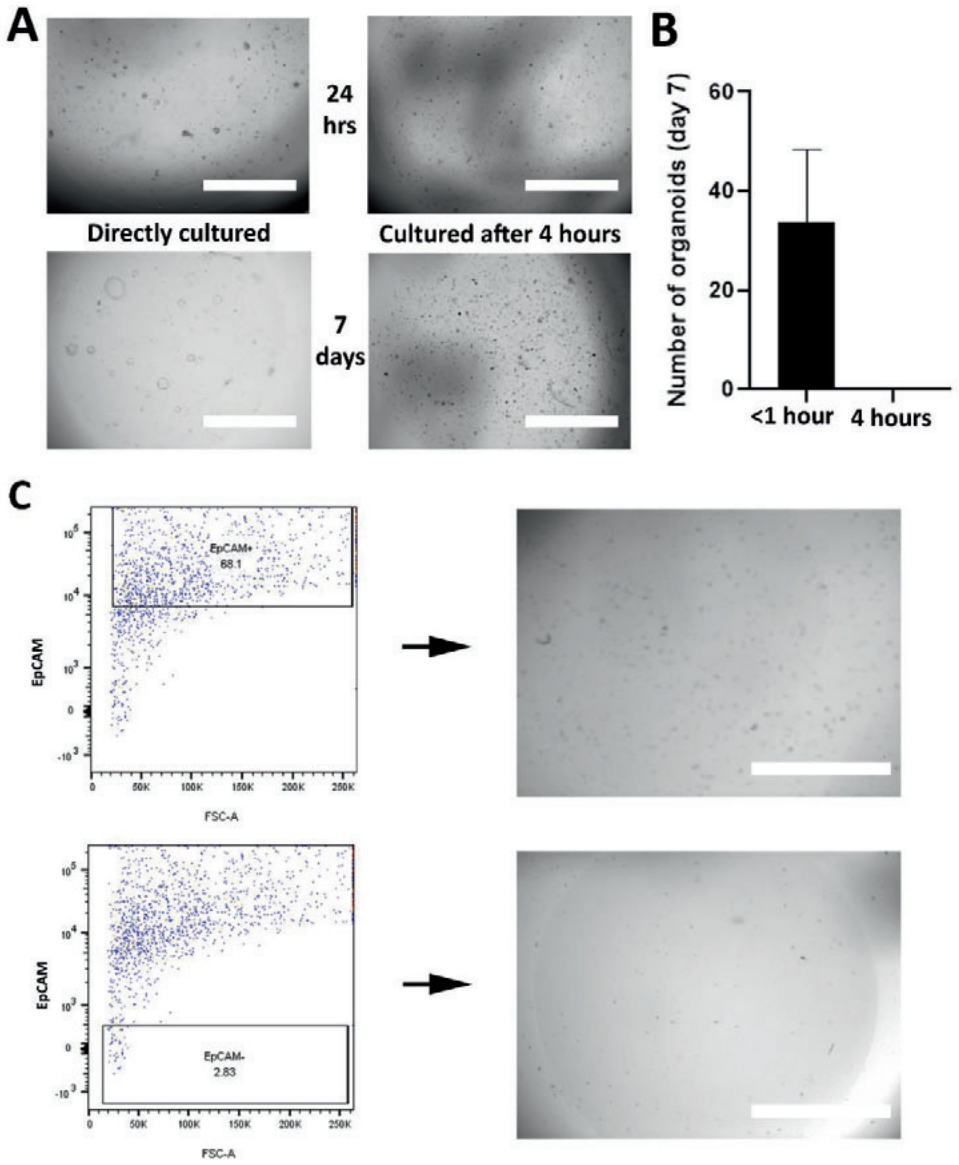

Figure S2. Culture of ERCP-derived BCOs directly or after four hours of storage at 4°C.
(a) On the left, bile samples were directly processed for organoid culture. While on the right, the bile samples were first stored at 4°C for four hours before being cultured as organoids. As shown in the bottom two pictures, bile samples directly cultured formed organoids after 7 days, while bile processed after 4 hours did not. Scale bars indicate 2mm. **(b)** Initiation of organoid cultures from ERCP-derived bile, cultured after < 1 hour or 4 hours of storage at 4°C, showing no outgrowth of organoids after a 4-hour storage period (n=3). *Indicates a significant difference ($p<0.05$). **(c)** $EpCAM^+$ and $EpCAM^-$ flow cytometry sorted cells from bile resulted in no viable organoids after two weeks of culture.

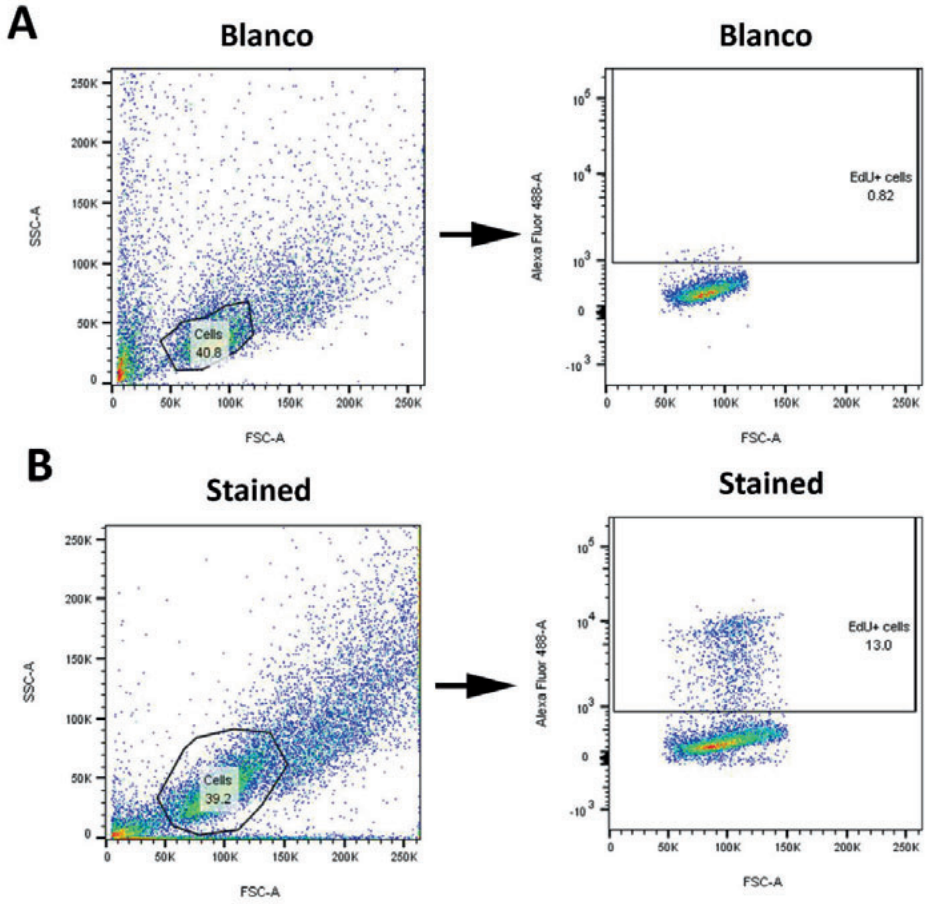

Figure S3. Gating strategy of EdU staining in BCOs.
(a) Top row unstained bile organoids (n=3, donors 1-3). First, cells were selected using forward-sideward scatter and next analysed on the Alexa-Fluor 488 spectrum. In **(b)** stained organoids are displayed.

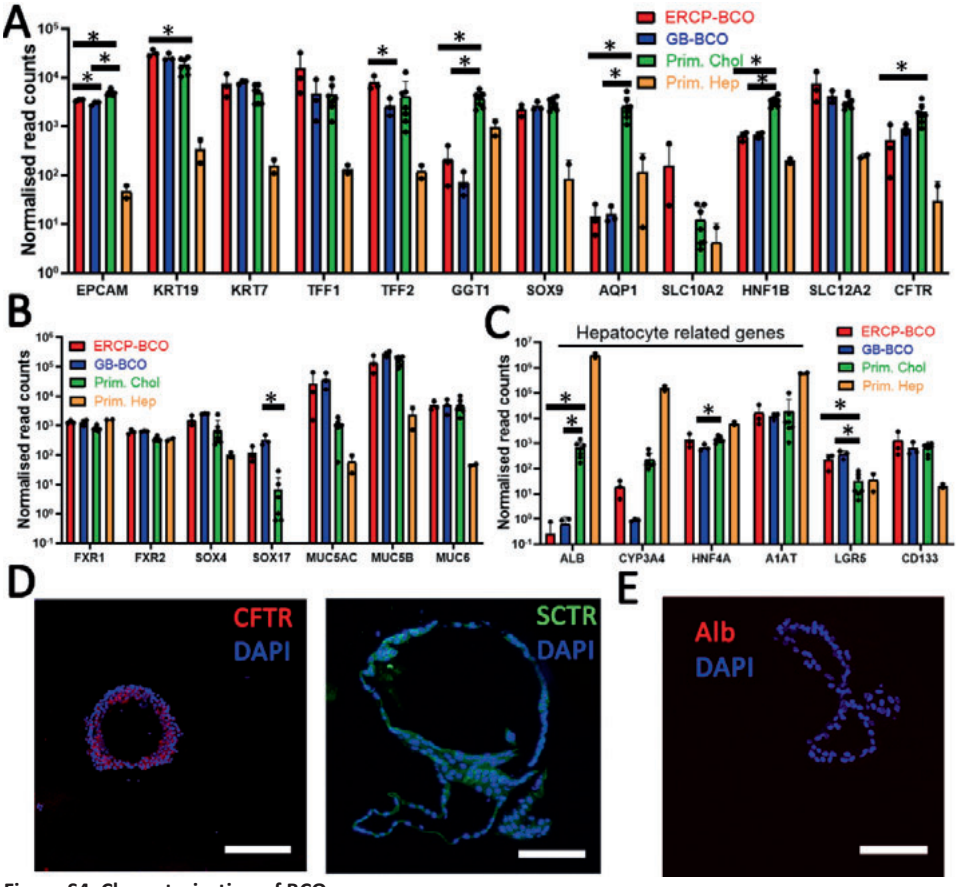

Figure S4. Characterization of BCOs.

(a-c) Normalized read counts from RNAsequencing data for BCOs obtained from gallbladder-derived bile (n=3, BCO1-3) and ERCP-derived bile (n=3, BCO5-7) compared to expression-data of primary cholangiocytes obtained from common bile duct (n=7) as published[9] and from 2D-cultured primary hepatocytes (n=2) as published by Schneeberger *et al.*[10]. All genes were significantly different expressed between primary cholangiocytes and hepatocytes (not indicated), except for TFF1, TFF2, SLC10A2, LGR5, FXR2, SOX4, SOX17, MUC5AC, and MUC6. All hepatocyte related genes in panel C were significantly lower in ERCP-BCOs and GB-BCOs compared to hepatocytes (not indicated). *indicates a significant difference between ERCP-BCOs, GB-BCOs and primary cholangiocytes ($p<0.01$). **(d)** Protein expression by immunofluorescence of the cholangiocyte markers: CFTR (red, left) and SCTR (green, right) with nuclei being counterstained (DAPI, blue) on BCOs (n=3, pictures displayed are from BCO5 and 7). **(e)** Protein expression by immunofluorescence shows absence of the hepatocyte marker: Albumin (red) in BCOs (n=3, BCO1, 5 and 7). Nuclei are counterstained with DAPI (blue). In both panels the scale bars indicate 200 µm.

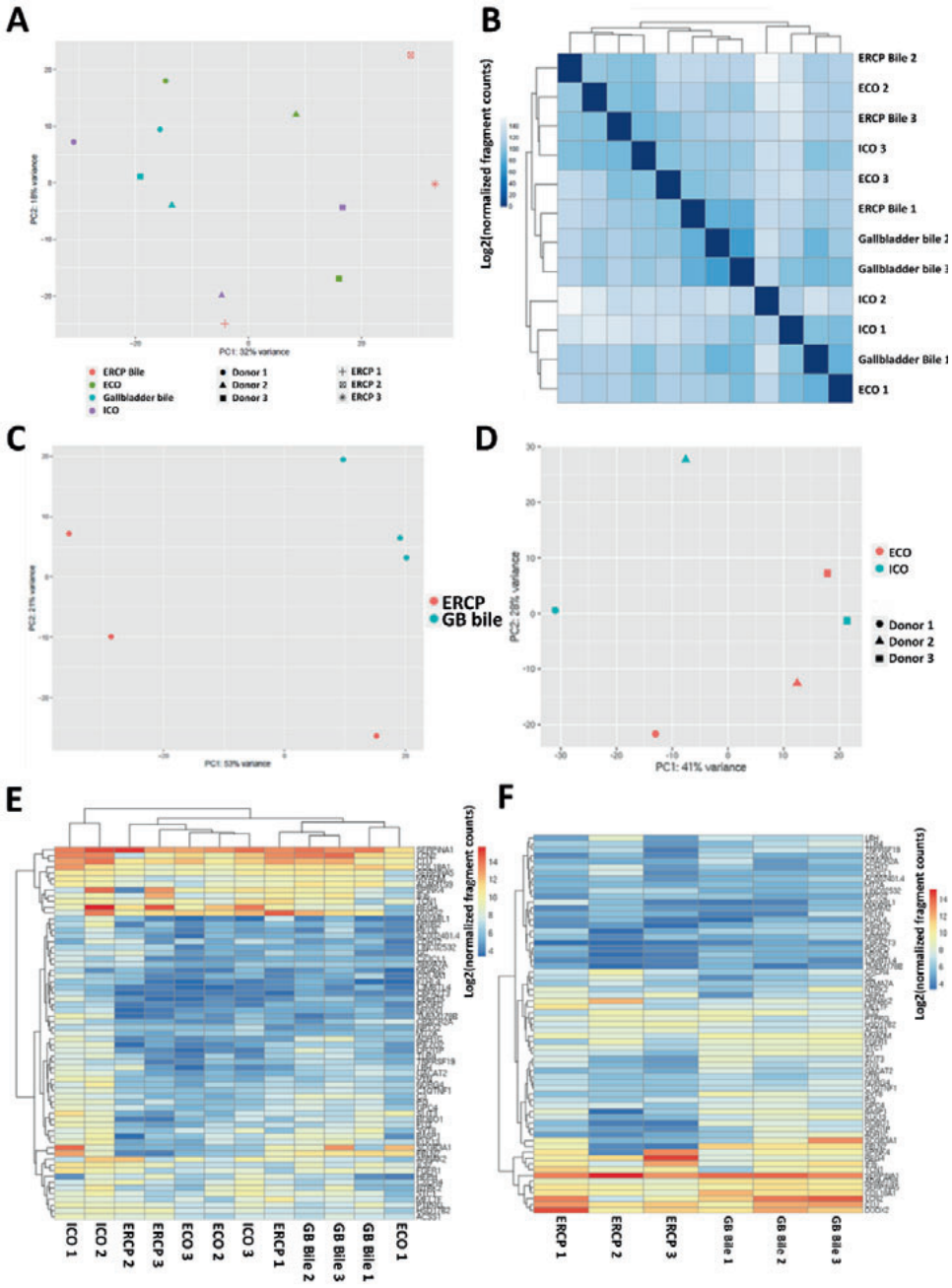

Figure S5. Expression of DEgenes beween ICOs and ECOs on organoid samples.

(a) Principal component analysis (PCA) of top 500 most variable genes between BCOs (ERCP-derived, n=3 BCO5-7 and gallbladder-derived, n=3, BCO1-3), displayed on all organoid sample types, showing no

clear clustering pattern between sources, but overall, a high correlation to each other. **(b)** Heatmap-clustering showing sample-to-sample distances on the same samples as used in the PCA plot, showing no clear clustering on either source or donor. **(c)** Principal component analysis (PCA) of ERCP-derived BCOs and gallbladder-derived BCOs. **(d)** PCA plot of ICOs vs ECOs. Indicates that ICO3 overlaps with ECO gene expression profiles. **(e)** Heatmap based upon ICO upregulated DEgenes on all 12 organoid samples, showing that ICO 1 and ICO 2 have an unique expression profile for ICO-specific genes compared to all other samples. **(f)** Heatmap of ICO-upregulated genes on all BCO samples, showing limited expression of these genes.

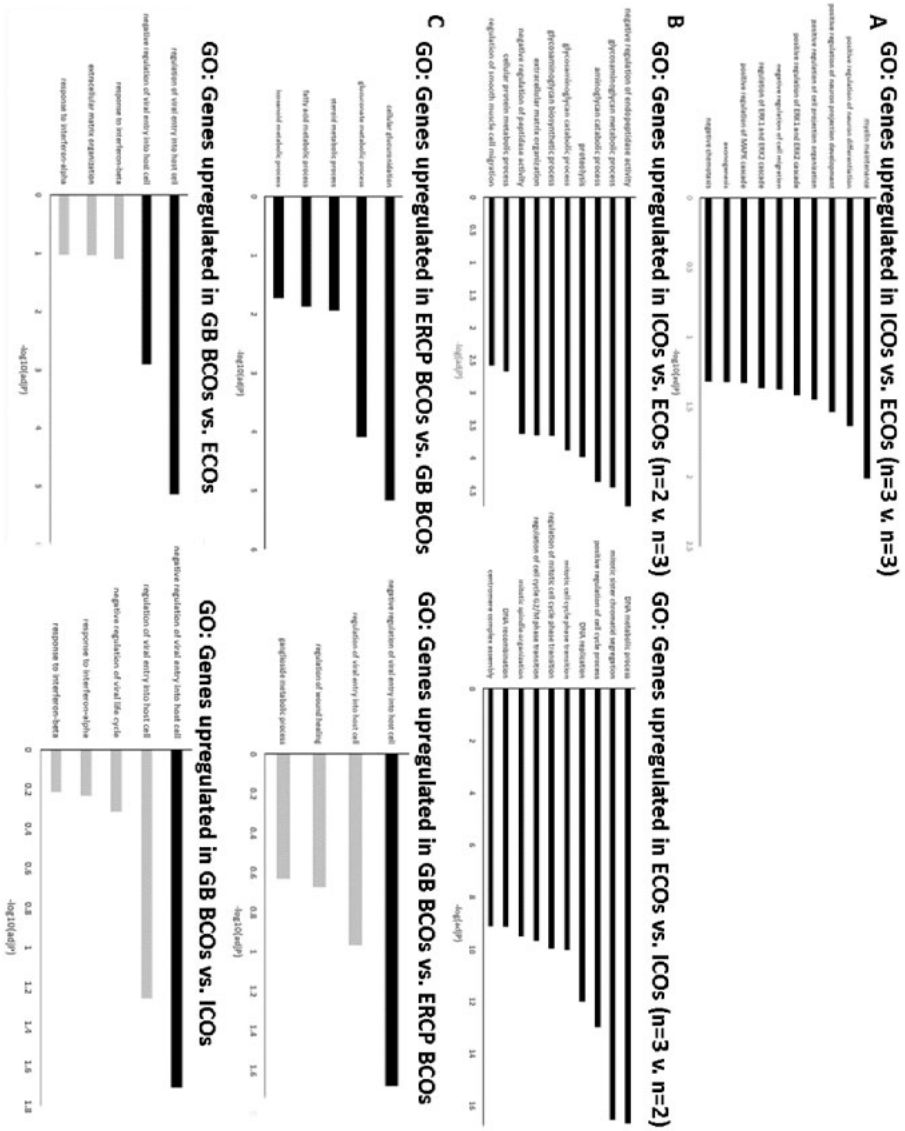

Figure S6. Pathway analysis in cholangiocyte organoids from different sources.
(a) Pathways analysis between ICOs and ECOs (n=3) revealed that certain pathways are enriched in ICOs compared to ECOs. No pathways were found to be significantly upregulated in ECOs compared to ICOs. **(b)** After exclusion of ICO 3, pathways analysis between ICOs (n=2) and ECOs (n=3) revealed that certain pathways are enriched in ICOs compared to ECOs. Interestingly, this analysis revealed that ECOs have significantly upregulated cell-proliferative pathways such as DNA replication and cell-cycle pathways. These results correspond to our EdU data (Figure 3D) in which the two lowest proliferating ICO samples were ICO 1 and ICO 2 and ICOs were significantly less proliferative compared to ECOs. **(c)** Pathway

analysis between different sources of BCOs showed a significant enrichment of metabolic-synthesis associated pathways in ERCP-derived BCOs compared to gallbladder-derived BCOs. No differences were found between ERCP BCOs and ICOs or ECOs. In contrast, GB-derived BCOs showed upregulation of viral-host interaction related pathways to both COs and ECOs as well as ERCP-derived BCOs. All experiments performed in Figure S6 are with donors 1-3.

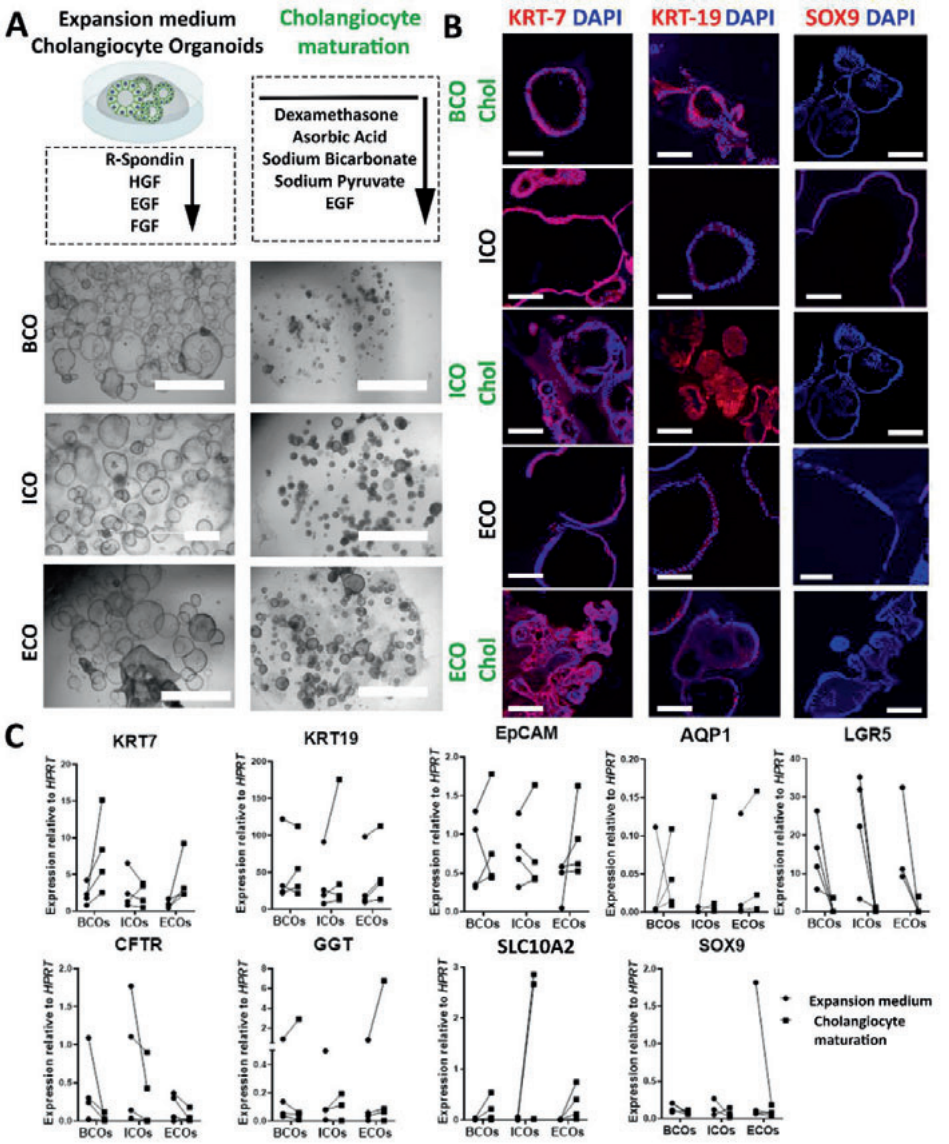

Figure S7. Cholangiocyte organoids from all three sources can be partially matured using an established cholangiocyte-differentiation protocol.

(a) Schematic overview and pictures of cholangiocyte-organoids (COs) from bile (BCO), intrahepatic biopsies (ICOs) or extrahepatic biopsies (ECOs) in either cholangiocyte maturation or in canonical-WNT stimulating conditions. Upon cholangiocyte maturation, 2D growth and smaller organoid size could be observed in multiple cultures in COs from all three sources. Scale bars indicate 2000µm. **(b)** Immunofluorescence images of protein expression in COs in differentiated and undifferentiated status for the cholangiocyte markers KRT-7, KRT-19 and SOX9. Images of BCOs in expansion medium for these

proteins are displayed in Figure 2B. Upon cholangiocyte maturation, KRT-7 and KRT-19 expression seems more pronounced. While clear SOX9 expression could only be detected in one sample of an ICO upon cholangiocyte maturation. Scale bars indicate 100 µm. **(c)** Gene-expression by qRT-PCR relative to the housekeeper gene *HPRT1* for cholangiocyte maturation and paired organoids cultured in canonical-WNT stimulating conditions from all three sources (n=3), for either mature cholangiocyte markers (cytokeratin-*KRT-7*, *KRT19*, *CFTR*, *GGT*, *ASBT*, *EpCAM, AQP1* and *CFTR*) or stemness/cholangiocyte progenitor markers (*LGR5* and *SOX9*). ICOs, ECOs and BCOs had higher expression of *KRT7*, *ASBT*, *AQP1* and *KRT19* in a similar manner after maturation, while *EpCAM* and *GGT* gene-expression remained stable. Upon cholangiocyte maturation the expression of the WNT-target gene *LGR5* and the cholangiocyte progenitor marker *SOX9* was lower in all cultures from all sources. In contrast, the expression of mature cholangiocyte marker *CFTR* was lower in the cholangiocyte maturation protocol for organoids from all three sources. As forskolin (a cAMP-activator) was removed from the cholangiocyte maturation medium, the organoids cultured in these conditions are considerably smaller (Figure S8A) compared to organoids in expansion medium. The downregulation of *CFTR* could be the result of less activation by forskolin and subsequent lack of swelling, as was previously published.[11] However, overall our results indicate that no complete maturation is reached *in vitro* with this protocol, but in contrast to upregulation of hepatocyte-markers, here all organoid sources behave similar. All experiments performed in Figure S8 are with donors 1-3.

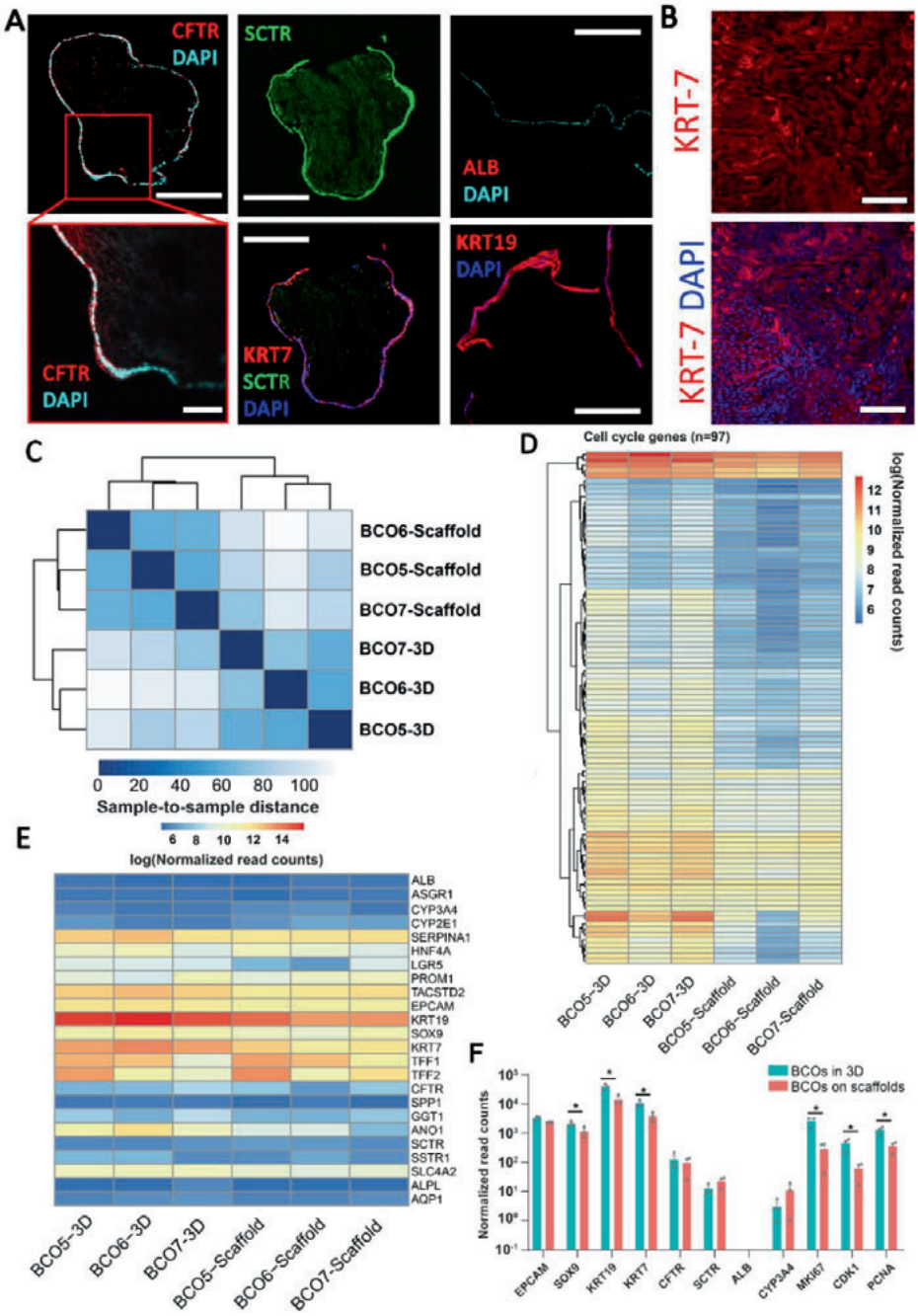
A
CFTR
DAPI
SCTR
ALB
DAPI
CFTR
DAPI
KRT7
SCTR
DAPI
KRT19
DAPI
B
KRT-7
KRT-7 DAPI
C
BCO6-Scaffold
BCO5-Scaffold
BCO7-Scaffold
BCO7-3D
BCO6-3D
BCO5-3D
0 20 40 60 80 100
Sample-to-sample distance
D
Cell cycle genes (n=97)
log(Normalized read counts)
12
11
10
9
8
7
6
BCO5-3D
BCO6-3D
BCO7-3D
BCO5-Scaffold
BCO6-Scaffold
BCO7-Scaffold
E
6 8 10 12 14
log(Normalized read counts)
ALB
ASGR1
CYP3A4
CYP2E1
SERPINA1
HNF4A
LGR5
PROM1
TACSTD2
EPCAM
KRT19
SOX9
KRT7
TFF1
TFF2
CFTR
SPP1
GGT1
ANO1
SCTR
SSTR1
SLC4A2
ALPL
AQP1
BCO5-3D
BCO6-3D
BCO7-3D
BCO5-Scaffold
BCO6-Scaffold
BCO7-Scaffold
F
BCOs in 3D
BCOs on scaffolds
Normalized read counts
EPCAM
SOX9
KRT19
KRT7
CFTR
SCTR
ALB
CYP3A4
MKI67
CDK1
PCNA

Figure S8. BCOs can successfully recellularize EHBD-scaffolds with tissue-like cholangiocyte cells.
(a) Immunofluorescence staining of sections of BCO-recellularized scaffolds demonstrating presence of the mature cholangiocyte markers CFTR (red, upper/bottom left panel), SCTR (green, upper middle panel), KRT-7 (red, bottom middle panel), KRT-19 (red, bottom right panel) and absence of the hepatocyte related marker albumin (red, upper right panel). All sections are stained with DAPI (nuclei, cyan or dark blue). Scale bars indicate 200 µm. **(b)** Whole mount confocal images of immunofluorescence staining KRT-7 (red, upper panel) and KRT-7 and DAPI (nuclei, blue bottom panel) of repopulated EHBD scaffolds with BCOs, scale bars indicate 100µm. **(c)** Heatmap of sample-to-sample distances, showing a clear clustering based on the culture condition. **(d)** Heatmap showing the cell cycle gene expression from the samples in the 2 conditions. **(e)** Heatmap of the expression levels of a few selected hepatocyte and cholangiocyte markers between the 2 culture conditions. **(f)** Bar plot showing the expression of selected known cholangiocyte markers (*EPCAM*, *SOX9*, *KRT19*, *KRT7*, *CFTR*, and *SCTR*), hepatocyte markers (*ALB* and *CYP3A4*), and cell cycle related markers (*MKI67*, *PCK1*, and *PCNA*) in both conditions. *Indicates a significant difference ($p<0.05$ adjusted for multiple testing).

References

1. Broutier L, Andersson-Rolf A, Hindley CJ, *et al*. Culture and establishment of self-renewing human and mouse adult liver and pancreas 3D organoids and their genetic manipulation. Nat. Protoc. 2016;11:1724–1743.
2. Sampaziotis F, Justin AW, Tysoe OC, *et al*. Reconstruction of the mouse extrahepatic biliary tree using primary human extrahepatic cholangiocyte organoids. Nat. Med. 2017;23:954–963.
3. Huch M, Gehart H, Boxtel R van, *et al*. Long-term culture of genome-stable bipotent stem cells from adult human liver. Cell. 2015;1–14.
4. Soroka CJ, Assis DN, Alrabadi LS, *et al*. Bile-Derived Organoids From Patients With Primary Sclerosing Cholangitis Recapitulate Their Inflammatory Immune Profile. Hepatology. 2019 Sep;70(3):871-882.
5. Sampaziotis F, de Brito MC, Geti I, *et al*. Directed differentiation of human induced pluripotent stem cells into functional cholangiocyte-like cells. Nat Protoc. 2017 Apr;12(4):814-827.
6. Sampaziotis F, de Brito MC, Madrigal P, *et al.* Cholangiocytes derived from human induced pluripotent stem cells for disease modeling and drug validation. Nat Biotechnol. 2015;33(8):845-852.
7. Verstegen MMA, Roos FJM, Burka K, *et al.* Human extrahepatic and intrahepatic cholangiocyte organoids show region-specific differentiation potential and model cystic fibrosis-related bile duct disease. Sci Rep. 2020 Dec 14;10(1):21900.
8. Willemse J, Roos FJM, Voogt IJ, *et al.* Scaffolds obtained from decellularized human extrahepatic bile ducts support organoids to establish functional biliary tissue in a dish. Biotechnol Bioeng. 2021 Feb;118(2):836-851.
9. Rimland CA, Tilson SG, Morell CM, *et al.* Regional differences in human biliary tissues and corresponding in vitro derived organoids. Regional Differences in Human Biliary Tissues and Corresponding In Vitro-Derived Organoids. Hepatology. 2021 Jan;73(1):247-267.
10. Schneeberger K, Sánchez-Romero N, Ye S, *et al.* Large-Scale Production of LGR5-Positive Bipotential Human Liver Stem Cells. Hepatology. 2020 Jul;72(1):257-270.
11. Van Mourik P, van Haaren P, Kruisselbrink E, *et al.* R117H-CFTR function and response to VX-770 correlate with mRNA and protein expression in intestinal organoids. J Cyst Fibros. 2020 Sep;19(5):728-732.

7

CHAPTER 7

Human bile contains cholangiocyte organoid initiating cells which expand as functional cholangiocytes in non-canonical WNT stimulating conditions.

Floris JM Roos, Monique MA Verstegen,
Laura Muñoz Albarinos, Henk P Roest, Jan-Werner Poley,
Geert WM Tetteroo, Jan NM IJzermans, Luc JW van der Laan

Frontiers in Cell and Developmental Biology 2021 Feb 9;8:630492.

Abstract

Diseases of the bile duct (cholangiopathies) remain a common indication for liver transplantation, while little progress has been made over the last decade in understanding the underlying pathophysiology. This is largely due to lack of proper *in vitro* model systems to study cholangiopathies. Recently, a culture method has been developed that allows for expansion of human bile duct epithelial cells grown as extrahepatic cholangiocyte organoids (ncECOs) in non-canonical WNT stimulating conditions. These ncECOs closely resemble cholangiocytes in culture and have shown to efficiently repopulate collagen-scaffolds that could act as functional biliary tissue in mice. Thus far initiation of ncECOs required tissue samples, thereby limiting broad patient-specific applications. Here we report that bile fluid, which can be less invasively obtained and with low risk for the patients, is an alternative source for culturing ncECOs. Further characterization showed that bile-derived cholangiocyte organoids (ncBCOs) are highly similar to ncECOs obtained from bile duct tissue biopsies. Compared to the previously reported bile cholangiocyte organoids cultured in canonical WNT-stimulation conditions, ncBCOs have superior function of cholangiocyte ion-channels and are able to respond to secretin and somatostatin. In conclusion, bile is a new, less invasive, source for patient-derived cholangiocyte organoids and makes their regenerative medicine applications safer and more feasible.

Introduction

Cholangiopathies are associated with significant morbidity and mortality.[1,2] Insight in the underlying pathophysiology and treatment options is incomplete, mostly due to the lack of good model systems to culture and expand primary human cholangiocytes.[3] Recently, Sampaziotis *et al.*[4] described a method to expand primary human cholangiocytes from extrahepatic bile duct biopsies and culture them as three-dimensional (3D) organoids. These so-called Extrahepatic Cholangiocyte Organoids (ncECOs) retained most biliary characteristics in culture and were successfully used to bioengineer artificial ducts that, after transplantation in mice, act as functional bile ducts. The culture of ncECOs is driven by non-canonical WNT-signaling (ncECOs) stimulated by R-spondin in combination with Dickkopf-related protein-1 (DKK-1). Also *in vivo*, non-canonical WNT-stimulation is important for cholangiocyte homeostasis and proliferation responses to bile duct injury.[5,6] Although highly effective, to grow these organoids either a tissue biopsy from the gallbladder or a brush via an endoscopic retrograde cholangiopancreatography (ERCP) is needed.[4,7] These options are potentially harmful to patients[8] or are procedures not regularly performed. This limits broad patient-specific disease modeling and regenerative medicine applications. To avoid the need for tissue-derived samples, we explored the use of human bile as an alternative, less invasive, source for patient-derived ncECOs. A recent study published by Soroka *et al.*[9] showed feasibility of culturing cholangiocyte organoids from bile, obtained by endoscopic retrograde cholangiopancreatography (ERCP). The expansion of these bile-derived organoids were driven by canonical WNT-signaling originally described for the growing intrahepatic cholangiocyte organoids (ICOs).[10] This canonical WNT-signaling is stimulated by R-spondin, providing a cholangiocyte with a more stem cell-like phenotype compared to *in vivo* cholangiocytes.[9,11-14] Moreover, these canonical WNT stimulation culture conditions will likely result in a different cell phenotype than observed under non-canonical WNT conditions.[4] Since, bile duct tissue derived ECOs cultured in canonical-WNT conditions (cECOs) do upregulate WNT-target genes, while ncECOs do not.[4,15] Currently it is unknown whether under non-canonical WNT-stimulated conditions cholangiocyte organoids can be expanded from bile and retain a more cholangiocyte-like phenotype. Therefore, the aim of this study is to initiate and expand non-canonical WNT driven cholangiocyte organoids from bile (ncBCOs) and to compare these to canonical-WNT driven bile cholangiocyte organoids (cBCOs) from the same bile samples and to ncECOs from (paired) bile duct tissue.

Materials and Methods

Bile and tissue collection

Fresh bile (1 mL) was collected from patients receiving an ERCP (n=8) for their regular treatment (complete list of patients Table S1). In addition, bile (3 mL) was collected *ex vivo* from gallbladders after surgical removal (n=8). Bile from gallbladders was collected from donor livers allocated for liver transplantation (n=8). Additionally, tissue samples were collected from gall bladders (n=5), either collected after cholecystectomy (n=1) at the IJsselland hospital, Capelle aan de IJssel, The Netherlands, or were along with liver biopsies (n=3) or extrahepatic bile duct (EHBD, n=4) biopsies, collected from gall bladders from donor livers allocated for liver transplantation (n=4). All bile samples were stored immediately on ice and were processed as soon as possible after collection. All patients or their next of kin consented with the use of their bile or tissue for research purposes by signing an informed consent, and the use of this material was approved by the Medical Ethical Committee of the Erasmus MC, Rotterdam (MEC-2014-060, MEC-2016-743 and MEC 2018-1174).

Generation and culture of canonical and non-canonical WNT stimulated cholangiocyte organoids from bile and tissue

For the initiation (of culture) of canonical WNT stimulated bile or intrahepatic or extrahepatic bile duct tissue cholangiocyte organoids (cBCOs, cICOs and cECOs, respectively), and non-canonical WNT stimulated extrahepatic bile duct tissue (ncECOs) we used protocols similar to the ones previously published.[4,9,10,11,15] For detailed methodology please refer to supplementary material and methods. Human ncBCOs (n=16) were cultured from one mL (ERCP) or three mL of bile (gallbladder), depending on the source. Bile was centrifuged at 453*g* for 5 minutes at 4˚C, supernatant was removed, and the cell pellet was washed twice with excess cold William's-E Medium (WE). Finally, the pellet was suspended in WE and filtered through a 70 µm cell strainer to remove debris. Afterwards, cells were plated out in a 25µL droplets of basement membrane extract (BME, Cultrex) and cultures medium (WE with supplements) was added according to the standard ncECO protocol.[4,7] Medium was changed twice a week and cultures were split in a 1:2 to 1:10 ratio depending on the number and size of organoids grown. Cultures were routinely checked for mycoplasma contamination, which came back negative. All experiments with ncECOs and ncBCOs were performed with passage five or higher, unless stated otherwise. For a complete overview of the nomenclature and culture conditions for cholangiocyte organoids and patient characteristics see Table S1 and Table S3.

Flow-cytometry of bile-derived cells and ncBCOs

Fresh human bile was obtained from patients immediately after collection via ERCP (n=3) and stored at 4˚C during transportation. Bile was transferred to a 15mL Falcon tube and

centrifuged for 5 minutes at 4˚C, supernatant was removed, and the cell pellet was washed twice with WE. ncBCOs were made single cell by incubation with Trypsin-EDTA (TE) for 25 to 40 min, at 37°C. Cells were washed in WE and put through a cell 70 µm cell strainer. Samples were blocked in 1% bovine serum albumin (BSA)-PBS for 15 minutes. TROP2 antibody (Invitrogen; rabbit monoclonal conjugated to Alexa Fluor-488, clone MR54, used 1:100) was added (30 min, on ice) and cells were subsequently measured on a Canto flow cytometer (BD Biosciences).

RNA extraction, cDNA synthesis and RT-qPCR

RNA was harvested by addition of 700µl of QIAzol lysis reagent (Qiagen) per two 25µL domes of ncECO (n=6), ncBCO (n=6) and cBCOs (n=6). RNA-extraction and subsequent cDNA synthesis was performed as previously published.[16] In short, RNA was isolated using a miRNeasy kit (Qiagen) according to the manufacturers protocol. RNA concentration was measured using a NANOdrop 2000 (ThermoFisher). 500ng cDNA was prepared using 5x PrimeScript RT Master Mix in a 2720 thermal cycler (Applied Biosystems). RT-qPCR was performed with the primer sets provided in Table S2. All RT-qPCR data are presented as mean with a 95% confidence interval. RT-qPCR values are relative to the housekeeping gene Hypoxanthine-guanine-fosforibosyl-transferase *(HPRT)* or Glyceraldehyde 3-phosphate dehydrogenase (*GAPDH)* and for visual interpretation multiplied by 10^5 or 10^6.

Immunohistochemistry (IHC)

IHC was performed according to standard procedures as previously described for cICOs, liver-biopsies obtained from donors allocated for transplantation were taken along as control.[10] In short, formalin-fixed, paraffin-embedded bile duct biopsies were sectioned (4µm thick) and processed according to standard procedures. Antigen retrieval was performed in citrate buffer (pH 6.0) for 10 min. in sub boiling temperatures and non-specific reactions were blocked by incubation with 10% goat serum in a 1% bovine serum albumin (BSA)-PBS solution. The sections were exposed to primary antibodies overnight at 4°C. Cytokeratin (KRT)19 and KRT7 antibodies (both Dako were used in 1:100 dilution in 1% BSA-PBS). The antibody for Cystic Fibrosis Transmembrane Conductance Regulator (CFTR, EMD Millipore Corp.) was used in a 1:200 dilution of 1%BSA-PBS. Sections were subsequently incubated with Envision+ system horseradish peroxidase anti-mouse secondary antibody (Dako) at room temperature for 60 min., before staining with 3'-diaminobenzidine (DAB). Nuclei were stained by haematoxylin. Analysis was done with a Carl zeiss Axioskop 20 microscope and images were taken with a Nikon Digital Side DS-5M camera.

Gene-array selection based qRT-PCR

Twenty genes were selected from the online published Microarray gene expression data corresponding to the heat map (Figure 1D) published in Sampaziotis *et al*.[4]. Out of the gene

expression heatmap, 10 genes were selected which have a similar expression between primary human cholangiocytes and ncECOs, five genes were selected which have higher expression in ncECOs compared to primary human cholangiocytes and five genes which have lower expression in ncECOs compared to primary human cholangiocytes. Additionally, 15 genes known to be WNT-target/stem cell related or hepatocyte and cholangiocyte specific, were selected[10] and their expression was assessed by RT-qPCR. The selected genes and correlating primer sets are listed in Table S2. The details on the ncECOs and ncBCOs used are described in Table S1. A Z-stack heat-map was created by unsupervised hierarchical clustering in R (version 3.5.1, R Core Team) supplemented with package Gplots (version 3.0.1).

Swelling of cholangiocyte organoids

To assess functionality of secretin and somatostatin, a slight modification of the Forskolin-Induced Swelling (FIS) assay as developed by Dekkers *et al.*[17] was applied. For this, ncECOs and ncBCOs organoids were incubated for 30 min with 3 µM calcein-green (Invitrogen), stimulated with secretin (10 µM) or secretin and somatostatin (100 µM) and analysed by confocal live cell microscopy at 37˚C for 120 min (LSM710, Zeiss). The total or single organoid area (XY plane) increase relative to t=0 of secretin treatment was quantified using velocity imaging software (Improvision) and compared to non-stimulated controls. Cell debris and unviable structures were manually excluded from image analysis.

Gamma-Glutamyltransferase (GGT) Assay

Ten microliters of supernatant of cholangiocyte organoids from bile (ncBCOs, n=3) and from tissue (ncECOs, n=3) were collected. Next GGT activity colorimetric assay kit (MAK089; Sigma-Aldrich) was used according to the manufacturer's protocol.

Rhodamine 123 transport assay

Functionality of the multi drug resistance-1 (MDR-1) transporter was performed according to standard protocol using a commercially available Rhodamine 123 assay (Sigma Aldrich).[4] Rhodamine 123 transport was determined by incubating the cultures with Rhodamine 123 (100 µM, Sigma Aldrich) for 5 min. at 37°C. Subsequently, specificity of the MDR-1 transporter was determined by blocking the transporter with Verapamil (10 µM, Sigma Aldrich) for 30 min at 37˚C prior to Rhodamine 123 incubation (100 µM, Sigma Aldrich). Confocal analysis was performed to determine MDR-1 activity. Images were acquired with a Leica SP5 confocal microscope (LEICA) equipped with a 488 nm laser.

Ussing chamber assay

ncECOs, ncBCOs, cICOs and cBCOs (all n=3) were collected from 10, 25 µL domes. Organoids were collected in WE, centrifuged (453g, 5 min, 4˚C) and the supernatant was removed. Organoids were mechanically broken by pipetting up and down and were spun down again.

A single cell suspension was made through incubation of the organoids in 1 mL Trypsin-EDTA (TE) for 25 to 40 min, at 37°C. Cells were washed in WE and put through a cell 70µm cell strainer. Approximately $3x10^5$ cells were resuspended in 200 µm WE-medium with supplements[4] and seeded on transwell inserts (24 well plate 6.5mm, Corning). Medium was changed twice per week. To check confluency, electrophysiological analysis (TEER) was performed after 4 days. The confluent transwells were placed in an Ussing chamber set up to analyse functional cholangiocyte-specific transporter channels (CFTR and Ca^{2+} dependent Cl^- channel) using Acquire & Analyze Software 2.3 (Physiologic Instruments, San Diego, California). For detailed methodology of the conditions please see supplementary material and methods.

RNA isolation for microarray

Total RNA was isolated from cECOs using the miRNEAsy mini kit (Qiagen, Hilden, Germany) according to the manufacturer's protocol and eluted in 30 µL of RNAse-free water. RNA concentration and integrity were determined using a Nanodrop 2000 (Thermo Fisher Scientific, Waltham MA, USA) and a Bioanalyzer 2100 (Agilent Technologies, Santa Clara CA, USA), respectively. A total of 300 ng RNA was reversed transcribed, amplified and biotin-labeled using the Illumina TotalPrep RNA Amplification Kit (Ambion-Life Technologies, Carlsbad CA, USA) according to the manufacturer's guidelines. HumanHT-12 v4 Expression BeadChips (Illumina, San Diego CA, USA) were overnight hybridized with 750 ng cRNA, washed, stained and scanned on an iScan and analyzed using GenomeStudio V2011.1 software (both from Illumina, Inc.).

Microarray analysis

Microarray analysis was based upon the publically available data of ncECOs from ArrayExpress E-MTAB-4591 (Sampaziotis *et al.*[4]), cICOs (n = 3) from the ArrayExpress E-MTAB-9044 (Roos *et al*.[19]), and the novel data generated for cECOs (deposited at Array Express, E-MTAB-9807). Bead types missing in one or more arrays were excluded, and the resulting non-normalized raw probe data set was combined with the open datasets. The file, describing for each probe AVG_Signal and Detection Pval, was loaded into R using the limma package (Ritchie *et al*.[20]. limma powers differential expression analyses for RNA-sequencing and microarray studies. Nucleic Acids Research 43, e47). Probes that were present at least once (Detection Pval <0.01) were considered as being expressed (21,929 probes) and used for further analysis. Following filtering, the data were background subtracted, normalized, and log2 transformed using the VSN package (Huber *et al.*[21]). The heatmap was conducted in R using heatmap.2 functions.

Statistical analysis

All analyses were conducted using SPSS software (statistical Product and Service solutions, version 22, SSPS Inc, Chicago, IL, USA) and graphs were performed using GraphPad Prism 7.0 (GraphPad Software Inc., USA). Continuous variables were tested using an independent T-test or Mann-Whitney-U test and presented with normal distribution as means with standard error of the mean and if not normally distributed, they are presented as range. Gene array unsupervised hierarchical clustering data was statistically analysed using Pearson's correlation was calculated between the eight samples (reference ncBCO 10). In all tests, a P-value of <0.05 was considered significant.

Results

Cholangiocyte organoids in non-canonical WNT stimulating conditions can successfully be expanded from human bile

In Figure 1A, a schematic overview of the culture protocol for bile cholangiocyte organoids (ncBCOs) from bile is displayed. As shown in Figure 1B, ncBCOs could be successfully cultured from bile obtained from multiple organ donors or patients with different underlying liver- or biliary diseases (n=15). Donor, patient and culture characteristics are shown in Table S1. ncBCOs could be initiated from both ERCP- and gallbladder-bile with a high success rate (15 from 16, 94%). Morphologically ncECOs and ncBCOs looked similar under bright-field microscopy (Figure 1B). Recent evidence showed that primary human cholangiocytes are Trop2 positive.[21] Thus to investigate if primary cholangiocytes are present in bile we looked at Trop2^{pos} cells. A shown in Figure 1C, the Trop2^{pos} cell population was the highly dominated population within the bile samples (mean percentage 62.20±2.69). To confirm that ncBCOs resemble their Trop2^{pos} organoid-initiating population *in vitro*, we performed flow-cytometry analysis on ncBCOs. As indicated by Figure 1C, almost all cells found within are organoids are indeed Trop2^{pos} (mean percentage 95.43±0.67) highlighting their resembles to primary cholangiocytes. Similar to ncECOs, ncBCOs rapidly expanded and could be passaged approximately one time a week in a 1:3 ratio. ncBCOs could be passaged for at least 15 passages (>3 months) (Figure 1D).

ncBCOs and ncECOs have similar gene- and protein-expression profiles

To determine the phenotype of ncBCOs, gene expression of a selected number of cholangiocyte-specific genes was assessed and compared to ncECOs using qRT-PCR.[4] Organoid lines included for qRT-PCR analysis were almost all (4 out of 6) paired from the same donor to overcome donor variances. Additionally, samples were from patients with a similar disease (ncBCO8 and ncECO11), or with a relatively healthy bile duct (ncBCO10 and ncECO12). Details of the origin of the organoids are shown in Table S1). Expression of cholangiocyte markers KRT19, KRT7, hepatocyte nuclear factor-1beta (HNF1β), CFTR, Trefoil Factor 1 (TFF1), Trefoil Factor 2 (TFF2) and biliary progenitor marker sex-determining region Y (Sox)9 was assessed. As shown in Figure 2A, these cholangiocyte markers were highly expressed in ncECOs and ncBCOs and no significant differences in expression was observed. As a control, the expression of hepatocyte markers albumin (ALB) and CYP3A4 compared to liver-tissue biopsies, as well as the WNT-target gene Leucine-rich repeat-containing G-protein coupled receptor 5 (LGR5) and the stem cell marker prominin-1, also known as CD133, was determined (Figure 2B). Compared to liver biopsies that mostly consists of hepatocytes, the expression of the hepatocyte markers albumin and Cyp3A4 was 17500-114970 times and 32 to 260 times lower in ncECOs and ncBCOs, respectively (Figure 2B), highlighting the resemblance of ncECOs and ncBCOs with cholangiocytes. Furthermore, no differences in

gene expression for LGR5 and CD133 could be determined between ncECOs and ncBCOs. To further confirm that ncBCOs have a similar gene expression profile as ncECOs, the expression of 35 genes (for gene selection see material and methods) was determined in ncBCOs and ncECOs using cluster analyses. Pearson correlation coefficient showed no major differences between the expression of these genes in both organoid types (Figure 2C). To confirm that the organoids are polarized, a CFTR-staining was performed, as shown in Figure 2D. CFTR is predominantly expressed on the luminal side of our ncBCOs, resembling the *in vivo* situation in the liver (Figure 2D). Furthermore, immunohistochemistry staining of KRT7 and KRT19 confirmed expression of both cholangiocyte markers in the cytoplasm of ncBCO and ncECOs. Moreover, histology revealed a typical columnar-like epithelium in the organoids, with the nucleus located basolateral, similar to primary cholangiocytes in tissue biopsies (Figure 2E).

Both ncBCOs and ncECOs have cholangiocyte functionality in vitro

Cholangiocytes influence bile quality by secretion of ions via either CaCl and Anoctamin-1 (ANO1) transporter channels or via an increase of cAMP which regulates CFTR.[22] Basolateral secretin and somatostatin receptors regulate intracellular cAMP concentrations.[22] As displayed in Figure 3A and 3B, ncBCOs responded to stimulation of secretin similar to the *in vivo* situation by showing an increase (2.21±0.48 fold change) in diameter (t=120) compared to t=0 minutes. The ncECOs responded similarly (mean fold change 1.74±0.22). Addition of somatostatin reduced the induced swelling (1.69±0.187 increase in ncBCOs and 1.41±0.14 for ncECOs), confirming functional secretin and somatostatin receptors in ncBCOs. The capability to export drugs was confirmed in ncBCOs by imaging effective transport of Rhodamine 123 by the multidrug resistance protein-1 (MDR1).[4] The complete abrogation of fluorophore transport to the lumen of the organoids by Verapamil, confirmed MDR-1 dependency (Figure 3C). Both findings are in line with the previously published results for ncECOs.[4] Previous work by Sampaziotis *et al.*[4] showed that activity of GGT in ncECOs is similar to primary cholangiocytes. To investigate if the GGT activity of ncBCOs is in line with ncECOs, we cultured both ncECOs and ncBCOs and analysed the culture supernatant for GGT-activity. As shown in Figure 3D we demonstrate that GGT excretion is similar between ncBCOs and ncECOs (7.77±1.10 vs.8.59±0.34, p=0.63) as measured by ELISA. Since activity of ncECOs and primary cholangiocytes is also similar, it seems plausible that ncBCOs resemble GGT activity similar to that off primary cholangiocytes. Organoids are normally grown in a 3D setting, making it difficult to access the cells' luminal side. In cholangiocytes, both the ANO1 and CFTR channel are located at the luminal side. To overcome the hurdle of accessing this side, both ncBCOs and ncECOs were grown as 2D monolayers and ion-channel functionality was addressed in an ussing chamber. As shown in Figure 3E, ncECOs and ncBCOs both responded to activation with forskolin (cAMP-activator) which was completely inhibited by addition of GlyH-101, a CFTR-inhibitor, to the luminal side. Additionally, stimulation by UTP (luminal) and inhibition (by T16Ainh-A01, luminal) demonstrated the presence of functional ANO1 in both

organoid types. Combined, this demonstrate that ncBCOs and ncECOs are very similar type organoids that both represent cholangiocyte-like characteristics.

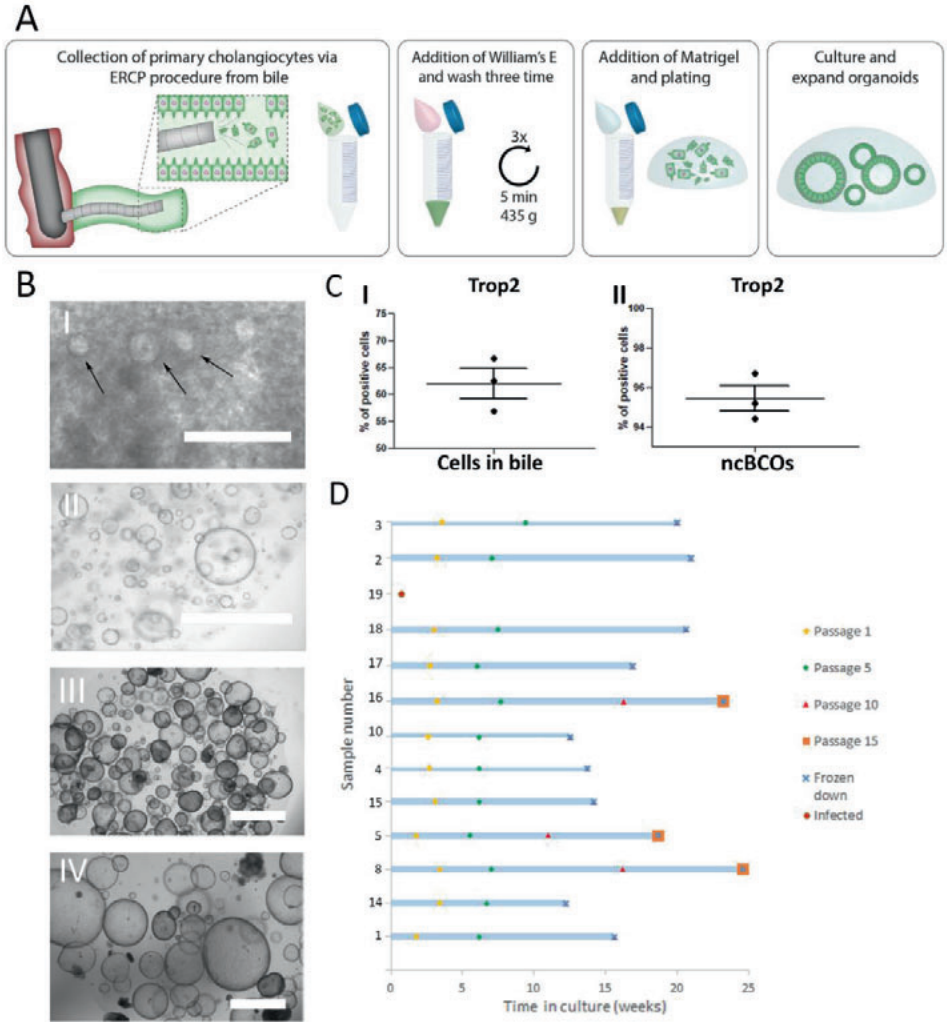

Figure 1. Creation and culturing of Bile Cholangiocyte Organoids in non-canonical WNT stimulating conditions (ncBCOs).

(a) Schematic representation of initiation of ncBCOs from ERCP collected bile. First bile is collected via an ERCP-procedure (1 mL) Organoid-initiating cells (viable cholangiocytes) are present in bile and bile should be quickly transferred on ice for processing. Next the bile is diluted and washed a total of three times with Williams'-E medium, to remove all bile from the cells. If a lot of debris is present, additionally cells could be passed through a 70µm cell strained. Subsequently, a hydrogel (matrigel, Corning or base membrane extract, Cultrex) is added and the cells are plated out in 25µL hydrogel droplets and cholangiocytes are expended as organoids. **(b) (i)** A representative image of ncBCOs at passage 0 (P0) after 5 days in culture. **(ii)** P5 ncBCOs showing mostly cyst-like organoids. (**iii**) A representative of an

extrahepatic cholangiocyte organoid in non-canonical WNT stimulating conditions (ncECO) P3. **(iv) nc**ECO passage P5. All scale bar indicates 1000µm. **(c) (i)** Trop2 flow cytometry of all cells counted as an event in bile, indicating that Trop2^{pos} cells are dominantly present in bile, in **(ii)** the mean percentage of Trop2^{pos}cells in ncBCOs are displayed. **(d)** Number of passages of the thirteen ncBCOs cultured before cryopreservation and storage.

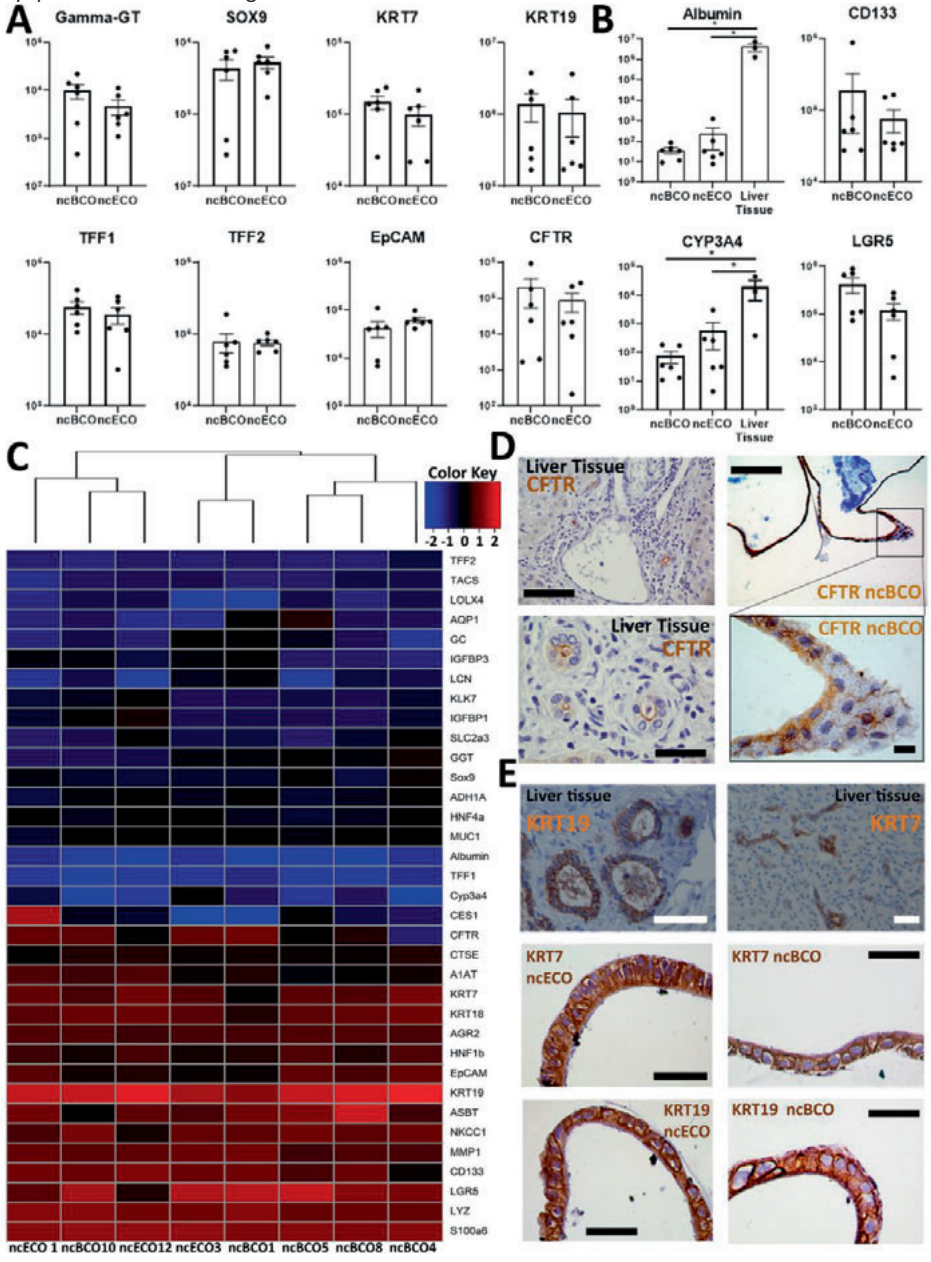

Figure 2. Gene- and protein-expression between ncBCOs and ncECOs is similar.
(a) Gene expression profiles of selected genes between ncECOs (n=6) and ncBCOs (n=6) for eight mature cholangiocyte-related genes relative to the reference gene *HPRT* (for characteristics of organoid lines or gene and primer details see Table S1 and S2). Error bars are presented as standard error of the mean (SEM). **(b)** Gene expression profiles of selected hepatocyte-and stemness/WNT-target-genes between ncECOs (n=6), ncBCOs (n=6) and liver-biopsies (n=3) relative to the reference gene *HPRT.* Indicating that ncECOs and ncBCOs have very low expression of hepatocyte-related genes: Albumin and Cyp3A4 and they have similar expression of stemness/WNT-target-related genes. Error bars are presented as SEM. **(c)** Gene expression profiles of ncBCOs and ncECOs are highly similar for these 35 selected genes. The included genes were selected based on published results by Sampaziotis *et al.* Figure 1D[4] along with additional WNT-target, cholangiocyte and hepatocyte related genes[10] and were quantified by qRT-PCR (see Methods and Table S2). Euclidean hierarchical clustering did not show a significant segregation of gene expression between ncECOs and ncBCOs. **(d)** Immunohistochemistry (IHC) staining of cystic fibrosis transmembrane conductance regulator (CFTR) in ncBCOs showing polarization of our organoids and luminal CFTR expression, similar to liver biopsies, top row scale bars indicate 200µm, bottom scale bars indicate 50 µm. **(e)** Immunohistochemistry of ncBCOs and ncECOs showing comparable staining of cytokeratin, (KRT)19 and KRT7. Moreover, it reveals a columnar like cell, resembling primary cholangiocytes as shown on liver tissue coupes. All scale bars in IHC pictures of ncECOs and ncBCOs represent 25µm, and all scale bars from the liver biopsy pictures represent 100µm. *indicates a statistical significant difference (P<0.05).

ncBCOs retain secretin receptor responsiveness and increased ion-channel activity in vitro compared to cBCOs

Soroka *et al.*[9] created bile cholangiocyte organoids (cBCOs), using the established culture conditions by Huch *et al.* created for cICOs.[10] To investigate if there are differences between ncBCOs and cBCOs we created organoids from bile samples and cultured them using both protocols (n=3). We analysed gene expression profiles using qRT-PCR. First, we assessed expression of the WNT target gene LGR5 and several cholangiocyte-related genes. As indicated in Figure S1A expression of all genes tested was similar in ncBCOs and cBCOs (Figure S1A). To investigate potential donor-variations between samples, we also compared the expression profiles between cECOs and ncECOs for the same cholangiocyte and WNT-target genes by micro-array. As shown in Figure S1B, the expression profiles of biological replicates for both culture conditions did not differ. Moreover, the overall expression profiles of cECOs and ncECOs are similar, although the differences in culture conditions seems to cause clustering of specific genes, indicating that this is an important factor driving gene expression profiles. In line with this observation, the mean gene expression of functional cholangiocyte channels, transporters, and enzymes NKCC1, ASBT, CFTR, GGT and AQP1 are significantly higher in ncBCOs compared to cBCOs (Figure 4A). This was an interesting finding and to further confirm differences in functional receptors and ion-channels, we performed the ussing chamber assay using 2D grown ncBCOs and cBCOs. As a control both the tissue-derived organoids (ncECOs and cICOs) from the original publications were created.[4,10]

As shown in Figure 4B and Figure S2 only organoids cultured in in the non-canonical WNT-stimulated medium (ncBCOs and ncECOs) could respond to addition of secretin and somatostatin. This indicates that functional SCTR and SSTR are only present in cholangiocyte organoids cultured in this specific medium. In contrast, organoid cultured in the canonical-WNT stimulated conditions (cICOs and cBCOs) did not respond to secretin or somatostatin. Moreover, it seems that although all four-organoid types could respond to forskolin and this response was specifically inhibited by addition of GlyH-101 (a specific CFTR-inhibitor), demonstrating functional CFTR-channels in all organoids, this effect was more pronounced in organoids cultured under the non-canonical WNT-stimulated conditions. To investigate the reason for the differences in functionality of cholangiocyte organoids in different culture conditions we looked at gene expression profiles as analysed by gene-array of publically available and novel generated data of cICOs, cECOs and ncECOs. All cICOs and cECOs were matched for donors (n=3). As shown in Figure 4C, the gene expression of almost all mature cholangiocyte-related enzymes, channels and receptors[17] was higher in non-canonical WNT-related conditions, similar to the results of the qRT-PCR analysis (Figure 4A). This suggest that lack of functional SCTR is the result of low or absent SCTR gene expression in organoids under canonical-WNT conditions. Interestingly, cICOs and cECOs cluster together, indicating that culture conditions overshadow differences related to the region of origin (e.q. from intra- or extrahepatic).

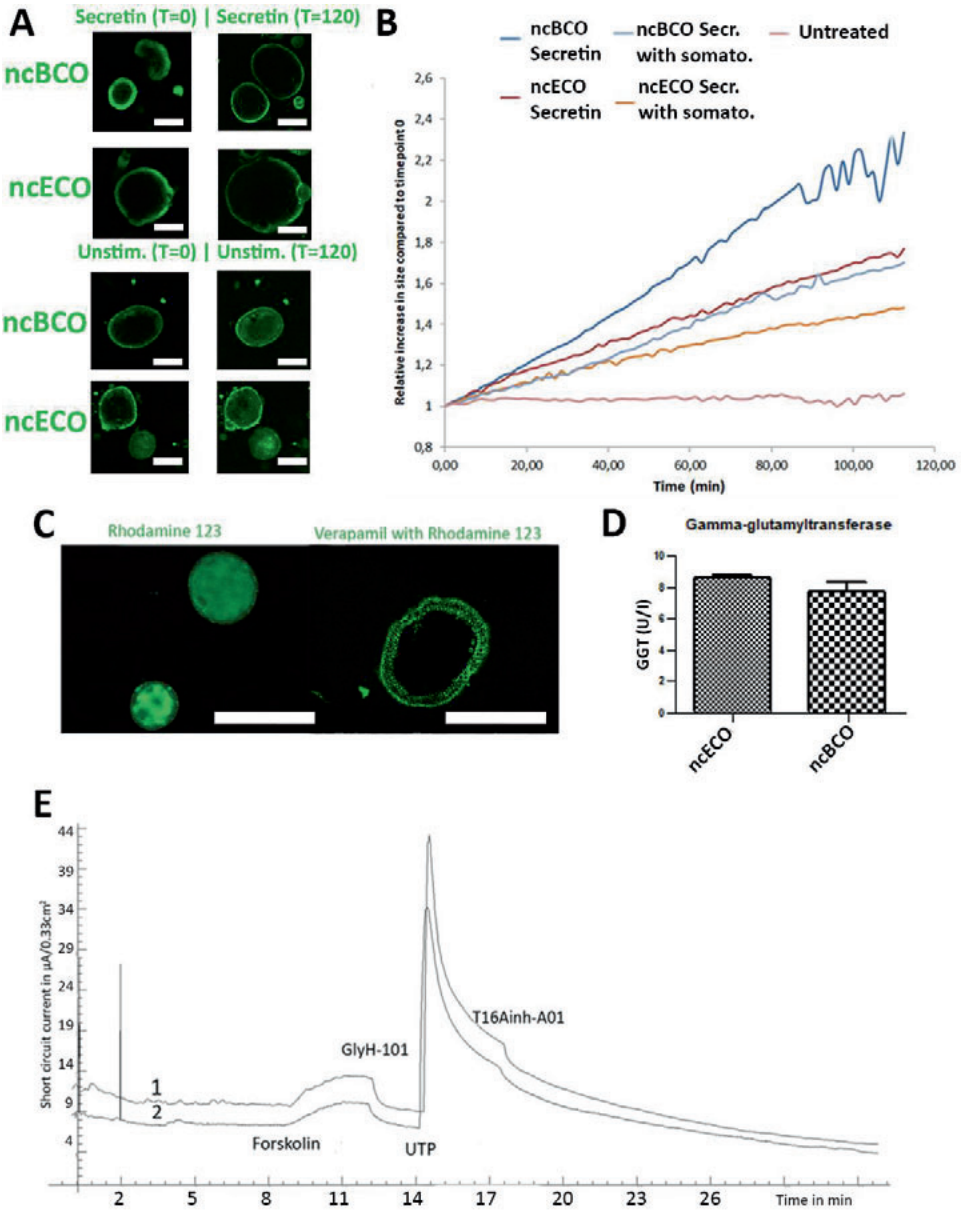

Figure 3. ncBCOs and ncECOs both have functional cholangiocyte activity.

(a) Representative images of selected ncECOs and ncBCOs at time is 0 minutes and time is 120 minutes of measurements in the secretin and unstimulated (unstimulated) groups. **(b)** Quantification of organoid swelling in ncECOs and ncBCOs in different groups, scale bars indicate 50µm. **(c)** ncBCOs show clear MDR-1 activity as Rhodamine 123 was actively transported out of the cells into the lumen of the organoid. Specificity was confirmed by inhibition with Verapamil. **(d)** Gamma-Glutamyltransferase

(GGT) activity (U/l) as measured by ELISA in both ncECOs and ncBCOs supernatants (n=3), scale bars indicate 100µm. **(e)** Representative ion-channel functionality of 2D-grown ncBCOs (line 1) and ncECOs (line 2) in an Ussing-chamber. Stimulation with cAMP-activator, forskolin, resulted in an increase in short circuit current, demonstrating CFTR-mediated activity (Cystic Fibrosis Transmembrane Conductance Regulator). This was completely blocked by CFTR-inhibitor, GlyH-101. Also, calcium-depended chloride excretion ion-channel activity, specifically stimulated by UTP and inhibited by T16Ainh-A01, was identical between ncBCOs and ncECOs.

To further investigate the influence of culture conditions, we changed the medium in the different organoid cultures. As shown in Figure S3A, it seems that culture conditions for the classical cholangiocyte markers do not differ in BCOs, with the exception for the expression of HNF1β between cBCOs and ncBCOs in this series. Interestingly, although BCOs are initiated in medium containing canonical-WNT stimulation, switching them to non-canonical WNT stimulating medium alters the gene expression profiles for genes related to function (Figure 3B). This change in medium directed the switched cBCO gene expression profile to become more closely related to bile cholangiocyte organoids initiated in non-canonical WNT conditions and expression of ASBT and GGT was significantly higher under non-canonical WNT stimulated conditions. A similar effect for these genes was observed when switching ncBCOs to canonical WNT stimulating conditions (Figure S3B). These results suggest that cholangiocyte organoids cultured in different conditions are very similar but differences might be induced by the culture conditions.

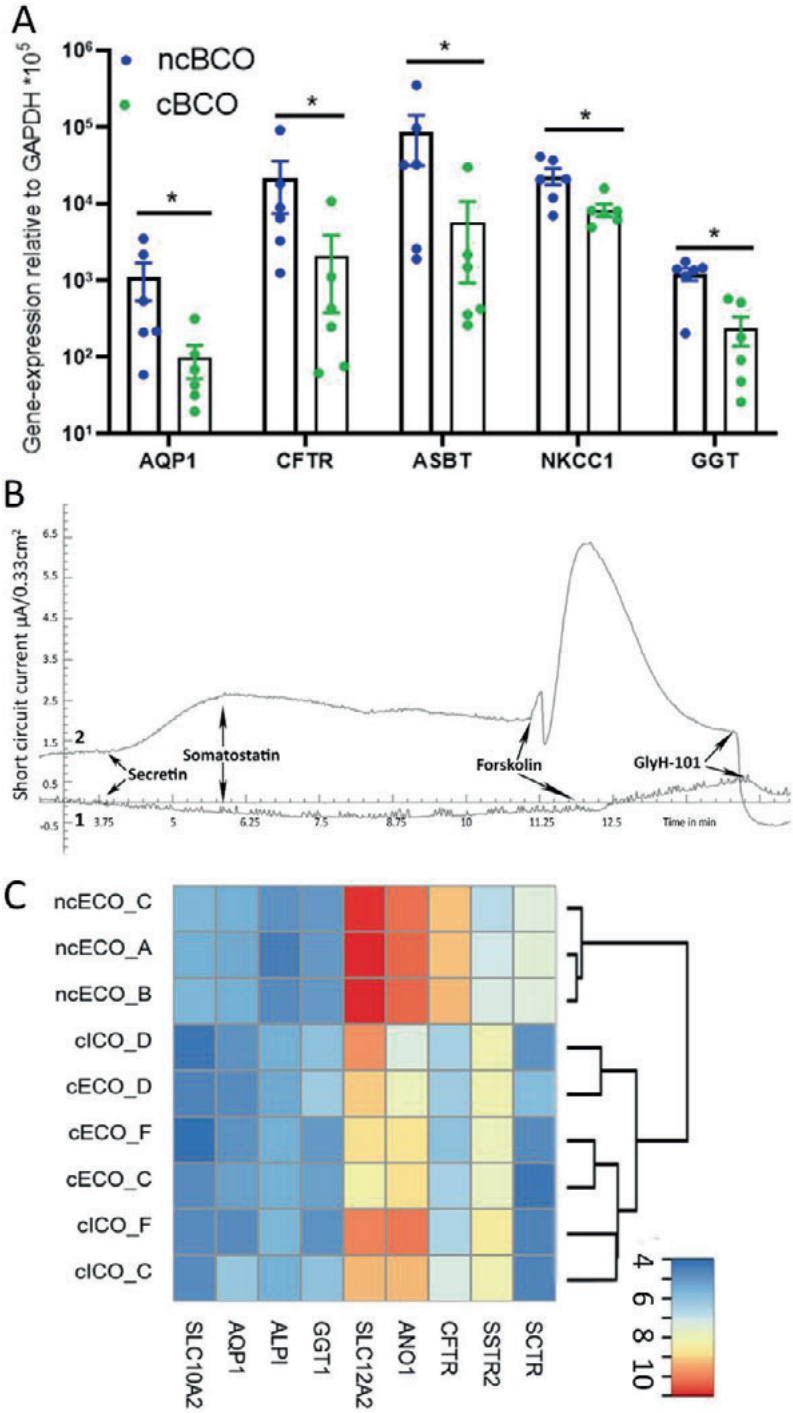
A
ncBCO
cBCO
Gene-expression relative to GAPDH *10^5
AQP1
CFTR
ASBT
NKCC1
GGT
B
Short circuit current µA/0.33cm²
Secretin
Somatostatin
Forskolin
GlyH-101
Time in min
C
ncECO_C
ncECO_A
ncECO_B
cICO_D
cECO_D
cECO_F
cECO_C
cICO_F
cICO_C
SLC10A2
AQP1
ALPI
GGT1
SLC12A2
ANO1
CFTR
SSTR2
SCTR

Figure 4. ncBCOs retain secretin receptor responsiveness and increased ion-channel activity *in vitro* compared to cBCOs.
(a) qRT-PCR of ncBCOs and cBCOs (both, n=6), for cholangiocyte specific channels and transporters. Showing a significant upregulation ($p<0.05$, as indicated by *) for AQP1, CFTR, ASBT, NKCC-1 and GGT in ncBCOs compared to cBCOs. Error bars are displayed as SEM. **(b)** Representative ion-channel functionality of 2D-grown bile cholangiocyte organoids in non-canonical WNT-stimulated conditions (ncBCOs, line 2) and bile cholangiocyte organoids in canonical-WNT stimulated organoids (cBCOs, line 1) in an Ussing-chamber, Stimulation with cAMP-activator (forskolin), resulted in an increase in short circuit current, however secretin stimulation (to the basolateral side) only gave a response in the ncBCOs. In similar fashion, somatostatin (basolateral addition) only gives a response in ncBCOs and not in cBCOs, while CFTR-inhibition via GlyH-101 (luminal addition), resulted in an inhibition of the channel in both organoid-types. Indicating the presence of functional CFTR channels in both organoids, but only somatostatin and secretin-receptors are functional in ncECOs. Moreover, it seems that CFTR-function is higher in organoids in non-canonical WNT stimulating conditions compared to organoids in canonical-WNT stimulating conditions. **(c)** Heatmap and clustering based expression of cholangiocyte related gene expression as analysed by gene-array for functional enzymes (ALPI and GGT1), channels (SLC12A2 –also known as NKCC1-, SLC10A2 – also known as ASBT-, AQP1, ANO1 and CFTR) and receptors (SCTR and SSTR) between cICOs (n=3), cECOs (n=3) and ncECO (n=3). Color key represents the log2 transformed signal intensities after variance stabilizing normalization.

Discussion

In this study we demonstrate that primary biliary epithelial cells (cholangiocytes) collected from bile can be cultured and expanded efficiently *in vitro* while retaining their cholangiocyte characteristics. We show that these ncBCOs, could be efficiently initiated from ERCP and gallbladder bile and could be cultured long-term. In addition, we show that ncBCOs have similar characteristics when compared to ncECOs as described by Sampaziotis *et al.*[4]. Similar gene expression profiles were found in both types of organoids, and both were found to behave as cholangiocytes in functional assays. This study furthermore provides evidence that ncBCOs are distinct from the previously published cBCOs.[9] The non-canonical WNT stimulation of ncBCOs seem to preserve the cholangiocyte-specific basolateral receptor activity *in vitro*. This is the first study demonstrating expansion of non-canonical WNT stimulated cholangiocyte organoids from bile. Recent publications show that cholangiocyte organoids in non-canonical WNT stimulating conditions can be cultured from intra- and extra hepatic biopsies as well as from brushes collected from the common bile duct.[4,7] The use of biopsies and ERCP brushes as a source for biliary organoids provides promising source for *in vivo* collected cholangiocytes as well. Of note, the use of brushes is associated with more complications for the patient when compared to the collection of liquid biopsies from bile.[23,24] Surgical procedures to obtain gallbladders or biopsies are especially risk full in patients with advanced liver cirrhosis[25,26], a potential target population. This is obviously an unwanted risk which limits the patient-specific applications. Moreover, bile allows for inclusion of patients with rare diseases and can model disease-progression *in vitro*, as liquid biopsies can be easily collected during routine (clinical) procedures which patients already undergo for their regular treatment at progressive time-points. Thus, ERCP-derived bile is a relatively safe source for patient-derived cholangiocyte organoids. We show that bile derived from the gallbladder is also a source of cholangiocyte organoids. We included gallbladder bile-derived organoids to study donor variations[11,15], since matched collection of gallbladder bile and gallbladder-tissue from the same patient could be easy accomplished. Some patients are not eligible for ERCP and thus a percutaneous transhepatic cholangiography drainage (PTCD) is performed in these specific patients. Since we demonstrate that multiple sources of bile can be used for ncBCOs, bile collected via PTCD might represent an additional source in this specific subgroup.

Cholangiocytes organoids, either initiated from tissue or bile in both culture conditions, are most likely risen from primary cholangiocytes.[4,27-29] In line with previous publications, we confirmed the presence of a Trop2^{pos} population in bile, which is considered the population that resembles primary cholangiocytes.[21] Since primary cholangiocytes are most likely the cell-of-origin for these organoid cultures, it are the culture conditions which are responsible for the difference in gene expression and functionality *in vitro*. ncBCOs are cultured in medium with components typically stimulating the non-canonical WNT-pathway, while

cBCOs are cultured in WNT/β-catenin stimulated conditions, usually responsible for maintaining stem cell-like characteristics in cell culture. Recent evidence indicates that non-canonical WNT signaling is important in cholangiocyte homeostasis and proliferation.[29,30] Both publications showed that, although WNT ligands seem important in homeostasis of biliary epithelium *in vivo*, this was independent of the canonical WNT–related genes AXIN2, LGR5 and β-catenin. This demonstrates that it is actually non-canonical WNT signaling which drives ductal reprogramming. In contrast, Planas-Paz *et al.* discovered that LGR5-depended WNT/β-catenin signaling is necessary for expansion of intrahepatic cholangiocytes, cultured as cICOs, *in vitro*.[29] In line with these results several publications have reported that WNT/β-catenin-LGR5 signaling is upregulated in canonical-WNT driven cholangiocyte-organoid cultures, while markers for mature cholangiocytes (like CFTR) are downregulated compared to primary cholangiocytes.[21,29,30] Thus, suggesting that organoids initiated under these WNT/β-catenin stimulated culture conditions require these specific signals for growth and alter their gene expression profile by expressing WNT/β-catenin related target genes, although this does not seem to be essential for ductal reprogramming in *in vivo* biliary epithelium.

This *in vitro* study might validate that the use of non-canonical WNT cell culture conditions results (for some aspects) in a more mature cholangiocyte *in vitro,* compared to WNT/β-catenin-stimulated conditions. Here we show that ncBCO have higher expression of mature cholangiocyte-channel genes compared to cBCOs. In addition, gene expression as analysed by gene-array shows that expression of the functional cholangiocyte-related genes such as ANO1, NKCC1, CFTR, GGT, AQP1 and the basolateral receptor SCTR is higher in non-canonical WNT stimulated cholangiocyte organoids when compared to WNT/β-catenin cultured organoids from tissue. Moreover, ncBCOs (and ncECOs) have functionality of the typical cholangiocyte-receptors: secretin and somatostatin while cBCOs (and cICOs) do not. Interestingly, our analysis provides evidence that there is some plasticity in cholangiocyte organoids since we demonstrate that gene expression profiles in BCOs change depending on the culture conditions. In line with our hypothesis, the functional-related genes ASBT and GGT are upregulated when culture medium is switched from canonical WNT to non-canonical WNT stimulating compounds. Also, other genes (HNF1β and PROM1) are differently expressed after switching. Together, our results indicate that culture conditions most probably drive the expression of specific genes in cholangiocyte organoids and that cholangiocytes might be more mature under non-canonical WNT stimulating conditions. It is important to note that ncECO were shown capable of forming functional bile duct tissue *in vivo* after repopulating collagen scaffolds and transplantation in mice.[4] The strength of using bile as a minimally invasive source of organoid-initiation cells for culturing cholangiocyte organoids, is that it allows for patient-specific organoid cultures and thereby avoids immunological responses after transplantation.

In conclusion, our studies confirm and extend the studies previously reported on extrahepatic cholangiocyte organoids[4], demonstrating that these cholangiocyte organoids can efficiently and reproducibly be initiated from bile collected from patients with a broad spectrum of underlying biliary diseases. Given that ncECOs and ncBCOs are highly similar, an important amenity of ncBCOs is that they are reproducibly initiated from bile which is collected relatively easily and in a less invasive manner opposed to surgically rendered tissue biopsies. Moreover, they seem to represent a more mature cholangiocyte compared to the previously published cBCO[9]. With this, the expansion and use of cholangiocyte organoids that are acquired with low complication hazard from patients, becomes feasible for personalized disease modeling and regenerative medicine.

References

1. Murray KF, Carithers RL Jr. AASLD practice guidelines: Evaluation of the patient for liver transplantation. Hepatology. 2005 Jun;41(6):1407-32.
2. Levitsky J. Operational tolerance: Past lessons and future prospects. Liver Transpl. 2011 Mar;17(3):222-32.
3. Sampaziotis F, Segeritz CP, Vallier L. Potential of human induced pluripotent stem cells in studies of liver disease. Hepatology. 2015 Jul;62(1):303-11.
4. Sampaziotis F, Justin AW, Tysoe OC, *et al.* Reconstruction of the mouse extrahepatic biliary tree using primary human extrahepatic cholangiocyte organoids. Nat Med. 2017 Aug;23(8):954-963.
5. Cui S, Capecci LM, Matthews RP. Disruption of planar cell polarity activity leads to developmental biliary defects. Dev Biol. 2011 Mar 15;351(2):229-41.
6. Strazzabosco M, Fabris L. Development of the bile ducts: essentials for the clinical hepatologist. J Hepatol. 2012 May;56(5):1159-70.
7. Tysoe OC, Justin AW, Brevini T, *et al.* Isolation and propagation of primary human cholangiocyte organoids for the generation of bioengineered biliary tissue. Nat Protoc. 2019 Jun;14(6):1884-1925.
8. Seeff LB, Everson GT, Morgan TR, *et al.* Complication rate of percutaneous liver biopsies among persons with advanced chronic liver disease in the HALT-C trial. Clin Gastroenterol Hepatol. 2010;8(10):877-883.
9. Soroka CJ, Assis DN, Alrabadi LS, *et al.* Bile-Derived Organoids From Patients With Primary Sclerosing Cholangitis Recapitulate Their Inflammatory Immune Profile. Hepatology. 2019 Sep;70(3):871-882.
10. Huch M, Gehart H, van Boxtel R, *et al.* Long-Term Culture of Genome-Stable Bipotent Stem Cells from Adult Human Liver. Cell. 2015 Jan 15; 160(1-2): 299–312.
11. Rimland CA, Tilson SG, Morell CM, *et al.* Regional differences in human biliary tissues and corresponding *in vitro* derived organoids. Epub ahead of print 29 March 2020.
12. Barker N, Huch M, Kujala P, *et al.* Lgr5(+ve) stem cells drive self-renewal in the stomach and build long-lived gastric units *in vitro*. Cell Stem Cell. 2010 Jan 8;6(1):25-36.
13. Sato T, Stange DE, Ferrante M, *et al.* Long-term expansion of epithelial organoids from human colon, adenoma, adenocarcinoma, and Barrett's epithelium. Gastroenterology. 2011 Nov;141(5):1762-72.
14. Sato T, Vries RG, Snippert HJ, *et al.* Single Lgr5 stem cells build crypt-villus structures *in vitro* without a mesenchymal niche. Nature. 2009 May 14;459(7244):262-5.
15. Verstegen, MMA, Roos, FJM, Burka, K, *et al*. Human extrahepatic and intrahepatic cholangiocyte organoids show region-specific differentiation potential and model cystic fibrosis-related bile duct disease. Sci Rep, 2020. Epub ahead of print.
16. Roest HP, Ooms LSS, Gillis AJM, *et al.* Cell-free microRNA miR-505-3p in graft preservation fluid is an independent predictor of delayed graft function after kidney transplantation. Transplantation. 2019 Feb;103(2):329-335.
17. Dekkers JF, Wiegerinck CL, de Jonge HR, *et al.* A functional CFTR assay using primary cystic fibrosis intestinal organoids. Nat Med. 2013 Jul;19(7):939-45.

18. Roos FJM, Bijvelds MJC, Verstegen MMA, *et al.* Impact of hypoxia and AMPK on CFTR-mediated bicarbonate secretion in human cholangiocyte organoids. Am J Physiol Gastrointest Liver Physiol. 2021 Mar 3. doi: 10.1152/ajpgi.00389.2020. Epub ahead of print.
19. Ritchie ME, Phipson B, Wu D, *et al.* limma powers differential expression analyses for RNA-sequencing and microarray studies. Nucleic Acids Res. 2015 Apr 20;43(7):e47.
20. Huber W, von Heydebreck A, Sültmann H, *et al.* Variance stabilization applied to microarray data calibration and to the quantification of differential expression. Bioinformatics. 2002;18 Suppl 1:S96-104.
21. Aizarani N, Saviano A, Sagar, *et al.* A human liver cell atlas reveals heterogeneity and epithelial progenitors. Nature. 2019 Aug;572(7768):199-204.
22. Boyer JL. Bile formation and secretion. Comprehensive Physiology. 2013;3(3):1035–1078.
23. Vandervoort J, Soetikno RM, Montes H, *et al.* Accuracy and complication rate of brush cytology from bile duct versus pancreatic duct. Gastrointest Endosc. 1999 Mar;49(3 Pt 1):322-7.
24. Korc P, Sherman S. ERCP tissue sampling. Gastrointest Endosc. 2016 Oct;84(4):557-71.
25. Currò G, Iapichino G, Melita G, *et al*. Laparoscopic cholecystectomy in Child-Pugh class C cirrhotic patients. JSLS. 2005 Jul-Sep;9(3):311-5.
26. Strömberg J, Hammarqvist F, Sadr-Azodi O, *et al*. Cholecystectomy in Patients with Liver Cirrhosis. Gastroenterol Res Pract. 2015;2015:783823.
27. Hu H, Gehart H, Artegiani B, *et al.* Long-Term Expansion of Functional Mouse and Human Hepatocytes as 3D Organoids. Cell. 2018 Nov 29;175(6):1591-1606.
28. Aloia L, McKie M, Vernaz G, *et al.* Epigenetic remodeling licences adult cholangiocytes for organoid formation and liver regeneration. Nat Cell Biol. 2019 Nov;21(11):1321-1333.
29. Planas-Paz L, Sun T, Pikiolek M, *et al.* YAP, but Not RSPO-LGR4/5, Signaling in Biliary Epithelial Cells Promotes a Ductular Reaction in Response to Liver Injury. Cell Stem Cell. 2019 Jul 3;25(1):39-53.
30. Pepe-Mooney BJ, Dill MT, Alemany A, *et al.* Single-Cell Analysis of the Liver Epithelium Reveals Dynamic Heterogeneity and an Essential Role for YAP in Homeostasis and Regeneration. Cell Stem Cell. 2019 Jul 3;25(1):23-38.

Supplementary Information

Materials and Methods

Generation and culture of canonical and non-canonical WNT stimulated cholangiocyte organoids from bile and tissue

For the initiation (of culture) of bile cholangiocyte organoids in canonical-WNT stimulating conditions (cBCOs, n=6), we used a protocol similar to the one previously published by Soroka *et al.*[1]. In short, organoids were initiated from a maximum of three mL of bile collected *ex vivo* and from one millilitre of bile collected *in vivo*. Bile was washed twice for five minutes with cold Advanced (Adv)DMEM/F12 (supplemented with 1% penicillin/streptomycin, Life Technologies; 1% Hepes 1 M, Fisher Scientific; 1% Ultra-glutamine 200mM, Fisher Scientific and 0.2% Primocin, Invivogen) at 453g and suspended in 8 mL of cold AdvDMEM/F12. Subsequently, the supernatant was removed and the pellet was suspended in 3 mL of AdvDMEM/F12 and passed through a 100 µm cell strainer to remove debris. After a third wash, the pellet was collected and plated out in a hydrogel (Matrigel, Corning, or diluted Basement Membrame Extract, BME, Cultrex). Medium was added according to the previously described protocol.[2,3] The first three days the medium was supplemented with 1% anti-anti (Gibco) to prevent bacterial- or fungal infections.

Tissue-derived intrahepatic cholangiocyte organoids in canonical-Wnt stimulating conditions (cICOs, n=3) and extrahepatic cholangiocyte organoids in canonical-Wnt stimulating conditions (cECOs, n=3) were initiated and cultured as previously published.[2-4] In short, liver or extrahepatic bile duct biopsies (0.5-1.0 cm^3) were digested using a collagenase solution in (2.5 mg/ml collagenase A1, Roche) EBBS (Hyclone, Thermoscientific) for 30 min at 37 ˚C. Digestion was stopped by adding cold supplement AdvDMEM/F12 filtered through a 70 µm cell strainer. The cell suspension was spun down for 5 minutes, 4˚C at 453*g*. Pellet was harvested in a hydrogel and specific medium was added according to protocol.[2,3] Medium was changed twice a week and organoids were passaged in a 1:2 to 1:8 ratio according to growth. Cultures were negative for mycoplasma contamination (data not shown).

The ncECO cultures (n=6) were initiated and maintained as previously published.[5] In short, cells were scraped from the inside of the gallbladders or from the inside of an extrahepatic bile duct (n=1) and collected in cold William's-E Medium (WE). The cells were centrifuged at 453*g* for 5 minutes at 4˚C, subsequently supernatant was removed, and the cell pellet was washed twice with excess cold WE. Next the pallet was collected and plated out in either matrigel or 70% BME diluted with WE and medium was added according to the standard protocol.[5]

Additionally, to investigate the influence of culture conditions on BCOs. Bile cholangiocyte organoids were either created from the same bile samples (n=3) either under cBCO conditions or ncBCO conditions. After three passages a switch from cBCO to ncBCO conditions and from ncBCO conditions to cBCO conditions was performed. Two passages later RNA was harvested from these 4 conditions per donor sample and analysed by qRT-PCR.

Ussing Chamber Measurement conditions

The temperature of the chambers was kept 37 °C by warm water bath circulation. Each chamber consisted of 3 mL modified Meyler solution (128 mmol/liter NaCl, 4.7 mmol/liter KCl, 1.3 mmol/liter $CaCl_2$, 1.0 mmol/liter $MgCl_2$, 0.3 mmol/liter Na_2HPO_4, 0.4 mmol/liter NaH_2PO_4, 20 mmol/liter $NaHCO_3$, 10 mmol/liter HEPES, supplemented with glucose (10 mmol/liter) in 95% O_2, 5% CO_2 at pH 7.3). Current was clamped and every second current was recorded. Two voltage spikes (5 millivoltage) were given, to measure resistance along the epithelial layers (*V=I*R; TEER*). CFTR-dependent anion secretion was activated by adding 20 µM Secretin (Sigma) basolateral or 10 µM Forskolin (Sigma) to both sides of the cells and inhibited by addition of GlyH-101 (20 µM, apical side, Calbiochem) or 100 µM Somatostatin (Sigma) basolateral. Calcium (Ca^{2+}) depended chloride (Cl^-) channels (CaCC) were stimulated by UTP (50 µM, apical side, Sigma) and inhibited by T16Ainh-A01 (50 µM, apical side, Tocris).

Table S1. Donor and culture characteristics of organoids included.

Age patient (years)	Gender	Cells Source	Donor Type; Indication ERCP/surgery	Culture type	Successful Culture	Characterized at Passage #	Gene expression
13	M	GB, GBB	DBD	ncECO 1, ncBCO 1	+	5-9	+
26	M	GBB	DCD	ncBCO 7**, cBCO 7**	+	5	+
29	M	ERCP	Bile stones	ncBCO 14	+	ND	-
30	M	ERCP	PSC	ncBCO 8 cBCO 8	+	5	+
35	F	GBB, GB	DBD	ncBCO 5, ncECO 5	+	5	+
41	F	EHBD	PSC	ncECO 11	+	5	+
47	M	GBB	DCD	ncBCO 6**, cBCO 6**	+	5	+
50	M	GB	Bile stones	ncECO 12	+	5-8	+
51	F	ERCP	AS	ncBCO 15	+	ND	-
52	M	GBB, GB	DCD	ncBCO 4, ncECO 4	+	5-9	+
54	M	EHBD	DBD	cECO D*	+	5	-
54	F	ERCP	Papiladenoma	ncBCO 10	+	5-8	+
56	F	EHBD	DCD	cECO C*	+	5	-
57	M	Liver, GBB, GBB	DCD	cICO 2, cBCO 2, ncBCO 2	+	5 5 5	+ (only cBCO)
58	F	ERCP	AS	ncBCO 16	+	ND	-
59	M	GB, GBB, GBB, Liver	DBD	ncECO 3, cBCO 3, ncBCO 3 cICO 3	+	5-8 5 5 5	+
67	M	Liver	DCD	cICO 13	+	5	+
67	F	EHBD	Cryptogenic Cirrhosis	cECO F*	+	5	-
70	M	ERCP	Bile stones	ncBCO 17	+	ND	-
72	M	ERCP	Bile stones	ncBCO 18	+	ND	-
73	F	ERCP	AS	ncBCO 19	-	ND	-
75	F	GBB	DBD	ncBCO 9**, cBCO 9**	+	5	+

Abbreviations: AS: Anastomotic bile duct Stricture, ncBCO: Bile Cholangiocyte Organoid in non-canonical WNT stimulating conditions, EHBD: Extrahepatic Bile Duct, cECOs: extrahepatic cholangiocyte organoids in canonical WNT stimulating conditions, cICOs: intrahepatic cholangiocyte organoids in canonical WNT stimulating conditions, cBCO: Bile Cholangiocyte Organoids organoids in canonical Wnt stimulating conditions, DBD: Donation after Brainstem Death, DCD: Donation after Circulatory Death, ncECO: Extrahepatic Cholangiocyte Organoids in non-canonical Wnt stimulating conditions, ERCP: Endoscopic Retrograde Cholangiopancreaticography, F: Female, GB: Gallbladder, GBB: Gallbladder Bile, M: Male, PSC: Primary sclerosing Cholangitis, ND: Not Determined. *These organoid cultures were only analysed for Micro Array analysis. **Used for switching experiment (ncBCOs, are only used for the switching experiment).

Table S2. List of genes and primers used.

Gene		Primer sequence (5' à 3')
KRT7	F	GGGGACGACCTCCGGAATAC
	R	CTTGGCACGCTGGTTCTTGA
KRT19	F	GCACTACAGCCACTACTACACGA
	R	CTCATGCGCAGAGCCTGTT
HNF1β	F	TCACAGATACCAGCAGCATCAGT
	R	GGGCATCACCAGGCTTGTA
HPRT	F	CTATAAATTCTTTGCTGACCTGCG
	R	CTTCGTGGGGTCCTTTTCACC
ALB	F	CTGCCTGCCTGTTGCCAAAGC
	R	GGCAAGGTCCGCCCTGTCATC
GAPDH	F	CTTTTGCGTCGCCAGCCGAG
	R	CCAGGCGCCCAATACGACCA
HNF4α	F	GTACTCCTGCAGATTTAGCC
	R	CTGTCCTCATAGCTTGACCT
AQP1	F	GGCCAGCGAGTTCAAGAAGAA
	R	TCACACCATCAGCCAGGTCAT
NKCC1	F	CCAAGGATGTGGTAGTAAGTGT
	R	GATTCTTTTTTCAACAGTGGTTGA
GGT	F	TGGTGGACATCATAGGTGGGGA
	R	ATGACGGCAGCACCTCACTT
ASBT	F	GGTGGCCTTTGACATCCTCCC
	R	GCATCATTCCGAGGGCAAGC
SOX9	F	ACCAGTACCCGCACTTGCAC
	R	GCGCCTTGAAGATGGCGTTG
EpCAM	F	GACTTTTGCCGCAGCTCAGGA
	R	AGCAGTTTACGGCCAGCTTGT
CFTR	F	TGGCGGTCACTCGGCAATTT
	R	TCCAGCAACCGCCAACAACT
LGR5	F	GTCAGCTGCTCCCGAATCCC
	R	TGAAACAGCTTGGGGGCACA
Cyp3A4	F	CAAAGAGCAACACAGAGCTGAA
	R	CAGAGGTGTGGGCCCTGGAAT
KRT18	F	TCCAAAAGACCACCACCCGCC
	R	TGCTCCCCAAAGTGTACCCTGC
CES1	F	GCCCGGAACCACAGAGATGCT
	R	AGCTCATCCCCGTGGTCTCCT
CD133	F	CCTGGGGCTGCTGTTTATTA
	R	TGGCACTGTGGGGAGGGTCTC

Gene		Primer sequence (5'à 3')
LOLX4	F	CTGGGCCGGACTGACTTTCGT
	R	CTTGTGCCCCTCAGCCACCTT
MMP1	F	GGCCCACAAACCCCAAAAGCG
	R	CGGGTAGAAGGGATTTGTGCGC
AGR2	F	TCCTAGCCGCCGACTCACACA
	R	GGTTTGACTGTGGTATCTCTGGCG
KLK7	F	ACCACCTGTACTGTCTCCGGCT
	R	AACCTTCGTGCAGTCCTGGGG
IGFBP1	F	GGCACAGGAGACATCAGGAGA
	R	CACCAGCAGAGTCCCGCCTC
SLC2a3	F	ATTGCTCTTCCCCTCCGCTGC
	R	CCTCAAAAGTCCTGCCACGGGT
TFF1	F	ACAAGCTGCTGTACACGGACA
	R	AAGTTTCCAGGGCCGGGCAAT
TFF2	F	TCTGTCCTGCCTCCCTGATCCA
	R	CTCTGGCACGTGAATCCCGGT
GC	F	ATGGCCAAAGAGCTGCCTGA
	R	TGGGCAGCTGGCATGAAGTA
A1AT	F	TGAGGAGAGCAGGAAAGGACA
	R	CTCAGCCAGGGAGACAGG
ALDH1A	F	TGAAGTCATCGGTCGGCTTGA
	R	ACCCCTACGATGACACTTGTGCC
LYZ	F	GGCAAAACCCCAGGAGCAGTT
	R	TGCCACCCATGCTCTAATGCCT
AGR2	F	TCCTAGCCGCCGACTCACACA
	R	GGTTTGACTGTGGTATCTCTGGCC
S100A6	F	GGCAGGGAGGGTGACAAGCA
	R	CCTCCTGGTCCTTGTTCCGGT
TACSTD2	F	CGAGCTTGTAGGTACCCGGCG
	R	TGCGCCGAGGAATCAGGAAGC
LCN2	F	ACCACATCGTCTTCCCTGTCCC
	R	ATCACCAACAGGGAGATTGC
LGR5	F	GTCAGCTGCTCCCGAATCCC
	R	TGAAACAGCTTGGGGGCACA
CTSE	F	ATTGGCTCCCCACCACAGAA
	R	CTGGACTGGGAAGGCTGGA

Table S3. Overview of cholangiocyte organoids cultured in this manuscript.

Name	Abbreviation	Source	Culturing conditions	Protocol/ reference
Bile Cholangiocyte Organoid in canonical WNT stimulating conditions	cBCO	Bile	Canonical WNT	Soroka *et al.*[1]
Intrahepatic Cholangiocyte Organoid in canonical WNT stimulating conditions	cICOs	Intrahepatic cholangiocytes via a liver biopsy	Canonical WNT	Huch *et al.*[2]; Broutier *et al.*[3]
Extrahepatic Cholangiocyte Organoid in canonical WNT stimulating conditions	cECOs	Extrahepatic cholangiocytes from an extrahepatic bile duct biopsy	Canonical WNT	Rimland *et al.*[4]
Extrahepatic Cholangiocyte Organoid in non-canonical WNT stimulating conditions	ncECO	Extrahepatic cholangiocytes	Non-canonical WNT	Sampaziotis *et al.*[5]; Tysoe *et al.*[6]
Bile Cholangiocyte Organoid in non-canonical WNT stimulating conditions	ncBCO	Bile	Non-canonical WNT	This protocol

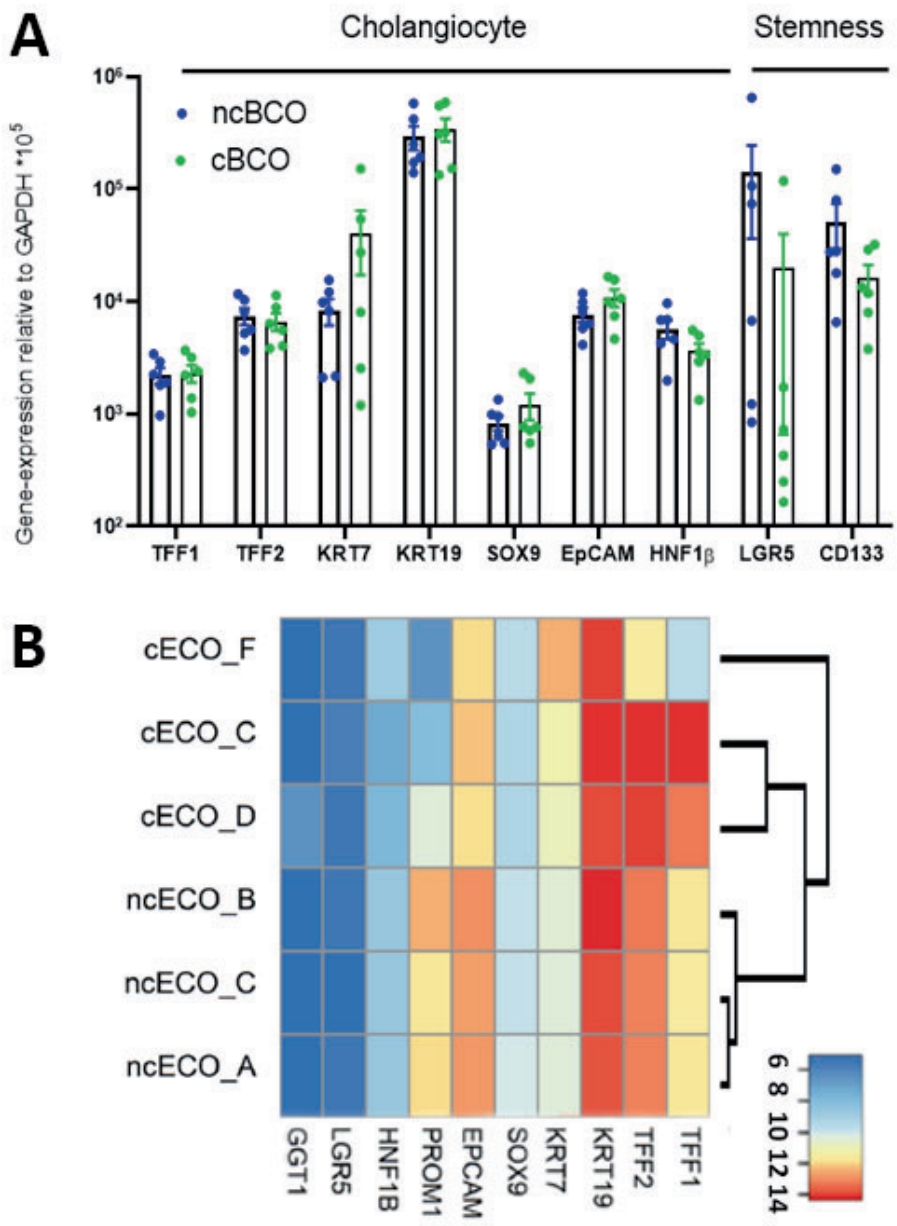

Figure S1. Classical cholangiocyte markers are similar expressed between non-canonical WNT and canonical-WNT stimulating conditions.

(a) qRT-PCR showing comparison between ncBCOs (n=6) and cBCOs (n=6) for different cholangiocyte- and stemness/Wnt-target related genes, relative to the housekeeping gene *GAPDH*, error bars are

presented with standard error of the mean. **(b)** Gene expression as analysed by Micro Array for ncECOs (n=3) and cECOs (n=3) for the similar genes as displayed in panel a. Color key represents the log2 transformed signal intensities after variance stabilizing normalization.

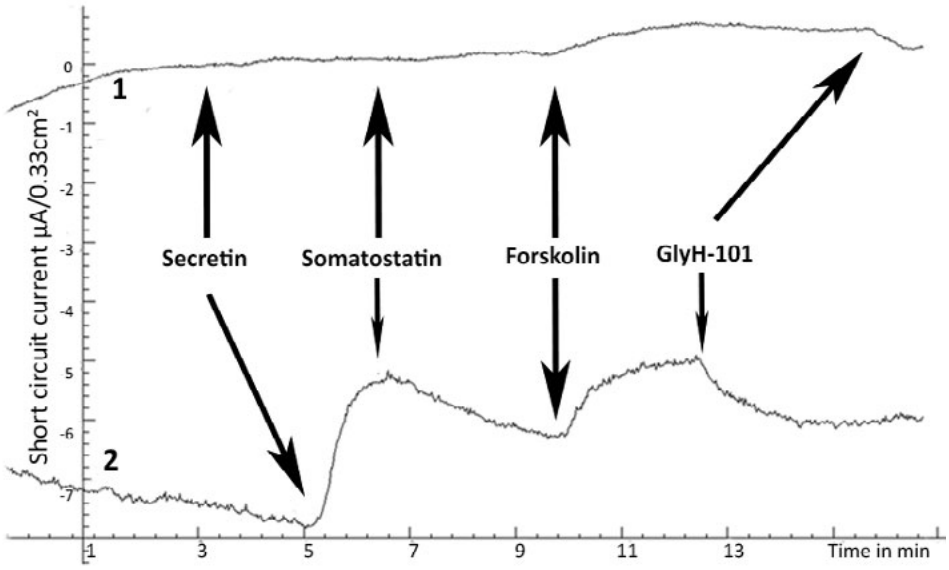

Figure S2. Cholangiocyte related and ion-channel and basolateral receptor activity in ncECOs and cICOs.

Representative ion-channel functionality of 2D-grown tissue derived canonical-Wnt stimulated organoids (cICOs, line 1) and tissue derived non-canonical WNT stimulated organoids (ncECOs, line 2) in an Ussing-chamber. Stimulation with cAMP-activator(forskolin), resulted in an increase in short circuit current, however secretin stimulation (to the basolateral side) only gave a response in the ncECOs. In similar fashion, somatostatin (basolateral addition) only gives a response in ncECOs and not in cICOs, while Cystic Fibrosis Transmembrane Conductance Regulator (CFTR)-inhibitor, GlyH-101 (luminal addition), resulted in an inhibition of the channel in both organoid-types. Indicating the presence of functional CFTR channels in both organoids, but only somatostatin and secretin-receptors are functional in ncECOs. Moreover, the CFTR responses in ncECOs seems more pronounced compared to cICOs.

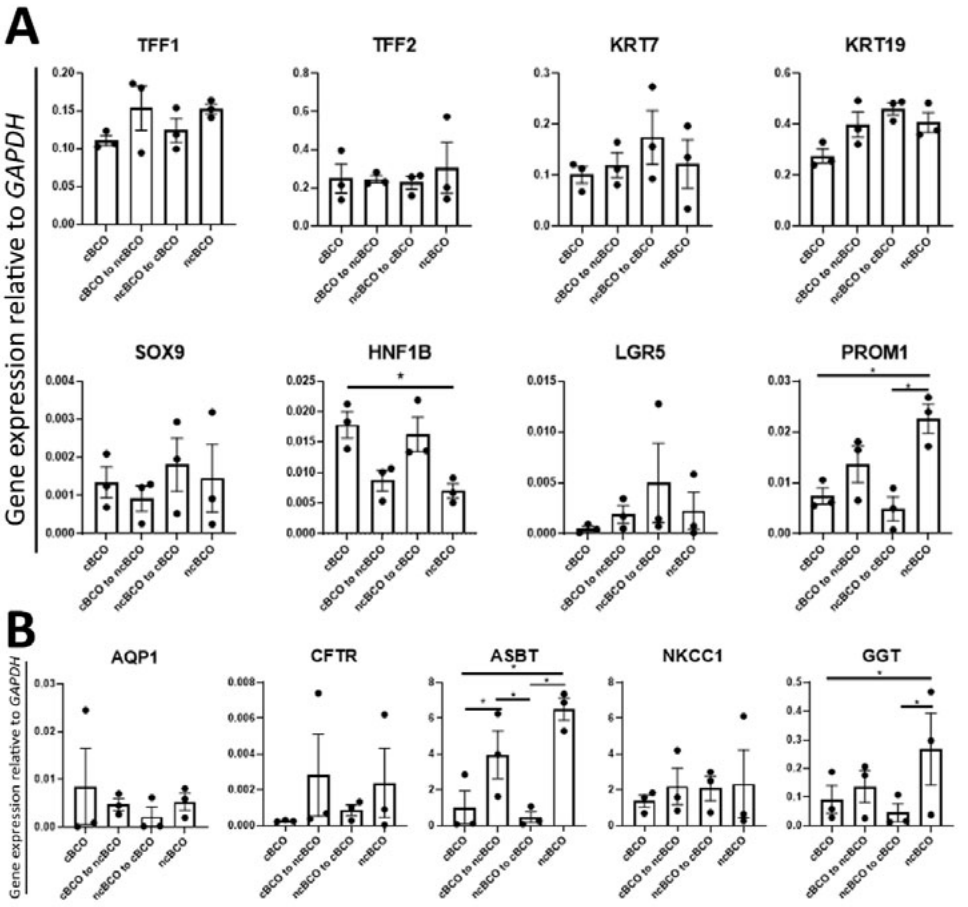

Figure S3. Gene expression profiles of bile cholangiocyte organoids under different culture conditions.

(a) Gene expression profiles as analysed by qRT-PCR for BCOs started up in either canonical WNT (cBCOs) or non-canonical WNT culture (ncBCOs) conditions for the classical cholangiocyte and stem cell/Wnt-target genes. After three passages pallet was split in half and organoids were either continued in their original conditions or switch to the other (n=3, all conditions). Error bars indicate standard error of the mean. **(b)** Gene expression profiles of the cholangiocyte markers related to function as analysed by qRT-PCR for the same samples as displayed in panel a. Error bars indicate standard error of the mean. *is considered a significant difference ($p<0.05$).

References

1. Soroka CJ, Assis DN, Alrabadi LS, *et al.* Bile-Derived Organoids From Patients With Primary Sclerosing Cholangitis Recapitulate Their Inflammatory Immune Profile. Hepatology. 2019 Sep;70(3):871-882.
2. Huch M, Gehart H, van Boxtel R, *et al.* Long-Term Culture of Genome-Stable Bipotent Stem Cells from Adult Human Liver. Cell. 2015 Jan 15; 160(1-2): 299–312.
3. Broutier L, Andersson-Rolf A, Hindley CJ, *et al.* Culture and establishment of self-renewing human and mouse adult liver and pancreas 3D organoids and their genetic manipulation. Nat Protoc. 2016 Sep;11(9):1724-43.
4. Rimland CA, Tilson SG, Morell CM, *et al.* Regional differences in human biliary tissues and corresponding *in vitro* derived organoids. Epub ahead of print 29 March 2020.
5. Sampaziotis F, Justin AW, Tysoe OC, *et al.* Reconstruction of the mouse extrahepatic biliary tree using primary human extrahepatic cholangiocyte organoids. Nat Med. 2017 Aug;23(8):954-963.
6. Tysoe OC, Justin AW, Brevini T, *et al.* Isolation and propagation of primary human cholangiocyte organoids for the generation of bioengineered biliary tissue. Nat Protoc. 2019 Jun;14(6):1884-1925.

8

CHAPTER 8

Human branching cholangiocyte organoids recapitulate embryonic bile duct development.

Floris JM Roos, Gilles S van Tienderen*, Haoyu Wu*, Ignacio Bordeu*, Dina Vinke, Laura Muñoz Albarinos, Kathryn Monfils, Sabrah Niesten, Ron Smits, Jorke Willemse, Daniel J Kunz, Maurice de Wit, Pim J French, Ludovic Vallier, Jan NM IJzermans, Richard C Bàrtfai, Hendrik Marks, Ben D Simons, Martin E van Royen, Monique MA Verstegen×, Luc JW van der Laan×

* these authors contributed equally;
× shared senior authorship.

Cell Stem Cell, Manuscript in revision.

Abstract

Adult tissue-derived cholangiocyte organoids show great promise for regenerative therapies and modeling of bile duct diseases. *In vitro*, their cyst-like morphology does not recapitulate the complex bifurcated architecture of intrahepatic bile ducts. Here, we report a new culture method which induces branching morphogenesis in organoids making it is more suited for studying intrahepatic biliary diseases. These branching cholangiocyte organoids (BRCO) self-organize into large complex tubular structures closely resembling bile duct branches, while single cell transcriptomic and functional analysis showed high similarity with primary cholangiocytes. The branching growth mimics bile duct development and is dependent on JAG1/NOTCH2 signaling. Furthermore, when applying the culture method to cholangiocarcinoma organoids (CCAO) this induced the formation of tumor-like structures *in vitro*. In contrast to previous organoid protocols, the branching CCAO architecture resembles the primary tumors, have a transcriptomic profile more closely to the primary tumor and show clear cancer-specific drug resistance. In conclusion, a complex, self-organizing, growth pattern can be induced in cholangiocyte organoids recapitulating branching morphogenesis in culture. This provides an improved model to study bile duct development and diseases.

Introduction

The biliary tree is a complex tubular system comprised by the extrahepatic bile duct (EHBD) and the intrahepatic bile ducts (IHBDs), that transport bile to the duodenum.[1-3] Cholangiocytes (biliary epithelial cells) line these ducts, providing a physical barrier to bile, and modify the bile composition.[4,5] Although IHBDs and EHBDs have very similar types of cholangiocytes, there are large morphological differences. Most importantly, IHBDs display a complex branching architecture, while the EHBD does not. Branching is a common phenomenon in organogenesis of mammalian species. It is the result of the complex interaction between tissue mechanics, molecular signaling and cell fate dynamics. Many organs, such as breasts (mammary glands), salivary glands, kidney, lung, pancreas (pancreatic ducts) and liver (bile ducts), display a branched architecture.[6] For all these organs, organoid culture methods have been developed which provide opportunities to study branching duct formation *in vitro*. For bile ducts, several organoid types have been established.[7-12] However, these cholangiocyte organoids form cyst-like structures with a fluid-filled lumen surrounded by a monolayer of epithelial cells and do not form complex branching structures.

Here, we report the establishment of branching cholangiocyte organoids (BRCOs) from human adult IHBDs. *In vitro*, BRCOs grow into self-renewing, self-organizing structures that appear as complex branching structures. BRCO cells closely resemble mature cholangiocytes on a single cell transcriptome level and recapitulate the heterogeneity of cholangiocytes present *in vivo*.[13-16] BRCOs exhibit mature cholangiocyte functional properties, such as ion transport and alkaline phosphatase (ALP) activity.[5] We demonstrate that ductal growth in BRCOs is tip-driven, that their dynamics and spatial organization are behaving according to probabilistic rules, and that tubular formation in BRCOs mimics development as seen *in situ*. Furthermore, organoids derived from an Alagille syndrome patient, suffering from defective bile duct formation due to a defective *JAGGED1* gene[17-19], were unable to form branches due to absence of NOTCH2 signaling. Finally, we demonstrate that branching cholangiocarcinoma (CCA) organoids (BRCCAOs) can be formed from organoids derived from primary CCA tumors.[20] BRCCAOs closely resemble the primary tumor-tissue architecture and transcriptomic profile and provide a better model for drug responses to clinically relevant chemotherapeutics. Overall, these results demonstrate the unique aspects of this new organoid model for studying (malignant) biliary diseases and embryonic bile duct development.

Materials and Methods

Cell lines

L-Wnt3a, 293T-HA-Rspo1-Fc and Noggin HEK-293 cell lines were used as described to generate conditioned media for organoid culture (secreting WNT3A, R-Spondin and Noggin). Cells were cultured in a humidified 5% CO_2 atmosphere at 37°C as previously described.[21,22]

Tissue and tumor collection

Tissue biopsies from liver (circa 0.5-3 cm^2, n=14) and extrahepatic bile duct (EHBD, circa 0.5-3 cm^3 n=3) were obtained from donor livers (n=12) or explant livers (n=2) during liver transplant procedures (for details see Table S1) performed at the Erasmus MC, Rotterdam, the Netherlands. The use of tissue biopsies and livers deemed unsuitable for transplantation was approved by the MEC of the Erasmus MC, (MEC-2012-090, MEC-2014-060). Fetal liver samples were collected via the CASA clinic in Leiden and Rotterdam and the use of fetal tissues was approved by the MEC of the Erasmus MC (MEC-2006-202). Additionally, cholangiocarcinoma (CCA) tumor tissue biopsies (n=3) from both perihilar and intrahepatic CCA (see Table S1) were obtained through liver resections performed at the Erasmus MC (MEC-2013-143). Biopsies were stored at 4˚C in University of Wisconsin (UW, Bridge to Life Ltd. Belzer Cold Storage Solution) preservation solution during transport. For a complete overview of characteristics of patients or donors from whom biopsies were obtained, please see Table S1. All patients or their next of kin gave written informed consent to use their tissue.

Generation and culture of (tumor) organoids

Organoids from (adult and fetal) liver- and EHBD biopsies were processed, initiated, and expanded as previously published.[7,11,21] Biopsies were digested by incubation with 4 mL collagenase digestion solution (2.5 mg/mL collagenase A1, Sigma) in Earle's Balanced Salt Solution (EBSS, Hyclone, ThermoFisher scientific) for 30 min at 37°C. Digestion solution was diluted by adding cold Advanced (Adv)DMEM/F12 (GIBCO, supplemented with 100 µg/mL penicillin/streptomycin, Fisher Scientific; HEPES 1M, Fisher Scientific; 1% Ultraglutamine 200mM, Fisher Scientific and Primocin, Invivogen) and centrifuged for 5 minutes, 4˚C at 453g. The cell suspension was filtered through a 70 µm Nylon cell strainer and centrifuged for 5 minutes, 4˚C at 453g. Supernatant was removed and the cell pellet was suspended in cold (4°C) or 25µL Basement Membrane Extract (BME, Cultrex) diluted with 30% of AdvDMEM/F12 which was allowed to solidify for 30-45 minutes at 37°C before 250µL start-up expansion medium (SEM) was added.[21] SEM consists of supplemented AdvDMEM/F12 (GIBCO, supplemented with 100 µg/mL penicillin/streptomycin, Life Technologies; Hepes 1M, Fisher Scientific; 1% Ultraglutamine 200mM, Fisher Scientific and Primocin, Invivogen) supplemented with 1% N2 (GIBCO) and 1% B27 (GIBCO), 1.25 mM N-Acetylcysteine (Sigma),

10 nM gastrin (Sigma), 50 ng/mL EGF (Peprotech), 10% RSPO1 conditioned media (homemade), 10% Noggin conditioned media (homemade), 30% WNT conditioned media (homemade), 10 µM (Y27632, Bioconnect), 10 µM hES cell cloning recovery solution (Tebu-bio), 100 ng/mL FGF10 (Peprotech), 25 ng/mL HGF (Tebu-bio), 10 mM Nicotinamide (Sigma), 5 µM A83.01 (Sanbio), and 10 µM Forskolin (Sigma). SEM was replaced with canonical-WNT stimulating expansion medium (EM), consisting of the same components without NOGGIN, WNT, Y27632, and hES cell cloning recovery solution, after three days.[21] Finally, branching organoids were created by switching culture conditions to non-canonical WNT stimulating conditions, consisting of William's E medium (WE, ThermoFisher Scientific) supplemented with 10 mM nicotinamide (Sigma), 17 mM sodium bicarbonate (Sigma), 0.2 mM 2-phospho-L-ascorbic acid trisodium salt (Sigma), 6.3 mM sodium pyruvate (Gibco), 14 mM glucose (Sigma), 20 mM HEPES (Fisher Scientific), ITS + premix (Life Technologies), 0.1 µM dexamethasone (Sigma), 2 mM Ultraglutamine (Fisher Scientific), 100 µg/mL penicillin/streptomycin (Fisher Scientific), 20 ng/mL EGF (Peprotech), 10% RSPO1 conditioned media (homemade) and 100 ng/mL DKK-1 (Abcam Ltd), after 3 passages.[9,12]
Cholangiocarcinoma organoids (CCAOs) were initiated and expanded as previously described.[20] Processing and initiation of these organoids was similar to ICO counterparts described above, except tissue digestion was extended to 2 hours for tumor tissue that, after visual inspection, still had relatively large undigested tissue fragments left. BRCCAOs were created by switching culture medium to non-canonical WNT stimulating conditions after a minimum of 3 passages in expansion medium.

Time-lapse bright field microscopy

BRCOs (n=3, multiple wells over time) were cultured in glass bottom 96 well plates (SensoPlate™ 24 well, Greiner Bio-One) and imaged using bright field microscopy using an Opera Phenix system (PerkinElmer), equipped with a 10x air objective (NA 0.3), in non-confocal modus. Every 30 minutes, for 110 hours, a small z-stack was acquired to ensure optimal optical focus in several points of the growing organoid. The images were concatenated to create a time-lapse and observe growth of the organoids. Additional time-lapse analysis was performed with the addition of A83-01 (1µM) to inhibit the transforming growth factor beta (TGF-β) pathway, known to be involved in branching morphogenesis.[6]

Transmission Electron Microscopy (TEM)

To perform TEM, BRCOs were fixated in 1.6% glutaraldehyde and were stored at 4°C until processed. Subsequently, post fixation was performed using 1% osmium tetroxide for one hour. Next, acetone rinses were performed (8 times 15 minutes with increased percentage of acetone) and samples were infiltrated with 1:1 100% acetone:epoxy embedding medium for two days. First, they were embedded for one hour at room temperature, followed by an embedding at 40°C overnight, and finally a 24-hour step of embedding at 60°C. Subsequently,

ultrathin sections of 60 a 70 nm were created at a 6-degree angle at speed of 1 mm/s with a Diatome Diamond knife and an electronic microscope ultra-microtome (Leica UC7). Finally, ultrathin sections were imaged using a FEI Talos transmission electron microscope (Thermo Scientific), equipped with a 4K CMOS camera; samples were imaged using 80 kV.

Hematoxylin and Eosin (H&E) and Immunofluorescence (IF) staining

Organoids were fixed for 10 minutes using 4% paraformaldehyde removing the hydrogel. Samples were paraffin embedded and cut as 4 µm thick slides. Subsequently, H&E staining was performed according to standard protocols. H&E-stained slides were imaged with Zeiss Axiokop 20 microscope and captured with a Nikon DS-U1 camera. If immunofluorescence was performed, slides were permeabilized with 0.1% Triton X-100 diluted in phosphate buffered saline (PBS) for 15 minutes. Subsequently, they were exposed to 10% goat serum diluted in 1% Bovine Serum Albumin (BSA)-PBS to prevent nonspecific antibody binding. Primary antibodies (for antibodies used and dilutions, see Table S2) were added to the organoids and incubated overnight at 4˚C. Finally, incubation with the secondary antibody took place for 60 minutes at room temperature and cell nuclei were stained with DAPI (Vectashield, Vectorlabs). Analysis took place on a SP5 confocal microscope (LEICA) equipped with a 405, 488 and 561 nm laser. Images were analyzed using ImageJ (version 1.52p, supplemented with FIJI).

Whole mount confocal IF staining

To evaluate protein expression of organoids, IF was performed using whole mount confocal microscopy with selected antibodies. In short, organoids were fixed for 10 minutes using 4% paraformaldehyde removing the hydrogel. Next, they were permeabilized with 0.1% Triton X-100 diluted in PBS for 15 minutes. Subsequently, they were exposed to 10% serum diluted in 1% BSA-PBS to prevent nonspecific antibody binding. Primary antibodies were added to the organoids and incubated overnight at 4˚C. Incubation with the secondary antibody took place for 60 minutes at room temperature. Additional cytoskeletal staining with Phalloidin Alexa Fluor™ 488 (1:200, ThermoFisher) and nuclear staining with DAPI was performed. Samples were imaged using a Leica 20X water dipping lens on Leica DM6000 CFS microscope with a LEICA TCS SP5 II confocal system or an Opera Phenix HCS system (PerkinElmer) equipped with a 20x air objective (NA 0.4) and 40x water immersion objective (NA 1.1). For detection on the Opera Phenix system, DAPI was excited with a 405 nm solid state laser and detected at 435-480 nm. EdU incorporation, Phalloidin Alexa Fluor 488, and the Ki67 immune labeling were excited at 488 and 561 nm and detected at 500-550 nm and 570-630 nm, respectively. Images were processed using ImageJ (version 1.52p, with FIJI).

Stable Isotope labeling by amino acids in cell culture (SILAC) sample preparation
Lyophilized samples were rehydrated in 200 µL extraction buffer with 100 mM ammonium bicarbonate with 8 M urea, and homogenized using a Bioruptor®Plus (Diagenode SA, Seraing, Belgium) at 4°C for 20 cycles, 15 s ON/OFF. Samples were centrifuged (14000 g, 15 min) and the protein content of supernatants was determined using Pierce BCA Protein Assay Kit (Thermo Scientific, Waltham, MA, USA). 30 µg of protein was further processed further by reduction with 5 mM tris-2-carboxyethyl phosphine for 30 min at 37°C, alkylated with 10 mM iodoacetamide for 45 min at room temperature, followed by overnight trypsin digestion at 37°C. Digestion was stopped by addition of formic acid (FA) to a pH < 3. Samples were desalted using C18 reversed-phase spin columns (Harvard Apparatus, Holliston, MA, USA) according to manufacturer's instructions. After desalting, samples were resuspended in 2% acetonitrile (ACN), 0.1% FA and the peptide concentrations were determined using a NanoDrop 2000c Spectrophotometer (Thermo Scientific).

Liquid chromatography (LC)–mass spectrometry (MS)/MS analysis
The LC MS/MS analysis was performed on Tribrid mass spectrometer Orbitrap Fusion equipped with a Nanospray source and coupled with an EASY-nLC 1000 ultrahigh pressure liquid chromatography (UHPLC) pump (ThermoFisher Scientific, San Jose, CA). One microgram of peptides was loaded and concentrated on an Acclaim PepMap 100 C18 precolumn (75 µm x 2 cm, ThermoFisher Scientific, Waltham, MA) and then separated on an Acclaim PepMap RSLC column (75 µm x 25 cm, nanoViper, C18, 2 µm, 100 Å) with the column temperature of 45°C. Peptides were eluted by a nonlinear 2h gradient at the flow rate of 300 nL/min from 2% solvent B (0.1% FA/ACN, Merck)/98% Solvent A (0.1% FA in water, Merck) to 40% solvent B. The Orbitrap Fusion was operated in the positive data-dependent acquisition (DDA) mode. Full MS survey scans from m/z 375-1500 with a resolution 120,000 were performed in the Orbitrap detector. The automatic gain control (AGC) target was set to 4 × 105 with an injection time of 50 ms. The most intense ions (up to 20) with charge states 2-7 from the full MS scan were selected for fragmentation. MS2 precursors were isolated with a quadrupole mass filter set to a width of 1.2 m/z. Precursors were fragmented by Higher Energy Collision Dissociation (HCD) and detected in Orbitrap detectors with a resolution of 30,000. The normalized collision energy (NCE) in HCD cells was set at 30%. The values for the AGC target and injection time were 5 × 104 and 54 ms, respectively. The duration of dynamic exclusion was set 45 s and the mass tolerance window 10 ppm.

SILAC Data analysis
Analysis of raw files was performed with MaxQuant (version 1.6.17.0). The resulting peak lists were searched in Andromeda against a reviewed human UniProtKB database (release 2021_02), complemented with the standard MaxQuant contaminant database. Enzyme specificity was set to trypsin/P with a maximum of two missed cleavages. Precursor mass

tolerance was set to 4.5 ppm and fragment ion mass tolerance to 20 ppm. Carbamidomethylation of cysteine was used as fixed modification and deamidation (Asparagine and Glutamine), oxidation (Methionine), hydroxyproline and acetylation were considered as variable modifications. The false discovery rate (FDR) was set to 0.01 for both peptides and proteins. The "match between runs" option was enabled with default settings to match identifications across samples. The mass spectrometry proteomics data have been deposited to the ProteomeXchange Consortium via the PRIDE partner repository[23].

RNA extraction, cDNA synthesis and RT-qPCR

Total RNA was collected after removal of the culture medium by adding 700µL of QIAzol lysis reagent (Qiagen) to a 24 well containing organoids (two 25µL BME domes). RNA was isolated using the miRNeasy kit (Qiagen) according to the manufacturer's protocol[24] and the concentration was measured using a NANOdrop 2000 (ThermoFisher). cDNA from 500ng RNA was prepared using 5x PrimeScript RT Master Mix in a 2720 thermal cycler (Applied Biosystems). RT-qPCRs were conducted on an Applied Biosystems StepONE Plus Real-Time PCR machine (Applied Biosystems), according to the manufacturer's guidelines, with 45 cycles of amplification. Reactions consist of 10 µL SYBR™ Green PCR Master Mix (Thermofisher Scientific), 1 µL of primers (Applied Biosystems/Life Technologies), 4 µL sterile milliQ water, and 5 µL of diluted cDNA. Threshold levels were manually set at 0.25 for all miRNA assays, and the upper Cq limit for reliable detection was set at 35 cycles. RT-qPCR was performed with the primer sets provided in Table S3. All RT-qPCR data are presented as mean with a 95% confidence interval. RT-qPCR values are relative to the housekeeping gene Hypoxanthine-guanine-fosforibosyl-transferase *(HPRT)* or Glyceraldehyde 3-phosphate dehydrogenase *(GAPDH)*.

(Trans)differentiation to hepatocytes

BRCOs and matching ICOs (from the same patient, n=3 individual patients) were differentiated to hepatocytes. The hepatocyte differentiation protocol used was adapted from Huch *et al.* with slight modifications (Clevers *et al.* patent: WO2017149025A1)[25], as published by Verstegen *et al.*[11] Medium consisted of 5 days of EM supplemented with BMP7 (Peprotech, 25 ng/mL) for ICOs and 5 days of non-canonical WNT stimulating conditions supplemented with BMP7 (25 ng/mL) for BRCOs. Then, the cultures were passaged and medium was changed to the differentiation medium (DM): AdvDMEM/F12 medium supplemented with 1% N2 and 1% B27 and containing EGF (50 ng/mL), gastrin (10 nM), HGF (25 ng/mL), FGF10 (100 ng/mL), A83-01 (5 µM), DAPT (10 µM), BMP7 (25 ng/mL), iCRT3 (Sigma, 25µM, iWP2 (Sanbio, 3 µM), Carbachol (Sigma, 100µM), CHIR99021 (Sigma, 3µM), and dexamethasone (30 µM). Differentiation medium was changed every 3-4 days and the total differentiation protocol took 14 days (including pre-treatment with BMP7). Differentiation was accessed by gene expression analysis of genes associated with

hepatocyte maturation (Albumin –*ALB*-, *HNF4α*, *MRP2* and alpha-1-anti trypsin –*SERPINA1*-) and stemness/WNT-target gene (*LGR5*) by RT-qPCR, and ELISA for A1AT (AssayMax™ Human alpha-1-Antitrypsin kit, AssayPro) and Albumin. A1AT ELISA was performed on supernatant of the organoids (n=3, all conditions) according to the manufacturer's instructions. The assay was performed in duplo, and the readout was done on a microplate reader at a wavelength of 450 nm (CytoFluor series 4000, Applied Biosystems). Furthermore, hepatocyte function was assessed using a human albumin ELISA as previously described (Bethyl laboratories, Montgomery, TX, USA).[26] First, plates were coated with a Human Albumin antibody (ThermoFisher, A80-229A 1:200) and incubated for 1 hour at room temperature, afterwards plates were washed. Subsequently, blocking was performed using 1% BSA-PBS for 30 minutes and samples were incubated for 1 hour at room temperature. Reaction was detected by adding a detection antibody (ThermoFisher, A80-129P, 1:10000) for 1 hour at room temperature and plates were washed extensively afterwards. TMB substrate (ThermoFisher) was added and after turning blue the reaction was halted by stopping buffer (1M Sulfuric Acid, Sigma) addition. All measurements were performed in duplo and human serum (Bethyl, 1:200 diluted) was taken along as a positive control. Readout was performed on a microplate reader at a wavelength of 450 nm (CytoFluor series 4000, Applied Biosystems).

Gamma-Glutamyltransferase (GGT) functionality

Supernatant (10µL) of BRCOs (n=3) and ICOs (n=3) was collected. Activity was determined using a colorimetric assay kit (MAK089; Sigma-Aldrich), freshly made medium was taken along as a negative control. The equivalent serum GGT activity in IU/L was calculated following the manufacturer's instructions by multiplying the average increase in absorbance over 30 minutes.

Alkaline Phosphatase functionality

ALP staining was carried out on BRCOs and ICOs (both, n=3) using the 5-bromo-4-chloro-3-indolyl-phosphate/nitro blue tetrazolium (BCIP/NBT, Promega) color development substrate. 5 mL of WE were mixed with 33µl of NBT and subsequently with 16.5µl of BCIP. 500µL of substrate mix was added to each well (24 well plate) and readout was performed after 30 minutes.

Rhodamine-123 transport functionality

Functionality of the Multi Drug Resistance (MDR)-1 transporter was assessed using the Rhodamine-123 assay.[10] Specificity was determined by blocking MDR-1 transporter with Verapamil (10 µM, Sigma Aldrich) for 30 min at 37˚C prior to Rhodamine-123 incubation (100 µM, Sigma Aldrich). Subsequently nuclei were counterstained by Hoechst 33342 (Sigma) and confocal images were acquired using a Leica SP5 confocal microscope (LEICA) equipped with a 405 and 488 nm laser.

Secretin, somatostatin and cholangiocyte ion-channel functionality

To assess functionality of secretin and somatostatin, a slight modification of the Forskolin-Induced Swelling (FIS) assay as developed by Dekkers *et al.*[27] for testing cystic fibrosis transmembrane conductance regulator (CFTR) was applied. For this, BRCOs and ICOs were incubated for 30 min with 3 µM calcein-green (Sigma), stimulated with secretin (10 µM) or secretin and somatostatin (100 µM) and analyzed by confocal live cell microscopy at 37˚C for 120 min (LSM710, Zeiss). The total or single organoid area (XY plane) increase relative to t=0 of secretin treatment was quantified using velocity imaging software (Improvision) and compared to non-stimulated controls. Cell debris and unviable structures were manually excluded from image analysis. To further confirm CFTR-functionality we performed an ussing chamber assay as previously published.[28] BRCOs were seeded on a transwell culture plate (24 well plate 6.5mm, Corning) to grow them in a 2D fashion. Prior to seeding of the cells, transwell inserts were coated with 5% matrigel (Corning) in PBS for 2 hours. Fully expanded domes of organoids were collected in WE and centrifuged (453*g*, 5 min, 4˚C). After removal of the supernatant, organoids were mechanically broken by vigorously up and down pipetting. The organoid suspension was spun down again and the cell pellet was made single cell by digestion in Trypsin-EDTA (TE) for 25 to 40 min at 37°C. Cells were washed in WE and sieved through a cell 70 µm cell strainer. Approximately $3x10^5$ cells were suspended in 200 µL WE with components medium and seeded on transwell inserts. Medium was changed every 3-4 days. To check confluence, the cells were examined by daily microscopy and electrophysiological analysis was performed after 4 days. Upon forming a confluent monolayer, transwells were placed in an Ussing chamber (Physiologic instruments) set up to analyze functional cholangiocyte-specific transporter channels (CFTR and Ca^{2+}- activated Cl^- channel) using Acquire & Analyze Software 2.3 (Physiologic Instruments, San Diego, California). The temperature of the chambers was kept at 37°C by warm water bath circulation and chambers were gassed with 95%O_2, 5%CO_2. Each chamber consisted of 3mL modified Meyler solution (128 mmol/liter NaCl, 4.7 mmol/liter KCl, 1.3 mmol/liter $CaCl_2$, 1.0 mmol/liter $MgCl_2$, 0.3 mmol/liter Na_2HPO_4, 0.4 mmol/liter NaH_2PO_4, 20 mmol/liter $NaHCO_3$, 10 mmol/liter HEPES, supplemented with glucose (10 mmol/liter) at pH 7.3). Current was clamped and every second short circuit current (Isc) was recorded. CFTR-dependent anion secretion was activated by adding Forskolin (3µL, 10mM) to both sides of the cells, and GlyH-101 (3µL, 20mM, apical). Calcium (Ca^{2+}) activated chloride (Cl-) channels (CaCC) were stimulated by UTP (3µL, 50mM, apical) and inhibited by T16Ainhibitor-A01 (3µL, 50mM, apical). The Isc measurements are presented as µA/cm^2. Data was visualized using Excel (Microsoft).

Cell proliferation assessment

Cell proliferation was determined using 5-Ethynyl-2'-deoxyuridine (EdU)-incorporation (ThermoFisher), performed according to the manufacturer's protocol. In short: EdU (10µM) was added to the medium and incubated for 4 hours at 37˚C degrees. BRCOs, ICOs, CCAOs and BRCCAOs were dissociated into single cell suspension via Trypsin-EDTA and suspended in 200µL of 1%BSA-PBS to be analyzed by flow cytometry according to protocol (Canto flow cytometer, BD Biosciences). The gating strategy was performed as previously published.[29] In short gating was based on forward scatter (FSC) and sideward scatter (SSC). Doublets were gated out via a single cell gate (height vs. width). EdU positivity gate was based on the background expression of FITC in organoids without EdU incorporation. Subset analysis was done using Flowjo (version v10.6.1, BD) analysis software. To determine the location of the proliferative cells in BRCOs and CCAOs, EdU incorporation was performed on fixated cells (as previously described for IF staining) by adding EdU (10µM) to the medium. Next click-it labeling was performed according to the manufacturer's instructions. Subsequently nuclei were counterstained by DAPI and confocal images were acquired using the Opera Phenix system (PerkinElmer).

Preparation of single-cell suspensions and FACS

Organoids (ICO and BRCO lines 6, 7 and 10) were incubated with Calcein for 45 min at 37^{o}C before dissociation for live staining of the cells. To get single cells, organoids were then dissociated and digested by 0.05% Trypsin-EDTA following the online protocol.[30] Single-cells were obtained using the flow cytometer FACS Aria (BD Biosciences) equipped with a 130 µm nozzle. Only GFP positive cells (living cells) were sorted into 384-well plates containing a unique CEL-seq primer and 5 µL mineral oil (Sigma, M5310) per well. Plates were stored at -80 ^{o}C until they were processed.

Single-cell RNA library preparation

Single-cell RNA libraries were prepared according to the mCEL-seq2 protocol.[31] Briefly, plates were thawed on ice, and then 100 nL lysis buffer (0.2% Triton X-100, 2mM dNTPs, 1:50.000 ERCC ExFold RNA spike-in (Thermo, 4456739)) was dispensed per well using the Nanodrop Ns-2 Stage (BioNex). SuperScript™ II Reverse Transcriptase (Invitrogen, 18064-14) was used in reverse transcription reaction mix following the protocol, 4 ^{o}C for 5 min; 25 ^{o}C for 10 min; 42 ^{o}C for 60 min; 70 ^{o}C for 10 min. 960 nL second-strand reaction mix containing *E. coli* DNA ligase (NEB, M0205L), *E. coli* DNA polymerase I (NEB, M0209L) and Random hexamer (sigma, 11034731001) were used per well for second-strand synthesis with the following protocol, 16°C for 2 hours. Next, cDNA from one 384-well plate was pooled, and *in vitro* transcription was performed using the MEGAscript™ T7 Transcription Kit (Invitrogen, AMB 1334-5) by incubating the reaction at 37°C for 14 hours. Afterwards, the amplified RNA was fragmented and cDNA was converted using Superscript II and the random octamer primer. Libraries were

amplified for 9 cycles using Phusion® High-Fidelity PCR Master Mix (NEB, M0531S) with the Nextflex primers, and quantified on the bio-analyzer using DNA high-sensitivity kit. Barcoded libraries were sequenced on an Illumina NextSeq 500 with 42+38bp paired-end reads at a depth of 24.2-32 million reads per plate.

Single-cell RNA-seq data analysis

Left read of paired-end reads contains the barcode information with 1-8bp to be the unique molecular identifier (UMI), 9-16bp to be the cell barcodes followed by polyT stretch. Barcode information from left reads were first extracted and added to the corresponding right reads using extract function from UMI-tools 1.0.0.[32] Right reads of read pairs were aligned to an artificial human genome (hg38) containing sequences of 92 ERCC spike-ins using STAR-2.7.0f[33] with default settings. Aligned reads were assigned to genes using featureCount 1.6.4[34] with the following parameter, -g gene_id. For each cell, the number of UMIs per gene was counted and the gene-cell matrixes were generated using count function from UMI-tools 1.0.0 with the following settings, --per-gene, --per-cell. For the downstream analysis, gene-cell matrixes were merged per donor and imported into R. Seurat 3.0[35] was used for data filtering, normalization, scaling, clustering, marker identification and visualization following the standard process. Briefly, Seurat objects were generated from the combined gene-cell matrixes per donor and cells that are not with the following criteria (1000< UMIs < 25000, mt%<50%) were filtered out. Then, UMIs were log normalized, and number of total UMIs and mitochondrial gene expression were regressed out during the data scaling. Seurat objects of different donors were integrated using the functions FindIntegrationAnchors and IntegrateData from Seurat to minimize the biological effects. Pathway analysis was performed using Enrichr web tool[36] with the significantly differentially expressed genes as input. In addition, the previous published datasets by both Sampaziotis *et al.*[37] (ArrayExpress: E-MTAB-8495) and Aizarani *et al*.[13] (GEO accession number: GSE124395) were integrated within our own dataset using Seurat integration[35] and analyzed as previously described.

Organoid clearing and imaging

Small blocks of agarose were fixed and stained using DAPI (Vectashield). After staining, organoids were optically cleared using a previously established protocol.[38] Organoids in agarose were firstly put in 50% PBS and 50% methanol for 30 minutes. Subsequently, they were put in 100% methanol overnight and treated with 50% 1:2 benzyl alcohol/benzyl benzoate (BABB) and 50% methanol for 30 minutes. Finally, clearing was completed by putting the organoids in 100% BABB and storing them at 4°C until imaging. For imaging, organoids are placed in a 24 well glass bottom imaging plate (SensoPlate™ 24 well, Greiner Bio-One). Complete organoids were imaged in 3D using the Opera Phenix HCS system (Perkin Elmer) in confocal modus (spinning disk) equipped with two sCMOS cameras. After a pre-scan (5x objective) to select the area of interest, the organoids were imaged with a 20x air

objective (NA 0.4, field of view is 421394 μm^2). Nuclear DAPI was excited with a 405 nm solid state laser and detected using a 435-480 band pass filter. The large Z-stacks with a step-size of 3.6 µm (optimal for these optics), ranging from below to above the organoid of interest was tiled to cover the predetermined area of interest. Individual images were exported as TIFF files and subsequently reconstructed.

Segmentation of the ductal network

The ductal networks of (n=3) BRCOs were reconstructed manually using a purpose-built graphical user interface (GUI) (implemented in MATLAB R2020a, The MathWorks, Inc., Natick, Massachusetts, USA). This GUI allowed us to locate and mark the lumen of ducts as well as bifurcation events in medium sized organoids, resulting in a three-dimensional reconstruction of the ductal networks (see Figures 5C and S5D-E). In general, when working with *in vivo* or *ex vivo* tissues, it is easy to recognize the main duct of a branching tissue, this corresponds to the duct that connects the whole tree to the exterior of the organ, as is the case of the common bile duct in the biliary tree. The main duct represents the root of a branching tree and can be used as a reference to extract its structural and topological features. A challenge of working with *in vitro* cultures, such as BRCOs, was that there is no notion of a main duct that could be used as the root. We could, nevertheless, define the root as the initial duct, from which the whole tree nucleated. Unfortunately, it was impractical to track this location from when the organoids were seeded to when they were imaged, thus the root location was inferred from the data. As organoids were cultured in 3D conditions and grew in a uniform and isotropic fashion, we defined the location of the root around the geometric center of the organoids (see blue marker in Figs. 5D and S5D). The statistical properties of the branching trees were observed to vary slightly with different choices of the location of the root around the geometric center of the BRCOs (data not shown).

Construction of the branching tree

To analyze the structure and topology of branching trees we focused on the sequence of branching and termination events within the tree. For this, we reduced the ductal reconstruction to an effective tree network, where nodes in the tree represent either branching events (nodes with degree 3) or end-points (nodes with degree 1, see Figs. 5H). The node degree corresponds to the number of edges (ducts) that span from a given node.

End-to-end-point distance distribution

The distribution of distances between all nodes in a complex network relates to the network spectrum, and provides a topological measure that is independent of the existence of a root node. Inspired by this, we measured the distribution of distances between every pair of end-nodes in the ductal tree. This distance was measured in units of tree levels, i.e. the distance measures the number of ducts that separate both end-points.

Termination probability

A branching tree can be characterized by hanging it from its root (see Reconstruction of branching network, and Figs. 5G and S5E). After defining the root as level zero (level i=0), every branching node and end-node can be identified by its level (or distance) from the root node. To measure the termination probability (q_i) as a function of the level (i) we then measured, for every level, the fraction of the total number of nodes in that level that correspond to end-nodes (nodes of degree 1) (Figure 5I). A value of $q_i<1/2$ indicates a net expansion of the tree, as bifurcations are more likely than end-points. On the contrary $q_i>1/2$ amounts to a contraction of the tree, with a larger proportion of end-nodes, while $q_i=1/2$defines a critical regime, where branching and termination events are balanced. It was previously observed that a stochastic branching and terminating dynamics of tip-drive growth self-organizes, in the long term into a balanced regime (qi=1/2), where active tips form a propagating front at the periphery of the expanding tissue.[39] Thus, the existence of a plateau around qi=1/2, is a good indication of an underlying stochastic dynamics of growth (see Figure 5I).

Subtree size and persistence

A subtree was defined as a subset of the whole tree that has a sub-root (or common ancestor) at a level greater than zero (i>0). To measure the subtree size and persistence we considered only subtrees whose common ancestor lied in generation i=4 (see example in Figure 5G). The subtree size corresponded to the total number of ducts in a given subtree, while the subtree persistence measured the number of levels spanned by the subtree. This choice for the pruning generation (i=4) was arbitrary, but kept fixed when analyzing both experimental networks and numerical simulations, in order to make their results comparable.

Projected area and circularity

For BRCCAOs, reconstruction of the full ductal network was infeasible due to the lack of a well-defined internal ductal structure. To compare BRCCAOs to BRCOs and also to the model proposed, we quantified their 2D-projected area and circularity. This was done by analyzing bright field images of BRCCAOs (n=21) and BRCOs (n=24) after 7-8 days of culture. The outline of the organoids was traced manually, and their total area (*A*) and perimeter (*P*) measured (see Figure 7E). It is worth noting that because organoids tend to grow radially in every direction, the projected area may be used to estimate their volume. To assess the organoid morphology, we measured the circularity of their projected area, defined as the ratio $4\pi A/P^2$ (see Figure 7E). This measure, sometimes referred to as compactness, is independent of the sizes of the organoids, and takes a maximum value of 1 when the object is a perfect circle, and approaches zero as the outline of the objects get rougher. Organoids with lower values of circularity are characterized by having more and longer ductal outgrowths, while organoids with circularity closer to 1 have a more compact, spheroidal shape.

Model of branching and termination dynamics

To model the growth dynamics of branching organoids, we use a variation of Branching and Annihilating Random Walk (BARW) model previously proposed to describe the process of branching morphogenesis in the mammary gland and kidney.[39] Active tips are modeled as particles that perform a persistent random walk, leaving a trail along the traversed path corresponding to the ductal structure of the network. Active tips are subject to Possonian branching events, i.e. branching occurs at a constant rate such that the timing between consecutive branching events is uncorrelated and follows an exponential distribution. As the time between consecutive branching events is directly proportional to the length of the ducts, this model also predicts an exponential distribution of duct lengths. However, experimental observation showed that short ducts were less abundant than expected from a purely exponential distribution (see Figure 5E), suggesting the existence of a short-term memory in the branching dynamics that prevents a tip from undergoing two consecutive rounds of branching in a very short period of time. This was accounted for in the model by introducing a refractory period τmeasured from the time of the last branching event which prevented a tip from undergoing another round of branching before the refractory period had elapsed. A Poisson branching process with a refractory time is known as a *renewal process*, where for a single tip, the time between events (waiting times, Δt) follows

$$p_\tau(\Delta t) = \Theta(\Delta t - \tau) s e^{-s(\Delta t - \tau)}$$

where s is the branching rate, and $\tau$the refractory period. The step-function $\Theta(x)$ is zero for $x < 0$,and one for $x \geq 0$,and ensures that tips do not branch during the refractory period. For this renewal process, the mean time between branching events in given tip is $< \Delta t >= \tau + 1/s$.

A comparison between the empirical and predicted distribution of duct lengths revealed an overabundance of long duct in BRCOs (Figs. 5E and S5F). These long ducts were mostly located in the periphery of organoids and seemed to have a decreased branching frequency. Based on experimental observations we considered two types of tip interactions: a termination mechanism, by which a tip may arrest its growth when coming within the inhibition radius (R_a) of another particle, and a second longer-ranged mechanism by which a tip is repelled from existing tips and/or ducts. As the organoids are grown in free 3D space, we run our numerical simulations considering an infinite system size. Simulations were terminated either when all tips became inactive, or when the predefined maximum simulation time was reached. As in *vitro* branching organoids do not have a defined directionality of growth, we initialize our simulations with a Y-shaped rudimentary tree that could elongate and branch from all three ends, with all branches lying in the same plane and separated by an angle $\pi/3$ between them. The root node was defined as the intersection

point of all three branches. This choice of initial state was implemented in order to mimic the initial state of experimental BRCOs.

Numerical simulations of the BARW model

Simulations of the BARW were performed by implementing a Gillespie (stochastic) algorithm, where active tips branch with a rate $s = \sigma$ and elongate with rate $r = 1$. Tip termination was implemented by introduction of an inhibition radius R_a. Tip termination occured when a tip got within the inhibition radius of another particle (tip or duct). Based on the observations that tips elongated freely as long as the don't collided with other ducts, and to prevent tips from terminating due to the presence of their own duct, tips only sensed other particles that lie in the half-space in front of them, considering the front as their direction of motion. In the three-dimensional simulation, given the position $r_1 = (x_1, y_2, z_3)$ of an active tip elongating in a direction defined by the polar and azimuthal angles (θ, ϕ) in spherical coordinates, an elongation event implied a translation of the active tip from position $r_1$to position

$$r_2 = r_1 + (Lsin(\theta')cos(\phi'), Lsin(\theta')sin(\phi'), Lcos(\theta')),$$

where the step length was fixed to unity, $L = 1$. The direction (θ', ϕ') related to the orientation of the parent particle (θ, ϕ) by

$$(\theta', \phi') = (\theta, \phi) + \delta\theta(Arcos(1 - 2u_1) - \pi/2, u_2),$$

where the second term on the right-hand side corresponds to a random noise distributed uniformly on a 2D sphere, with$u_1 \in U([0,1[)$ and $u_2 \in U([-\pi, \pi])$, and$\delta\theta \in [0,1]$ is the noise intensity. When $\delta\theta = 0$, there is no noise in the system and ducts grow following a perfect straight line, with infinite persistence. For positive values of $\delta\theta$, ducts deviate from a strait line as they grow, with $\delta\theta = 1$corresponding to a random walk. A self-avoidance mechanism was introduced as described by Hannezo *et al*.[39] This implementation considers that a tip in position $r_i$could sense a repulsive force from all other r_j particles within a repulsion radius R_a, i.e. $|r_i - r_j| \leq R_a$. Additionally, we considered that the affected tip could only sense those particles in the half-space in front of it, as described for the inhibition process. Considering direction of the center of mass of all repelling particles with respect to the location of the tipr_i

$$p_i = \frac{\sum_j \ (r_i - r_j)}{\left|\sum_j \ (r_i - r_j)\right|},$$

then the active tip suffered, at each elongation event, an additional displacement opposite to the direction of the repelling particles of the form $-f_r r_i$, where $f_r$corresponded to the strength of the repulsive force. During a branching event two new branches were generated

forming and angle α between them. The locations of the new branches were defined as described by Hannezo *et al.*[39]. The parent duct and the two daughter branches were considered coplanar, and the angle of rotation of the two daughter branches with respect to the plane perpendicular to the parent duct was chosen randomly from a uniform distribution. A refractory period $\tau$was also introduced, such that if a given tip underwent a branching event at time t, the same tip could only branch again after time $t + \tau$ has been reached. This refractory time was independent for each active tip, and accounted for a maturation period before a tip can branch again.

Estimating model parameter from BRCO data

In three-dimension, the BARW has two key parameters that must be defined, the branching-to-elongation rate ratio σ, which measures how often a tip branches in relation to its elongation, and the inhibition radius R_a. From live imaging of growing organoids (Video S4), we estimated the duct elongation speed to be on the order of $5\ \mu m/h$. From this, and the average duct length between two bifurcation events, the value for σ was estimated $\sigma = 0.023 \pm 0.005$ (SD) between the (n=3) BRCO samples. Through fitting, we found that the lower bound $\sigma = 0.018$ achieved the best results. It is worth noting that the elongation rate of $5\ \mu m/h$ is an approximated measure that may have contribution both from tip elongation and tissue reorganisation in BRCOs. The inhibition radius was set to$R_a = 100\ \mu m$, which was estimated from the typical size of a growing tip.

From the above we could equate the simulation step size $L$to $5\ \mu m$, and a unit of simulation time to $1\ h$. As organoids were cultured for approximately 7-8 days, we set the maximum simulation time to 8 days (192 hours). The refractory period was adjusted by exploring a range of parameter values between 0 to 10 hours, and we found that a value of $\tau = 5\ h$ gave good qualitative agreement with the data. The repulsion radius R_r was set to $R_r = 1.2R_a = 120\ \mu m$, with a repulsive strength of $f_r = 0.2$. These parameters were adjusted to provide qualitative agreement with experimental observations of tip-tip repulsion (see Video S4), yet the quantitative measures depended weakly on small variations to f_r.

Unfortunately, the clearing and preparation of BRCOs for imaging removed their structural support, and in consequence, BRCOs appear as flattened objects in confocal images. The clearing evidently perturbed the location and straight nature of their ducts. For instance, measuring the relative deviation $(L_d - l_d)/l_d$, of the true ducts' length L_d from the straight distance between branch points l_d, gave a value of 0.5 when measured from cleared BRCOs, indicating a large tortuosity of BRCO ducts. However, this was not compatible with bright field and live imaging observations that showed a remarkable persistence in the ductal elongation process. We found that for BRCOs, a noise amplitude $\delta\theta = 0.03$ gave good qualitative agreement with observations. Small variations of this parameter did not affect the quantitative measurements of organoid morphology or topology. A similar issue arises when attempting to measure the typical angle between offspring branches (see Figure S5I), which

revealed a typical value of $95°$, but and extremely large variation ($SD = 50°$), likely as a consequence of the clearing process. In the numerical simulations we considered that the angle α between offspring branches was uniformly distributed, $\alpha \in U([80°, 110°])$. Quantitative measurements showed little sensitivity to changes in the distribution of values of α.

Model parameter for simulation or BRCCAOs

As BRCAAOs lacked a well-defined branching network, it was impossible to reconstruct its ductal structure and estimate parameters for this system. Instead, we hypothesized how the different model parameters could have been affected based on empirical observation. Bright field and confocal images revealed that BRCCAOs have a particularly compact structure, unlike in BRCOs where ducts are dispersed. This dense nature of BRCCAOs, as indicated by a smaller size of BRCCAOs compared to BRCOs after 7-8 days of culture (Figure 7E), was an indication that the tip-duct and tip-tip interaction mechanisms might be compromised. To account for this in model, we considered the extreme case were both the inhibition $(R_a)$and repulsion (R_r) radii are zero, eliminating tip-tip and tip-duct interaction altogether. Moreover, the dense organization of BRCCAOs was also reflected on the morphology of their boundary. These organoids were characterized by having a well-defined boundary, without long duct protruding outwards (as was the case in BRCOs), which was quantified by measuring the organoid circularity (Figure 7E). From the perspective of the BARW model, this implies that BRCCAOs have a reduced capacity to form elongated, persistent ducts, which may be accounted for in the model by increasing the noise amplitude, which we set to $\delta\theta = 0.1$.

Goodness of fit

Comparison between the distributions of duct lengths, subtree sizes and persistence, end-to-end node distances, and termination probability were done using a goodness of fit statistic R^2. Given a set of $n$of experimental measurement $(x_1, x_2, \ldots, x_n)$,whose average value is given by $\underline{x}$, and a corresponding set of theoretical predictions $(y_1, y_2, \ldots, y_n)$, then

$$R^2 = 1 - \frac{\sum_{i=1}^{n} (x_i - y_i)^2}{\sum_{i=1}^{n} (x_i - \underline{x})^2},$$

which takes values in [0,1]. A value of $R^2 = 1$, if the prediction fits the data perfectly.

DAPT, BMS493 and Chimeric Jagged 1 assay

Effect of inhibiting the retinoic acid receptor on BRCOs was evaluated by adding BMS493 (1µM, Sigma) for 120 hours to the culture medium of BRCOs.[34] Additionally, the effect of inhibiting the NOTCH receptor on branching was assessed by incubating BRCOs with DAPT (50 µM) for ten days. Normal BRCOs and BRCOs exposed to vehicle control (DMSO) were taken along as a control. Similarly, in a dose dependent (50ng/mL; 80ng/mL; 100ng/mL;

200ng/mL and 500ng/mL) testing manner recombinant Human Jagged 1 Fc Chimera (Biotechne; RZL2220041) was added to the culture conditions of the ICOs derived from the Alagille Syndrome patient to improve branching in these organoids. To evaluate branching morphogenesis over time, the process was captured by transmission microscopy (EVOS® FL Cell Imaging System, ThermoFisher) for all medium additions.

Western Blot assay

For western blotting samples from ICOs (n=3) and ICOs from the (corrected) Alagille patient were obtained. The organoids were lysed with house made 2x Laemmli Sample Buffer (Bio-Rad, 161-0737) supplemented with 1,4-Dithithreitol (DTT; 0.1M) for 5 minutes at 95°C. Protein concentrations were evaluated with the bicinchoninic acid (BCA) protein assay (ThemoFisher Scientific; 23227) according to the manufacturer's protocol. Protein samples migrated through a sulfate polyacrylamide gel (7%) in running buffer for 105 minutes at 100 V and were blotted to a polyvinlylideenfluoride membrane (Merck Chemicals BV; IPFL85R) using blotting buffer for 2 hours at 250 mA. Molecular weight of proteins was determined using precision plus protein dual color standard (Bio-Rad; 1610374) 250 kDa marker. Membranes were blocked with Odyssey blocking buffer (Westburg BV; 927-40000) for 1 hour at room temperature. Subsequently, membranes were incubated overnight at 4°C with a polyclonal antibody to Jagged1 and a monoclonal β-actin antibody. Followed by one hour incubation with secondary antibodies after washing. Immunoblots were scanned by Odyssey 3.0 (Clx) imaging system and analyzed using Image Studio Lite (Version 5.2).

DNA processing and sequencing of JAG1

Two full domes (25 µL) of ICOs derived from an AGS patient were collected by centrifuging in a 15 mL tube for 5 minutes, 4°C at 453 g. DNA was isolated from the obtained pellet using QIAamp Micro DNA kits (Qiagen) according to the manufacturer's protocol. Subsequently, the concentration was measured on a NANOdrop 2000 (ThermoFisher). Using Sanger sequencing (Macrogen) and Multiplex Ligation-dependent Probe Amplification analysis (Probemix P184, version C3; MRC Holland) a large heterozygous deletion was detected. Further sequence of the mutated strand was determined by PCR amplification using GoTaq (Promega Benelux BV; M7805) and Q5 high-fidelity DNA polymerase according to manufacturer's protocol (NEB; M0491), subsequently amplicons were Sanger sequenced until the exact mutation was obtained. The used primers are listed in Table S3.

Bulk RNA-seq of primary tumor and tumor organoids

RNA from CCA primary tissue and CCAOs and BRCCAOs (n=3 biological replicates) was collected in lysis buffer (QIAzol lysis reagent, Qiagen) and the RNA was isolated using the miRNeasy mini kit (Qiagen) as previously described under the subheading RNA-isolation. Bulk RNA-seq was performed by Novogene (Beijing, China) resulting in 20-30 million, 150 nucleotides long, paired-end reads. Sequencing data were uploaded to the Galaxy Web

platform public server usegalaxy.org.[40] Sequences were trimmed for adapters using Trim Galore! (Version 0.4.3.1), and mapped using RNA STAR (version 2.6.8a)[33] against the human reference genome (GRCh38). Mapped reads were translated to counts using FeatureCounts (version 2.0.1)[34] applying the built-in hg38 genome annotation file. CCA primary tissue bulk RNA-seq data from patient CCA1 was retrieved from a previously published manuscript (accession number GSE84073)[20] and incorporated into our dataset. Raw counts were batch corrected using ComBat-seq[41] (available via sva package version 3.36.0) using a negative binomial regression model. Analysis of differential expression was performed using edgeR[42] (version 3.32.1) and Limma86 (version 3.46.0)[43] R packages. Genes were considered differentially expressed when the adjusted p-value was <0.05 (Benjamini Hochberg FDR corrected). Subsequent GSEA on the log2FC values was done using fgsea[44] (version 1.16.0) and gage[45] (version 2.40.1) R packages. To increase specificity, fgsea results were filtered using gage results so that only pathways which are significant and in the same direction in both methods are retained. To assess similarity between tissue and organoid, we filtered total genes to only include DE genes between CCAOs and BRCCAOs. This set of genes was used to create a Pearson's correlation matrix.

In vitro drug assay on (BR)CCAOs

CCAOs (n=3) and matching BRCCAOs (n=3) were dissociated to single cells or small clumps with tripLE (ThermoFisher; 12604013) for 3 x 5 minutes at 37˚C while applying mechanical disruption through pipetting. TrypLE was inactivated by adding cold AdvDMEM/F12, centrifuged for 5 minutes (4˚C at 453 g) and counted for plating out at a concentration of 5000 cells/5 µL BME in 96 well plates (Cellstar). Organoids were cultured for three days. Subsequently, a concentration dilution series of gemcitabine (range 10nM-10µM), cisplatin, or a combination of both compounds was added and cell viability was measured using CellTiter-Glo (Promega) after 72 hours. All experimental conditions were tested in biological and technical triplicate. An experimental concentration range was determined and dose-response curves were fitted using nonlinear least squares regression fitting.

Statistical analyses

presented are expressed as mean ± standard deviation (SD) unless otherwise specified. Data other than sequencing data were analyzed and plotted using Prism Software 8.0 (GraphPad). Biological and technical replicates are specified in the Figure legends for each experiment. In all tests, a P value of <0.05 is considered significant and was determined by two-tailed Student's t test, unless otherwise specified in the Figure legends. When comparing more than two means, significance was assessed by ANOVA tests.

Results

Establishment of branching cholangiocyte organoids

Branching cholangiocyte organoids were established by applying a 'two-stage culture method'. First, intrahepatic cholangiocyte organoids (ICOs, n=20) were initiated from liver biopsies using standard conditions in expansion medium.[7] After three passages, the expansion medium was replaced by the “branching-initiation” medium after which most ICOs morphologically changed to a branching pattern (Figure 1A). BRCOs could be induced from 14/20 (70%) individual ICO lines, cultured from a variety of liver biopsies. (Table S1). No underlying patient characteristics that could possibly compromise branching development, such as donor age, donor type or liver disease, could be identified. As shown in Figure S1A, branching cholangiocyte organoids (BRCOs) could only be established from ICOs and not from extrahepatic cholangiocyte organoids. Interestingly, although the branching morphogenesis is a developmental process, only adult ICOs and not fetal intrahepatic cholangiocyte organoids could develop to BRCO (n=3, Figure S1B, Table S1). Mostly, the BRCO cultures consist of a mix of branching and non-branching (cyst-like) organoids, at variable ratios (Figure S1C). In contrast, once established, BRCOs could be passaged long-term while maintaining the branching architecture (>20 passages), indicating that when BRCOs are formed, they remain their characteristics under external perturbations.

BRCO cells resemble primary cholangiocytes

BRCOs self-organize and continue to grow and expand through the elongation of existing branches and the formation of new branches via bifurcations and trifurcations, giving rise to complex ramified architectures (Figure 1B and online Video S1). We observed morphological variabilities between BRCOs, which might arise from their non-stereotypic branching dynamics and differences in their initial seeding pattern (Figure S1D). When analyzed by electron microscopy, we found that individual cells within BRCOs displayed ultrastructural features of columnar epithelial cells, such as microvilli and tight junctions (Figure 1C, indicated by arrows). Immunofluorescence staining’s for cholangiocyte markers cytokeratin (KRT)19 and 7, showed expression in all cells, highlighting the resemblance of BRCOs to primary cholangiocytes (Figure 1D, Figure S1E and online Video S2). The nuclei are located at the basolateral side of the cells, with the bulk of the cytoplasm being to the lumen, suggesting cell polarization. Mature cholangiocyte markers for secretin receptor (SCTR) and cystic fibrosis transmembrane conductance regulator (CFTR) were expressed at the basolateral or luminal side of the tubes, respectively (Figure S1E). Finally, positive staining for tight-junction marker zonula occludens (ZO-1) was pronounced at the luminal side of the tubes (Figure S1E), and F-actin staining revealed the presence of an open lumen while showing increased activity across the luminal side, likely due to staining of microvilli (Figure 1D, Figure S1E and online Video S3). These cholangiocyte-typic features were similar to the *in vivo* situation.[5]

Interestingly, some cells located at the tips of BRCOs were albumin positive (Figure S1E). Gene expression analyses of BRCOs by qRT-PCR showed expression of typical biliary markers such as *KRT19*, *KRT7*, Hepatocyte nuclear factor-1 beta (*HNF-1β*), Trefoil Factor 1 (*TFF1*) and *TFF2* (Figure 1E).[15] In contrast to ICOs[7], BRCOs highly express classic hepatocyte-related genes such as *SERPINA1* (also known as alpha-1 antitrypsin), Albumin (*ALB*), and *CYP3A4* (Figure 1E), which is also found in primary cholangiocytes[13] and which is in line with the positive albumin staining. In contrast, BRCOs showed limited expression of the shared progenitor/mature cholangiocyte markers *SOX9* and *TROP2*, while the WNT-target gene leucine-rich-repeat-containing G-protein-coupled receptor *(LGR)5* was severely downregulated (P<0.0001), compared to ICOs.[7]

BRCOs recapitulate functional bile ducts in vitro

Bright field and confocal imaging of BRCOs suggested that the BRCO architecture consists of a single open lumen (Figure 1A and D and Figure S1E). This was confirmed by active transport of fluorescent rhodamine-123 into the lumen of BRCOs via multi-drug-receptor-1 (MDR1). Within the lumen, rhodamine-123 could freely diffuse, revealing a network of connected ducts (Figure 2A). Blocking MDR1 transporter by verapamil, completely blocked the transport of rhodamine-123 and caused the fluorescence to reside within the BRCO cells (Figure 2B). *In vivo*, cholangiocytes regulate bile flow and composition by transportation, secretion, and absorption of ions, bile substances, and water.[5] In order to demonstrate the presence of these functions in BRCOs, we first assessed secretin and somatostatin receptor activity. As shown in Figure 2C, upon secretin stimulation BRCOs swell by active ion transport and increased osmolality. Clearly, swollen BRCOs loss their slender tubular structures. Somatostatin significantly inhibited swelling (secretin 1.3±0.03 swelling vs. somatostatin addition 1.15±0.05, p=0.01, Figure 2D). These results demonstrate the functionality of both receptors, as well as the likely presence of functional ion and water transportation via CFTR and aquaporins. Ion channel activity was confirmed in a monolayer of BRCOs using an ussing chamber set up. Forskolin stimulated, and GlyH-101 (CFTR-inhibitor) inhibited short circuit current (Isc), indicating functional CFTR-activity (Figure 2E). Similarly, upon incubation with uridine 5'-triphosphate, an increase of Isc was observed, which was specifically inhibited by T16Ainh-A01, indicating anoctamin-1 (ANO1) activity. Furthermore, activity of important cholangiocyte-related enzymes was tested. Similar to cholangiocytes *in vivo*[46], alkaline phosphatase activity was present and primarily located on the luminal side of the BRCOs (Figure 2F), while gamma-glutamyl transferase (GGT)-activity was also clearly detectable in BRCOs (Figure 2G).

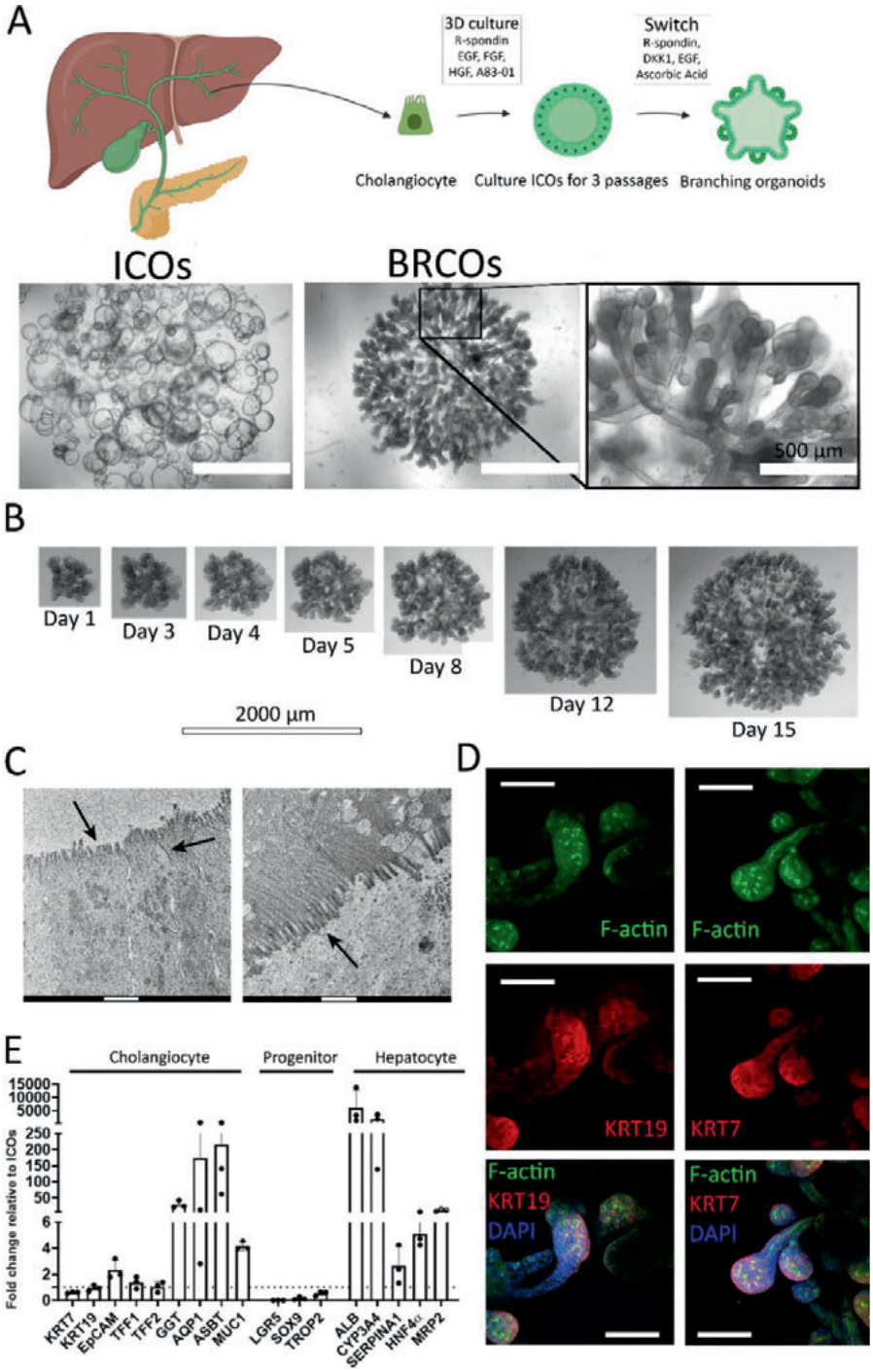
A
3D culture
R-spondin
EGF, FGF,
HGF, A83-01
Switch
R-spondin,
DKK1, EGF,
Ascorbic Acid
Cholangiocyte
Culture ICOs for 3 passages
Branching organoids
ICOs
BRCOs
500 µm
B
Day 1
Day 3
Day 4
Day 5
Day 8
Day 12
Day 15
2000 µm
C
D
F-actin
F-actin
KRT19
KRT7
F-actin
KRT19
DAPI
F-actin
KRT7
DAPI
E
Cholangiocyte
Progenitor
Hepatocyte
Fold change relative to ICOs
15000
10000
5000
250
200
150
100
50
6
4
2
0
KRT7
KRT19
EpCAM
TFF1
TFF2
GGT
AQP1
ASBT
MUC1
LGR5
SOX9
TROP2
ALB
CYP3A4
SERPINA1
HNF4α
MRP2

Figure 1. Establishment and characterization of branching cholangiocyte organoids.
(a) Schematic overview of BRCO culture. Intrahepatic cholangiocytes are obtained from a liver biopsy and cultured as ICOs. After three passages, culture conditions are switched and BRCOs are formed. **(b)** Growth over (two weeks) time of BRCOs. **(c)** Transmission electron microscopy images of single cells of BRCOs, in the left panel arrows indicate microvilli (left) and a tight junction (right). In the right panel the arrow points to microvilli, scale bars indicate 1 µm. **(d)** Whole mount confocal images of BRCOs for cytokeratin (KRT) 19 and KRT7 (both red), F-actin (green) staining, nuclei are counterstained with DAPI (blue), scale bar indicates 100 µm. **(e)** BRCOs bulk gene-expression measured by qRT-PCR for cholangiocyte, progenitor-related/WNT-target genes and hepatocytes markers. Values are displayed as fold change compared to ICOs (n=3). All experiments in Figure 1C-E are with lines 2-4. Panel B is with BRCO line 1.

Finally, to investigate if we could induce hepatocyte-like differentiation within BRCOs, we applied a hepatocyte differentiation protocol.7,11 After 14 days of differentiation, BRCOs lost their tubular structures and acquired a denser, more cyst-like morphology (Figure 2H), as observed previously for ICOs in differentiation conditions.7,8 Expression of hepatocyte markers decreased in BRCOs after differentiation, while the opposite was observed for LGR5 expression (Figure 2I), that increased in BRCOs. When looking at hepatocyte specific synthetic function, clearly protein secretion levels of A1AT and albumin in the culture medium was significantly reduced in BRCOs after hepatic differentiation (Figure 2J). Collectively, these results indicate that BRCOs recapitulate functional properties of intrahepatic bile ducts and although some expression of hepatocyte-related genes was observed in BRCOs, hepatic functionality was limited in both expansion and hepatic differentiation conditions, indicating that likely only biliary cells are present in BRCOs.

Single cell transcriptomic reveals that BRCOs differ from ICOs but are similar to primary cholangiocytes

To further investigate the transcriptomic differences between ICOs and BRCOs at a single cell resolution, as well as to capture the cellular heterogeneity within BRCOs, we performed single-cell RNA sequencing. (scRNAseq) In total, 3456 cells were analyzed using CEL-seq2[31] collected from three matched BRCOs and ICOs cultures established from the same donors (Figure 3A). Using a stringent quality threshold, a similar number of cells (1105 for BRCOs and 1429 for ICOs) were retained, and comparable numbers of genes and UMIs were detected from BRCOs and ICOs (Figure S2A-C). To determine different populations, we performed clustering analysis and applied Uniform Manifold Approximation and Projection (UMAP) for the visualization. Batch correction (see methods) was performed to minimize the biological effects of different donors.

Two main groups of cells separated based on different culture conditions were observed (Figure 3B and online Sup. File 1). Cells from individual donors were evenly distributed across both clusters, suggesting adequate batch correction (Figure S2D). Cluster analysis revealed

seven sub-clusters (Figure 3B) of which clusters 5 and 7 were mainly cells in the G2M and S phases of the cell cycle. ICO cells had high expression of *Ki67*, (83.4% versus 16.6% in BRCOs, Figure S2E). Mature cholangiocytes *in vivo*, are generally quiescent but can proliferate in response to injury or damage.[47-49] Looking at the differences in cell-cycle phases, significantly more G1 cells in BRCOs were found (avg. 75.1%), compared to ICOs (avg. 65.8%; $p<0.05$, Figure S2E). A similar trend was observed in proliferation experiments as demonstrated by EdU incorporation. EdU was incorporated in more cells in ICOs (23.9% ± SD 11.2 EdU^+ cells, n=3), compared to BRCOs (10.6% ± SD 2.1, p=0.11, n=3, Figure S2F), indicating a possible lower proliferating activity in BRCOs. We further explored transcriptomic differences in the non-dividing cell clusters. We identified significantly higher expression of 204 genes in BRCOs and 272 genes ICOs (Figure S3G, Sup. File 2). Pathway analysis demonstrated that genes upregulated in BRCOs are mostly involved in multiple metabolic processes, while genes with more prominent expression in ICOs are enriched in localization of Cajal body pathway, normally found in proliferative cells (Figure S3H). Taken together, these results suggest that BRCOs are less proliferative than ICOs.

Subsequently, we investigated the gene expression of known mature cholangiocyte markers or immature (progenitor) cholangiocytes.[15] Although cells from both organoid types express mature cholangiocyte markers such as *EPCAM*, *CD24*, *SOX9*, *KRT7* and *KRT19*, we observed significantly decreased expression of *SOX9*, *KRT7* and *KRT19* in BRCOs (Figure 3C and 3D). Interestingly, previous data indicates that *KRT19* is upregulated in ICOs when compared to primary cholangiocytes[13]. In contrast, mature cholangiocyte genes *SPP1* and *LYZ* are significantly higher expressed in BRCOs compared to ICOs (Figure 3C and 3D). In addition, the ICO cells express high levels of *MUC5AC* and *MUC5B*, two markers that are normally expressed in intestinal cells and gastrointestinal cancers, but are hardly detectable in BRCO cells (Figure 3C and 3D) or $EPCAM^+$ cells *in vivo*.[13] Furthermore, we noticed higher expression of *SERPINA1*, *ALB* and *CYP2E1* in BRCOs, confirming the observations by qPCR gene expression analysis (Figure 1E). To investigate if BRCOs display transcriptomic profiles that better resemble primary human cholangiocytes *in vivo*, we performed gene set enrichment analysis (GSEA) using a previously published dataset of cholangiocyte organoids and their corresponding tissue.[8] For this, the enrichment of differentially expressed genes between BRCO and ICO was analyzed compared to common bile duct, pancreatic bile duct and gallbladder tissue and their corresponding organoids.[8] We found that BRCO genes were significantly more enriched in gene sets reflecting the primary tissue (Figure 4A). In contrast and as expected, ICO gene enrichment was found only to correspond with organoids and not the biliary epithelium (Figure 4A). In summary, the scRNAseq analysis shows that BRCOs differ from ICOs, and display less proliferative and stem-like features compared to ICOs and, more importantly, better correspond to mature cholangiocytes.

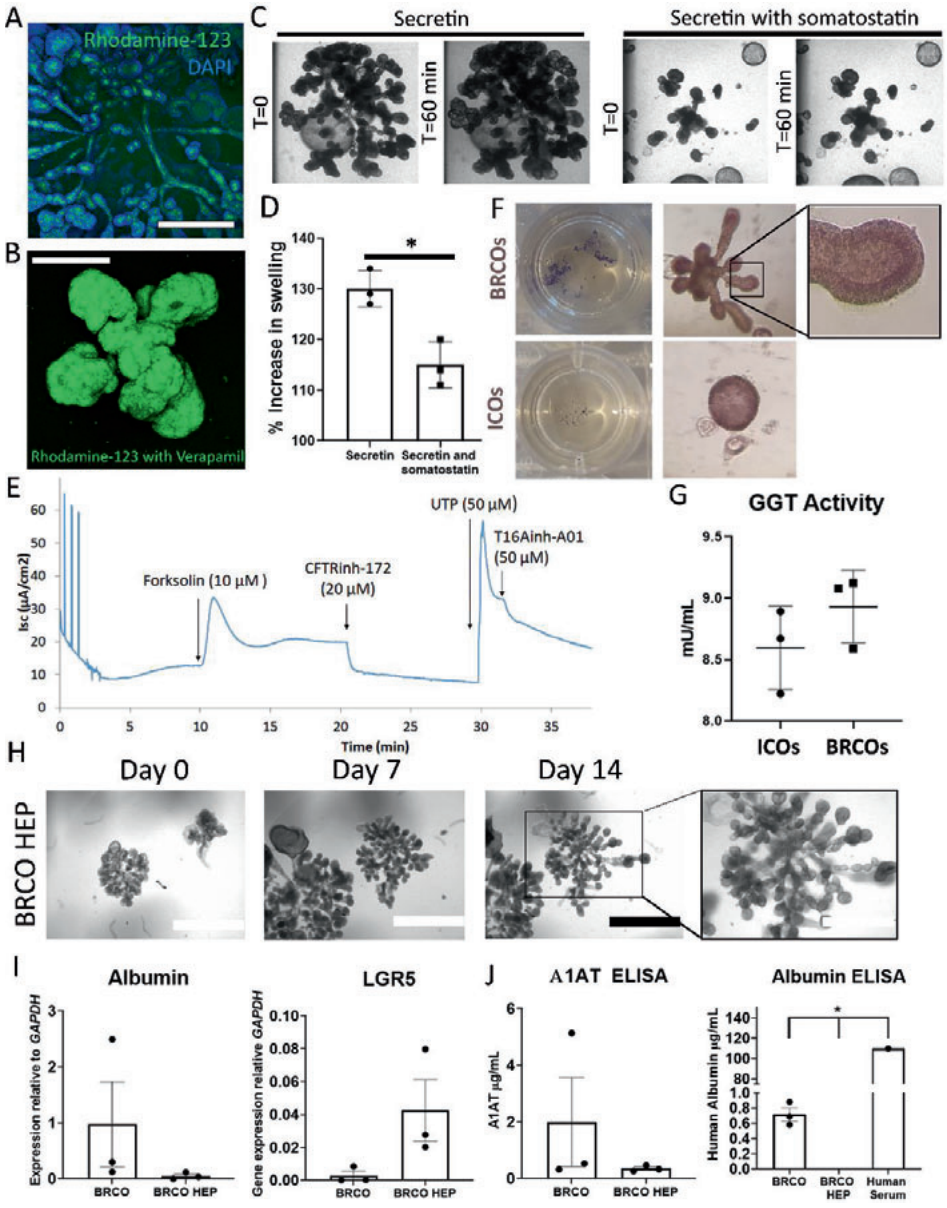

Figure 2. BRCOs resemble functional intrahepatic bile ducts *in vitro.*

(a) Max-projection of whole mount confocal image of rhodamine-123 (green), nuclei are counterstained with DAPI (blue). **(b)** Max-projection of whole mount confocal image of rhodamine-123 (green) after verapamil addition, scare bars in a and b indicate 100 µm. **(c)** BRCOs at T=0 minutes and T=60 minutes stimulated by secretin and secretin with somatostatin pre-treatment. **(d)** Quantification of the swelling assay in c. **(e)** Ussing chamber experiment of 2D grown BRCOs, demonstrating functional

CFTR and ANO-1. **(f)** ALP activity in BRCOs and ICOs. **(g)** GGT activity in BRCOs compared to ICOs. Experiments a-g are performed on biological triplicates ICOs and BRCOs 3, 4 and 6. **(h)** Bright field images of BRCOs cultured in hepatocyte-differentiation conditions, scale bars indicate 1000 µm and upon zoom 200µm. **(i)** qRT-PCR for mRNA of *ALB* and *LGR5* in BRCOs and after hepatocyte-differentiation. **(j)** Human A1AT and Albumin secretion as measured via ELISA BRCOs and after hepatocyte-differentiation. As a positive control, albumin was also detected in a human serum sample (n=1). Experiment i and j are performed on lines 6-8. *indicates significant difference ($p<0.05$).

Proteomics of BRCOs confirms differences with ICOs and similarities with cholangiocytes

To investigate differences in protein production between BRCOs and ICOs, we performed SILAC-based mass spectrometry (Figure S3A). A clear segregation of BRCO and ICO clusters was observed when applying principal component analysis (Figure S3B). We found an overlap of 653 proteins that were produced in all samples, however no differential expression between these proteins was detected (Figure S3C). Therefore, we focused on investigating uniquely produced proteins in the two organoid types. We observed that BRCOs produced far more unique proteins than ICOs (702 vs. 132, Figure S3D and F). Furthermore, we noticed that some genes that were differently expressed in scRNAseq analysis, correspond to the production of 36 unique proteins (Figure S3E and Sup. File 2-3). Finally, we investigated how these proteins correlate to highly expressed proteins present in primary (gallbladder) cholangiocytes according to the human protein atlas.[50] As shown in Figure S3G, the important cholangiocyte channels SLC12A2 and ABCC3, as well as PDL1 and CLDN2, were solely present in BRCOs. In contrast, ICOs produced CCL20, a protein associated with the biliary disease primary sclerosing cholangitis.[51]

Cellular heterogeneity in BRCOs in relation to heterogeneity of primary intrahepatic cholangiocytes

Next, we focused on the transcriptomic heterogeneity within BRCO cells (Figure 4B). Besides cluster 4, which mainly contains cells from G2M and S phases of the cell cycle, we identified 3 sub-clusters in BRCOs, similar to the UMAP analysis (Figure 3B). Recent evidence indicates that there is heterogeneity in epithelial cells along the biliary tracts, with a subset of intrahepatic cholangiocytes expressing hepatocyte-related genes.[13,14] Interestingly, only BRCO cells, in cluster 1, expressed hepatocyte-related genes: *GC*, *PCK1*, *ALB* and *CYP2E1* (Figure 3C and Figure S4C and D). These are likely the cells surrounding the tips of the BRCOs which stained positive for albumin protein (Figure S1E). In addition, we identified expression of cholangiocyte markers *TACSTD2*, *TFF1* and *TFF2* in cluster 2 and 3, which are not present in cluster 1 (Figure 4B). Moreover, in sub-cluster 2 a small group of cells expressing *LGR5* was detected (Figure 4B). To investigate the location of cells from specific clusters within the BRCOs, differentially expressed genes were selected. Of these, *CLDN2* was highly expressed in cluster 1 and 2, and almost absent in cluster 3. Immunostainings revealed the presence of highly expressing *CLDN2* cells in the tips (cluster 1, albumin staining) and along the distal part

of the tubes (cluster 2, Figure S1E), suggesting that cells from cluster 3 are likely located at the proximal part of the ductal structures. Together, these results suggest that cells from cluster 2 and 3 represent the mature cholangiocyte compartment located in the tubular structures, with a few *LGR5*$^{+}$ cells in cluster 2 maintaining some stem cell-like features.[13]

To further investigate the different cell types (clusters) within BRCOs, we compared the results from our scRNAseq analysis to the published human adult liver cell atlas.[13,15] For this, only parenchymal cells (ie. hepatocytes) and EPCAM^{+} cells/cholangiocytes were included and compared to the cell sub-clusters of BRCOs and ICOs. ICOs, that were also described in the published cell atlas, were used as controls. As shown in Figure 4C, ICO cells from both studies grouped together suggesting proper batch correction. As already shown in Figure 4A, we confirmed that the majority of BRCO cells are more closely related to primary EPCAM^{+}/cholangiocytes than ICO cells (Figure 4C). Looking into more detail, BRCO cells from cluster 1 (red, hepatocyte marker expressing cells) indeed grouped together with primary hepatocytes (Figure 4C). In contrast, BRCO cells from cluster 2 (green, mature cholangiocyte like cells) are closer to the primary cholangiocyte and EPCAM^{+} cells, leaving a few *LGR5*$^{+}$ cells separated from the other cells in cluster 2 (Figure 4C). BRCO cells from cluster 3 are in between the EPCAM^{+}/cholangiocyte and hepatocyte clusters (Figure 4C) and may miss an *in vivo* counterpart.

Finally, to confirm the transcriptomic similarities between BRCOs and primary cholangiocytes and to compare BRCOs to ICO cultured in the same conditions (Tysoe *et al.*[12]) as BRCOs, we integrated our data with previously published scRNA seq data from these specific ICOs[37] and its matching primary intrahepatic cholangiocytes (Figure S4A). Overall, we found that ICOs cultured in both conditions[7,9] were separated and clearly clustered, while cells from BRCO and primary cholangiocytes were more scattered. When performing subset analysis in BRCOs, it is clear that especially cluster 1 and 3 demonstrate a correlation to primary intrahepatic cholangiocytes (Figure S4B). In addition, the *Ki67*$^{+}$ cluster of BRCOs are close to the proliferating cells from both ICOs (Figure S4B and C). However, in line with our previous observation, BRCOs express *Ki67* and *LGR5* to a lesser extent than both types of ICOs (Figure S4C and D). In contrast, BRCOs express hepatocyte markers such as *ALB* and *GC*, as do these primary cholangiocytes (Figure S4C and D). Taking together, our analysis revealed that BRCOs have a unique transcriptome distinct from previous published cholangiocyte organoids, that closely resembles primary cholangiocytes and represents the heterogeneity present in EPCAM^{+} cells *in vivo*.

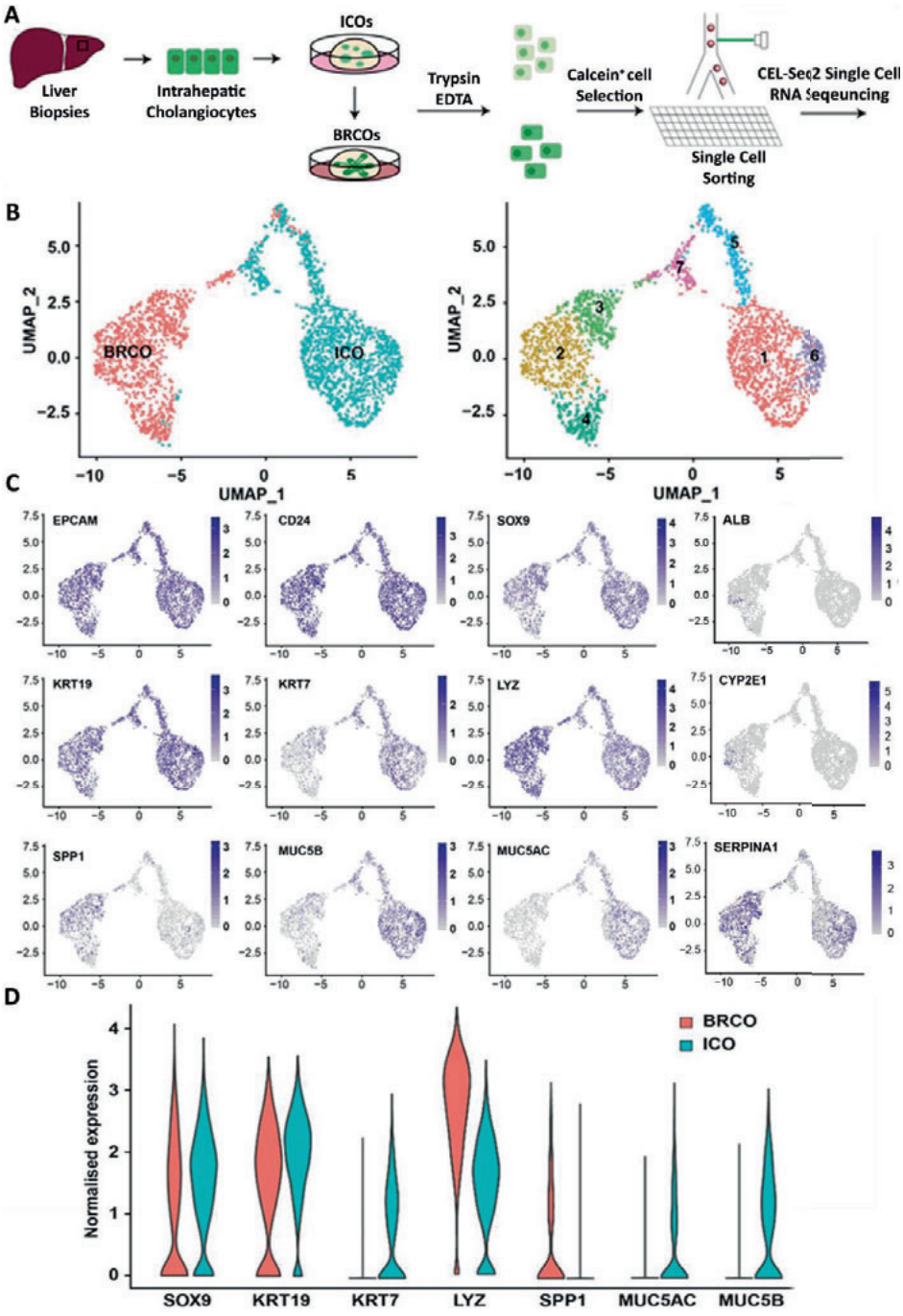
A
Liver Biopsies
Intrahepatic Cholangiocytes
ICOs
BRCOs
Trypsin EDTA
Calcein+ cell Selection
CEL-Seq2 Single Cell RNA Sequencing
Single Cell Sorting
B
UMAP_2
UMAP_1
BRCO
ICO
C
EPCAM
CD24
SOX9
ALB
KRT19
KRT7
LYZ
CYP2E1
SPP1
MUC5B
MUC5AC
SERPINA1
D
Normalised expression
BRCO
ICO
SOX9
KRT19
KRT7
LYZ
SPP1
MUC5AC
MUC5B

Figure 3. Single cell transcriptomics demonstrates that BRCOs consist of cholangiocyte-like cells that differ from ICOs.

(a) Schematic overview of the single cell RNA sequencing experiment. Both ICOs and BRCOs (n=3 matched for donor) were treated with Trypsin-EDTA and single calcein^{+} cells were sorted into 384-well plates. **(b)** UMAP plots of single cells from ICO and BRCO colored by different cell types (left), and colored by cluster number (right). Cells that share similar transcriptome profiles are grouped as clusters. **(c)** UMAP plots showing expression levels of general mature and immature cholangiocyte (organoids) genes (*EPCAM*, *CD24*, *SOX9*, *KRT19*, *KRT7*, *LYZ*, *SPP1*, *MUC5B* and *MUC5AC*) and hepatocyte related genes (*ALB*, *CYP2E1* and *SERPINA1*). **(d)** Expression violin plot showing the transcription levels of significantly different expressed cholangiocyte related genes from c.

BRCOs show essential traits of branching morphogenesis in vitro

Since BRCOs display a branching morphology, we investigated if their growth dynamics and spatial organization is conform known morphogenetic programs. EdU incorporation and Ki67 stainings showed that proliferating cells were almost exclusively located in the peripheral tips of the organoids (Figure 5A and 5B, Figure S5A and S5B). This peripheral location of cell proliferating is consistent with tip-driven branching, a feature shared with other branching organs during development.[39] Another feature of branching morphogenesis is the avoidance of shunt formation by induction of growth arrest when a tip encounters other (submerged) ducts. In BRCOs we observed no shunts, but found branch growth to stop when a tip neared another duct (Figure S5C), explaining the observed absence of cell proliferation in sub-peripheral regions of BRCOs. Besides growth inhibition or even arrest of the tips to avoid contact of already existing branches, we occasionally observed avoidance of tips by actively growing to another direction when they came close to other branches, as shown in online Video S4. This observation suggests that steric constraints are also important for tip termination to occur.

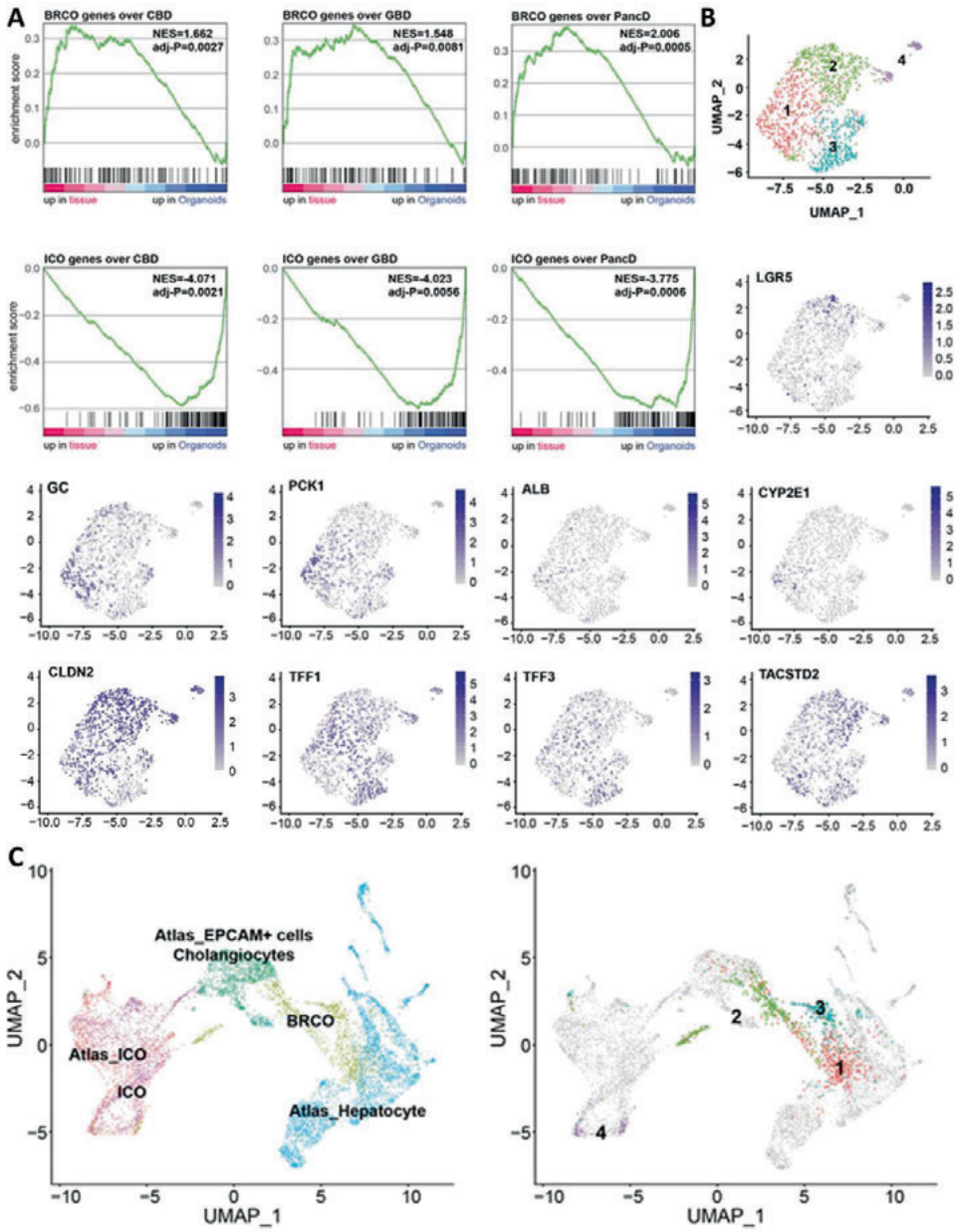

Figure 4. Transcriptomic heterogeneity in subsets of BRCO cells resembles that of primary cholangiocytes.

(a) GSEA analysis of BRCO versus ICO as compared to the lists of differentially expressed genes between primary cholangiocytes and corresponding organoids from the common bile duct (CBD, on the left), gallbladder bile duct (GBD, in the middle), and pancreatic bile duct (PancBD, on the right). DE gene lists

from *Rimland et al.*[8] were used and genes were ranked according to expression level in cholangiocytes (left side) and organoids (right side). Enrichment of BRCO genes is displayed on top and enrichment of ICO genes at the bottom. **(b)** UMAP plot of single cells from BRCOs colored by different clusters and the transcription levels of *LGR5*, selected hepatocyte (*GC*, *PCK1*, *ALB*, and *CYP2E1*), and cholangiocyte markers (*TACSTD2*, *CLDN2*, *TFF1* and *TFF3*). **(c)** UMAP plots of single cells from the integration analysis of ICOs, hepatocytes and cholangiocytes. The plot on the left is colored based on cell types, and the one on the right highlights BRCO cells according to the clusters in Figure 4B.

BRCOs follow probabilistic rules of branching and termination

To gain further insight into the growth dynamics of BRCOs, we reconstructed the spatial organization and topology of the full ductal network of three individual BRCOs at day five till day eight of culture (Figure 5C, D and Figure S5D). Quantitative analysis of duct lengths, defined as the length between consecutive branch points, revealed an approximately exponential distribution (Figure 5E). This implies that the timing between consecutive bifurcation events is random and is therefore not correlated. Such behavior is consistent with a non-stereotypical program, where branching events are regulated locally and not via global (extrinsic) cues. A more detailed analysis revealed a lower abundance of shorter ducts than expected from a purely exponential length distribution (Figure S5E). This indicates that tips may undergo a maturation and enlargement process before branching, which decreases the likelihood of shorter ducts to be present. Together with the evidence for tip-driven growth and termination, these observations fit the model of stochastic growth and branching patterns of BRCOs *in vitro*, similar to the branching ducts observed *in vivo*.[39] Within this framework, known as the Branching Annihilating Random Walk (BARW), growing tips undergo a "random walk" giving rise to a random trail of immobile ductal cells. According to this model, growing tips also undergo a random pattern of (stochastic) bifurcations, leading to branching and an exponential distribution of duct lengths. Active tips terminate growth irreversibly when they come within a critical distance, termed the annihilation radius, of a neighboring duct or tip. To test whether BRCO growth fits the BARW model we quantified the ductal network organization and represented this as binary branching trees (see Methods, Figure 5F, and Figure S5F). We then determined the probability (q_i) that a tip terminates at branch level (i) (Figure 5H, I and S5G, Methods). We also assessed the distribution of the subtree size (Figure 5G) and persistence (Figure 5J and K) and found that subtrees can comprise two to dozens of branches that were able to extend in length for up to nine levels. Adjusting the ratio of the branch rate to elongation rate, we found that the BARW model reproduced the heterogeneous subtree organization (R^2=0.89 and R^2=0.97, respectively). Also, the distribution of tip-to-tip distances (R^2=0.91, Figure S5H) fitted the model. These quantitative analyses show that branching and terminating dynamics in BRCOs fit the BARW model and, as shown *in vitro*, results in a ductal network without shunting. In conclusion, BRCOs are characterized by a non-stereotypical, locally regulated branching structure, similar to that observed in other branching contexts *in vivo*.

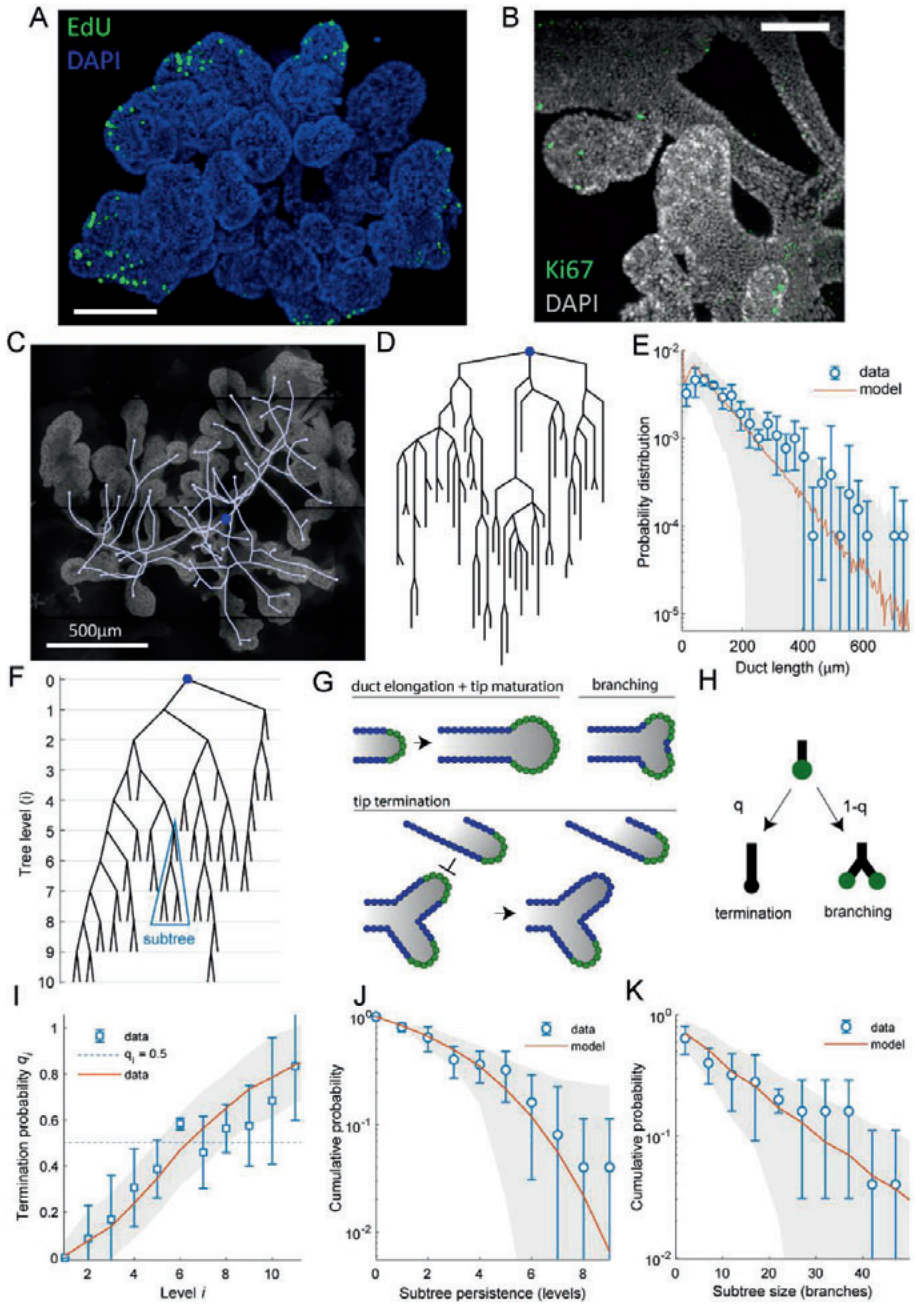

Figure 5. BRCOs grow according to branching and annihilating random walk dynamics with tip maturation.

Max-projections of confocal images of **(a)** EdU incorporation (green) and **(b)** Ki67 (green)immunofluorescence staining. Nuclei are counterstained with DAPI blue and grey), scale bars indicate 500µm (a) and 200 µm (b). **(c)** BRCO overlaid with the reconstructed ductal network (gray lines), the source is indicated in blue. **(d)** Planar representation of the reconstructed ductal networks (source node in blue). **(e)** Duct-length distribution for BRCOs (blue, n=3) and model prediction in orange (R^2=0.56). **(f)** Schematic of the processes in the BARW model proposed. **(g)** Branching tree representation of the ductal network with subtree size distribution (blue) used in the BARW model, the source node is shown in blue. **(h)** Schematics for the termination probability (q) and branching probability (1-q). Comparison of experimental measurements and model for **(i)** Termination probability (R^2 =0.89), and the cumulative probability for **(j)** subtree persistence (R^2=0.97) and **(k)** sizes (R^2=0.89). For **(e)** and **(i-k)**, experimental measurements appear in blue (error bars correspond to the SD), and results of the model appear in orange (shaded area shows the SD from >1000 realizations). All experiments conducted in this Figure were performed on BRCO10 and a technical duplicate of BRCO9.

Key liver developmental pathways are replicated in BRCOs

Increasing evidence indicates that primary cholangiocytes express WNT-ligands but use non-canonical WNT-signaling and YAP-signaling for self-replication and bile duct regeneration.[14,52] BRCOs are grown in conditions that both stimulate (RSPO1) and inhibit (Dickkopf-related protein 1 –DKK1) canonical WNT signaling. In addition, they are established from ICO cultures that severely upregulate WNT/β-catenin target genes.[9,13] Thus, we investigated if the different culture conditions of BRCOs and ICOs affect signaling pathways by examining genes involved in pathways crucial for liver development. [53-55] From the genes known to be involved in the WNT/β-catenin pathway, we detected lower expression of *LGR5* and *AXIN2* in BRCOs when compared to ICOs (Figure S6A), confirming previous results (Figure 1E, 3D and S4C). In contrast and as expected, downstream targets of the non-canonical WNT planar cell polarity (PCP) pathway, *JUN* and *JUND*, were highly elevated in BRCOs (Figure S6A). With respect to the YAP/HIPPO pathway, we assessed the expression of *YAP1* and known downstream targets.[52,53] In both organoid types we could detect *YAP1* expression, which was slightly higher in BRCOs (Figure S6B). However, downstream targets were hardly detectable except for *KLF6* (Figure S6B).

JAG1/NOTCH2 signaling is essential for branching morphogenesis in vitro

Several signaling pathways are known to be involved in branching morphogenesis. For instance, the TGF-β receptor signaling pathway has been implied as termination signal. Pathway analysis of the single cell transcriptomics indicated high activity of the TGF-β pathway in BRCOs (Figure S6C). This may confirm activation of the tip termination signals during *in vitro* branching development[6]. However, inhibition of TGF-β via A81-01 did not result in arrest of branching *in vitro* (Online Video S5). Similarly, blockage of retinoic acid synthesis, an important pathway for biliary development[56], did not affect growth or branching dynamics (Figure S6D). Another established signal involved in bile duct development is the NOTCH pathway. Appropriate JAG1/NOTCH2 signaling in hepatoblasts is

required for intrahepatic bile duct development. Inadequate NOTCH signaling, as seen in patients with Alagille syndrome, results in a deficient tubular formation.[17] The single cell transcriptomics shows no significant differences for *NOTCH2* and *JAG1* expression between BRCOs and ICOs, but a trend to higher expression was noticed (Figure 6A). To further investigate the potential involvement of the NOTCH pathway, ICOs were initiated from an AGS patient carrying a mutated copy of the *JAGGED1* gene.[57] To determine the exact mutation, MLPA analysis on AGS ICOs was performed. One large heterozygous deletion in *JAG1* was found, and Sanger sequencing identified two large deletions (of 3473 base pairs (bp) and 4811 bp), starting from the last 7 bp of exon 10 and exceeding to the first 27 bp of exon 24. RTq-PCR analyses confirmed the presence of relatively short mRNA products in AGS ICOs, while no such mRNA product could be detected in healthy ICOs (S6E and F). As potential compensation of mutated *JAG1*, AGS ICOs had higher expression of *NOTCH2* compared to healthy ICOs (Figure S6G). Western Blot analysis confirmed the reduced expression of wild type JAG1 protein in AGS ICOs and the presence of a mutated JAG1 protein (Figure 6B). In addition, immunofluorescence showed a clear difference in JAG1 localization. Healthy ICOs predominantly expressed JAG1 at the plasma membrane, while this localized expression was absent in AGS ICOs (Figure 6C). Although proliferation was diminished in AGS ICOs compared to healthy ICO (22.7%±5.8SD vs. 4.1%±0.3 D, p=0.01 Figure 6D), they formed normal cystic organoids. However, upon switching to branching-initiation medium AGS ICOs failed to show branching morphogenesis, stopped proliferating and underwent cell death (Figure 6E). Addition of exogenous chimeric JAG1 protein to AGS ICOs did not rescue these effects (Figure S6H), which may be due to limited receptor access or the haploinsufficiency.[58] However, the involvement of NOTCH signaling in branching morphogenesis was confirmed in healthy BRCOs by using the NOTCH-inhibitor DAPT. At first, BRCOs are forming (24 hours), however within 150 hours of DAPT treatment, existing branches are retracting, the formation of new branches is completely prevented and partially remodeled to cystic organoids (Figure 6F). In summary, these results suggest that appropriate JAG1/NOTCH2 signaling is essential for branching morphogenesis in BRCOs.

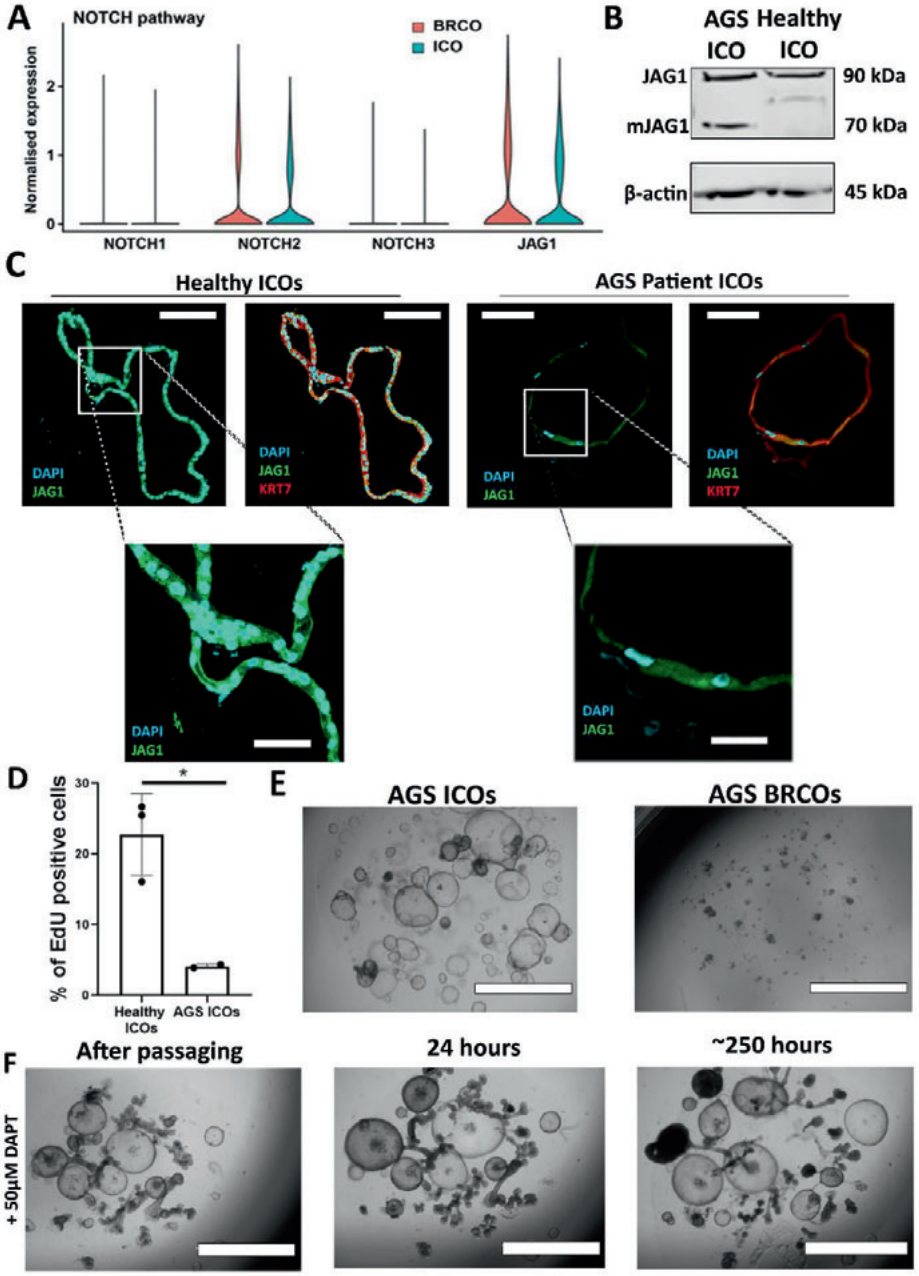

Figure 6. JAG1/NOTCH2 signaling is essential for branching morphogenesis in BRCOs.
(a) Violin plots showing the expression of selected genes in single cells involved in the NOTCH pathway cells for BRCOs (red) and ICOs (green)**. (b)** JAGGED1 protein expression analyzed via Western Blotting

in AGS ICOs and healthy ICOs. β-actin was taken along as a loading control. **(c)** Immunofluorescence staining of healthy ICOs (left) and AGS ICOs (right) for JAGGED1 (green), KRT-7 (Red) and Nuclei (DAPI, cyan). Scale bars indicate 100 µm and 25 µm upon zoom. **(d)** Percentage of EdU positive cells as analyzed by flow cytometry in healthy ICOs (n=3) and AGS ICOs (n=2, technical replication). **(e)** Organoids from an AGS patient cultured in ICO (left) and BRCO conditions (right). Scale bars indicate 1000µm. **(f)** Effect of NOTCH signaling inhibitor DAPT (50 µM) on healthy BRCOs. Scale bars indicate 2000 µm. Panel a is created using ICO and BRCO lines 6,7 and 10, all other panels are performed with biological triplicates (ICO12, 15 and 16). *indicates significant difference ($p<0.05$).

Cholangiocarcinoma organoids in branching conditions undergo morphological and gene expression changes resembling the primary tumor

One of the hallmarks of cancer is the disturbance of morphological cues resulting typical dysplastic tumor architecture. Since BRCOs demonstrate a complex architecture, we hypothesized that our culture protocol could also aid in modelling cholangiocarcinoma. To test this hypothesis, three different CCAO lines were cultured under branching conditions (BRCCAOs). A gradually and substantial change in morphology occurred in all lines within two weeks of culture, forming dense spheroidal organoids with branch-like outgrowths (Figure 7A and S7A). H&E staining of BRCCAOs showed the formation of multiple peripheral branches with a lumen, variable in diameter, surrounded by compact layers of cells (Figure 7B) and showed a striking resemblance to the primary tumor (Figure 7C). Branches were more tightly packed together compared to BRCOs, and adhered to multiple other tubular structures, resembling dysregulated growth of CCAs *in vivo* (Figure 7B and C). BRCCAOs showed widespread KRT7 expression (Figure S7B), a well-established marker for CCA tumor cells.[59] Expression of ZO-1, related to both morphogenesis and polarization in tissue[60], was not exclusively membrane-bound, indicating a lack of cellular polarization in BRCCAOs, in contrast to healthy BRCOs (Figure S1F and S7C). In addition, BRCCAOs showed no evidence of tip-driven proliferation but instead showed proliferation in both tips and ducts, demonstrated by EdU incorporation (Figure 7D) and confirmed by Ki67 staining (Figure S7D). In general, proliferation rates were not statically different between CCAOs and BRCCAOs (5.1% ± SD 0.3 vs. 9.2% ± SD 3.1, p=0.1, Figure S7E). The disorganized proliferation patterns demonstrate that growth is not exclusively tip-driven, as seen in BRCOs, but might reflect a compromised tip-inhibition mechanism, resulting in an irregular growth pattern, with tightly packed branching-like structures. Quantitively, measurements indicate that BRCCAOs were significantly smaller and more circularly than BRCOs (Figure 7E). Qualitatively, the structure of BRCCAOs could be recapitulated in the BARW model proposed for BRCOs by limiting tip-duct interactions (see Methods for details). Subsequently, the model produced dense and disorganized structures, and reproduced the size-reduction observed in BRCCAOs compared to BRCOs (Figure S7F and G). Furthermore, the model indicated that BRCCAOs seem to have an internal and an external structure filled with active tips, as was already seen in the cultures

(Figure 7E and S7F and G). This data shows that BRCCAOs consist of cholangiocarcinoma cells that have a perturbed structure resembling the tumor-like morphology.

To assess if the morphological changes are corroborated by changes in gene expression, bulk transcriptome analysis of BRCCAOs was performed (n=3) and compared to CCAOs. After normalization, the expression of 15.140 genes was compared in both types of tumor organoids and a pronounced difference in overall gene expression between them was found (PCA analysis, PC2, Figure S7H). In total we detected 149 DE genes (Sup. File 4), of which 22 overlapped with ICOs and BRCOs (Figure 3B). Despite the relatively large interpatient variability (PC1, Figure S7H), DE genes were consistently expressed in each tumor organoid line (Figure S7I). Of note, regulators of MAPK activity *DUSP1* and *DUSP5*, key effectors of cellular growth and survival[61], were among the most DE genes (Figure 7F). Similar to BRCOs, *JUN* and *JUND*[62] were upregulated in BRCCAOs, indicating activation of the PCP signaling pathway. GSEA analyses revealed that CCAOs have higher expression of genes related to cellular proliferation pathways (Figure 7G and S7J), while BRCCAOs show higher expression of genes related to complex cellular pathways (Figure 7G), including tumor-associated hypoxia (NES 2.85)[63]. Interestingly, TGF-β signaling, a pathway directly linked to metastasis and chemo-resistance[64], was upregulated in BRCCAOs compared to CCAOs (Figure S6C). To investigate whether the BRCCAO transcriptome is more closely related to the one of the primary tumor tissues, a gene correlation analyses was performed. For this, we integrated and filtered RNAseq data of patient-paired CCA tumor tissue based on the DE genes between BRCCAOs and CCAOs. As expected, the highest correlation coefficient (CC >0.97) was observed within the three CCAOs lines and within the three BRCCAOs lines. When comparing the CCAO and BRCCAO conditions, only a low correlation coefficient was observed (CC 0.59±0.06). Interestingly, when comparing organoids to primary tumor tissue, BRCCAOs showed a high correlation to CCA tumor (CC 0.80 ± SD 0.05, Figure 7H). The correlation of CCAOs and CCA tumor was much lower (CC 0.55 ± SD 0.08). Overall, our analyses revealed striking differences between the transcriptome of CCAOs and BRCCAOs, and it shows that the transcriptome of BRCCAO more closely resembles the gene expression profile of the primary cholangiocarcinoma tumor.

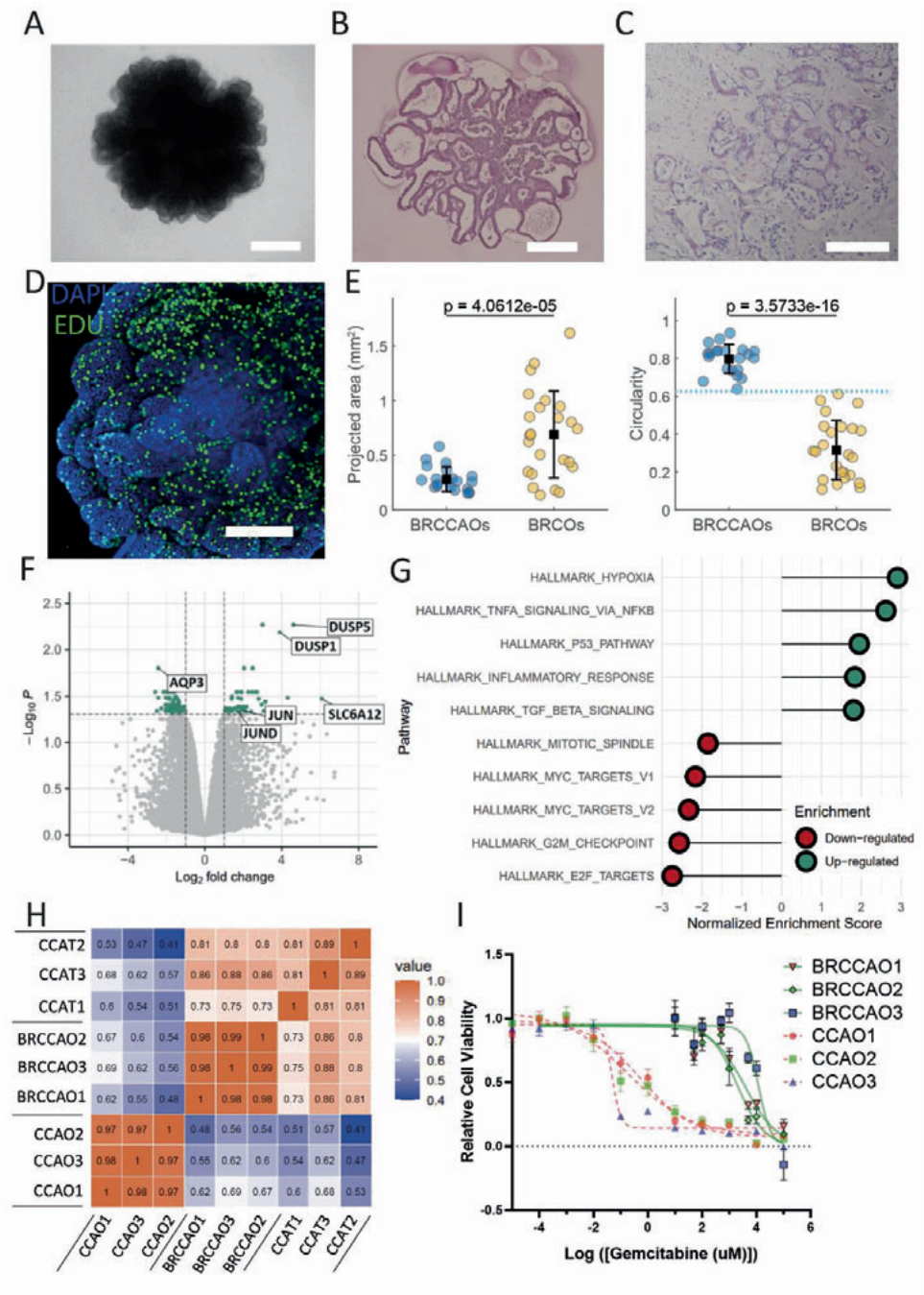
A
B
C
D
DAPI
EDU
E
p = 4.0612e-05
Projected area (mm²)
BRCCAOs
BRCOs
p = 3.5733e-16
Circularity
BRCCAOs
BRCOs
F
−Log10 P
Log2 fold change
DUSP5
DUSP1
AQP3
JUN
JUND
SLC6A12
G
HALLMARK_HYPOXIA
HALLMARK_TNFA_SIGNALING_VIA_NFKB
HALLMARK_P53_PATHWAY
HALLMARK_INFLAMMATORY_RESPONSE
HALLMARK_TGF_BETA_SIGNALING
HALLMARK_MITOTIC_SPINDLE
HALLMARK_MYC_TARGETS_V1
HALLMARK_MYC_TARGETS_V2
HALLMARK_G2M_CHECKPOINT
HALLMARK_E2F_TARGETS
Pathway
Enrichment
Down−regulated
Up−regulated
Normalized Enrichment Score
H
CCAT2
CCAT3
CCAT1
BRCCAO2
BRCCAO3
BRCCAO1
CCAO2
CCAO3
CCAO1
value
I
Relative Cell Viability
Log ([Gemcitabine (uM)])
BRCCAO1
BRCCAO2
BRCCAO3
CCAO1
CCAO2
CCAO3

Figure 7. Characterization and comparative analysis of BRCCAOs shows improved *in vitro* modelling of CCA.
(a) Representative bright field image of cholangiocarcinoma organoids grown in branching conditions (BRCCAOs). **(b)** H&E staining of a cross-sectioned BRCCAO. **(c)** H&E staining of a cross-sectioned primary cholangiocarcinoma tissue. **(d)** Max projection image of whole-mount confocal image of EdU (green) incorporation. Nuclei are counterstained by DAPI (blue). **(e)** 2D-projeced area (left) and circularity (right) of BRCAAOs and BRCOs (p-values obtained from two-sample t-tests). **(f)** Volcano scatter plot of statistical significance (adj. p-value) versus Log2FC showing DE genes between CCAOs and BRCCAOs. Positive log2 fold change indicates increased expression in BRCCAOs and relevant genes are highlighted. **(g)** Pathway analyses of DE genes showing normalized enrichment score significantly upregulated in BRCCAOs (green) or CCAOs (red). **(h)** Correlation matrix of transcriptomic profiles of matched tumor tissue (CCAT), BRCCAOs and CCAOs. A value of 1 represents complete correlation, and a value of 0 represents no significant correlation. **(i)** Dose-response curves after 72h treatment with gemcitabine and cisplatin generated from luminescence signal intensity relative to control. Biological replicates are plotted separately. All scale bars indicate 200 µm, except panel c where it indicates 100µm. All experiments were performed with three pairs of BRCCAOs and CCAOs and performed in Duplo.

As cholangiocarcinomas in vivo, BRCCAOs are chemo resistant

As the gene expression profile of BRCCAOs much better reflects the gene expression of primary CCA tumors, we postulate that the responses to drug treatments in BRCCAOs better reflect the drug responses of primary tumors. Although used as the golden standard for palliative treatment, it is well documented that primary CCA tumors are quite resistant to gemcitabine and/or cisplatin chemotherapy.[65] Therefore, we incubated CCAOs and BRCCAOs with gemcitabine and/or cisplatin for 72 hours, to mimic single and combinational therapies. Similar to previously published results[66], CCAOs were shown to be resistant to cisplatin monotherapy. Also, BRCCAOs were resistant to cisplatin monotherapy (data not shown). When combining cisplatin (10µM) with different doses of gemcitabine, a clear dose-dependent response on cell viability was observed (Figure 7I). A remarkable difference in response was observed between BRCCAOs and CCAOs. The CCAOs showed the highest sensitivity for the combination treatment with an average IC50 value for gemcitabine of 0.388 µM. The sensitivity of BRCCAOs for gemcitabine was at least a 10.000-fold higher with an average IC50 of 5760 µM ($p<0.001$, Figure 7I). This effect might be related to the differences in cell proliferation rate, as has been described for primary tumors.[67] Therefore, we assessed the proliferation levels in both organoid types in the time-period before the treatment, but no significant difference was observed between CCAOs and BRCCAOs (Figure S7K). This indicates that other drug resistance factors, other than the proliferation rate, are involved in the insensitivity of BRCCAOs for gemcitabine and cisplatin. In summary, these results clearly demonstrate that BRCCAOs better mimic *in vivo* CCA tumor tissue on a transcriptional level, resulting in a high resistance to chemotherapeutics compared to CCAOs. Gemcitabine and cisplatin combinational therapy only provides patients a modest benefit in overall survival[68] and BRCCAOs appear to reproduce this response more closely than CCAOs.

Discussion

With the establishment of the branching cholangiocyte organoid culture system, we have demonstrated that intrahepatic cholangiocytes derived from adult liver biopsies can be expanded *in vitro* as self-organizing branching epithelial bile ducts. The transcriptomic profile of BRCOs closely resembles that of *in vivo* intrahepatic cholangiocytes. Moreover, we show that BRCOs are capable of mimicking bile duct development *in vitro* driven by NOTCH2 signaling, making BRCOs a potential unique model for studying Alagille syndrome. Finally, we demonstrate that this culture method can also be applied to cholangiocarcinoma modeling. BRCCAOs form structures with disorganized growth-patterns, and BRCCAO gene expression profiles resemble those of the original tumor. Furthermore, drug-responses in BRCCAOs were more reminiscent of the *in vivo* tumor response. These results demonstrate that the newly developed culture method provides a novel and unique *in vitro* model for studying biliary development as well as (non-)cancerous biliary diseases.

The introduction of cholangiocyte organoids[69] from human adult tissue as described by Huch *et al.*[7] and Sampaziotis *et al.*[9] largely overcame the challenges of long-term culture of cholangiocytes. However, both protocols form organoids consisting of a polarized monolayer of cells with a central cavity, independent of the region where the organoid-initiating cells were obtained from.[7,9] Due to the lack of tubular formation *in vitro*, these models represent a suboptimal model for studying intrahepatic bile duct formation and disease. The unique architecture of the BRCOs developed here, provide a solution to study tubular formation. We show that the formation of BRCOs is driven by NOTCH2 signaling and that it follows a tip-driven branching and termination dynamics that is similar to other tissues *in vivo*.[70,71] These typical dynamics indicate that tips bifurcate following probabilistic rules, yet arrest their growth in crowded regions, adequately representing organ development. This makes BRCOs a convenient *in vitro* model to study biliary development and diseases, such as AGS related bile duct paucity, without the need for (suboptimal) animal models.

BRCOs are the first cholangiocyte organoid system derived from adult tissue cells that demonstrates such an extensive and complex branching morphology. Importantly, when cholangiocytes are solely exposed to either culture-condition, or switching occurs in opposite directions, the organoids become cystic in shape. This indicates that branching *in vitro* can only be established under specific circumstances. During embryonic development the intrahepatic bile ducts develop from a monolayer of progenitor cells, the ductal plate (DP).[72-74] DP-formation is WNT/β-catenin-dependent, but cholangiocyte differentiation and subsequent bile duct formation during later stages of embryonic development, relies on non-canonical WNT signaling.[13,14,75]

To grow BRCOs, we follow this same pattern of development. First, we start with a monolayer of cells, cultured primarily under WNT/β-catenin signaling, indicated by high expression of *AXIN2 and LGR5* in ICOs compared to BRCOs. After switching, β-catenin independent WNT signaling is also promoted, as confirmed by high expression of the PCP pathway associated genes *JUN and JUND*.[75,76] Furthermore, we show that by inhibiting NOTCH signaling (Figure 6B), or by a combination of inhibiting NOTCH and WNT signaling, BRCOs transform back to cysts (Figure 2H). Thus, by mimicking the subsequent activity of different pathways involved in biliary development *in vitro,* we established BRCOs. Similar approaches might create branching organoids derived from other organs as well.

Previous studies on cholangiocyte (organoids) demonstrate that there are subtle, but important, local microenvironment-driven differences between intra- and extrahepatic cholangiocytes.[8,37] Moreover, these cholangiocytes have distinct embryonic origins and have a unique predisposition for cholangiopathies, such as Alagille syndrome in intrahepatic bile ducts. Interestingly, *JAG1* is only highly expressed in intrahepatic cholangiocytes[37] and is essential for proper tubular development. In line with these results, only organoids derived from intrahepatic cholangiocytes are capable of forming BRCOs under influence of adequate JAG1/NOTCH signaling. Surprisingly, fetal-ICOs did not form tubular structures *in vitro*. *In vivo,* the first tubular structures form around week 12, but proper intrahepatic development only starts from week 20.[77] The gestational age of the fetal livers used in this study is between 17-18 weeks, suggesting that livers might have been too young to demonstrate branching *in vitro.*

Importantly, recent transcriptome studies of cholangiocytes demonstrated extensive heterogeneity in the biliary compartment. In cholangiocytes, a subset of cells expresses high levels of hepatocyte-related genes such as *ALB, SERPINA1 and HNF4α*[13,14,37,52], suggested to be the cholangiocytes that can transdifferentiate to hepatocytes.[13,78] As shown in Figure 4B, BRCOs show a similar aspect of cholangiocyte heterogeneity as indicated by the hepatocyte marker expression cluster 1, previously unseen in cholangiocyte organoids[7,9] (Figure 3C and S4C and D). However, we were unable to create hepatocyte-like cells in BRCOs or further upregulate hepatocyte markers under transdifferentiation protocols (Figure 2I-J, S1F). Nevertheless, the high correlation to primary intrahepatic cholangiocytes makes BRCOs an exceptionally good model to study mature cholangiocytes *in vitro.* In addition, subsequent studies could focus on co-culturing BRCOs with hepatocyte (-like cells) and investigate if epithelial livers can be established *in vitro.*

WNT signaling pathways are frequently dysregulated in a variety of cancers[59,79], providing a rationale for the pathophysiological role of the different culture conditions in BRCCAOs. In a clinical setting, elevated levels of DKK1 are related to lymphatic metastasis and poor prognosis in CCA[80], indicating a more aggressive tumor phenotype. Furthermore, a phase II

clinical trial with an anti-DKK1 antibody in CCA patients is currently underway[81], showing the importance of the culture conditions we described here, in a tumor setting. BRCCAOs show a unique phenotype, characterized by a dense organization of branch outgrowths compared to healthy BRCOs. BRCCAOs phenotype is consistent with a branching morphogenesis model with a hindered capacity to inhibit tip growth or to produce elongated ducts. The clear difference in growth patterns between healthy and tumor organoids was not well recapitulated by previous CCA and cholangiocyte organoids. In addition, BRCCAOs exhibit features of an uncontrolled, undirected growth that is also seen in tumors *in vivo*.[82] In recent years, organoids have been appreciated for their ability to recapitulate patient characteristics. Here, we show that transcriptionally, BRCCAOs are more representative of *in vivo* patient tumor tissue, while upregulating important tumor-related pathways, such as hypoxia and TGF-β signaling, showcasing the complex cellular behavior in BRCCAOs. However, considering high single cell inter-tumor heterogeneity present in CCAs *in vivo*[83], it remains a question to what extent BRCCAOs are able to represent this heterogeneity. Extending the single-cell RNAseq to BRCCAOs could provide more granularity on the transcriptomic changes occurring, and the possible subpopulations that are affected.

Clinically, a main hurdle for management of CCA remains the lack of response to treatment.[59] Although in recent years the number of trials utilizing targeted therapies have increased[84,85], the need for novel therapies is still present. Preclinical models that better recapitulate this (chemo)resistance could aid this process. The significant increase in chemo resistance shown by BRCCAOs resembles the patient situation and paves the way for developing novel strategies to overcome CCA chemo resistance *in vitro*. Interestingly, similar to BRCOs, we observed activation of the JNK pathway in BRCCAOs. Integration between JNK and β-catenin has been shown to regulate cancer development.[86] Furthermore, *JUND* has been shown to mediate JNK-stimulated survival and anti-apoptotic signaling in collaboration with NF-κB[87], another upregulated pathway in BRCCAOs, hinting at a relationship between these important signaling pathways and the observed chemo resistance. Further studies shall focus on uncovering the molecular basis of the mechanisms for chemoresistance that are present in these organoids.

In conclusion, our results indicate that BRCOs represent organoids that recapitulate both the complex morphological architecture as well as the transcriptomic heterogeneity present in human intrahepatic bile ducts. They represent a novel and unique model for studying human bile duct development and associated (malignant) diseases.

References

1. Castaing D. Surgical anatomy of the biliary tract. HPB (Oxford). 2008;10(2):72-76.
2. Zong Y, Stanger BZ. Molecular mechanisms of bile duct development. Int. J. Biochem. Cell Biol. 2011;43:257–264.
3. Si-Tayeb K, Lemaigre FP, Duncan SA. Organogenesis and development of the liver. Dev Cell. 2010;18(2):175-189.
4. Strazzabosco M, Fabris L. Functional anatomy of normal bile ducts. Anat Rec (Hoboken). 2008;291(6):653-660.
5. Boyer JL. Bile formation and secretion. Compr Physiol. 2013 Jul;3(3):1035-78.
6. Hannezo E, Simons BD. Multiscale dynamics of branching morphogenesis. Curr Opin Cell Biol. 2019 Oct;60:99-105.
7. Huch M, Gehart H, Boxtel R van, *et al.* Long-term culture of genome-stable bipotent stem cells from adult human liver. Cell. 2015;1–14.
8. Rimland CA, Tilson SG, Morell CM, *et al.* Regional differences in human biliary tissues and corresponding *in vitro* derived organoids. Hepatology. 2021 Jan;73(1):247-267.
9. Sampaziotis F, Justin AW, Tysoe OC, *et al*. Reconstruction of the mouse extrahepatic biliary tree using primary human extrahepatic cholangiocyte organoids. Nat. Med. 2017;23:954–963.
10. Sampaziotis F, de Brito MC, Madrigal P, *et al.* Cholangiocytes derived from human induced pluripotent stem cells for disease modeling and drug validation. Nat Biotechnol. 2015 Aug;33(8):845-852.
11. Verstegen MMA, Roos FJM, Burka K, *et al.* Human extrahepatic and intrahepatic cholangiocyte organoids show region-specific differentiation potential and model cystic fibrosis-related bile duct disease. Sci Rep. 2020 Dec 14;10(1):21900.
12. Tysoe OC, Justin AW, Brevini T, *et al.* Isolation and propagation of primary human cholangiocyte organoids for the generation of bioengineered biliary tissue. Nat Protoc. 2019 Jun;14(6):1884-1925.
13. Aizarani N, Saviano A, Sagar, *et al*. A human liver cell atlas reveals heterogeneity and epithelial progenitors. Nature. 2019 Aug;572(7768):199-204.
14. Planas-Paz L, Sun T, Pikiolek M, *et al.* YAP, but Not RSPO-LGR4/5, Signaling in Biliary Epithelial Cells Promotes a Ductular Reaction in Response to Liver Injury. Cell Stem Cell. 2019 Jul 3;25(1):39-53.e10.
15. Segal JM, Kent D, Wesche DJ, *et al.* Single cell analysis of human foetal liver captures the transcriptional profile of hepatobiliary hybrid progenitors. Nat Commun. 2019 Jul 26;10(1):3350.
16. MacParland SA, Liu JC, Ma XZ, *et al.* Single cell RNA sequencing of human liver reveals distinct intrahepatic macrophage populations. Nat Commun. 2018;9(1):4383.
17. Li L, Krantz ID, Deng Y, *et al*. Alagille syndrome is caused by mutations in human Jagged1, which encodes a ligand for Notch1. Nat Genet. 1997;16(3):243-251.
18. Oda T, Elkahloun AG, Pike BL, *et al.* Mutations in the human Jagged1 gene are responsible for Alagille syndrome. Nat Genet. 1997;16(3):235-242.
19. McDaniell R, Warthen DM, Sanchez-Lara PA, *et al.* NOTCH2 mutations cause Alagille syndrome, a heterogeneous disorder of the notch signaling pathway. Am J Hum Genet. 2006;79(1):169-173.
20. Broutier L, Mastrogiovanni G, Verstegen MMA, *et al.* Human primary liver cancer-derived organoid cultures for disease modeling and drug screening. Nat Med. 2017;23(12):1424-1435.

21. Broutier L, Andersson-Rolf A, Hindley CJ, *et al.* Culture and establishment of self-renewing human and mouse adult liver and pancreas 3D organoids and their genetic manipulation. Nat Protoc. 2016 Sep;11(9):1724-43.
22. Barker N, Huch M, Kujala P, *et al.* Lgr5(+ve) stem cells drive self-renewal in the stomach and build long-lived gastric units in vitro. Cell Stem Cell. 2010 Jan 8;6(1):25-36.
23. Vizcaíno JA, Deutsch EW, Wang R, et al. ProteomeXchange provides globally coordinated proteomics data submission and dissemination. Nat Biotechnol. 2014 Mar;32(3):223-6.
24. Roest HP, Ooms LSS, Gillis AJM, *et al.* Cell-free MicroRNA miR-505-3p in Graft Preservation Fluid Is an Independent Predictor of Delayed Graft Function After Kidney Transplantation. Transplantation. 2019 Feb;103(2):329-335.
25. Clevers H, Gehart H. WO2017149025 - IMPROVED DIFFERENTIATION METHOD. Retrieved from Https://patentscope.wipo.int/search/en/detail.jsf?docId=WO2017149025&tab=PCTBIBLIO, accessed upon May 1st 2020.
26. Vanwolleghem T, Libbrecht L, Hansen BE, *et al*. Factors determining successful engraftment of hepatocytes and susceptibility to hepatitis B and C virus infection in upa-Scid mice. J Hepatol. 2010 Sep;53(3):468-76.
27. Dekkers JF, Wiegerinck CL, de Jonge HR, *et al.* A functional CFTR assay using primary cystic fibrosis intestinal organoids. Nat Med. 2013 Jul;19(7):939-45.
28. Roos FJM, Bijvelds MJC, Verstegen MMA, *et al.* Impact of hypoxia and AMPK on CFTR-mediated bicarbonate secretion in human cholangiocyte organoids. Am J Physiol Gastrointest Liver Physiol. 2021 Mar 3. Epub ahead of print.
29. Roos FJM, Verstegen MMA, Muñoz-Albarinos L, *et al.* Human bile contains cholangiocyte organoid initiating cells which expand as functional cholangiocytes in non-canonical WNT stimulating conditions. Front Cell Dev Biol. 2021 Feb 9;8:630492.
30. Zilionis R, Nainys J, Veres A, *et al.* Single-cell barcoding and sequencing using droplet microfluidics. Nat Protoc. 2017 Jan;12(1):44-73.
31. Hashimshony T, Senderovich N, Avital G, *et al.* CEL-Seq2: sensitive highly-multiplexed single-cell RNA-Seq. Genome Biol. 2016 Apr 28;17:77.
32. Smith T, Heger A, Sudbery I. UMI-tools: modeling sequencing errors in Unique Molecular Identifiers to improve quantification accuracy. Genome Res. 2017 Mar;27(3):491-499.
33. Dobin A, Davis CA, Schlesinger F, *et al.* STAR: ultrafast universal RNA-seq aligner. Bioinformatics. 2013;29(1):15-21.
34. Liao Y, Smyth GK, Shi W. featureCounts: an efficient general purpose program for assigning sequence reads to genomic features. Bioinformatics. 2014 Apr 1;30(7):923-30.
35. Butler A, Hoffman P, Smibert P, *et al*. Integrating single-cell transcriptomic data across different conditions, technologies, and species. Nat Biotechnol. 2018 Jun;36(5):411-420.
36. Kuleshov MV, Jones MR, Rouillard AD, *et al.* Enrichr: a comprehensive gene set enrichment analysis web server 2016 update. Nucleic Acids Res. 2016 Jul 8;44(W1):W90-7.
37. Sampaziotis F, Muraro D, Tysoe OC, *et al*. Cholangiocyte organoids can repair bile ducts after transplantation in the human liver. Science. 2021 Feb 19;371(6531):839-846.
38. van Royen ME, Verhoef EI, Kweldam CF, *et al.* Three-dimensional microscopic analysis of clinical prostate specimens. Histopathology. 2016 Dec;69(6):985-992.
39. Hannezo E, Scheele CLGJ, Moad M, *et al.* A Unifying Theory of Branching Morphogenesis. Cell. 2017 Sep 21;171(1):242-255.
40. Afgan E, Baker D, van den Beek M, *et al.* The Galaxy platform for accessible, reproducible and collaborative biomedical analyses: 2016 update Nucleic Acids Res. 2016 Jul 8;44(W1):W3-W10.

41. Hang Y, Parmigiani G, Johnson WE. *ComBat-seq*: batch effect adjustment for RNA-seq count data. NAR Genom Bioinform. 2020 Sep;2(3):lqaa078.
42. Robinson MD, McCarthy DJ, Smyth GK. edgeR: a Bioconductor package for differential expression analysis of digital gene expression data. Bioinformatics. 2010 Jan 1;26(1):139-40.
43. Ritchie ME, Phipson B, Wu D, Hu Y, Law CW, Shi W, Smyth GK. limma powers differential expression analyses for RNA-sequencing and microarray studies. Nucleic Acids Res. 2015 Apr 20;43(7):e47.
44. Korotkevich G, Sukhov V, Sergushichev A. Fast gene set enrichment analysis. BioRxiv. 2019, doi: 10.1101/060012.
45. Salzberg SL, Phillippy AM, Zimin A, *et al.* GAGE: A critical evaluation of genome assemblies and assembly algorithms. Genome Res. 2012 Mar;22(3):557-67.
46. Alvaro D, Benedetti A, Marucci L, *et al*. The function of alkaline phosphatase in the liver: regulation of intrahepatic biliary epithelium secretory activities in the rat. Hepatology. 2000 Aug;32(2):174-84.
47. LeSage GD, Benedetti A, Glaser S, *et al*. Acute carbon tetrachloride feeding selectively damages large, but not small, cholangiocytes from normal rat liver. Hepatology. 1999 Feb;29(2):307-19.
48. LeSage GD, Glaser SS, Marucci L, *et al*. Acute carbon tetrachloride feeding induces damage of large but not small cholangiocytes from BDL rat liver. Am J Physiol. 1999 May;276(5):G1289-301.
49. Maroni L, Haibo B, Ray D, et al. Functional and structural features of cholangiocytes in health and disease. Cell Mol Gastroenterol Hepatol. 2015 Jul 1;1(4):368-380.
50. Uhlén M, Fagerberg L, Hallström BM, *et al.* Tissue-based map of the human proteome. Science. 2015 Jan 23;347(6220):1260419.
51. Jiang X, Karlsen TH. Genetics of primary sclerosing cholangitis and pathophysiological implications. Nat Rev Gastroenterol Hepatol 2017;14:279-295
52. Pepe-Mooney BJ, Dill MT, Alemany A, *et al.* Single-Cell Analysis of the Liver Epithelium Reveals Dynamic Heterogeneity and an Essential Role for YAP in Homeostasis and Regeneration. Cell Stem Cell. 2019 Jul 3;25(1):23-38.e8.
53. Goessling W, North TE, Lord AM, *et al.* APC mutant zebrafish uncover a changing temporal requirement for wnt signaling in liver development. Dev Biol. 2008;320(1):161-174.
54. McLin VA, Rankin SA, Zorn AM. Repression of Wnt/beta-catenin signaling in the anterior endoderm is essential for liver and pancreas development. Development. 2007;134(12):2207-2217.
55. Yimlamai D, Christodoulou C, Galli GG, *et al.* Hippo pathway activity influences liver cell fate. Cell. 2014 Jun 5;157(6):1324-1338.
56. Koike H, Iwasawa K, Ouchi R, *et al.* Modelling human hepato-biliary-pancreatic organogenesis from the foregut-midgut boundary. Nature. 2019 Oct;574(7776):112-116.
57. Oda T, Elkahloun AG, Pike BL, *et al.* Mutations in the human Jagged1 gene are responsible for Alagille syndrome. Nat Genet. 1997;16(3):235-242.
58. McCright B, Lozier J, Gridley T. A mouse model of Alagille syndrome: Notch2 as a genetic modifier of Jag1 haploinsufficiency. Development. 2002 Feb;129(4):1075-82.
59. Banales JM, Cardinale V, Carpino G, *et al.* Cholangiocarcinoma: current knowledge and future perspectives consensus statement from the European Network for the Study of Cholangiocarcinoma (ENS-CCA). Nature Reviews Gastroenterology & Hepatology. 2016 May;13(5):261-80.
60. Odenwald MA, Choi W, Buckley A, *et al.* ZO-1 interactions with F-actin and occludin direct epithelial polarization and single lumen specification in 3D culture. Journal of cell science. 2017 Jan 1;130(1):243-59.

61. Nunes-Xavier C, Roma-Mateo C, Rios P, *et al.* Dual-specificity MAP kinase phosphatases as targets of cancer treatment. Anti-Cancer Agents in Medicinal Chemistry (Formerly Current Medicinal Chemistry-Anti-Cancer Agents). 2011 Jan 1;11(1):109-32.
62. Lamb JA, Ventura JJ, Hess P, *et al.* JunD mediates survival signaling by the JNK signal transduction pathway. Molecular cell. 2003 Jun 1;11(6):1479-89.
63. Bhandari V, Hoey C, Liu LY, *et al.* Molecular landmarks of tumor hypoxia across cancer types. Nature genetics. 2019 Feb;51(2):308-18.
64. Colak S, Ten Dijke P. Targeting TGF-β signaling in cancer. Trends in cancer. 2017 Jan 1;3(1):56-71.
65. Banales JM, Marin JJ, Lamarca A, *et al.* Cholangiocarcinoma 2020: the next horizon in mechanisms and management. Nature Reviews Gastroenterology & Hepatology. 2020 Sep;17(9):557-88.
66. Li L, Knutsdottir H, Hui K, *et al.* Human primary liver cancer organoids reveal intratumor and interpatient drug response heterogeneity. JCI insight. 2019 Jan 24;4(2).
67. Gupta A, Gautam P, Wennerberg K, *et al.* A normalized drug response metric improves accuracy and consistency of anticancer drug sensitivity quantification in cell-based screening. Communications biology. 2020 Jan 23;3(1):1-2.
68. Valle J, Wasan H, Palmer DH, *et al.* Cisplatin plus gemcitabine versus gemcitabine for biliary tract cancer. New England Journal of Medicine. 2010 Apr 8;362(14):1273-81.
69. Marsee A, Roos FJM, Verstegen MMA, *et al*. Building consensus on definition and nomenclature of hepatic, pancreatic, and biliary organoids. Cell Stem Cell. 2021 May 6;28(5):816-832
70. Scheele CL, Hannezo E, Muraro MJ, *et al*. Identity and dynamics of mammary stem cells during branching morphogenesis. Nature. 2017 Feb 16;542(7641):313-317
71. Sznurkowska MK, Hannezo E, Azzarelli R, *et al.* Defining Lineage Potential and Fate Behavior of Precursors during Pancreas Development. Dev Cell. 2018 Aug 6;46(3):360-375.
72. Zong Y, Panikkar A, Xu J, *et al*. Notch signaling controls liver development by regulating biliary differentiation. Development. 2009;136(10):1727-1739.
73. Kodama Y, Hijikata M, Kageyama R, *et al*. The role of notch signaling in the development of intrahepatic bile ducts. Gastroenterology. 2004;127(6):1775-1786.
74. Geisler F, Strazzabosco M. Emerging roles of Notch signaling in liver disease. Hepatology. 2015;61(1):382-392.
75. Lade AG, Monga SP. Beta-catenin signaling in hepatic development and progenitors: which way does the WNT blow?. Dev Dyn. 2011;240(3):486-500.
76. Chen Y, Chen Z, Tang Y, *et al.* The involvement of noncanonical Wnt signaling in cancers. Biomed Pharmacother. 2021 Jan;133:110946.
77. Roskams T, Desmet V. Embryology of extra- and intrahepatic bile ducts, the ductal plate. Anat Rec (Hoboken). 2008 Jun;291(6):628-35.
78. Raven A, Lu WY, Man TY, *et al.* Cholangiocytes act as facultative liver stem cells during impaired hepatocyte regeneration. Nature. 2017 Jul 20;547(7663):350-354.
79. Zimmerli D, Hausmann G, Cantù C, *et al*. Pharmacological interventions in the Wnt pathway: inhibition of Wnt secretion versus disrupting the protein-protein interfaces of nuclear factors. Br J Pharmacol. 2017 Dec;174(24):4600-4610.
80. Shi RY, Yang XR, Shen QJ, *et al.* High expression of Dickkopf-related protein 1 is related to lymphatic metastasis and indicates poor prognosis in intrahepatic cholangiocarcinoma patients after surgery. Cancer. 2013 Mar 1;119(5):993-1003.

81. Goyal L, Sirard C, Schrag M, *et al*. Phase I and Biomarker Study of the Wnt Pathway Modulator DKN-01 in Combination with Gemcitabine/Cisplatin in Advanced Biliary Tract Cancer. Clin Cancer Res. 2020 Dec 1;26(23):6158-6167.
82. Chung YE, Kim MJ, Park YN, *et al*. Varying appearances of cholangiocarcinoma: radiologic-pathologic correlation. Radiographics. 2009 May-Jun;29(3):683-700.
83. Zhang M, Yang H, Wan L, *et al.* Single-cell transcriptomic architecture and intercellular crosstalk of human intrahepatic cholangiocarcinoma. J Hepatol. 2020 Nov;73(5):1118-1130.
84. Javle M, Lowery M, Shroff RT, Weiss KH, *et al.* Phase II Study of BGJ398 in Patients With FGFR-Altered Advanced Cholangiocarcinoma. J Clin Oncol. 2018 Jan 20;36(3):276-282.
85. Abou-Alfa GK, Macarulla T, Javle MM, *et al*. Ivosidenib in IDH1-mutant, chemotherapy-refractory cholangiocarcinoma (ClarIDHy): a multicentre, randomised, double-blind, placebo-controlled, phase 3 study. Lancet Oncol. 2020 Jun;21(6):796-807.
86. Nateri AS, Spencer-Dene B, Behrens A. Interaction of phosphorylated c-Jun with TCF4 regulates intestinal cancer development. Nature. 2005 Sep 8;437(7056):281-5.
87. Lamb JA, Ventura JJ, Hess P, *et al.* JunD mediates survival signaling by the JNK signal transduction pathway. Mol Cell. 2003 Jun;11(6):1479-89.

Supplementary Information

Table S1. Patient and organoid culture characteristics.

Culture type	Age patient (years)	Gender	Cell Source	Donor Type/ Surgical Indication	Cultured until passage
ICO 1, ECO 1, BRCO 1	67	M	Liver-, EHBD biopsy	DCD	25
ICO 2, ECO 2, BRCO 2	75	F	Liver-, EHBD biopsy	DBD	15
ICO 3, ECO 3, BRCO 3	47	M	Liver-, EHBD biopsy	DBD	15
ICO 4, BRCO 4	65	F	Liver biopsy	DBD	20
ICO 5, BRCO 5	41	M	Liver biopsy	DBD	15
ICO 6, BRCO 6	50	M	Liver biopsy	DBD	15
ICO 7, BRCO 7	80	F	Liver biopsy	DBD	15
ICO 8, BRCO 8	75	F	Liver biopsy	DBD	10
ICO 9, BRCO 9	58	M	Liver biopsy	DBD	10
ICO 10, BRCO 10	22	F	Liver biopsy	DCD	10
ICO 11, BRCO 11	72	M	Liver biopsy	DBD	10
ICO 12, BRCO 12	51	F	Liver biopsy	DBD	15
ICO 13, BRCO 13	72	F	Liver biopsy (explant liver)	Toxic-induced acute liver failure	15
ICO 14, BRCO 14	43	F	Liver biopsy (explant liver)	Alcoholic induced liver cirrhosis	15
ICO 15	78	F	Liver biopsy	DBD	15
ICO 16	50	F	Liver biopsy	DCD	15
AGS ICO	47	F	Liver biopsy (explant liver)	Alagille Syndrome	15
Fetal-ICO 1	18-20 weeks	unknown	Fetal Liver	Explant fetal liver	8
Fetal-ICO 2	18-20 weeks	unknown	Fetal Liver	Explant fetal liver	8
Fetal-ICO 3	18-20 weeks	unknown	Fetal Liver	Explant fetal liver	7
CCAO 1, BRCCAO 1	34	F	pCCA	Cholangiocarcinoma (surgical resection)	n/a
CCAO 2, BRCCAO 2	59	M	iCCA	Cholangiocarcinoma (surgical resection)	n/a
CCAO 3, BRCCAO 3	76	F	iCCA	Cholangiocarcinoma (surgical resection)	n/a

Abbreviations. ICO: intrahepatic cholangiocyte organoids, ECO: extrahepatic cholangiocyte organoids, BRCO: branching cholangiocyte organoids, EHBD: extrahepatic bile duct, DCD: donation after circulatory death, DBD: donation after brain death, AGS: Alagille Syndrome, CCAO: cholangiocarcinoma organoid, BRCCAO: Branching cholangiocarcinoma organoid, pCCA: perihilar cholangiocarcinoma, iCCA: intrahepatic cholangiocarcinoma, n/a: not applicable.

Table S2. List of antibodies used.

Antibody	Raised	Manufacturer-Reference	Dilution/concentration
Albumin	Mouse	Sigma-Aldrich: A6684	1:500
KRT-7	Mouse	DAKO: M7018	1:100
KRT-19	Mouse	DAKO: M0888	1:100
CFTR	Mouse	EMD Millipore Corp: MAB3484	1:100
MUC-1	Mouse	ThermoFisher Scientific: MA5-14077	1:500
SCTR	Rabbit	Abcam: AB234830	1:100
CLDN2	Mouse	ThermoFisher Scientific: 32-5600	1:100
ZO-1	Rabbit	ProteinTech: 21773-1-AP	1:100
MIB-1	Rabbit	Ventana: GG1661	2.0 µg/mL
JAG1	Mouse	Biomatik: CAU25271	1:1000
β-actin	Rabbit	Santa Cruz Biotech Inc. sc-47778	1:1000
Alexa Fluor 555	Goat – polyclonal (anti-mouse)	ThermoFisher Scientific: A21422	1:200
Alexa Fluor 488	Goat – polyclonal (anti-rabbit)	ThermoFisher Scientific: A32731	1:200
IRDye – 680LT	Goat – polyclonal (anti-mouse)	LI-COR Biosciences: 926-68020	1:10000
IRDye – 800CW	Goat – polyclonal (anti-rabbit)	LI-COR Biosciences: 926-32213	1:10000

Table S3. List of genes and primers used

Gene		Primer sequence (5' à 3')	Gene		Primer sequence (5'à 3)
KRT7	F	GGGGACGACCTCCGGAATAC	SERPINA1	F	GAGGAGAGCAGGAAAGGACA
	R	CTCAGCCAGGGAGACAGG		R	CTTGGCACGCTGGTTCTTGA
GGT	F	TGGTGGACATCATAGGTGGGGA	KRT19	F	GCACTACAGCCACTACTACACGA
	R	ATGACGGCAGCACCTCACTT		R	CTCATGCGCAGAGCCTGTT
ASBT	F	GGTGGCCTTTGACATCCTCCC	TFF2	F	TCTGTCCTGCCTCCCTGATCCA
	R	GCATCATTCCGAGGGCAAGC		R	CTCTGGCACGTGAATCCCGGT
SOX9	F	ACCAGTACCCGCACTTGCAC	HPRT1	F	TATAAATTCTTTGCTGACCTGCG
	R	GCGCCTTGAAGATGGCGTTG		R	CTTCGTGGGGTCCTTTTCACC
EpCAM	F	GACTTTTGCCGCAGCTCAGGA	ALB	F	CTGCCTGCCTGTTGCCAAAGC
	R	AGCAGTTTACGGCCAGCTTGT		R	GGCAAGGTCCGCCCTGTCATC
CFTR	F	TGGCGGTCACTCGGCAATTT	GAPDH	F	CTTTTGCGTCGCCAGCCGAG
	R	TCCAGCAACCGCCAACAACT		R	CCAGGCGCCCAATACGACCA
LGR5	F	GTCAGCTGCTCCCGAATCCC	HNF4α	F	GTACTCCTGCAGATTTAGCC
	R	TGAAACAGCTTGGGGGCACA		R	CTGTCCTCATAGCTTGACCT
CYP3A4	F	AGCAAAGAGCAACACAGAGCTGAA	AQP1	F	GGCCAGCGAGTTCAAGAAGAA
	R	CAGAGGTGTGGGCCCTGGAAT		R	TCACACCATCAGCCAGGTCAT
TFF1	F	ACAAGCTGCTGTACACGGACA	β-catenin	F	GAAAATCCAGCGTGGACAATG
	R	AAGTTTCCAGGGCCGGGCAAT		R	TTGTCAGTTCAGGGATTGC
MRP2	F	TGGGATGAAAGGTCATCCTTTACGG	MUC1	F	CTGTCAGTGCCGCCGAAAG
	R	GGGGCCAGGAGCCATAGGTA		R	CGTGCCCCTACAAGTTGGCA
TACSTD2 /TROP2	F	CGAGCTTGTAGGTACCCGGCGm	JAG1_ n11/24	F	GGAGCAAGTCTGGAGACAGCC
	R	TGCGCCGAGGAATCAGGAAGC		R	TGAATGGACGGATCGCCTGC
JAGe24	F	TGAATGGACGGATCGCCTG	JAG1_ e25/26	F	GGCACTGCCAGATAATCCCTCG
	R	TTGTTCGCTGAAGGGGAAG	JAG1_e25	R	TCAGCGAGCTGTTTCCATCA
JAG1_e9	R	ATCCTTGATGGGGACCGTGT	JAG1_e26 /10	R	TCTCCTAATAACTGTTCCCACGG
JAG1_11	F	GCCAAACCTTGTGTAAACGC	JAG1_e9	F	ACAGAAGACGAGCGTGTGGC

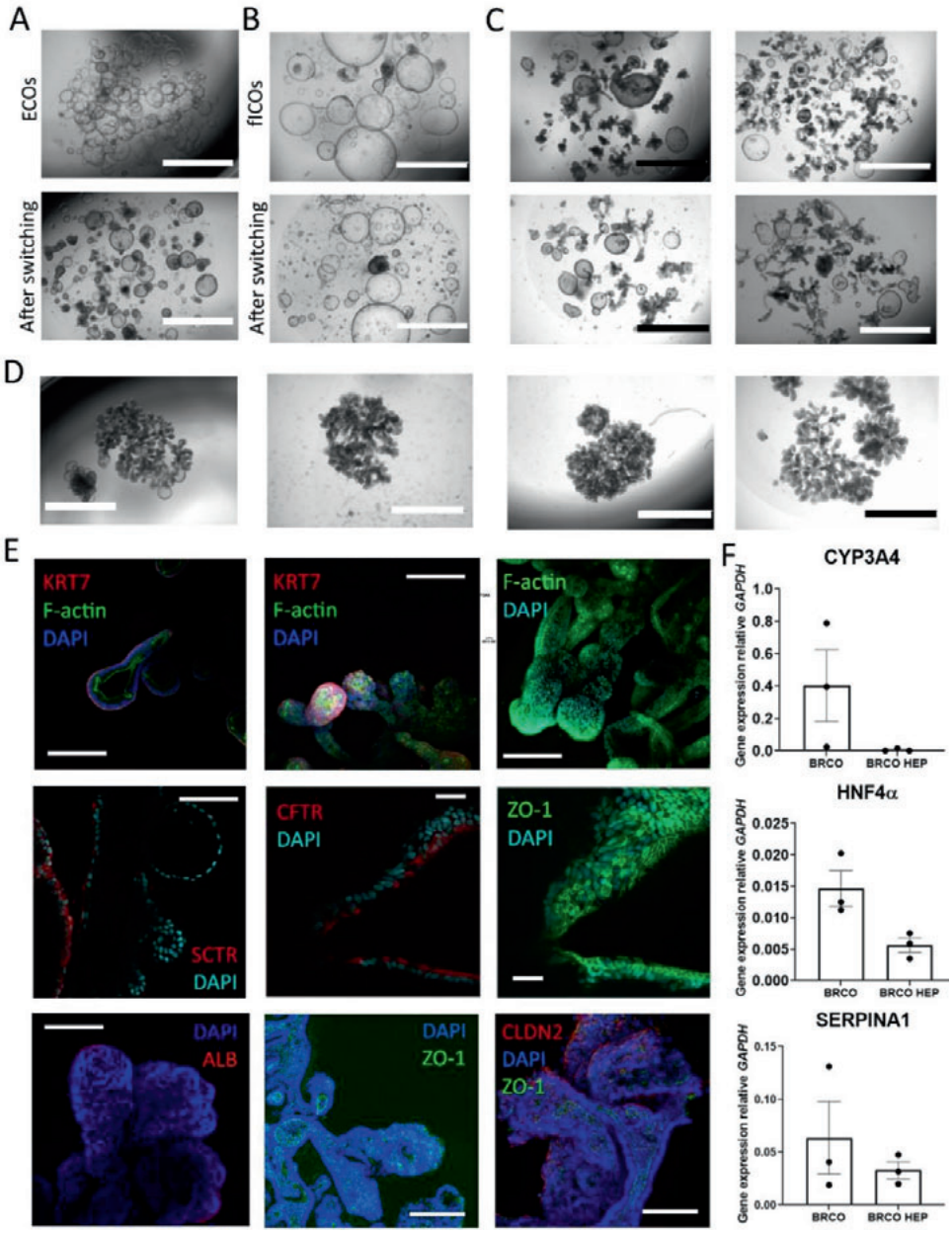

Figure S1. BRCOs represent complex tubular cholangiocyte organoids that can only be established from intrahepatic cholangiocytes.

(a) Organoids derived from the extrahepatic part of the biliary tree do not form BRCOs after switching (n=3). **(b)** Organoids derived from fetal liver biopsies do not form BRCOs after switching culture

conditions (n=3). **(c)** The percentage of BRCOs differs between cultures after switching. **(d)** Different examples of BRCOs from 4 different individual donors, scale bars in a-d represent 2000 µm. **(e)** Whole mount confocal images of BRCOs reveal the presence of polarized cholangiocyte like cells across an open tubular lumen, similar to the *in vivo* situation, scale bars indicate 100 µm. **(f)** gene-expression as analyzed by qRT-PCR for mature hepatocyte-related genes in BRCOs in expansion and when cultured in hepatocyte-differentiation medium. Values are displayed relative to the housekeeping gene *GAPDH* (all experiments with ECOs and BRCOs in Figure S2 are performed with lines 1-3 for Figure a-e and panel F with line 6-8).

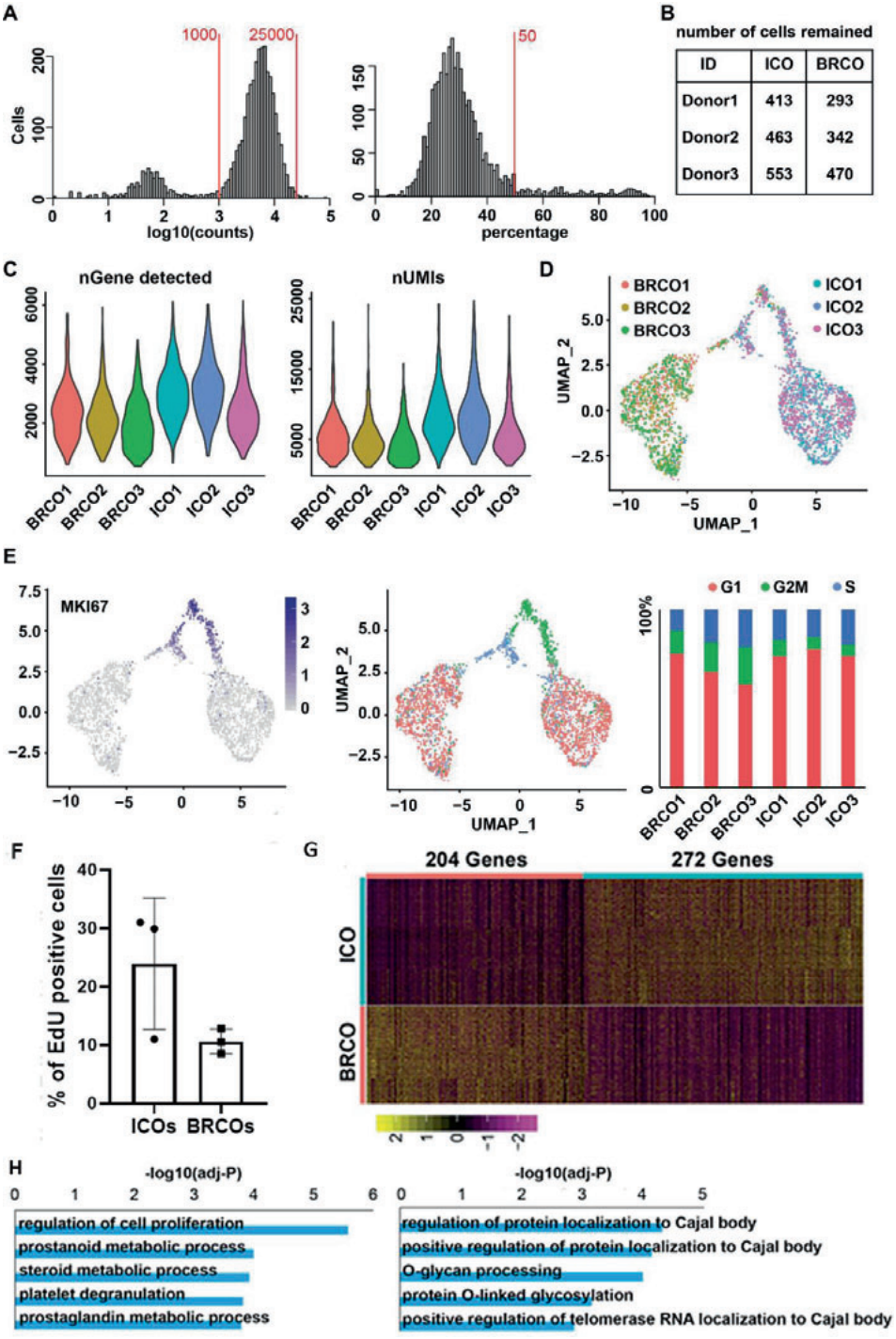
A
1000
25000
50
Cells
log10(counts)
percentage
B
number of cells remained
ID | ICO | BRCO
Donor1 | 413 | 293
Donor2 | 463 | 342
Donor3 | 553 | 470
C
nGene detected
nUMIs
BRCO1
BRCO2
BRCO3
ICO1
ICO2
ICO3
D
UMAP_1
UMAP_2
E
MKI67
G1
G2M
S
F
% of EdU positive cells
ICOs
BRCOs
G
204 Genes
272 Genes
ICO
BRCO
H
-log10(adj-P)
regulation of cell proliferation
prostanoid metabolic process
steroid metabolic process
platelet degranulation
prostaglandin metabolic process
regulation of protein localization to Cajal body
positive regulation of protein localization to Cajal body
O-glycan processing
protein O-linked glycosylation
positive regulation of telomerase RNA localization to Cajal body

Figure S2. BRCOs are significantly limited in their proliferation compared to ICOs.
(a) Histograms showing the numbers of UMIs (in log10 format) in each cell on the left, and percentage of mitochondrial gene expression per cells on the right. Only the cells following the criteria (1000 < unique transcripts < 25000, MT% < 50%) are used for the analysis. **(b)** Number of ICO and BRCO cells from different donors remained after the filtering. **(c)** Violin plots of numbers of detected genes (on the left) and UMIs (on the right) from both ICOs and BRCOs. Cells are grouped based on the cell types and donors. **(d)** UMAP plot showing the single cells colored by cell types and donors. **(e)** Expression UMAP plot for MKI67 gene. Color bar indicates log2 normalized read counts (on the left). UMAP plot of single cells colored by different cell-cycle phases (G1, G2M, and S phases), and the distribution of cells by cell-cycle phase (on the right). Cells are grouped by cell types and donors. **(f)** Percentage of positive single cells in organoids after 4 hours of EdU incorporation as analyzed by flow cytometry on paired BRCO and ICO samples (n=3). **(g)** Heatmap of the differentially expressed genes up-regulated in BRCOs (n=204 genes) and ICOs (n=272 genes). **(h)** GO analysis (biological process) for the same gene sets from the DE gene analysis. Only the top five most significant pathways are listed here.

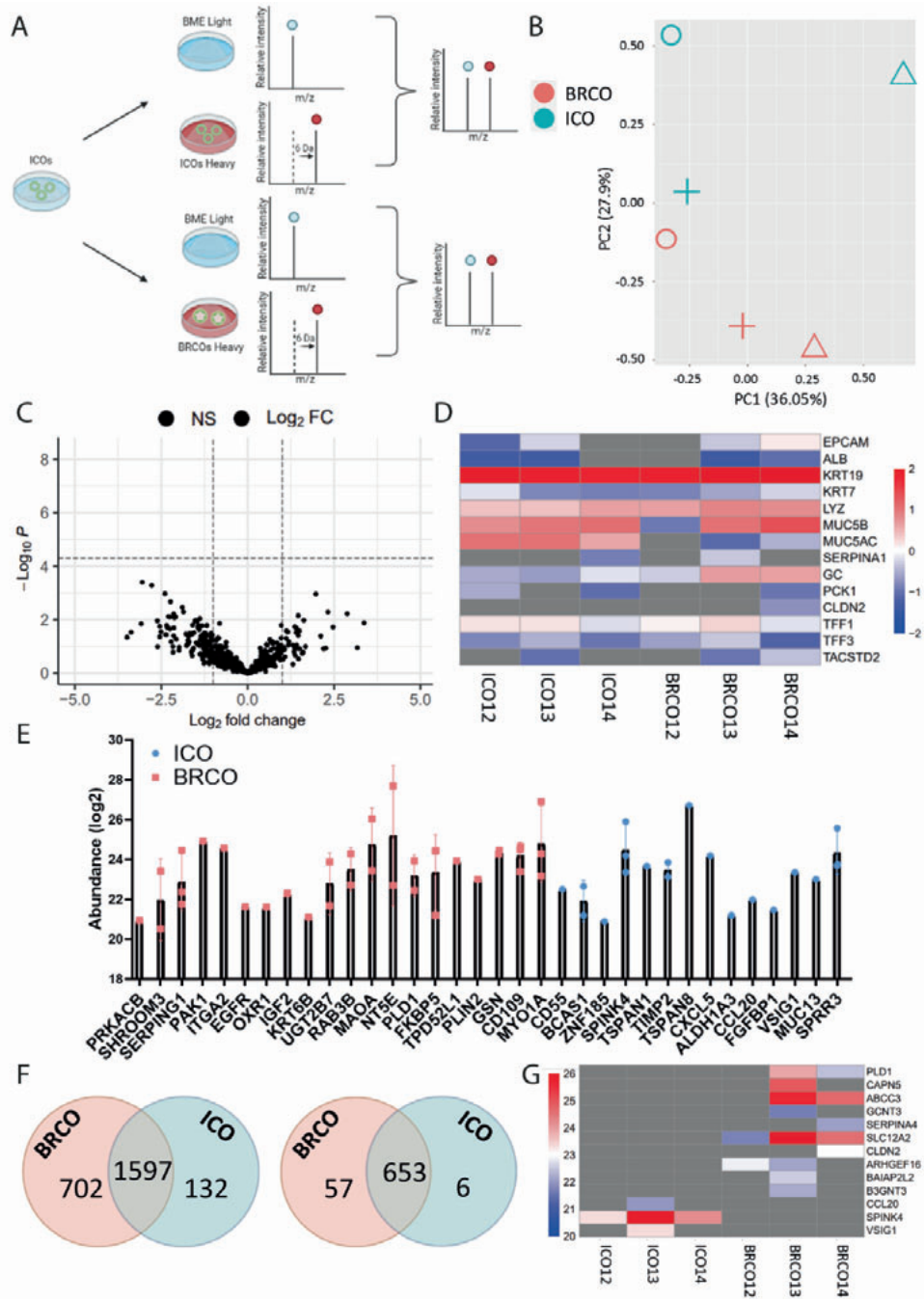
A
BME Light
ICOs
ICOs Heavy
BME Light
BRCOs Heavy
Relative intensity
m/z
6 Da
B
BRCO
ICO
PC2 (27.9%)
PC1 (36.05%)
C
NS
Log2 FC
−Log10 P
Log2 fold change
D
EPCAM
ALB
KRT19
KRT7
LYZ
MUC5B
MUC5AC
SERPINA1
GC
PCK1
CLDN2
TFF1
TFF3
TACSTD2
ICO12
ICO13
ICO14
BRCO12
BRCO13
BRCO14
E
ICO
BRCO
Abundance (log2)
PRKACB
SHROOM3
SERPING1
PAK1
ITGA2
EGFR
OXR1
IGF2
KRT6B
UGT2B7
RAB3B
MAOA
NT5E
PLD1
FKBP5
TPD52L1
PLIN2
GSN
CD109
MYO1A
CD55
BCAS1
ZNF185
SPINK4
TSPAN1
TIMP2
TSPAN8
CXCL5
ALDH1A3
CCL20
FGFBP1
VSIG1
MUC13
SPRR3
F
BRCO
ICO
702
1597
132
BRCO
ICO
57
653
6
G
PLD1
CAPN5
ABCC3
GCNT3
SERPINA4
SLC12A2
CLDN2
ARHGEF16
BAIAP2L2
B3GNT3
CCL20
SPINK4
VSIG1
ICO12
ICO13
ICO14
BRCO12
BRCO13
BRCO14

Figure S3. Protein expression analysed by SILAC reveals differences between BRCOs and ICOs.
(a) Schematic overview of the experiment. **(b)** PCA plot displaying overall protein abundance values of paired BRCOs and ICOs. Intensity values were transformed using variance stabilizing transformation before plotting. The different shapes represent different organoid lines. Only proteins present in all conditions were taken into consideration. **(c)** A volcano scatter plot of statistical significance (adj. P-value <0.05) vs. magnitude of change (Log2FC) showing no overall DE proteins present between BRCOs and ICOs. Only proteins present in all conditions were used for analysis. **(d)** Heatmap showing protein abundance levels of previously described cholangiocyte (organoid) markers (EPCAM, KRT19, KRT7, LYZ, MUC5B, TACSTD2, TFF1, and TFF3) and hepatocyte related markers (ALB, GC, PCK1, and SERPINA1). All data was transformed and z-scored per sample (see legend). Grey values represent non-detected protein levels in the sample. **(e)** Interleaved scatter plot of matched exclusive proteins and DEGenes from the scRNAseq analysis for both BRCOs and ICOs. Each dot represents an overlap in that particular gene and corresponding protein for a sample. **(f)** Protein overlaps and exclusivity when applying loose criteria (present in 1 of 3 samples, not present in 3 of 3 samples of other group, left) and stringent criteria (present in 3 of 3 samples, not present in 3 of 3 samples of another group, right). **(g)** Uniquely produced proteins according to loose criteria in BRCOs and ICOs, correlated to DE proteins in primary cholangiocytes (from the gallbladder) as previously described.[26] All experiments performed in this Figure are with lines 12-14 (3 biological replicates for ICOs and BRCOs).

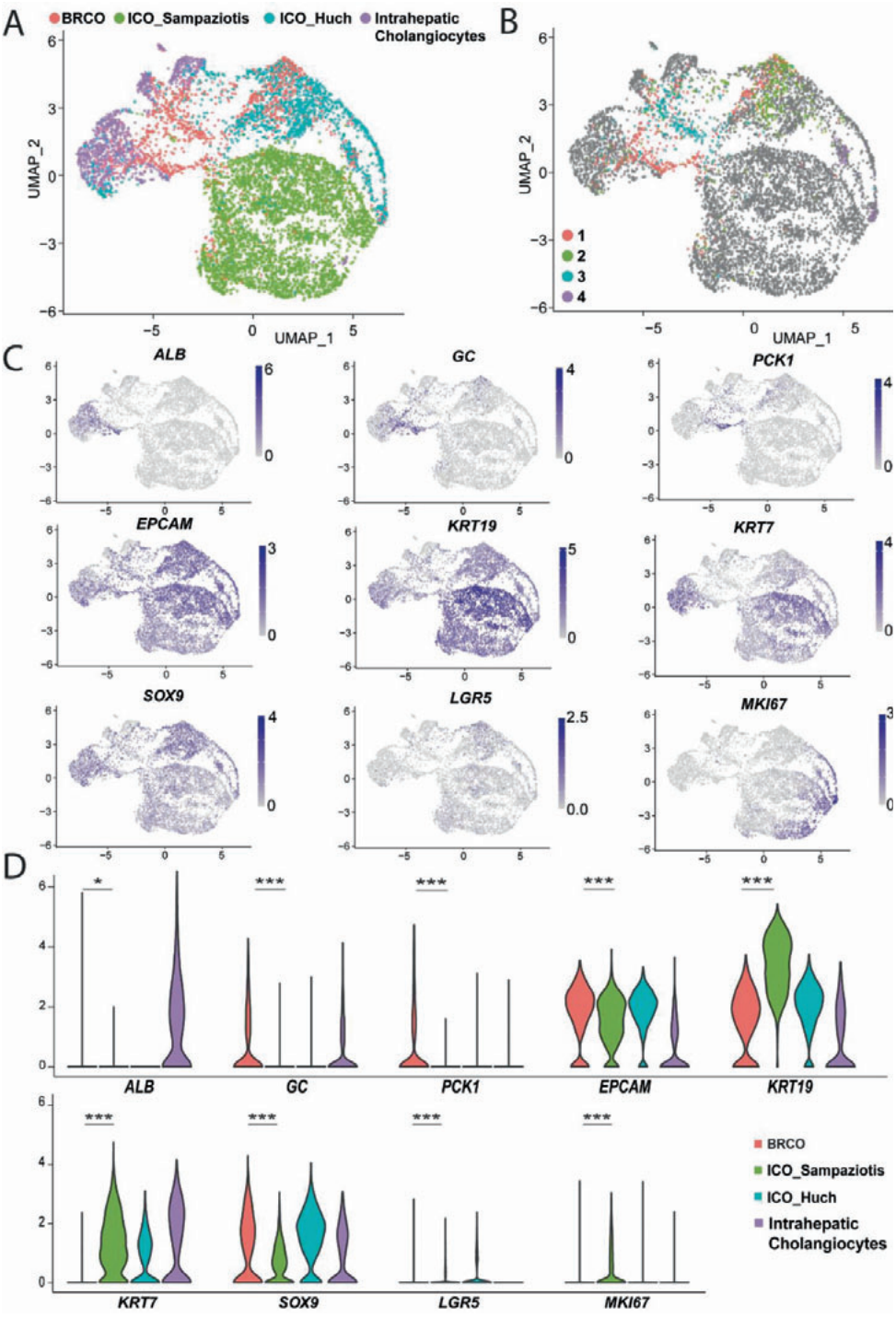
A
BRCO
ICO_Sampaziotis
ICO_Huch
Intrahepatic Cholangiocytes
UMAP_2
UMAP_1
B
1
2
3
4
C
ALB
GC
PCK1
EPCAM
KRT19
KRT7
SOX9
LGR5
MKI67
D
ALB
GC
PCK1
EPCAM
KRT19
KRT7
SOX9
LGR5
MKI67
BRCO
ICO_Sampaziotis
ICO_Huch
Intrahepatic Cholangiocytes

Figure S4. scRNAseq. demonstrate transcriptomic differences between BRCOs and ICOs.
(a) UMAP plots of single cells isolated from ICOs cultured according to Huch *et al.* [7] (n=3, ICO_Huch), BRCOs (n=3), and integrated with the scRNAseq data from Sampaziotis *et al.*[37] consisting of ICOs cultured according to Tysoe *et al*.[12] (n=1, ICO_Sampaziotis) and matching intrahepatic cholangiocytes (n=1). Cells colored by different cell types (on top). **(b)** UMAP plots of the different clusters present in BRCOs (cluster 1-4) of Figure 4B, and colored matched according to Figure 4B. **(c)** UMAP plots showing expression levels of previously described cholangiocyte organoid markers (*EPCAM*, *SOX9*, *KRT19* and *KRT7*), WNT-target gene *LGR5*, proliferation marker *Ki67* and hepatocyte related markers (*ALB*, *GC* and *PCK1*). **(d)** Expression violin plot showing the transcription levels of the selected genes in **c**. Only transcriptomic differences between ICO_Sampaziotis and BRCOs are shown. * P<0.05, *** p<0.001 by Wilcox test.

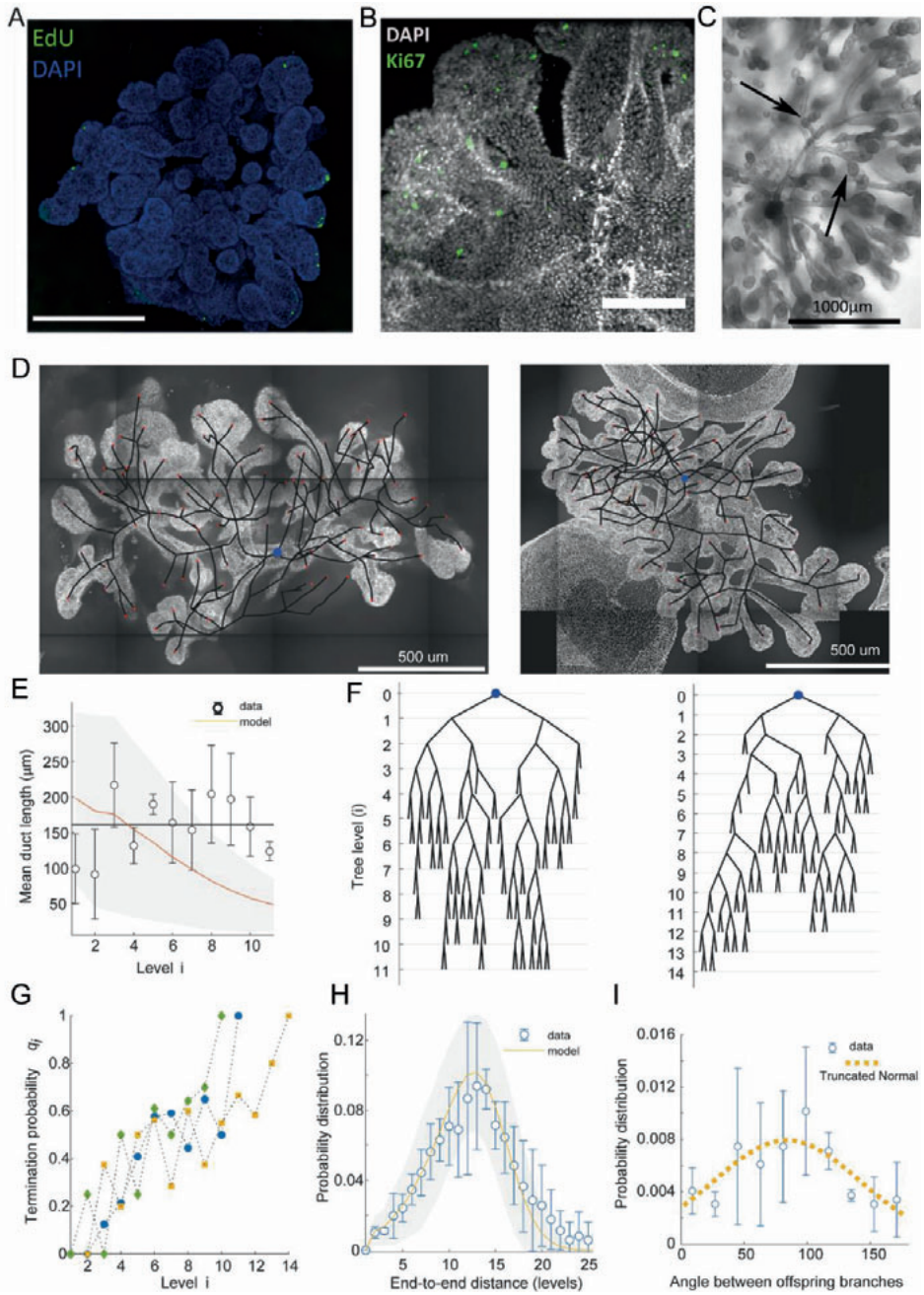
A
EdU
DAPI
B
DAPI
Ki67
C
1000µm
D
500 um
500 um
E
data
model
Mean duct length (µm)
Level i
F
Tree level (i)
G
Termination probability q_i
Level i
H
data
model
Probability distribution
End-to-end distance (levels)
I
data
Truncated Normal
Probability distribution
Angle between offspring branches

Figure S5. BRCOs network reconstruction and statistics.
(a-b) Max-projection of confocal image of EdU (green) incorporation and Ki67 (green), nuclei are counterstained with DAPI (blue and grey), scale bars indicate 500µm (left) and 200 µm (right). **(c)** Close-up of the internal ductal structure of a BRCO, arrows indicate arrested tips. **(d)** Single z-slice of two 3D confocal BRCO images overlaid with the full reconstructed ductal networks (gray lines), the position identified as the sources are indicated in blue. **(e)** Average duct-length as a function of the level in the tree, markers indicate the average and error bars the SD from three n = 3 repeats, the model predictions are shown in orange and its SD by the shaded area. **(f)** Branching tree corresponding to the organoids shown in panels **(d)**, left organoids is left tree and the right organoids is the right tree. **(g)** Termination probability as a function of the level in the tree, for each independent repeat. **(h)** End-to-end node distance distribution obtained from experiments (blue, error bars show the SD), and model (orange, shaded area = SD). **(i)** Distribution of angles formed by two offspring branches, measured from n=3 samples, showing peak around 95 degrees. All experiment conducted in this Figure are performed on BRCO10 and a technical duplicate of BRCO 9.

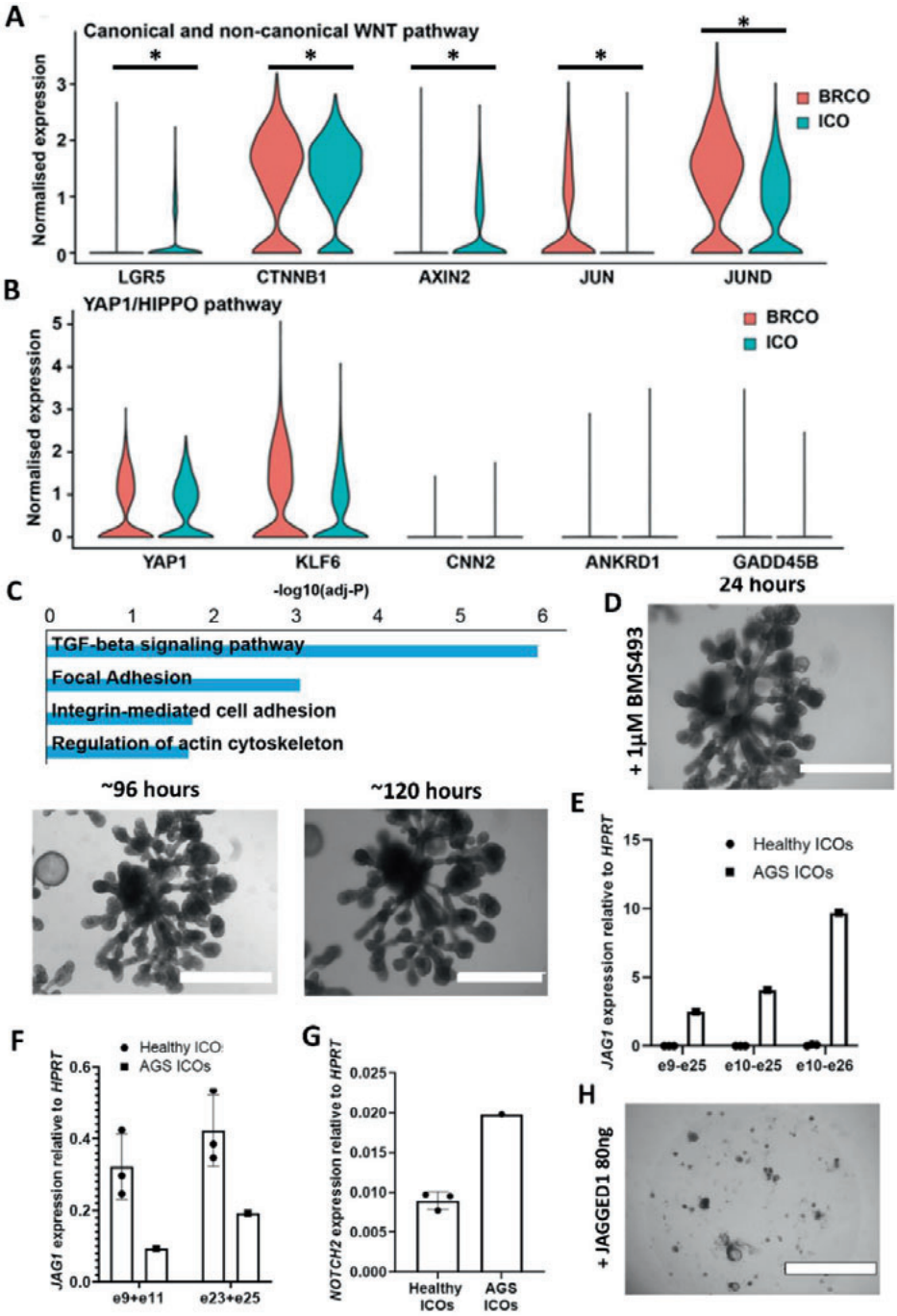
A
Canonical and non-canonical WNT pathway
Normalised expression
BRCO
ICO
LGR5
CTNNB1
AXIN2
JUN
JUND
B
YAP1/HIPPO pathway
Normalised expression
BRCO
ICO
YAP1
KLF6
CNN2
ANKRD1
GADD45B
C
-log10(adj-P)
TGF-beta signaling pathway
Focal Adhesion
Integrin-mediated cell adhesion
Regulation of actin cytoskeleton
D
24 hours
+ 1µM BMS493
~96 hours
~120 hours
E
JAG1 expression relative to HPRT
Healthy ICOs
AGS ICOs
e9-e25
e10-e25
e10-e26
F
JAG1 expression relative to HPRT
Healthy ICOs
AGS ICOs
e9+e11
e23+e25
G
NOTCH2 expression relative to HPRT
Healthy ICOs
AGS ICOs
H
+ JAGGED1 80ng

Figure S6. Pathways important for branching in BRCOs.
(a-b) Violin plots showing the expression of selected genes involved in different pathways (*LGR5*, *CTNNB1*, *AXIN2*, *JUN*, and *JUND* from WNT pathway; *YAP1*, *KLF6*, *CNN2*, *ANKRD1*, and *GADD45B* from YAP1/HIPPO pathway). Cells were grouped based on the cell types. **(c)** Cytoskeletal pathway analysis of ICOs and BRCOs (n=3) obtained via scRNAseq. **(d)** BMS493 addition (1µM) does not inhibit branching 120 hours of culture, scale bars indicate 200 µm. **(e-f)** JAG1 expression of specific exons in healthy (n=3) and AGS ICOs relative to *HPRT*. **(g)** qPCR of *NOTCH2* in healthy ICOs (n=3) compared to AGS ICOs relative to *HPRT*. **(h)** Chimeric JAGGED1 addition to culture media does not result in formation of BRCOs in the AGS patient after switching culture conditions. Experiments in panel a-c (scRNAseq) are performed with ICOs and BRCO 6,7 and 10. Panel d with ICOs and BRCOs 7-9 and f-h with ICO 12, 15 and 16. * P<0.05 by Wilcox test.

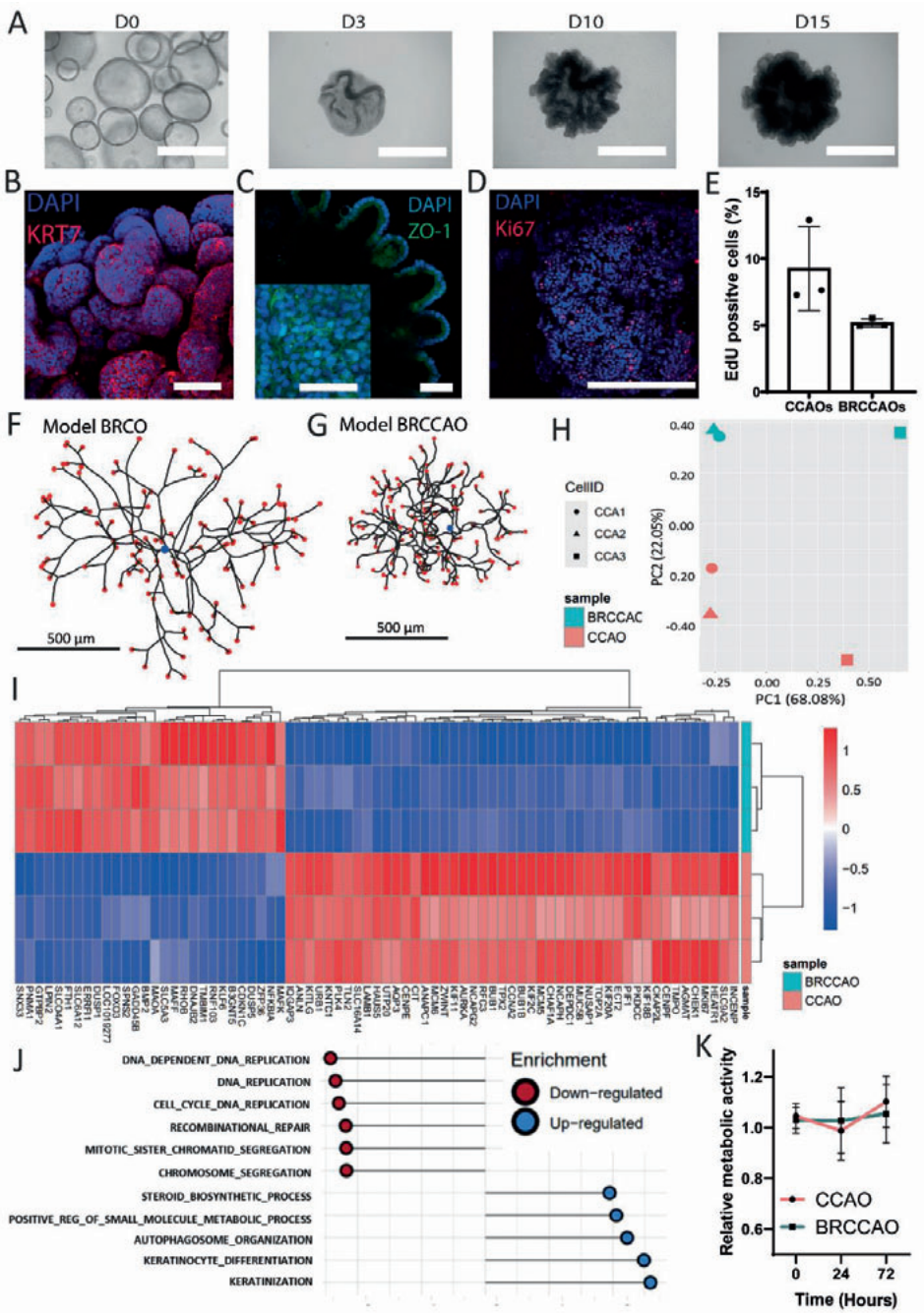
A
D0
D3
D10
D15
B
DAPI
KRT7
C
DAPI
ZO-1
D
DAPI
Ki67
E
EdU possitve cells (%)
CCAOs
BRCCAOs
F
Model BRCO
500 µm
G
Model BRCCAO
500 µm
H
CellID
CCA1
CCA2
CCA3
sample
BRCCAC
CCAO
PC2 (22.05%)
PC1 (68.08%)
I
sample
BRCCAO
CCAO
J
DNA_DEPENDENT_DNA_REPLICATION
DNA_REPLICATION
CELL_CYCLE_DNA_REPLICATION
RECOMBINATIONAL_REPAIR
MITOTIC_SISTER_CHROMATID_SEGREGATION
CHROMOSOME_SEGREGATION
STEROID_BIOSYNTHETIC_PROCESS
POSITIVE_REG_OF_SMALL_MOLECULE_METABOLIC_PROCESS
AUTOPHAGOSOME_ORGANIZATION
KERATINOCYTE_DIFFERENTIATION
KERATINIZATION
Enrichment
Down-regulated
Up-regulated
K
Relative metabolic activity
CCAO
BRCCAO
Time (Hours)

Figure S7. Additional characterization of BRCCAOs.

(a) Bright field images of growth of BRCAOs. T=0 is defined as the day of switching medium from expansion medium to non-canonical WNT stimulating medium. Total time period is 15 days. Scale bars indicate 400 µm. **(b)** Whole mount confocal image of BRCCAO for KRT7 (red), nuclei are counterstained by DAPI (blue), scale bar indicates 200 µm. **(c)** Immunofluorescence staining of BRCCAOs for Zonula occludens-1 (ZO-1, green) and nuclei (DAPI, blue) indicating no cell polarization in the branching structures. Bottom-left shows a magnification of the center (non-branching part) of the same BRCCAO with ZO-1 signal indicating cell polarity and tight junction presence. Scale bars indicate 100 µm**. (d)** Whole mount confocal image of Ki67, a marker for proliferation, showing no evidence for tip-driven growth occurring. Scale bar indicates 400 µm. **(e)** Percentage of positive cells for EdU incorporation as analyzed by flow cytometry in CCAOs and BRCCAOs (n=3). **(f)** Representative BRCO and in **(g)** a BRCCAO obtained from numerical simulations of the theoretical model, scale is equal for both schematics (see Methods for parameter values). **(h)** PCA plot displaying paired CCAOs and BRCCAOs. **(i)** Heatmap of top 75 DE genes when comparing BRCCAOs and CCAOs. **(j)** GSEA of the top 5 GO: biological processes up and downregulated in BRCCAOs. **(k)** Metabolic activity indicating cellular activity over the period of 72h before addition of (chemo)therapeutics. No significant difference can be observed. All experiments for BRCCAOs and CCAOs are performed with the biological triplicates.

PART IV

REGENERATIVE MEDICINE

IV

9

CHAPTER 9

Scaffolds obtained from decellularized human extrahepatic bile ducts support organoids to establish functional biliary tissue in a dish.

Jorke Willemse, Floris JM Roos, Iris J Voogt, Ivo J Schurink, Marcel C Bijvelds, Hugo R de Jonge, Luc JW van der Laan, Jeroen de Jonge, Monique MA Verstegen

Biotechnology and Bioengineering 2021 Feb;118(2):836-851.

Abstract

Biliary disorders can lead to life-threatening disease and are also a challenging complication of liver transplantation. As there are limited treatment options, tissue engineered bile ducts could be employed to replace or repair damaged bile ducts. We explored how these constructs can be created by seeding hepatobiliary LGR5$^+$ organoids onto tissue-specific scaffold. For this, we decellularized discarded human extrahepatic bile ducts (EBD) that we recellularized with organoids of different origin, that is, liver biopsies, extrahepatic bile duct biopsies, and bile samples. Here, we demonstrate efficient decellularization of EBD tissue. Recellularization of the EBD extracellular matrix (ECM) with the organoids of extrahepatic origin (EBD tissue and bile derived organoids) showed more profound repopulation of the ductal ECM when compared with liver tissue (intrahepatic cholangiocyte) derived organoids. The bile duct constructs that were repopulated with extrahepatic cholangiocytes organoids expressed mature cholangiocyte-markers and had increased electrical resistance, indicating restoration of the barrier function. Therefore, the organoids of extrahepatic sources are identified to be the optimal candidate for the development of personalized tissue engineered EBD constructs.

Introduction

Biliary complications, such as bile leaks and anastomotic strictures, occurring after donation after circulatory death (DCD) liver transplantation (LT) are common and a major cause of posttransplant complications and morbidity.[1,2] In DCD LT, the biliary epithelial lining of the extrahepatic bile ducts (EBD) is more prone to damage, due to the prolonged warm ischemia period in the donor. This results in a higher incidence of ischemia type biliary lesions, which leads to more diffuse nonanastomotic biliary strictures, when compared with donation after brain death (16% vs. 3%).[3,4] Current treatment options, such as endoscopic retrograde cholangiopancreatography and hepaticojejunostomy, often fail to restore biliary drainage and up to 65% of patients with ischemic cholangiopathy after LT require retransplantation.[4] Personalized regenerative medicine strategies could prevent the need for retransplantation of the whole liver in case the donor liver is failing due to aforementioned complications. Damaged extrahepatic bile duct (EBD) can be replaced with functional tissue engineered constructs, preferably built using the autologous cells. These strategies can potentially relief the intense pressure on the already limited donor organ pool. The EBD is not merely a “simple tube” that transports cytotoxic bile, as the EBD contains complex tortuous networks of peribiliary glands (PBG) and blood vessels. The PBG can be found in- (intramural) and outside (extramural) the wall of the EBD and play an important role in maintaining homeostasis and bile duct regeneration after injury.[5] The PBG are surrounded by small blood vessels, which are also known as the peribiliary vascular plexus. Recreating these small glandular and tortuous structures *in vitro* with high precision is challenging. Therefore, the use of decellularized extracellular matrix (ECM) could be an interesting alternative for recreating EBD tissue *in vitro*, where the decellularized ECM functions as a scaffold or the EBD.[6] The decellularized scaffolds need to be repopulated with biliary cells to restore the vital barrier function of the bile duct against the cytotoxic bile. Human LGR5^{+} cholangiocyte organoids are an interesting source of functional biliary cells, as organoids offer long-term stable *in vitro* expansion of cholangiocytes.[7,8] This allows for the generation of large numbers of autologous cells *in vitro* from relatively small (liquid) biopsy samples. The organoid cultures can be established from liver biopsies (intrahepatic cholangiocyte organoids [ICO])[8], EBD tissue (extrahepatic cholangiocyte organoids [ECO])[9,10], and bile samples (bile-cholangiocyte organoids [BCO]).[11] The cells that give rise to these cholangiocyte organoids are EPCAM positive and organoids from all three sources maintain cholangiocyte-specific markers (e.g., EPCAM, cytokeratin 7 [KRT-7] or cytokeratin 19 [KRT-19]) and functionality.[7-12] Furthermore, relative small biopsies (0.5–1.0 g tissue or 1 mL of bile) are adequate to initiate cultures, which subsequently can yield millions of cells.[13,14] These characteristics make the organoids ideal cell sources for the repopulation of decellularized EBD scaffolds in an effort to create functional tissue engineered bile ducts *in vitro*. However, whether cholangiocyte organoids from all three sources are capable of efficient repopulation and restore the vital barrier

function of the EBD, is yet to be determined. Therefore, we aimed to develop an *in vitro* model for bile duct tissue engineering in which the recellularization capacity and, moreover, bile duct functionality after recellularization of the cholangiocyte organoids collected from the three sources, can be assessed. We first developed an efficient decellularization protocol for human EBD tissue to obtain ductal ECM. Subsequently, ICO, ECO, and BCO were expanded and used to recellularize the decellularized EBD scaffold. Confluency was used as a measure for the seeding efficiency of the epithelial monolayer. Furthermore, we analyzed expression of cholangiocyte markers and tested biliary function of the tissue engineered constructs.

Materials and Methods

Sample procurement for decellularization

Biopsies of healthy EBD tissue (N = 26) were collected during LT. Before transplantation, the duct of the donor organ is shortened to make the anastomosis with the recipients' bile duct. The removed section (usually 3–10 mm) was stored in Belzer UW cold storage solution (UW; Bridge to Life) at 4°C. Four segments (3–5 mm by 3–5 mm) were cut from the biopsy. One segment was used for organoid initiation (see sample procurement for organoid initiation, N = 5). The second segment was fixed in 4% paraformaldehyde (PFA; Fresenius Kabi) for histological analysis. The two other segments were snap frozen in liquid nitrogen and stored at −80°C for biochemical analysis purposes. The remaining EBD tissue was stored in 1× phosphate-buffered saline (PBS) at −20°C until decellularization. The use of these biopsies for research purposes was approved by the Medical Ethical Council (MEC) of the Erasmus University Medical center (MEC-2014-060) and patients gave their written informed consent. Full length EBD tissue (average length: 3–5 cm, N = 8) was obtained from human research livers. These livers were deemed unsuitable for clinical transplant procedures in the EuroTransplant zone by all transplant centers, due to a variety of reasons, such as steatosis and/or age (N = 8). No organ retrieval was initiated for research purposes only. In all cases, next of kin gave informed consent for research to Transplant Coordinators of the Dutch Transplantation Society (NTS). The use of research liver was approved by the Erasmus MC medical ethics committee (MEC-2012-090). After organ procurement, the liver was stored in UW organ preservation fluid (Bridge to life) on ice and shipped to the Erasmus MC, where the EBD was surgically removed from the liver. Small biopsy samples were taken in a similar manner as previously described, except for organoid initiation. The remaining EBD tissue was placed in PBS and stored at −20°C.

Sample procurement for organoid initiation

Biopsies of liver tissue (0.5–2 cm^3; N = 5) and EBD tissue (N = 5) were obtained for organoid initiation during LT at the Erasmus University Medical Center Rotterdam from healthy donor tissue (N = 3) and diseased explant tissue (N = 2; recurrent primary sclerosing cholangitis and Wilson's disease). Liver and EBD biopsies were donor or patient paired. The use of these biopsies for research purposes was approved by the Medical Ethical Council or the Erasmus University Medical Center (MEC-2014-060) and written informed consent was given by the next of kin of the donor or by patients. Biopsies were stored and transported in UW preservation fluid on ice. Bile (1 mL) was collected from patients (N = 3) undergoing ERCP procedures during treatment for primary sclerosing cholangitis, bile leakage, or choledocholithiasis. The use of bile samples for research purposes was approved by the Medical Ethical Council of the Erasmus University Medical Center (MEC-2016-743). All patients gave written informed consent. Samples were stored and transported on wet ice.

Decellularization

The EBD was washed with dH_2O until all traces of blood or bile were removed from the EBD. The lumen of the full-length EBD was flushed using a blunt needle. Subsequently, the ductal tissue was incubated with Trypsin-EDTA (TE) (0.05%, Gibco) for 30 min at 37°C on an orbital shaker. TE was washed away with dH_2O for 15 min. Subsequently, the EBD was placed in 50 ml of 4% Triton-X-100 + 1%NH_3 (T×100 solution) on an orbital shaker at room temperature (RT). T×100 solution was replaced every 30 min until 10 cycles were reached. The EBD tissue was placed in 50 mL dH_2O for 5 min. and dH_2O was refreshed 10 times. The decellularized EBD tissue was stored in 50 mL dH_2O at 4°C for 5–7 days to remove traces of T×100. dH2O was refreshed every 1 or 2 days. The decellularized duct was incubated with DNase solution (Table S1) for 4 hours at 37°C on an orbital shaker. Afterwards, the EBD was placed in 50 mL 0.9% saline solution, which was refreshed three times. Biopsy samples were taken for histological and DNA analysis.

Histology

PFA-fixed samples were embedded in paraffin and sectioned at 4 µm. Sections of before and after decellularization samples were stained with hematoxylin and eosin (H&E) or 4',6-diamidino-2-phenylindole (DAPI; Vectashield, Vectorlabs). H&E-stained slides were imaged with Zeiss Axiokop 20 microscope and captured with a Nikon DS-U1 camera. DAPI stained slides were analyzed using EVOS microscope (Thermo Fisher Scientific). Immunohistochemistry (IHC) staining was performed on before and after decellularization samples with Collagen Type I and Collagen type IV (Table S4). Antigen retrieval was performed in citrate buffer (pH = 6.0) at subboiling temperatures for 10 min. Primary antibodies were incubated over night at 4°C. Envision + system horseradish peroxidase antirabbit secondary antibody (DAKO) was incubated at RT for 60 min, before staining with 3'-diaminobenzidine and counterstained with hematoxylin.

Scanning electron microscopy

Small PFA-fixed biopsies (before and after decellularization, N = 2) were dehydrated with ethanol and hexamethyldisilazane (Sigma) series before gold sputtering (15 µm) using a Quorum Q300TD sputtering device (Quorumtech). Biopsies were imaged with a JSM-7500F field emission electron microscope (JEOL).

Biochemical analysis

The wet weight of the samples was weighed before performing analysis. DNA was isolated using a QIAamp DNA mini-Kit (Qiagen) following the manufacturer's protocol. DNA content was measured using a NanoDrop spectrophotometer (Thermo Fisher Scientific; N = 11) and corrected for the corresponding wet weight of the measured sample (ng DNA/mg wet weight tissue). The quality and length of DNA base pairs (BP) was measured using a 2100 BioAnalyzer

(Agilent technologies) using a DNA-1000 kit (Agilent Technologies). Total collagen content of the samples was determined using a Total Collagen Kit (Quickzyme Biosciences, N = 9). Collagen content was measured in a clear 96-well plate at 570 nm using an Omega POLARstar Microplate reader (BMG labtech). The content was corrected for the wet weight of the corresponding samples (µg Collagen/mg wet weight tissue). Sulfated glycosaminoglycan (sGAG) was determined using a Blyscan glycosaminoglycan assay (Biocolor; N=15). Samples were digested in a Papain (Sigma) solution (10 mg/mL) at 65°C for 8 hours. sGAG was isolated from the sample digest according the manufacturers protocol. The sGAG content was measured by absorbance measurements (680 nm) in a clear 96-well plate using a model 680 XR microplate reader (Bio-Rad).

Recellularization

Organoid initiation was similar as previously described (ICO and ECO).[8,9] See Figure 1B for a schematic overview of organoid initiation and the section "Sample procurement for organoid initiation" for more details on tissue procurement. In short, biopsies were minced, digested in 2.5 mg/mL collagenase type A (Sigma) for 20 min at 37°C. The cell suspension was strained (70 µm cell strainer) and washed in cold Advanced DMEM/F12 (Adv^+, Table S2). After centrifugation (1500RPM, 5 min., 4°C) the remaining cell pellet was suspended in reduced growth factor basement membrane matrix (BME, Cultrex) solution (70% BME, 30% cold Adv^+). The mixture was plated in 25 µL droplets in a 48-well suspension culture plate (Greiner). The BME solidified at 37°C for 30–45 min before startup medium (SM, Table S3) was added. After 3 days SM was replaced with expansion medium (EM, Table S3).

Initiation bile-cholangiocyte organoids

The obtained bile was suspended in 8 mL cold Adv^+, centrifuged (1500RPM, 5 min., 4°C) and the supernatant was removed. This procedure was repeated once. The remaining cell pellet was suspended in 3 mL cold Adv+, strained (100 µm cell strainer) and centrifuged. The cell pellet was suspended in 70% BME solution and cells were treated similar to ICO and ECO.

Culturing organoids

EM was refreshed of all three types of organoids every 3 to 4 days. Organoids were split in 1:4 to 1:6 ratios every 7 to 10 days depending on proliferation rate of the cells by mechanical dissociation and replating of organoids fragments in fresh BME.

Preparation of the ECM

Full length decellularized EBD was cut open along the longitudinal axis (Figure 1A). Circular discs (Ø 3 mm) were cut using disposable dermal biopsy punches (Stiefel). The discs were collected in 50 mL 1× PBS and washed in PBS three times. This was repeated with Adv^+ and with Adv^+ supplements with 10× concentration Pen/Strep and primocin. The discs were

incubated overnight at 37°C. The discs were washed in Adv^+. The ECM was placed in the middle of a 48-well 45 min before addition of cells. Residual Adv^+ was removed from the surface and side of the discs.

Recellularization experiments

Organoids were harvested by removing the BME droplets from the wells using cold Adv^+, as previously described (see Figure 1C for a schematic overview). In general, a full BME droplet (average yield: $6.0 * 10^4$ cells, SD: $\pm 2.0 * 10^4$ cells per dome) was used per ECM disc. After removal of BME from the cell pellet, 1 mL TE was added. The suspension was incubated at 37°C until organoid fragments were dissociated into a single cell suspension. The cells were counted using disposable cell counting chambers (Kova). About 10 µL cell suspension was added to the center of the ECM discs.

The samples were incubated at 37°C for 2 hours before 500 µL EM supplemented with 10 µM Y27632 was added to the wells. EM +Y27632 was replaced with EM after 3 days and medium was refreshed every 3 or 4 days. The ECM-cell construct was kept in culture for up to 21 days. Organoid cultures in BME served as a control. After 21 days experiments were terminated. About 4–6 samples were fixed in 4% PFA for 20 min. These samples were used for histological analysis or whole mount staining. These 4–6 samples were lyzed in 700µL Qiazol lysis reagent (Qiagen) and stored at −80°C for quantitative polymerase chain reaction (qPCR) analysis.

Ussing chamber experiments

Larger segments (W: 1 cm, L: 2 cm) of ECM were cut from the EBD using a scalpel. The recellularization procedure was similar to the circular discs recellularization, however, the cell number was increased five-fold (see Figure 1D for a schematic overview). About 5*10 µL cell suspension droplets were used for each segment. Furthermore, EM was refreshed every 1–2 days. After 21 days the segment was cut in two equal sized parts. Each part was placed in an Ussing slider (P2303A, area: 0.10 cm^2, Physiologic Instruments, Figure S2) and subsequently placed in the Ussing chamber (Physiologic Instruments). Decellularized ECM was used as a control for the Ussing chamber experiments. The Ussing chambers were filled with Meyler's medium (Table S7) supplemented with 10 mM glucose. The Ussing chambers were kept at 37°C and a 95% O_2 5% CO_2 gas mixture was bubbled through the chambers. A VCC MC8 voltage clamp module (Physiologic Instruments) was used to clamp the potential difference at 0 mV. The short circuit current (Isc) was recorded using Acquire and Analyze 2.3 software (Physiologic Instruments). Trans epithelial electrical resistance (TEER) measurements was measured by applying three 5 mV spikes. The resistance was calculated according to Ohm's law R = V/I. The resistance of the recellularized constructs was calculated bysubtracting measured resistance value of decellularized ECM ($R_{organoids}=R_{constructs}-R_{decellularized\ ECM}$) $R_{organoids}$ was subsequently corrected for the surface area (A = 0.10 cm^2) of the Ussing slide and TEER = $R_{organoids} * A_{tissueslide}$. Finally, ion-channel activity was

measured. CFTR- dependent anion secretion was activated by adding forskolin (10 µM) to the basolateral side of the constructs and inhibited by addition of GlyH-101 (20 µM, apical). The calcium activated chloride channels (CaCC) were stimulated by addition of UTP (50 µM, apical).

Immunohistochemistry of organoids

Organoids were cultured in BME, fixed in 4% PFA and embedded in paraffin. Subsequently, IHC staining was performed as described previously for the IHC procedure in the histology Section (2.2.1). The primary antibodies (Cytokeratin 7 (KRT-7) and cytokeratin 19 (KRT-19; Table S4) were incubated overnight at 4°C. The secondary antibody (Table S5) was incubated at RT for 60 min. Whole mount confocal imaging was performed on 4% PFA fixed recellularized scaffolds. Recellularized ECM samples were permeabilized with 0.1% Triton-X-100 in 1× PBS for 20 min. The samples were blocked in 5% serum in 1× PBS for 60 min. The primary antibodies (see Table S4) were incubated overnight at 4°C. The secondary antibody (Table S5) was incubated at RT for 60 min. KRT-7 and KRT-19 samples were additionally stained with Phalloidin Alexa Fluor 488 (Thermo Fisher Scientific). All samples were stained with DNA-staining DAPI. Samples were imaged using a Leica ×20 water dipping lens on Leica DM6000 CFS microscope with a LEICA TCS SP5 II confocal system. Images were processed and analyzed using ImageJ.

qPCR gene expression analysis

Qiazol lyzed samples were homogenized using a TissueRuptor (Qiagen). Messenger RNA (mRNA) isolation was performed with the miRNeasy kit according to the manufacturers' protocol. RNA content was measured using a Nanodrop and complementary DNA (500 ng) was prepared using 5× PrimeScript RT Master Mix and a 2720 thermal cycler (Applied Biosystems). qPCR was performed according to standard procedures with SYBR select master mix for SFX (Applied Biosystems) on a StepOnePlus real time PCR System (Applied Biosystems). All the tested primer sets are listed in Table S6. GAPDH, B2M, and HPRT were used as reference genes. The geometrical average of the three housekeeping genes was used as previously described[15] for determining the dCt of the genes.

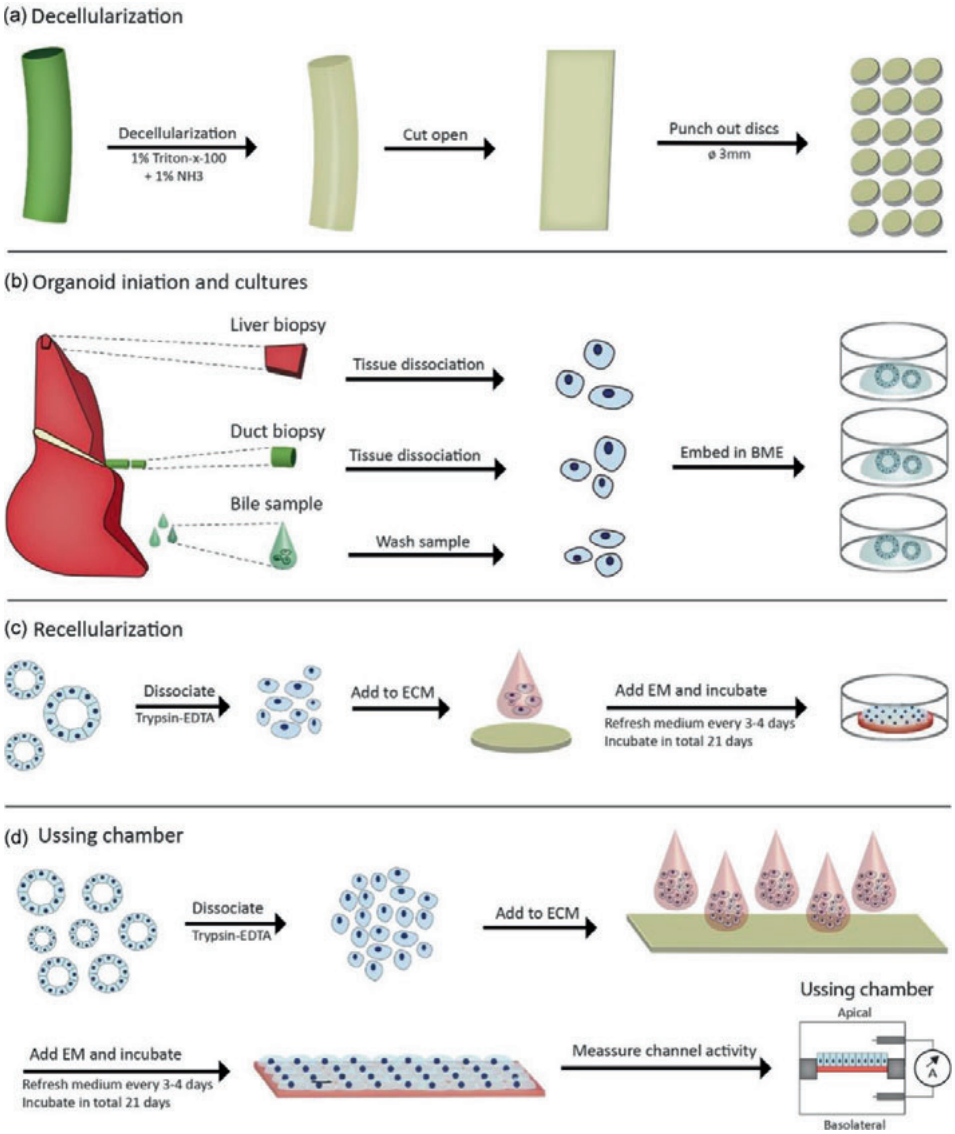

Figure 1. Graphical representation of human EBD decellularization and recellularization procedures. **(a)** Decellularization of EBD tissue was performed with T×100 solution. After decellularization the full-length EBD was cut open along the longitudinal axis and circular discs (Ø3 mm) are punched using a dermal biopsy punch. **(b)** Organoids were initiated from three different sources; intrahepatic cholangiocytes via liver tissue (ICO), EBD tissue (ECO), and bile samples (BCO). The cells obtained from these sources were embedded in BME and cultured as per normal protocol. **(c)** Recellularization experiments start with dissociation of the organoids. A suspension of single cells (10 µL) was added to the ECM and kept in culture for up to 21 days. **(d)** Recellularization experiments for Ussing Chamber

were performed in a similar manner as the normal recellularization experiments. After a 21-day culture period, the recellularized construct was carefully placed inside the Ussing chamber setup, followed TEER and ion-channel activity measurements in Ussing chambers. BCO, bile-cholangiocyte organoids; BME, basement membrane matrix; EBD, extrahepatic bile duct; ECM, extracellular matrix; ECO, extrahepatic cholangiocyte organoids; ICO, intrahepatic cholangiocyte organoids; TEER, trans epithelial electrical resistance.

Data analysis

Analysis of data was performed with Prism (version 8.0, Graphpad Software). Data from DNA, RNA, total collagen, sGAG content, and Nuclei per mm^2 is displayed as mean ± standard deviation (SD). Nonpaired t-test were performed to analyze means. Analysis of variance on ranks was performed for the quantified nuclei data. qPCR data is displayed as 2^{-dCt} in "before–after" graphs, were "before" represents the BME controls and "after" the recellularized constructs of the same donor/patient. Wilcoxon matched pairs tests were performed on qPCR data.

Results

All EBD samples showed severe signs of denudation before decellularization, as no confluent layers of cholangiocytes could be found (Figures 2B and 2D). This was likely the result of ischemia. Due to the denudation, no cholangiocyte RNA of adequate quality could be obtained from fresh EBD tissue. During decellularization, the bile ducts underwent a slight change in color from yellow/white to white (Figure 2A). The decellularization procedure did not affect the dimensions of the EBD, as no shrinking or expansion was witnessed (Figures 2A and S1). However, loose connective tissue fibers surrounding the bile ducts (Figures 2A and S1), detached as a result of gentle agitation on the rocker and was washed away during replacement of T×100 solution. This connective tissue did not contain muscle, extramural PBG or blood vessel structures. Full length EBDs were cut open along the longitudinal axis after the decellularization procedure was completed and showed typical "golf ball-like" surface macroscopically (Figure 2A). The decellularization procedure did not affect the macroscopic architecture of the luminal side of the duct. All cells were efficiently removed during the decellularization procedure (Figure 2B) and no dsDNA (Figure 2C) was detected in the decellularized EBD. DNA quantification (Figure 2G) showed a significant ($p < .001$) decrease in DNA content to 11.9 ng DNA (SD: ±9.2 ng). No fragment of dsDNA could be detected by the BioAnalyzer after decellularization (Figure S1), confirming complete decellularization. The fibrous ultrastructure of the ECM remained intact and was not affected by the procedure as shown by Scanning electron microscopy (SEM; Figure 2D). IHC staining of the decellularized bile ducts for Collagen I and IV showed that these proteins remain present (Figure 2E,F). The total collagen content did not differ significantly ($p = .69$) before (64.9 μg/mg wet tissue, SD: ±21.0 μg/mg) and after decellularization (57.6 μg/mg wet ECM, SD: ±12.9 μg/mg). The sGAG content decreased significantly ($p < .001$) after decellularization (before: 16.4 μg/mg wet tissue, SD: ±6.8 μg/mg; after: 1.4 μg/mg wet ECM, SD: ±1.1 μg/mg), which could be due to the detachment and subsequent removal of connective tissue on the outside of the ductal tissue, however, this was not further determined. Organoids from all three ductal sources proliferated well, were spherical in shape (Figure S2) and were comparable with organoids as previously described by other publications.[8-11] The organoids were KRT-7 and KRT-19 positive (Figure S2). Differences in proliferation patterns were noticed, however, these were attributed to donor-donor variances, as patient/donor paired organoids showed similar characteristics (data not shown). Similar findings were also mentioned by other publications.[8] Furthermore, no significant differences were noted between organoids derived from healthy donor or liver patients, as all organoids were similar in size, shape or proliferation patterns.

Bright field microscopic evaluation of the recellularization experiments was limited as a result of the density of the ECM. However, viable cells surrounding the scaffolds were detected 24 h after initiating the recellularization with organoids from all three sources (Figure 3A). After

7–10 days transparent rim was seen surrounding the edge of the ECM disc in ECO and BCO recellularized samples. In ICO samples, this rim was inconsistent and did not fully cover the entire disc. Cyst-like structures were seen inside the rim (Figure 4A). Between Day 15 and 18 these cystic structures disappeared in ECO and BCO samples and an uninterrupted rim encapsulated the edges of these samples after 21 days (Figure 3A). Cells with columnar phenotypes surrounded the ductal ECM (Figure 3C). This was not consistent with ICO recellularized samples, which had either cells with a flattened phenotypes or cystic structures after 21 days (Figures 3B and 3D).

Whole mount confocal analysis with F-actin staining showed that confluent monolayers covered the entire surface of ECM discs recellularized with ECO and BCO (Figure 3G, H). "Honey comb" -like structure were visible at ×40 magnification (Figure S2), showing that F-actin is located at the edges of the cell membranes, where the cells attach to each other. ECM repopulated with ICO did not reveal similar patterns. Three out of five samples from this source failed to form a confluent layer on the entire surface of the ductal ECM (Figures 3I and S2). The two other samples lacked "honey comb" - like structures. The "success rate" as determined by the number of samples which were fully repopulated upon examination with whole mount confocal imaging is 40% for ICO (Figure 3J), whereas this rate was 100% for ECO and BCO. Quantification of nuclei per set area (Figure S2 contains representative images for all conditions) revealed that ICO repopulated samples contain significantly ($p < .01$) less nuclei per mm^2 (17.1 nuclei per mm^2, SD: ±6.3) than ECO (24.9 nuclei per mm^2, SD: ±4.2) and BCO (25.0 nuclei per mm^2, SD: ±4.6). The difference between completely repopulated ICO samples (confluent, 20.5 nuclei per mm^2, SD: ±5.2) with the partially repopulated ICO samples (not confluent, 12.9 nuclei per mm^2, SD: ±4.8) was also significant ($p < .01$, Figure S2). Even after full repopulation with ICO, the number of nuclei per set area was lower when compared with samples repopulated with ECO and BCO, however, this difference is not significant.

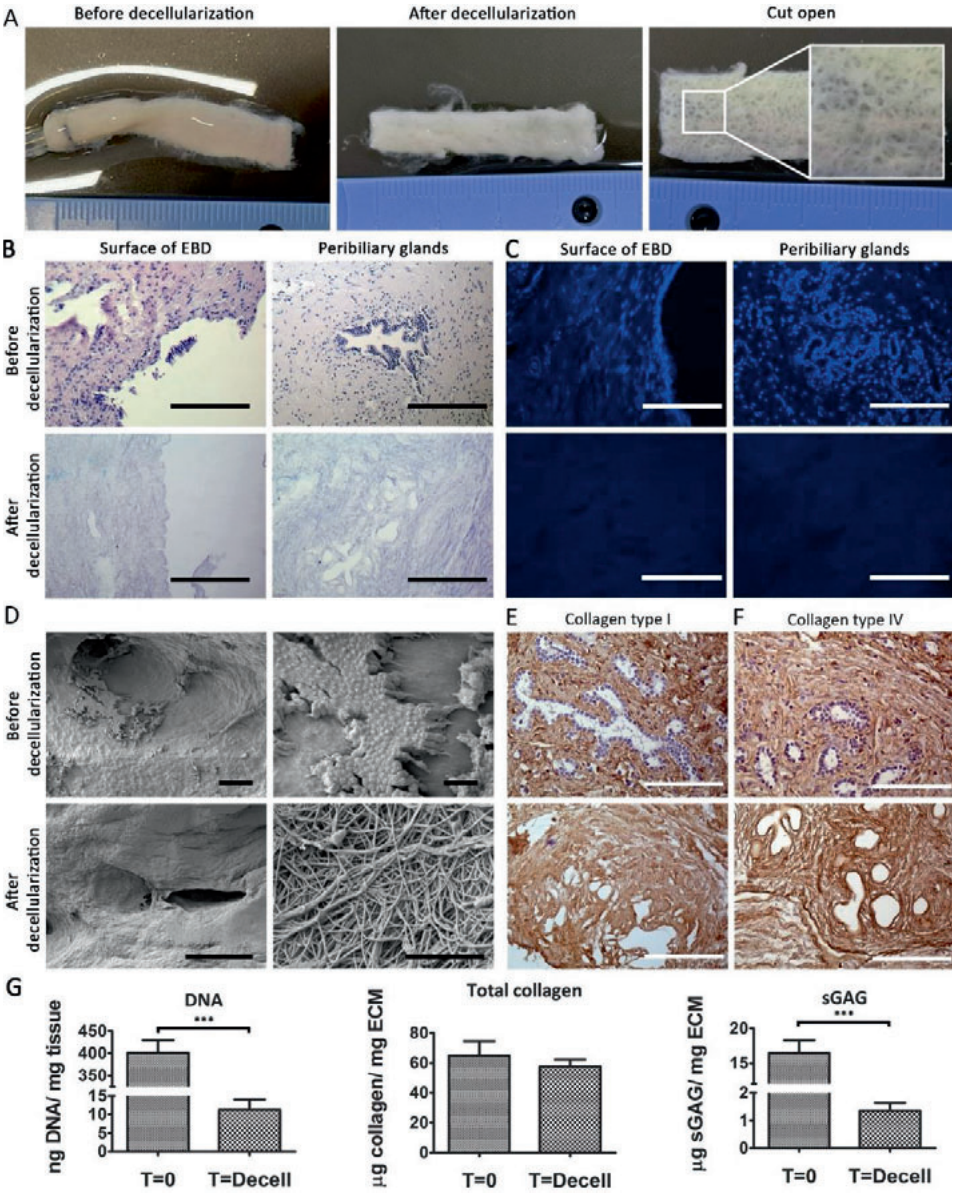

Figure 2. Decellularization of human extrahepatic bile duct tissue is feasible.

(a) Macroscopic images of before and after decellularization. The ostia of the PBG are visible (outtake). **(b)** Before and after decellularization images of H&E-stained paraffin slides showing the surface of the EBD (left) and intramural PBG (right). Scale bars represent: 200 µm. **(c)** DAPI staining revealed that after decellularization no visible dsDNA is present in the decellularized ECM on the surface of the EBD or in the PBGS. Scale bars represent: 200 µm. **(d)** Scanning electron microscopy images before

decellularization shows the expected denudation of the extrahepatic bile duct as only a few cells can be seen at two different magnifications from the same sample. After decellularization all cells were removed and the ultrastructure of the ECM remains intact as is shown by two different magnifications from the same sample. Scale bars represent 200 µm left side, 10 µm top right, 1 µm bottom right. **(e)** Collagen Type I remains present after decellularization. Scale bars represent: 200 µm. **(f)** Collagen type IV remains present in the PBG after decellularization. Scale bar represents: 200 µm. **(g)** Results from the biochemical analyses. DNA drops significantly (***p < .001) after decellularization to 11.9 ng DNA (SD ± 9.2 ng DNA). Total collagen content does not differ significantly (N = 9). sGAG content decreases significantly (***p < .001) to 1.4 µg sGAG/mg ECM (SD± 1.0 µg sGAG; N = 15). DAPI, 4′,6-diamidino-2-phenylindole; EBD, extrahepatic bile duct; ECM, extracellular matrix; H&E, hematoxylin and eosin; PBG, peribiliary glands; sGAG, sulfated glycosaminoglycan.

Interestingly, a decrease in KRT-7 (approximately ECO: 8-fold, BCO: 2.3-fold, and ICO: 1.6-fold decrease) and KRT-19 (approximately ECO: 2.5-fold, BCO: 2-fold, and ICO: 1.7-fold decrease) was measured, whereas KRT-7 and KRT-19 staining showed that on protein level these proteins are still expressed. Recently, it was shown that there is no significant differential gene expression of KRT-7 and KRT-19 between primary extrahepatic cholangiocytes and ECO.[9] Expression of mature cholangiocyte markers MUC-1, TFF-1, TFF-2, EPCAM, TROP-2, and HNF-1β remained stable. KI-67 expression, as indicator for cell proliferation, decreased when recellularized with ECO and BCO, whereas in some of the ICO samples this was inconclusive. The ICO samples, which reached confluency had a decrease in KI-67 expression (1.6-fold, 33-fold, and 50-fold), whereas nonconfluent ICO samples had an increase (4.4 and 1.2-fold) in expression when compared with matched BME controls. In all cases, an increase in Vimentin expression was measured after recellularization (ECO: 3.8-fold, BCO: 1.6-fold, and ICO: 9.7-fold increase) indicating that cells were undergoing epithelial-to-mesenchymal transition.
Expression of the cholangiocyte-specific transporter and channel genes CFTR, SLC-4a2, and SLC10a2 (ASBT) was also detected (Figure S3) suggesting that the cells could be capable of performing anion and bile salt transport functions. Recellularization on ECM discs did not affect expression of hepatocyte markers Albumin, CYP-3a4, ABCB11 (BSEP), and HNF-4α (Figure S3). No apparent hierarchical clustering could be found between recellularized samples or organoids from the same patients in BME. Similarly, no clustering could be found between organoids derived from healthy donors or patients (data not shown). Expression of cholangiocyte marker cytokeratin-7 (KRT-7) differed between ECO, BCO and ICO repopulated ECM (Figure 4A-C), as KRT-7 expression was lower in ICO samples compared with ECO and BCO. Cholangiocyte marker cytokeratin-19 (KRT-19) expression was similar for all repopulated ECM samples (Figure 4D-F). Protein expression of Zone Occludens-1 (ZO-1) was also seen in ECM samples recellularized with organoids from all three types, however, expression was seen in different patterns (Figure 4G-I). In ECO and BCO samples, ZO-1 was located in between cells, showing that tight junctions formed between individual cells (Figure 4G, H). The XZ-plane revealed that ZO-1 expression was found at the luminal side, whereas

nuclei are located at the basolateral side of the cells. This indicates cholangiocyte-like polarization of the cells on ECO and BCO recellularized samples. Again, ICO showed a different pattern, as these cells lacked the “honey comb” -like structured, had flattened phenotypes and no polarization was witnessed (Figure 4I). Specific gene expression analysis showed a decrease in expression of LGR5 (WNT target gene) after recellularization when compared with matched BME controls (Figure 5). ICO showed an approximate four-fold decrease, whereas ECO had a 6.5-fold and BCO a 10-fold decrease after recellularization. SOX-9 (biliary progenitor marker) expression of BCO samples (both BME controls and recellularized samples) was higher compared with SOX-9 expression of ECO and ICO samples. Focusing on BCO samples only, the SOX-9 expression decreased threefold after recellularization when compared with matched BME controls. Expression of NOTCH-2 was increased (approximately ECO: 3.5-fold, BCO: 6.1-fold, and ICO: 3.1-fold) after recellularization, indicating differentiation to cholangiocytes.

Whole mount confocal analysis of ductal ECM recellularized with ECO or BCO after staining with acetylated α-tubulin revealed presence of primary cilia in these samples (Figure 6A-D). The XZ-plane revealed that cilia can be found on the apical side of the cells similar to the *in vivo* situation (Figure 6A-D, XZ plane). No acetylated α-tubulin was detected in ICO-repopulated scaffolds. ICO recellularized samples were not assessed for functionality testing, as these organoids failed to fully repopulate the ductal ECM. The Ussing chamber experiments required larger ECM samples (L: 2 cm, W: 1 cm) and therefore the number of cells used was increased fivefold (approx. 3.0×10^5 cells per segment). Recellularization patterns were similar to those of the circular ductal ECM. However, due to the increased number of cells, EM had to be refreshed more often. During the last 7 days of the 21-day period, medium was refreshed every 24 hours. Recellularized constructs had TEER of 17.8 Ω·cm^2 (SD: ±1.4 Ω·cm2) and 21.1 Ω·cm2 (SD: ±4.7 Ω·cm^2) for ductal ECM recellularized with ECO and BCO, respectively (Figure 6E). No fresh tissue was used as a control, due to the severity of denudation of EBD tissue. CFTR-channel activity was induced by addition of forskolin (cAMP agonist). The segments repopulated with ECO showed a relatively small response (Figure 6F), whereas no change in Isc was detected for BCO samples (Figure 6G). Both the ECO and BCO recellularized constructs responded to GlyH-101 induced blockage of the CFTR-channel with a reduction in anion secretion. This indicates that CFTR-channels in the BCO recellularized ECM constructs were already active, presumably caused by the presence of forskolin in EM. Subsequent activation of CaCC with the purinergic Ca^{2+} agonist UTP caused a transient increase in Isc in both samples. UTP was added to the luminal side of the constructs, thus the response indicates proper polarization of the epithelial cell layer with both CFTR and CaCC channels localized at the apical cell surface. Decellularized ECM was taken along as a negative control and did not respond to any of the additions (Figure S2).

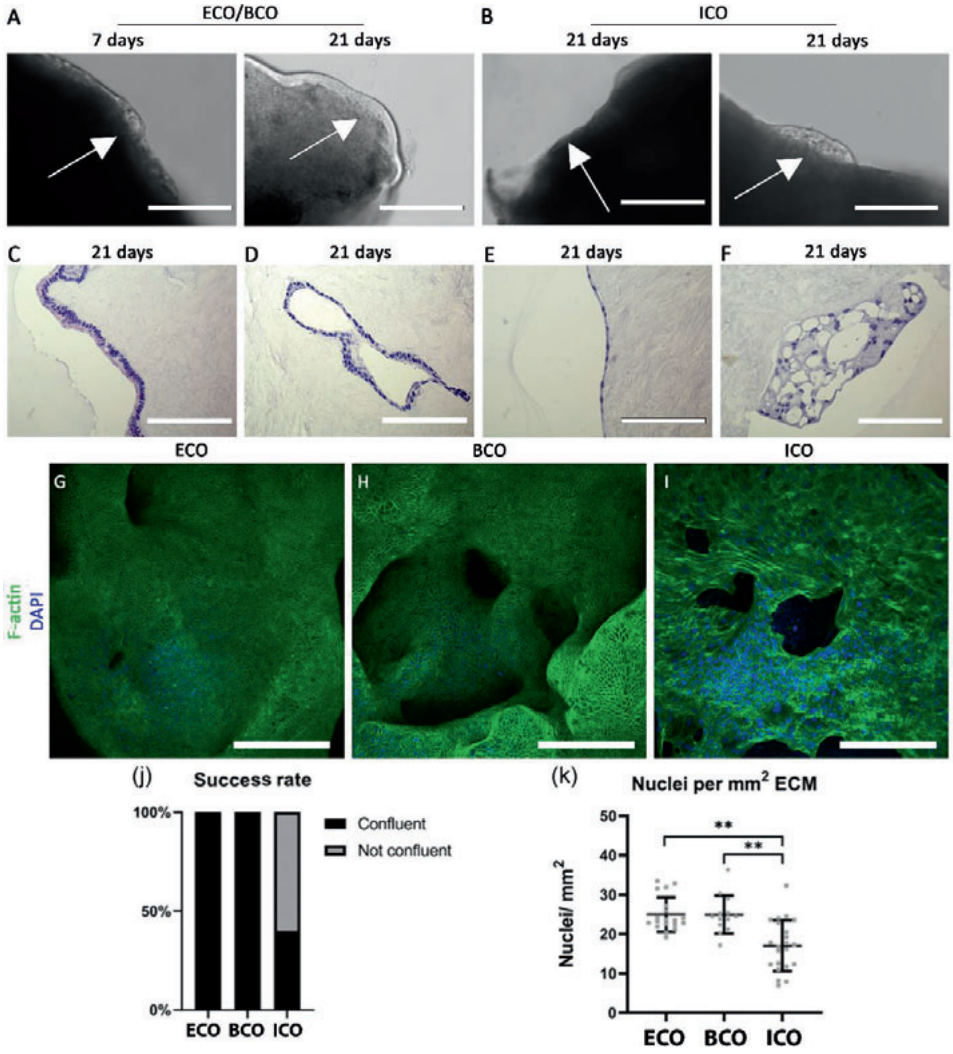

Figure 3. ECO and BCO can fully repopulate the luminal surface of ductal ECM.

(a) Decellularized ECM were not transparent. Only cells surrounding the edges of the scaffold can be monitored. After 24 h cells can be found surrounding the ECM of ECO and BCO recellularized samples. After 7 days a semitransparent rim appeared, which contained cystic structures (white arrow). After 21 days no cystic structures could be detected (scale bars: 200 µm). **(b)** ICO were less efficient in recellularization of ductal ECM, as they formed thin edges surrounding the ECM. ICO showed either a cystic-phenotype or flattened phenotype after 21-days (scale bars: 200 µm). **(c)** ECO and BCO that encapsulated the luminal surface of the ECM had a columnar phenotype, where the nucleus was located to the apical side of the ECM. **(d)** Cells were found inside the lumen of the ostia of the PBG. **(e)** ICO lack the columnar phenotype. Cells are flattened in shape. **(f)** In some cases, where ICO fail to recellularize the ductal ECM, cystic structures are seen after 21 days. Scale bars **(c–f)** 200 µm. **(g–i)** F-actin staining

on whole mounted samples. **(g** and **h)** ECO and BCO are capable of forming confluent layers on the luminal surface of the ductal ECM. Ostia of PBG **(h)** are also repopulated. **(i)** ICO expresses a different phenotype, as recellularization was not completed. Scale bar GHI: 200 µm. **(j)** The "success rate" as determined by the percentage of completely repopulated samples. For ECO and BCO the success rate was 100% as organoids from each donor or patient formed confluent layers ($N = 5$ ECO and $N = 3$ BCO). For ICO this percentage was 40%, as organoids from only two donors or patients were capable of forming confluent layers. The other three donor or patient ICO formed flattened layers with holes. **(k)** The number of nuclei counted per mm^2. ECO and BCO have 24.9 nuclei (SD: ±4.2) and 25.0 nuclei (SD: ±4.6) per mm^2 respectively. The nuclear density of ICO differs significantly with ECO and BCO repopulated samples (**$p < .01$). ICO repopulated samples contained 17.1 nuclei per mm^2 (SD: ±6.3). Success rate **(j)** and nuclear density **(k)** were determined by examination and analysis of five whole mount confocal Z-stacks of each source ($N = 4$ ECO and ICO, $N = 3$ BCO). BCO, bile-cholangiocyte organoids; ECM, extracellular matrix; ECO, extrahepatic cholangiocyte organoids; ICO, intrahepatic cholangiocyte organoids; PBG, peribiliary glands.

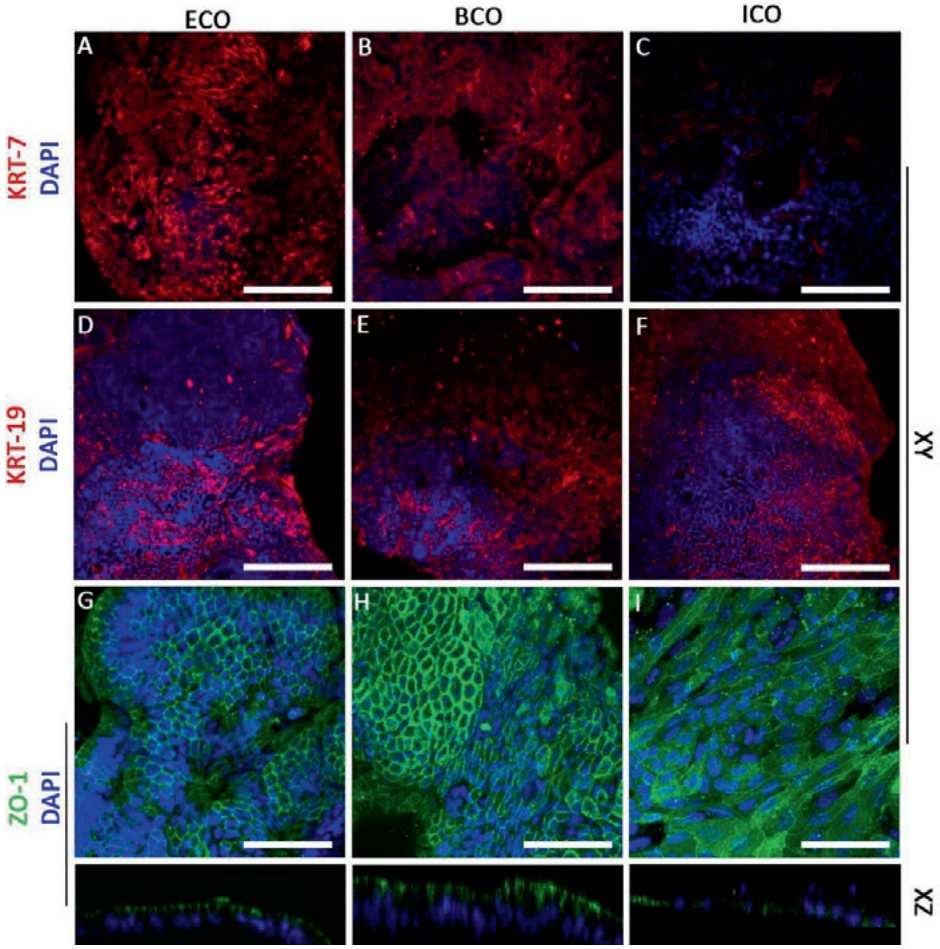

Figure 4. Organoids derived from EBD tissue or bile samples can be used to repopulate the apical surface of ductal ECM.

(a–c) ECO and BCO express cytokeratin-7 (KRT-7), whereas ICO showed lower expression of KRT-7. **(d–f)** cytokeratin-19 (KRT-19) expression was similar between ECO, BCO, and ICO. **(k–m)** Zone Occludens-1 (ZO-1) expression showed that ECO and BCO had a "honey comb" -like phenotype. ZO1 was located on the luminal side (XZ plane), whereas nuclei were located at the basolateral side, indicating cholangiocyte-like polarization of the cells. ICO recellularized samples had a flattened phenotype and no polarization of ZO-1 was detected. Scale bars: (a–f) = 200 µm and (g–i) = 100 µm. BCO, bile-cholangiocyte organoids; ECM, extracellular matrix; ECO, extrahepatic cholangiocyte organoids; ICO, intrahepatic cholangiocyte organoids.

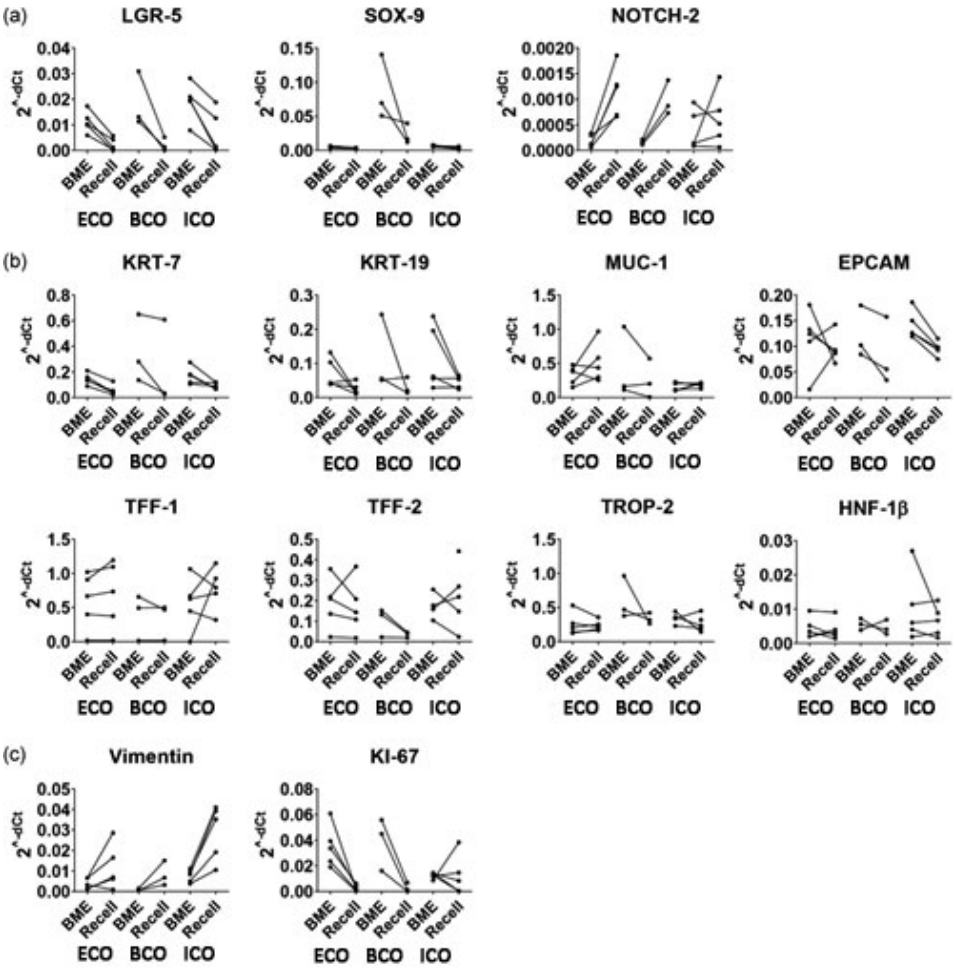

Figure 5. mRNA expression data before (BME) and after recellularization (Recell) on top of the ductal ECM of matched organoids from different origins.

Cholangiocyte differentiation or stem cell markers are shown in panel **(a)**. Cholangiocyte-specific genes are shown in panel **(b)**. Proliferation (KI-67) and epithelial-to-mesenchymal transition marker (Vimentin) are displayed in panel **(c)**. The RT-qPCR data is displayed as 2^{-dCt}. Wilcoxon signed rank test did not reveal any significant differences between the marched BME and recellularized samples. BME, basement membrane matrix; ECM, extracellular matrix; mRNA, messenger RNA; RT-qPCR quantitative reverse-transcription polymerase chain reaction.

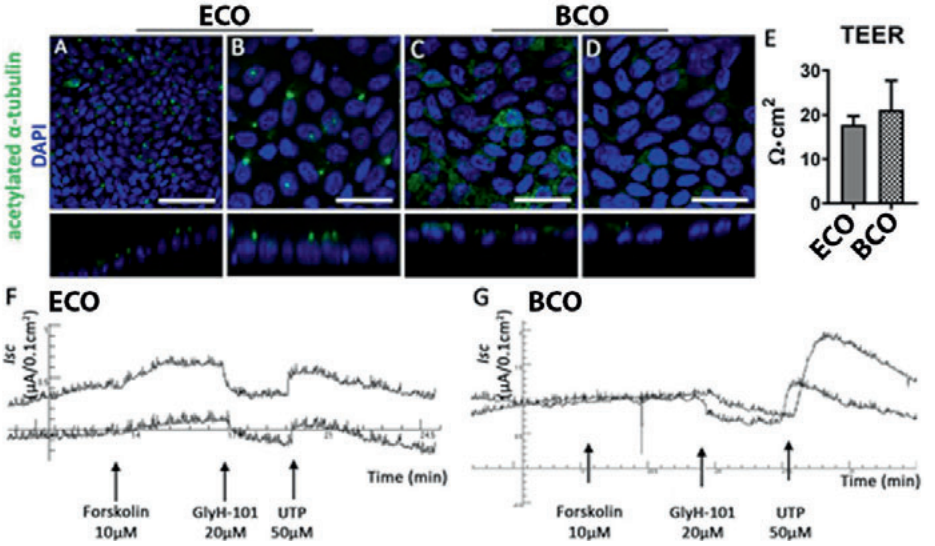

Figure 6. Functional bile duct constructs can be created *in vitro* using ECO or BCO.

(a–d) Acetylated α-tubulin staining shows the presence of cilia in ECO and BCO recellularized samples. Scale bars: (a) 100 μm, **(b–d)**: 50 μm. **(e)** TEER measurements show an increase in resistance compared to decellularized ECM (N = 3 measurements per sample). **(f)** and **(g)**: Ussing chamber experiments showing short circuit current (Isc) changes upon consecutive addition of Forskolin (a cAMP agonist), GlyH-101 (CFTR inhibitor), and UTP (Ca^{2+} agonist and CaCC activator) of ECO recellularized ECM (f, N = 2) and BCO recellularized ECM (g, N = 2). After addition of Forskolin a small response in ECO samples was recorded, but not in the BCO samples. GlyH-101 successfully blocked CFTR-channel activity in both samples, as a decrease Isc was recorded. Addition of 50 μM UTP showed an increase in current for both samples indicating the presence of CaCC. BCO, bile-cholangiocyte organoids; CaCC, calcium activated chloride channels; ECM, extracellular matrix; ECO, extrahepatic cholangiocyte organoids; TEER, trans epithelial electrical resistance.

Discussion

The ability to engineer personalized functional EBD constructs *in vitro* may have considerable impact on the management of biliary complications after LT. Here, we demonstrated efficient decellularization of human EBD tissue and showed preservation of the ultrastructure of the EBD. Subsequent successful recellularization with cells derived from ECO and BCO, but not from ICO, was shown. The recellularized ductal ECM expressed mature cholangiocyte markers (such as KRT-7, KRT-19, NOTCH-2, TFF-1, and TFF-2) and demonstrated cholangiocyte-specific ion-channel functionality. This provides proof of principle that in the near future, patient-specific, transplantable and functional EBD tissue constructs could be engineered *in vitro*, which can be used to replace or repair damaged EBD tissue *in vivo*.

The use of decellularization strategies for ductal tissue engineering purposes has previously shown successful in animal models. Cheng *et al*.[16] successfully transplanted a decellularized ureter, splinted by a silicone stent or a T-tube, in guinea pigs. In parallel, Struecker *et al.*[17] transplanted porcine abdominal aorta, which was recellularized with autologous cholangiocytes, in a porcine model. However, ureter or aorta ECM does not resemble the architecture of human EBD as these structures are lacking the complex PBG architecture.

Decellularization of human EBD tissue was efficient and did not damage the architecture of the ECM. The loss of connective tissue surrounding the EBD could account for the decrease in sGAG content, although this was not further quantified. The decrease of sGAG did not appear to impact the formation of confluent cell-layers, as ECO and BCO successfully repopulated the surface of the ductal ECM. Further analysis of the repopulated ductal ECM showed cholangiocyte-like cells, which expressed cholangiocyte markers on RNA and protein level. Furthermore, they had a functional barrier allowing measurements of vectoral transport of anions through cholangiocyte-specific ion-channels (CFTR and CaCC). These responses could not be compared with healthy and viable EBD-tissue, as all EBD tissue obtained from LT procedures showed extensive denudation of the cholangiocyte monolayer and did not possess a functional barrier anymore. However, the responses measured were in similar order of magnitude as the responses measured for human gall bladder epithelium.[18]

Although ICO expressed similar cholangiocyte markers, they were less successful in fully repopulating the bile duct ECM. This difference in recellularization efficiency could be explained by regional differences in human biliary tissues. The extrahepatic and intrahepatic bile ducts are of different embryonic origin, arising from different progenitors during embryonic development.[19] This results in transcriptional differences between EBD or IBD cholangiocytes. Rimland *et al.*[9] recently demonstrated that these differences are retained *in vitro* in the organoids initiated from different sources. Therefore, organoids of extrahepatic origin could be best suited to repopulate the decellularized ECM of the EBD. ICO, on the other hand, could potentially be more useful for repopulation of decellularized IBD[20] which is vital for creating for functional liver tissue constructs *in vitro*.

Biliary organoids are an alternative source of primary cholangiocytes of which expansion *in vitro* is challenging.[21] The organoids were obtained from healthy donors or from patient material (see Section "*Sample procurement for organoid initiation*" for indications). No significant differences between healthy or "diseased" organoids were witnessed in manner of proliferation or mRNA expression profiles, and there was no difference in recellularization capacity. This indicates that autologous cells from patients could be used for personalized regenerative medicine purposes. BCO can obtained through less invasive ERCP procedures, making BCO more ideal for personalized purposes. ECO from donors could be used as an alternative when patient-derived cells are not available.

Biliary $LGR5^+$ organoids offer specific advantages when used in tissue engineering over other cell sources, such as induced pluripotent stem cells (iPSC), mostly because organoids are less prone to (epi)genetic variation.[8,22]

Furthermore, iPSC requires extensive reprogramming and differentiation protocols, whereas no differentiation protocols were needed to create functional EBD constructs *in vitro*. The organoids already express mature cholangiocyte markers TFF-1, TFF-2, and MUC-1.[23,24] In addition, extrahepatic organoids have shown to be efficiently used for ductal tissue engineering purposes *in vivo*. Sampaziotis *et al.*[10] demonstrated that extrahepatic organoids can successfully replace extrahepatic bile duct in mice, albeit that the culture medium for initiating and expanding the organoids differed from ours. Furthermore, they used an artificial collagen scaffold, which lacks tissue-specific architecture, such as the PGBs. Therefore, the use of collagen scaffolds might be less optimal for long-term homeostasis of the engineered bile duct. An advantage of applying decellularization strategies is that these architectural features do remain present after decellularization of EBD.

However, several "hurdles" have to be taken before decellularized and repopulated human ductal ECM can be clinically used. First and foremost, a translational step from the small two-dimensional sections to three-dimensional (3D) tubular structures has to be made. This involves increasing the surface area that needs to be recellularized and an increase in the number of cells. Subsequently, there will be an increase in oxygen and nutrient consumption and it is likely that this translation requires more complex culture systems, such as perfusion-based bioreactors. Furthermore, maintaining viability of cholangiocytes after transplantation would require the development of a blood vessel network. Struecker *et al.*[17] showed feasibility of transplanting a bile duct construct solely with cholangiocytes in a large animal model without forming blood vessels (before transplantation). This could suggest that a preformed blood vessel network is not required, as formation of blood vessel after implantation appeared to be adequate. However, this study was performed in healthy animals and more research is required whether this holds true for patients with defective EBD tissue.

Another important issue is the use of non GMP-compliant basement membrane extracts, such as Matrigel or Cultrex BME, for the initiation and expansion of organoids. These extracts

are created from mouse tumor tissue[25,26] and are limiting the clinical applications of the organoids and subsequently of recellularized EBD constructs.[14] To overcome this "hurdle," clinically relevant and well-defined culture substrates are required. Alternative candidates have already been investigated for organoids cultures.[27-29]

In conclusion, we show successful recellularization of decellularized EBD tissue using cholangiocyte organoids. Both ECO and BCO are promising cell sources to be used in personalized biliary tissue engineering, as they maintain cholangiocyte-marker expression, showed restored barrier function and possessed cholangiocyte-specific ion-channel activity. In this study, we identified BCO as the most suitable candidate for future use in building functional 3D tubular EBD constructs. This is mostly due to easy access and minimally invasive collection of bile from patients.

References

1. Hessheimer AJ, Cárdenas A, García-Valdecasas JC, *et al*. Can we prevent ischemic-type biliary lesions in donation after circulatory determination of death liver transplantation? Liver Transpl. 2016 Jul;22(7):1025-33.
2. de Vries Y, von Meijenfeldt FA, Porte RJ. Post-transplant cholangiopathy: Classification, pathogenesis, and preventive strategies. Biochim Biophys Acta Mol Basis Dis. 2018 Apr;1864(4 Pt B):1507-1515.
3. Blok JJ, Detry O, Putter H, Rogiers X, *et al.* Eurotransplant Liver Intestine Advisory Committee. Longterm results of liver transplantation from donation after circulatory death. Liver Transpl. 2016 Aug;22(8):1107-14.
4. Foley DP, Fernandez LA, Leverson G, *et al.* Biliary complications after liver transplantation from donation after cardiac death donors: an analysis of risk factors and long-term outcomes from a single center. Ann Surg. 2011 Apr;253(4):817-25.
5. de Jong IEM, van Leeuwen OB, Lisman T, *et al.* Repopulating the biliary tree from the peribiliary glands. Biochim Biophys Acta Mol Basis Dis. 2018 Apr;1864(4 Pt B):1524-1531.
6. Crapo PM, Gilbert TW, Badylak SF. An overview of tissue and whole organ decellularization processes. Biomaterials. 2011 Apr;32(12):3233-43.
7. Aloia L, McKie MA, Vernaz G, *et al.* Epigenetic remodeling licences adult cholangiocytes for organoid formation and liver regeneration. Nat Cell Biol. 2019 Nov;21(11):1321-1333.
8. Huch M, Gehart H, van Boxtel R, *et al.* Long-term culture of genome-stable bipotent stem cells from adult human liver. Cell. 2015 Jan 15;160(1-2):299-312.
9. Rimland CA, Tilson SG, Morell CM, *et al.* Regional Differences in Human Biliary Tissues and Corresponding In Vitro-Derived Organoids. Hepatology. 2021 Jan;73(1):247-267.
10. Sampaziotis F, Justin AW, Tysoe OC, *et al.* Reconstruction of the mouse extrahepatic biliary tree using primary human extrahepatic cholangiocyte organoids. Nat Med. 2017 Aug;23(8):954-963.
11. Soroka CJ, Assis DN, Alrabadi LS, *et al.* Bile-Derived Organoids From Patients With Primary Sclerosing Cholangitis Recapitulate Their Inflammatory Immune Profile. Hepatology. 2019 Sep;70(3):871-882.
12. Aizarani N, Saviano A, Sagar, Mailly L, *et al.* A human liver cell atlas reveals heterogeneity and epithelial progenitors. Nature. 2019 Aug;572(7768):199-204.
13. Schneeberger K, Sánchez-Romero N, Ye S, *et al.* Large-Scale Production of LGR5-Positive Bipotential Human Liver Stem Cells. Hepatology. 2020 Jul;72(1):257-270.
14. Willemse J, Lieshout R, van der Laan LJW, *et al.* From organoids to organs: Bioengineering liver grafts from hepatic stem cells and matrix. Best Pract Res Clin Gastroenterol. 2017 Apr;31(2):151-159.
15. Vandesompele J, De Preter K, Pattyn F, *et al.* Accurate normalization of real-time quantitative RT-PCR data by geometric averaging of multiple internal control genes. Genome Biol. 2002 Jun 18;3(7):RESEARCH0034.
16. Cheng Y, Xiong XZ, Zhou RX, *et al*. Repair of a common bile duct defect with a decellularized ureteral graft. World J Gastroenterol. 2016 Dec 28;22(48):10575-10583.
17. Struecker B, Hillebrandt KH, Raschzok N, *et al.* Implantation of a Tissue-Engineered Neo-Bile Duct in Domestic Pigs. Eur Surg Res. 2016;56(1-2):61-75.

18. Chinet T, Fouassier L, Dray-Charier N, *et al.* (1999). Regulation of electrogenic anion secretion in normal and cystic fibrosis gallbladder mucosa. Hepatology. 1999 Jan;29(1):5-13.
19. Zong Y, Stanger BZ. Molecular mechanisms of bile duct development. Int J Biochem Cell Biol. 2011 Feb;43(2):257-64.
20. Willemse J, Verstegen MMA, Vermeulen A, *et al.* Fast, robust and effective decellularization of whole human livers using mild detergents and pressure controlled perfusion. Mater Sci Eng C Mater Biol Appl. 2020 Mar;108:110200.
21. Tabibian JH, Trussoni CE, O'Hara SP, *et al.* Characterization of cultured cholangiocytes isolated from livers of patients with primary sclerosing cholangitis. Lab Invest. 2014 Oct;94(10):1126-33.
22. Rebuzzini P, Zuccotti M, Redi CA, *et al.* Achilles' heel of pluripotent stem cells: genetic, genomic and epigenetic variations during prolonged culture. Cell Mol Life Sci. 2016 Jul;73(13):2453-66.
23. Segal JM, Kent D, Wesche DJ, *et al.* Single cell analysis of human foetal liver captures the transcriptional profile of hepatobiliary hybrid progenitors. Nat Commun. 2019 Jul 26;10(1):3350.
24. MacParland SA, Liu JC, Ma XZ, *et al.* Single cell RNA sequencing of human liver reveals distinct intrahepatic macrophage populations. Nat Commun. 2018 Oct 22;9(1):4383.
25. Benton G, Arnaoutova I, George J, *et al.* Matrigel: from discovery and ECM mimicry to assays and models for cancer research. Adv Drug Deliv Rev. 2014 Dec 15;79-80:3-18.
26. Hughes CS, Postovit LM, Lajoie GA. Matrigel: a complex protein mixture required for optimal growth of cell culture. Proteomics. 2010 May;10(9):1886-90.
27. Giobbe GG, Crowley C, Luni C, *et al.* Extracellular matrix hydrogel derived from decellularized tissues enables endodermal organoid culture. Nat Commun. 2019 Dec 11;10(1):5658.
28. Gjorevski N, Sachs N, Manfrin A, *et al.* Designer matrices for intestinal stem cell and organoid culture. Nature. 2016 Nov 24;539(7630):560-564.
29. Krüger M, Oosterhoff LA, van Wolferen ME, *et al.* Cellulose Nanofibril Hydrogel Promotes Hepatic Differentiation of Human Liver Organoids. Adv Healthc Mater. 2020 Mar;9(6):e1901658.

Supplementary Information

Table S1: DNase solution

Component	Concentration	Brand
DNase 1	5U/L	Sigma
NaCl	0.9% 100mL	Sigma
$CaCl_2$	100mM	Sigma
$MgCl_2$	100mM	Sigma

Table S2: Medium supplement for Advanced DMEM/ F12.

Component	Amount	Concentration	Brand
Advanced DMEM/F12	500mL		Gibco
HEPES	5mL	1M	Life technologies
L-Glutamin	5mL	100X	Life technologies
Primocin	1mL	500mg/mL	Invivogen
Pen/Strep	5mL	10000 U/mL	Life technologies

Table S3: Medium formulation for Start Up Medium (SEM)* and Expansion Medium (EM).

Component	Concentration	Brand
Adv^+		Gibco
N2	1%	Gibco
B27	2%	Gibco
N-Acetylcystein	1,25 mM	Sigma
gastrin	10 nM	Sigma
EGF	50 ng/mL	Peprotech
FGF10	100 ng/mL	Peprotech
HGF	25 ng/mL	Peprotech
nicotinamide	10nM	Sigma
A83.01	5 µM	Tocris
Forskolin	10 µM	Torcris
R-Spondin	10%	Conditioned medium
WNT*	30% WNT	Conditioned medium
Noggin*	25 ng/mL	Conditioned medium
Y27632*	10µM	Tocris
hES cell cloning recovery solution*	1:1000 dilution	Stemgent

Table S4: List of primary antibodies used for Immunohistochemistry or Whole mount confocal. Antibodies with ** are only used for whole mount confocal.

Antibody	Raised in	Dilution	Supplier
Collagen Type I	Rabbit	1:60	Novus biologicals
Collagen Type IV	Rabbit	1:50	Novus biologicals
Acetylated α-tubulin**	Mouse	1:100	Sigma
ZO1**	Rabbit	1:100	Proteintech
KRT 7**	Mouse	1:100	Dako
KRT 19**	Mouse	1:100	Dako

Table S5: List of fluorescent labeled secondary antibodies.

Secondary antibody	Raised in	Against	Dilution	Supplier
Alexa 555	Goat	Mouse	1:100	Fisher scientific
Alexa 488	Goat	Rabbit	1:100	Fisher scientific

Table S6: List of qPCR primers.

Primer	Forward sequence 5'to 3'	Reverse sequence 5'to 3'
GAPDH	CTTTTGCGTCGCCAGCCGAG	CCAGGCGCCCAATACGACCA
HPRT-1	ACCAGTCAACAGGGGACATAA	CTTCGTGGGGTCCTTTTCACC
B2M	GTGTCTGGGTTTCATCCATC	GGCAGGCATACTCATCTTTT
LGR-5	GTCAGCTGCTCCCGAATCCC	TGAAACAGCTTGGGGGCACA
KRT-7	GGGGACGACCTCCGGAATAC	CTTGGCACGCTGGTTCTTGA
KRT-19	GCACTACAGCCACTACTACACGA	CTCATGCGCAGAGCCTGTT
EPCAM	GACTTTTGCCGCAGCTCAGGA	AGCAGTTTACGGCCAGCTTGT
TROP-2	CGAGCTTGTAGGTACCCGGCG	TGCGCCGAGGAATCAGGAAGC
SOX-9	ACCAGTACCCGCACTTGCAC	GCGCCTTGAAGATGGCGTTG
HNF-1β	TCACAGATACCAGCAGCATCAGT	GGGCATCACCAGGCTTGTA
NOTCH-2	CATCTGGATGGGCTGGTGCC	AGGATGATTTCATACCCCGAGTGC
TTF-1	ACAAGCTGCTGTACACGGACA	AAGTTTCCAGGGCCGGGCAAT
TTF-2	TCTGTCCTGCCTCCCTGATCCA	CTCTGGCACGTGAATCCCGGT
MUC-1	CTGTCAGTGCCGCCGAAAGA	CGTGCCCCTACAAGTTGGCA
KI-67	CTACGGATTATACCTGGCCTTCC	AGGAAGCTGGATACGGATGTCA
Vimentin	CGGGAGAAATTGCAGGAGG	TGCTGTTCCTGAATCTGAGC
SLC-4a2	GAAGATTCCTGAGAATGCCG	GTCCATGTTGGCACTACTCG
AQP-1	GGCCAGCGAGTTCAAGAAGAA	TCACACCATCAGCCAGGTCAT
CFTR	TGGCGGTCACTCGGCAATTT	TCCAGCAACCGCCAACAACT
ASBT	GGTGGCCTTTGACATCCTCCC	GCATCATTCCGAGGGCAAGC
BSEP	TGAGCCTGGTCATCTTGTG	TCCGTAAATATTGGCTTTCTG
Albumin	CTGCCTGCCTGTTGCCAAAGC	GGCAAGGTCCGCCCTGTCATC
CYP-3a4	AGCAAAGAGCAACACAGAGCTGAA	CAGAGGTGTGGGCCCTGGAAT
HNF-4α	GTACTCCTGCAGATTTAGCC	CTGTCCTCATAGCTTGACCT

Table S7: Composition of Meyler's medium used in the Ussing chambers.

Concentration	Compound
128mM	NaCl
4.7mM	KCl
1.3mM	$CaCl_2$
1mM	$MgCl_2$
0.3mM	Na_2HPO_4
0.4mM	NaH_2PO_4
20mM	$NaHCO_3$
10mM	HEPES

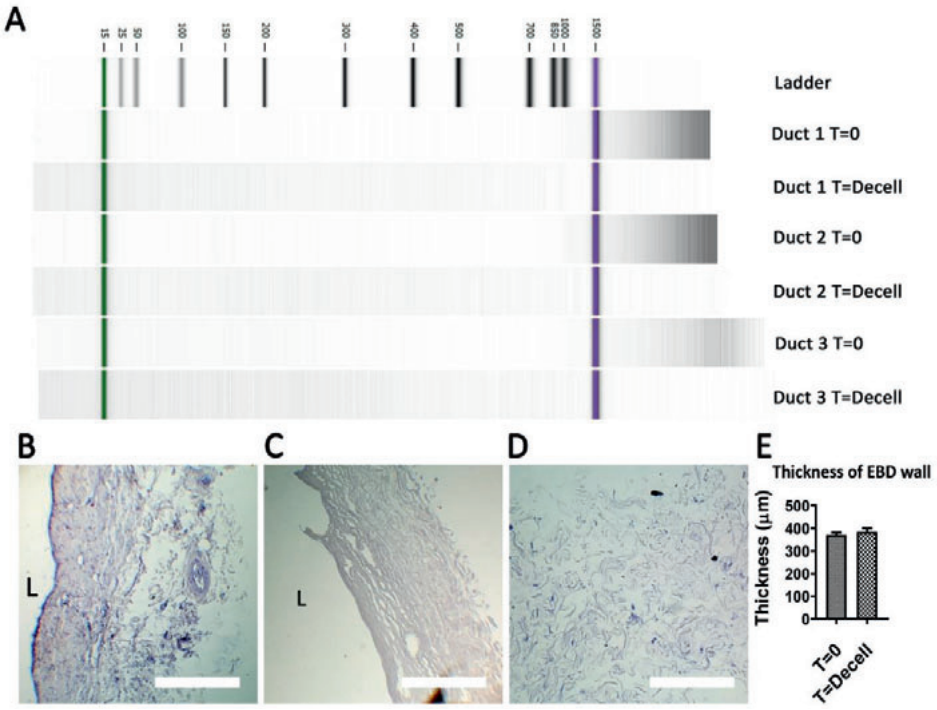

Figure S1. Extrahepatic bile ducts can successfully decellularized.

(a) No double stranded DNA was found after decellularization as shown by the results of the BioAnalyzer. For this, paired samples (n=3) before (T=0) and after decellularization (T=decell) were analyzed. Histological analysis by HE staining of a bile duct sample before decellularization (T=0) **(b)** and after decellularization (T=Decell) **(c)**. L indicates the luminal side of the EBD. Scale bars: 400µm. **(d)** HE staining of loose connective tissue that was removed from the EBD during the decellularization procedure. The connective tissue did not contain blood vessels, muscle fibers and/or PBG. Scale bar: 100µm. **(e)** The decellularization procedure did not affect the thickness of the EBD wall (P=0.856) as was measured on HE-sections of before decellularized EBD samples (N=6 different samples per condition, N=10 independent measurements per sample).

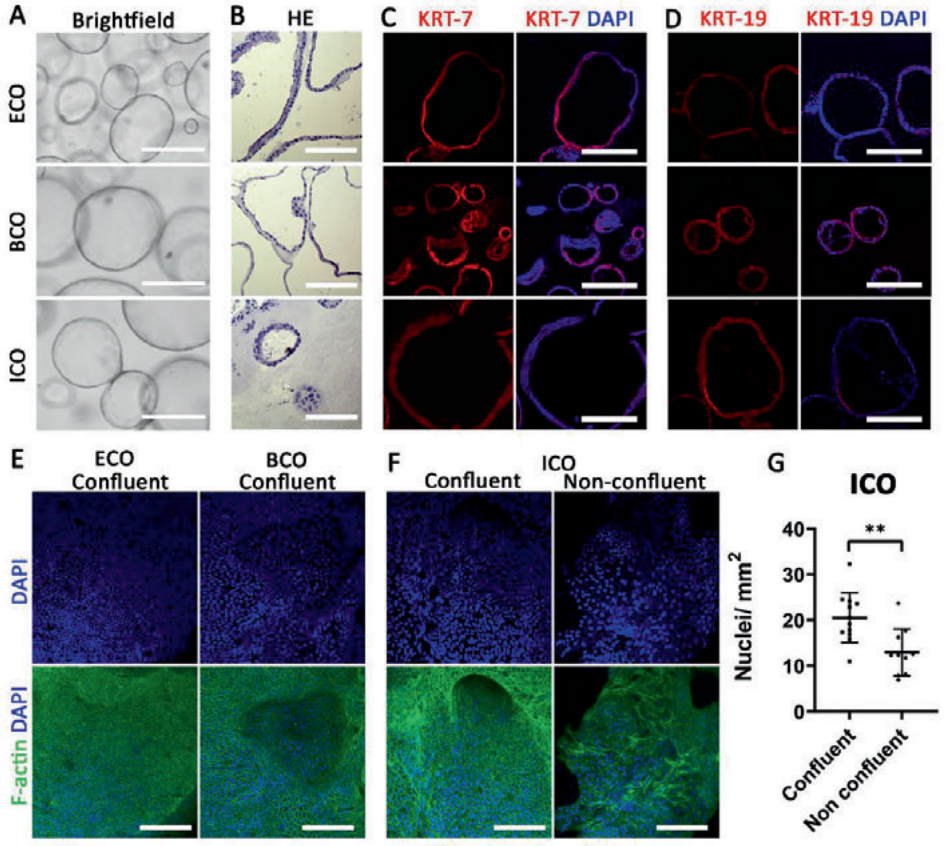

Figure S2. Organoids from all three sources represent biliary epithelial organoids.
(a) Bright field pictures of ECO, BCO and ICO grown in BME. Organoids from all three sources are spherical in shape. Scale bars: 400µm. **(b)** HE images of ECO (top), BCO (middle) and ICO (bottom) grown in BME. Scale bars: 400µm. KRT-7 **(c)** and KRT-19 **(d)** staining of ECO (top), BCO (middle) and ICO (bottom) of organoids cultured in BME show that organoids are KRT-7 and KRT-19 positive. Scale bars: 200µm. **(e, f)**: Whole mount confocal images after recellularization of the decellularized ECM with ECO (**e**, left column), BCO, (**e**, right column) and ICO **(f)**. ECO and BCO samples were completely confluent and had the highest nuclear density. F-actin + DAPI staining revealed 'honey comb'-like structures on the surface of the repopulated ECM. Image representative for N=4 independent bile duct scaffolds recellularized with N=5 ECO and N=3 BCO lines. Scale bars: 100µm. **(f)**: ICO were less capable of fully repopulating the surface of the decellularized ECM, as DAPI staining revealed differences in nuclear density between confluent (left column) and non-confluent (right column). 'Honey comb'-like structures are seen in confluent samples, but not in non-confluent samples. Scale bars: 100µm. **(g)** There is a significant difference (**, $P<0.01$) between the number of nuclei per mm^2 grown for CO repopulated scaffolds. Fully repopulated (confluent) samples (N=2 for ICO) yielded 20.5 nuclei per mm^2 (SD: ±5.2), whereas the nuclear density was 12.9 nuclei per mm^2 (SD: ±4.8) for the non-confluent samples (N=3 for ICO).

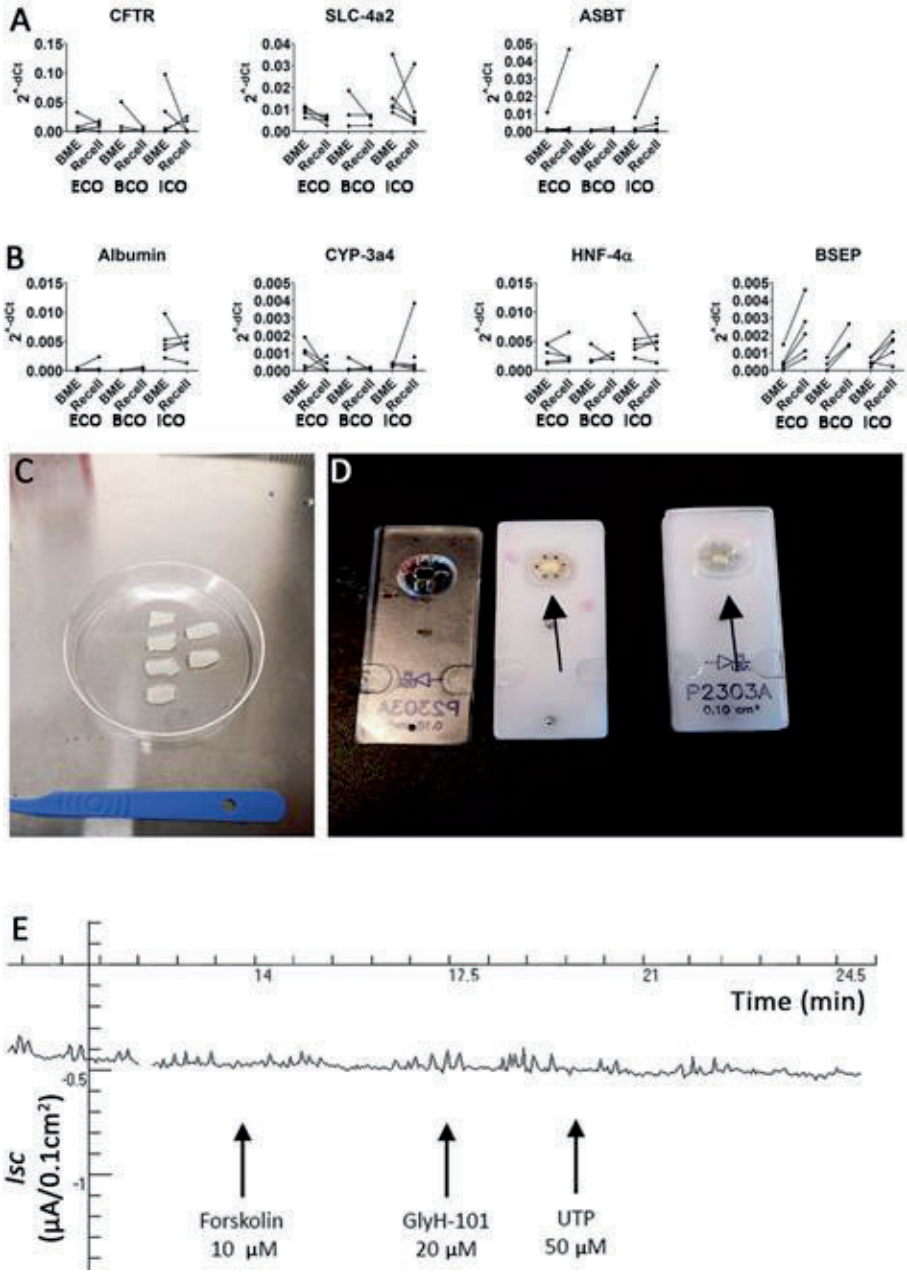

Figure S3. Organoids after recell remain commited to their biliary lineage.

(a, b) Gene expression analysis (RT-qPCR) of recellularized ECM for cholangiocyte-related genes (CFTR, SLC-4a2 and ASBT) **(a)** and hepatocyte-related genes (Albumin, CYP-3a4, HNF-4α and BSEP) **(b)**. The RT-qPCR data is displayed as 2^{-dCt} and each recellularized sample (after) is connected to a matched BME

control (before). No significant differences were found in the expression of these cholangiocyte (CFTR, SLA-4a2 and ASBT) and hepatocyte (Alb, Cyp3A4, HNF4a and BSEP) genes, according to the Wilcoxon signed rank test. **(c)** Larger ductal ECM scaffolds (L:2cm, W: 1cm) were used to assess the TEER and vectoral Ion-transport by CFTR functionality in the repopulated bile ducts using an Ussing chamber set up. **(d)** the recellularized scaffolds were placed inside the Ussing chamber holders. The black arrows indicate the scaffolds, which were placed over a set of needles to hold them in place. **(e)** The Ussing chamber results of decellularized ECM negative control (without cells) (N=1). No response to added components was detected.

PART V

DISCUSSION

V

10

CHAPTER 10

GENERAL DISCUSSION AND CONCLUSIONS

PART I – INTRODUCTION AND DEFINITIONS

Cholangiopathies remain a major challenge for the field of hepatology and hepatobiliary surgery. This is reflected in the fact that approximately 20% of all adult liver transplantations is for a biliary disease and up to 80% of pediatric liver transplantation have underlying biliary illnesses.[1,2] This is partially due to a lack of knowledge in understanding biliary pathophysiology and, subsequently, the inability to develop successful treatments. Moreover, the lack of sufficient replacement tissue for bile ducts has resulted in the continuous use of liver transplantation as a treatment for extrahepatic biliary diseases. Among other factors, suboptimal *in vitro* and *in vivo* models for studying bile ducts as well the inability to culture primary cholangiocytes contributed to this delay in progress.[3] This all changed with the introduction of the "bipotential liver-derived organoids", by Huch *et al.* in 2015.[4] In **chapter two** of this thesis, the definition of an organoid was redefined, in close collaboration with 60 experts in the field, and the name giving of organoids initiated from different parts of the liver, biliary system and pancreas was unified. The **"**bipotential liver-derived organoids", mainly used in this thesis, were redefined as intrahepatic cholangiocyte organoids (ICOs). Furthermore, the usefulness of cholangiocyte organoids for studying the development and diseases of the biliary tree was investigated. **Part II** focuses on their disease modelling capabilities *in vitro*. And, in **Part III**, novel cholangiocyte-organoid models were developed, which were used in **Part IV** to investigate regeneration of the extrahepatic bile duct *in vitro*.

PART II – DISEASE MODELING

Post-transplant cholangiopathy or the development of a non-anastomotic biliary stricture (NAS) is a severe and feared complication of the bile duct pathology after liver transplantation.[5-8] Recent evidence demonstrated that NAS develops due to a failure of regeneration from specific areas of the bile ducts.[9-11] However, which factors play a role in damaging the bile duct during transplantation is still largely unknown. Multiple studies showed a relationship between a lack of luminal bicarbonate and the development of several cholangiopathies (Primary Sclerosing Cholangitis and Primary Biliary Cholangitis).[12] In cholangiocytes, bicarbonate is transported to the lumen of the bile duct by the Anion-Exchanger 2 (AE2) transporter. AE2 exchanges luminal chloride (Cl^-), excreted via the luminal channels cystic fibrosis conductance transmembrane regulator (CFTR) and anoctamin-1 (ANO1), for intracellular bicarbonate.[13] This highlights the potential relevance of CFTR, ANO1, and AE2 in maintaining proper bicarbonate (HCO_3^-) secretion. Insufficient bicarbonate secretion is indicated by an acidotic bile. Research shows that acidotic bile during transplantation is associated with the development of NAS.[14] Therefore, it has been

suggested that this 'bicarbonate umbrella theory' might also contribute to the development of NAS.

Based on this data, ICOs were used to investigate this hypothesis **in chapter three**. First, it was demonstrated that the organoids described by Huch and colleagues[4] closely resembled primary cholangiocytes on gene-array based expression profiles and that ICOs have presence of functional cholangiocyte-specific ion-channels. Next, it was shown that hypoxia negatively influences the activity of CFTR and ANO1, which subsequently results in increased cell death when cholangiocytes are exposed to bile under these conditions. Finally, the reseach showed that it was possible to rescue CFTR activity during hypoxia by addition of an AMPkinase-inhibitor. An interesting observation, during the conducted research, was the capacity of the CFTR channel to transport bicarbonate directly into the lumen of the bile. This suggests a dual-role for the channel (both directly and indirectly via AE2) in maintaining the bicarbonate umbrella.

Chapter four elaborates upon this finding. Cystic Fibrosis (CF) is an autosomal recessive genetic disease which negatively effects the function of the CFTR-protein. Since CFTR is expressed in multiple organs such as the intestines, the lungs, the pancreas, and the bile ducts, it will result in a multi system disease.[15-17] Recent therapies have emerged that are capable of treating the pulmonary-related issues in up to 90% of affected patients.[18,19] With the improvement in treating CF-related lung disease, patients have a prolonged life expectancy and nowadays 10% of the CF-population will develop CF-related liver disease due to the defect in the bile ducts.[20,21] However, an affected liver is a late complication of CF, which is in sheer contrast to the intestinal- and lung related complications. Thus, to investigate if CFTR behaves differently in different organs, intestinal and cholangiocyte organoids were compared from both healthy and (treated) CF-donors. The results of **chapter four** demonstrated that CFTR predominantly secretes Cl^- in intestinal organoids, while cholangiocytes can secrete HCO_3^- in a 1:1 ratio in healthy individuals. In contrast, organoids from CF-patients treated with Trikavta[18,19], in both intestinal- and biliary epithelial cells, mainly secreted Cl^- via CFTR after partially rescuing CFTR-activity. Interestingly, cholangiocyte organoids from healthy individuals primarily secreted Cl^- via the ANO1-channel, while the ratio of Cl^-: HCO_3^- secretion via ANO1 is almost 1:1 in treated and untreated CF-patients. Thus, it seems that cholangiocytes from CF-patients might have a compensatory mechanism for secretion of HCO_3^- and that activation of ANO1 could be the reason that CF-related liver disease is relatively mild compared to other complications.

Limitations, implications and future directions of Part II

The research conducted in **Part II** determined the crucial role CFTR plays in developing multiple bile-duct diseases. When looking at the bicarbonate umbrella, historically, the anion-exhanger-2 (AE2) transporter was the main focus of attention. AE2 exchanges

intracellular bicarbonate for extracellular chloride. Thus, it was assumed that AE2 was the only channel capable of excreting bicarbonate in the lumen. The model, displayed in **chapter three** and **four**, demonstrated that human cholangiocytes are able to excrete bicarbonate via ANO1 and CFTR as well. However, it would be interesting to investigate the role AE2 plays within the set-up. Potentially, this could be achieved by creating a knock-out of AE2 in ICOs and create a 2D monolayer of these organoids. Another, valuable addition to the work would be to measure bicarbonate secretion and pH, directly. So far, bicarbonate excretion was defined as the anion fraction excreted in the absence of chloride, but to investigate this in more detail for each channel, a direct measurement would be essential. Finally, for future experiments, it is important to make note of the relative proportion between number of cholangiocytes and the volume of bile added to the monolayer. Because, perhaps a super-physiological excess of bile was given in relation to the number of cholangiocyte organoid cells in the monolayer in the hypoxia experiments. This may explain why bile-related cell death could not be prevented with conventional cell death inhibitors under these conditions. One important new finding is the direct transport of bicarbonate by the CFTR-channel in the organoid model. The primary function of cholangiocytes is bicarbonate secretion and **chapter four** shows that in healthy individuals CFTR can predominantly secrete bicarbonate. This finding is in clear contrast to the CFTR-protein in epithelial cells derived from the intestine, which mostly secrete chloride. Furthermore, evidence was provided that ANO1 can be autologous stimulated to secrete additional bicarbonate in patients without functional CFTR (CF-patients). The finding that cholangiocytes can secrete chloride and bicarbonate via an additional channel distinguishes them from epithelial cells of the lung and intestine. This might explain why CF-related liver disease, as a consequence of bile stasis, is relatively mild and uncommon compared to complications in other organs. Since the effect of Trikafta, the golden standard, could be limited to chloride secretion via CFTR in certain tissues, additional therapeutic interventions for CF-patients could focus on either the ANO1 channel in cholangiocytes or secretion of bicarbonate via CFTR. However, it should be noted that the conducted reseach only examined one CF-patient with a homozygous Δ508 mutation. It is needed to extend the study with organoids from different patients with similar mutations as well as from CF-patients with heterozygous Δ508 mutations. If the results would be consistent across CF-patients with different underlying mutations, this would imply that further CF-related liver reseach could be focused on bicarbonate transport and ANO-1 functionality in chongiocytes.

PART III – NOVEL ORGANOID SOURCES AND MODELS

Extrahepatic cholangiocyte organoids

The protocol for culturing intrahepatic cholangiocyte organoids, as established by Huch *et al.*[4], resulted in a major leap forward in understanding liver biology. However, it also created

several new questions. In the research conducted, Huch *et al*.[4] demonstrated that biliary cells derived from liver biopsies could be cultured as organoids. These cells could be (trans)differentiated to the hepatocyte lineage and used for modeling of both cholangiocyte- and hepatocyte diseases. However, a variety of articles published hypothesized that extrahepatic cholangiocytes differ from their intrahepatic counterparts.[13] To investigate this, in **chapter five** cholangiocyte organoids were established from extra- and intrahepatic biopsies. Subsequently, the similarities and differences between both organoids were investigated. Using RNA sequencing, it was demonstrated that there are very limited differences in gene expression between both cell types *in vitro*. This observation was supported by a study published around the same time, in which the authors confirmed these findings.[22] In addition, they demonstrated that this finding contrasts the gene expression of cholangiocytes from different regions of the biliary tree, where larger differences are found.[22] Surprisingly, only intrahepatic-derived, but not extrahepatic-derived cholangiocyte organoids were capable of differentiation to hepatocyte-like-cells. A possible explanation for this discrepancy between gene expression profiles and functionality may be the role of the local microenvironment in which cells are cultured. The cells were removed from their normal niche and cultured in a different extracellular matrix and local microenvironment compared to the *in vivo* situation. *In vitro*, both organoid types are cultured in the same environment. This might lead to a bias in gene expression profiling (not completely resembling the *in vivo* situation). In addition, a difference in functionality might be due to intrinsic variants between cells as determined by their anatomic region or epigenetic profiling. This hypothesis was confirmed by Sampaziotis *et al*. in a study in which they showed that all cholangiocytes are likely to be derived from one cell type, but regional differences occur due to their local niche.[23] Furthermore, they confirmed that the differences between primary cholangiocytes and cholangiocyte organoids are indeed the result of the microenvironment.[23]

Bile cholangiocyte organoids (BCOs)

Cholangiocyte organoids have an enormous potential to be used in clinical applications.[23] They resemble their tissue of origin and thus can be used for patient-specific disease modeling and regenerative medicine applications.[4] However, to make the transition from the bench to the clinic, a minimally-invasive matter for obtaining organoid-initiation cells is necessary. Preferably, these cells need to be collected during routine clinical procedures. This is something that cannot be achieved by culturing organoids from tissue. Thus, the reseach conducted in **chapter six and seven** investigated if bile, normally produced by hepatocytes and modified by cholangiocytes[13], could be an alternative source to biopsies for culturing cholangiocyte organoids. **Chapter six** demonstrated that culturing organoids from bile, obtained from a variety of sources during routine clinical procedures, is feasible. Moreover, it was shown that these cells are similar in their gene- and protein expression to organoids cultured from extrahepatic biopsies. Based on their transcriptome, as obtained via RNA

sequencing, it was demonstrated that although organoids from different locations are highly similar, bile cholangiocyte organoids still retain a regional landscape. Thus, BCOs derived from ERCP-bile mostly represent cholangiocytes from the common bile duct, while BCOs derived from bile within the gall bladder are closest to gall bladder cholangiocytes. Functionally, BCOs mostly resemble extrahepatic bile duct-tissue derived organoids, as they have the inability to differentiate to hepatocytes. This finding makes it likely to assume that bile cholangiocyte organoids originate from shredding of local cells from the extrahepatic bile duct. Thus, the next step was to investigate if these cells could repopulate human extracellular matrix derived from decellularized[24] extrahepatic bile ducts. Amazingly, BCOs could do this in a very successful manner. Moreover, the differences between BCOs cultured on scaffolds and in a hydrogel were analyzed and it was observed that BCOs cultured on EHBD scaffolds clustered more closely to primary cholangiocytes from the common bile duct, indicating that the local microenvironment is important for cholangiocyte plasticity.

Chapter seven focused on a new culture method for creating cholangiocyte organoids. Sampaziotis *et al.* demonstrated in 2017 that cholangiocyte organoids could also be cultured using a combination of canonical-WNT and non-canonical WNT stimulated factors.[25] In contrast, cholangiocyte organoids, as described by Huch *et al.*[4], rely solely on canonical-WNT stimulation. Furthermore, they showed that their organoids were capable of populating scaffolds which successfully could be transplanted as common bile ducts *in vivo.*[25] Considering the strong regenerative potential described by the authors, the question was raised whether these organoids could also be cultured from bile. **Chapter seven** presents data showing that this is possible. In line with the previous publication of **chapter six**, it was shown that bile cholangiocyte organoids resemble their tissue counterparts on genomic, proteomic, and functional levels. Finally, when comparing the two organoid types cultured from bile, it was observed that the gene and protein expression profiles were quite similar. However, it was noted that the gene expression of cholangiocyte channels and transporters (CFTR, Aquaporin 1, and both the basolateral secretin- and somatostatin receptors), are more strongly upregulated in organoids cultured according to the Sampaziotis protocol, suggesting that these organoids more closely resemble tissue-derived cholangiocytes. [13]

Branching cholangiocyte organoids

The biliary tree consists of two major structures: the intra- and extrahepatic bile ducts. The extrahepatic bile duct has a single lumen structure (the common bile duct), which after divarication of the cystic duct, forms the common hepatic duct.[26] The hepatic duct bifurcates into a right- and left part, enters the liver, and starts to give rise to the intrahepatic bile ducts. Inside the liver, the bile ducts form a complex branching network of dividing bile ducts throughout the liver all the way up to the peripheral parts.[26] This complex branching morphology was currently lacking in the cholangiocyte organoid models.[4,25] In **chapter eight,**

a novel method is described that successfully allows branching morphogenesis to occur in cultures of cholangiocyte organoids. These branching cholangiocyte organoids (BRCOs) closely resemble the transcriptomic profile of mature cholangiocytes as demonstrated by single cell RNA sequencing. Furthermore, evidence was provided that the proliferating cells are located at the tips of the ducts, similar to embryonic development of the intrahepatic bile ducts *in vivo.* Based upon this observation, it was demonstrated that BRCOs mimic biliary development *in vitro* by comparing the model computationally with a previously established model for branching formation.[27] Subsequently, factors that could be essential for duct formation *in vitro* were investigated. Previous studies highlight the potential role for NOTCH2, since (among other evidence) patients suffering from Alagille Syndrome (AGS, disrupted NOTCH2/JAG1 signaling), display bile duct paucity.[28] Indeed, organoids obtained from a patient suffering from AGS did not form any BRCOs and suffered from cell-death. Unfortunately, the genetic affected *JAGGED1* could not be corrected via CRISPR-Cas9 technology.[29] Thus, the definitively evidence, that demonstrated that BRCOs rely on NOTCH2/JAG1 to display a branching phenotype, was not obtained. Finally, it was shown that cholangiocarcinoma (CCA, bile duct cancer)-organoids[30], behave significantly different compared to the previously established model.[30] Branching CCA organoids more closely resembled the transcriptomic profile of the primary tumor, but also displayed a more representative response to different drug-therapeutic additions. Finally, in contrast to the organized tip-driving branching healthy cells display, CCA organoids (under branching conditions) show highly disorganized growth patterns similar to tumor-behavior. Thus, overall, the results indicate the importance and relevance of this novel culture-method. Overall, with the work conducted in **Part III**, a significant contribution was made in obtaining new insights in bile duct regeneration and the applicability of organoid cultures for patient-specific therapies.

Limitations, implications and future directions of Part III

Recent evidence suggested that the quiescent liver stem cell might not exist[31], but that it could actually be a direct trans differentiation of (certain) mature cholangiocytes which contribute to hepatocyte regeneration.[32] In line with these results, Huch *et al.* showed that their cholangiocyte organoids, obtained from intrahepatic bile ducts, are capable of differentiation to hepatocytes *in vitro.* In contrast, organoids derived from extrahepatic biopsies could not. A possible explanation for this difference in functionality between intra- and extrahepatic cholangiocytes, is that the embryonic stem cell population differs. Intrahepatic cholangiocytes develop from the hepatoblast, a common progenitor to both cholangiocyte and hepatocytes.[33] Meanwhile, extrahepatic cholangiocytes arise from a shared progenitor with the pancreas.[33] Thus, it would be interesting to investigate if extrahepatic cholangiocytes also have transdifferentation capacities, but to pancreatic cells instead of hepatocytes. Another essential question that needs to be answered is how non-

canonical WNT driven cholangiocyte organoids compare to primary tissue and to canonical-WNT stimulated organoids. Or to be more precise, would these differences only matter *in vitro* or also for possible transplantation *in vivo*? Evidence suggests that canonical-WNT cultured cholangiocyte organoids closely resemble the (epi)genetic profiling of cholangiocytes undergoing ductal reprogramming, thus resembling a more proliferative cholangiocyte.[31,34] So far, it is unclear if cholangiocytes rely on WNT/β-catenin signaling for proliferation *in vivo*, but studies actually suggest they do not.[34,35] In line with these studies, when compared to (non-) proliferative biliary epithelium cells, canonical-WNT stimulated organoids severely upregulate stem cell markers and WNT/β-catenin related signaling.[31,35] This is in contrast to the transcriptome of organoids cultured from organs that rely on WNT/β-catenin signaling for regeneration. For instance, in the intestines no upregulation of these canonical-WNT associated genes is observed.[36] Furthermore, based upon single-cell RNA sequencing data, it was demonstrated that cholangiocyte organoids in non-canonical WNT stimulating conditions closely resemble primary cholangiocytes[23], suggesting that these might be closer to the primary tissue. For a definitive answer, a side-to-side comparison between both organoid-types and primary tissue needs to be performed. By using bile as a source for organoid cultures, a protocol was developed that is capable of creating patient-specific cholangiocyte organoids obtained from *in vivo* material, without the need for invasive surgical interventions. Patient-specific organoids provide the ability to follow patients during their disease-progression since organoids recapitulate the status of the patient is reflected *in vitro*[4]. Follow-up of patients on multiple time points with subsequent analysis of gene expression profiles *in vitro* might contribute to a better understanding of underlying biology and disease-progression. This could provide new clues essential for clinical decision making. For instance, when new mutations are being found, known to resemble a pre-malignant stadium, personalized treatment considerations can be made based upon these observations. In addition, it would be very valuable to investigate if CCA organoids can be cultured from bile. Research indicates that CCA organoids can be cultured from tissue specimens obtained from surgical resections or biopsies, while maintaining their resemblance to the *in vivo* tumor.[30] Interestingly, researchers showed that these tumor-organoids can be used for personalized drug screening options. Unfortunately, only a minority of patients receive a surgical intervention and thus organoids can only be cultured from these patients.[37] If cholangiocarcinoma-organoids could successfully be established from bile, this would massively extend the target audience and therefore could contribute in obtaining more treatment options for the majority of cholangiocarcinoma patients. Finally, to overcome the shortcoming of studying cholangiocytes in itself without taking their anatomical shapre in consideration, a protocol for establishment of BRCOs was developed. However, a major deficiency to the protocol is the lack of additional hepatic cell types and specific extracellular matrix. Thus, although BRCOs show a remarkably resemblance to mature bile ducts, they only represent the cholangiocyte epithelial compartment. However,

in contrast to the previously established ICOs, BRCOs show transcriptomic heterogeneity comparable to the primary tissue as shown by single-cell RNA sequencing. Another disadvantage of the system would be that culturing BRCOs is very labor intensive which makes them unsuitable for large scale regenerative experiments. On the other hand, their unique morphology and structures make them very suited to study biliary development to such an extent that the use of animal models for this become redundant. Interestingly, BRCOs can only be established from adult intrahepatic, but not extrahepatic organoids. Importantly, next to studying intrahepatic development, BRCOs can also be used to study specific (non)-cancerous biliary diseases in a unique manner, compared to previously published systems.[4,30] All in all, BRCOs will hopefully contribute to the development of novel therapeutic strategies and in understanding underlying pathophysiology of biliary diseases.

PART IV – REGENERATIVE MEDICINE

Cholangiocyte organoids are initiated from primary cholangiocytes and acquire a highly proliferative state *in vitro*.[34] A similar process that is observed *in vivo* when cholangiocytes are dividing to restore damage or maintain homeostasis.[35] Since cholangiocyte organoids do not resemble an organoid with a hierarchical stem cell-differentiated cell population, for instance as seen in intestinal organoids[38], they are potentially very useful for tissue-engineering or regenerative medicine applications. However, to engineer an extrahepatic bile duct *in vitro,* there is also a need for scaffold on which the cells can grow. To make sure the scaffold is complementary to the cells, it must resemble the tissue-of-origin to a certain extent.[39] Therefore, the perfect scaffold would be a human extrahepatic bile duct without cells. One of the technologies to obtain tissue scaffolds is called decellularization[40]; with this process all cells are removed and the extracellular matrix proteins remain unaffected and can be recellularized with for instance organoids. Thus, the research of **chapter nine** was set-out to investigate if a decellularization protocol for extrahepatic bile ducts could be established and whether these scaffolds can successfully be recellularized with cholangiocyte organoids. **Chapter nine** demonstrated that human extrahepatic bile ducts can successfully be emptied of cells, without compromising the integrity and protein compartment of the extracellular matrix (ECM). Seeding cholangiocyte organoids derived from bile or the extrahepatic bile duct on the bile duct ECM resulted in successfully repopulated bile duct scaffolds including the biliary crypts. Surprisingly, intrahepatic cholangiocyte organoids could repopulate parts of these scaffolds, but were not very successful in fully covering them. Finally, cholangiocyte-functionality of these tissue engineered bile ducts was demonstrated by showing an increase in epithelial resistance and active ion-transport of the CFTR and ANO1 channels.

Limitations, implications and future directions of Part IV

Although scaffolds were not repopulated as a tubular 3D-duct, the study of **chapter nine** provides the first evidence that human extrahepatic bile ducts can be functionally

recellularized by cholangiocyte organoids after decellularization. However, subsequent studies should focus on creating 3D tubular structures and investigate if these constructs resemble fully functional extrahepatic bile ducts *in vitro* and *in vivo.* Most importantly, the engineered biliary tissue should maintain a functional barrier against the toxic bile[13], without extensive cholangiocyte cell-death. Another important question is to see if these constructs will induce vascularization or angiogenesis upon transplantation *in vivo* and therefore are capable of long-term functional survival *in vivo*. Preliminary data suggests that this could be the case, but definitive studies should be performed.[25,41-43] In addition, organoids are historically grown in matrigel or BME, all which are based upon Engelbreth-Holm-Swarm mouse sarcoma cells making organoids incompatible with good clinical practice guidelines. Thus, novel clinical grade hydrogels or scaffolds should be developed to expand organoids in order to be used in clinical applications.[44] Currently, strategies to create clinically grade hydrogels are investigated, one of which is based on using decellularized organs as a base for the hydrogel to grow organoids in. Recent evidence has demonstrated that cholangiocyte organoids cultured in decellularized pig intestine hydrogel are similar compared to organoids cultured in the classic mouse-sarcoma hydrogels.[45] These novel approaches provide promising culture-techniques for transferring organoid cultures to the clinic. Finally, by using organoids derived from bile, a technique was used that makes it feasible to create patient-specific extrahepatic bile ducts *in vitro*. This specificity ensures that, if transplanted, the donor tissue will not be rejected by the patient's immune response. Moreover, the extrahepatic bile ducts used here, were obtained from livers rejected for transplantation. By doing so in the future, this approach could potentially help relieve some tension on the organ-donor pool by transplanting patient-specific extrahepatic bile duct constructs, instead of livers for extrahepatic diseases.

CONCLUSIONS

Cholangiocyte organoids have emerged as promising new model for studying the bile duct development, regeneration and diseases *in vitro*. In the studies presented in this thesis, the scientific organoid community was unified and the possibilities to translate *in vitro* knowledge to improve the outcome of patients with cholangiopathies in the clinic was explored. It was shown that cholangiocyte organoids are suitable for modeling biliary diseases and the importance of the local origin of cholangiocytes was described. In addition, the use of decellularized bile ducts provided the first proof-of-concept that these cells can be used for tissue engineering purposes of the human extrahepatic bile duct *in vitro*. These constructs have the potential to be successfully transplanted in humans. Together with the regenerative potential of cholangiocyte organoids, this thesis indicates that cholangiocyte organoids can contribute to overcoming the donor supply problem.

11

CHAPTER 11

NEDERLANDSE DISCUSSIE EN CONCLUSIES

DEEL I – INTRODUCTIE EN DEFINITIES

Ziekten van de galwegen (cholangiopathieën) zijn een groot probleem binnen de hepato-pancreato-biliaire chirurgie en hepatologie. Dit blijkt onder andere uit de indicaties voor levertransplantatie. Zo'n 5% van alle levertransplantaties bij volwassen wordt uitgevoerd vanwege de galwegziekte primaire scleroserende cholangitis (PSC). Daarnaast zijn galwegcomplicaties na een transplantatie één van de meest frequente oorzaken voor een re-transplantatie en is bij kinderen het percentage van galwegziekten (circa 80%) de nummer één indicatie voor een levertransplantaties.[1,2] Het continue vergaren van kennis over de ziekteontwikkeling en het bedenken en optimaliseren van effectieve therapieën is een belangrijk speerpunt in leverziekten en levertransplantatie-gerelateerd onderzoek. Echter, de voortgang van dit onderzoek wordt mede beperkt door het gebrek aan goede *in vitro* en *in vivo* modellen om galwegziekten mee te bestuderen. De grootste uitdaging hierin is het kweken van primaire galwegcellen, dat nagenoeg onmogelijk is met de huidige technieken. Hierdoor is het onhaalbaar om voldoende galwegweefsel te maken in het laboratorium om ziekten te bestuderen, maar is er ook onvoldoende materiaal op handen om nieuwe galwegweefsel te maken voor eventuele klinische toepassing.[3] Deze opgaven kunnen mogelijk worden opgelost met de introductie van "bipotente lever stamcel organoïden" zoals die zijn beschreven voor het eerst in 2015.[4] In **hoofdstuk twee** van dit proefschrift werd de definitie van deze specifieke organoïd geherdefinieerd, in nauwe samenwerking met 60 experts binnen het veld, als intrahepatische galweg organoïden. Vervolgens zijn de mogelijkheden van deze galweg organoïden voor het bestuderen van de galwegen verder onderzocht en beschreven in dit proefschrift. In **deel II** van deze thesis is onderzocht of galweg organoïden in staat zijn om cholangiopathieën te modelleren *in vitro*. Daarnaast is **deel III** gericht op het ontwikkelen van nieuwe galweg organoïd modellen. Dit is onder andere gedaan om de transitie van deze cellen naar de kliniek te bespoedigen. Tenslotte is **deel IV** van deze thesis gericht op de potentie van deze organoïden om de galwegen te regenereren.

DEEL II – ZIEKTE MODELLERING

Post-transplantatie cholangiopathie of de ontwikkeling van niet-anastomotische galwegstricturen (NAS) is een zeer ernstige en gevreesde complicatie na een levertransplantatie.[5-8] Recent onderzoek heeft aangetoond dat een gebrek aan galwegregeneratie, mogelijk vanuit een tekort aan specifieke galwegcel populaties, een belangrijke rol speelt in het ontwikkelen van deze complicatie.[9-11] Echter, welke factoren exact een rol spelen bij het ontstaan van de initiële schade is nog grotendeels onbekend. Verschillende studies hebben gekeken naar de relatie tussen een potentiële beschermende rol van bicarbonaat voor de galwegcel en het ontwikkelen van diverse cholangiopathieën.[12] Dat de "bicarbonaat paraplu" daadwerkelijk een rol speelt bij het ontstaan van verschillende

galwegziekten is reeds aangetoond.[12] Daarnaast bleek uit recentelijke klinische data dat het hebben van een zuurder pH in gal (hetgeen duidt op te weinig basisch bicarbonaat) op het moment van een levertransplantatie, een risico is voor het ontwikkelen van post-transplantatie cholangiopathieën.[13]

Op basis van deze studies is in **hoofdstuk drie** onderzocht of de bicarbonaat paraplu theorie ook daadwerkelijk een rol kan spelen bij het ontwikkelen van NAS. Het onderzoek heeft zich voornamelijk gericht op de effecten van hypoxie op ion-kanaal activiteit in galweg organoïden gewkweekt als een 2D-monolaag.[4] Allereerst laten gen-expressie profielen zien dat intrahepatische galweg organoïden, qua transcriptoom, erg lijken op primaire galwegcellen en dat zij functionele galwegcel specifieke ion-kanalen hebben. Vervolgens is aangetoond dat een gebrek aan zuurstof een negatieve invloed heeft op de activiteit van zowel het cystic fibrosis transmembrane conductance regulator (CFTR)-kanaal als op het calcium-geactiveerde chloride kanaal (CaCC), ook wel anoctamine (ANO)1 genoemd.[14] Als vervolgens gal werd toegevoegd aan het model, dan werd een additionele sterfte van de cellen waargenomen onder deze lage-zuurstof periode. Tenslotte werd aangetoond dat toevoeging van een AMPkinase remmer zorgt voor een verbetering van de activiteit van het CFTR-eiwit in de absentie van zuurstof. Tevens laat het onderzoek zien dat het CFTR-eiwit naast chloride ook direct bicarbonaat kan transporteren richting de luminale zijde van de galwegcel. Dit impliceert dat CFTR zowel direct als indirect bijdraagt aan het in stand houden van de bicarbonaat paraplu, namelijk direct via secretie van bicarbonaat richting het lumen van de galwegen en indirect via secretie van chloride, welke vervolgens via het anion exchanger-2 (AE2) kanaal wordt uitgewisseld voor intracellulair bicarbonaat.

In **hoofdstuk vier** is voortgebouwd op deze observatie. Cystische fibrose (CF) is een autosomaal recessieve ziekte die de functionaliteit van het CFTR-eiwit aantast. Het CFTR-eiwit komt tot expressie in veel verschillende organen zoals: de longen, de alvleesklier, de darmen, maar ook de galwegen.[15-17] Het defect in de galwegen zorgt bij een kleine groep van CF-patiënten voor leverfalen en de noodzaak tot een levertransplantatie. Gelukkig heeft recentelijk onderzoek aangetoond dat er voor 90% van alle CF-patiënten nu effectieve medicatie (Trikafta) is.[18,19] Echter, om de effectiviteit van deze medicijnen te bepalen is er alleen gekeken naar de long-gerelateerde complicaties. Gezien het feit dat CF-gerelateerde leverschade relatief laat en weinig voorkomt ten opzichte van (bijvoorbeeld) darm-gerelateerde complicaties,[20,21] is in **hoofdstuk vier** onderzocht hoe CFTR-functie in de galwegen zich verhoudt tot de darmen. Dit is gedaan in cellen van gezonde donoren met functioneel CFTR en in een cellen van een CF-patiënt (dysfunctioneel CFTR). In gezonde donoren kan CFTR in galwegcellen zowel chloride als bicarbonaat in vergelijkbare mate kan uitscheiden, dit is in tegenstelling tot CFTR in epitheliale cellen van de darm waar dit voornamelijk chloride bleek te zijn. In darm- en galweg organoïden van patiënten met CF, waarbij de CFTR-functie gedeeltelijk werd gecorrigeerd door middel van Trikafta[18,19], bleek in

beide gevallen CFTR voornamelijk chloride uit te scheiden. Een interessante additionele bevinding was dat galwegcellen van gezonde mensen voornamelijk chloride via het ANO1 kanaal secreten, terwijl dit in (Trikafta-behandelde) cellen van CF-patiënten voornamelijk bicarbonaat bleek te zijn. Het lijkt er dus op dat galwegcellen in CF-patiënten mogelijk een autoloog compensatoir mechanisme, middels additionele activatie van het ANO1 kanaal, voor de uitscheiding van bicarbonaat hebben.

Limitaties, implicaties en toekomstige directies van deel II

Het onderzoek uit **deel II** heeft vastgesteld dat CFTR een belangrijke rol speelt bij het ontwikkelen van galwegziekten. Als er wordt gekeken naar de bicarbonaat paraplu is er historisch altijd veel aandacht voor het AE2 kanaal geweest. Dit kanaal wisselt intracellulair bicarbonaat uit voor extracellulair chloride. Deze interesse in AE2 is ontstaan vanuit de gedachte dat alleen AE2 bicarbonaat naar luminaal kan transporteren in de galwegcel. Het model uit **hoofdstuk drie** heeft zich gericht op de rol van CFTR (en ANO1), echter het zou interessant zijn om te kijken naar de mate waarin AE2 bijdraagt aan bicarbonaat transport. Een optie om dit te onderzoeken zou zijn door een AE2 gendefect te maken, bijvoorbeeld door een zogenaamd knock-out model van galweg organoïden te maken, en deze dan als een 2D monolaag te laten groeien. Andere essentiële aanvullingen op het project zouden metingen van direct bicarbonaat transport en pH-waarden zijn. Tot op heden zijn deze proeven helaas niet gelukt. In de huidige experimenten is daarom bicarbonaat excretie gedefinieerd als ion-transport in de absentie van chloride, maar om met zekerheid de gesecreteerde bicarbonaat fractie te onderzoeken is een directe meting nodig. Tenslotte, is het belangrijk om te realiseren dat er in het model een overmaat aan (toxisch) gal in verhouding tot cellen werd toegevoegd. Het is dan ook belangrijk om in het vervolg rekening te houden met deze cellaag:gal verhouding. Dit zou kunnen bijdragen aan het bepalen van de effectiviteit van medicamenteuze interventies. Daarnaast demonstreert het onderzoek uit **hoofdstuk vier** de unieke capaciteiten van het CFTR-eiwit in galwegcellen. Één van de belangrijkste functies van de galwegcel is het secreten van bicarbonaat, het werk uit **hoofdstuk vier** toont aan dat het CFTR-kanaal van galwegcellen, in gezonde donoren, bicarbonaat kan uitscheiden richting het lumen. Dit is een duidelijk contrast met de functie van het CFTR-eiwit in epitheliale cellen van de darm, welke voornamelijk chloride uitscheiden. Daarnaast laten de resultaten zien dat het ANO1 kanaal de uitscheidingsfunctie van bicarbonaat gedeeltelijk kan overnemen in patiënten met disfunctioneel CFTR (CF-patiënten). Het feit dat galwegcellen een additioneel ion-kanaal hebben, dat zowel bicarbonaat als chloride kan secreten, onderscheidt hen van bijvoorbeeld epitheliale cellen vanuit de long of darmen. Dit potentiële compensatoire mechanisme kan een reden zijn voor het relatief late en milde beloop van galweg-gerelateerde complicaties ten opzichte van darm- en long problematiek in CF-patiënten. Tenslotte toont het onderzoek aan dat het effect van de Trikafta behandeling, op CFTR, gelimiteerd kunnen zijn tot chloride-secretie. Daarom

zou het van toegevoegde waarde zijn als nieuwe therapeutische interventies zich ook richten op secretie van bicarbonaat via CFTR. Echter, een belangrijke beperking van het onderzoek is dat slechts één CF-patiënt met een homozygote Δ508 mutatie geïncludeerd is. Om verder te onderzoeken of het model toepasbaar is voor een bredere CF-patiëntenpopulatie is het noodzakelijk dat deze experimenten worden herhaald in cellen van patiënten met zowel eenzelfde- als een andere CF-mutatie.

DEEL III – NIEUWE ORGANOÏD BRONNEN EN MODELLEN

Organoïden van extrahepatische galwegcellen

De publicatie van Huch *et al.*[4] in 2015 bleek een grote sprong voorwaarts te zijn in het kweken van galwegcellen. In dit onderzoek werd aangetoond dat vanuit intrahepatische galwegen, verkregen via leverbiopten, galweg organoïden kunnen worden gekweekt.[4] Deze cellen kunnen gedeeltelijk worden ge(trans)differentieert naar een levercel, alsmede worden gebruikt om ziekten van de intrahepatische galwegen (Alagille Syndroom) te modelleren. Meerdere publicaties hebben aangetoond dat galwegcellen in de lever mogelijk verschillen van galwegcellen gelegen buiten de lever.[22] Om deze hypothese verder te onderzoeken, zijn in **hoofdstuk vijf** organoïden gekweekt vanuit biopten van de extrahepatische galweg. Vervolgens is onderzocht hoe deze cellen zich verhouden tot hun intrahepatische variant. Middels genetische analyse ("bulk RNA sequencing") van beide soorten organoïden werd aangetoond, tegelijkertijd met een publicatie van collega's uit een andere onderzoeksgroep[22], dat er nagenoeg geen verschil is tussen beide organoïden in gen-expressie. Diezelfde studie toonde ook aan dat er tussen gen-expressie profielen van het primaire weefsel (intra- en extrahepatich) juist wel grote verschillen zitten.[22] Ook interessant is het feit dat alleen galweg organoïden verkregen vanuit cellen gelegen in de lever, ook daadwerkelijk meer kunnen gaan lijken op levercellen, in tegenstelling to galweg organoïden vanuit de extrahepatische galweg. Een mogelijk verklaring hiervoor is dat de kweekcondities waarin de organoïden worden gekweekt, deze gen-expressie kunnen doen veranderen. Dit resulteert vervolgens in een vergelijkbaar gen-expressie profiel, maar door de intrinsieke verschillen van de cellen tot een verschil in functionaliteit. Deze hypothese kon worden bevestigd in een publicatie van Sampaziotis *et al.* waarbij zij het RNA van primaire galwegcellen van de gehele galboom hebben ontrafeld middels "single cell" RNA sequencing.[23] Zij toonden aan dat er subtiele verschillen zijn in het transcriptoom van galwegcellen, maar dat deze inderdaad ontstaan door lokale omgevingsfactoren. Er is dus eigenlijk één galwegcel die, indien noodzakelijk, zich kan aanpassen aan de lokale omgeving, ook als deze wordt gekweekt als organoïd.[23]

Galweg organoïden vanuit gal

Galweg organoïden hebben een enorme potentie om te worden gebruikt voor persoonlijke geneeskunde. Echter, om de transitie van het laboratorium naar de kliniek te maken, moet het verkrijgen van materiaal om galweg organoïden te maken zo eenvoudig en minimaal invasief mogelijk zijn. Dit is niet het geval voor biopten verkregen vanuit de intra- of extrahepatische galwegen.[4] Daarom is in **hoofdstuk zes en zeven** onderzocht of vanuit de vloeistof gal, geproduceerd door de lever, organoïden kunnen worden gemaakt.[14] Het onderzoek uit **hoofdstuk zes** laat zien dat dit mogelijk is. Gal heeft als groot voordeel dat het verkregen kan worden op verschillende manieren gedurende de routinebehandeling van een patiënt. Wij demonstreren dat galweg organoïden, gemaakt vanuit gal, gelijk zijn aan galweg organoïden gekweekt vanuit biopten van de intra- en extrahepatische galweg. Als vervolgens het gehele RNA wordt vergeleken met organoïden uit verschillende regio's van de galboom, middels RNA sequencing, dan resulteert dit globaal in een gelijkwaardig gen-expressieprofiel. Daarentegen, konden er nog wel subtiele aanwijzingen worden gevonden voor hun regionale afkomst. Zo komen organoïden verkregen middels ERCP-gal het meest overeen met galwegcellen vanuit de extrahepatische galweg (daar waar de ERCP plaatsvindt) en hebben organoïden geweekt vanuit gal van de galblaas een expressieprofiel het meeste gelijksoortig aan galwegcellen vanuit de galblaas. Bovendien werd aangetoond dat, net als organoïden verkregen vanuit de extrahepatische galweg, organoïden vanuit gal niet kunnen differentiëren naar een levercel. Dit maakt de kans groot dat organoïden vanuit gal (grotendeels) afkomstig zijn van cellen die oorspronkelijk in de extrahepatische galweg hebben gezeten. Daarnaast is onderzocht of organoïden vanuit gal in staat zijn om matrix, van menselijk extrahepatisch galwegweefsel, te bekleden. Dit bleken zij zeer succesvol te kunnen. Tenslotte werd vastgesteld dat onder invloed van deze matrix de galweg organoïden hun gen-expressieprofielen aanpassen en dat deze profielen meer gaan lijken op primaire galwegcellen verkregen vanuit een extrahepatische galweg. In **hoofdstuk zeven** wordt ingegaan op een nieuwe methode voor het kweken van galweg organoïden, ontwikkelt door Sampaziotis en collega's.[25] Zij gebruikten deze cellen om humane extrahepatische galwegweefsel *in vitro* te maken, waarna ze deze zelf gecreëerde galweg succesvol hebben getransplanteerd in een muismodel.[54] Gezien de enorme potentie van deze nieuwe cellen voor regeneratieve geneeskunde, is onderzocht of deze cellen ook vanuit gal kunnen worden gecreëerd. Dat deze opzet succesvol is, werd beschreven in **hoofdstuk zeven**. Net als eerder beschreven in **hoofdstuk zes**, is er nauwelijks verschil tussen organoïden vanuit gal of verkregen vanuit extrahepatisch galweg weefsel. Tenslotte zijn beide galweg organoïden, gekweekt vanuit gal, met elkaar vergeleken. Het bleek dat zij grotendeels gelijk waren op gen- en eiwitexpressie, behalve als er specifiek naar functionele galwegcel-gerelateerde kanalen of receptoren wordt gekeken.[14] De kanalen CFTR, Aquaporine 1 en de secretine- en somatostatine receptoren kwamen namelijk veel hoger tot expressie in galweg organoïden gekweekt volgens het nieuwe kweekprotocol van Sampaziotis. Daarnaast bleek ook de

functie van bepaalde receptoren (secretine en somatostatine) en het ion-kanaal CFTR vele malen hoger in dit protocol.

Vertakkende galweg organoïden

De galboom bestaat uit twee belangrijke delen, de intra- en de extrahepatische galweg. De extrahepatische galweg bestaat uit een enkele structuur (ductus choledochus) die na aftakking van de ductus cysticus de ductus hepaticus communis vormt.[26] Deze splitst vervolgens in een rechter en linker tak en mondt dan uit in de intrahepatische galwegen. Deze intrahepatische galwegen vormen een complex vertakkend netwerk van steeds smaller wordende galwegen door de gehele lever.[26] Deze specifieke morfologie van de intrahepatische galwegen werd niet gemodelleerd *in vitro* met de huidige galweg organoïd protocollen.[4,25] Daarom is in **hoofdstuk acht** een nieuwe kweekmethode ontwikkeld om deze vertakkende intrahepatische organoïden succesvol te kunnen kweken. Het onderzoek toonde, middels "single-cell RNA sequencing", aan dat het transcriptoom van individuele cellen van deze vertakkende organoïden een hoge mate van gelijkheid vertonen met primaire galwegcellen gelegen in de lever. Daarnaast liet het zien dat de delende cellen in deze organoïden zich bevinden in de uiteinden van de ducten. Dit komt overeen met waar de delende cellen zich bevinden tijdens de embryonale ontwikkeling van de intrahepatische galwegen. Gebaseerd op deze observatie is onderzocht of deze organoïden embryonale galwegontwikkeling konden modelleren. Dit bleek inderdaad het geval, de groei van deze vertakkende organoïden vertoont namelijk een grote mate van overeenkomst met een eerder gevalideerd mathematisch model voor de ontwikkeling van vertakkende humane organen.[27] Vervolgens is gekeken welke factoren essentieel zijn voor duct formatie *in vitro*. Eerder onderzoek had reeds aangetoond dat NOTCH2 signalen een essentiële rol hierin kunnen spelen. Dit is onder andere gesuggereerd, doordat patiënten die lijden aan het syndroom van Alagille (AGS, defect in NOTCH2/JAGGED1 signaal) slecht ontwikkelde intrahepatische galwegen hebben.[28] In lijn met deze observatie konden organoïden, verkregen van een patiënt met AGS, niet vertakken in deze condities. Helaas waren de CRISPR-Cas9 experimenten[29], om het gemuteerde *JAGGED1* te corrigeren, onsuccesvol. Daarom is niet om ontstreden kunnen vaststellen dat organoïden NOTCH2/JAG1 nodig hebben om te vertakken. Verder, werd aangetoond dat cholangiocarcinoom (CCA, galwegkanker) -organoïden, zich significant anders gedragen in deze condities, ten opzichte van het eerder gepubliceerde protocol om CCA organoïden te kweken.[30] Ook blijkt dat het transcriptoom van vertakkende CCA meer overeenkomt met de primaire tumor, en dat deze cellen ook representatiever reageren als zij worden blootgesteld aan verschillende medicamenteuze interventies. Tot slot, werd gedemonstreerd dat, in tegenstelling tot gezonde vertakkende organoïden die zeer georganiseerde groei vertonen, deze organisatie niet aanwezig is in vertakkende CCA organoïden. Hier was zeer gedesorganiseerde groei waar te nemen, vergelijkbaar met de wilde woekering van primaire tumoren. Samenvattend tonen

deze resultaten de toepassing van deze nieuwe kweekconditie voor het modelleren van galwegziekten van gezond- en tumorweefsel.

Limitaties, implicaties en toekomstige directies van deel III

Met het creëren van deze verscheidende nieuwe galweg organoïd modellen is een belangrijke wetenschappelijke- en patiëntgerichte bijdrage geleverd aan het vakgebied. Recent onderzoek suggereert dat (een subpopulatie) van intrahepatische galwegcellen kan (trans) differentiëren tot een levercel.[31,32] Dit is in tegenstelling tot de klassieke gedachte dat er specifieke stamcelpopulaties actief kunnen worden in de lever die – indien noodzakelijk– kunnen differentiëren tot galweg- en levercellen. Het principe van de (trans) differentiërende intrahepatische galwegcel kan worden gemodelleerd *in vitro*. Een galweg organoïd verkregen van de extrahepatische galwegcel kan dit niet (*in vitro*). Een mogelijke verklaring hiervoor is het verschil in embryonale origine tussen beide cellen. De intrahepatische galwegcel ontstaat vanuit hepatoblasten gedurende de embryonale ontwikkelingsfase. Hepatoblasten zijn foetale lever stamcellen, die kunnen differentiëren tot lever- en galwegcellen.[33] De extrahepatische galwegcel ontstaat uit een stamcel waaruit ook de ductale structuren van het pancreas ontwikkelen.[34] Een interessante vervolgstudie zou dan ook zijn om te onderzoeken of extrahepatische galwegcellen ook tweevoudige differentiatie capaciteiten hebben, maar in plaats van naar levercellen, kunnen differentiëren richting ductale pancreascellen. Een andere vervolgstap zou zijn om te kijken naar het verschil in gen-expressie profiel tussen primair galwegweefsel en organoïden gekweekt in beide protocollen. Er lijken namelijk verschillen te zijn tussen non-canonical WNT (Sampaziotis protocol[25]) en canonical-WNT gekweekte galweg organoïden (Huch protocol[4]). Het is dan ook goed mogelijk dat deze verschillen in protocollen het ene type organoïd geschikter maakt voor een bepaald experiment dan het andere en vice versa.[34] Of deze verschillen ook belangrijk zijn voor eventuele transplantatie *in vivo* moet nog worden uitgezocht. Het is namelijk nog maar de vraag of galwegcellen *in vivo* prolifereren onder invloed van WNT/β-catenine signalen of dat dit onder invloed is van non-canonical WNT-signalen.[35] Nieuw onderzoek suggereert het laatste. Deze theorie wordt verder gesteund door het feit dat galweg organoïden, gekweekt volgens een non-canonical-WNT protocol een grotere overeenkomst hebben met primair galwegweefsel op basis van gen-expressie (middels single cell RNA sequencing), dan canonical-WNT gekweekte organoïden.[23] Verder is bekend dat organen, die duidelijk canonical-WNT behoeftig zijn voor homeostase, zoals de darm, een grote mate van overlap in hun gen-expressie profielen vertonen met organoïden gekweekt onder deze condities.[36] Dit in tegenstelling tot galwegcel-organoïden, gekweekt onder canonical-WNT stimulatie. Deze cellen laten namelijk een enorme verhoging van klassieke WNT/β-catenine signalen ten opzichte van primaire galwegcellen zien.[31,35] Wel is duidelijk geworden dat er regionale verschillen zijn in de galwegen; zowel *in vivo* als *in vitro.* Deze verschillen worden gedeeltelijk gecreëerd onder invloed van galcompositie.[23] Interessant is ook het feit dat deze regionale

verschillen niet alleen gelden voor de gezonde situatie, maar ook in ziektes van de galwegen. Zo manifesteren ziekten zich niet alleen verschillend in intra-en extra hepatische galwegen, maar komen deze soms specifiek voor in slechts één van beide. Het zou dan ook van toegevoegde waarde zijn om te onderzoeken of bepaalde extrahepatische galwegziektes alleen kunnen worden gemodelleerd in extrahepatische galweg organoïden model, of dat er verschillen zijn tussen intra- en extrahepatische organoïden van bijvoorbeeld patiënten met alleen intrahepatische PSC.

Verder werd een protocol ontwikkeld waardoor, buiten chirurgische ingrepen om, patiënt-specifieke galweg organoïden gedurende hun routinebehandeling kunnen worden gemaakt vanuit gal. Dit houdt in dat patiënten nu eenvoudig kunnen worden vervolgd tijdens de (soms onvermijdelijke) progressie van hun ziekte *in vitro*. Dit zou een belangrijke klinische consequentie kunnen hebben. Immers, wanneer er eventuele nieuwe mutaties worden gevonden *in vitro*, dan reflecteert dit de huidige status van de patiënt.[4] Mochten hierbij pre-maligne mutaties worden gedetecteerd, dan zou een behandelplan hierop kunnen worden aangepast. Ook kan deze methode meer inzichten vergaren over de onderliggende biologie van deze (eventuele) progressie. Of daadwerkelijk ziekteprogressie met galweg organoïden kan worden gemodelleerd moet eerst nog worden uitgezocht. Daarnaast zou een belangrijke toegevoegde waarde zijn om te onderzoeken of galwegkanker (cholangiocarcinoom) – organoïden ook vanuit gal kunnen worden gekweekt. Recentelijk onderzoek heeft namelijk aangetoond dat een cholangiocarcinoom, verkregen vanuit tumorweefsel, kan worden gekweekt als organoïd waarbij de originele tumor *in vitro* wordt gerepresentateerd.[30] Een belangrijke toepassing van het model is dat de onderzoekers aantoonden dat deze organoïden kunnen worden gebruikt voor het testen van tumor-specifieke therapieën. Echter, momenteel komt slecht een minderheid van de patiënten met een cholangiocarcinoom in aanmerking voor een operatieve ingreep en kan dus alleen van deze groep materiaal worden verkregen voor een organoïden-kweek.[37] Door gebruik te maken van gal als nieuwe bron voor cholangiocarcinoom organoïden zou de patiëntenpopulatie kunnen worden uitgebreid en daardoor kan een bijdrage worden geleverd aan de behandeling van deze niet-operabele meerderheid. Tenslotte is het eerste humane *in vitro* model ontwikkeld dat vanuit volwassen galwegcellen een vertakkende morfologie vertoont. Echter, ondanks de unieke morfologie, die vertakkende galweg organoïden vertonen, gaat het ook hier alleen om een organoïd bestaande uit epitheliale cellen. Belangrijke additionele hepatische cellen en specifieke matrix ontbreken nog in dit model en het toevoegen van deze cellen zou een goede vervolgstap zijn. Daarentegen, vertonen zij een hele hoge mate van overeenkomst met het transcriptoom van primair intrahepatisch galweg epitheel. Individuele cellen van deze organoïden zijn onder andere instaat om de transcriptomische heterogeniteit van intrahepatische galwegcellen te recapituleren. Dit maakt ze dus erg geschikt als model voor intrahepatische galwegen. Nadelig is wel het feit dat het protocol erg arbeidsintensief is, zeker in vergelijking met eerder gepubliceerde galweg organoïd protocollen.[4,23] Dit maakt het

gebruik van deze cellen voor potentiële regeneratieve experimenten onhandig en niet de eerste keuze. Aan de andere kant zijn vertakkende galwegcel organoïden juist geschikt voor specifieke doeleinden. Zo kunnen ze worden gebruikt om de ontwikkeling van galwegen te modelleren, hetgeen zou kunnen zorgen voor minder gebruik van diermodellen. Een verdere interessante observatie was dat alleen vanuit de adulte intrahepatische galwegcellen deze vertakkende organoïden kunnen worden gekweekt. Een mogelijke verklaring hiervoor is dat er niet de beschikking was over primair weefsel van relatief oude foetale levers (>18 weken, het moment waarop de vertakkende galwegen ontstaan). Het zou dan ook interessant zijn om te onderzoeken of organoïden verkregen vanuit dit weefsel wel vertakkende structuren kunnen vormen. Daarnaast is aangetoond dat deze organoïden kunnen worden gebruikt voor het bestuderen van zeldzame galwegziekten, zoals het Alagille Syndroom en galwegkanker. Ze kunnen dit voor beide ziektes op een unieke manier ten opzichte van eerdere studies.[4,30] Daarom is er de hoop dat dit nieuwe *in vitro* model zal bijdragen aan de kennis en de behandeling van galwegziekten.

DEEL IV – REGENERATIEVE GENEESKUNDE

Galweg organoïden, gekweekt met het Huch protocol[4], worden geïnitieerd vanuit gedifferentieerde galwegcellen die een *in vitro* proces ondergaan waardoor ze frequenter delen, vergelijkbaar met ductale herprogrammering voor galwegcellen *in vivo*.[26] Organoïd-vorming is dus eenzelfde proces als het herstel van schade aan de galwegen *in vivo*.[35] Doordat een galweg organoïd alleen bestaat uit galwegcellen en niet uit stamcellen, zoals bijvoorbeeld het geval is voor intestinale organoïden[38], zijn galweg organoïden in potentie uitermate geschikt voor herstel van gedifferentieerd galwegepitheel. Echter, om galwegen *in vitro* te creëren heb je ook gespecialiseerde matrix, het liefst één die ook de specifieke architectuur van het beoogde orgaan nabootst, nodig waarop deze cellen kunnen groeien. Een optie voor het verkrijgen van deze matrix is het decellularizeren (leeg maken van cellen) van orgaanweefsel.[39,40] In **hoofdstuk negen** is succesvol extrahepatische galweg weefsel gedecellulariseerd. Als vervolgens galweg organoïden verkregen vanuit de extrahepatische galweg of vanuit gal deze extracellulaire matrix (ECM) scaffolds koloniseren, dan resulteert dit in het succesvol bekleden van de gehele matrix (inclusief de galweg crypten). Dit in tegenstelling tot galweg organoïden verkregen vanuit de intrahepatische galwegen, die niet in staat bleken een confluente monolaag te vormen.

Limitaties, implicaties en toekomstige directies van deel IV

Ondanks dat ECM scaffolds alleen werden gepopulariseerd in 2D en niet in een volledige 3D-buisstructuur, is dit het eerste bewijs dat humane galwegen succesvol kunnen worden leeggemaakt van cellen en functioneel kunnen worden hersteld door gebruik te maken van galweg organoïden. Vervolgexperimenten zullen moeten aantonen dat dit repopuleren ook

lukt in een buisstructuur en er zal verder onderzoek moeten plaatsvinden of deze structuren op dezelfde wijze functioneren als een humane extrahepatische galweg *in vitro* en *in vivo*. Belangrijk is dat het construct in staat moet zijn om bescherming te kunnen bieden tegen gal, zonder dat dit resulteert in celdood.[13] Verder is het van belang dat, na transplantatie, er neovascularisatie van het construct zal plaatsvinden waardoor het kan overleven. Dat dit in potentie kan gebeuren is reeds aangetoond.[41-43] Het definitieve bewijs voor deze constructen zal echter moeten worden vergaard in een *in vivo* transplantatiemodel. Echter, een belangrijk obstakel dat eerst moet worden overwonnen, voordat daadwerkelijk organoïden (of constructen) naar mensen kunnen worden getransplanteerd, is het vinden van een alternatief voor hydrogellen verkregen van muis sarcomacellen. Hydrogellen zijn essentieel voor het kweken van organoïden, maar klassiek gebruikte hydrogelen, zoals matrigel, beperken de toepasbaarheid voor gebruik in mensen.[44] Een mogelijke oplossing is het maken van hydrogellen vanuit gedecellularizeerde menselijke organen. Een recentelijke publicatie heeft aangetoond dat galweg organoïden gekweekt in een hydrogel gemaakt van gedecellularizeerde varkensdarm vergelijkbaar zijn met organoïden gekweekt in de muis-sarcoom hydrogellen (matrigel).[45] Ook moet er worden gekeken welke bron van organoïden het beste kan worden gebruikt voor klinische toepassingen. Gal lijkt hiervoor de ideale oplossing. Organoïden kunnen hier minimaal-invasief worden verkregen, waardoor er vervolgens patiënt-specifieke constructen kunnen worden gemaakt. Vooral, omdat er gebruik is gemaakt van galwegenmatrix verkregen van levers afgewezen voor transplantatie, biedt deze manier van hergebruik van de galwegen een unieke kans om nieuw extrahepatisch galwegweefsel te maken die in de toekomst kan worden getransplanteerd zonder immuunreactie.

CONCLUSIES

Galweg organoïden bieden tot nu toe ongekende mogelijkheden voor het bestuderen van galwegen *in vitro*. In dit proefschrift is de basis gelegd om deze cellen in de toekomst te kunnen gebruiken in de kliniek, is de toepasbaarheid van deze cellen om de biologie van de galwegen te bestuderen uitgebreid en is de wetenschappelijke gemeenschap rondom galweg organoïden verenigd. Tevens is aangetoond dat galwegcel organoïden geschikt zijn om galwegziekten te modelleren en is het belang van de lokale oorsprong van deze cellen beschreven. De bevinding dat deze cellen de potentie kunnen hebben om nieuwe galwegen *in vitro* te creëren, en dat deze in de nabije toekomst kunnen worden toegevoegd aan een beschadigd transplantaat biedt unieke mogelijkheden om meer donorlevers geschikt te maken voor transplantatie.

References discussion

1. Lazaridis KN, LaRusso NF. The Cholangiopathies. Mayo Clin Proc. 2015;90(6):791-800.
2. Spada M, Riva S, Maggiore G, Cintorino D, Gridelli B. Pediatric liver transplantation. World J Gastroenterol. 2009;15(6):648-674.
3. Sampaziotis F, Segeritz CP, Vallier L. Potential of human induced pluripotent stem cells in studies of liver disease. Hepatology. 2015;62(1):303-311.
4. Huch M, Gehart H, van Boxtel R, *et al.* Long-term culture of genome-stable bipotent stem cells from adult human liver. Cell. 2015;160(1-2):299-312.
5. Thethy S, Thomson BNj, Pleass H, *et al.* Management of biliary tract complications after orthotopic liver transplantation. Clin Transplant. 2004;18(6):647-653.
6. Hampe T, Dogan A, Encke J, *et al.* Biliary complications after liver transplantation. Clin Transplant. 2006;20 Suppl 17:93-96.
7. Verdonk RC, Buis CI, Porte RJ, Haagsma EB. Biliary complications after liver transplantation: a review. Scand J Gastroenterol Suppl. 2006;(243):89-101.
8. Wojcicki M, Milkiewicz P, Silva M. Biliary tract complications after liver transplantation: a review. Dig Surg. 2008;25(4):245-257.
9. Hansen T, Hollemann D, Pitton MB, *et al.* Histological examination and evaluation of donor bile ducts received during orthotopic liver transplantation--a morphological clue to ischemic-type biliary lesion?. Virchows Arch. 2012;461(1):41-48.
10. Brunner SM, Junger H, Ruemmele P, *et al.* Bile duct damage after cold storage of deceased donor livers predicts biliary complications after liver transplantation. J Hepatol. 2013;58(6):1133-1139.
11. Karimian N, Op den Dries S, Porte RJ. The origin of biliary strictures after liver transplantation: is it the amount of epithelial injury or insufficient regeneration that counts?. J Hepatol. 2013;58(6):1065-1067.
12. Beuers U, Hohenester S, de Buy Wenniger LJ, *et al.* The biliary HCO(3)(-) umbrella: a unifying hypothesis on pathogenetic and therapeutic aspects of fibrosing cholangiopathies. Hepatology. 2010;52(4):1489-1496.
13. Boyer JL. Bile formation and secretion. Compr Physiol 2013;3:1035–78.
14. Watson CJE, Kosmoliaptsis V, Randle LV, *et al.* Normothermic Perfusion in the Assessment and Preservation of Declined Livers Before Transplantation: Hyperoxia and Vasoplegia-Important Lessons From the First 12 Cases. Transplantation. 2017;101(5):1084-1098.
15. Cohn JA, Strong TV, Picciotto MR, *et al.* Localization of the cystic fibrosis transmembrane conductance regulator in human bile duct epithelial cells. Gastroenterology. 1993;105(6):1857-1864.
16. Kinnman N, Lindblad A, Housset C, *et al.* Expression of cystic fibrosis transmembrane conductance regulator in liver tissue from patients with cystic fibrosis. Hepatology. 2000;32(2):334-340.
17. O'Sullivan BP, Freedman SD. Cystic fibrosis. Lancet. 2009;373(9678):1891-1904.
18. Middleton PG, Mall MA, Dřevínek P, *et al.* Elexacaftor-Tezacaftor-Ivacaftor for Cystic Fibrosis with a Single Phe508del Allele. N Engl J Med. 2019;381(19):1809-1819.
19. Heijerman HGM, McKone EF, Downey DG, *et al.* Efficacy and safety of the elexacaftor plus tezacaftor plus ivacaftor combination regimen in people with cystic fibrosis homozygous for the F508del mutation: a double-blind, randomised, phase 3 trial [published correction appears in Lancet. 2020 May 30;395(10238):1694].

20. Ooi CY, Durie PR. Cystic fibrosis from the gastroenterologist's perspective. Nat Rev Gastroenterol Hepatol. 2016;13(3):175-185.
21. Debray D, Narkewicz MR, Bodewes FAJA, *et al.* Cystic Fibrosis-related Liver Disease: Research Challenges and Future Perspectives. J Pediatr Gastroenterol Nutr. 2017;65(4):443-448.
22. Rimland CA, Tilson SG, Morell CM, *et al.* Regional differences in human biliary tissues and corresponding *in vitro* derived organoids. Hepatology. 2021 Jan;73(1):247-267
23. Sampaziotis F, Muraro D, Tysoe OC, *et al.* Cholangiocyte organoids can repair bile ducts after transplantation in the human liver. Science. 2021 Feb 19;371(6531):839-846.
24. Rana D, Zreiqat H, Benkirane-Jessel N, *et al*. Development of decellularized scaffolds for stem cell-driven tissue engineering. J Tissue Eng Regen Med. 2017;11(4):942-965.
25. Sampaziotis F, Justin AW, Tysoe OC, *et al.* Reconstruction of the mouse extrahepatic biliary tree using primary human extrahepatic cholangiocyte organoids. Nat Med. 2017;23(8):954-963.
26. Banales JM, Huebert RC, Karlsen T, *et al.* Cholangiocyte pathobiology. Nat Rev Gastroenterol Hepatol. 2019;16(5):269-281.
27. Hannezo E, Scheele CLGJ, Moad M, *et al.* A Unifying Theory of Branching Morphogenesis. Cell. 2017 Sep 21;171(1):242-255.e27.
28. Deutsch GH, Sokol RJ, Stathos TH, Knisely AS. Proliferation to paucity: evolution of bile duct abnormalities in a case of Alagille syndrome. Pediatr Dev Pathol. 2001 Nov-Dec;4(6):559-63.
29. Hsu PD, Lander ES, Zhang F. Development and applications of CRISPR-Cas9 for genome engineering. Cell. 2014 Jun 5;157(6):1262-1278.
30. Broutier L, Mastrogiovanni G, Verstegen MM, *et al.* Human primary liver cancer-derived organoid cultures for disease modeling and drug screening. Nat Med. 2017;23(12):1424-1435.
31. Aizarani N, Saviano A, Sagar, *et al.* A human liver cell atlas reveals heterogeneity and epithelial progenitors. Nature. 2019;572(7768):199-204.
32. Raven A, Lu WY, Man TY, *et al.* Cholangiocytes act as facultative liver stem cells during impaired hepatocyte regeneration [published correction appears in Nature. 2018 Mar 14;555(7696):402]. Nature. 2017;547(7663):350-354.
33. Zong Y, Stanger BZ. Molecular mechanisms of bile duct development. Int J Biochem Cell Biol. 2011;43(2):257-264.
34. Aloia L, McKie MA, Vernaz G, *et al.* Epigenetic remodeling licences adult cholangiocytes for organoid formation and liver regeneration. Nat Cell Biol. 2019;21(11):1321-1333.
35. Planas-Paz L, Sun T, Pikiolek M, *et al.* YAP, but Not RSPO-LGR4/5, Signaling in Biliary Epithelial Cells Promotes a Ductular Reaction in Response to Liver Injury. Cell Stem Cell. 2019;25(1):39-53.e10.
36. Fujii M, Matano M, Toshimitsu K, *et al.* Human Intestinal Organoids Maintain Self-Renewal Capacity and Cellular Diversity in Niche-Inspired Culture Condition. Cell Stem Cell. 2018;23(6):787-793.e6.
37. Nagino M, Ebata T, Yokoyama Y, *et al.* Evolution of surgical treatment for perihilar cholangiocarcinoma: a single-center 34-year review of 574 consecutive resections. Ann Surg. 2013;258(1):129-140.
38. Sato T, Vries RG, Snippert HJ, *et al.* Single Lgr5 stem cells build crypt-villus structures *in vitro* without a mesenchymal niche. Nature. 2009;459(7244):262-265.
39. Badylak SF, Freytes DO, Gilbert TW. Extracellular matrix as a biological scaffold material: Structure and function. Acta Biomater. 2009;5(1):1-13.

40. Rana D, Zreiqat H, Benkirane-Jessel N, *et al.* Development of decellularized scaffolds for stem cell-driven tissue engineering. J Tissue Eng Regen Med. 2017;11(4):942-965.
41. Miyazawa M, Torii T, Toshimitsu Y, *et al.* A tissue-engineered artificial bile duct grown to resemble the native bile duct. Am J Transplant. 2005;5(6):1541-1547.
42. Cushieri A, Baker PR, Anderson RJ, Holley MP. Total and subtotal replacement of the common bile duct: effect of transhepatic silicone tube stenting. Gut. 1983;24(8):756-760.
43. Christensen M, Laursen HB, Rokkjaer M, *et al.* Reconstruction of the common bile duct by a vascular prosthetic graft: an experimental study in pigs. J Hepatobiliary Pancreat Surg. 2005;12(3):231-234.
44. Saheli M, Sepantafar M, Pournasr B, *et al.* Three-dimensional liver-derived extracellular matrix hydrogel promotes liver organoids function. J Cell Biochem. 2018;119(6):4320-4333.
45. Giobbe GG, Crowley C, Luni C, *et al.* Extracellular matrix hydrogel derived from decellularized tissues enables endodermal organoid culture. Nat Commun. 2019;10(1):5658

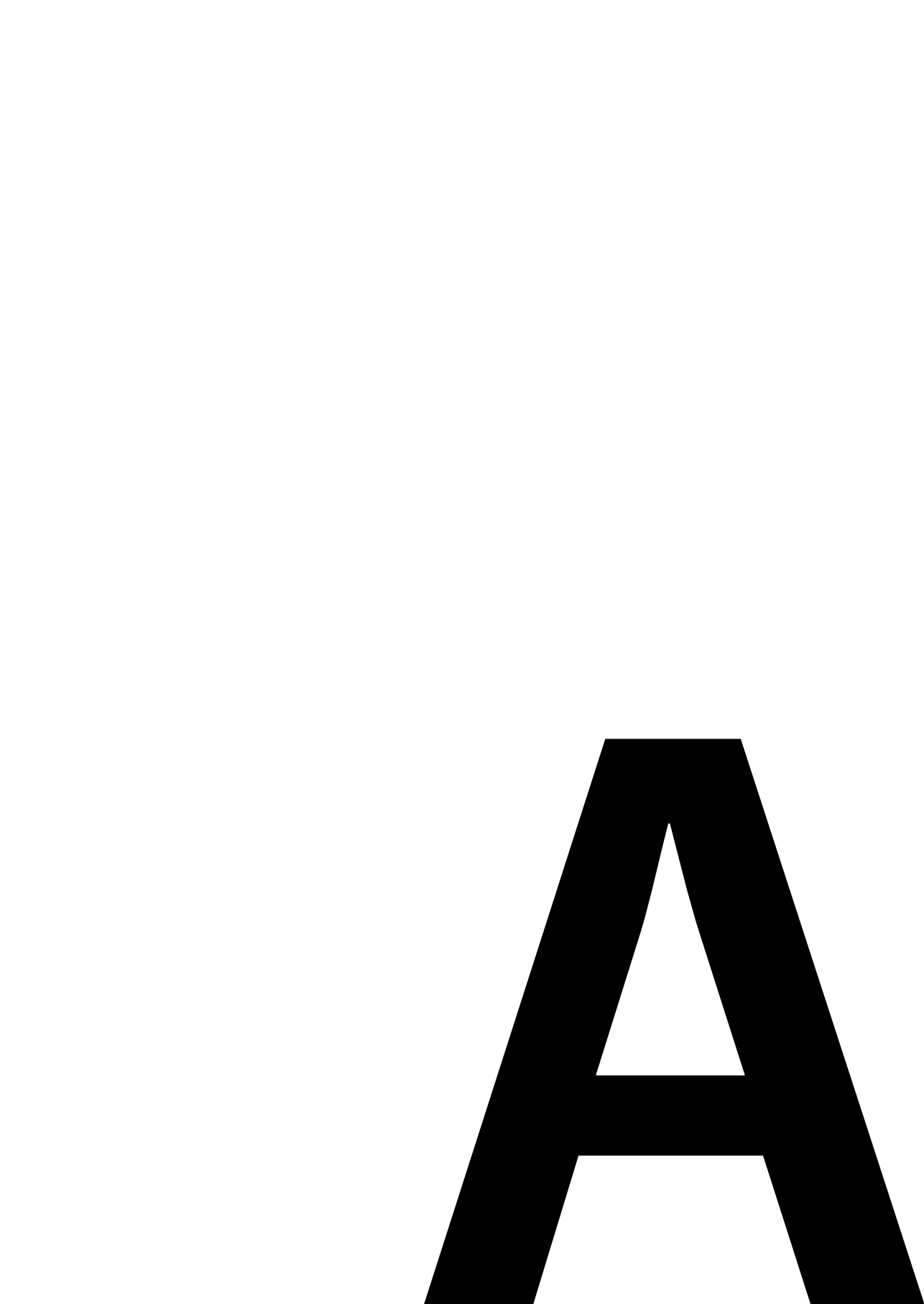

APPENDICES

PhD portfolio

Bibliography

Curriculum Vitae

Dankwoord

PHD PORTFOLIO

PhD Candidate Floris J.M. Roos
Department Surgery
Promotoren Prof.dr. J.N.M. IJzermans & Prof. dr. L.J.W. van der Laan
Co-promotor Dr. ing. M.M.A. Verstegen
Research period June 2017 –May 2021

1. PhD Training	Year	Workload	ECTS
Courses			
Gastroenterology Seminar, Department of Gastroenterology and Hepatology, Erasmus MC, Rotterdam	2017 - 2020	150 hours	7.0
Integrity in scientific research, dept. of Medical Ethics and philosophy, Erasmus MC, Rotterdam	2017	8 hours	0.3
Basic Introduction course on SPSS, MolMed, Erasmus MC, Rotterdam	2017	20 hours	1.0
Basic Confocal Microscopy, Optical Image Center, Erasmus MC, Rotterdam	2018	8 hours	-
Photoshop and lllustrator CC 2019 Workshop for PhD-students, MolMed, Erasmus MC, Rotterdam	2019	16 hours	0.3
Biomedical English Writing Course, MolMed, Erasmus MC, Rotterdam	2019	40 hours	2.0
Oral Presentations	**Year**	**Workload**	**ECTS**
The role of recipient epithelial cells in regeneration after liver transplantation: Different kinetics of chimerism for hepatocytes and bile duct epithelial cells, 29th Boot conference, Nederlandse Transplantatie Vereniging (NTV), Zeist	2017	8 hours	0.3
The role of recipient epithelial cells in regeneration after liver transplantation: Different kinetics of chimerism for hepatocytes and bile duct epithelial cells, 23rd Annual Congress of the International Liver Transplantation Society (ILTS), Prague, Czech Republic	2017	8 hours	0.3
The role of recipient epithelial cells in regeneration after liver transplantation: Different kinetics of chimerism for hepatocytes and bile duct epithelial cells, Annual Science Surgery Day, Erasmus Medical Center	2018	8 hours	0.3
Bile as a non-invasive source of cholangiocyte organoids for developing patient-specific disease modeling and personalized regenerative medicine, Symposium voor Experimentele Onderzoeken Heelkundige Specialismen, Rotterdam	2018	8 hours	0.3
Bile as a non-invasive source of cholangiocyte organoids for developing patient-specific disease modeling and personalized regenerative medicine, Najaarscongres, Nederlandse Vereniging voor de Heelkunde, Ede	2018	8 hours	0.3

Bile as a non-invasive source of cholangiocyte organoids for developing patient-specific disease modeling and personalized regenerative medicine, Annual Science Surgery Day, Erasmus Medical Center	2019	8 hours	0.3
Identification of new drug targets to prevent ischemia-induced bile toxicity using a human biliary organoid model, 9th Dutch Liver Retreat, Nederlandse Vereniging voor Hepatologie (NVH), Spier	2019	8 hours	0.3
Bile as a non-invasive source of cholangiocyte organoids for developing patient-specific disease modeling and personalized regenerative medicine, 32nd Boot conference, NTV, Amsterdam	2019	8 hours	0.3
Identification of new drug targets to prevent ischemia-induced bile toxicity using a human biliary organoid model, 32nd Boot conference, NTV, Amsterdam	2019	8 hours	0.3
Bile as a non-invasive source of cholangiocyte organoids for developing patient-specific disease modeling and personalized regenerative medicine, 54th International Liver Conference (ILC) of the European Association for the study of the Liver (EASL), Vienna, Austria	2019	8 hours	0.3
Bile as a non-invasive source of cholangiocyte organoids for developing patient-specific disease modeling and personalized regenerative medicine, 25th Annual Congress of the ILTS, Toronto, Canada	2019	8 hours	0.3

1. PhD Training - Poster Presentations	**Year**	**Workload**	**ECTS**
The effectiveness of non-surgical interventions in biliary duct complications after liver transplantation, 29th Boot conference, NTV, Zeist	2017	8 hours	0.3
The role of recipient epithelial cells in regeneration after liver transplantation: Different kinetics of chimerism for hepatocytes and bile duct epithelial cells, 52nd ILC of the EASL, Amsterdam	2018	8 hours	0.3
Bile as a non-invasive source of cholangiocyte organoids for developing patient-specific disease modeling and personalized regenerative medicine, Stem Cells & Organoids in Development & Disease, International Society for Stem Cell Research, Amsterdam	2019	8 hours	0.3
Identification of new drug targets to prevent ischemia-induced bile toxicity using a human biliary organoid model, 54th ILC of the EASL, Vienna, Austria	2019	8 hours	0.3

1. PhD Training Attended (international) conferences and seminars	Year	Workload	ECTS
7th Dutch Liver Retreat, NVH, Spier	2016	10 hours	0.4
Dutch Association of Gastroenterology (NVGE), Spring meeting, Veldhoven	2016	16 hours	0.6
Dutch Association of Gastroenterology, Spring Meeting, Veldhoven	2017	16 hours	0.6
29th Bootcongres, NTV, Zeist 52nd ILC of the EASL, Amsterdam 23rd Annual Congres of the ILTS, Prague, Czech Republic	2017	16 hours	0.6
Dutch Association of Gastroenterology, Fall Meeting, Veldhoven	2017	16 hours	0.6
8th Dutch Liver Retreat, NVH, Spier	2018	10 hours	0.4
Annual Science Surgery Day, dept. of Surgery, Erasmus MC	2019	6 hours	0.2
30th Bootcongres, NTV, Rotterdam	2018	16 hours	0.6
32nd Erasmus Liver Day	2018	8 hours	0.3
SEOHS, Rotterdam	2018	8 hours	0.3
9th Dutch Liver Retreat, NVH, Spier	2019	10 hours	0.4
Annual Science Surgery Day, dept. of Surgery, Erasmus MC	2019	6 hours	0.2
31st Bootcongres, NTV, Amsterdam	2019	16 hours	0.6
54nd ILC of the EASL, Vienna, Austria	2019	36 hours	0.9
25rd Annual ILTS conference, Toronto, Canada	2019	36 hours	0.9
10th Dutch Liver Retreat, NVH, Spier	2020	16 hours	0.6
55nd ILC of the EASL (digital)	2020	20 hours	0.7

Awards and Grants received	Year	Awarded
Grant: Coolsingel Stichting	2016	€15.000
Best Abstract Boot conference, NTV, Zeist	2017	
Grant: Anna&Maurits de Kock Stichting with Jorke Willemse	2018	€35.000
Best Oral Presentation, SEOHS, Rotterdam	2018	€500
1st Price, 'Nel Kreeft' Award, Science Surgery Day, Erasmus MC	2019	
Grant: Astellas "Trans(p)la(n)t(at)ion Research Award", NTV, Amsterdam	2019	€5.000
ILTS "Rising Star Award" for top research, Toronto, Canada	2019	€1.500
Young Investigator Award, 54th ILC of the EASL, Vienna, Austria	2019	€800
Erasmus Trustfunds, Internship Grant	2019	€500
'Onderzoeksbeurs', NVH	2020	€500
'Scholingsbeurs', NTV	2020	€500
EASL Regenerative Hepatology: 'Albert Geerts Fellowship'	2021	€40.000

2. Teaching	Year	Workload	ECTS
Lecturing			
Chimerism during Transplantation, Gastroenterology and Transplantation Minor, Erasmus MC	2018-2020	12 hours	0.7
ROEM Meeting, Cholangioyte Organoids, Erasmus MC	2018	4 hours	0.1
Experimental Progress in Transplantation, Junior Medicine, Erasmus MC	2020	4 hours	0.1
Supervision			
Systematic Review of three Bachelor Students groups, Minor Gastroenterology and Transplantation, Erasmus MC	2017-2020	32 hours	1.0
Systematic Review of two Bachelor Students Groups, "Keuzeonderwijs Transplantatiegeneeskunde", Erasmus MC	2017-2019	20 hours	0.7
2. Teaching - Supervision			
Master graduation project Kim Heckmans, Biomedical Science, Leiden University (six months)	2018	192 hours	6.9
Master graduation project Laura Muñoz-Albarinos, Molecular Medicine, Erasmus MC (eight months)	2019	256 hours	9.2
Master graduation project Sabrah Niesten, Nano Biology, University of Delft (seven months)	2019-2020	224 hours	8.0
Master graduation project Dina Vinke (eight months), Regenerative Medicine and Technology, University of Utrecht	2020-2021	256 hours	9.2
3. Extracurricular	**Year**	**Workload**	**ECTS**
Peer reviewing of manuscripts: Canadian Journal of Gastroenterology, Liver International, Stem Cell Reports	2018-2021	16 hours	0.6
Organizing Committee Dutch Liver Retreat	2020-2022	40 hours	

BIBLIOGRAPHY

Roos FJM, Poley JW, Polak WG, Metselaar HJ. Biliary complications after liver transplantation; recent developments in etiology, diagnosis and endoscopic treatment. Best Practice & research: Clinical Gastroenterology. 2017 Apr;31(2):227-235.

Verstegen MMA, **Roos FJM***, Burka K*, Gehart H, Jager M, de Wolf M, Bijvelds MJC, de Jonge HR, Ardisasmita AI, van Huizen NA, Roest HP, de Jonge J, Koch M, Pampaloni F, Fuchs SA, Schene IF, Luider TM, van der Doef HPJ, Bodewes FAJA, de Kleine RHJ, Spee B, Kremers GJ, Clevers H, IJzermans JNM, Cuppen E, van der Laan LJW. Scientific Reports. 2020 Dec 14;10(1):21900. *these authors contributed equally.

Willemse J, **Roos FJM**, Voogt IJ, Schurink IJ, Bijvelds M, de Jonge HR, van der Laan LJW, de Jonge J, Verstegen MMA. Scaffolds obtained from decellularized human extrahepatic bile ducts support organoids to establish functional biliary tissue in a dish. Biotechnology and Bioengineering. 2021 Feb;118(2):836-851.

Roos FJM, Verstegen MMA, Muñoz Albarinos L, *et al.* Human bile contains cholangiocyte organoid initiating cells which expand as functional cholangiocytes in non-canonical Wnt stimulating conditions. Frontiers in Cell and Developmental Biology. 2021 Feb 9;8:630492.

Roos FJM, Bijvelds MJC*, Verstegen MMA*, Roest HP, Metselaar HJ, Polak WG, Jonge HR, IJzermans JNM, van der Laan LJW. Impact of hypoxia and AMPK on CFTR-mediated bicarbonate secretion in human cholangiocyte organoids. American Journal of Physiology-Gastrointestinal and Liver Physiology. 2021 May 1;320(5):G741-G752. *these authors contributed equally.

Roos FJM*, Marsee A*, Verstegen MMA; HPB Organoid Consortium[#], Gehart H, de Koning E, Lemaigre F, Forbes SJ, Peng WC, Huch M, Takebe T, Vallier L, Clevers H, van der Laan LJW[×], Spee B[×]. Building Consensus on Definition and Nomenclature of Hepatic, Pancreatic and Biliary Organoids. Cell Stem Cell. 2021 May 6;28(5):816-832. *these authors contributed equally, #for author list of HPB organoid consortium, please see Table S1 of chapter 2, ×shared senior authorship.

Roos FJM*, Wu H*, Willemse J, Lieshout R, Muñoz Albarinos LA, Kan YY, Poley JW, Bruno MJ, de Jonge J, Bártfai R, Marks H, IJzermans JNM, Verstegen MMA[×], van der Laan LJW[×]. Cholangiocyte organoids from human bile retain a local phenotype and can repopulate bile ducts *in vitro*. Clinical and Translational Medicine. 2021;11(12):e566. *these authors contributed equally, ×shared senior authorship.

Bijvelds MJC, **Roos FJM**, Meijsen KF, Roest HP, Verstegen MMA, Janssens HM, van der Laan LJW, de Jonge HR. Rescue of chloride and bicarbonate transport by elexacaftor-ivacaftor-tezacaftor in organoid-derived CF intestinal and cholangiocyte monolayers. Journal of Cystic Fibrosis. 2021 Dec 15:S1569-1993(21)02165-2.

PUBLICATIONS OUTSIDE THE SCOPE OF THIS THESIS

Roos FJM, IJzermans JNM, van der Laan LJW. Reply to "Detection and Analysis of Circulating Epithelial Cells in Liquid Biopsies from Patients with Liver Disease": Implications for Transplant Chimerism. Gastroenterology. 2019 May;156(6):1932-1933.

Willemse J, **Roos FJM**, Voogt IJ, Schurink IJ, Bijvelds M, de Jonge HR, van der Laan LJW, de Jonge J, Verstegen MMA. Cover Image, Biotechnology and Bioengineering, Volume 118, Number 2, February 2021. Cover image was based upon Scaffolds obtained from decellularized human extrahepatic bile ducts support organoids to establish functional biliary tissue in a dish.

van der Laan LJW, **Roos FJM**, Verstegen MMA. Bile Duct Repair in Human Liver Grafts: Effective Cholangiocyte Organoid Engraftment and Plasticity. Hepatology. 2021 Oct;74(4):2287-2289.

Shi S, Verstegen MMA, Roest HP, Ardisasmita AI, Cao W, **Roos FJM**, de Ruiter PE, Niemeijer M, Pan Q, IJzermans JNM, van der Laan LJW. Recapitulating Cholangiopathy-Associated Necroptotic Cell Death In Vitro Using Human Cholangiocyte Organoids. Cellular and Molecular Gastroenterology and Hepatology. 2021 Oct 23;13(2):541-564.

CURRICULUM VITAE

Floris Johan Maria Roos werd geboren op 1 juli 1992 te ’s-Gravenhage. Na het behalen van zijn VWO-diploma aan het Dalton Voorburg, te Voorburg begon hij in 2010 met de Bachelor Geneeskunde aan de Universiteit van Rotterdam. Gedurende zijn gehele Universitaire studie heeft hij gewerkt als student-assistent aan de Vaat-en Transplantatiechirurgie van het Erasmus MC. Het is alhier waar zijn passie voor de Heelkunde en de lever ontstond. Tijdens zijn co-schappen werd zijn voorkeur voor de Heelkunde verder bevestigd, waarna hij werd verkozen om deel te nemen aan het “Dedicated Schakeljaar” Heelkunde 2016 (begeleiders dr. T.M.A.L. Klem en dr. B.P.L. Wijnhoven) en begon hij met onderzoek te doen naar de galwegen, hetgeen resulteerde in zijn eerste publicatie. Het opgestarte onderzoek kon worden uitgebreid tot volwaardig promotietraject binnen het Laboratorium voor Experimentele Transplantatie en Intestinale Chirugie (LETIS) onder begeleiding van prof.dr. Luc van der Laan, prof.dr. Jan IJzermans en dr. Monique Verstegen in het Erasmus MC en heeft hij de mogelijkheid gekregen om het onderzoek uit te breiden in het Jeffrey Cheah Biomedical Centre Instituut aan de Universiteit van Cambridge (begeleiders prof.dr. Ludovic Vallier en dr. Fotis Sampaziotis), helaas werd dit vanwege de COVID-19 pandemie voortijd beëindigd. Hij is voor zijn werk meervoudig beloond met prijzen op (inter)nationale congressen (o.a. Rising Star Award, International Liver Transplantation Society, 2019 Toronto en Best Abstract Bootcongres van de Nederlandse Transplantatie Vereniging 2017 en 2019). Tijdens zijn promotieonderzoek was hij actief betrokken bij het onderwijs van de Heelkunde en behoorde hij tweevoudig tot de organisatie van de “Dutch Liver Retreat”, het landelijk experimentele congres van der lever georganiseerd door de Nederlandse Vereniging voor Hepatologie. Momenteel, heeft hij opnieuw de kans gekregen om te werken aan de Universiteit van Cambridge en werkt hij daar als klinische research associate op de afdeling Heelkunde en in het Cambridge Stem Cell Institute**.** Floris woont in Cambridge, Verenigd Koninkrijk.

Floris Johan Maria Roos was born 1st of July 1992 in the Hague (The Netherlands). After obtaining his high school degree he started studying Medicine in Rotterdam. During his study-period he worked at several wards in the Erasmus MC. It is here were his interest in the liver and Surgery was raised. During his internships this interest continued and was he selected to enroll in the “Dedicated Schakeljaar” 2016 program at the department of Surgery (supervisors dr. T.M.A.L. Klem and dr. B.P.L. Wijnhoven) and started conducting research into the bile ducts, resulting in his first publication. Elaborating on this project a PhD-trajectory was initiated under supervision of prof. dr. Luc van der Laan, prof.dr. Jan IJzermans en dr. Monique Verstegen in the Erasmus MC and he performed an internship at the University of Cambridge (supervisor prof.dr. Ludovic Vallier and dr. Fotis Sampaziotis), which was prematurely ended due to the COVID-19 pandemic. He has won numerous awards and grants during the trajectory as well as being an active participant in education for young Medical students. Currently, he restarted working at the University of Cambridge as a clinical research fellow on cholangiocyte organoids/clinician at the surgical ward. Floris lives in Cambridge, United Kingdom.

DANKWOORD

Ik ben ontzettend blij en content dat het daadwerkelijk gelukt is om dit proefschrift te maken. Deze thesis was er nooit gekomen zonder de hulp van jullie allemaal. Graag wil ik dan ook iedereen van harte bedanken die heeft meegeholpen hieraan, een aantal van jullie wil ik extra in het zonnetje zetten.

Hooggeleerde L.J.W. van der Laan, beste **Luc**. Bovenstaande geldt in het bijzonder voor jou. Jij hebt mij tijdens mijn masterstage onder je hoede genomen en *echt* grootgebracht in het doolhof van basaal wetenschappelijk onderzoek. Je enthousiasme en creativiteit heb ik altijd enorm gewaardeerd en ik heb altijd het gevoel gehad alsof wij vele handen op één buik waren, die als we eenmaal begonnen met filosoferen over één kleine vraag eindigden met een twee uur durend gesprek. Daarom kon ik het ook altijd prima hebben als manuscripten weer eens maanden bij je op het bureau bleven liggen. Ik kan mij geen betere begeleider voor mijn onderzoek voorstellen en ik hoop dat wij samen de komende jaren het onderzoek kunnen voortzetten.

Hooggeleerde J.N.M. IJzermans, beste **Jan**. Onze eerste ontmoeting, waarbij ik kwam vragen om onderzoek bij u te mogen doen, zal ik nooit vergeten. U stelde scherpe en relevante vragen, waar ik voor mijn gevoel niet altijd een goed antwoord op had. Gelukkig heeft u mij een kans willen geven en hebben wij samen dit mooie avontuur beleefd. Ik waardeer altijd ieder telefoontje en gesprek (vaak over al het andere dan wetenchap) die we hebben gehad, zowel privé (ook tijdens slechte periodes), als over werk. U heeft me altijd mijn gang laten gaan zonder ofwel de klinische relevantie te benadrukken, dan wel –de altijd terechte- kritische noot te leveren. Waarvoor veel dank.

Zeergeleerde M.M.A. Verstegen, beste **Monique**. De eerste twee jaar van dit traject was je zijdelings betrokken; langzaamaan werd het duidelijk dat Luc professor ging worden en we dus opzoek moesten naar een nieuwe co-promotor. Ik ben ontzettend blij dat jij dit bent geworden. Ik denk dat de dagen waar ik niet binnenviel in je kamer om “één korte vraag” te stellen in de afgelopen jaren op één hand te tellen zijn. Ondanks dat schrijven van manuscripten niet mijn grootste specialiteit bleken, worstelde je je hier altijd doorheen en was je altijd de eerste die het weer volledig gereviseerd terugstuurde. Vele hoogtepunten van mijn proefschrift waren nooit gelukt zonder jou, heel veel dank.

Hooggeleerde M.P. Peppelenbosch, beste **Maikel**. Zelden heb ik zo gelachen om een professor als hij ging speechen of langskwam op EE-830 en zelden heb ik zoveel bewondering gehad voor iemands parate kennis en wetenschapsdrift. Ik heb groot bewondering voor uw creativiteit en het enorm brede veld van wetenschap dat u bestudeert. Bedankt voor alle goede vrijdag middag gesprekken en scherpe vragen, ik ben ontzettend blij dat u deelneemt in mijn lees commissie.

Hooggeleerde U.H.W. Beuers, beste **Ulrich**. Ik denk dat wij elkaar voor het eerst ontmoette op de DLR van 2015. Iedere volgende keer dat wij elkaar zagen konden we altijd

een goed praatje maken (over onderzoek) en toonde u altijd interesse in wat wij hier aan t doen waren in Rotterdam. Ik ben blij dat uw lab ook langzaam organoïden aan het incorporeren is om cholangiocyten mee te bestuderen en dat u als cholangiocyten expert wilt deenemen in mijn lees commissie.

Hooggeleerde S.W.C. van Mil, beste **Saskia**. Dank u wel voor het plaatsnemen in mijn lees commissie. Ik kijk ernaar uit om op een later moment met u van gedachten te wisselen over het proefschrift.

Zeergeleerde K. Schneeberger, beste **Kirsten**. Hartelijk dank voor het plaatsnemen in mijn grote commissie. Als een expert binnen het Nederlandse organoïden veld en één die oog heeft voor de toekomst vooral met betrekking tot klinische toepassingen ben ik erg blij dat u wilt deelnemen aan de discussie, ik kijk ernaar uit.

Highly learned, L. Vallier and very learned F. Sampaziotis, dear **Ludovic** and **Fotis.** I am forever within your dept. You were willing to listen to a "fanboi" of your work during a congress and gave him the opportunity to come and work with you in Cambridge. Both of you helped raise the scientific value of my research and helped me establish multiple papers on cholangiocyte organoids. I am very grateful that both of you were willing to come and participate in my committee and I look forward to the discussion.

Hooggeleerde R. Shiri - Sverdlov, beste **Ronit**. Wij kennen elkaar sinds verschillende DLR-congressen in Spier en hebben zelfs meermaals het congres samen mogen organiseren. Ik heb altijd genoten van het prettig samenwerken, maar ook van uw scherpe opmerkingen en vragen tijdens presentaties. Ik kijk ernaar uit om dit voor te zetten tijdens de verdediging.

Hooggeleerde H.J. Metselaar, beste **Herold**. Voor u geldt, dat dit proefschrift zelfs nooit was geïnitieerd zonder uw hulp. Vanaf jongs af aan ben ik onder uw vleugels mogen opgroeien en u heeft mij geïntroduceerd bij prof. van der Laan en prof. IJzermans, veel dank voor dit al.

I want to thank the additional members of the steering committee of our consensus paper: **Prof. H. Clevers, Prof. T. Takebe, Prof. E. de Koning, Prof. H. Gehart, Prof. F. Lemaigre, dr. M. Huch, dr. W. Peng, Prof. Forbes** but especially **dr.** B. (**Bart**) Spee and **Ary Marsee.** Dear Ary, we had a lot of fun writing this article and talking to all the experts in the field. I couldn't imagine doing this project with anyone else, we really worked together and gave it our best. We became good friends and will continue to work together in the future for sure. Thank you for your English revisions of my discussion and good luck with your thesis as well as being a newly dad! Beste **Bart**, jij initieerde dit project en kwam bij ons uit en gunde mij ook nog eens een eerste auteur positie. Hartstikke bedankt hiervoor het was een eer om mede de kar te mogen trekken.

To **prof. B. Simons, Ignacio**, **Daniel, Haoyu, dr. M. van Royen, dr. R. Bártfai and dr. H. Marks,** thank you for the valid collaborating on our branching organoids project. Without your help it would never have become such a nice story.

Lieve collega (onderzoekers) van de Heelkunde, de MDL en het Laboratorium van de MDL met wie ik de afgelopen jaren heb mogen samenwerken en borrelen, bedankt. Jullie hebben dit proefschrift tot één groot leuk avontuur gemaakt, een aantal hebben dat extra in het bijzonder gedaan.

"Luc's apprentices", Lieve **Jasmijn**, **Jorke** en **Ruby**. Vanaf de allereerste dag dat wij samenwaren hebben we een ongelofelijk leuke klik gehad. Na vier jaar gaat er denk ik geen week voorbij dat we elkaar niet appen (het hoogtepunt van de appgroep was vaak woensdagochtend tussen 9:00 en 10:30), met elkaar lachen en ondersteunen. Op een mooie vriendschap voor het leven en heel veel succes met jullie laatste loodjes.

Jorke of tegenwoordig dr. Willemse. Ik ben altijd onder de indruk van je geweest vanwege jouw snelheid op de racefiets, jouw kunde om enorme hoeveelheden alcohol naar binnen te werken zonder dronken te worden, maar bovenal je kennis binnen dit vakgebied. Als de twee meest uitgesproken ego's binnen onze groep zijn we in de afgelopen vier jaar ook wel eens kort gebotst, maar dat duurde dan ook maar vijf minute en eindigde altijd met een knuffel (ook al hield je daar niet van). De duct-recell en de ILTS in Toronto met jou waren beide hoogtepunten tijdens mijn PhD. Ik ben onwijs blij om je aan mijn zijde te mogen hebben als **paranimf**; als ik flauwval, ik reken op je.

All collega's binnen **groep Luc. Gilles** het was echt onwijs leuk dat jij bij ons kwam werken halverwege mijn traject. Ik heb altijd heerlijk met je kunnen lachen, bier drinken en sporten. Veel succes in de komende jaren en ik ben ervan overtuigd dat we elkaar nog zullen zien. **Ivo** and **Shaojun** (hopefully I finally spell your name correctly), you both were my (almost) Medical Doctors partners in the lab. Which was nice, cause sometimes instead of talking about cell-matrix interactions it is also nice to talk about clinic-related stuff. Good luck to you both with the last straws and we will see each other soon during your defenses! Dr. **H(enk) Roest**, Kameradski, Tovaritsj! Dankjewel voor alle hulp altijd met welke vorm dan ook van het analyseren, visualiseren van gen-expressie data. Mr. qPCR is een eretitel die je met verve hebt verdiend, maar ook altijd de borrels (sorry nog voor die ene keer met die fles wijn…), pingpongen en fietstochten op weg naar het EMC waren altijd erg gezellig. **Petra**, **Yik** en **Kubra**, dankjewel voor alles altijd tiptop in orde te maken en het ondersteunen met kweken. In het bijzonder **Petra** veel dank voor jouw hulp met altijd alle differentiatie projecten. Je was van onschatbare waarde.

Bastiaan, mijn metgezel van de Heelkunde op het lab! Wat was het jammer dat jij het EE8 kamer al zo snel weer ging verlaten. Ik heb altijd onwijs kunnen lachen om je fameuze uitspraken: "Zijn er nog roddels." "Zo'n unit." en "Carole Baskin killed her husband". Het was iedere week weer een plezier om je te verslaan met pingpong, succes de komende 2 jaar nog met het genezen van HCC, zet hem op!

Michiel, van iedereen die eerder wegging dan ik van het lab, mis ik jou het meest. De lunches waren een heerlijk filosofisch moment, je wist altijd een zeer uitgesproken mening haaks op

de mijne te kiezen waardoor er leuke en interessante discussies volgden. Daarnaast altijd in voor een gezellige vrijmibo of buien de werktijd om activiteit. Veel succes met het afronden van je promotie en het schoppen tot MDL-arts. **Vincent,** we hebben langdurig mogen samenwerken en het was dan ook jammer toen je het lab verliet. Bedankt voor alle leuke gesprekken, goede lab adviezen en vele biertjes. Tot snel in de endoscopie kamer!
Lieve Lisette, wij zijn al zolang vrienden! Wat was het jammer toen je naar het hoge Noorden ging verhuizen. Er is niemand die mij zo aan het lachen kan maken als jij, ik waardeer je directe oprechtheid enorm. Dinertjes samen (zeker bij Boca's) zijn altijd gezellig en niets is leuker dan me samen met jou vol proppen! Bedankt voor al je steun en zeker ook op de moeilijkste momenten en bedankt dat je helemaal uit het Noorden bent overgekomen!
Lieve Caroline, mijn beste jeugdvriendin sinds (ik denk nu bijna) 15 jaar? Ik koester onze vriendschap enorm en niets is heerlijker dan een goede vriend te hebben buiten het (bio)Medische wereldje om waartegen je af en toe lekker kan aanzeiken!
Dan zijn er nog mijn twee oude kamergenootjes van Ca-411: **Rosalie en Kasper**. Dankjewel voor jullie goede opvoeding. Kasper, jouw ongelooflijke enthousiasme is ongeëvenaard en Rosalie jouw algemene kennis (over iedere zaak ter wereld) en vriendelijkheid is iets waar ik heel lekker op ga. Het is denk ik tijd voor een cola zerotje! ☺

Mijn tennisteampje aka de helden van de competitie: Martijn, Paul, Niels en Wing. Al zolang vrienden wat kan je hier nog tegen zeggen. Tennis was al jarenlang de perfecte afleiding tijdens werk, iedere zondag superfit klaar voor competitie! Het bier en de borrelplank smaakte altijd goed ☺ **Daphne** bedankt voor alle leuke en zware uitputtende crawlende momenten in de vroege morgen. Als mede de wijntjes achteraf! Tot snel op zaterdag en op het volgende congres! #duimpjebokshandschoen. **Ruben** en **Lisette**, bedankt voor alle gezelligheid, gegolf en borrels!

To all the **colleagues from the Laboratory** who made life fun and my research better: Amy, Robbie, Lucia, Monique, Lauke, Thijmen, Lisanne, Gülce, Suk-Yee, Kateryna, Sunrui, Gertine, Patrick, Anthonie, Gwenny, Ron, Auke and all the rest Thank you for all the parties, the vrijmibo's, the pubquizes and trips towards Germany for the Oktoberfest. It was truly great and memorable. In het bijzonder de **CF-groep: Nathasha** en **Kelly**: we hebben met zijn drieën heerlijk samengewerktdit maakte het doen van experimenten vele malen leuker. **Dr. M. Bijvelds** en **prof. H. de Jonge**, wat was het altijd heerlijk om te filosoferen over ion-transporten en signaling in cholangiocyten. Ik kan jullie niet genoeg bedanken voor de bijdrage die jullie hebben geleverd aan mijn proefschrift. To everybody in **Cambridge**, thank you fort he warm welcome and I look forward to drinking and doing science with you all!

Iedereen die heeft geholpen met het verkrijgen van **materialen**: het **LTx-team,** de **HPB-chirurgen**, **dr. Wojtek Polak,** bedankt altijd voor alle steun en jouw hulp bij het ischemie

project, **dr. Jeroen de Jonge** bedankt dat ik mocht bijdragen aan jullie onwijze gave decell en recell projecten, de **verpleging van de MDL-scopie afdeling**, **prof. M. Bruno** en **dr. Jan-Werner Poley**. Jullie zijn allemaal onbetaalbaar geweest voor mijn promotie, bedankt! Aan **dr. T. Klem** en **dr. B. Wijnhoven** bedankt dat jullie mij de kans hebben gegeven om deel te nemen aan het Schakeljaar programma, uiteindelijk heeft het onderzoek dat we toen geïnitieerd hebben direct geleidt tot mijn promotietraject. En tenslotte in het bijzonder **de secretaresses** van de Heelkunde (**Carola** en **Anita**), maar zeker **Leonie** van de MDL mag niet worden vergeten. Zonder jullie lag dit boekje nu nog ergens rond te zweven tussen wal en schip. Lieve **May** en **Amir** bedankt voor alle interesse in mijn onderzoek, goede gesprekken en gastvrijheid over de afgelopen jaren!

Dan de mensen die echt niet mogen worden vergeten: **mijn familie**. Allereerst mijn broertjes Martijn, **Maurits** en **Friso**. Maupie en Willy ik denk dat geen app-groep zo actief is geweest in de afgelopen jaren als TV-kijken (nu re-named naar OSM-kijken). Ik heb iedere dag wel één moment heel hard moeten lachen. Ik heb genoten van jullie ontwikkeling -en dan bedoel ik niet alleen in spiermassa toename- en ik kan niet trotser op jullie zijn. Maurits, ik ben onwijs blij dat je naast me staat vandaag als 2de **paranimf**. Jarenlang samen een kamer gedeeld bij mama en papa thuis, net als ik Geneeskunde gaan studeren en we zien elkaar nog iedere week. Ik kan me geen betere paranimf bedenken. Friso, inmiddels fulltime de brauw jonge met een “Zlatan-achtige” bluf attitude waar je trots op kan zijn. Dankjewel voor alle steun, etentjes, het corrigeren van mijn Nederlandse introductie en de biertjes; als je me nu eens kan laat winnen met OSM zijn we helemaal goed! **Martijn,** de 2de van de familie die (mogelijk) gaat promoveren, inmiddels heb je gezien wat het allemaal teweegbrengt, weer waar je aan begint… Dank voor alle goede gesprekken en advies over de afgelopen jaren, mede door jou zit ik nu aan de overkant van het kanaal.

Jaap, fantastische oom bedankt voor het mooie werk dat je hebt geleverd aan de illustraties van dit boekje. Ik ben erg blij dat jij het hebt gedaan en ook dat je het geregelde stalken geen probleem vond. Ik sta bij je in het (bier)krijt! **Ivo** en **Sophie** bedankt voor alle lieve support en vriendelijke woorden altijd. Lieve oom, bedankt voor alle inspiratie en (medische persoonlijke/familiaire) hulp gedurende de afgelopen jaren. Altijd zeer gewaardeerd en blij dat jullie erbij zijn, ik kijk ernaar uit om exact 22 jaar na jouw promotie ook te mogen verdedigen.

Lieve **mam** en **pap**, ik ben zeer blij dat jullie erbij kunnen zijn. De afgelopen jaren waren niet eenvoudig en soms vol ellende. Laten we er vandaag en de komende tijd betere tijden van maken en een gezellig feestje vieren. ☺ Dankjewel voor alle support en interesse gedurende mijn onderzoek en tot snel in Cambridge!

Lieve Talli, mijn steun en toeverlaat. Sorry voor, de soms stress momenten (indien er papers moesten worden gesubmit of als tripjes weer eens niet door gingen of als er halsoverkop moest worden teruggegaan). Dankjewel voor alles de afgelopen jaren en dankjewel dat je me alle ruimte hebt gegeven om naar Cambridge te verhuizen. Ik kijk uit naar ons volgende avontuur samen met onze 3de partner in crime **Kara**.